frontiers | Research Topics

Recent advances in papillary thyroid carcinoma: Diagnosis and predictive factors

Edited by
Erivelto Martinho Volpi and Jose Federico Carrillo

Published in
Frontiers in Endocrinology

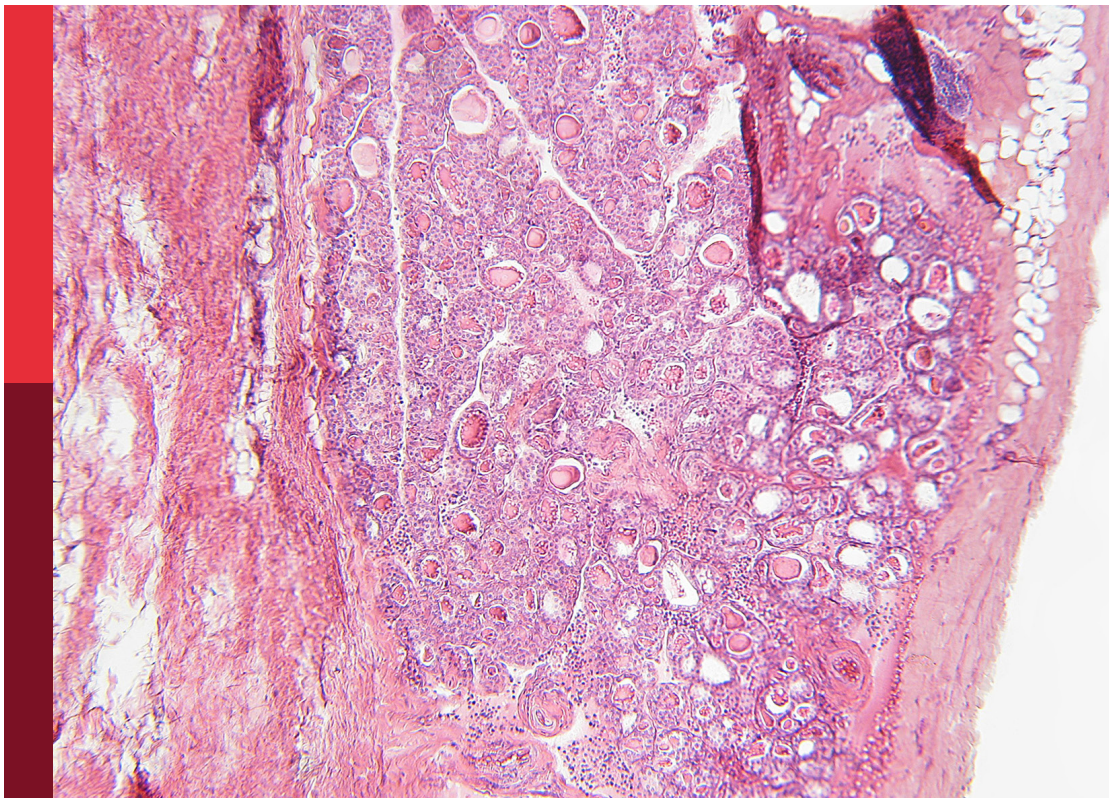

ISSN 1664-8714
ISBN 978-2-8325-3849-4
DOI 978-2-8325-3849-4

About Frontiers

Frontiers is more than just an open access publisher of scholarly articles: it is a pioneering approach to the world of academia, radically improving the way scholarly research is managed. The grand vision of Frontiers is a world where all people have an equal opportunity to seek, share and generate knowledge. Frontiers provides immediate and permanent online open access to all its publications, but this alone is not enough to realize our grand goals.

Frontiers journal series

The Frontiers journal series is a multi-tier and interdisciplinary set of open-access, online journals, promising a paradigm shift from the current review, selection and dissemination processes in academic publishing. All Frontiers journals are driven by researchers for researchers; therefore, they constitute a service to the scholarly community. At the same time, the *Frontiers journal series* operates on a revolutionary invention, the tiered publishing system, initially addressing specific communities of scholars, and gradually climbing up to broader public understanding, thus serving the interests of the lay society, too.

Dedication to quality

Each Frontiers article is a landmark of the highest quality, thanks to genuinely collaborative interactions between authors and review editors, who include some of the world's best academicians. Research must be certified by peers before entering a stream of knowledge that may eventually reach the public - and shape society; therefore, Frontiers only applies the most rigorous and unbiased reviews. Frontiers revolutionizes research publishing by freely delivering the most outstanding research, evaluated with no bias from both the academic and social point of view. By applying the most advanced information technologies, Frontiers is catapulting scholarly publishing into a new generation.

What are Frontiers Research Topics?

Frontiers Research Topics are very popular trademarks of the *Frontiers journals series*: they are collections of at least ten articles, all centered on a particular subject. With their unique mix of varied contributions from Original Research to Review Articles, Frontiers Research Topics unify the most influential researchers, the latest key findings and historical advances in a hot research area.

Find out more on how to host your own Frontiers Research Topic or contribute to one as an author by contacting the Frontiers editorial office: frontiersin.org/about/contact

Recent advances in papillary thyroid carcinoma: Diagnosis and predictive factors

Topic editors

Erivelto Martinho Volpi — Centro de referencia no ensino do diagnóstico por imagem (CETRUS), Brazil

Jose Federico Carrillo — National Institute of Cancerology (INCAN), Mexico

Citation

Volpi, E. M., Carrillo, J. F., eds. (2023). *Recent advances in papillary thyroid carcinoma: Diagnosis and predictive factors*. Lausanne: Frontiers Media SA. doi: 10.3389/978-2-8325-3849-4

Table of contents

frontiers | Frontiers in Endocrinology

TYPE Editorial
PUBLISHED 15 September 2023
DOI 10.3389/fendo.2023.1283397

OPEN ACCESS

EDITED AND REVIEWED BY
Claire Perks,
University of Bristol, United Kingdom

*CORRESPONDENCE
Jose Federico Carrillo
josejosecarr@gmail.com

RECEIVED 26 August 2023
ACCEPTED 30 August 2023
PUBLISHED 15 September 2023

CITATION
Volpi EM, Ramirez-Ortega MC and Carrillo JF (2023) Editorial: Recent advances in papillary thyroid carcinoma: diagnosis and predictive factors. *Front. Endocrinol.* 14:1283397. doi: 10.3389/fendo.2023.1283397

Editorial: Recent advances in papillary thyroid carcinoma: diagnosis and predictive factors

Erivelto Martinho Volpi[1], Margarita Carmen Ramirez-Ortega[2] and Jose Federico Carrillo[3]*

[1]Head and Neck Department, Centro de Referencia no Ensino do Diagnóstico por Imagem (CETRUS), São Paulo, Brazil, [2]Departamento de Farmacología, Instituto Nacional de Cardiologia Ignacio Chavez, Mexico City, Mexico, [3]Head and Neck Department, National Institute of Cancerology (INCAN), Mexico City, Mexico

KEYWORDS

differentiated thyroid carcinoma, TERT (telomerase reverse transcriptase) in thyroid carcinoma, Radioiodine resistance in differentiated thyroid carcinoma, CEUS (Contrast enhanced ultrasound) in thyroid cancer, BRAFV600 mutation in thyroid carcinoma, FNAB (fine needle aspiration biopsy) in thyroid nodules

Editorial on the Research Topic
Recent advances in papillary thyroid carcinoma: diagnosis and predictive factors

In this Research Topic, novel strategies are presented to discern genomic and molecular basis, early and accurate diagnosis of Papillary thyroid carcinoma(PTC), as well as predictive factors for recurrence, which help in the design of new treatment strategies. Figure 1.

Cell cycle-related lncRNAs (long non -coding protein RNA) signatures (CCLRSig) are investigated by Li et al., utilizing the TCGA. They identify five signatures (FOXD2-AS1, LOC100507156, BSG-AS1, EGOT, and TMEM105) which predict the recurrence-free interval (RFI) in papillary PTC through Kaplan-Meier analyses, Receiver Operating Curve (ROC), and a Cox multivariate model. Further, a nomogram with clinicopathological features included gave an area under the curve (AUC) in ROC analyses, of 0.681 at five years. The higher risk scores determined by the aforementioned signature correlated with higher immune cell infiltration patterns which suggests a regulatory role from their findings to the immune processes of the malignancy.

Another paper by He et al., defines, with data extracted from the TCGA - in BRAFV-600 gene mutated thyroid carcinomas -STRA6 gene upregulation which defines the nature of the immune system activation and interaction of IL2-STAT5 pathway. Decreased activation of CD8+ T cells in the tissue harboring these thyroid carcinomas defines a higher potential for invasion and metastasis development, involving an increase in the epithelial-mesenchymal transition process, all of which worsens the prognosis of patients with upregulated STRA6. These facts open a new venue for the development of more precise therapeutic strategies.

Regarding genetics encoding papillary thyroid carcinoma (PTC), Li et al. analyzed patients with stages I and IV, comparing different stages of PTC using The Cancer Genome Atlas(TCGA) with edgeR technology and describe TIMP1, LOX, CD276, IFNA1, TLR2, and POSTN as key genes involved in the development of the malignancy. As well, the protein-

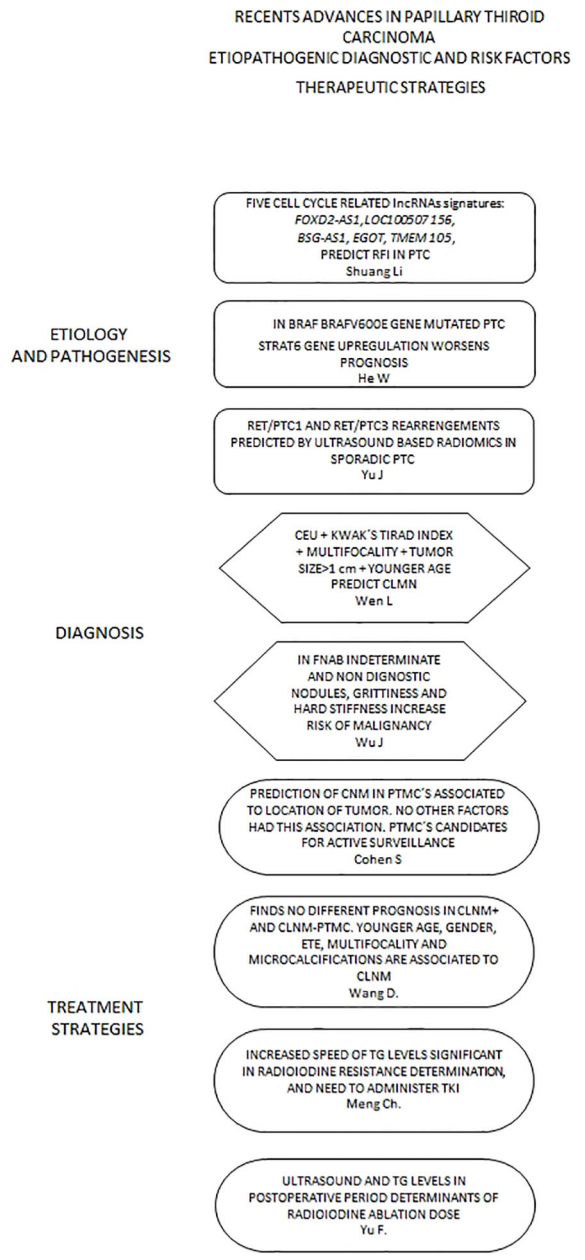

FIGURE 1
Presents a flow chart that displays relevant articles included in this topic according to different scopes regarding Papillary Thyroid Carcinoma. lncRNAs, long non-coding protein RNA; RFI, Recurrence Free Interval; PTC, Papillary Thyroid Carcinoma; CEU, Contrast-enhanced Ultrasound; CLNM, Central Lymph Node Metastasis; CNM, Cervical Node Metastases; FNAB, Fine Needle Aspiration Biopsy; PTMC, Papillary Thyroid Microcarcinoma; ETE, Extrathyroid Extension; TG, Thyroglobulin; TKI, Thyrosine Kinase Inhibitors.

protein interaction (PPI) of these genes was evaluated and finally, 47 miRNA and 44 transcription factors were described bound to the previously described genes. CD276, POSTN, and IFNA1 may be considered as new potential biomarkers associated with the prognosis of thyroid cancer. In addition, TF–miRNA–target gene regulatory is involved in the development of PTC. These findings explain different clinical courses in patients with similar histology features and PTC.

Yu et al., through ultrasound images (Radiomics) construct a nomogram to predict RET rearrangements in sporadic papillary thyroid carcinoma. Although non-selective determination of RET/PTC1 and RET/PTC3 is performed, future efforts and studies are warranted to describe mutations associated with high-risk characteristics (RET/PTC3) without the need for a gene test.

An article by Fang et al. describes a combination of contrast-enhanced ultrasound (CEU) characteristics in thyroid nodules, to increase the diagnostic accuracy of this method in partially cystic lesions. Briefly, the peak intensity index (P1<1), centrifugal perfusion, and heterogeneous enhancement were predictors of malignancy, with better results compared to Kwak´s Ti-Rads index; however, the cases number is small and the study was performed by only one individual, which warrants prospective and larger studies including different operators.

In the same order of ideas, Li et al. describe the usefulness of CEU combined with primary tumor ultrasound characteristics to predict the presence of clinical (cN1a) and pathologic central lymph node metastasis (pN1a). They find tumor size >1cm, multifocality, and younger age combined with hyperenhancement in areas close to the primary tumor as indicative of cN1a metastases, which if validated in larger studies could lead to new paradigms regarding indications for central lymph node dissection. Regarding pN1a lesions, these were associated with young age, large size, and multifocality.

Prediction of BRAF mutations according to elastographic and gray-scale features of thyroid nodules ultrasound (although not including benign lesions) is reported by Wang et al. Although nowadays $BRAF^{v600}$-mutation associated to high-risk prognosis in differentiated thyroid cancer is debated (1), the association of the ultrasonographic features (Radiomics) to the presence of this mutation is suggested and probably, in future studies, the association of these characteristics to other mutations like TERT (telomerase reverse transcriptase) promoter mutations chr-5, 1,295,228 C>T (C228T) and 1,295,250 C>T (C250T)) (2), will help to design more accurate surgical approaches and adjuvant therapies.

Although containing a small number of cases, the report from Xue et al. finds a color doppler ultrasound characterized by a spoked-wheel figure in thyroid nodules to be highly specific to detect papillary carcinoma, which has a 100% accuracy compared to grey-scale ultrasound (16%). This paper represents another interesting contribution to detect non-invasively the presence of thyroid cancer, and likely high-risk prognostic factors, although the prevalence of spoke-wheel blood flow is low in thyroid nodules (0.1%).

The use of Computerized Tomography (CT) Radiomics combined with clinical features of thyroid nodules to predict extrathyroidal extension (ETE) is described by Yu et al. They describe age, gender, tumor size, and a Rad-score (CT radiomics) as associated with ETE with an AUC (area under the curve) greater than 0.75 in the Receiver Operating Curve (ROC) analyses, which demonstrates a high efficiency for this nomogram. Larger studies on this subject are warranted and designed to obtain definitive external validation and improvement of this nomogram.

Regarding the prognosis of papillary microcarcinoma in T1N0M0 Stage, Qian et al. report, with the propensity score-matched (PSM) analyses, similar prognoses for patients treated with and without

surgery in a series obtained from the SEER database, which adds support to the active surveillance strategy in these lesions, although the retrospective nature of the study, the lack of some clinical and pathological data expected from cases analyzed from the SEER and the small number of patients which did not have surgery, although elective candidates, warrant the need to perform larger and prospective studies.

Another clinical study by Zhao and Gong explores the SEER database and a PSM analyses the long-term effect of radioactive iodine (131I) in patients with low and intermediate risk. Although a retrospective study extracted from the SEER database, a beneficial effect was demonstrated on the whole with the administration of I131, specifically in patients >55 years of age, with multifocality and extrathyroid extension. In microcarcinomas, N0, unifocal and no extrathyroid extension cases the effect of radioiodine is nil.

ine needle aspiration biopsy (FNAB) of thyroid nodules has high accuracy; however, in spite of the TIRADs score and Bethesda system development, the presence of indeterminate and non-diagnostic categories in significant and cellular punctures, confers higher relevance to clinical findings as has been reported in previous studies (3). The paper from Wu et al. brings over again the subject regarding nodule clinical characteristics during FNAB procedures, and they find grittiness and hard stiffness as major aids in making decisions regarding nodules with indeterminate diagnosis. These facts warrant future large prospective studies to include the combination of FNAB, clinical, and radiologic factors to increase the diagnostic accuracy of this test, especially in the aforementioned Bethesda category.

Zhang et al. describe in a cohort of patients aged ≥65 years a nomogram that included ten factors: age, gender, marital status, histologic type, grade, TNM stage, surgery status, and tumor size, and predicted overall survival (OS) in their cohorts either in training and in external validation. This nomogram allowed the development of software that accurately predicted OS in geriatric patients. Surgery added better OS in high-risk patients. Although other nomograms (4) have been developed the application proposed is of major value in this specific population.

Eng et al. reports-with the identification of single nucleotide variants- progression of BTG (Benign thyroid goiter) to papillary thyroid carcinoma through FANCD1 (BRCA2) and FANCD2 genes, and hypothesize that papillary thyroid cancer related to goiter (PCb) and non-related to goiter (PCa) have different pathways of development. PCb was induced by Jak-STAT and Notch signaling pathways and PCa by thyroid kinase pathways activation. They propose independent mechanisms for the development of papillary thyroid cancer in patients with BTG, stating that PCb is not an intermediate stage in the development of thyroid cancer.

A very interesting report by Wang et al. performs a multivariate analysis of clinical factors and ultrasound characteristics to predict cervical node metastasis (CNM). Age, gender, nodule size, multifocality, contact extent with thyroid capsule ≥25%, maximal elastography ≥48.4, and interrupted capsule at CEUS in the multivariate analyses allowed calculation of CNM in thyroid carcinoma, with a ROC (Receiver Operating Curve) analyses with more than 80% predictive capability. Further studies are warranted for external validation of these results.

A clinical and genetic markers nomogram was created and validated by Ma et al. where they predict the presence of central lymph node metastases (CLNM) in papillary carcinoma patients clinically and ultrasonographically negative for CNM. Gender, Hashimoto´s thyroiditis, extrathyroidal extension, presence of TERT promoter, and NRas mutations were found significantly associated with CLNM. Of note, this study identifies as well the non-significant association of BRAFV600 mutation to risk factors and overall prognosis in papillary thyroid carcinoma.

A paper by Cohen et al. describes the prognostic factors of Papillary thyroid microcarcinoma (PTMC) associated with CNM and consequently its candidacy for active surveillance. They only find the location of the tumor either superior or inferior pole lesion as definers of CNM. Size, irregular margins, closeness to the capsule of the trachea and thyroiditis were non-associated to locoregional metastases. As an aside, in their study they consider microcarcinomas as nodules up to 2.7 cm and 1 cm in ultrasound and pathology diagnosis, respectively, and propose a definition of microcarcinomas further for lesions up to 1.5-2 cm by ultrasound.

A study in the same line by Wang et al. constructs a nomogram for the prediction of CLNM in PTMC. These authors find -using ultrasound, clinical, and pathological factors -that younger age, gender, ETE, multifocality and microcalcifications are the most significant ones associated with the presence of CLNM. Of note, DFS (disease-free survival) did not show a significant difference when comparing CLNM+ and CLNM- patients, which gives further support to the active surveillance policy in PTMC cases.

CT (Computerized Tomography) has not been considered a major tool for diagnosing CNM. An innovative article by Zhu et al. uses different contrast enhancements determined by CT in HU(Hounsfield Units), regarding lymph nodes(ENHU), esternocleidomastoid muscle(EMHU), and plain lymph node (PNHU) scans. They find that values of ENHU, ENHU-PNHU, ENHU-EMHU, and ENHU/EMHU are significantly related to high accuracy regarding detection of CNM with receiver-operating curve (ROC) analyses performed with higher than 0.8 area under the curve. This is one of the few manuscripts yet to exist regarding the use of CT in early- stage thyroid carcinoma.

Radioactive iodine resistant (RAIR) cases with metastatic disease are analyzed according to thyroglobulin and TSH change speed in the manuscript by Meng et al. Although the concept has been raised in previous reports and is considered by some authors as an important criterion to determine radioactive iodine-resistant malignancies (5), they construct a nomogram based on Thyroglobulin stimulated (Ts) differences at ablation and first recurrence: Ts1-Ts2: ΔTgs, as well as Thyroid Stimulant Hormone levels at same periods: TSHs1-TSH2= ΔTSHs. A ratio ΔTgs/ΔTSHs considering these two differences ≤1.5 as well as older age predicts rapid progression of the disease for these patients, which makes closer monitoring imperative, along with considering early administration of TKI agents.

The study by Yu et al., —although not including the extrathyroid extension factor (ETE)—designs a nomogram with two variants

including overall ultrasound characteristics (first variant) and seven precise ultrasonographic signs (aspect transverse ratio, cystic change, microcalcification, mass hyperecho, echogenicity, lymphatic hilum structure, and vascularity) which together with Tg and TgAb levels are associated to residual disease or CLNM. This analysis presents a worthwhile tool to determine the best ablation radioiodine dose.

Author contributions

EV: Conceptualization, Formal Analysis, Investigation, Project administration, Supervision, Visualization, Writing – original draft, Writing – review & editing. MR-O: Conceptualization, Data curation, Formal Analysis, Investigation, Methodology, Visualization, Writing – original draft, Writing – review & editing. JC: Conceptualization, Data curation, Formal Analysis, Methodology, Project administration, Supervision, Validation, Visualization, Writing – original draft, Writing – review & editing.

Conflict of interest

The authors declare that the research was conducted in the absence of any commercial or financial relationships that could be construed as a potential conflict of interest.

The author(s) declared that they were an editorial board member of Frontiers, at the time of submission. This had no impact on the peer review process and the final decision

Publisher's note

References

1. Henke LE, Pfeifer JD, Ma C, Perkins SM, DeWees T, El-Mofty S, et al. BRAF mutation is not predictive of long-term outcome in papillary thyroid carcinoma. *Cancer Med* (2015) 4(6):791–9. doi: 10.1002/cam4.417

2. Liu R, Xing M. TERT promoter mutations in thyroid cancer. *Endocr Relat Cancer* (2016) 23(3):R143–55. doi: 10.1530/ERC-15-0533

3. Carrillo JF, Frias-Mendivil M, Ochoa-Carrillo FJ, Ibarra M. Accuracy of fine-needle aspiration biopsy of the thyroid combined with an evaluation of clinical and radiologic factors. *Otolaryngol Head Neck Surg* (2000) 122(6):917–21. doi: 10.1016/S0194-59980070025-8

4. Wang J, Zhanghuang C, Jin L, Zhang Z, Tan X, Mi T, et al. Development and validation of a nomogram to predict cancer-specific survival in elderly patients with papillary thyroid carcinoma: a population-based study. *BMC Geriatr* (2022) 22(1):736. doi: 10.1186/s12877-022-03430-8

5. Mutsuddy P, Jeon S, Yoo SW, Zhang Y, Chowdhury MSA, Kim J, et al. Optimization of serum thyroglobulin measured at different time points for prognostic evaluation in differentiated thyroid carcinoma patients. *Med (Baltimore)* (2020) 99(14):e19652. doi: 10.1097/MD.0000000000019652

frontiers in Endocrinology

ORIGINAL RESEARCH
published: 08 December 2021
doi: 10.3389/fendo.2021.783670

Value of Contrast-Enhanced Ultrasound in Partially Cystic Papillary Thyroid Carcinomas

Fengkai Fang[1†], Yi Gong[2†], Liyan Liao[3], Fei Ye[2], Zhongkun Zuo[2], Zhang Qi[1], Xiaodu Li[1] and Chengcheng Niu[1]*

[1] Department of Ultrasound Diagnosis, The Second Xiangya Hospital, Central South University, Changsha, China, [2] Department of Thyroid Surgery, The Second Xiangya Hospital, Central South University, Changsha, China, [3] Department of Pathology, The Second Xiangya Hospital, Central South University, Changsha, China

Partially cystic papillary thyroid carcinomas (PCPTCs) are rarely reported papillary thyroid carcinomas (PTCs) and are usually misdiagnosed as benign nodules. The objective of this study was to provide the various sonographic characteristics of partially cystic thyroid nodules for differentiation between malignant and benign nodules, including those for conventional ultrasound (US) and contrast-enhanced ultrasound (CEUS). Twenty-three PCPTC patients and 37 nodular goiter patients were enrolled in this study. We evaluated the size, cystic percentage, solid echogenicity, calcification, vascularity, and CEUS parameters for each nodule. The final diagnosis of all patients was confirmed *via* surgery. Univariate analysis demonstrated that compared with benign nodular goiters, PCPTCs more frequently presented with calcification, hypoechogenicity of the solid part, hypoenhancement, heterogeneous enhancement, centrifugal perfusion, peak intensity index <1, time to peak index ≥1, and area under the curve index <1 on preoperative US and CEUS. Binary logistic regression analysis demonstrated that heterogeneous enhancement, centrifugal perfusion, and peak intensity index <1 are independent CEUS characteristics related to malignant PCPTCs and can be used for their differentiation from benign nodular goiters (all $p < 0.05$). Our study indicated that preoperative CEUS characteristics may serve as a useful tool to distinguish malignant PCPTCs from benign thyroid nodules.

Keywords: thyroid carcinomas, partially cystic thyroid nodules, thyroid ultrasonography, partially cystic papillary thyroid carcinomas (PCPTCs), contrast-enhanced ultrasound (CEUS)

OPEN ACCESS

Edited by:
Eleonora Molinaro, University of Pisa, Italy

Reviewed by:
Carla Gambale, University of Pisa, Italy
Michael Cordes, University of Erlangen Nuremberg, Germany

***Correspondence:**
Chengcheng Niu
niuchengcheng@csu.edu.cn

[†]These authors have contributed equally to this work

Specialty section:
This article was submitted to Cancer Endocrinology, a section of the journal Frontiers in Endocrinology

Received: *26 September 2021*
Accepted: *15 November 2021*
Published: *08 December 2021*

Citation:
Fang F, Gong Y, Liao L, Ye F, Zuo Z, Qi Z, Li X and Niu C (2021) Value of Contrast-Enhanced Ultrasound in Partially Cystic Papillary Thyroid Carcinomas. Front. Endocrinol. 12:783670. doi: 10.3389/fendo.2021.783670

INTRODUCTION

Thyroid carcinomas have a mostly solid composition, but those with predominant cystic changes (>50% of the nodule) can be observed in 2.5%–6.0% of all thyroid carcinoma cases (1, 2). In a prospective study, 213 partially cystic thyroid nodules in 196 patients who had consecutively undergone prospective sonographic diagnosis and ultrasonography-guided fine-needle aspiration biopsy (US-FNAB) were included, and the rate of malignancy for partially cystic thyroid nodules was 5.2% (3). Thyroid nodules can be classified as cystic or almost completely cystic, spongiform, mixed cystic and solid, solid, or almost completely solid according to their composition as

ascertained by ultrasonography (4). However, to our knowledge, there are few studies that have investigated sonographic features as predictors for the diagnosis of malignant partially cystic thyroid nodules.

US-FNAB is the preferred method for the preoperative diagnosis of benign and malignant thyroid lesions. Current guidelines consider a size ≥1 cm (in nodules with high suspicion), 1.5–2.0 cm (in nodules with any suspicious US features), or 2.0 cm (in nodules without any suspicious US features) as a criterion for US-FNAB, regardless of the cystic portion (5). However, US-FNAB has a high rate of nondiagnostic and false-negative results for the diagnosis of partially cystic thyroid nodules (6).

Contrast-enhanced ultrasound (CEUS), as a relatively novel ultrasound (US) technique, has great significance value in the diagnosis of collapsing benign cystic or predominantly cystic thyroid nodules when combined with clinical history according to the 2020 Chinese guidelines for ultrasound malignancy risk stratification of thyroid nodules (7, 8). However, very few published studies have reported the use of CEUS for predominant cystic thyroid carcinomas. To our knowledge, this is the first article describing the CEUS features and corresponding histopathology of PCPTCs. Hence, the aim of the present study was to provide CEUS characteristics for PCPTCs in order to distinguish them from benign nodules.

MATERIALS AND METHODS

Patients

The study was approved by the Ethical Committee of the Second Xiangya Hospital of Central South University in China and was performed in accordance with the Declaration of Helsinki for human studies. The requirement of informed consent from human subjects is sometimes waived by institutional review boards (IRBs) for protocols that include a retrospective review of images acquired for clinical diagnostic purposes. From June 2017 to August 2021, 27 partially cystic thyroid carcinoma patients who received conventional US and CEUS examinations were retrospectively enrolled in this case-control study. The inclusion criteria were as follows: 1) patients with mixed echoic thyroid nodules that were confirmed as PTCs with partial cystic degeneration by pathologic examinations after surgery; 2) no invasive procedure such as thyroid surgery or FNA was previously performed. Four patients were excluded because they had different types of thyroid cancers: two medullary thyroid carcinomas and two follicular carcinomas. For patients with multifocal PTCs, only the largest was selected. Finally, 23 patients with 23 PCPTCs were included in this study. In addition, from August 2017 to August 2021, 37 patients with 37 mixed echoic thyroid nodules who received conventional US and CEUS examinations were recruited for this study as a control group. The inclusion criteria were as follows: 1) patients with mixed echoic thyroid nodules that were confirmed to be nodular goiters by pathologic examination after surgery; 2) no invasive procedure such as thyroid surgery or FNA was previously performed. For patients with multifocal thyroid nodules, only the largest was selected. Finally, 37 patients with 37 nodular goiters were included in this study. Ultimately, 60 mixed echoic thyroid nodules in 60 patients were enrolled in the study.

Conventional US

A Siemens Acuson S3000 US scanner (Siemens Medical Solutions, Mountain View, CA, USA) equipped with 9L4 (4–9 MHz) and 18L6 (6–18 MHz) linear array transducers was used for conventional US, and a 9L4 linear array transducer was used for CEUS. All examinations were performed by the same operator with 15 years of experience in thyroid ultrasound diagnosis and 10 years of experience in performing CEUS to prevent bias from different operators and to ensure optimized image quality. All selected thyroid nodules were evaluated by conventional B-mode US and color-Doppler US for the following US features: size (the largest diameter), cystic percentage (≥50% or <50%), solid part echogenicity (hypoechogenicity or isoechogenicity), calcification (present or absent), and internal vascularity (present or absent).

The nodules were classified according to the Thyroid Imaging Reporting and Data System (TI-RADS) proposed by Kwak et al. (9). According to that classification, five US suspicious features (solid component, hypoechogenicity or marked hypoechogenicity, microlobulated or irregular margins, taller-than-wide shape, and presence of microcalcifications) were applied to categorize the thyroid nodules: TI-RADS score 3 (no suspicious US features), 4a (one suspicious US feature), 4b (two suspicious US features), 4c (three or four suspicious US features), and 5 (five suspicious US features). In this study, hypoechogenicity was applied for the solid part of these mixed echoic thyroid nodules.

CEUS and Analysis

CEUS was performed using contrast pulsed sequencing (CPS) technology [mechanical index (MI) = 0.07]. SonoVue (Bracco, Italy) was injected intravenously as a bolus of 3.0 ml *via* a 20-gauge antecubital vein cannula, followed by a saline flush of 5 ml, with the timer started simultaneously. Thyroid nodule imaging lasted at least 60 s. The CEUS videos were digitally recorded and analyzed with CEUS software (Contrast Dynamics, Mountain View, CA, USA). Time-intensity curves (TICs) of the thyroid within selected regions of interest (ROIs) were acquired, and the contrast enhancement features of thyroid nodules were applied according to our previous study (10). After comparison with the surrounding thyroid parenchymal enhancement, the contrast enhancement features were classified as follows: enhancement type (hyperenhancement, isoenhancement, hypoenhancement), perfusion pattern (centripetal perfusion, the perfusion of microbubbles from the periphery to the center of nodule; centrifugal perfusion, the perfusion of microbubbles from the center to the periphery of nodule), enhancement uniformity (homogeneous, the microbubbles were evenly distributed; heterogeneous, the microbubbles were unevenly distributed), peak intensity (PI; expressed as a percentage), time to peak (TP; expressed in seconds), and area under the curve (AUC; expressed in percentage by seconds). The PI, TP, and AUC of the nodules are reported as indices by the ratio of the ROI of the

nodules to the ROI of the thyroid parenchymal tissue. PI index represents the ratio of the quantitative values of peak intensity of the nodule to the quantitative values of thyroid parenchymal tissue. If the average quantitative values of nodule were higher or equal to that of the thyroid parenchymal tissue, the PI index was expressed as ≥1; if this was not the case, the PI index was expressed as <1. Similarly, TP index ≥1 meant that the time to peak of the nodule was slower or equal to that of the thyroid parenchymal tissue; AUC index ≥1 meant that the area under the curve of the nodule was higher or equal to that of the thyroid parenchymal tissue.

Reference Standard

FNA Bethesda cytology (BC) diagnoses were divided into six categories according to the Bethesda System (5). The histopathological results after surgery were used as the reference standard for the final diagnosis of PTCs or nodular goiters.

Statistical Analysis

The statistical analysis was performed with SPSS version 21.0 software (SPSS, Chicago, IL, USA). Continuous data are presented as the mean and standard deviation (SD) and compared by the independent t-test. Categorical data were presented as percentages and analyzed by the chi-square test. Binary logistic regression was used to assess significant CEUS features and their independent association with malignant partially cystic thyroid nodules. The sensitivity, specificity, accuracy, positive predictive value (PPV), and negative predictive value (NPV) of TI-RADS for differentiation between benign and malignant thyroid nodules were calculated. A statistically significant difference was determined when $p < 0.05$.

RESULTS

A total of 60 patients with 60 partially cystic thyroid nodules (23 malignant and 37 benign) were included in the analysis. For malignant thyroid nodules, the FNA cytology diagnoses for 23 nodules were as follows: one (4.3%) nodule was BC 3 (atypia or follicular lesion of undetermined significance), three (13.1%) nodules were BC 4 (follicular neoplasm or suspicious for a follicular neoplasm), seven (30.4%) nodules were BC 5 (suspicious for malignancy), and 12 (52.2%) nodules were BC 6 (malignant). All nodules were confirmed as PTC by pathologic examinations after surgery. For benign thyroid nodules, 16 patients had malignant-looking thyroid nodules on the other thyroid lobe, and FNA cytology was carried out for the malignant thyroid nodules. Thus, 16 patients with PTCs on the other thyroid lobe were confirmed by pathologic examinations after total thyroidectomy; 16 benign thyroid nodules on this thyroid lobe were also confirmed by histopathology. The FNA cytology diagnoses for the other 21 nodules were as follows: six (28.6%) nodules were BC 3, and 15 (71.4%) were BC 2 (benign).

The clinical characteristics of the patients are outlined in **Table 1**. The average ages of PCPTC patients and nodular goiter patients were 41.74 ± 9.99 years (range: 29–63 years) and 51.92 ± 9.55 years (range: 25–68 years), respectively, and PCPTC patients were younger than nodular goiter patients in this study ($p < 0.05$). Male patients constituted 26.1% of PCPTC patients and 5.4% of nodular goiter patients; thus, female patients accounted for a larger proportion of nodular goiters than PCPTCs ($p < 0.05$). Thirteen (56.5%) PCPTC patients and 31 (83.8%) nodular goiter patients had multifocal thyroid nodules, and nodular goiter patients had many more thyroid nodules per patient than PCPTC patients in this study ($p < 0.05$).

The US characteristics of partially cystic thyroid nodules are outlined in **Table 2**. The mean diameters were 29.35 ± 12.21 mm (range: 9–51 mm) for malignant partially cystic thyroid nodules and 32.97 ± 14.39 mm (range: 10–68 mm) for benign partially cystic thyroid nodules. In the malignant thyroid nodule group, six (26.1%) nodules had cystic percentage greater than 50% (**Figure 1**), 21 (91.3%) nodules had calcifications (**Figure 1**), 18 (78.3%) nodules exhibited hypoechogenicity in the solid part of the partially cystic nodules (**Figure 1**), and five (21.7%) nodules exhibited isoechogenicity in the solid part. Seventeen (73.9%) nodules had internal blood flow. For the CEUS parameters, 10 (43.5%) nodules exhibited hypoenhancement (**Figure 2**), and 22 (95.7%) nodules had heterogeneous enhancement (**Figure 2**), which meant that the microbubbles in the majority of the nodules were unevenly distributed. Twenty (87.0%) nodules had a centrifugal perfusion pattern, and three nodules (13.0%) had a centripetal perfusion pattern (**Figure 2**), indicating that most of the nodules received a perfusion of microbubbles from the center to the periphery. The quantitative CEUS parameters showed that 14 (60.1%) nodules had a PI index <1 (**Figure 2**), 14 (60.9%) nodules had a TP index ≥1, and 21 (91.3%) nodules had an AUC index <1 (**Figure 2**). In the benign thyroid nodule group, 15 (40.5%) nodules had a cystic percentage greater than 50%, 29 (78.4%) nodules had an absence of calcification, 15 (40.5%) nodules exhibited hypoechogenicity in the solid part, and 22 (59.5%) nodules exhibited isoechogenicity in the solid part. Twenty-three (62.2%) nodules had internal blood flow. For the CEUS parameters, 31 (83.8%) nodules exhibited hyperenhancement or isoenhancement, 30 (81.1%) nodules had uniform enhancement, and 34 (91.9%) nodules had a centripetal

TABLE 1 | Clinical characteristics of the PCPTCs and nodular goiters.

Characteristics	PCPTCs (n = 23)	Nodular goiter (n = 37)	p Value
Age (years)	41.74 ± 9.99	51.92 ± 9.55	0.000*
Male sex	6 (26.1)	2 (5.4)	0.045*
Multifocality	13 (56.5)	31 (83.8)	0.020*

*$p < 0.05$ was considered a significant difference.
PTPTC, partially cystic papillary thyroid carcinoma.

TABLE 2 | Ultrasound characteristics of the PCPTCs and nodular goiters.

Characteristics	PCPTCs (n = 23)	Nodular goiter (n = 37)	p Value
Conventional US parameters			
Size (mm)	29.35 ± 12.21	32.97 ± 14.39	0.320
Cystic percentage			0.282
≥50%	6 (26.1)	15 (40.5)	
<50%	17 (73.9)	22 (59.5)	
Calcification			0.000*
Present	21 (91.3)	8 (21.6)	
Absent	2 (8.7)	29 (78.4)	
Solid part echogenicity			0.004*
Hypoechogenicity	18 (78.3)	15 (40.5)	
Isoechogenicity	5 (21.7)	22 (59.5)	
Internal vascularity			0.408
Present	17 (73.9)	23 (62.2)	
Absent	6 (26.1)	14 (37.8)	
CEUS parameters			
Enhancement type			
Hypo-	10 (43.5)	6 (16.2)	0.020*
Hyper- or iso-	13 (56.5)	31 (83.8)	
Enhancement uniformity			0.000*
Homogeneous	1 (4.3)	30 (81.1)	
Heterogeneous	22 (95.7)	7 (18.9)	
Perfusion			0.000*
Centripetal	3 (13.0)	34 (91.9)	
Centrifugal	20 (87.0)	3 (8.1)	
PI index			0.000*
≥1	9 (39.1)	31 (83.8)	
<1	14 (60.9)	6 (16.2)	
TP index			0.001*
≥1	14 (60.9)	7 (18.9)	
<1	9 (39.1)	30 (81.1)	
AUC index			0.000*
≥1	2 (8.7)	28 (75.7)	
<1	21 (91.3)	9 (24.3)	

*$p < 0.05$ was considered a significant difference.
PI, peak intensity; TP, time to peak; TP, time to peak time; AUC, area under the curve; PCPTC, partially cystic papillary thyroid carcinoma.

perfusion pattern. The quantitative CEUS parameters showed that 31 (83.8%) nodules had a PI index ≥1, 30 (81.1%) nodules had a TP index <1, and 28 (75.7%) nodules had an AUC index ≥1. The univariate analysis indicated that the PCPTCs more frequently presented with calcification, hypoechogenicity of the solid part, hypoenhancement, heterogeneous enhancement, centrifugal perfusion, PI index <1, TP index ≥1, and AUC index <1 for preoperative US and CEUS compared to benign thyroid nodules (all $p < 0.05$).

For evaluation of the value of CEUS parameters in PCPTCs, a binary logistic regression analysis was performed for all of the statistically significant CEUS variables ($p < 0.05$). The results indicated that enhancement uniformity (B = 4.080, OR = 59.166, 95% CI = 1.928–1,815.846, p = 0.020), centrifugal perfusion (B = 4.502, OR = 90.157, 95% CI = 4.443–1,829.637, p = 0.003), and PI index <1 (B = 5.515, OR = 248.279, 95% CI = 1.655–37241.707, p = 0.031) were independent characteristics related to the PCPTC nodules that could be used to differentiate them from benign nodular goiters (**Table 3**).

Heterogeneous enhancement, centrifugal perfusion, and PI index <1 were independent characteristics related to PCPTCs that could be used to differentiate them from benign thyroid nodes; therefore, we chose these CEUS parameters for the diagnosis of PCPTCs. If the thyroid nodule had more than 2 (≥2) of the above three CEUS characteristics, the thyroid nodule was classified as a malignant thyroid nodule; if the thyroid nodule had less than 2 (<2) of the above three CEUS characteristics, the thyroid nodule was classified as a benign thyroid nodule. Then, the combination diagnosis of Kwak TI-RADS classification and CEUS characteristics was calculated. If the thyroid nodule had a Kwak TI-RADS 4b score and/or CEUS ≥2, the thyroid nodule was classified as a malignant thyroid nodule; if the thyroid nodule had a Kwak TI-RADS 4a score and/or CEUS <2, the thyroid nodule was classified as a benign thyroid nodule. The diagnostic performance of the different methods for differentiation between benign and malignant thyroid nodules is outlined in **Table 4**. The Kwak TI-RADS with a cutoff value of 4a/4b score achieved an Az value of 0.851, with an accuracy of 86.7% (52/60). The CEUS characteristics with a cutoff value of CEUS ≥2 achieved an Az value of 0.924, with an accuracy of 91.7% (55/60). The combination of Kwak TI-RADS and CEUS achieved an Az value of 0.897, with a cutoff value of 4a/4b or CEUS ≥2, and had an accuracy of 88.3% (53/60), which was better than that of Kwak TI-RADS. However, there was no significant difference with respect to diagnostic accuracy for differentiation between benign and malignant thyroid nodules among all groups ($p > 0.05$).

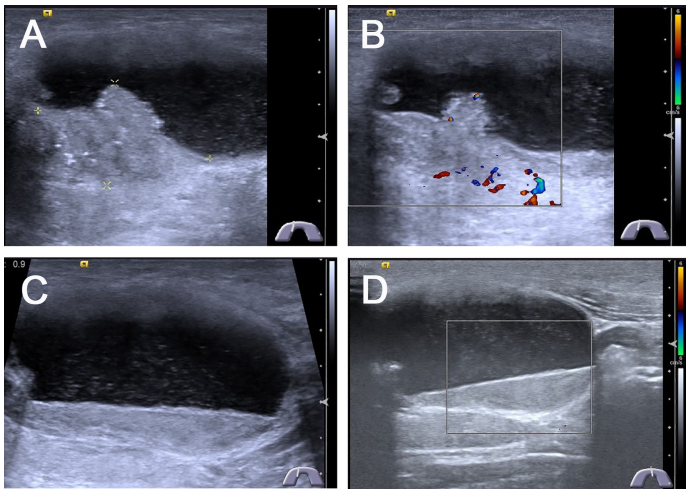

FIGURE 1 | Conventional ultrasonography images of predominantly cystic papillary thyroid carcinoma. **(A)** Longitudinal gray-scale sonography revealed a predominantly cystic 4.2 × 2.4 × 2.7 cm^3 thyroid nodule with a little solid portion abutted on the side of the cyst wall in the thyroid isthmus, the cystic portion was more than 90% of the thyroid node. **(B)** CDFI showed poor blood flow signals in the solid portion of the thyroid nodule. **(C)** Most portions of this thyroid node were cystic with a lot of mobile silt-like isoechoic substance. **(D)** CDFI showed no blood flow signals in the silt-like isoechoic substance.

Of 23 PCPTCs patients, 14 (60.1%) patients had central cervical lymph node metastasis. Histopathological examination of samples using hematoxylin and eosin (H&E) staining showed a predominantly PCPTC with a cystic percentage greater than 90% (**Figure 3**), revealing the thick cystic wall of the mass (3–6 mm) (**Figures 3A, B**) and the solid part abutting on the base side of the cyst wall (**Figures 3C, D**). Many nipple-like bulges were seen on both the cyst wall and the solid part. Meanwhile, some nipple-like bulges (black arrows indicated) were also observed in the central lymph nodes (**Figures 3E, F**), which indicated that those lymph nodes were metastatic for thyroid carcinoma.

DISCUSSION

Partially cystic thyroid nodules are common on ultrasonography and are considered to be a result of the cystic degeneration of either neoplastic or non-neoplastic nodules (11). Although partially cystic thyroid nodules are traditionally interpreted as having a low risk of malignancy, some studies have reported that the frequency of malignancy among partially cystic thyroid nodules varies from 5.2% to 17.6% (3, 6, 12, 13). A study by Kim et al. (14) compared the disease-free survival of 553 PTCs with cystic changes according to the percentage of cystic component (two groups: 25% or 50%) of the thyroid nodules and found that the proportion of the cystic component in PTCs did not affect disease-free survival. In this study, 56 patients (10.1%) were confirmed to have tumor recurrence within the follow-up period, while the independent predictors of recurrence were pathologic size, male sex, and lymph node metastasis. Therefore, it is vital to differentiate malignant thyroid nodules from benign partially cystic thyroid nodules using preoperative ultrasonography and/or US-FNAB.

Some studies have reported the conventional sonographic features of partially cystic thyroid nodules associated with malignancy. Lee et al. (12) reported that partially cystic thyroid nodules with a predominantly solid component (solid portion was >50%), an eccentrically placed solid component, and the presence of microcalcifications were all associated with malignancy. Kim et al. (3) reported that partially cystic thyroid nodules had an eccentric solid portion with an acute angle, and microcalcifications were significantly associated with malignancy. Park et al. (15) reported the malignant sonographic features of an entire partially cystic thyroid nodule and its internal solid portion. A taller-than-wide shape and spiculated or microlobulated margins were associated with malignancy in partially cystic thyroid nodules. Furthermore, an eccentric solid configuration, non-smooth margin, hypoechogenicity, and microcalcifications of the internal solid portion were significantly associated with malignancy. In our study, most PCPTCs had an eccentric solid portion with microcalcifications, which was consistent with recent reports (3, 12, 15). However, the acute angle of the internal solid portion, the taller-than-wide shape, and the spiculated or microlobulated margin of the entire nodule were not shown in our study (15). In a study by Henrichsen et al. (1), 360 malignant thyroid nodules that had been surgically removed were analyzed, nine (2.5%) of which were 51%–100% cystic. Of the nine malignancies (cystic portion >50%), four (44%) demonstrated increased vascularity either in a nodule or in thickened walls (1). In our study, some PCPTCs showed poor blood flow signals in the internal solid portion of the thyroid nodule, which was similar to the Color Doppler Flow Imaging (CDFI) findings of solid PTCs reported by other studies (10, 16). However, there are very few reports regarding the CEUS findings of malignant partially cystic thyroid nodules.

CEUS, as a novel technique for detecting microvessels of tissues, has been widely applied in improving the diagnostic

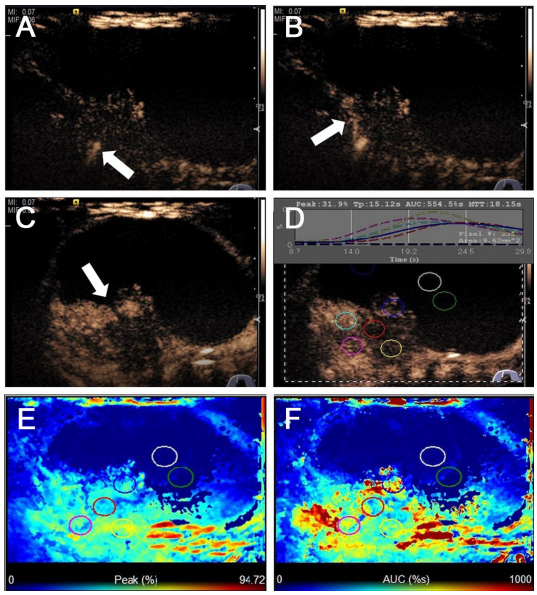

FIGURE 2 | CEUS images of predominantly cystic papillary thyroid carcinoma. **(A)** CEUS image showed a slight enhancement from the bottom of the solid portion at 9 s. **(B)** The enhancement from the bottom to the periphery of the solid portion at 15 s. **(C)** All the solid portions of this nodule heterogeneously enhanced and reached its peak [time to peak (TTP)] at 23 s. **(D)** TICs displayed the wash-in time of 9 s, TTP of 15 s, PI of 31.9%, and AUC of 554.5% s for the solid portion of this thyroid nodule, and the cystic portion of the nodule has no enhancement. **(E)** The parametric color map showed that the solid portion was almost a majority of green with a little blue, the cystic portion was totally blue, which indicated that the PIs for the center of the solid portion was almost equal to those of the periphery of the solid portion. **(F)** The parametric color map showed the solid portion was heterogeneous with a mixture of green, yellow, and red, and the cystic portion was totally blue, which indicated that the AUC for the center of the solid portion was lower than those of the periphery of the solid portion.

accuracy of thyroid nodules. Deng et al. (17) reported that hypoenhancement on CEUS correlated highly with a malignant diagnosis of thyroid nodules (sensitivity: 82.1%, specificity: 84.9%, accuracy: 84.0%, PPV: 71.9%, and NPV: 91.0%). Ma et al. (18) found that heterogeneous enhancement on CEUS showed the best diagnostic performance for papillary thyroid microcarcinoma, with the highest PPV of 88.0%, an accuracy of 83.7%, and a relatively high specificity of 83.9%. However, mixed cystic nodules or almost cystic nodules (cystic portion >75%) were excluded from previous studies due to the demand for elastography (10, 17, 18). In our study, 43.5% of PCPTCs showed hypoenhancement, 95.7% of PCPTCs showed heterogeneous enhancement, and 87% of PCPTCs exhibited centrifugal perfusion, which is inconsistent with the CEUS enhancement of solid PTCs reported in previous studies (10, 19, 20). Compared with benign nodular goiters, PCPTCs more frequently had hypoenhancement, heterogeneous enhancement, centrifugal perfusion, PI index <1, TP index ≥1, and AUC index <1 on preoperative CEUS. Binary logistic regression analysis demonstrated that heterogeneous enhancement, centrifugal perfusion, and PI index <1 are independent CEUS characteristics related to malignant PCPTCs that can be used to differentiate them from benign nodular goiters (all $p < 0.05$). This may be due to increased neovascularization in the malignant nodules; however, the invasive growth characteristics of malignant nodules also destroyed the new blood vessels, formed small tumor thrombi in the necrotic vessels, and led to the occlusion of small blood vessels. Therefore, the degree of CEUS enhancement not only is related to the number of blood vessels but also depends on the state of internal blood vessel function. Especially in PCPTCs with cystic percentage greater than 90%, the solid portion on the cyst wall of the thyroid nodule had few blood vessels around the papillary protrusion in the cyst wall based on the H&E histopathological staining results, which was consistent with the heterogeneous hypoenhancement on CEUS. These results may be explained by the fact that the inner solid portion of the malignant nodule was often located at the base of the papillary protrusion in the cyst wall, and the blood vessels around the lesion easily invaded outward, resulting in ischemic necrosis of the inner solid portion near the side of the cystic portion and continuous cystic degeneration. Furthermore, the inner solid portion of the malignant nodule was located at the base of the papillary protrusion in the cyst wall, and the blood vessels around the lesion easily invaded outward, which may lead to central cervical lymph node metastasis.

This study had several limitations. First, an unavoidable selection bias may have existed, and some patients with suspicious malignancies might not have been enrolled in this study because they did not have surgery. Second, the nodule sizes studied for comparison between the two groups ranged from a few millimeters to tens of millimeters; these size differences might affect the US characteristics of PCPTCs. Third, all conventional US and CEUS examinations were performed by a single experienced operator, which means that the study was not

TABLE 3 | Multivariate logistic regression analysis of CEUS characteristics related to PCPTCs distinguishing from nodular goiters.

Characteristics	Partial regression coefficient, β	Odds ratio	95% Confidence interval	p Value
Heterogeneous enhancement	4.080	59.166	1.928–1,815.846	0.020*
Centrifugal perfusion	4.502	90.157	4.443–1,829.637	0.003*
PI index <1	5.515	248.279	1.655–37,241.707	0.031*

**p < 0.05 was considered a significant difference.*
PCPTC, partially cystic papillary thyroid carcinoma.

TABLE 4 | Diagnostic performance for discrimination between PCPTCs and nodular goiters.

Methods	Cutoff score	Sensitivity, %	Specificity, %	Accuracy, %	PPV, %	NPV, %	Az (95% CI)
TI-RADS	4a/4b	78.3	91.9	86.7	85.7	87.2	0.851 (0.738–0.963)
CEUS	CEUS ≥2	95.7	89.2	91.7	84.6	97.1	0.924 (0.848–1.000)
TI-RADS+CEUS	4a/4b or CEUS ≥2	95.7	83.8	88.3	78.6	96.9	0.897 (0.811–0.984)

TIRADS, Thyroid Imaging Reporting and Data System; CEUS, contrast-enhanced ultrasound; PPV, positive predictive value; NPV, negative predictive value; CI, confidence interval; PCPTC, partially cystic papillary thyroid carcinoma.

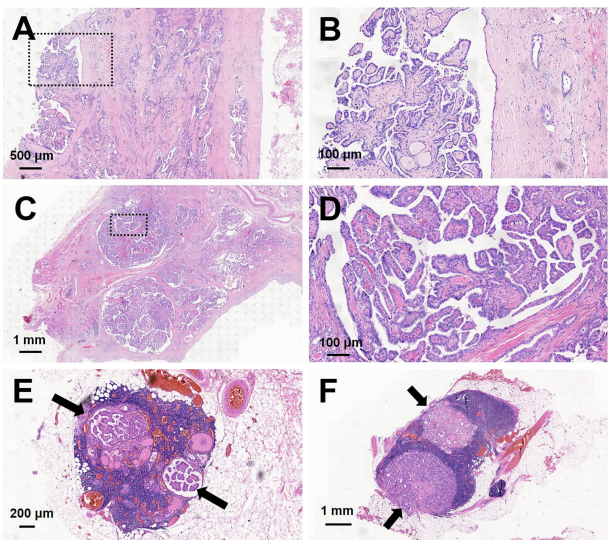

FIGURE 3 | Hematoxylin and eosin (H&E) staining of predominantly cystic papillary thyroid carcinoma and central cervical lymph nodes. The thick cystic wall of the mass showed a lot of nipple-like bulges: **(A)** magnification, ×20; **(B)** magnification, ×100. The solid portion of the mass showed a lot of nipple-like bulges: **(C)** magnification, ×10; **(D)** magnification, ×100. Some nipple-like bulges (black arrows indicated) were shown in two central cervical lymph nodes: **(E)** magnification, ×25; **(F)** magnification, ×10.

operator independent. Because subjective interference caused by other examiners might exist, further studies with more operators performing each examination are needed. Fourth, this was a small-scale retrospective study, which may have caused the inaccurate evaluation of the effect on CEUS parameters by the different nodule sizes of the two groups. Thus, a large-scale prospective study is needed to clarify these findings in the future.

CONCLUSION

PCPTCs are extremely rare cystic PTCs, and very few studies describe their ultrasonographic imaging features and related pathologic findings. On preoperative US and CEUS, PCPTCs more frequently presented with calcification, hypoechogenicity of the solid part, hypoenhancement, heterogeneous enhancement, centrifugal perfusion, PI index <1, TP index ≥1, and AUC index <1 compared with benign nodular goiters. Binary logistic regression analysis demonstrated that heterogeneous enhancement, centrifugal perfusion, and PI index <1 are independent CEUS characteristics related to malignant PCPTCs that can be used to differentiate them from benign nodular goiters. Thus, preoperative CEUS characteristics may serve as a useful tool to distinguish malignant PCPTCs from benign thyroid nodules and thus effectively supplement conventional US.

DATA AVAILABILITY STATEMENT

The raw data supporting the conclusions of this article will be made available by the authors without undue reservation.

ETHICS STATEMENT

The studies involving human participants were reviewed and approved by the Ethical Committee of the Second Xiangya Hospital, Central South University. The patients/participants provided their written informed consent to participate in this study. Written informed consent was obtained from the individual(s) for the publication of any potentially identifiable images or data included in this article.

AUTHOR CONTRIBUTIONS

CN contributed to the conception and design of the work. FF and YG participated in the data analysis and article writing. LL, FY, ZZ, ZQ, and XL participated in the data collection and patients' follow-up. All authors contributed to the article and approved the submitted version.

FUNDING

This project was funded by the National Natural Science Foundation of China (81974267) and the Science and Technology Innovation Program of Hunan Province (2021RC3033).

REFERENCES

1. Henrichsen TL, Reading CC, Charboneau JW, Donovan DJ, Sebo TJ, Hay ID. Cystic Change in Thyroid Carcinoma: Prevalence and Estimated Volume in 360 Carcinomas. *J Clin Ultrasound* (2010) 38(7):361–6. doi: 10.1002/jcu.20714
2. Chan BK, Desser TS, McDougall IR, Weigel RJ, Jeffrey RB Jr. Common and Uncommon Sonographic Features of Papillary Thyroid Carcinoma. *J Ultrasound Med* (2003) 22(10):1083–90. doi: 10.7863/jum.2003.22.10.1083
3. Kim DW, Lee EJ, In HS, Kim SJ. Sonographic Differentiation of Partially Cystic Thyroid Nodules: A Prospective Study. *AJNR Am J Neuroradiol* (2010) 31(10):1961–6. doi: 10.3174/ajnr.A2204
4. Tessler FN, Middleton WD, Grant EG, Hoang JK, Berland LL, Teefey SA, et al. ACR Thyroid Imaging, Reporting and Data System (TI-RADS): White Paper of the ACR TI-RADS Committee. *J Am Coll Radiol* (2017) 14(5):587–95. doi: 10.1016/j.jacr.2017.01.046
5. Haugen BR, Alexander EK, Bible KC, Doherty GM, Mandel SJ, Nikiforov YE, et al. 2015 American Thyroid Association Management Guidelines for Adult Patients With Thyroid Nodules and Differentiated Thyroid Cancer: The American Thyroid Association Guidelines Task Force on Thyroid Nodules and Differentiated Thyroid Cancer. *Thyroid* (2016) 26(1):1–133. doi: 10.1089/thy.2015.0020
6. Bellantone R, Lombardi CP, Raffaelli M, Traini E, De Crea C, Rossi ED, et al. Management of Cystic or Predominantly Cystic Thyroid Nodules: The Role of Ultrasound-Guided Fine-Needle Aspiration Biopsy. *Thyroid* (2004) 14(1):43–7. doi: 10.1089/105072504322783830
7. Zhou J, Yin L, Wei X, Zhang S, Song Y, Luo B, et al. A. Vascular Ultrasound Group of the Society of Ultrasound in Medicine of the Chinese Medical, T. Chinese Artificial Intelligence Alliance for and U. Breast: 2020 Chinese Guidelines for Ultrasound Malignancy Risk Stratification of Thyroid Nodules: The C-TIRADS. *Endocrine* (2020) 70(2):256–79. doi: 10.1007/s12020-020-02441-y
8. Peng Q, Niu C, Zhang Q, Zhang M, Chen S, Peng Q. Mummified Thyroid Nodules: Conventional and Contrast-Enhanced Ultrasound Features. *J Ultrasound Med* (2019) 38(2):441–52. doi: 10.1002/jum.14712
9. Kwak JY, Han KH, Yoon JH, Moon HJ, Son EJ, Park SH, et al. Thyroid Imaging Reporting and Data System for US Features of Nodules: A Step in Establishing Better Stratification of Cancer Risk. *Radiology* (2011) 260(3):892–9. doi: 10.1148/radiol.11110206
10. Peng Q, Niu C, Zhang M, Peng Q, Chen S. Sonographic Characteristics of Papillary Thyroid Carcinoma With Coexistent Hashimoto's Thyroiditis: Conventional Ultrasound, Acoustic Radiation Force Impulse Imaging and Contrast-Enhanced Ultrasound. *Ultrasound Med Biol* (2019) 45(2):471–80. doi: 10.1016/j.ultrasmedbio.2018.10.020
11. Li W, Zhu Q, Jiang Y, Zhang Q, Meng Z, Sun J, et al. Partially Cystic Thyroid Nodules in Ultrasound-Guided Fine Needle Aspiration: Prevalence of Thyroid Carcinoma and Ultrasound Features. *Med (Baltimore)* (2017) 96(46):e8689. doi: 10.1097/MD.0000000000008689
12. Lee MJ, Kim EK, Kwak JY, Kim MJ. Partially Cystic Thyroid Nodules on Ultrasound: Probability of Malignancy and Sonographic Differentiation. *Thyroid* (2009) 19(4):341–6. doi: 10.1089/thy.2008.0250
13. Garcia-Pascual L, Barahona MJ, Balsells M, del Pozo C, Anglada-Barcelo J, Casalots-Casado J, et al. Complex Thyroid Nodules With Nondiagnostic Fine Needle Aspiration Cytology: Histopathologic Outcomes and Comparison of the Cytologic Variants (Cystic vs. Acellular). *Endocrine* (2011) 39(1):33–40. doi: 10.1007/s12020-010-9409-2
14. Kim JY, Kim EK, Lee HS, Kwak JY. Conventional Papillary Thyroid Carcinoma: Effects of Cystic Changes Visible on Ultrasonography on Disease Prognosis. *Ultrasonography* (2014) 33(4):291–7. doi: 10.14366/usg.14028
15. Park JM, Choi Y, Kwag HJ. Partially Cystic Thyroid Nodules: Ultrasound Findings of Malignancy. *Korean J Radiol* (2012) 13(5):530–5. doi: 10.3348/kjr.2012.13.5.530
16. Sun CY, Lei KR, Liu BJ, Bo XW, Li XL, He YP, et al. Virtual Touch Tissue Imaging and Quantification (VTIQ) in the Evaluation of Thyroid Nodules: The Associated Factors Leading to Misdiagnosis. *Sci Rep* (2017) 7:41958. doi: 10.1038/srep41958
17. Deng J, Zhou P, Tian SM, Zhang L, Li JL, Qian Y. Comparison of Diagnostic Efficacy of Contrast-Enhanced Ultrasound, Acoustic Radiation Force Impulse Imaging, and Their Combined Use in Differentiating Focal Solid Thyroid Nodules. *PloS One* (2014) 9(3):e90674. doi: 10.1371/journal.pone.0090674PONE-D-13-30329[pii
18. Ma HJ, Yang JC, Leng ZP, Chang Y, Kang H, Teng LH. Preoperative Prediction of Papillary Thyroid Microcarcinoma *Via* Multiparameter Ultrasound. *Acta Radiol* (2017) 58(11):1303–11. doi: 10.1177/0284185117692167
19. Chen S, Niu C, Peng Q, Tang K. Sonographic Characteristics of Papillary Thyroid Carcinoma With Coexistent Hashimoto's Thyroiditis in the Preoperative Prediction of Central Lymph Node Metastasis. *Front Endocrinol (Lausanne)* (2021) 12:556851. doi: 10.3389/fendo.2021.556851
20. Hong YR, Yan CX, Mo GQ, Luo ZY, Zhang Y, Wang Y, et al. Elastography, and Contrast Enhanced US Features of Papillary Thyroid Microcarcinoma Predict Central Compartment Lymph Node Metastases. *Sci Rep* (2015) 5:7748. doi: 10.1038/srep07748

Conflict of Interest: The authors declare that the research was conducted in the absence of any commercial or financial relationships that could be construed as a potential conflict of interest.

this article, or claim that may be made by its manufacturer, is not guaranteed or endorsed by the publisher.

frontiers in Endocrinology

ORIGINAL RESEARCH
published: 24 January 2022
doi: 10.3389/fendo.2021.810630

Ultrasound and Contrast-Enhanced Ultrasound Characteristics Associated With cN1 and Microscopic pN1 in Papillary Thyroid Carcinoma

Wen Li[1,2†], Shusheng Qiu[3†], Ling Ren[2], Qiuyang Li[2], Shaowei Xue[2], Jie Li[4], Yan Zhang[2] and Yukun Luo[1,2*]*

[1] Department of Ultrasound, Medical School of Chinese People's Liberation Army (PLA), Beijing, China, [2] Department of Ultrasound, The First Medical Center, Chinese PLA General Hospital, Beijing, China, [3] Department of Surgery, ZiBo Central Hospital, Zibo, China, [4] Department of Pathology, The First Medical Center, Chinese PLA General Hospital, Beijing, China

OPEN ACCESS

Edited by:
Michele Caraglia,
University of Campania Luigi Vanvitelli, Italy

Reviewed by:
Giovanni Docimo,
University of Campania Luigi Vanvitelli, Italy
Jeffrey A. Knauf,
Cleveland Clinic, United States

***Correspondence:**
Yukun Luo
luoyk301@126.com
Yan Zhang
zhangyaner301@126.com

[†]These authors have contributed equally to this work and share first authorship

Specialty section:
This article was submitted to Cancer Endocrinology, a section of the journal Frontiers in Endocrinology

Received: 07 November 2021
Accepted: 29 December 2021
Published: 24 January 2022

Citation:
Li W, Qiu S, Ren L, Li Q, Xue S, Li J, Zhang Y and Luo Y (2022) Ultrasound and Contrast-Enhanced Ultrasound Characteristics Associated With cN1 and Microscopic pN1 in Papillary Thyroid Carcinoma. Front. Endocrinol. 12:810630. doi: 10.3389/fendo.2021.810630

Objectives: Lymph node metastases (LNMs) could be stratified into clinical N1 (cN1) and microscopic pN1 (pathological N1), which bear different biological behavior and prognosis. Our study aimed to investigate the associations between LNMs and primary tumor's US (ultrasound) and CEUS (contrast-enhanced ultrasound) characteristics based on the stratification of LNMs into cN1 and microscopic pN1 in papillary thyroid carcinoma (PTC).

Methods: From August 2019 to May 2020, 444 consecutive PTC patients who underwent preoperative neck US and CEUS evaluation were included. According to regional lymph node status, the patients were classified into cN1 group versus cN0 (clinical N0) group and microscopic pN1 group versus pN0 (pathological N0) group. For multiple PTCs, the largest one was selected for the evaluation of US, CEUS and clinical features. Univariate and multivariate analyses were performed to determine independent predictors of cN1 and microscopic pN1.

Results: 85 cN1 versus 359 cN0 patients and 117 microscopic pN1 versus 242 pN0 patients were analyzed. Multivariate logistic regression analysis showed that <55-years-old (OR: 2.56 (1.08–6.04), male [OR: 2.18 (1.22–3.91)], large size [OR: 2.59 (1.71–3.92)], calcification [OR: 3.88 (1.58–9.51)], and hyper-enhancement [OR: 2.78 (1.22–6.30)] were independent risk factors of cN1, while <55-years-old [OR: 1.91 (1.04–3.51)], large size [OR: 1.56 (1.003–2.42)], multifocality [OR: 1.67 (1.04–2.66)] were independent risk factors of microscopic pN1.

Conclusions: For patients with PTC, young age, male, large size, calcification, and hyper-enhancement were independent predictors of cN1, while young age, large size and multifocality were independent predictors of microscopic pN1.

Keywords: ultrasound, contrast-enhanced ultrasound, papillary thyroid carcinoma, lymph node metastasis, cN1, microscopic pN1

INTRODUCTION

Papillary thyroid carcinoma (PTC) is the most common thyroid carcinoma, comprising more than 90% of all thyroid cancers (1). Most PTC patients have good prognosis. However, cervical lymph node metastases (LNMs) are common in PTCs and could increase the recurrence risk and mortality outcomes of PTCs (2, 3). Central compartment dissection has been performed for the PTC patients prone to LNMs (4), yet it might increase the likelihood of morbidity, including hypocalcemia and is unnecessary for those with low-risk LNMs. In addition, postoperative radioiodine therapy might be considered for aggressive PTCs (5). Therefore, it is essential to evaluate the risk factors of LNMs and establish a procedure to screen preoperatively for aggressive PTCs, thereby assisting with the therapeutic planning.

Although ultrasound is the preferred imaging modality for the assessment of LNMs in PTC patients (4), preceding studies (3, 6) found that conventional ultrasound missed 33–90% of LNMs in PTC patients. Instead of direct detection, investigators focused on the sonographic features of PTCs to predict LNMs, and contrast-enhanced ultrasound (CEUS) has also been utilized to screen for aggressive PTCs from indolent ones and predict LNMs.

Some investigations (7–13) have explored the PTC's US and CEUS features associated with LNMs and confirmed their values in predicting LNMs. However, LNMs could be stratified into clinical N1 (cN1, observed on US) and microscopic pN1 (pathological N1), which might bear different biological behavior and prognostic values. cN1 PTCs are deemed to be more aggressive and have worse prognosis than microscopic pN1 PTCs (1, 4, 14–17). Very similar recurrence risks and mortality outcomes could be seen in patients with pN0 and microscopic pN1 (1). The differences in biological behavior and prognosis between cN1 and microscopic pN1 might signify that the characteristics of US and CEUS of primary tumor could also be different.

Hence, the present study aimed to investigate the associations between LNMs and each of the US and CEUS characteristics of PTCs based on the stratification of LNMs into cN1 and microscopic pN1.

MATERIALS AND METHODS

Patients

This retrospective study was conducted from August 2019 to May 2020. The inclusion criteria were as follows: 1. Patients who underwent open surgery (initial therapy); 2. The definitive pathological diagnosis was PTC; 3. Both conventional US and CEUS examinations were carried out within one month before operation. The following were excluded: 1. Central lymph node (level VI) dissection was not performed; 2. Patients with other subtypes of thyroid carcinomas. Thus, a total of 444 patients (331 females and 113 males; mean age, 43.50 ± 11.08 years; range, 18-69 years) were identified and enrolled. For multifocal PTCs, the largest one was selected. Ultimately, 444 PTC lesions (median size, 1.0 (0.7,1.5) cm) were chosen for this study.

This study was approved by Medical Ethics Committee of Chinese PLA General Hospital (S2019-178-02) and the written informed consents were waived because the patients' data were assessed retrospectively and anonymously.

Stratification of LNMs

LNMs include cN1 and microscopic pN1. cN1 is defined as clinically detectable macroscopic LNMs which could be observed on US. Microscopic pN1 could only be detected by histopathologic review. For the cN1 unconfirmed by preoperative cytology, they should be validated by postoperative pathology in our study. For this purpose, we matched the suspicious LNMs observed on US to the corresponding lymph nodes on pathology based on location and size. As long as any of them was demonstrated by postoperative pathology, the cN1 would be established in our study.

According to the regional lymph node status, the patients were classified into cN1 group versus cN0 group [including microscopic pN1 and pN0 (pathological N0)] and microscopic pN1 group versus pN0 group.

Conventional US and CEUS Examinations

This investigation was carried out with machines from four vendors: a Mindray Resona7 (Shenzhen, China) equipped with a L14-5WU transducer for conventional US and a L11-3U for CEUS, a Philips iU22 (Bothell, WA, USA) equipped with a L12-5 transducer for conventional US and a L9-4 for CEUS, an ACUSON Sequoia (Siemens, Germany) equipped with a 18L6 for conventional US and a 10L4 for CEUS as well as an ACUSON S2000 (Siemens, Germany) equipped with a 9L4 transducer for conventional US and CEUS. Patients were scanned in supine position with neck fully exposed. By grayscale ultrasound, the size, position, composition, echogenicity, shape, margin, calcification and halo of the nodule were thoroughly examined. The regional lymph nodes were also meticulously scrutinized.

The largest plane of the tumor was chosen and US machine was then switched to CEUS mode. And the focus was always placed deeper than the examined nodule to diminish the microbubble disruption. The contrast medium was SonoVue (Bracco Imaging S.p.A, Milan, Italy), which was administered intravenously through the antecubital vein as a bolus at a dose of 1.8-2.0 mL followed by 5 mL of saline flush. The real-time microbubble perfusions within the nodules and surrounding tissues were observed for a minimum of 2 min and recorded in the hard drive of the system.

Image Interpretation and Analysis

Two sonologists (Y.K.L. and Y.Z.) with more than 10 years of experience in thyroid ultrasonography, were blinded to the clinicopathological information and performed a retrospective review of the US and CEUS sonograms independently. Discrepancies in the interpretation were resolved by consensus.

Concerning the US features, the following were evaluated for each nodule: composition (solid or almost completely solid, others), echogenicity (hyperechoic or isoechoic, hypoechoic, very hypoechoic), shape (wider-than-tall, taller-than-wide), margin (smooth, lobulated or irregular), calcification (absent, present),

halo (absent, present), suspicious extrathyroidal extension on US (absent, present). The following characteristics were used to evaluate the suspicious extrathyroidal extension on US: the nodule abuts the thyroid capsule, which displays the signs of interruption (loss of the echogenic capsule line); and the nodule interrupts the capsule and invades the surrounding tissues (18–20). With respect to the regional lymph nodes, according to the previous studies (21–26), US-based detection of highly suspicious LNM was based on the following features: 1) microcalcification; 2) cystic change; 3) hyper-echogenicity; 4) rounded shape with increased anteroposterior diameter; 5) peripheral vascularization; 6) irregular margin and loss of hilum. The suspicious lymph nodes on US were routinely recommended for fine needle biopsy in our institution.

The thyroid nodules were assessed on CEUS relative to the surrounding thyroid parenchyma. Compared to that of the surrounding thyroid tissue, the peak intensity of the nodule was classified into (1): hypo-enhancement (2), iso-enhancement (3), hyper-enhancement. According to the preceding studies (27, 28), the presence of tumor-adjacent hyper-enhancement area(s) was indicative of high invasiveness of tumors. This feature was defined as the hyper-enhancement area(s) abutting on tumor. The ring, band-like or patchy enhancement area(s) could be observed in this feature. As to the hyper-enhancement nodules, this feature presented the extension of enhancement region.

Histological Analysis

All specimens were classified in accordance with the WHO Classification of Tumors of Endocrine Organs (4th edition) by experienced pathologists who were blinded to the medical history and sonographic findings. Pathological diagnosis was considered as the gold standard for the study.

Statistical Analysis

The statistical software used in this study was SPSS, version 21.0 (SPSS Inc, Chicago, IL). *P* value of <0.05 was considered statistically significant. The patients were categorized as cN1 group versus cN0 group and microscopic pN1 group versus pN0 group. Continuous variables with normal distribution were summarized as mean ± standard deviation, otherwise they were presented as median (lower quartile, upper quartile). Categorical variables were summarized as frequencies and percentages. Continuous variables were assessed using the unpaired Student *t* test or Mann Whitney U test. Categorical variables were evaluated by Pearson's chi-square or Fisher's exact test. Variables, that were significant in the univariate analysis or were clinically relevant, were selected into a binary logistic regression model using an enter method to further identify the independent risk factors associated with cN1 and microscopic pN1 separately and establish the prediction models. Odds ratios (ORs) with 95% confidence intervals (CIs) were calculated. The receiver operating characteristic (ROC) curves obtained by MedCalc were used to determine the best cut-off values for the continuous variables (tumor size) and to assess the models' diagnostic performance. The corresponding area under the ROC curve (AUC), sensitivity, and specificity were calculated at the optimal cut-off values.

RESULTS

Histological Findings

444 PTCs included 5 aggressive variants (only tall cell variant) and 439 non-aggressive variants, including classical, follicular, oncocytic and warthin-like variants. LNMs were found in 202 patients (45.50%). Among them, 85 patients were found cN1 and 117 were found microscopic pN1. In 85 cN1 patients, at least one involved lymph node could be observed on US. 44 of 85 cN1 patients were confirmed by preoperative cytology and the rest were demonstrated by postoperative pathology based on the size and location. Extra-nodal extension occurred in 15 of 85 cN1 patients, which was documented in the operative report.

Thus, 85 cN1 patients versus 359 cN0 patients (including 117 microscopic pN1 patients and 242 pN0 patients) and 117 microscopic pN1 patients versus 242 pN0 patients were analyzed in our study (**Figure 1**).

Comparison of PTC's US and CEUS Features Between cN1 Patients and cN0 Patients

The age, gender, size, multifocality, extrathyroidal extension on US, calcification and enhancement intensity differed significantly between patients with cN1 and cN0 ($p<0.05$) (**Table 1**). However, there were no significant differences in composition, echogenicity, shape, margin, halo as well as tumor-adjacent hyper-enhancement area(s) ($p>0.05$) (**Table 1**).

Multivariate Logistic Regression Analysis for cN1

Multivariate logistic regression analysis was performed for all significant variables identified in the univariate analysis. Among them, size was added to the multivariate model as a continuous variable. Additionally, given that the PTCs with halo (encapsulated tumors) tend to present rich blood supply but highly favorable prognosis (29), this feature was also added to the multivariate model to check for possible confounding effects.

The predictive factors for cN1 were <55-years-old (OR: 2.56 (1.08–6.04), *p*: 0.032), male (OR: 2.18 (1.22–3.91), *p*: 0.009), size (OR: 2.59 (1.71–3.92), $p<0.0001$), calcification (OR: 3.88 (1.58–9.51), *p*: 0.003), and hyper-enhancement (OR: 2.78 (1.22–6.30), *p*: 0.015) (**Figure 2**), whereas the others were dependent on cN1 ($p>0.05$). The AUC was 0.557 for age (95% CI: 0.510–0.604), 0.612 for gender (95% CI: 0.565–0.657), 0.749 for size (95% CI: 0.706–0.789), 0.630 for calcification (95% CI: 0.584–0.675), and 0.658 for enhancement intensity (95% CI: 0.612–0.702), respectively. The best cut-off value of tumor size was >1.4 cm.

An equation was established with the significant predictive factors: logit (*p*) = -5.289 + 0.902 × age + 0.736 × gender + 0.919 × size + 0.575 × iso-enhancement + 0.876 × hyper-enhancement. The AUC of 0.802 (95% CI: 0.762–0.838) for equation suggested a significant difference compared with the single factors ($p<0.05$ for all) (**Figure 3**). The calcification showed the highest sensitivity (92.94%) in predicting cN1, while enhancement intensity indicated the highest specificity (83.84%). The diagnostic accuracy of size was the highest (76.80%) (**Table 2**).

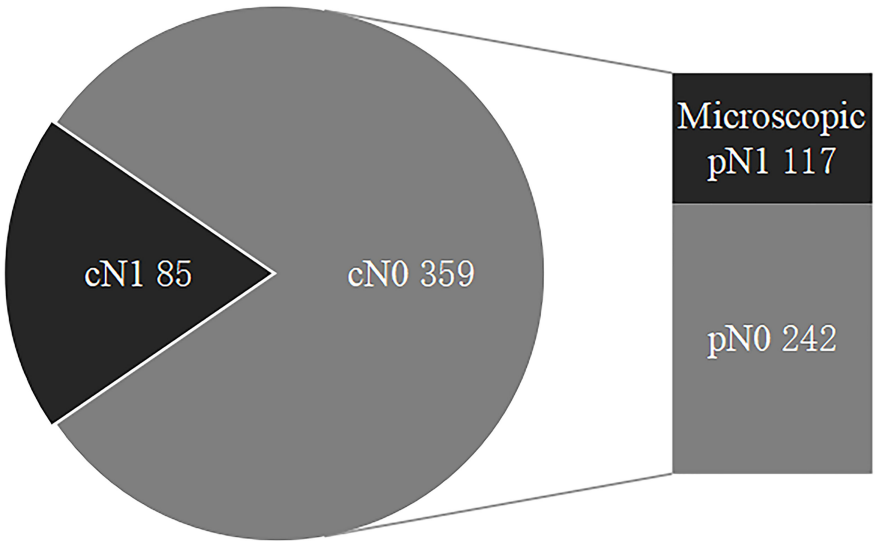

FIGURE 1 | The status of regional lymph nodes in papillary thyroid carcinoma. LNMs include cN1 and microscopic pN1, and cN0 are comprised of microscopic pN1 and pN0. LNMs, lymph node metastases; cN1, clinical N1; Microscopic pN1, microscopic pathological N1; cN0, clinical N0; pN0, pathological N0.

TABLE 1 | Clinical and sonographic characteristics of cN1 PTCs and cN0 PTCs.

Characteristics	cN1 PTCs (n = 85)	cN0 PTCs (n=359)	*P* value
Age, y	38.71 ± 10.87	44.63 ± 10.84	<0.0001*
<55	77 (90.59)	284 (79.11)	0.015*
Gender			<0.0001*
Male	37 (43.53)	76 (21.17)	
Size (Maximum diameters, cm)	1.50 (1.00,2.45)	1.00 (0.60,1.20)	<0.0001*
Multifocality	51 (60.00)	152 (42.34)	0.003*
Suspicious extrathyroidal extension on US			<0.001*
Absent	14 (16.47)	130 (36.21)	
Present	71 (83.53)	229 (63.79)	
Composition			0.877
Solid or almost completely solid	83 (97.65)	354 (98.61)	
Others	2 (2.35)	5 (1.39)	
Echogenicity			0.083
Hyperechoic or isoechoic	2 (2.35)	1 (0.28)	
Hypoechoic	74 (87.06)	303 (84.40)	
Very hypoechoic	9 (10.59)	55 (15.32)	
Shape			0.311
Wider-than-tall	38 (44.71)	139 (38.72)	
Taller-than-wide	47 (55.29)	220 (61.28)	
Margin			0.935
Smooth	3 (3.53)	16 (4.46)	
Lobulated or irregular	82 (96.47)	343 (95.54)	
Presence of calcification	79 (92.94)	240 (66.85)	<0.0001*
Presence of halo	14 (16.47)	38 (10.58)	0.129
Enhancement intensity			<0.0001*
Hypo-enhancement	14 (16.47)	129 (35.93)	
Iso-enhancement	37 (43.53)	172 (47.91)	
Hyper-enhancement	34 (40.00)	58 (16.16)	
Presence of tumor-adjacent hyper-enhancement area (s)	18 (21.18)	91 (25.35)	0.422

cN1, clinical N1; cN0, clinical N0; PTC, papillary thyroid carcinoma.
Data were presented in mean ± standard deviation, median (lower quartile, upper quartile) and number (percent).
**These p values are of <0.05.*

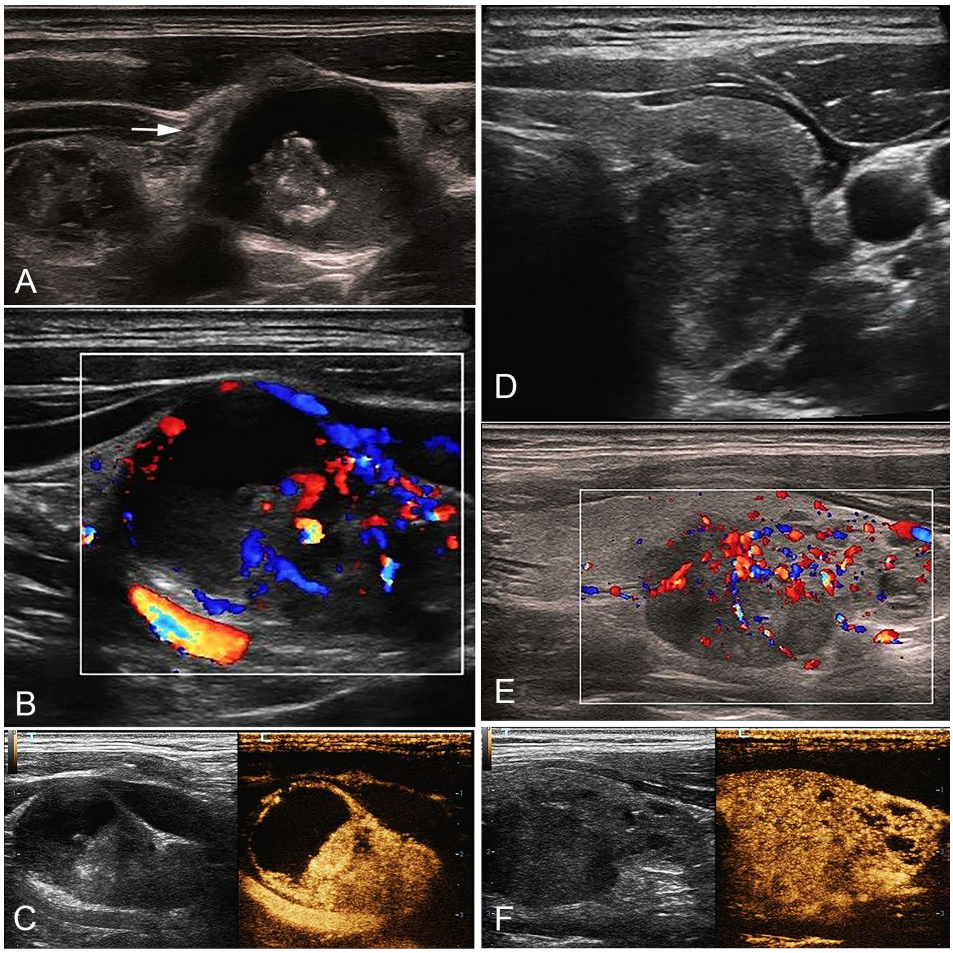

FIGURE 2 | A 35-year-old male with cN1 PTC. **(A)** Sonogram of the largest metastatic lymph node (arrow) in level IV indicates irregular margin, loss of hilum, calcification, hyper-echogenicity, and cystic change in the node. **(B)** CDFI shows non-hilar vascularization. **(C)** CEUS indicates heterogeneous hyper-enhancement and perfusion defect in the node. **(D)** Sonogram of the PTC lesion shows a solid hypo-echogenic nodule with irregular margin and a taller than wide shape, measuring 1.2*1.4*1.9cm. **(E)** CDFI indicates abundant blood flow signals. **(F)** CEUS shows that the PTC lesion presents pervasive hyper-enhancement. PTC, papillary thyroid carcinoma; cN1, clinical N1; CDFI, color doppler flow imaging; CEUS, contrast-enhanced ultrasound.

Comparison of PTC's US and CEUS Features Between Microscopic pN1 Patients and pN0 Patients

Statistically significant differences were found in age, size, multifocality and calcification between microscopic pN1 patients and pN0 patients ($p<0.05$) (**Table 3**). But there were no significant differences in gender, extrathyroidal extension on US, composition, echogenicity, shape, margin, halo, enhancement intensity as well as tumor-adjacent hyper-enhancement area(s) ($p>0.05$) (**Table 3**).

Multivariate Logistic Regression Analysis for Microscopic pN1

To control more confounders, the variables added to the multivariate analysis were identical to those added to the multivariate analysis of cN1. The predictive factors for microscopic pN1 were <55-years-old (OR: 1.91 (1.04–3.51), *p*: 0.036), size (OR: 1.56 (1.003–2.42), *p*: 0.049), multifocality (OR: 1.67 (1.04–2.66), *p*: 0.033). The AUC was 0.541 for age (95% CI: 0.488–0.593), 0.601 for size (95% CI: 0.548–0.652), and 0.566 for multifocality (95% CI: 0.513–0.618), respectively. The best cut-off value of tumor size was >1.0 cm.

An equation was also created using the significant predictive factors: logit (p) = -1.853 + 0.609 × age + 0.391 × size + 0.502 × multifocality. The AUC of the predictive equation was 0.639 (95% CI: 0.586–0.688), higher than the single factors ($p<0.05$ for age and multifocality, but not for size) (**Figure 4**). The age had the highest sensitivity (84.62%) in predicting microscopic pN1, whereas the size indicated the highest specificity (70.25%). The size also achieved the highest accuracy (63.23%) (**Table 4**).

DISCUSSION

LNMs can be classified into cN1 and microscopic pN1, which might vary in biological behavior and prognosis. cN1 is defined as clinically detectable macroscopic LNMs which could be observed

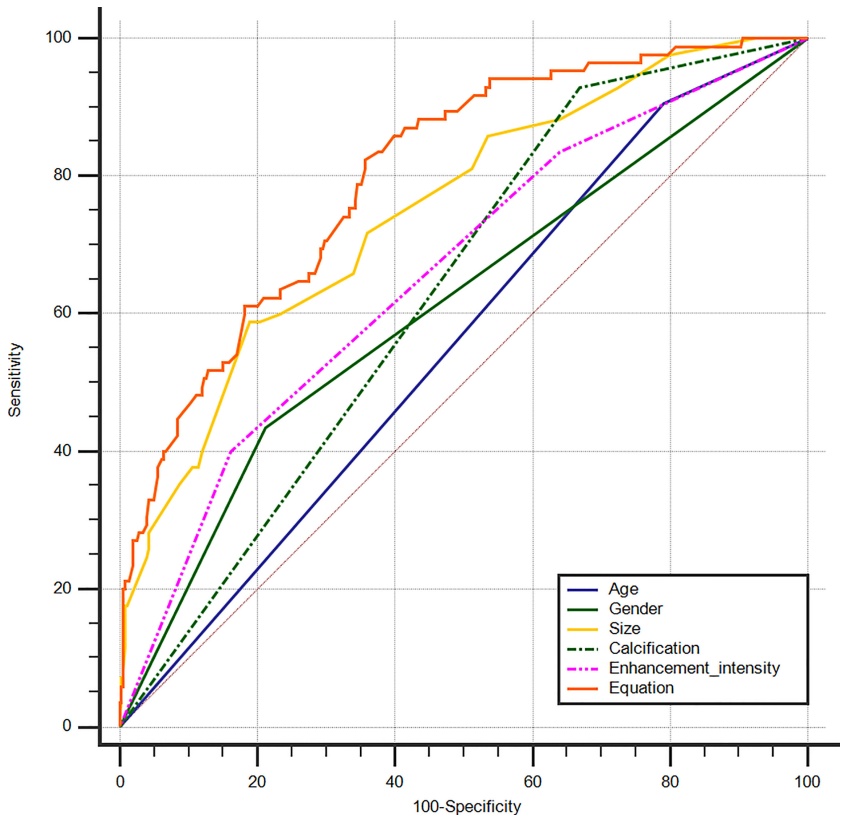

FIGURE 3 | ROC curves of PTC age (AUC=0.557), gender (AUC=0.612), size (AUC=0.749), calcification (AUC=0.630), enhancement intensity on CEUS (AUC=0.658) and Equation (AUC=0.802) for the prediction of cN1. ROC, receiver operating characteristic; PTC, papillary thyroid carcinoma; AUC, area under the curve; CEUS, contrast-enhanced ultrasound; cN1, clinical N1.

TABLE 2 | ROC analysis for predicting cN1 in PTCs.

Characteristics	AUC	95% CI	Sensitivity	Specificity	Accuracy
Age	0.557	0.510–0.604	90.59%	20.89%	34.23%
Gender	0.612	0.565–0.657	43.53%	78.83%	72.07%
Size*	0.749	0.706–0.789	58.82%	81.06%	76.80%
Calcification	0.630	0.584–0.675	92.94%	33.15%	44.59%
Enhancement intensity	0.658	0.612–0.702	40.00%	83.84%	75.45%
Predictive equation	0.802	0.762–0.838	82.35%	64.35%	67.79%

ROC, receiver operating characteristic; cN1, clinical N1; PTC, papillary thyroid carcinoma; AUC, area under the curve; CI, confidence interval.
**The best cut-off value of tumor size was >1.4 cm.*

on US. Microscopic pN1 could only be found by histopathology. Microscopic pN1 carries a smaller recurrence risk than cN1 but possesses similar recurrence risks and mortality outcomes with pN0 (1, 4, 14–17). Microscopic pN1 might have little impact on the risk of structural recurrence and disease specific survival (1). Consequently, it could be hypothesized that primary tumor's US and CEUS features associated with cN1 and microscopic pN1 might differ. Our study explored the connections between LNMs and primary tumor's US and CEUS characteristics based on the stratification of LNMs into cN1 and microscopic pN1 and confirmed this hypothesis.

We discovered that independent risk factors for cN1 were <55-years-old, male, large size, calcification and hyper-enhancement, while those for microscopic pN1 were <55-years-old, large size and multifocality. CEUS, a pure blood pool imaging technique, could be used to assess the blood perfusion of tumors (30). As the angiogenesis is essential in the occurrence, development, invasion, and metastasis of PTCs, it could be speculated that PTCs with hyper-enhancement (rich blood supply) possessed high invasiveness and an increased probability of LNMs, which could further develop into clinically detectable LNMs (cN1). In our study, hyper-enhancement on CEUS was correlated with cN1

TABLE 3 | Clinical and sonographic characteristics of microscopic pN1 PTCs and pN0 PTCs.

Characteristics	Microscopic pN1 PTCs (n = 117)	pN0 PTCs (n = 242)	*P* value
Age, y	42.75 ± 11.11	45.54 ± 10.61	0.022*
<55	99 (84.62)	185 (76.45)	0.074
Gender			0.243
Male	29 (24.79)	47 (19.42)	
Size (Maximum diameters, cm)	1.00 (0.70,1.45)	0.80 (0.60,1.20)	0.002*
Multifocality	60 (51.28)	92 (38.02)	0.017*
Suspicious extrathyroidal extension on US			0.430
Absent	39 (33.33)	91 (37.60)	
Present	78 (66.67)	151 (62.40)	
Composition			1.000
Solid or almost completely solid	115 (98.29)	239 (98.76)	
Others	2 (1.71)	3 (1.24)	
Echogenicity			0.470
Hyperechoic or isoechoic	0 (0)	1 (0.41)	
Hypoechoic	103 (88.03)	200 (82.65)	
Very hypoechoic	14 (11.97)	41 (16.94)	
Shape			0.277
Wider-than-tall	50 (42.74)	89 (36.78)	
Taller-than-wide	67 (57.26)	153 (63.22)	
Margin			0.907
Smooth	5 (4.27)	11 (4.55)	
Lobulated or irregular	112 (95.73)	231 (95.45)	
Presence of calcification	88 (75.21)	152 (62.81)	0.019*
Presence of halo	11 (9.40)	27 (11.16)	0.612
Enhancement intensity			0.264
Hypo-enhancement	48 (41.03)	81 (33.47)	
Iso-enhancement	49 (41.88)	123 (50.83)	
Hyper-enhancement	20 (17.09)	38 (15.70)	
Presence of tumor-adjacent hyper-enhancement area (s)	28 (23.93)	63 (26.03)	0.668

Microscopic pN1, microscopic pathological N1; pN0, pathological N0; PTC, papillary thyroid carcinoma.
Data were presented in mean ± standard deviation, median (lower quartile-upper quartile) and number (percent).
**These p values are of <0.05.*

rather than with microscopic pN1. The similar conclusion was drawn by other studies (7, 10) that hyper-enhancement on CEUS suggested a high risk of LNMs. In these studies, the LNMs included both cN1 and microscopic pN1. It has been reported that calcification was an independent predictor of LNMs for patients with PTC (31–33). In our study, calcification was associated with cN1, but not with microscopic pN1. Male is associated with a worse prognosis, constituting a non-independent adverse prognostic factor (34, 35). Some studies (36, 37) have reported that male was an independent predictor of LNMs in patients with PTC. In our study, male was connected with cN1 rather than microscopic pN1. Size is an independent prognostic factor of PTCs and has been demonstrated to be associated with LNMs by many studies (7–9, 11, 12). This conclusion was validated in our study. The optimal cut-off value of size for the prediction of cN1 was 1.4cm, whereas that for the prediction of microscopic pN1 was 1.0cm. Previous studies (31, 32, 37) found that young age was connected with LNMs. This conclusion was demonstrated in our study, although Jianming Li et al. (36) reported that old age was a risk factor of LNMs. Multifocality has been reported to be associated with an increased risk of LNMs (8, 32, 37, 38) and it was identified to be an independent risk factor of microscopic pN1 in our study.

The eighth edition of the American Joint Committee on Cancer (AJCC) Manual mentions that the current challenge for clinical staging is that the conventional US cannot confidently classify the lymph nodes as clinically negative lymph nodes (cN0) or clinically positive lymph nodes (cN1) before Surgery (1). According to our study, for PTCs with the predictive factors of cN1, very careful scrutiny of neck ultrasound was needed to screen for the potential macroscopic LNMs. If suspicious or indeterminate lymph nodes were found, lymphatic or intravenous CEUS should be recommended (21, 22, 39), thereby increasing the confidence in diagnosis and biopsy, and improving the detection rate of LNMs, especially for junior sonologists. For cN0 patients with PTC, the predictive factors (young age, large size and multifocality) were suggestive of an increased probability of microscopic LNMs. It might be better that prophylactic central compartment dissection was performed for patients with these factors.

A more demolitive surgery is accompanied by a risk of increased postoperative complications, such as neck hematoma, hypoparathyroidism, and recurrent laryngeal nerve injury (40–42). Therefore, it is of great significance to accurately identify LNMs before surgery, which could impact on the extent of surgery. Our findings could serve as preoperative supplementary markers for determining the status of LNMs, thereby enhancing the accuracy and detection rate of LNMs and assisting the surgeons in determining the optimal extent of surgery.

Our study had some limitations. First, this is a retrospective, single-center study. Second, our institution is a tertiary referral hospital. Additionally, many patients with papillary thyroid

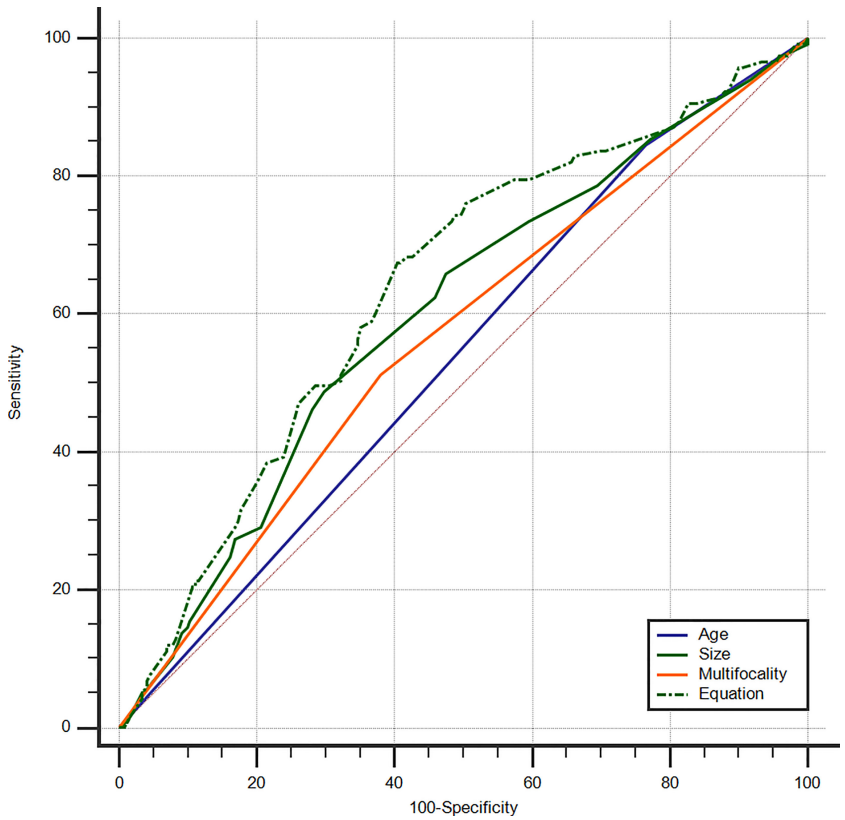

FIGURE 4 | ROC curves of PTC age (AUC=0.541), size (AUC=0.601), multifocality (AUC=0.566), and Equation (AUC=0.639) for the prediction of microscopic pN1. ROC, receiver operating characteristic; PTC, papillary thyroid carcinoma; AUC, area under the curve; Microscopic pN1, microscopic pathological N1.

TABLE 4 | ROC analysis for predicting microscopic pN1 in PTCs.

	AUC	95% CI	Sensitivity	Specificity	Accuracy
Age	0.541	0.488–0.593	84.62%	23.55%	43.45%
Size*	0.601	0.548–0.652	48.72%	70.25%	63.23%
Multifocality	0.566	0.513–0.618	51.28%	61.98%	58.50%
Predictive equation	0.639	0.586–0.688	67.52%	59.50%	62.12%

ROC, receiver operating characteristic; Microscopic pN1, microscopic pathological N1; PTC, papillary thyroid carcinoma; AUC, area under the curve; CI, confidence interval.
**The best cut-off value of tumor size was >1.0 cm.*

microcarcinoma were subjected to active surveillance or thermal ablation therapy rather than surgery. Therefore, surgery patients in our hospital might have the higher staging and sample selection bias might exist. A multi-center study was needed to solve these problems. Third, our study cohort lacked postoperative follow-up data. Future studies should investigate postoperative follow-up sonography in our institution and compare recurrence and survival rates.

In conclusion, PTCs with the risk factors, including <55-years-old, male, large size, calcification and hyper-enhancement, have an increased probability of cN1. Cervical lymph nodes should be carefully scrutinized. For cN0 patients with PTC, young age, large size and multifocality were associated with an increased likelihood of microscopic pN1. Prophylactic central compartment dissection might be appropriate for these patients.

DATA AVAILABILITY STATEMENT

The raw data supporting the conclusions of this article will be made available by the authors, without undue reservation.

ETHICS STATEMENT

The studies involving human participants were reviewed and approved by Medical Ethics Committee of Chinese PLA General Hospital. The ethics committee waived the requirement of written informed consent for participation. Written informed consent was obtained from the individual(s) for the publication of any potentially identifiable images or data included in this article.

AUTHOR CONTRIBUTIONS

The conception and design of the study: WL, SQ, YZ, and YL. Acquisition of data: WL and SQ. Analysis and interpretation of data: LR, QL, SX, and JL. Drafting the article: WL and SQ. The article and final approval of the version to be submitted: YZ and YL.

FUNDING

This work was supported by grants (81901746 to YZ) from National Natural Science Foundation of China, grants (81771834 to YL) from National Natural Science Foundation of China, and grants (2019MBD-040 to YL) from Chinese PLA General Hospital.

REFERENCES

1. Tuttle RM, Morris LF, Haugen BR, Shah JP, Sosa JA, Rohren E, et al. Thyroid - Differentiated and Anaplastic Carcinoma. In: MB Amin, SB Edge, FL Greene, DR Byrd, RK Brookland and MK Washington, editors. *AJCC Cancer Staging Manual*, *8 ed*. Chicago: Springer (2017). p. 873–90.
2. Sipos JA. Advances in Ultrasound for the Diagnosis and Management of Thyroid Cancer. *Thyroid Off J Am Thyroid Assoc* (2009) 19(12):1363–72. doi: 10.1089/thy.2009.1608
3. Baek SK, Jung KY, Kang SM, Kwon SY, Woo JS, Cho SH, et al. Clinical Risk Factors Associated With Cervical Lymph Node Recurrence in Papillary Thyroid Carcinoma. *Thyroid Off J Am Thyroid Assoc* (2010) 20(2):147–52. doi: 10.1089/thy.2008.0243
4. Haugen BR, Alexander EK, Bible KC, Doherty GM, Mandel SJ, Nikiforov YE, et al. American Thyroid Association Management Guidelines for Adult Patients With Thyroid Nodules and Differentiated Thyroid Cancer: The American Thyroid Association Guidelines Task Force on Thyroid Nodules and Differentiated Thyroid Cancer. *Thyroid Off J Am Thyroid Assoc* (2016) 26 (1):1–133. doi: 10.1089/thy.2015.0020
5. Luster M, Aktolun C, Amendoeira I, Barczyński M, Bible KC, Duntas LH, et al. European Perspective on 2015 American Thyroid Association Management Guidelines for Adult Patients With Thyroid Nodules and Differentiated Thyroid Cancer: Proceedings of an Interactive International Symposium. *Thyroid Off J Am Thyroid Assoc* (2019) 29(1):7–26. doi: 10.1089/thy.2017.0129
6. Moo TA, McGill J, Allendorf J, Lee J, Fahey T, et al. 3rdImpact of Prophylactic Central Neck Lymph Node Dissection on Early Recurrence in Papillary Thyroid Carcinoma. *World J Surg* (2010) 34(6):1187–91. doi: 10.1007/s00268-010-0418-3
7. Zhan J, Zhang LH, Yu Q, Li CL, Chen Y, Wang WP, et al. Prediction of Cervical Lymph Node Metastasis With Contrast-Enhanced Ultrasound and Association Between Presence of BRAF(V600E) and Extrathyroidal Extension in Papillary Thyroid Carcinoma. *Ther Adv Med Oncol* (2020) 12:1758835920942367. doi: 10.1177/1758835920942367
8. Wang Y, Nie F, Wang G, Liu T, Dong T, Sun Y. Value of Combining Clinical Factors, Conventional Ultrasound, and Contrast-Enhanced Ultrasound Features in Preoperative Prediction of Central Lymph Node Metastases of Different Sized Papillary Thyroid Carcinomas. *Cancer Manage Res* (2021) 13:3403–15. doi: 10.2147/cmar.S299157
9. Tao L, Zhou W, Zhan W, Li W, Wang Y, Fan J. Preoperative Prediction of Cervical Lymph Node Metastasis in Papillary Thyroid Carcinoma *via* Conventional and Contrast-Enhanced Ultrasound. *J Ultrasound Med Off J Am Inst Ultrasound Med* (2020) 39(10):2071–80. doi: 10.1002/jum.15315
10. Hong YR, Yan CX, Mo GQ, Luo ZY, Zhang Y, Wang Y, et al. Conventional US, Elastography, and Contrast Enhanced US Features of Papillary Thyroid Microcarcinoma Predict Central Compartment Lymph Node Metastases. *Sci Rep* (2015) 5:7748. doi: 10.1038/srep07748
11. Liu Y, Zhou H, Yang P, Zhou Y, Wu J, Chen C, et al. Contrast-Enhanced Ultrasonography Features of Papillary Thyroid Carcinoma for Predicting Cervical Lymph Node Metastasis. *Exp Ther Med* (2017) 14(5):4321–7. doi: 10.3892/etm.2017.5087
12. Zhan J, Diao X, Chen Y, Wang W, Ding H. Predicting Cervical Lymph Node Metastasis in Patients With Papillary Thyroid Cancer (PTC) - Why Contrast-Enhanced Ultrasound (CEUS) was Performed Before Thyroidectomy. *Clin Hemorheol Microcirc* (2019) 72(1):61–73. doi: 10.3233/ch-180454
13. Sun F, Zou Y, Huang L, Shi Y, Liu J, Cui G, et al. Nomogram to Assess Risk of Central Cervical Lymph Node Metastasis in Patients With Cn0 Papillary Thyroid Carcinoma. *Endocr Pract Off J Am Coll Endocrinol Am Assoc Clin Endocrinologists* (2021) 27(12):1175–82. doi: 10.1016/j.eprac.2021.06.010
14. Randolph GW, Duh QY, Heller KS, LiVolsi VA, Mandel SJ, Steward DL, et al. The Prognostic Significance of Nodal Metastases From Papillary Thyroid Carcinoma can be Stratified Based on the Size and Number of Metastatic Lymph Nodes, as Well as the Presence of Extranodal Extension. *Thyroid Off J Am Thyroid Assoc* (2012) 22(11):1144–52. doi: 10.1089/thy.2012.0043
15. Asimakopoulos P, Shaha AR, Nixon IJ, Shah JP, Randolph GW, Angelos P, et al. Management of the Neck in Well-Differentiated Thyroid Cancer. *Curr Oncol Rep* (2020) 23(1):1. doi: 10.1007/s11912-020-00997-6
16. Gorshtein A, Benbassat C, Robenshtok E, Shimon I, Hirsch D. Response to Treatment Is Highly Predictable in Cn0 Patients With Papillary Thyroid Carcinoma. *World J Surg* (2016) 40(9):2123–30. doi: 10.1007/s00268-016-3507-0
17. Bardet S, Malville E, Rame JP, Babin E, Samama G, De Raucourt D, et al. Macroscopic Lymph-Node Involvement and Neck Dissection Predict Lymph-Node Recurrence in Papillary Thyroid Carcinoma. *Eur J Endocrinol* (2008) 158(4):551–60. doi: 10.1530/eje-07-0603
18. Chung SR, Baek JH, Choi YJ, Sung TY, Song DE, Kim TY, et al. Sonographic Assessment of the Extent of Extrathyroidal Extension in Thyroid Cancer. *Korean J Radiol* (2020) 21(10):1187–95. doi: 10.3348/kjr.2019.0983
19. Lamartina L, Bidault S, Hadoux J, Guerlain J, Girard E, Breuskin I, et al. Can Preoperative Ultrasound Predict Extrathyroidal Extension of Differentiated Thyroid Cancer? *Eur J Endocrinol* (2021) 185(1):13–22. doi: 10.1530/eje-21-0091
20. Ramundo V, Di Gioia CRT, Falcone R, Lamartina L, Biffoni M, Giacomelli L, et al. Diagnostic Performance of Neck Ultrasonography in the Preoperative Evaluation for Extrathyroidal Extension of Suspicious Thyroid Nodules. *World J Surg* (2020) 44(8):2669–74. doi: 10.1007/s00268-020-05482-6
21. Hong YR, Luo ZY, Mo GQ, Wang P, Ye Q, Huang PT. Role of Contrast-Enhanced Ultrasound in the Pre-Operative Diagnosis of Cervical Lymph Node Metastasis in Patients With Papillary Thyroid Carcinoma. *Ultrasound Med Biol* (2017) 43(11):2567–75. doi: 10.1016/j.ultrasmedbio.2017.07.010
22. Wei Y, Yu MA, Niu Y, Hao Y, Di JX, Zhao ZL, et al. Combination of Lymphatic and Intravenous Contrast-Enhanced Ultrasound for Evaluation of Cervical Lymph Node Metastasis From Papillary Thyroid Carcinoma: A Preliminary Study. *Ultrasound Med Biol* (2021) 47(2):252–60. doi: 10.1016/j.ultrasmedbio.2020.10.003
23. Zhan J, Diao XH, Chen Y, Wang WP, Ding H. Homogeneity Parameter in Contrast-Enhanced Ultrasound Imaging Improves the Classification of Abnormal Cervical Lymph Node After Thyroidectomy in Patients With Papillary Thyroid Carcinoma. *BioMed Res Int* (2019) 2019:9296010. doi: 10.1155/2019/9296010
24. Chen L, Chen L, Liu J, Wang B, Zhang H. Value of Qualitative and Quantitative Contrast-Enhanced Ultrasound Analysis in Preoperative Diagnosis of Cervical Lymph Node Metastasis From Papillary Thyroid Carcinoma. *J Ultrasound Med Off J Am Inst Ultrasound Med* (2020) 39 (1):73–81. doi: 10.1002/jum.15074
25. Xiang D, Hong Y, Zhang B, Huang P, Li G, Wang P, et al. Contrast-Enhanced Ultrasound (CEUS) Facilitated US in Detecting Lateral Neck Lymph Node Metastasis of Thyroid Cancer Patients: Diagnosis Value and Enhancement Patterns of Malignant Lymph Nodes. *Eur Radiol* (2014) 24(10):2513–9. doi: 10.1007/s00330-014-3288-5
26. Leboulleux S, Girard E, Rose M, Travagli JP, Sabbah N, Caillou B, et al. Ultrasound Criteria of Malignancy for Cervical Lymph Nodes in Patients Followed Up for Differentiated Thyroid Cancer. *J Clin Endocrinol Metab* (2007) 92(9):3590–4. doi: 10.1210/jc.2007-0444

27. Zhang Y, Zhang X, Li J, Cai Q, Qiao Z, Luo YK. Contrast-Enhanced Ultrasound: A Valuable Modality for Extracapsular Extension Assessment in Papillary Thyroid Cancer. *Eur Radiol* (2021) 31(7):4568–75. doi: 10.1007/s00330-020-07516-y
28. Vraka I, Panourgias E, Sifakis E, Koureas A, Galanis P, Dellaportas D, et al. Correlation Between Contrast-Enhanced Ultrasound Characteristics (Qualitative and Quantitative) and Pathological Prognostic Factors in Breast Cancer. *In Vivo (Athens Greece)* (2018) 32(4):945–54. doi: 10.21873/invivo.11333
29. Chan JKC. The Thyroid Gland. In: CDM Fletcher, editor. *Diagnostic Histopathology of Tumors, 5th ed*. Philadelphia: Elsevier (2021). p. 1265.
30. Sidhu PS, Cantisani V, Dietrich CF, Gilja OH, Saftoiu A, Bartels E, et al. The EFSUMB Guidelines and Recommendations for the Clinical Practice of Contrast-Enhanced Ultrasound (CEUS) in Non-Hepatic Applications: Update 2017 (Long Version). *Ultraschall der Med (Stuttgart Germany 1980)* (2018) 39(2):e2–e44. doi: 10.1055/a-0586-1107
31. Liu J, Jia X, Gu Y, Chen X, Guan L, Yan J, et al. Thyroid Parenchyma Microcalcifications on Ultrasound for Predicting Lymph Node Metastasis in Papillary Thyroid Carcinoma: A Prospective Multicenter Study in China. *Front Oncol* (2021) 11:609075. doi: 10.3389/fonc.2021.609075
32. Shi WY, Hu MX, Zhu Q, Xia CX, Zhao Y, Zhou YJ, et al. Study of Ultrasonographic Features in Predicting Reginal Lymph Node Metastasis in Patients With Papillary Thyroid Carcinoma. *Zhonghua yi xue za zhi* (2016) 96 (27):2165–8. doi: 10.3760/cma.j.issn.0376-2491.2016.27.011
33. Chen J, Li XL, Zhao CK, Wang D, Wang Q, Li MX, et al. Conventional Ultrasound, Immunohistochemical Factors and BRAF(V600E) Mutation in Predicting Central Cervical Lymph Node Metastasis of Papillary Thyroid Carcinoma. *Ultrasound Med Biol* (2018) 44(11):2296–306. doi: 10.1016/j.ultrasmedbio.2018.06.020
34. Rosai J, Saavedra JA, Asioli S, Baloch ZW, Bogdanova T, Chen H, et al. Papillary Thyroid Carcinoma. In: RV Lloyd, RY Osamura, G Kloppel and J Rosai, editors. *WHO Classification of Tumors of Endocrine Organs, 4 ed*. Lyon: IARC (2017). p. 81–91.
35. Chan JKC. The Thyroid Gland. In: CDM Fletcher, editor. *Diagnostic Histopathology of Tumors, 5th ed*. Philadelphia: Elsevier (2021). p. 1264.
36. Jianming L, Jibin L, Linxue Q. Suspicious Ultrasound Characteristics Correlate With Multiple Factors That Predict Central Lymph Node Metastasis of Papillary Thyroid Carcinoma: Significant Role of HBME-1. *Eur J Radiol* (2020) 123:108801. doi: 10.1016/j.ejrad.2019.108801
37. Ma B, Wang Y, Yang S, Ji Q. Predictive Factors for Central Lymph Node Metastasis in Patients With Cn0 Papillary Thyroid Carcinoma: A Systematic Review and Meta-Analysis. *Int J Surg (Lond Engl)* (2016) 28:153–61. doi: 10.1016/j.ijsu.2016.02.093
38. Wang W, Su X, He K, Wang Y, Wang H, Wang H, et al. Comparison of the Clinicopathologic Features and Prognosis of Bilateral Versus Unilateral Multifocal Papillary Thyroid Cancer: An Updated Study With More Than 2000 Consecutive Patients. *Cancer* (2016) 122(2):198–206. doi: 10.1002/cncr.29689
39. Liu Z, Wang R, Zhou J, Zheng Y, Dong Y, Luo T, et al. Ultrasound Lymphatic Imaging for the Diagnosis of Metastatic Central Lymph Nodes in Papillary Thyroid Cancer. *Eur Radiol* (2021) 31(11):8458–67. doi: 10.1007/s00330-021-07958-y
40. Gambardella C, Patrone R, Di Capua F, Offi C, Mauriello C, Clarizia G, et al. The Role of Prophylactic Central Compartment Lymph Node Dissection in Elderly Patients With Differentiated Thyroid Cancer: A Multicentric Study. *BMC Surg* (2019) 18(Suppl 1):110. doi: 10.1186/s12893-018-0433-0
41. Conzo G, Calò PG, Gambardella C, Tartaglia E, Mauriello C, Della Pietra C, et al. Controversies in the Surgical Management of Thyroid Follicular Neoplasms. Retrospective Analysis of 721 Patients. *Int J Surg (Lond Engl)* (2014) 12(Suppl 1):S29–34. doi: 10.1016/j.ijsu.2014.05.013
42. Conzo G, Docimo G, Ruggiero R, Napolitano S, Palazzo A, Gambardella C, et al. Surgical Treatment of Papillary Thyroid Carcinoma Without Lymph Nodal Involvement. *Il Giornale di chirurgia* (2012) 33(10):339–42.

Conflict of Interest: The authors declare that the research was conducted in the absence of any commercial or financial relationships that could be construed as a potential conflict of interest.

Publisher's Note: All claims expressed in this article are solely those of the authors and do not necessarily represent those of their affiliated organizations, or those of the publisher, the editors and the reviewers. Any product that may be evaluated in this article, or claim that may be made by its manufacturer, is not guaranteed or endorsed by the publisher.

frontiers | Frontiers in Endocrinology

ORIGINAL RESEARCH
published: 22 April 2022
doi: 10.3389/fendo.2022.872153

Radiomic Model for Determining the Value of Elasticity and Grayscale Ultrasound Diagnoses for Predicting BRAF^{V600E} Mutations in Papillary Thyroid Carcinoma

Yu-guo Wang[1†], Fei-ju Xu[2†], Enock Adjei Agyekum[2†], Hong Xiang[3], Yuan-dong Wang[4], Jin Zhang[2], Hui Sun[5], Guo-liang Zhang[6], Xiang-shu Bo[2], Wen-zhi Lv[7], Xian Wang[2], Shu-dong Hu[8*] and Xiao-qin Qian[2*]*

[1] Department of Ultrasound, Jiangsu Hospital of Integrated Traditional Chinese and Western Medicine, Nanjing, China, [2] Department of Ultrasound, Affiliated People's Hospital of Jiangsu University, Zhenjiang, China, [3] Department of Pediatrics, Affiliated Hospital of Jiangsu University, Zhenjiang, China, [4] Department of Radiotherapy, Affiliated People's Hospital of Jiangsu University, Zhenjiang, China, [5] Department of Pathology, Affiliated People's Hospital of Jiangsu University, Zhenjiang, China, [6] Department of General Surgery, Affiliated People's Hospital of Jiangsu University, Zhenjiang, China, [7] Department of Artificial Intelligence, Julei Technology, Company, Wuhan, China, [8] Department of Radiology, Affiliated Hospital of Jiangnan University, Wuxi, China

BRAF^{V600E} is the most common mutated gene in thyroid cancer and is most closely related to papillary thyroid carcinoma(PTC). We investigated the value of elasticity and grayscale ultrasonography for predicting BRAF^{V600E} mutations in PTC.

Methods: 138 patients with PTC who underwent preoperative ultrasound between January 2014 and 2021 were retrospectively examined. Patients were divided into BRAF^{V600E} mutation-free group (n=75) and BRAF^{V600E} mutation group (n=63). Patients were randomly divided into training (n=96) and test (n=42) groups. A total of 479 radiomic features were extracted from the grayscale and elasticity ultra-sonograms. Regression analysis was done to select the features that provided the most information. Then, 10-fold cross-validation was used to compare the performance of different classification algorithms. Logistic regression was used to predict BRAF^{V600E} mutations.

Results: Eight radiomics features were extracted from the grayscale ultrasonogram, and five radiomics features were extracted from the elasticity ultrasonogram. Three models were developed using these radiomic features. The models were derived from elasticity ultrasound, grayscale ultrasound, and a combination of grayscale and elasticity ultrasound, with areas under the curve (AUC) 0.952 [95% confidence interval (CI), 0.914–0.990], AUC 0.792 [95% CI, 0.703–0.882], and AUC 0.985 [95% CI, 0.965–1.000] in the training dataset, AUC 0.931 [95% CI, 0.841–1.000], AUC 0. 725 [95% CI, 0.569–0.880], and AUC 0.938 [95% CI, 0.851–1.000] in the test dataset, respectively.

OPEN ACCESS

Edited by:
Akira Sugawara,
Tohoku University, Japan

Reviewed by:
Ting Wang,
Guangzhou First People's Hospital, China
Fumihiko Furuya,
University of Yamanashi, Japan

***Correspondence:**
Xian Wang
wangxian8812@126.com
Shudong Hu
hsd2001054@163.com
Xiao-qin Qian
yz_tyz1030@126.com

†These authors have contributed equally to this work and share the first authorship

Specialty section:
This article was submitted to Thyroid Endocrinology, a section of the journal Frontiers in Endocrinology

Received: 09 February 2022
Accepted: 23 March 2022
Published: 22 April 2022

Citation:
Wang Y-g, Xu F-j, Agyekum EA, Xiang H, Wang Y-d, Zhang J, Sun H, Zhang G-l, Bo X-s, Lv W-z, Wang X, Hu S-d and Qian X-q (2022) Radiomic Model for Determining the Value of Elasticity and Grayscale Ultrasound Diagnoses for Predicting BRAF^{V600E} Mutations in Papillary Thyroid Carcinoma. Front. Endocrinol. 13:872153. doi: 10.3389/fendo.2022.872153

Conclusion: The radiomic model based on grayscale and elasticity ultrasound had a good predictive value for BRAF^{V600E} gene mutations in patients with PTC.

Keywords: ultrasonic examination, radiomic, papillary thyroid carcinoma, BRAF-V600E, model

INTRODUCTION

Papillary thyroid carcinoma (PTC) is the most common type of pathological thyroid cancer, accounting for approximately 80–90% of all thyroid cancers and with an annually increasing incidence (1, 2). Most patients have a low death rate, with a 10-year survival rate of > 90%; however, some histological subtypes are prone to extraglandular thyroid invasion, vascular invasion, a high postoperative recurrence rate, and distant metastasis rate. The BRAF^{V600E} gene encodes a protein-dependent kinase, an essential component of the mitogen-activated protein kinase pathway that plays a crucial role in the regulation of cell proliferation, differentiation, and apoptosis (3, 4). The BRAF^{V600E} gene has the highest mutation rate in thyroid cancer and is closely associated with PTC. The mutation of BRAF^{V600E} is an important factor in the PTC phenotype, which contributes to the diagnosis and differential diagnoses of PTC; additionally, the detection rate of PTC is 30–84% (4, 5). The BRAF^{V600E} mutation is closely related to PTC extrathyroid extension invasion and cervical lymph node metastasis, suggesting an invasion of patients with PTC (6, 7). The BRAF^{V600E} mutation was also included in the risk stratification of PTC in the 2015 American Thyroid Association Guidelines; therefore, the preoperative diagnosis of the BRAF^{V600E} mutation is closely related to the development of an appropriate surgical treatment plan to prevent the recurrence of PTC.

While recent studies have shown that grayscale ultrasound can predict the mutation of BRAF^{V600E} in PTC, the results are highly controversial (8, 9). Kabaker et al. reported that vertical and horizontal diameter ratios >1, an unclear boundary, low echo, calcification, and no halo were all associated with the BRAF^{V600E} mutation on ultrasound examination (10). Similarly, Hahn et al. reported that vertical and horizontal diameter ratios >1 were associated with BRAF^{V600E} gene mutations (11); however, some related scholars simultaneously reported that there were no ultrasonic characteristics related to the BRAF^{V600E} mutation (12, 13). Ultrasound radiomics (USR) is a branch of radiomics that is based on ultrasound examination, combined with genetic and clinical data, and employs artificial intelligence as a tool for high-throughput extraction and analysis of relevant tumor information, from structure to molecular cell function analysis, identify tissue and cell level characteristics that cannot be detected by visual reading or conventional quantitative technology, and provide auxiliary decision support for clinical diagnosis and prognosis (14, 15). With high throughput, it can transform the image data from the region of interest (ROI) of lesions into quantitative data with feature space, performing precise quantitative analysis. Previous studies have shown that ultrasonic histogram and texture analysis can help distinguish between benign and malignant thyroid nodules (15, 16); however, there are few reports regarding the ultrasonic image features of the BRAF^{V600E} mutation in PTC using the USR method (8, 9), and there is no further application of multimodal USR.

In this study, the USR features of PTC were analyzed based on grayscale and elasticity ultrasound to predict the risk of the BRAF^{V600E} mutation.

MATERIALS AND METHODS

Clinical Data

This study was approved by the Ethics Committee of Jiangsu University Affiliated People's Hospital, and all patients provided written informed consent. PTC patients who underwent a preoperative thyroid ultrasound examination, BRAF^{V600E} mutation detection, and surgery at Jiangsu University Affiliated People's Hospital between January 2014 and 2021, were retrospectively examined. **Figure 1** shows the enrolment procedure. The inclusion criteria were having undergone preoperative grayscale and elasticity ultrasound examination of the thyroid, with related ultrasound images and diagnostic results obtained; a maximum nodule diameter > 5 mm; a maximum nodule diameter > 5 mm, < 5 cm; postoperative pathology-confirmed PTC; and unilateral and single focal lesion. The exclusion criteria were unclear ultrasound images of nodules owing to artifacts and a maximum nodule diameter > 5 cm. Finally, 138 PTCs of 138 patients (mean age, 41.63 ± 11.36 [range, 25–65] years) were analyzed in this study. One hundred thirty-eight patients were divided into BRAF^{V600E} mutation-free group (n=75) and BRAF^{V600E} mutation group (n=63). The clinical information of the enrolled patients, including age, sex, nodule diameter, nodule location, nodule echo, nodule boundary, nodule internal and peripheral blood flow, nodule elastic grading, calcification, cervical lymph node metastasis, and BRAF^{V600E} mutation results were recorded.

Ultrasound and Elastic Ultrasound Examination

The Philips Q5 (both Healthcare, Eindhoven, Netherlands) and the GE LOGIC E20 (GE Medical Systems, American General) ultrasonic instrument (L12-5 linear array probe, frequency: 10–14 MHz) were used. The patients were placed in the supine position, and longitudinal and transverse continuous scanning were performed to obtain longitudinal and transverse images of the thyroid nodules. A coexisting diagram including the nodule diameter, nodule location, nodule echo, nodule boundary, blood flow in and around the nodule, elastic grading of the nodule, calcification, and cervical lymph node metastasis was observed. The elastic imaging mode was enabled, and the position and size of the sampling frame were adjusted on the cross-sectional image. The nodules were positioned at the center of the elastic

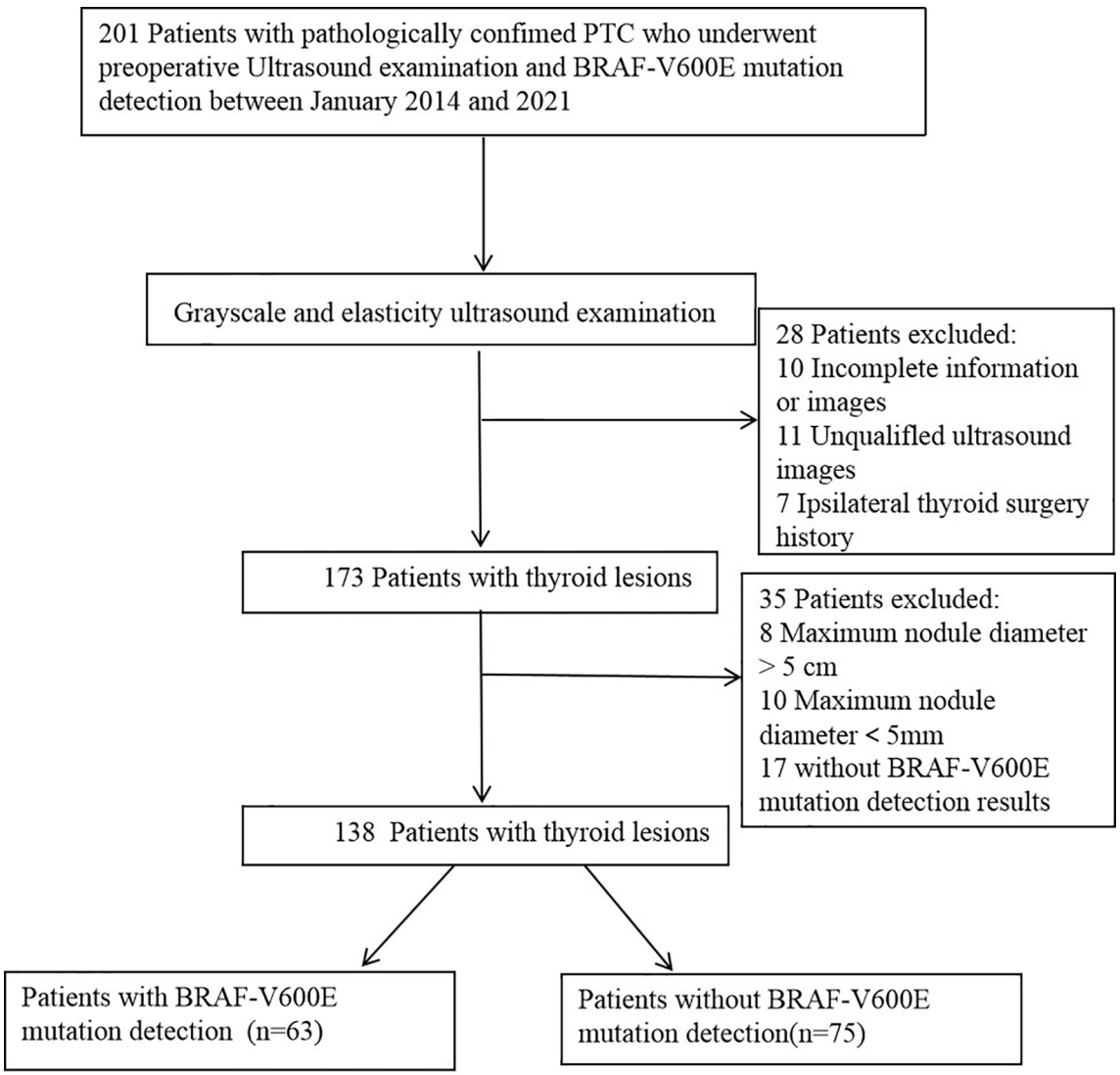

FIGURE 1 | Schematic diagram of the patient selection. PTC, papillary thyroid carcinoma.

imaging region, with the ROI more than four times the size of the nodules. The probe was perpendicular to the nodule, and pressure was applied in a steady manner (range 1–2 mm, 1–2 times/s). When the linear strain hint graph (green spring) indicated stability, the freeze key was pressed to obtain an elastic image; the color change in the ROI was observed (green indicated soft; red indicated hard), and the hardness of the nodule was scored based on elasticity. The grading standard of the elastic image was as follows: 1 point, nodules, and surrounding tissues were completely green; 2 points, nodules were red and green (mostly green); 3 points, mixed red and green distribution (mainly red); 4 points, nodules were completely red; and 5 points, the red coverage was greater than that of the nodule.

ROI Segmentation and Normalization

Thyroid ultrasound examinations were performed within one week before surgery. Two radiologists (with 9 and 10 years of experience in the diagnosis of thyroid diseases, respectively) blinded to the pathological and surgical records, completed the manual ultrasonic image segmentation independently. The ROIs were placed on the tumor mass without the surrounding tissue, the ROIs were manually sketched on each image using the ITK-SNAP software (http://www.itksnap.org). The tumor regions in the elasticity ultrasound images were sketched according to the grayscale images. Following the manual ROI segmentation, the z-score normalization method was used to standardize the grayscale and elasticity ultrasound images to obtain a standard normal distribution of image intensities.

Radiomic Feature Extraction and Feature Selection

The PyRadiomics platform from the medical image data was used to extract the standardized set of radiology characteristics (https://github.com/Radiomics/pyradiomics). In total, 479 radiomics features were extracted from the ultrasound images of each ROI. The grayscale features were extracted from the ROI of the grayscale images, and elastic features were extracted from the ROI of the elastic images. The interclass correlation coefficient (ICC) was used to evaluate the inter-observer and intra-observer consistency of feature extraction. ICC > 0.80 was considered excellent. Spearman's correlation analysis was used to select radiometric that were highly correlated with BRAF^{V600E} mutations. The redundant features identified by Spearman's correlation coefficient ≥0.8 were eliminated; the minimum redundancy maximum relevance (mRMR) algorithm was subsequently used to select the top 10 features with high relevance and low redundancy for the following analyses. After mRMR, the least absolute shrinkage and selection operator (LASSO) logistic regression method, using 10-fold cross-validation, was used to select the most useful BRAF^{V600E} mutation-related predictive features in the training dataset (**Figure 2**).

According to the result of the LASSO regression analysis, the mathematical expression of the BMUS and ES radiomic signatures are given as follows:

$$\begin{aligned}&\text{BMUSRadiomicsignature}\\&= 0.271 - 0.384 \times \text{wavelet . LH \_ glrlm \_ RanVariance} + 0.224\\&\times \text{wavelet . HH \_ glcm \_ Imc1} + 0.118\\&\times \text{wavelet . HL \_ glcm \_ InverseVariance} + 0.086\\&\times \text{wavelet . LH \_ glszm \_ SmallAreaEmphasis} + 0.058\\&\times \text{wavelet . LL \_ glcm \_ MCC} + 0.055\\&\times \text{wavelet . HH \_ glszm \_ SmallAreaLowGrayLevelEmphasis}\\&+ 0.51 \times \text{wavelet . LH \_ firstorder \_ Median} + 0.025\\&\times \text{wavelet . LH \_ glcm \_ Imc1}\end{aligned}$$

$$\begin{aligned}&\text{ESRadiomic signature}\\&= 0.307 + 0.521 \times \text{wavelet . HL \_ glszm \_ SmallAreaEmphasis}\\&- 0.426 \times \text{original \_ firstorder \_ Minimum} + 0.424\\&\times \text{wavelet . HL \_ glcm \_ MCC} + 0.384\\&\times \text{wavelet . HL \_ glrlm \_ HighGrayLevelRunEmphasis} - 0.073\\&\times \text{original \_ glszm \_ GrayLevelNonUniformityNormalized}\end{aligned}$$

Radiomic Model Construction and Validation

A single radiomics model using grayscale and elasticity ultrasound was generated using a linear combination of the selected features, weighted by the LASSO algorithm with non-zero coefficients. The combined grayscale and elasticity radiomics model was built based on multivariate analysis of the training dataset. Differences in the radiomics model between patients with and without the BRAF^{V600E} mutation were compared using the Mann–Whitney U test. The predictive performance of the radiomics model was evaluated using a receiver operating characteristic (ROC) curve, and the area under the curve (AUC), sensitivity, and specificity were calculated for both the training and test datasets.

Detection Method of BRAF Gene

More than two needles were used to puncture tissue, and DNA was extracted using the QIAamp Human Genome DNA Extraction Kit (QIAGEN). The NanoDrop 1000 (Thermo Fisher, USA) was used to measure DNA concentrations, which were ≥50ng/l. The PCR reaction system was set up in accordance with the PCR kit's specifications, which included a special probe, reaction solution, and pure water. The processed nucleic acid to be tested, as well as the positive and negative quality controls, were then added to the reaction system, centrifuged at 2000 rpm for 15 seconds to the bottom of the tube, and the PCR amplification reaction was carried out. The reaction conditions were set in accordance with the kit's specifications. Following the completion of the reaction, the negative quality control should have no S-type amplification curve and the positive quality control should have an S-type amplification curve and a Ct value of 30. The results of the BRAF gene to be tested are finally read after the above two conditions are met.

Statistical Analysis

Statistical analyses were performed using R software (version 3.6.1, https://www.r-project.org) and SPSS 20.0 software (SPSS, Inc., Chicago,IL). Descriptive statistics of continuous variables were expressed as mean ± standard deviation, and the age difference between the two groups was tested using the Student's t-test. The $\chi 2$ test showed that the gender difference between the two groups was statistically significant ($P<0.05$). To evaluate the best predictive models, AUCs in the ROC analysis were calculated.

RESULTS

Clinical Characteristics

In 138 patients with PTC, 78 cases were classical type, 49 cases were follicular type, and 6 cases were diffuse sclerosis type. The mutation rate of BRAF gene was 45.6% (63/138), 62.8% (49/78) and 16.3% (8/49). The mutation rate of diffuse sclerosing type was 33.3% (2/6) and that of hypercellular subtype was 80% (4/5). A total of 138 PTC patients, including 87 women (mean age, 41.81 ± 11.23 [range, 25–57] years) and 51 men (mean age, 43.82 ± 12.18 [range, 28–65] years). All patients were randomly divided into either the training group (n=96) or the test group (n=42) using a stratified sampling method, and the mutation and non-mutation groups were randomly divided at 7:3, respectively. A comparison

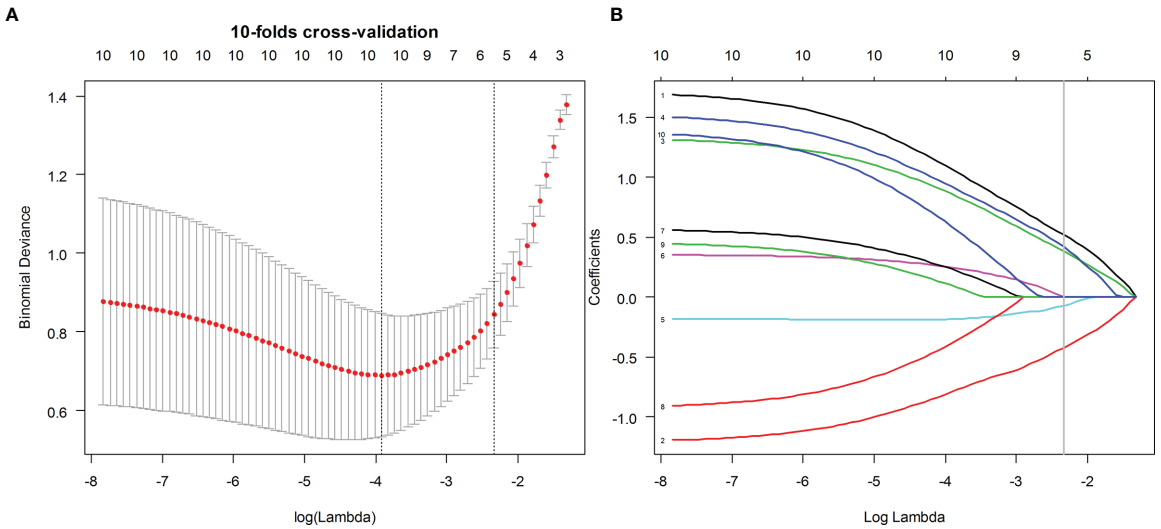

FIGURE 2 | Ultrasound image feature selection using the least absolute shrinkage and selection operator (LASSO) logistic regression model in the training dataset. **(A)** The 10-fold cross-validation and the minimal criteria process were used to generate the optimal penalization coefficient lambda in the LASSO model. **(B)** LASSO coefficient profiles of the BMUS and ES features. The dotted vertical line was drawn at the value selected by 10-fold cross-validation when the optimal λ resulted in eight (BMUS) and five (ES) nonzero coefficients, respectively.

of the clinical data and imaging comparisons of the 138 patients between the training and test groups is shown in **Table 1**. There were no significant differences in clinical characteristics between the two groups, including age and sex (P>0.05). There were also no significant differences in the mean nodule size (BRAF^{V600E} mutant group: 24.12 ± 8.6 mm; without BRAF^{V600E} mutant group: 23.98 ± 11.01 mm, P=0.928) or cervical lymph node metastasis (P=0.102) between the two groups. The relationship between the BRAF^{V600E} mutation and ultrasonic imaging characteristics is shown in **Table 2**.

Feature Selection

In total, 479 radiomic features were extracted from the grayscale and elasticity ultra-sonograms of each patient. The grayscale features were reduced to eight BRAF^{V600E} mutation-related features after Spearman's correlation analysis, mRMR, and LASSO algorithms were applied in the training cohort (**Figure 3**). Likewise, the elasticity features were reduced to five risk predictors in the training cohort (**Figure 3**). Favorable inter- and intra-observer reproducibility of feature extraction was achieved, with intra-observer ICCs of 0.487–0.965 and inter-observer ICCs of 0.543–0.982.

Model Construction and Validation

According to the grayscale and elastic ultrasound images in the training dataset, logistic regression values were the best classifier. First, we evaluated the performances of the three models in the training dataset and then validated them in the test dataset. The AUCs of the grayscale, elasticity, grayscale, and elasticity combination prediction model in the training dataset was 0.792 (95% CI, 0.703–0.882), 0.952 (95% CI, 0.914–0.990), and 0.985 (95% CI, 0.965–1.000), respectively. In the test dataset, the AUCs were 0.725 (95% CI, 0.569–0.880), 0.931 (95% CI, 0.841–1.000), and 0.938 (95% CI, 0.851–1.000), respectively. The results showed that the elastic prediction model or the combination of the grayscale and elastic prediction model was better than the grayscale prediction model. The AUC, accuracy, sensitivity, and specificity of the three models are shown in **Table 3**. The ROC curves of the three models are shown in **Figure 4**. The decision curve analysis (DCA) was applied in determining the clinical usefulness of the radiomic by calculating the net benefits at different threshold values in the combined training and validation cohort. The DCA showed that radiometric provided a higher overall net benefit than the all or no treatment strategy (**Figure 5**).

DISCUSSION

At present, mutations in the BRAF^{V600E} gene positively correlate with high-risk clinicopathological factors of PTC such as extraglandular invasion, cervical lymph node metastasis, and tumor stage III-IV, suggesting that the BRAF^{V600E} mutation may reflect the degree of malignancy of PTC (17, 18). It plays a key role in the development and evolution of PTC and can be used as an important indicator to objectively judge the invasiveness of PTC. We thus believe that by detecting BRAF^{V600E} mutations and expanding the scope of surgical resection for cases with BRAF^{V600E} mutation, active treatment can be optimized thereby enabling a better prognosis. Because of its strong association with aggressive clinic pathological outcomes and serious molecular derangements in PTC, the BRAF mutation has emerged as a unique and valuable molecular marker in the management of PTC. The preoperative prediction of BRAF^{V600E} mutations in

TABLE 1 | Clinical characteristics of the patients in the training and test cohorts.

Characteristic	Training cohort (n=96)	test cohort (n=42)	P-value
Age, mean ± SD (years)	41.78 ± 10.99	44.33 ± 12.81	0.152
Age (years)			
>45	48.63 ± 5.23	49.90 ± 5.89	0.218
≤45	34.61 ± 5.17	34.76 ± 7.87	0.670
Sex			
Male	36	15	0.851
Female	60	27	
Tumor size(mm), mean ± SD	26.04 ± 8.51	26.63 ± 8.55	0.074
Primary site			
Right lobe	28	15	0.318
Left lobe	30	16	
Isthmus	38	11	
Tumor location			
Upper pole	31	18	0.325
Lower pole	27	13	
Middle	38	11	
Composition			
Solid	56	19	0.269
Predominantly solid	40	23	
Elastic classification			
1	13	5	0.375
2	22	15	
3	15	7	
4	26	7	
5	20	8	
Cystic change			
With cystic change	52	20	0.579
Without cystic change	44	22	
Calcification			
Microcalcification	37	11	0.143
Macrocalcification	41	17	
Rim calcification	18	14	
Tumor border			
Clear	37	13	0.510
Less clear	31	18	
Fuzzy	28	11	
Cervical lymph node metastasis	61	31	0.327

patients with PTC is therefore of great significance for guiding their clinical treatment.

Liu et al. predicted the BRAF^{V600E} mutation in patients with PTC using gray-scale ultrasound radiomics, demonstrating the feasibility of using the USR method for analysis (15). When compared with a single ultrasound imaging mode, USR can delve into details behind PTC ultrasound images to determine the temporal and spatial heterogeneity of PTC, indicating the relationship between image features and BRAF^{V600E} mutations. USR can therefore be used as a noninvasive imaging method for the preoperative evaluation of BRAF^{V600E} mutations in patients with PTC. In our study, we developed a preoperative, radiomic ultrasound model to improve the prediction of the BRAF^{V600E} mutation in patients with PTC. The AUC of gray-scale radiomic sequence model, elastic radiomic sequence model, and multi-sequence (grayscale combined with elastic ultrasound) radiomic model in the training dataset was 0.792, 0.952, 0.985 respectively, and in the test dataset were 0.725, 0.931, 0.938, respectively. Our study shows that both the elastic radiomic sequence model and the multi-sequence (grayscale combined with elastic ultrasound) sequence model can well predict the BRAF^{V600E} mutation in the training dataset and test dataset. Elasticity ultrasound can estimate the corresponding conditions inside PTC tissues *via* an ultrasonic imaging method combined with digital image processing or digital signal processing technology. Elastography reflects the relative hardness of the lesion and its surrounding tissues, while the hardness of PTC tissues is closely related to its internal pathological structure; therefore, real-time tissue elastography can evaluate the anatomical structure and biological characteristics of PTC.

Bojunga et al. showed that elasticity ultrasound can effectively distinguish between benign and malignant thyroid nodules (19), while Moon et al. found that PTC elastography findings with a degree of high hardness were associated with extrathyroidal invasion (20). These studies provide a new perspective for the ultrasound diagnosis of BRAF^{V600E} mutation-positive and negative PTC. Recent studies have shown that owing to the different arrangement and composition of cells, elasticity indices of parts of tissues are different (21, 22); the higher the malignancy of PTC, the greater the hardness on elasticity ultrasound imaging. There were significant differences in the elastic modulus or hardness between patients with and without

TABLE 2 | Relationship between BRAF mutations and US imaging characteristics through visual assessment of papillary thyroid carcinomas.

	BRAF mutation (n=63)	No BRAF mutation (n=75)	P-value
Age, mean ± SD, years	38.03 ± 10.41	36.68 ± 10.05	0.377
Sex			
Male	22	29	0.724
Female	41	46	
Tumor size, mean ± SD	24.12 ± 8.6	23.98 ± 11.01	0.928
Composition			
Solid	33	42	0.733
Predominantly solid	30	33	
Solid part Echogenicity			
Markedly hypoechoic	41	20	0.000
Hypoechoic	10	21	
Isoechoic	9	14	
Hyperechoic	3	20	
Shape			
Irregular	32	43	0.443
Round to oval	31	32	
Vertical and horizontal diameter ratio			
≥1	41	27	0.001
<1	22	48	
Margin			
Spiculated/microlobulated	30	25	0.183
Ill-defined	21	28	
Smooth	12	22	
Calcification			
Microcalcification	26	22	0.127
Macrocalcification	27	31	
Rim calcification	10	22	
Final C-TIRADS category			
Low suspicion	16	31	0.058
Intermediate suspicion	17	23	
High suspicion	30	22	
Cervical lymph node metastasis	47	45	0.102

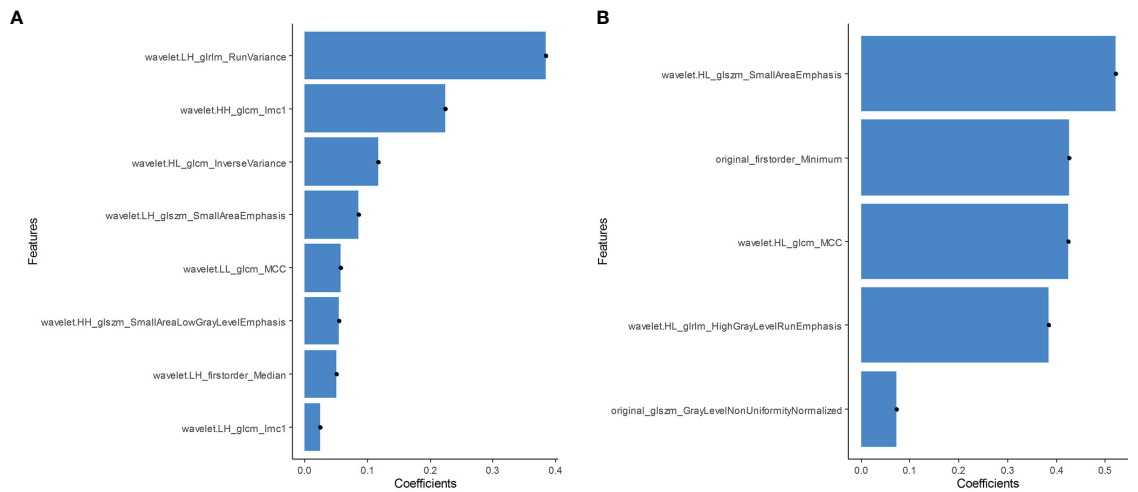

FIGURE 3 | **(A)** Grayscale features were reduced to eight BRAF^{V600E} mutation-related features in the training cohort. **(B)** The elasticity features were reduced to five risk predictors in the training cohort.

BRAF^{V600E} mutations based on the ultrasound images. Elasticity could directly and quantitatively reflect the absolute hardness of BRAF^{V600E} mutation-positive and negative PTC and better reflect the pathological characteristics of tissues. Therefore, multimodal USR was used in this study to predict the BRAF^{V600E} mutation in patients with PTC. A significant association was revealed between ultrasound radiomic features and the BRAF^{V600E} mutation in PTC; thus, our analysis provides

TABLE 3 | Performance of the sequences models.

Cohort	Model	AUC[a]	SEN[b] (%)	SPE[c] (%)	PPV[d]	NPV[e]	ACC[f] (%)	Cutoff value
dataset	grayscale	0.792 (0.703–0.882)	69.1	78.0	80.9	65.3	72.9	0.372
	elasticity	0.952 (0.914–0.990)	85.5	97.6	97.9	83.3	90.6	0.469
	grayscale + elasticity	0.985 (0.965–1.000)	96.4	97.6	98.1	95.2	96.9	0.628
Test dataset	grayscale	0.725 (0.569–0.880)	54.2	83.3	81.2	57.7	66.7	0.372
	elasticity	0.931 (0.841–1.000)	83.3	94.4	95.2	81.0	88.1	0.469
	grayscale + elasticity	0.938 (0.851–1.000)	83.3	1.0	1.0	81.8	90.5	0.628

[a]*AUC, area under the receiver operating characteristic curve.*
[b]*SEN, sensitivity.*
[c]*SPE, specificity.*
[d]*PPV, positive predictive value.*
[e]*NPV, negative predictive value.*
[f]*ACC, balanced accuracy.*

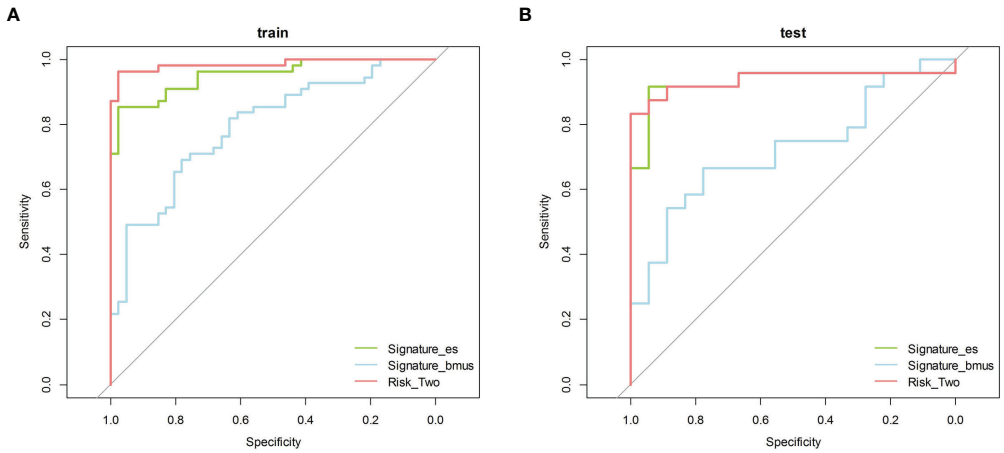

FIGURE 4 | The ROC curves of the three models. ROC, receiver operating characteristic. **(A)** Training cohort **(B)** Test cohort.

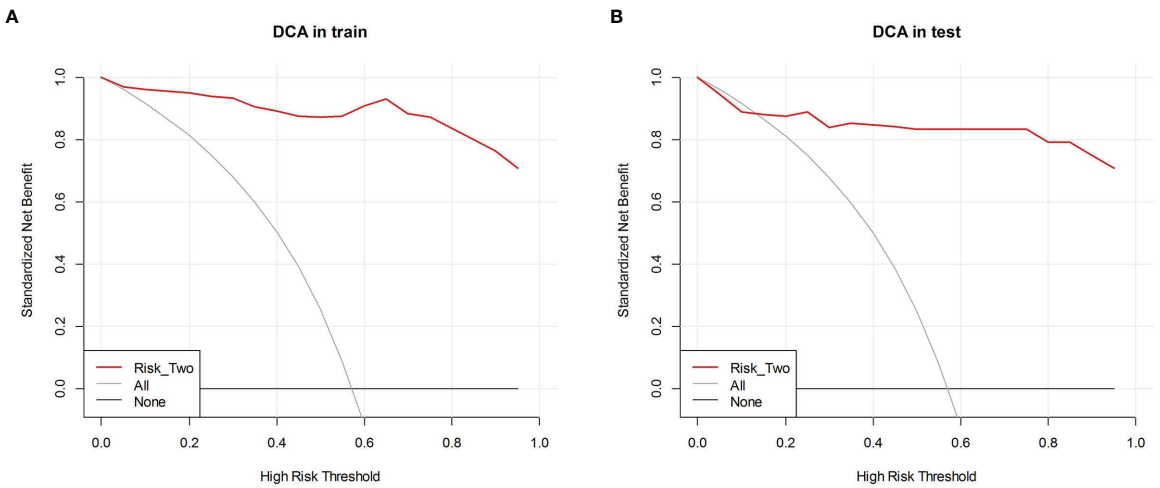

FIGURE 5 | Decision curve analysis (DCA) of each model in predicting BRAF^{V600E} Mutations for papillary thyroid carcinoma (PTC). The vertical axis measures standardized net benefit. The horizontal axis shows the corresponding risk threshold. The DCA showed using the risk_two radiomics (red curve) derived in the present study to predict BRAF^{V600E} Mutations provided the greatest benefit. **(A)** DCA in training cohort **(B)** DCA in the test cohort.

an alternative method that is noninvasive and convenient for the assessment of the BRAF^{V600E} mutation in patients. Using LASSO feature selection, 958 quantitative imaging features were reduced to 13 potential features (8 from grayscale and 5 from elasticity ultrasound) suitable for radiomic features analysis of the ultrasound datasets. Most of the selected imaging features were microscopic structural features of the tumor, including cellularity, and compression of the normal thyroid tissues by the tumor. We analyzed the relationship between radiomic features and the BRAF^{V600E} mutation and found 11 wavelet features, 1 first-order feature, and 1 texture feature that were significantly correlated with the BRAF^{V600E} mutation. According to the definitions of these texture features, these radiomic features can serve as a new tool for preoperative prediction of BRAF^{V600E} mutations in PTC patients.

There are some limitations to our study. First, this was a small sample retrospective study conducted at two institutions; thus, a selection bias may exist. In the future, we aim to conduct a multicenter study with a larger sample size. Second, only two ultrasound machines with similar parameters were used in this study to avoid the influence of equipment; however, parameter characteristics and patient-related factors may still affect the pixel intensity of the ultrasound images. Future studies should investigate several different types of ultrasonic instruments. Third, we focused on assessing the BRAF^{V600E} mutation in patients with PTC and did not study the gene in healthy individuals, which may have led to a selection bias. Finally, the lack of external validation data is a limitation of this study.

CONCLUSIONS

Our preliminary study suggests that elasticity ultrasound, combined with gray-scale ultrasound imaging, has significant clinical value for predicting BRAF^{V600E} mutation in patients with PTC. This can provide clinicians with a more accurate and noninvasive diagnosis of the BRAF^{V600E} mutation before surgery thereby optimizing treatment outcomes.

DATA AVAILABILITY STATEMENT

The original contributions presented in the study are included in the article/supplementary material. Further inquiries can be directed to the corresponding authors.

ETHICS STATEMENT

The studies involving human participants were reviewed and approved by Jiangsu University-affiliated peoples ethics committee. The patients/participants provided their written informed consent to participate in this study.

AUTHOR CONTRIBUTIONS

Conceptualization, Y-gW, F-jX, EA, XW, and X-qQ. Data curation, GZ, XB, W-zL, and SH. Formal analysis, F-jX, GZ, and W-zL. Funding acquisition, Y-gW, XW, S-dH, and X-qQ. Investigation, HX, Y-dW, and JZ. Methodology, EA, HS, and W-zL. Project administration, XW, S-dH, and X-qQ. Resources, Y-gW, F-jX, and SH. Software, HS, X-sB, and W-zL. Supervision, XW, SH, and X-qQ. Validation, Y-gW, F-jX, HX, Y-dW, and JZ. Visualization, Y-gW, F-jX, and X-sB. Writing – original draft, XW and X-qQ. Writing – review and editing, EA. All authors contributed to the article and approved the submitted version.

FUNDING

The authors disclose the receipt offinancial support for the research, authorship, and/or publication of this article from the Clinical Medicine Science and Technology Development Foundation of Jiangsu University (Project No. JLY2021001) and the Zhenjiang Commission of Science and Technology (Project No. SH2020046, Project No. SH2018050, and Project No. SH2018056). Guiding Project of Jiangsu Health Committee (Z2021071).

REFERENCES

1. Haugen BR, Alexander EK, Bible KC, Doherty GM, Mandel SJ, Nikiforov YE, et al. 2015 American Thyroid Association Management Guidelines for Adult Patients With Thyroid Nodules and Differentiated Thyroid Cancer: The American Thyroid Association Guidelines Task Force on Thyroid Nodules and Differentiated Thyroid Cancer. *Thyroid* (2016) 26:1–133. doi: 10.1089/thy.2015.0020
2. Tuttle RM, Haugen B, Perrier ND. Updated American Joint Committee on Cancer/Tumor-Node-Metastasis Staging System for Differentiated and Anaplastic Thyroid Cancer (Eighth Edition): What Changed and Why? *Thyroid* (2017) 27:751–6. doi: 10.1089/thy.2017.0102
3. Kure S, Ishino K, Kudo M, Wada R, Saito M, Nagaoka R, et al. Incidence of BRAF V600E Mutation in Patients With Papillary Thyroid Carcinoma: A Single-Institution Experience. *J Int Med Res* (2019) 47:5560–72. doi: 10.1177/0300060519873481
4. Czarniecka A, Oczko-Wojciechowska M, Barczyński M. BRAF V600E Mutation in Prognostication of Papillary Thy-Roid Cancer (PTC) Recurrence. *Gland Surg* (2016) 5:495–505. doi: 10.21037/gs.2016.09.09
5. Yan C, Huang M, Li X, Wang T, Ling R. Relationship Between BRAF V600E and Clinical Features in Papillary Thyroid Carcinoma. *Endocr Connect* (2019) 8:988–96. doi: 10.1530/EC-19-0246
6. Rashid FA, Munkhdelger J, Fukuoka J, Bychkov A. Prevalence of BRAFV600E Mutation in Asian Series of Papillary Thyroid Carcinoma—a Contemporary Systematic Review. *Gland Surg* (2020) 9:1878–900. doi: 10.21037/gs-20-430
7. Sun J, Zhang J, Lu J, Gao J, Ren X, Teng L, et al. BRAF V600E, and TERT Promoter Mutations in Papillary Thyroid Carcinoma in Chinese Patients. *PloS One* (2016) 11:e153319. doi: 10.1371/journal.pone.0153319
8. Yoon JH, Han K, Lee E, Lee J, Kim EK, Moon HJ, et al. Radiomics in Predicting Mutation Status for Thyroid Cancer: A Preliminary Study Using Radiomics Features for Predicting BRAFV600E Mutations in Papillary Thyroid Carcinoma. *PloS One* (2020) 15:e228968. doi: 10.1371/journal.pone.0228968
9. Yoon J, Lee E, Koo JS, Yoon JH, Nam KH, Lee J, et al. Artificial Intelligence to Predict the BRAFV600E Mutation in Patients With Thyroid Cancer. *PloS One* (2020) 15:e242806. doi: 10.1371/journal.pone.0242806
10. Kabaker AS, Tublin ME, Nikiforov YE, Armstrong MJ, Hodak SP, Stang MT, et al. Suspicious Ultrasound Characteristics Predict BRAFV600E-Positive Papillary Thyroid Carcinoma. *Thyroid* (2012) 22:585–9. doi: 10.1089/thy.2011.0274

11. Hahn SY, Kim TH, Ki CS, Kim SW, Ahn S, Shin JH, et al. Ultrasound and Clinicopathological Features of Pa-Pillary Thyroid Carcinomas With BRAF and TERT Promoter Mutations. *Oncotarget* (2017) 8:108946–57. doi: 10.18632/oncotarget.22430
12. Li Q, Yuan J, Wang Y, Zhai Y. Association Between the BRAF V600E Mutation and Ultrasound Features of the Thyroid in Thyroid Papillary Carcinoma. *Oncol Lett* (2017) 14:1439–44. doi: 10.3892/ol.2017.6276
13. Xu J, Chen Y, Dang Y, Dang YY, Chen M. Association Between Preoperative US, Elastography Features and Prognostic Factors of Papillary Thyroid Cancer With BRAFV600E Mutation. *Front Endocrinol (Lausanne)* (2020) 10:902. doi: 10.3389/fendo.2019.00902
14. Liu T, Ge X, Yu J, Guo Y, Wang Y, Wang W, et al. Comparison of the Application of B-Mode and Strain Elastography Ultrasound in the Estimation of Lymph Node Metastasis of Papillary Thyroid Carcinoma Based on a Radiomics Approach. *Int J Comput Assist Radiol Surg* (2018) 13:1617–27. doi: 10.1007/s11548-018-1796-5
15. Kwon MR, Shin JH, Park H, Cho H, Hahn SY, Park KW. Radiomics Study of Thyroid Ultrasound for Predicting BRAF Mutation in Papillary Thyroid Carcinoma: Preliminary Results. *AJNR Am J Neuroradiol* (2020) 41:700–5. doi: 10.3174/ajnr.A6505
16. Xu JM, Xu XH, Xu HX, Zhang YF, Guo LH, Liu LN, et al. Prediction of Cervical Lymph Node Metastasis in Patients With Papillary Thyroid Cancer Using Combined Conventional Ultrasound, Strain Elastography, and Acoustic Radiation Force Impulse (ARFI) Elastography. *Eur Radiol* (2016) 26:2611–22. doi: 10.1007/s00330-015-4088-2
17. Chen TY, Lorch JH, Wong KS, Barletta JA. Histological Features of BRAF V600E-Mutant Anaplastic Thyroid Carcinoma. *Histopathology* (2020) 77:314–20. doi: 10.1111/his.14144
18. Celik M, Bulbul BY, Ayturk S, Durmus Y, Gurkan H, Can N, et al. The Relation Between BRAFV600E Mutation and Clinicopathological Characteristics of Papillary Thyroid Cancer. *Med Glas (Zenica)* (2020) 17:30–4. doi: 10.17392/1086-20
19. Bojunga J, Mondorf A. Schilddrüsen-Elastografie [Thyroid Elastography]. *Laryngorhinootologie* (2019) 98:150–6. doi: 10.1055/a-0790-0885
20. Jiang M, Li C, Tang S, Lv W, Yi A, Wang B, et al. Nomogram Based on Shear-Wave Elastography Radiomics can Improve Preoperative Cervical Lymph Node Staging for Papillary Thyroid Carcinoma. *Thyroid* (2020) 30:885–97. doi: 10.1089/thy.2019.0780
21. Yi L, Qiong W, Yan W, Youben F, Bing H. Correlation Between Ultrasound Elastography and Histologic Characteristics of Papillary Thyroid Carcinoma. *Sci Rep* (2017) 7:45042. doi: 10.1038/srep45042
22. Li N, He JH, Song C, Yang LC, Zhang HJ, Li ZH. Nomogram Including Elastography for Prediction of Contralateral Central Lymph Node Metastasis in Solitary Papillary Thyroid Carcinoma Preoperatively. *Cancer Manag Res* (2020) 12:10789–97. doi: 10.2147/CMAR.S278382

Conflict of Interest: The authors declare that the research was conducted in the absence of any commercial or financial relationships that could be construed as a potential conflict of interest.

Publisher's Note: All claims expressed in this article are solely those of the authors and do not necessarily represent those of their affiliated organizations, or those of the publisher, the editors and the reviewers. Any product that may be evaluated in this article, or claim that may be made by its manufacturer, is not guaranteed or endorsed by the publisher.

frontiers | Frontiers in Endocrinology

ORIGINAL RESEARCH
published: 01 June 2022
doi: 10.3389/fendo.2022.874396

Extrathyroidal Extension Prediction of Papillary Thyroid Cancer With Computed Tomography Based Radiomics Nomogram: A Multicenter Study

Pengyi Yu[1,2†], Xinxin Wu[1,2†], Jingjing Li[1,2†], Ning Mao[3,4], Haicheng Zhang[3], Guibin Zheng[5], Xiao Han[1,2], Luchao Dong[1,2,6], Kaili Che[4], Qinglin Wang[4], Guan Li[4], Yakui Mou[1,2] and Xicheng Song[1,2*]*

[1] Department of Otorhinolaryngology, Head and Neck Surgery, Yantai Yuhuangding Hospital, Qingdao University, Yantai, China, [2] Shandong Provincial Clinical Research Center for Otorhinolaryngologic Diseases, Yantai, China, [3] Big data and Artificial Intelligence Laboratory, Yantai Yuhuangding Hospital, Qingdao University, Yantai, China, [4] Department of Radiology, Yantai Yuhuangding Hospital, Qingdao University, Yantai, China, [5] Department of Thyroid Surgery, Yantai Yuhuangding Hospital, Qingdao University, Yantai, China, [6] Second Clinical Medicine College, Binzhou Medical University, Yantai, Shandong, China

Objectives: To develop and validate a Computed Tomography (CT) based radiomics nomogram for preoperative predicting of extrathyroidal extension (ETE) in papillary thyroid cancer (PTC) patients

Methods: A total of 153 patients were randomly assigned to training and internal test sets (7:3). 46 patients were recruited to serve as an external test set. A radiologist with 8 years of experience segmented the images. Radiomics features were extracted from each image and Delta-radiomics features were calculated. Features were selected by using one way analysis of variance and the least absolute shrinkage and selection operator in the training set. K-nearest neighbor, logistic regression, decision tree, linear-support vector machine (linear -SVM), gaussian-SVM, and polynomial-SVM were used to build 6 radiomics models. Next, a radiomics signature score (Rad-score) was constructed by using the linear combination of selected features weighted by their corresponding coefficients. Finally, a nomogram was constructed combining the clinical risk factors with Rad-scores. Receiver operating characteristic (ROC) curve, decision curve analysis (DCA), and calibration curve were performed on the three sets to evaluate the nomogram's performance.

Results: 4 radiomics features were selected. The six models showed the certain value of radiomics, with area under the curves (AUCs) from 0.642 to 0.701. The nomogram

OPEN ACCESS

Edited by:
Paolo Miccoli, University of Pisa, Italy

Reviewed by:
Clara Ugolini, University of Pisa, Italy
Sabrina Rosaria Paparo, University of Pisa, Italy

***Correspondence:**
Xicheng Song
drxchsong@163.com
Yakui Mou
muykmd@126.com

†These authors have contributed equally to this work and share first authorship

Specialty section:
This article was submitted to Thyroid Endocrinology, a section of the journal Frontiers in Endocrinology

Received: *12 February 2022*
Accepted: *27 April 2022*
Published: *01 June 2022*

Citation:
Yu P, Wu X, Li J, Mao N, Zhang H, Zheng G, Han X, Dong L, Che K, Wang Q, Li G, Mou Y and Song X (2022) Extrathyroidal Extension Prediction of Papillary Thyroid Cancer With Computed Tomography Based Radiomics Nomogram: A Multicenter Study. Front. Endocrinol. 13:874396. doi: 10.3389/fendo.2022.874396

combining the Rad-score and clinical risk factors (radiologists' interpretation) showed good performance (internal test set: AUC 0.750; external test set: AUC 0.797). Calibration curve and DCA demonstrated good performance of the nomogram.

Conclusion: Our radiomics nomogram incorporating the radiomics and radiologists' interpretation has utility in the identification of ETE in PTC patients.

Keywords: papillary thyroid cancer, extrathyroidal extension (ETE), radiomics, contrast-enhanced CT, nomogram

HIGHLIGHTS

- Radiomics features were extracted from non-contrast and contrast-enhanced CT images, and Delta-radiomics features were calculated.
- 6 classifiers (KNN, LR, DT, linear-SVM, gaussian-SVM, and polynomial-SVM) were used to construct radiomics models and showed favorable discriminatory abilities.
- The nomogram model combining the radiomics and radiologists' interpretation showed good predictive performance.

INTRODUCTION

While thyroid cancer is one of the most common cancers worldwide, it has a very low mortality rate (1). Papillary thyroid cancer (PTC) is the most common histologic subtype of thyroid cancer (2, 3). In the 8th edition of AJCC (American Joint Committee on Cancer) (4), extrathyroidal extension (ETE), which was subdivided into gross ETE and microscopic ETE, refers to the primary tumor invades the surrounding structures including the strap muscles, trachea, vasculature, larynx, esophagus, and recurrent laryngeal nerve. Furthermore, ETE is an independent risk factor associated with lymph node metastasis and directly affects the clinical outcomes of PTC patients (5, 6). The 15-year survival rate of PTC patients with ETE is significantly lower than that of patients without ETE. Therefore, the diagnosis of ETE is essential for the treatment decision of PTC.

Ultrasound (US), magnetic resonance imaging (MRI), and Computed Tomography (CT) are common non-invasive imaging modality for preoperative ETE diagnosis. US has a high degree of accuracy and sensitivity for identifying ETE (~ 70%), but low specificity (27.2%-68.9%) leads to a high risk of false positive results (7, 8), and US relying on the experience level of the operator is subjective. MRI is slightly inferior to US but similar to CT with regards to accuracy (9). Young Lan Seo et al. (10), found that CT could accurately identify most types of ETE (i.e., esophageal invasion). Furthermore, contrast-enhanced computed tomography (CE-CT) offers an additional phase (venous phase) and three-dimensional images. However, it is difficult to accurately predict ETE based only on traditional images, and obtain the guidance needed for preoperative planning, because interpretation of the images depends on the experience level of the radiologist or surgeon. Besides, histopathological examination, which is the gold standard for diagnosing ETE, is an invasive method, and usually used to verify a preoperative assessment of ETE obtained by using non-invasive tools. Thus, a novel non-invasive tool is needed to help surgeons predict ETE and make clinical decisions prior to performing an operation.

In recent years, Radiomics, the high-throughput extraction of large amounts of image features from radiographic images, can be used to build a mineable high-dimensional database of original material obtained by machine learning (11). Radiomics can also be used to identify the underlying heterogeneity of images that can be difficult to detect with human eyes. Combined with Machine leaning, radiomics are generally used by researchers to predict the prognosis of patients with tumors and assess the impact of various diseases (12, 13). Until now, no study has built a predictive model of ETE using a CT radiomics nomogram adding to time sequential features and then validated the model in a multicenter study. We have achieved that goal.

In this study, we established an effective radiomics nomogram capable of predicting the ETE of PTC based on CT images.

METHODS

Patients

This was a retrospective, multicenter, and diagnostic study. From January 2019 to December 2019, 153 patients, which were collected consecutively from Yantai Yuhuangding Hospital, were randomly assigned to a training set or an internal test set at a ratio of 7:3 (**Figure 1A**). Additionally, 46 consecutive patients at Qilu Hospital of Shandong University were recruited to serve as an external test set from June 2019 to December 2019 (**Figure 1B**). The inclusion and exclusion criteria can be found in **Appendices**.

The protocol for this retrospective study was approved by the Institutional Review Board of The Affiliated Yantai Yuhuangding

Abbreviations: AJCC, American Joint Committee on Cancer; ANOVA, analysis of variance; AUC, area under the curve; CE-CT, contrast-Enhanced computed tomography; CI, confidence interval; CT, Computed Tomography; DCA, decision curve analysis; DT, decision Tree; ETE, extrathyroidal extension; ICCs, intra- and inter-class correlation coefficients; KNN, k-nearest neighbor; LASSO, least absolute shrinkage and selection operator; LR, logistic regression; MRI, magnetic resonance imaging; PTC, papillary thyroid cancer; ROC, Receiver Operating Characteristic; SVM, support vector machine; US, Ultrasound; VIF, variance inflation factor; VOI, volume of interest.

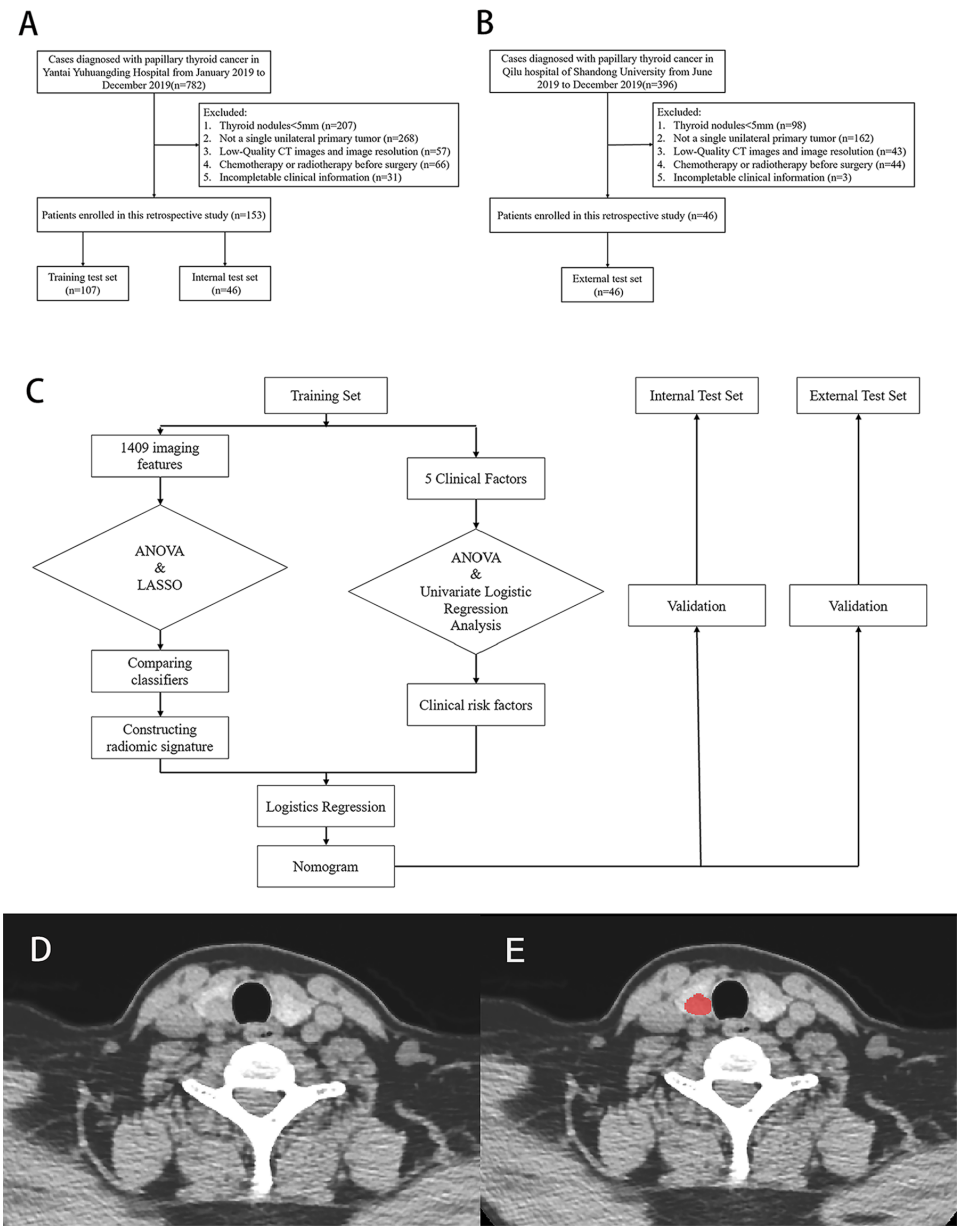

FIGURE 1 | Flow chart of patients' enrolment in **(A)** training, internal test set and **(B)** external test set. **(C)** Flow chart of study work. **(D, E)** Examples of regions of interest (ROIs) segmentation on contrast-enhanced computed tomography (CE-CT) images.

Hospital of Qingdao University. The requirement for obtaining written informed consent from the patients was waived by the review board. A study work flow diagram is shown in **Figure 1C**.

Radiologists' Interpretation of ETE

CT assessments of ETE were performed by two experienced radiologists, one with 15 years of experience and another with 5 years of experience. Both radiologists were blinded to histopathological results. Any disagreement was resolved by discussion or consultation with a third radiologist who had 20 years of experience. ETE was reported on CT images when at least one of the following CT criteria was fulfilled: 1) tumor in contact with 180° or more of the tracheal, esophageal, muscle or vascular circumference; 2) loss of normal structure; 3) a clinical symptom (e.g., ipsilateral vocal cord palsy) was present that could be explained by the CT images; 4) tumor showed poorly defined margin with heterogeneous signal intensity in adjacent soft tissue; 5) focal bulging out or disruption of the thyroid capsule by tumor; 6) more than 25% of perimeter of the tumor was abutting the thyroid capsule (10). Kendall's coefficient of concordance *W* (Kendall's *W*) was used to evaluate inter-radiologist agreement. *W* scores range between 0 and 1, which

was graded as very good (0.80 to 1.00), good (0.60 to 0.80), fair (0.40 to 0.60), moderate (0.20 to 0.40) or poor (<0.20) (14).

Image Segmentation

The Image Acquisition protocol is shown in **Appendices**. After that, a radiologist with 8 years of experience manually delineated the PTC regions of interest (ROI) (15) on non-contrast and venous phase CT images by using an ITK-SNAP (version 3.8.0; www.itksnap.org). Based on their traits, ROIs were manually delineated along the tumor contour on each transverse section and the ROIs in each slice constituted a volume of interest (VOI). A sample of segmentation process is shown in **Figures 1D, E**. Three months later, another two radiologists segmented the images of 30 patients who were randomly selected to assess the intra- and inter-observer reproducibility of radiomics features by intra- and inter-class correlation coefficients (ICCs). An ICC > 0.8 indicated an excellent agreement of radiomics features.

Feature Extraction

Before feature extraction, VOIs were prepossessed included gray value standardization, gray level discretization, and image resampling. A total of 2818 radiomics features were originally extracted from each VOI by using PyRadiomics (16) on Python (version 3.7). A total of 1409 sequential features based on time series were calculated as Delta $_{(\text{radiomics feature})}$, which was defined as the difference between features seen on the venous phase and non-contrast CT images. Delta $_{(\text{radiomics feature})}$ was calculated as follows:

$$\text{Delta}_{(\text{radiomics feature})} = \text{Feature}_{(\text{venous phase})} - \text{Feature}_{(\text{non-contrast phase})}$$

A total of 4227 features (containing radiomics features and sequential features) were identified for each patient containing 19 types of first order statistics, 13 types of Shape features, 28 types of Gray-Level Co-occurrence Matrix (GLCM) features, 16 types of Gray-Level Run-Length Matrix (GLRLM) features, 16 types of Gray Level SizeZone Matrix (GLSZM) features, and 56 types of sequential features.

Features Selection

The values of the extracted features were standardized with z scores by using mean and standard deviation values. Next a two-step procedure for dimensionality reduction and feature selection was devised. First, an analysis of variance (ANOVA) was performed to screen out discriminative features in the training set, with only features having a $P < 0.05$ being selected. Next, the least absolute shrinkage and selection operator (LASSO) method was used to reduce the dimensions of features, identify the most significant features (17), and make a second selection.

Radiomics Models Construction and Evaluation

K-Nearest Neighbor (KNN), Logistics Regression (LR), Decision Tree (DT), Linear-support vector machine (Linear-SVM), Gaussian-SVM, and Polynomial-SVM methods were used to construct radiomics models, respectively. Area under the curve (AUC) was regarded as a performance indicator and used to evaluate the performance of the radiomics-based models built by using each classifier. Finally, a radiomics signature (Rad-score) was calculated by using a linear combination of selected features weighted by the corresponding LASSO coefficients.

Clinical Risk Factors Selection and Nomogram Construction

In the training set, one-way ANOVA and multivariate logistic regression analysis were used to screen clinical risk factors including sex, age, primary site, tumor diameter, and radiologist interpretation to identify the clinical risk factors for ETE. To quantify the roles of the Rad-score and clinical risk factors in predicting ETE, both of those risk factors were included in a multivariate logistic regression analysis that was conducted using a backward-stepwise approach, where collinearity was considered and risk factors with a variance inflation factor (VIF) > 10 and a $P > 0.05$ were excluded. When the minimum Akaike information criterion was reached, the Akaike information was taken as the criterion, the stepwise procedure was stopped, and the final multivariate logistic regression constituted the nomogram.

Nomogram Validation

The nomogram's predictive performance was evaluated in the training set, internal test set, and external test set, respectively. The nomogram's performance was evaluated in terms of the receiver operating characteristic (ROC) curve. In particular, the comparison between the nomogram and radiologists' interpretation was illustrated in the same ROC curve. A decision curve analysis (DCA) was plotted for the entire set and applied in a clinical usefulness evaluation of the nomogram by calculating the net benefits at different threshold values in the training and test sets. In addition, a calibration (agreement between observations and prediction of ETE) curve was used to evaluate the agreement between actual status and ETE probabilities as predicted by the nomogram, accompanied by the Hosmer-Lemeshow test.

Statistical Analysis

All statistical analyses were performed using Python (version 3.6, https://www.python.org), R software (version 4.0.3, https://www.r-project.org), and SPSS (version 26.0, IBM Corp.). Scikit-Learn, a Python library, was used for selecting radiomics features and constructing a radiomics model. The modules of "feature-selection," "linear-model," "svm," "neighbors," "tree," and "metrics" were used for the entire procedure. The "rms" package in R software was used to select clinical risk factors, build the nomogram, and plot calibration curves. The "rmda" package was used to perform DCA. SPSS software was used to compare categorical variables (i.e., sex, T stage, primary site, radiologists' interpretation, and lymph node metastasis) by using the χ^2 test or Fisher's exact test. Continuous variables were compared by using the student's t test or Mann-Whitney U test, when appropriate. Statistical significance was two-sided, and a $P < 0.05$ was considered to be statistically significant.

RESULTS

Clinical Characteristics

The numbers of enrolled patients in the training set, internal test set, and external test set were 107, 46, and 46, respectively. There were no significant differences in sex, age, diameter, Thyroid Stimulating Hormone (TSH), Free Thyroxine (FT4), Free Triiodothyronine (FT3), and Primary site in each data set, but there was a significant difference in T stage. Details of clinical characteristics in the 3 sets are shown in **Table 1**. Radiologist A and radiologist B reported all CT imaging results with good inter-radiologist agreement (Kendall's W, 0.823).

Radiomics Features and Prediction Performance of the Radiomics-Based Models

A total of 4227 radiomics features were extracted from each patient's images. The intra-observer and inter-observer ICCs were 0.867 and 0.915, respectively, indicating an excellent agreement on radiomics features. Four radiomics features (Small Area Low Gray Level Emphasis, Gray Level Variance, Difference Entropy, and Busyness) in the training set were finally selected (**Figure 2**; **Table 2**).

Predictive models built by using KNN, LR, DT, Linear-SVM, Gaussian-SVM, and Polynomial-SVM, showed favorable discriminatory abilities for radiomics parameters with AUCs of 0.841 (95% Confidence Interval [CI], 0.769-0.900), 0.774 (95% CI, 0.683-0.853), 0.841 (95% CI, 0.772-0.897), 0.774 (95% CI, 0.680-0.854), 0.805 (95% CI, 0.710-0.879), and 0.815 (0.708-0.888), respectively, in the training set (Figure 3 A). In the internal test set, the six radiomics models also showed good performance with AUCs of 0.669 (95% Confidence Interval [CI], 0.394-0.568), 0.701 (95% CI, 0.480-0.767), 0.680 (95% CI, 0.516-0.795), 0.694 (95% CI, 0.508-0.788), 0.642 (95% CI, 0.454-0.600), and 0.681 (0.466-0.700), respectively (**Figure 3B**). Interestingly, in terms of AUC, the LR, which was later used to build the nomogram, demonstrated the best performance of the 6 models.

Development and Validation of the Radiomics Nomogram

The 4 features mentioned above were selected and their coefficients were plugged into a formula for calculating Rad-score as described below:

$$\begin{aligned}\text{Rad}-\text{score} = {} & \text{Small Area Low Gray Level Emphasis} * \\ & 0.0426553682266122 + \text{Gray Level Variance} * - \\ & 0.0238497391861649 + \text{Difference Entropy} * \\ & 0.0146833132887633 + \text{Busyness} * -0.00717595762541243\end{aligned}$$

The ANOVA and multivariate logistic regression analysis only identified radiologists' interpretation as being an independent ETE predictor (**Table 3**). The values of Rad-score and radiologists' interpretation for predicting the presence of ETE in PTC patients were quantified in our nomogram (score for each factor is shown in **Figure 4**). The radiomics nomogram showed a good prognostic capability, with AUCs of 0.860 (95% CI, 0.790-0.931), 0.750 (95%

TABLE 1 | Characteristic of enrolled patients in three sets.

		Training Set (n = 107)			Internal Test Set (n = 46)			External Test Set (n = 46)		
		ETE (n = 28)	Non-ETE (n = 79)	*P* value	ETE (n = 12)	Non-ETE (n = 34)	*P* value	ETE (n = 13)	Non-ETE (n = 33)	*P* value
Sex (M/F)		5/23	27/52	0.105	1/11	6/28	0.440	2/11	11/22	0.223
Age (Years)[a]		44.82 ± 12.41	47.14 ± 12.07	0.388	53.42 ± 13.06	48.88 ± 13.36	0.315	40.77 ± 14.66	39.39 ± 12.17	0.764
Diameter (mm)[a]		1.53 ± 0.81	1.41 ± 1.29	0.627	1.28 ± 0.65	1.86 ± 1.35	0.059	1.77 ± 0.61	1.78 ± 1.12	0.962
Hormone (mIU/L)[a]	TSH	2.53 ± 1.03	2.14 ± 1.31	0.480	4.43 ± 7.71	2.20 ± 1.57	0.362	123.92 ± 181.05	54.44 ± 84.77	0.30
	FT4	15.91 ± 3.02	16.01 ± 2.27	0.861	15.50 ± 1.90	16.24 ± 2.60	0.390	2.77 ± 1.94	2.26 ± 1.36	0.328
	FT3	4.84 ± 0.84	4.82 ± 0.61	0.936	5.08 ± 1.47	4.85 ± 0.74	0.504	11.95 ± 2.08	13.85 ± 2.06	0.01*
T Stage	T_1	6 (21.43)	61 (53.16)	<0.001*	4 (33.33)	22 (64.71)	0.014*	3 (23.08)	26 (78.78)	<0.001*
	T_2	1 (3.57)	14 (1.27)		1 (8.33)	9 (26.47)		0(0.00)	5 (15.15)	
	T_3	15 (53.57)	4 (45.57)		5 (41.67)	3 (8.82)		5 (38.46)	2 (6.06)	
	T_4	6 (21.43)	0 (0.00)		2 (16.67)	0 (0.00)		5 (38.46)	0 (0.00)	
Primary site	Left/right lobe	28 (100.00)	77 (97.47)	0.395	12 (100.00)	33 (97.06)	0.548	13 (100.00)	32 (96.97)	>0.999
	Isthmus	0 (0.00)	2 (2.53)		0 (0.00)	1 (2.94)		0 (0.00)	1 (3.03)	
Radiologists' Interpretation	correct	21 (75.00)	64 (81.01)	0.449	7 (58.33)	29 (85.29)	0.052	10 (76.92)	23 (69.70)	0.729
	incorrect	7 (25.00)	15 (18.99)		5 (41.67)	5 (14.71)		3 (23.08)	10 (30.30)	
LN Status	positive	19 (67.86)	32 (40.51)	0.013*	8(66.67)	10 (29.41)	0.157	10 (76.92)	18 (54.55)	0.197
	negative	9 (32.14)	47 (59.49)		4 (33.33)	24 (70.59)		3 (23.08)	15(45.45)	

The data are displayed as n (%) except otherwise noted.

[a]Mean ± standard deviation.

ETE, Extrathyroidal Extension; M, Male; F, Female; TSH, Thyroid Stimulating Hormone; FT4, Free Thyroxine; FT3, Free Triiodothyronine; LN, lymph node.

**P < 0.05*

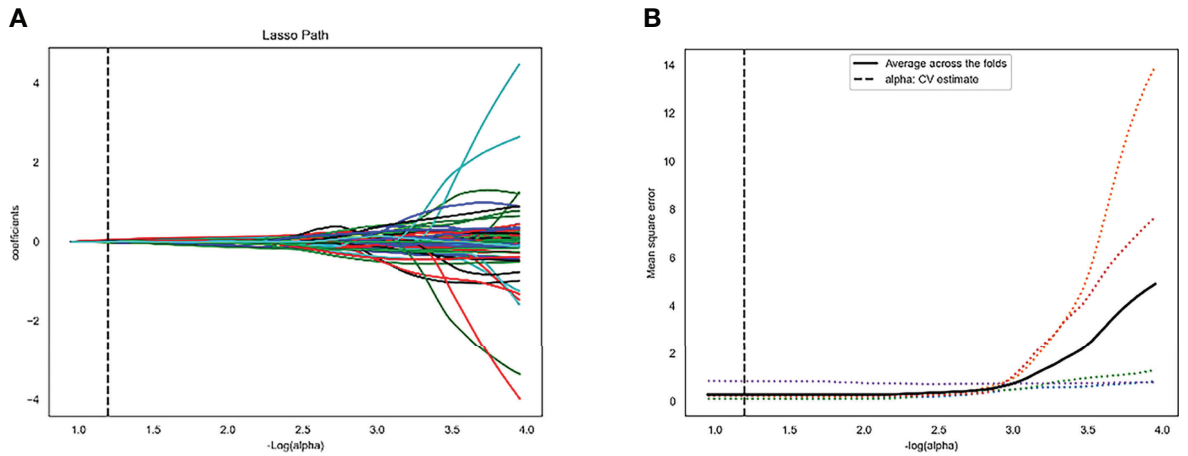

FIGURE 2 | Least absolute shrinkage and selection operator (LASSO) algorithm for radiomics features selection. **(A)** LASSO coefficient profiles of the 4 features. The y-axis represents coefficient of each feature. **(B)** Mean square error path.

CI, 0.579-0.921), and 0.797 (95% CI, 0.665-0.926) in the training, internal test, and external test sets, respectively (**Figures 3C–E**; **Table 4**). Furthermore, the radiomics nomogram had a more powerful predictive efficiency than the interpretation of radiologists with 5 and 10 years of experience, whose AUC in the training, internal test, and external test sets were 0.762 (95% CI, 0.667-0.858), 0.718 (95% CI, 0.560-0.876), and 0.733 (95% CI, 0.615-0.841), respectively (**Figures 3C–E**). In the external test set, the nomogram's accuracy (0.848 vs. 0.717) and specificity (0.909 vs, 0.697) were higher than those of radiologist's interpretation, reflecting a better prognostic performance of the radiomics nomogram; however, the sensitivity of the nomogram (0.692, 95% CI 0.389-0.896) was similar with that of radiologists' interpretation (0.769, 95% CI 0.460-0.938) (**Table 4**). We tested this nomogram to distinguish minimal and grossly ETE in internal and external test set, and achieved relatively good performance with AUC of 0.800 (0.578-1.000) and 0.722(0.390-1.000), sensitivity of 0.800 (0.299-0.989) and 0.500(0.092-0.908), specificity of 0.667 (0.412-0.856) and 0.889(0.507-0.994), and accuracy of 0.696 (0.471-0.868) and 0.769 (0.462-0.950) respectively. (**Figure 3F**). The DCA showed that radiomics nomogram could add more benefit than treat patients as all-ETE or non-ETE when the threshold probability ranged from 0.10 to 0.50 in internal test set and 0.12 to 0.75 in the external test set (**Figures 5A, B**). The calibration curve for the radiomics nomogram, when assessed by the Hosmer-Lemeshow test, yielded *P* of 0.48, 0.88, and 0.34 in the training set, internal test set, and external test set, respectively (**Figures 5C, D**), demonstrated good agreement between actual status and ETE probabilities as predicted by the nomogram in all three sets.

DISCUSSION

Most patients with PTC have a favorable long-term survival prognosis (18); however, ETE remains an independent risk factor affecting overall survival and clinical decision making (19). Therefore, it is crucial to create a powerful predictive tool that can help surgeons and inexperienced radiologists evaluate possible ETE and make a clinical decision regarding treatment. In this retrospective multicenter study, six predictive models were established for verifying that radiomics could be used to predict ETE. Furthermore, a nomogram was constructed based on radiomics information and clinical risk factors, and displayed an excellent ability to predict ETE, with AUCs of 0.750 and 0.797 in an internal test set and external test set, respectively. Those results indicated that the radiomics nomogram could serve as an independent medical decision-making tool, and satisfy the requirements of precision medicine.

Unlike previous studies (20–24), the present study investigated the value of radiomics with six classifiers. This result showed that radiomics could play a crucial role in ETE prediction. Nomograms based on radiomics have been widely

TABLE 2 | LASSO coefficient profiles of the 4 features.

Radiomics features	Phase	Feature type	Coefficient
Small Area Low Gray Level Emphasis	Non-contrast	GLSZM	0.0426553
Gray Level Variance	Non-contrast	GLSZM	-0.023849
Difference Entropy	Non-contrast	GLSZM	0.014683
Busyness	Non-contrast	GLSZM	-0.007175

LASSO, least absolute shrinkage and selection operator; GLSZM, gray-level size zone matrix.

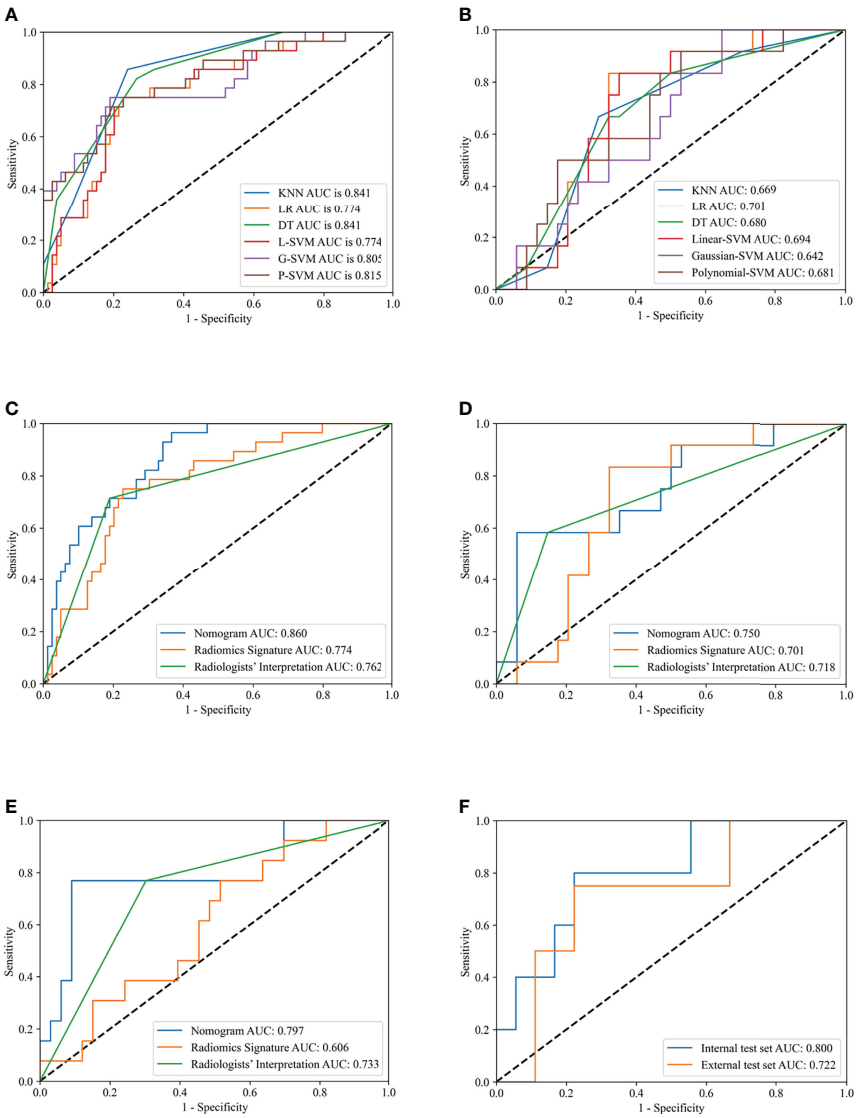

FIGURE 3 | Receiver operating characteristic (ROC) curves of different models in training and test sets. Receiver operating characteristic (ROC) curves of K-Nearest Neighbor (KNN), Logistics Regression (LR), Decision Tree (DT), Linear-support vector machine (Linear-SVM), Gaussian-SVM, and Polynomial-SVM models in the training **(A)** and internal test **(B)** set. ROC curves of nomogram, radiomics signature, and radiologists' interpretation in the training **(C)**, internal test **(D)**, external test **(E)** set. ROC curves of nomogram for division of minimal and gross extrathyroidal extension (ETE) in the internal test and external test set **(F)**.

TABLE 3 | The selection of clinical risk factors for ETE by ANOVA and univariate LR analysis.

Variables	ANOVA		Univariate LR Analysis	
	F Value	P	OR	P
Sex	2.642	0.107	NA	NA
Age	0.752	0.388	NA	NA
Primary Site	0.612	0.436	NA	NA
Tumor Diameter	0.065	0.799	NA	NA
Radiologist's Interpretation	33.412	<0.01*	1.506	<0.01*

ETE, extrathyroidal extension; ANOVA, analysis of variance; LR, logistic regression; OR, odds ratio; NA, not available.
**P < 0.05*

used to predict medical prognoses (25) and clinical outcomes by combining a Rad-score and clinical risk factors (26). The nomogram constructed in this study demonstrated an ability to generate individualized predictions that were useful for identifying and stratifying patients with PTC.

Some previous studies have been conducted on this topic (27, 28). Bin Chen et al. (27) and Xian Wang et al. (28) constructed radiomics nomograms for ETE prediction based on CT images and US images, respectively. Nevertheless, their studies lacked an external test set. Furthermore, those investigators only used a single classifier (logistic regression analysis) to evaluate the radiomics approach and build a nomogram. Their results showed that the nomogram had a discrimination ability (AUCs of 0.772 and

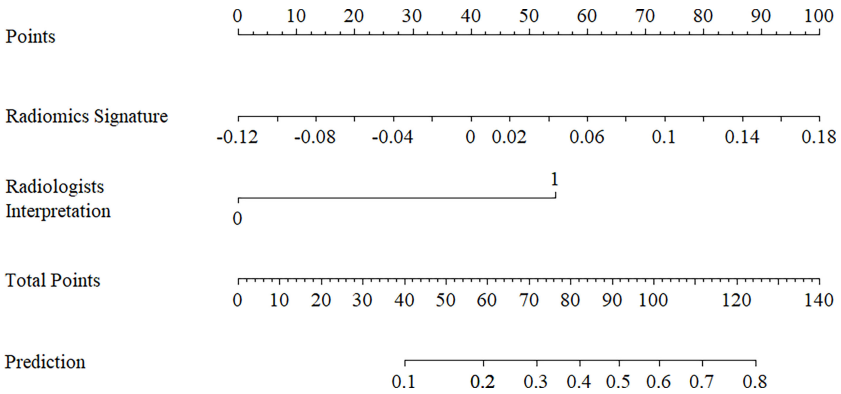

FIGURE 4 | Radiomics nomogram with radiomics signature (rad-score) and radiologists' interpretation incorporated.

TABLE 4 | Efficacies of the models predicting ETE in patients with PTC.

	AUC	Sensitivity	Specificity	Accuracy
Training Set				
Rad-score	0.774 (0.677-0.871)	0.722 (0.671-0.861)	0.750 (0.571-0.893)	0.757 (0.665-0.835)
Radiologists' interpretation	0.762 (0.667-0.858)	0.810 (0.712-0.886)	0.714 (0.536-0.857)	0.785 (0.695-0.859)
Nomogram	0.860 (0.790-0.931)	0.734 (0.633-0.853)	0.786 (0.643-0.929)	0.710 (0.615-0.794)
Internal Test Set				
Rad-score	0.701 (0.545-0.857)	0.706 (0.588-0.882)	0.583 (0.333-0.833)	0.674 (0.520-0.805)
Radiologists' interpretation	0.718 (0.560-0.876)	0.853 (0.706-0.971)	0.583 (0.333-0.833)	0.783 (0.636-0.891)
Nomogram	0.750 (0.579-0.921)	0.765 (0.584-0.886)	0.583 (0.333-0.833)	0.717 (0.565-0.840)
External Test Set				
Rad-score	0.606 (0.469-0.748)	0.692 (0.389-0.896)	0.485 (0.312-0.661)	0.543 (0.390-0.691)
Radiologists' interpretation	0.733 (0.615-0.841)	0.769 (0.460-0.938)	0.697 (0.511-0.838)	0.717 (0.565-0.840)
Nomogram	0.797 (0.665-0.926)	0.692 (0.389-0.896)	0.909 (0.745-0.976)	0.848 (0.711-0.937)

ETE, extrathyroidal extension; PTC, Papillary thyroid cancer; Rad-score, radiomics signature score; AUC, area under curves.

0.824, respectively, in an internal test set) for ETE classification that was similar to that of our nomogram (AUC = 0.750 in internal test set). When comparing the two nomograms, the nomogram developed in our multicenter study has notable advantages. First, the use of an external test set improved the reliability of our radiomics nomogram and proved that it had relatively good repeatability and generalization ability. This is the first study to use a CT radiomics nomogram adding to time sequential features which greatly enhanced a variety of features to predict ETE. However, no single feature was proven to be statistically significant, which means the time change of CT images may play a minor role in ETE prediction. Finally, the ability of this radiomics nomogram to predict ETE approximated that of experienced radiologists' interpretation, showing that the nomogram could be used to help surgeons make clinical decisions prior to performing surgery, and satisfy the requirements of precision medicine.

In addition, 4 selected features were all from non-contrast CT images, suggesting that there was no obvious advantage of features extracted from CE-CT images in ETE diagnosis. However, CE-CT is useful in ETE interpretation.

The limitations of this study are as follows: (1) PTCs with a diameter < 1 cm were included in the study, and may have been difficult to distinguish on CT images; this may have led to sample bias. To address this problem, any doubt was resolved by discussion or consultation with a third radiologist who had 20 years of experience. (2) The study's retrospective design may have led to selection bias. Prospective studies are needed to control for confounding variables. (3) A manual segmentation approach is time-consuming and may affect the precision of feature extraction in some cases; however, the ICCs for intra- and inter-observer agreement ranged from 0.809 to 0.923. Previous studies showed that the automatic segmentation method may facilitate the use of radiomics in busy clinical practice and lead to high degrees of intra- and inter-observer reproducibility (29–32). A further study will use automatic segmentation to draw the ROIs. (4) CE-CT leads to higher total radiation doses, longer examination times, and use of contrast medium, limiting its broad use in clinical practice. (5) Only the machine learning method was used, and previous studies have shown that deep learning methods have a certain value for predicting lymph node metastases and classifying PTC (33, 34); however, no study has ever constructed an ETE-prediction model by using deep learning methods. In light of this, we will focus on that in a subsequent study.

CONCLUSION

In this study, a non-invasive nomogram combined the Rad-score and radiologists' interpretation showing good

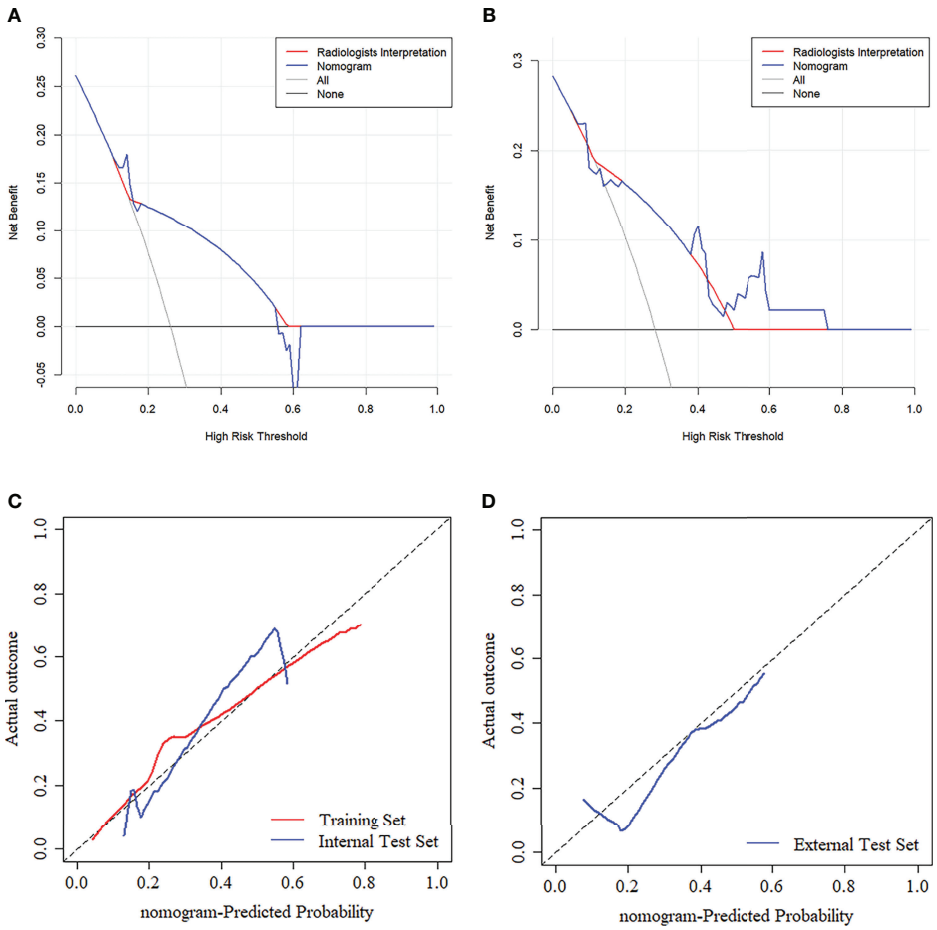

FIGURE 5 | **(A, B)** Decision curve analysis (DCA) for the prediction models in the internal and external test set. The y-axis represents the net benefits, while the x-axis represents the threshold probability. The blue line represents the radiomics nomogram. The red line represents the radiologists' interpretation model. The gray line represents the assumption that no patients were diagnosed as ETE. The horizontal black line represents the assumption that all patients were diagnosed as ETE. Calibration curves of radiomics nomogram in the training **(C)**, internal test **(C)**, and external test **(D)** sets. The diagonal line represents the perfect prediction of the radiomics nomogram.

repeatability and generalization ability for predicting ETE. This radiomics nomogram may also facilitate clinical decision-making; however, additional studies with larger sample sizes and more centers should be performed to improve the nomogram's efficiency.

DATA AVAILABILITY STATEMENT

The raw data supporting the conclusions of this article will be made available by the authors, without undue reservation.

ETHICS STATEMENT

The studies involving human participants were reviewed and approved by the Institutional Review Board of The Affiliated Yantai Yuhuangding Hospital of Qingdao University. Written informed consent for participation was not required for this study in accordance with the national legislation and the institutional requirements.

AUTHOR CONTRIBUTIONS

PY, XW, and JL implemented the literature searching and manuscript writing. KC, QW, and NM implemented the ETE interpretation. GL implemented ROI segmentation. HZ contributed to data analysis, figure making, and algorithm development. YM, GZ, XH, and LD identified the radiological characteristics of PTC and estimated and adjusted the accuracy of ROIs. XS, YM, and NM conducted the design, quality control, and data interpretation of this study. All authors

analyzed the data and their significance and were involved in the final editing and approval of the submitted article. All authors contributed to the article and approved the submitted version.

FUNDING

This work was supported by the Taishan Scholars Project (No. ts20190991).

ACKNOWLEDGMENTS

We thank professor Dexin Yu of Qilu Hospital of Shandong University provided CT images and clinical information of external test set in this study.

SUPPLEMENTARY MATERIAL

The Supplementary Material for this article can be found online at: https://www.frontiersin.org/articles/10.3389/fendo.2022.874396/full#supplementary-material

REFERENCES

1. Bray F, Ferlay J, Soerjomataram I, Siegel RL, Torre LA, Jemal A. Global Cancer Statistics 2018: Globocan Estimates of Incidence and Mortality Worldwide for 36 Cancers in 185 Countries. *CA Cancer J Clin* (2018) 68 (6):394–424. doi: 10.3322/caac.21492
2. *Cancer Stat Facts: Thyroid Cancer* (2020). Available at: https://seer.cancer.gov/statfacts/html/thyro.html.
3. Seib CD, Sosa JA. Evolving Understanding of the Epidemiology of Thyroid Cancer. *Endocrinol Metab Clin North Am* (2019) 48(1):23–35. doi: 10.1016/j.ecl.2018.10.002
4. Amin MB, Edge SB, Greene FL, Byrd DR, Brookland Rk, Washington MK, et al. (2017) AJCC Cancer Staging Manual. Chicago: American College of Surgeons press.
5. Park SY, Kim HI, Kim JH, Kim JS, Oh YL, Kim SW, et al. Prognostic Significance of Gross Extrathyroidal Extension Invading Only Strap Muscles in Differentiated Thyroid Carcinoma. *Br J Surg* (2018) 105(9):1155–62. doi: 10.1002/bjs.10830
6. Sapuppo G, Tavarelli M, Russo M, Malandrino P, Belfiore A, Vigneri R, et al. Lymph Node Location Is a Risk Factor for Papillary Thyroid Cancer-Related Death. *J Endocrinol Invest* (2018) 41(11):1349–53. doi: 10.1007/s40618-018-0865-5
7. Lee CY, Kim SJ, Ko KR, Chung KW, Lee JH. Predictive Factors for Extrathyroidal Extension of Papillary Thyroid Carcinoma Based on Preoperative Sonography. *J Ultras Med* (2014) 33(2):231–8. doi: 10.7863/ultra.33.2.231
8. Gweon HM, Son EJ, Youk JH, Kim JA, Park CS. Preoperative Assessment of Extrathyroidal Extension of Papillary Thyroid Carcinoma: Comparison of 2- and 3-Dimensional Sonography. *J Ultras Med* (2014) 33(5):819–25. doi: 10.7863/ultra.33.5.819
9. Kim H, Kim JA, Son EJ, Youk JH, Chung TS, Park CS, et al. Preoperative Prediction of the Extrathyroidal Extension of Papillary Thyroid Carcinoma With Ultrasonography Versus Mri: A Retrospective Cohort Study. *Int J Surg* (2014) 12(5):544–8. doi: 10.1016/j.ijsu.2014.03.003
10. Seo YL, Yoon DY, Lim KJ, Cha JH, Yun EJ, Choi CS, et al. Locally Advanced Thyroid Cancer: Can Ct Help in Prediction of Extrathyroidal Invasion to Adjacent Structures? *AJR Am J Roentgenol* (2010) 195(3):W240–4. doi: 10.2214/ajr.09.3965
11. Gillies RJ, Kinahan PE, Hricak H. Radiomics: Images Are More Than Pictures, They Are Data. *Radiology* (2016) 278(2):563–77. doi: 10.1148/radiol.2015151169
12. Bi WL, Hosny A, Schabath MB, Giger ML, Birkbak NJ, Mehrtash A, et al. Artificial Intelligence in Cancer Imaging: Clinical Challenges and Applications. *CA Cancer J Clin* (2019) 69(2):127–57. doi: 10.3322/caac.21552
13. Geras KJ, Mann RM, Moy L. Artificial Intelligence for Mammography and Digital Breast Tomosynthesis: Current Concepts and Future Perspectives. *Radiology* (2019) 293(2):246–59. doi: 10.1148/radiol.2019182627
14. Gisev N, Bell JS, Chen TF. Interrater Agreement and Interrater Reliability: Key Concepts, Approaches, and Applications. *Res Soc Adm Pharm* (2013) 9 (3):330–8. doi: 10.1016/j.sapharm.2012.04.004
15. Beurnier A, Jutant EM, Jevnikar M, Boucly A, Pichon J, Preda M, et al. Characteristics and Outcomes of Asthmatic Patients With Covid-19 Pneumonia Who Require Hospitalisation. *Eur Respir J* (2020) 56 (5):2001875. doi: 10.1183/13993003.01875-2020
16. Zwanenburg A, Vallières M, Abdalah MA, Aerts H, Andrearczyk V, Apte A, et al. The Image Biomarker Standardization Initiative: Standardized Quantitative Radiomics for High-Throughput Image-Based Phenotyping. *Radiology* (2020) 295(2):328–38. doi: 10.1148/radiol.2020191145
17. Sauerbrei W, Royston P, Binder H. Selection of Important Variables and Determination of Functional Form for Continuous Predictors in Multivariable Model Building. *Stat Med* (2007) 26(30):5512–28. doi: 10.1002/sim.3148
18. Roman BR, Morris LG, Davies L. The Thyroid Cancer Epidemic, 2017 Perspective. *Curr Opin Endocrinol Diabetes Obes* (2017) 24(5):332–6. doi: 10.1097/med.0000000000000359
19. Perrier ND, Brierley JD, Tuttle RM. Differentiated and Anaplastic Thyroid Carcinoma: Major Changes in the American Joint Committee on Cancer Eighth Edition Cancer Staging Manual. *CA Cancer J Clin* (2018) 68(1):55–63. doi: 10.3322/caac.21439
20. Limkin EJ, Sun R, Dercle L, Zacharaki EI, Robert C, Reuzé S, et al. Promises and Challenges for the Implementation of Computational Medical Imaging (Radiomics) in Oncology. *Ann Oncol* (2017) 28(6):1191–206. doi: 10.1093/annonc/mdx034
21. Lambin P, Leijenaar RTH, Deist TM, Peerlings J, de Jong EEC, van Timmeren J, et al. Radiomics: The Bridge Between Medical Imaging and Personalized Medicine. *Nat Rev Clin Oncol* (2017) 14(12):749–62. doi: 10.1038/nrclinonc.2017.141
22. Zheng YM, Xu WJ, Hao DP, Liu XJ, Gao CP, Tang GZ, et al. A Ct-Based Radiomics Nomogram for Differentiation of Lympho-Associated Benign and Malignant Lesions of the Parotid Gland. *Eur Radiol* (2021) 31(5):2886–95. doi: 10.1007/s00330-020-07421-4
23. Yang L, Yang J, Zhou X, Huang L, Zhao W, Wang T, et al. Development of a Radiomics Nomogram Based on the 2d and 3d Ct Features to Predict the Survival of Non-Small Cell Lung Cancer Patients. *Eur Radiol* (2019) 29 (5):2196–206. doi: 10.1007/s00330-018-5770-y
24. Ma X, Wei J, Gu D, Zhu Y, Feng B, Liang M, et al. Preoperative Radiomics Nomogram for Microvascular Invasion Prediction in Hepatocellular Carcinoma Using Contrast-Enhanced Ct. *Eur Radiol* (2019) 29(7):3595–605. doi: 10.1007/s00330-018-5985-y
25. Ji GW, Zhang YD, Zhang H, Zhu FP, Wang K, Xia YX, et al. Biliary Tract Cancer at Ct: A Radiomics-Based Model to Predict Lymph Node Metastasis and Survival Outcomes. *Radiology* (2019) 290(1):90–8. doi: 10.1148/radiol.2018181408
26. Iasonos A, Schrag D, Raj GV, Panageas KS. How to Build and Interpret a Nomogram for Cancer Prognosis. *J Clin Oncol* (2008) 26(8):1364–70. doi: 10.1200/jco.2007.12.9791
27. Chen B, Zhong L, Dong D, Zheng J, Fang M, Yu C, et al. Computed Tomography Radiomic Nomogram for Preoperative Prediction of Extrathyroidal Extension in Papillary Thyroid Carcinoma. *Front Oncol* (2019) 9:829. doi: 10.3389/fonc.2019.00829
28. Wang X, Agyekum EA, Ren Y, Zhang J, Zhang Q, Sun H, et al. A Radiomic Nomogram for the Ultrasound-Based Evaluation of Extrathyroidal Extension in Papillary Thyroid Carcinoma. *Front Oncol* (2021) 11:625646. doi: 10.3389/fonc.2021.625646
29. Chen X, Men K, Chen B, Tang Y, Zhang T, Wang S, et al. Cnn-Based Quality Assurance for Automatic Segmentation of Breast Cancer in Radiotherapy. *Front Oncol* (2020) 10:524. doi: 10.3389/fonc.2020.00524

30. Masood S, Fang R, Li P, Li H, Sheng B, Mathavan A, et al. Automatic Choroid Layer Segmentation From Optical Coherence Tomography Images Using Deep Learning. *Sci Rep* (2019) 9(1):3058. doi: 10.1038/s41598-019-39795-x
31. Liu C, Gardner SJ, Wen N, Elshaikh MA, Siddiqui F, Movsas B, et al. Automatic Segmentation of the Prostate on Ct Images Using Deep Neural Networks (Dnn). *Int J Radiat Oncol Biol Phys* (2019) 104(4):924–32. doi: 10.1016/j.ijrobp.2019.03.017
32. Ghavami N, Hu Y, Gibson E, Bonmati E, Emberton M, Moore CM, et al. Automatic Segmentation of Prostate Mri Using Convolutional Neural Networks: Investigating the Impact of Network Architecture on the Accuracy of Volume Measurement and Mri-Ultrasound Registration. *Med Imag Anal* (2019) 58:101558. doi: 10.1016/j.media.2019.101558
33. Zhu YC, AlZoubi A, Jassim S, Jiang Q, Zhang Y, Wang YB, et al. A Generic Deep Learning Framework to Classify Thyroid and Breast Lesions in Ultrasound Images. *Ultrasonics* (2021) 110:106300. doi: 10.1016/j.ultras.2020.106300
34. Lee JH, Ha EJ, Kim JH. Application of Deep Learning to the Diagnosis of Cervical Lymph Node Metastasis From Thyroid Cancer With Ct. *Eur Radiol* (2019) 29(10):5452–7. doi: 10.1007/s00330-019-06098-8

Conflict of Interest: Authors declared that the research was conducted in the absence of any commercial or financial relationships that could be construed as a potential conflict of interest.

frontiers | Frontiers in Endocrinology

TYPE Original Research
PUBLISHED 05 August 2022
DOI 10.3389/fendo.2022.944758

OPEN ACCESS

EDITED BY
Jose Federico Carrillo,
National Institute of Cancerology (INCAN), Mexico

REVIEWED BY
Akira Sugawara,
Tohoku University, Japan
Raúl Hernández Romero,
National Institute of Cancerology (INCAN), Mexico

*CORRESPONDENCE
Li Mei
523036921@qq.com
Xincai Qu
Quxc2008@126.com

†These authors have contributed equally to this work and share first authorship

SPECIALTY SECTION
This article was submitted to Cancer Endocrinology, a section of the journal Frontiers in Endocrinology

RECEIVED 15 May 2022
ACCEPTED 05 July 2022
PUBLISHED 05 August 2022

CITATION
Qian B, Hu L, Zhang S, Zhu J, Mei L, Huang T and Qu X (2022) Comparison of clinicopathological features and prognosis of papillary thyroid carcinoma and microcarcinoma: A population-based propensity score matching analysis.
Front. Endocrinol. 13:944758.
doi: 10.3389/fendo.2022.944758

Comparison of clinicopathological features and prognosis of papillary thyroid carcinoma and microcarcinoma: A population-based propensity score matching analysis

Bei Qian†, Longqing Hu†, Shoupeng Zhang, Junlin Zhu, Li Mei*, Tao Huang and Xincai Qu*

Department of Thyroid and Breast Surgery, Union Hospital, Tongji Medical College, Huazhong University of Science and Technology, Wuhan, China

Background: Overtreatment of papillary thyroid microcarcinoma (PTMC) has become a common concern. This study aimed to compare clinicopathological features between PTMC and papillary thyroid carcinoma (PTC) and to explore whether surgery can confer significant survival benefits in all patients with PTC or PTMC.

Methods: Data of 145,951 patients with PTC registered in Surveillance, Epidemiology, and End Results (SEER) database and 8,751 patients with PTC in our institution were retrospectively collected. Patients with tumors less than 10 mm in diameter were classified as PTMC cohort and the rest as PTC cohort. Clinicopathological features between PTMC and PTC were compared on the basis of SEER cohort and validated with institutional data. Survival analysis was conducted to explore the effect of surgery on the prognosis of patients. To minimize potential confounders and selection bias, we performed propensity score matching (PSM) analysis to match more comparable cohorts.

Results: Compared with PTC, PTMC exhibited the following characteristics: more common in women and whites, older age at diagnosis, lower proportion of follicular variants, intraglandular dissemination, extraglandular and capsular invasion, higher proportion of multifocality, fewer lymph node and distant metastases, and higher cancer-specific survival (CSS) and overall survival (OS) (all p-value < 0.05). Regarding treatment, patients with PTMC received a lower proportion of radiotherapy, chemotherapy, and total thyroidectomy but a higher proportion of lobectomy and/or isthmectomy. There was no significant difference in CSS for patients with PTMC at stage T1N0M0 with or without surgery (P = 0.36).

Conclusion: Generally, PTMC showed higher biological indolence than PTC, which meant a higher survival rate for patients in both OS and CSS. For patients

with PTMC at staged T1N0M0, active surveillance (AS) may be a potentially feasible management strategy. However, the maintenance of good medical compliance and the management of psychological burden cannot be ignored for patients included in AS.

KEYWORDS

papillary thyroid carcinoma (PTC), papillary thyroid microcarcinoma, (PTMC), propensity score matching (PSM), clinicopathological features, active surveillance (AS)

Background

Thyroid cancer (THCA) is the most common endocrine malignancy, increasing at incidence rate of at least 4.5% per year (1). It has been estimated that THCA will become the top four most common malignancy by 2030 (2). Papillary thyroid carcinoma (PTC) is the most common subtype of THCA, comprising 80% of all cases (3). Papillary thyroid microcarcinoma (PTMC) is PTC with a maximum tumor diameter of less than 10 mm (4), which is considered to significantly contribute to the increasing incidence of THCA (5). The current management standard for PTC is immediate surgical treatment, including total thyroidectomy with bilateral central lymph node dissection (CLND), unilateral thyroid lobectomy with CLND, or total thyroidectomy with bilateral CLND and lateral cervical LN dissection of the affected side. However, despite the incidence of PTC increasing, its mortality rate has remained relatively stable (6, 7). It was reported that, due to the indolence of PTC, most PTMC would either not progress or progress so slowly that it never leads to clinically meaningful disease over the patient's lifetime (8). In addition, the prevalence of occult PTC at autopsy in the general population was high, at 35.6% (9). Therefore, considering the very low disease-specific mortality and recurrence rates of PTMC and risk of surgical complications, the traditional management approach of immediate thyroid surgery for PTMC is being reconsidered (10). Currently, several studies have focused on the clinicopathological differences between PTC and PTMC and whether surgery is the preferred treatment by all patients with PTC. Although active surveillance (AS) was included in clinical guidelines in Japan in 2010 (11) and the United States in 2015 (12) as an alternative management strategy for low-risk PTMC, this strategy is still questioned by many thyroid doctors and patients due to the limited data available (13).

Propensity score matching (PSM) is a statistical method to ensure an even distribution of confounders and biases between treatment and control cohorts, improving comparability between cohorts (14). It has emerged as the preferred method of matching exposed and nonexposed patients in observational cohort studies, yielding estimates of effects similar to the results of randomized control trials (15). Therefore, using PSM, this study aimed to compare clinicopathological features between PTMC and PTC and explore whether surgery can confer significant survival benefits in all patients with PTC or PTMC.

Patients and methods

Data source and patient selection

Data of patients with PTC were extracted from 18 population-based cancer registries of the SEER database (https://seer.cancer.gov/) from 2000 through 2018 using the SEER*Stat program (version 8.3.9). The SEER database was a cancer incidence registry including about 30% of the US population. The extraction criteria were as follows: "Primary Site = C73.9-Thyroid gland" and "Behavior code ICD-0-3 = Malignant". The exclusion criteria were as follows: (1) nonpathological diagnosis; (2) non-papillary carcinoma as the histologic type; (3) unknown survival time; (4) unknown tumor size; (5) unknown surgery approach; and (6) unknown if surgery underwent. The variables extracted from eligible cases included the following: patient ID, age at diagnosis, sex, race/ethnicity, year of diagnosis, follicular variant, multifocality, laterality, tumor size, T stage, N stage, M stage, surgery of primary site, radiotherapy recode, chemotherapy recode, distant metastases record, number of lesions, follow-up months, number of metastatic lymph node (LN), distant metastasis record, SEER cause-specific death classification, and vital status recode (study cutoff used). In addition, data of patients with PTC diagnosed and treated in our institution from 2009 to 2020 were collected. Inclusion criteria were as follows: (1) pathological diagnosis was PTC; (2) clinicopathological information was complete and available; (3) surgery was underwent; and (4) informed consent was signed. The parameters collected included the following: patient ID, sex, age,

year of diagnosis, surgery approach, laterality, follicular subtype, multifocality, intraglandular dissemination, extraglandular invasion, capsular invasion, T stage, N stage, and M stage. The demographic and clinicopathological data of all eligible cases were retrospectively analyzed.

Cohort definition and variable recode

All eligible patients with PTC were divided into PTMC and PTC cohort according to whether tumor diameter ≤10 mm and then matched with propensity scores to obtain more comparable cohorts. In addition, patients with PTC or PTMC were divided into two cohorts according to whether they underwent surgery or not to explore the effect of surgery on prognosis of patients. The variables analyzed included all factors, age (≤55 or >55), sex (female or male), race (black, white, or other), follicular variant (yes or no), multifocality (yes or no), T stage, N stage, M stage, radiotherapy (yes or no), chemotherapy (yes or no), and surgery approach. The cutoff point for continuous variables such as age was generated by the "surv_cutpoint" function of the "Survminer" package in R. The primary outcomes investigated were cancer-specific survival (CSS) and overall survival (OS). CSS was classified on the basis of available death certificate information using SEER-defined variables. OS was defined as the time from diagnosis until death or last follow-up.

Study design

First, after initial screening, patients with PTC and PTMC were classified by year of diagnosis to roughly estimate incidence trends of PTC and PTMC over time. Second, statistical differences in clinicopathological parameters of the PTC and PTMC cohorts from the SEER database were compared before and after PSM and validated with our institution's cohort. Third, survival analysis was performed to compare the prognosis (both CSS and OS) between patients with PTC and those with PTMC, and between patients who underwent and those who did not perform surgery. Finally, the cohort of to whom surgery was recommended but not underwent was further selected and then matched with the cohort that underwent surgery using PSM. In addition, and survival analysis was applied to evaluate the difference in prognosis. This work has been reported following the STROCSS criteria (16).

Propensity score matching analysis

PSM analysis was used to match patients with PTC and those with PTMC. This method was also used to match patients who underwent surgery and those who were recommended but did not, to balance the potential baseline confounding factor (17). The "Matchit" package in R studio (http://www.r-project.org) was used to match the propensity score between cohorts, and the matching approach was set as the nearest neighbor algorithm with a matching ratio of 1:1 and a caliper value of 0.01 (18). The variables balanced using PSM included age, sex, race, year of diagnosis, laterality, multifocality, and follicular variant. The "Cobalt" package of R studio was applied to estimate kernel density and analyze standardized difference of means and to evaluate the covariate balance before and after matching (19). An absolute value of the mean difference less than 0.05 was considered as qualified matching.

Statistical analysis

Continuous variables with normal distribution were expressed as mean and standard deviation (SD) and as median and interquartile range (IQR) for nonnormally distributed variables. The Student's t-test (normally distributed) or Mann-Whitney U-test (nonnormally distributed) was used to compare continuous variables. Categorical variables were presented as frequencies and percentages (%) and analyzed using Fisher's exact test or Pearson $\chi 2$ test. A two-sided P-value <0.05 was considered statistically significant. R studio version 4.0.3 software (http://www.r-project.org) was used to perform all statistical analyses and visualization.

Ethics statement

This study was exempt from the approval processes of the Institutional Review Boards because no personal information about patients was sought and their identities will not be revealed in any publication. Informed consent was obtained from all patients for additional personal data.

Results

Demographic and clinicopathological characteristics of patients

A total of 145,951 patients registered in the SEER database from 2004 to 2018 and 8,751 patients treated at our center from 2009 to 2020 were included in this study. The detailed flow diagram showing the patient inclusion and exclusion criteria process in the SEER database is shown in Figure 1. The number of diagnosed cases per year is shown in Figure 2, indicating that the incidence of both PTC and PTMC was increased year by year. The mean age at diagnosis was 48.3 years (SD = 16.0) and 51.2 years (SD = 14.1) for PTC and PTMC, respectively. The median follow-up time was 66 months for PTC cohort (IQR: 29–111) and 70 months (IQR: 34–112) for PTC cohort. Compared

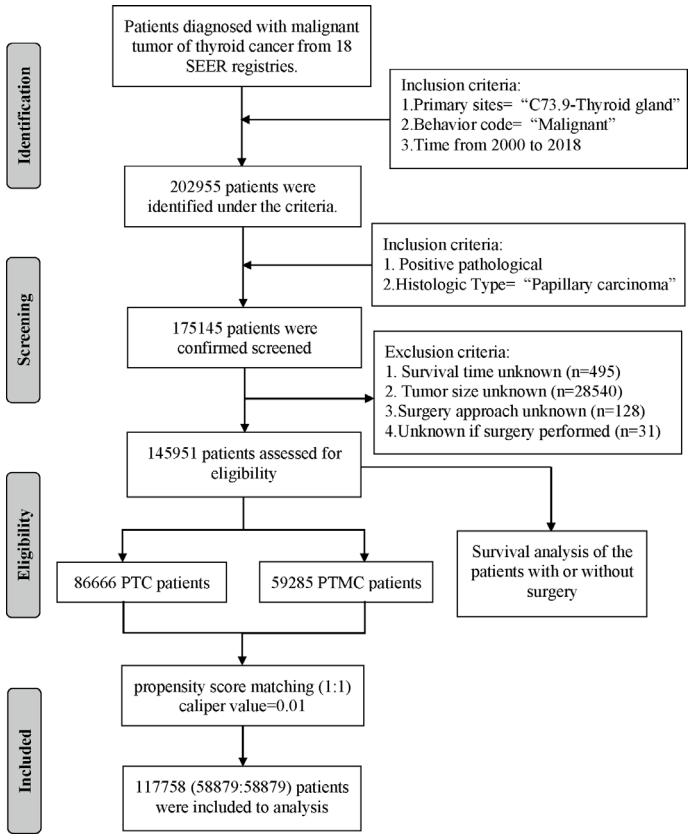

FIGURE 1
Flow diagram presenting the screening process in the SEER database.

with PTC, PTMC exhibited the following characteristics: more common in women (81.1% vs. 74.1%) and whites (82.2% vs. 80.1%), lower proportion of follicular variants (27.9% vs. 31.0%), higher proportion of multifocality (19.9% vs. 16.8%), and higher CSS (99.7% vs. 98.3%) and OS (94.3% vs. 92.7%) (all *p*-value <0.001).

Validation data from our institution also confirmed that, compared with PTC, PTMC was more common in women

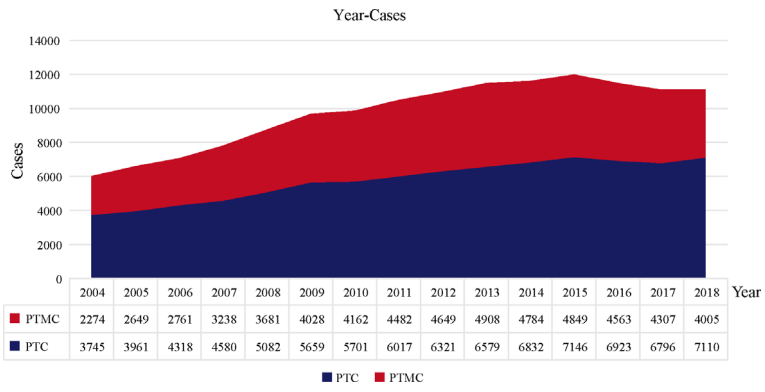

FIGURE 2
The number of PTC and PTMC cases diagnosed annually recorded in the SEER database consisting of 18 population-based cancer registries. PTC, papillary thyroid carcinoma; PTMC, papillary thyroid microcarcinoma.

(80.6% vs. 74.5%) and had older age at diagnosis (44.79 vs. 42.87), higher proportion of bilateral lesions (28.1% vs. 22.3%), lower proportion of follicular subtype (0.7% vs. 1.7%), and higher proportion of lobectomy and/or isthmectomy (21.3% vs. 14.7%) but lower proportion of total thyroidectomy (78% vs. 83%) (all the *p*-value<0.001). Detailed data are presented in Table 2.

PSM adjustment of patient characteristics

Patients with PTMC and PTC were 1:1 propensity matched with a caliper value of 0.01 to yield 58,879 matched pairs of patients. The clinicopathological comparison between the two cohorts is presented in Table 1 and Supplementary Table 1. After minimizing potential bias using PSM analysis, PTMC still showed consistently lower T, N, and M stages and fewer LN (11.9% vs. 30.8%) and distant metastases (0.3% vs. 1.5%) compared with PTC. In addition, the difference between PTMC and PTC in OS (94.3% vs. 91.9%) and CSS (99.7% vs. 98.1%) was more significant (all *p*-value <0.001). Meanwhile, as shown in Supplementary Table 1, compared with PTMC, PTC had more lung (0.7% vs. 0.1%), bone (0.3% vs. 0.1%), and distant LN (0.1% vs. 0) metastases. Together, these results meant that PTMC had a higher biological indolence than PTC. Regarding treatment, patients with PTMC had a lower proportion of radiotherapy (24.3% vs. 59.5%), chemotherapy (0.1% vs. 0.6%), and total thyroidectomy (72.2% vs. 87.3%) but a higher proportion of lobectomy and/or isthmectomy (21.5% vs. 7%) compared with patients with PTC (all *p*-value <0.001).

Validation data from our center also verified that, after PSM, PTC showed stably higher T staging and N staging and higher proportion of intraglandular dissemination (4.7% vs. 2.8%), extraglandular invasion (5.8% vs. 1.1%), and capsular invasion (55.9% vs. 42.1%) (all *p*-value <0.001), which supported the results of SEER data analysis. Detailed data are presented in Table 2. In addition, the comparison of clinicopathological features between the cohorts (patients who underwent surgery and those who were recommended but did not undergo surgery) is presented in Supplementary Table 2.

Assessment of covariate balance in matched groups

Assessment of the covariate balance in the matched cohorts was an important step to diagnose the quality of matched samples (20). In present study, the balance was defined as similarity in the empirical distributions of the full set of covariates between matched PTMC and PTC cohorts. As shown in Figures 3A, C analysis of standardized mean difference suggested that almost all covariates were less than 5%, far less than the 10% reported in the literature (21, 22), suggesting a good match. In addition, Kernel density estimation in Figures 3B, D indicated that, compared with the unmatched sample, the matched sample showed almost complete overlap, suggesting better comparability between the two cohorts. Therefore, our results jointly confirmed that the confounders and bias between the cohorts were well balanced, and the comparison was reliable.

Survival analysis outcomes in patients with PTC vs. those with PTMC

The survival analysis in Figure 4 suggested that the 5-year OS and 10-year OS of PTC were about 94% and 88%, respectively, and that of PTMC were about 96% and 91%, respectively. In addition, the 5-year CSS and 10-year CSS of PTC were about 98% and 97%, respectively, whereas the 5-year and 10-year CSS of PTMC were above 99%. Detailed data are presented in Table 3. In addition, PTMC showed a better prognosis than PTC for both OS and CSS under similar clinicopathological parameters such as age, sex, race, follicular variant, multifocality, and TNM staging (all *p*-value < 0.01).

Survival analysis outcomes in patients with and without surgery

Survival analysis in Figure 5 showed that the 5-year OS, 5-year CSS, 10-year OS, and 10-year CSS were about 95%, 99%, 90%, and 98%, respectively, in patients with PTC who underwent surgery, compared with about 62%, 86%, 50% and 82%, respectively, in patients with PTC without surgery. Similarly, the 5-year OS and 10-year OS of PMTC patients who underwent surgery were about 97% and 92%, respectively, whereas both the 5-year and 10-year CSS were above 99%. However, the 5-year OS and 10-year OS of patients with PTMC who did not undergo surgery were about 76% and 67%, respectively, whereas both the 5-year and 10-year CSS were about 98%. Detailed results are presented in Table 3.

In addition, analysis of patients at different TNM stages suggested that surgery improved CSS and OS in almost all patients (all *p*-value < 0.05), except patients with PTMC at stage T1N0M0. Figure 5O indicated that there was no significant difference in CSS for patients with PTMC at stage T1N0M0 with and without surgery ($p = 0.36$), although OS was statistically significant for this group of patients ($p < 0.0001$). As shown in Figure 6D, further survival analysis of patients underwent surgery and those who were recommended but did not undergo surgery also showed no statistical difference in CSS

10.3389/fendo.2022.944758

TABLE 1 Clinicopathological characteristics and statistical results of patients with PTC or PTMC recorded in SEER database before and after propensity score matching.

Characteristic	Level	Pre–Propensity Score Matching				Post–Propensity Score Matching			
		Overall	PTC	PTMC	P	Overall	PTC	PTMC	P
N		145,951	86,666	59,285		117,758	58,879	58,879	
Age, mean (SD)		49.4 (15.34)	48.3 (16.0)	51.2 (14.1)	<0.001	51.3 (14.5)	51.4 (14.9)	51.1 (14.1)	<0.001
Age group, n (%)	≤55 years	94,141 (64.5)	57,925 (66.8)	36,216 (61.1)	<0.001	71,811 (61.0)	35,670 (60.6)	36,141 (61.4)	0.005
	>55 years	51,810 (35.5)	28,741 (33.2)	23,069 (38.9)		45,947 (39.0)	23,209 (39.4)	22,738 (38.6)	
Sex, n (%)	Female	112,296 (76.9)	64,204 (74.1)	48,092 (81.1)	<0.001	95,215 (80.9)	47,516 (80.7)	47,699 (81.0)	0.178
	Male	33,655 (23.1)	22,462 (25.9)	11,193 (18.9)		22,543 (19.1)	11,363 (19.3)	11,180 (19.0)	
Race, n (%)	Black	9,224 (6.3)	5,207 (6.0)	4,017 (6.8)	<0.001	7,566 (6.4)	3,579 (6.1)	3,987 (6.8)	<0.001
	Other	18,595 (12.7)	12,077 (13.9)	6,518 (11.0)		13,134 (11.2)	6,621 (11.2)	6,513 (11.1)	
	White	118,132 (80.9)	69,382 (80.1)	48,750 (82.2)		97,058 (82.4)	48,679 (82.7)	48,379 (82.2)	
Follicular variant, n (%)	No	102,505 (70.2)	59,762 (69.0)	42,743 (72.1)	<0.001	84,431 (71.7)	42,031 (71.4)	42,400 (72.0)	0.017
	Yes	43,446 (29.8)	26,904 (31.0)	16,542 (27.9)		33,327 (28.3)	16,848 (28.6)	16,479 (28.0)	
Multifocality, n (%)	No	119,604 (81.9)	72,130 (83.2)	47,474 (80.1)	<0.001	94,681 (80.4)	47,566 (80.8)	47,115 (80.0)	0.001
	Yes	26,347 (18.1)	14,536 (16.8)	11,811 (19.9)		23,077 (19.6)	11,313 (19.2)	11,764 (20.0)	
Laterality (%)	A	144,908 (99.3)	85,948 (99.2)	58,960 (99.5)	<0.001	117,184 (99.5)	58,630 (99.6)	58,554 (99.4)	0.002
	B	1,043 (0.7)	718 (0.8)	325 (0.5)		574 (0.5)	249 (0.4)	325 (0.6)	
T stage, n (%)	T1	92,877 (63.6)	36,504 (42.1)	56,373 (95.1)	<0.001	81,569 (69.3)	25,582 (43.4)	55,987 (95.1)	<0.001
	T2	25,082 (17.2)	25,082 (28.9)	0 (0.0)		16,321 (13.9)	16,321 (27.7)	0 (0.0)	
	T3&T4	27,805 (19.1)	24,893 (28.7)	2,912 (4.9)		19,747 (16.8)	16,855 (28.6)	2,892 (4.9)	
	Tx	187 (0.1)	187 (0.2)	0 (0.0)		121 (0.1)	121 (0.2)	0 (0.0)	
N stage, n (%)	N0	99,385 (68.1)	52,560 (60.6)	46,825 (79.0)	<0.001	83,103 (70.6)	36,631 (62.2)	46,472 (78.9)	<0.001
	N1	34,964 (24.0)	27,923 (32.2)	7,041 (11.9)		25,145 (21.4)	18,133 (30.8)	7,012 (11.9)	
	Nx	11,602 (7.9)	6,183 (7.1)	5,419 (9.1)		9,510 (8.1)	4,115 (7.0)	5,395 (9.2)	
M stage, n (%)	M0	143,072 (98.0)	84,367 (97.3)	58,705 (99.0)	<0.001	115,676 (98.2)	57,374 (97.4)	58,302 (99.0)	<0.001
	M1	1,513 (1.0)	1,340 (1.5)	173 (0.3)		1,057 (0.9)	885 (1.5)	172 (0.3)	
	Mx	1,366 (0.9)	959 (1.1)	407 (0.7)		1,025 (0.9)	620 (1.1)	405 (0.7)	
Radiotherapy, n (%)	Yes	65,823 (45.1)	51,436 (59.3)	14,387 (24.3)	<0.001	49,365 (41.9)	35,055 (59.5)	14,310 (24.3)	<0.001
	No	80,128 (54.9)	35,230 (40.7)	44,898 (75.7)		68,393 (58.1)	23,824 (40.5)	44,569 (75.7)	
Surgery approach, n (%)	No surgery or surgery, NOS	2,705 (1.9)	2,125 (2.5)	580 (1.0)	<0.001	2,092 (1.8)	1,523 (2.6)	569 (1.0)	<0.001
	Local tumor resection	1,033 (0.7)	396 (0.5)	637 (1.1)		880 (0.7)	252 (0.4)	628 (1.1)	
	Lobectomy and/or isthmectomy	19,181 (13.1)	6,450 (7.4)	12,731 (21.5)		16,756 (14.2)	4,103 (7.0)	12,653 (21.5)	
	Near total thyroidectomy	4,912 (3.4)	2,381 (2.7)	2,531 (4.3)		4,091 (3.5)	1,576 (2.7)	2,515 (4.3)	

(Continued)

10.3389/fendo.2022.944758

TABLE 1 Continued

Characteristic	Level	Pre–Propensity Score Matching				Post–Propensity Score Matching			
		Overall	PTC	PTMC	P	Overall	PTC	PTMC	P
	Total thyroidectomy	118,120 (80.9)	75,314 (86.9)	42,806 (72.2)		93,939 (79.8)	51,425 (87.3)	42,514 (72.2)	
Chemotherapy, n(%)	Yes	513 (0.4)	430 (0.5)	83 (0.1)	<0.001	408 (0.3)	325 (0.6)	83 (0.1)	<0.001
	No	145,438 (99.6)	86,236 (99.5)	59,202 (99.9)		117,350 (99.7)	58,554 (99.4)	58,796 (99.9)	
Cancer-specific death, n (%)	Yes	1,643 (1.1)	1,490 (1.7)	153 (0.3)	<0.001	1,299 (1.1)	1,146 (1.9)	153 (0.3)	<0.001
	No	144,308 (98.9)	85,176 (98.3)	59,132 (99.7)		116,459 (98.9)	57,733 (98.1)	58,726 (99.7)	
Status, n(%)	Dead	9,711 (6.7)	6,312 (7.3)	3,399 (5.7)	<0.001	8,134 (6.9)	4,764 (8.1)	3,370 (5.7)	<0.001
	Alive	136,240 (93.3)	80,354 (92.7)	55,886 (94.3)		109,624 (93.1)	54,115 (91.9)	55,509 (94.3)	

PTC, papillary thyroid carcinoma; PTMC, papillary thyroid microcarcinoma; N/n, number; SD, standard deviation; NOS, not otherwise specified.

TABLE 2 Clinicopathological characteristics and statistical results of patients with PTC or PTMC recorded in our institution before and after propensity score matching.

Characteristic	Level	Pre–Propensity Score Matching				Post–Propensity Score Matching			
		Overall	PTC	PTMC	P	Overall	PTC	PTMC	P
N		8,751	4,456	4,295		6,998	3,499	3,499	
Age, mean (SD)		43.81 (11.31)	42.87 (11.93)	44.79 (10.54)	<0.001	43.92 (10.96)	43.98 (11.49)	43.87 (10.39)	0.689
Age group, n (%)	≤55 year	7,474 (85.4)	3,816 (85.6)	3,658 (85.2)	0.555	6,000 (85.7)	2,954 (84.4)	3,046 (87.1)	0.002
	>55 year	1,277 (14.6)	640 (14.4)	637 (14.8)		998 (14.3)	545 (15.6)	453 (12.9)	
Sex, n (%)	Male	1,968 (22.5)	1,135 (25.5)	833 (19.4)	<0.001	1,530 (21.9)	765 (21.9)	765 (21.9)	1
	Female	6,783 (77.5)	3,321 (74.5)	3,462 (80.6)		5,468 (78.1)	2,734 (78.1)	2,734 (78.1)	
Laterality, n (%)	Unilateral	6,550 (74.8)	3,464 (77.7)	3,086 (71.9)	<0.001	5,186 (74.1)	2,636 (75.3)	2,550 (72.9)	0.02
	Bilateral	2,201 (25.2)	992 (22.3)	1,209 (28.1)		1,812 (25.9)	863 (24.7)	949 (27.1)	
Surgery approach, n (%)	Surgery, NOS	69 (0.8)	64 (1.4)	5 (0.1)	<0.001	55 (0.8)	52 (1.5)	3 (0.1)	<0.001
	Local tumor resection	8 (0.1)	8 (0.2)	0 (0.0)		6 (0.1)	6 (0.2)	0 (0.0)	
	Lobectomy and/or isthmectomy	1,569 (17.9)	654 (14.7)	915 (21.3)		1,260 (18.0)	490 (14.0)	770 (22.0)	
	Near total thyroidectomy	55 (0.6)	30 (0.7)	25 (0.6)		41 (0.6)	22 (0.6)	19 (0.5)	
	Total thyroidectomy	7,050 (80.6)	3,700 (83.0)	3,350 (78.0)		5,636 (80.5)	2,929 (83.7)	2,707 (77.4)	
T stage, n (%)	T1	7,231 (82.6)	3,352 (75.2)	3,879 (90.3)	<0.001	5,773 (82.5)	2,611 (74.6)	3,162 (90.4)	<0.001
	T2	385 (4.4)	382 (8.6)	3 (0.1)		290 (4.1)	288 (8.2)	2 (0.1)	
	T3	579 (6.6)	383 (8.6)	196 (4.6)		457 (6.5)	319 (9.1)	138 (3.9)	
	T4	556 (6.4)	339 (7.6)	217 (5.1)		478 (6.8)	281 (8.0)	197 (5.6)	
N stage, n (%)	N0	4,446 (50.8)	1,727 (38.8)	2,719 (63.3)	<0.001	3,563 (50.9)	1,397 (39.9)	2,166 (61.9)	<0.001
	N1	4,305 (49.2)	2,729 (61.2)	1,576 (36.7)		3,435 (49.1)	2,102 (60.1)	1,333 (38.1)	
M stage, n (%)	M0	8,722 (99.7)	4,442 (99.7)	4,280 (99.7)	0.921	6,980 (99.7)	3,491 (99.8)	3,489 (99.7)	0.813
	M1	29 (0.3)	14 (0.3)	15 (0.3)		18 (0.3)	8 (0.2)	10 (0.3)	
Follicular subtype, n (%)	No	8,645 (98.8)	4,381 (98.3)	4,264 (99.3)	<0.001	6,953 (99.4)	3,478 (99.4)	3,475 (99.3)	0.765
	Yes	106 (1.2)	75 (1.7)	31 (0.7)		45 (0.6)	21 (0.6)	24 (0.7)	
Multifocality, n (%)	No	5,432 (62.1)	2,771 (62.2)	2,661 (62.0)	0.842	4,317 (61.7)	2,138 (61.1)	2,179 (62.3)	0.325
	Yes	3,319 (37.9)	1,685 (37.8)	1,634 (38.0)		2,681 (38.3)	1,361 (38.9)	1,320 (37.7)	
Intraglandular dissemination, n (%)	No	2,969 (33.9)	1,826 (41.0)	1,143 (26.6)	<0.001	2,332 (33.3)	1,343 (38.4)	989 (28.3)	<0.001

(Continued)

10.3389/fendo.2022.944758

TABLE 2 Continued

Characteristic	Level	Pre–Propensity Score Matching				Post–Propensity Score Matching			
		Overall	PTC	PTMC	P	Overall	PTC	PTMC	P
	Unknown	5,434 (62.1)	2,402 (53.9)	3,032 (70.6)		4,402 (62.9)	1,990 (56.9)	2,412 (68.9)	
	Yes	348 (4.0)	228 (5.1)	120 (2.8)		264 (3.8)	166 (4.7)	98 (2.8)	
Extratglandular invasion, n (%)	No	7,913 (90.4)	3,801 (85.3)	4,112 (95.7)	<0.001	6,312 (90.2)	2,972 (84.9)	3,340 (95.5)	<0.001
	Unknown	547 (6.3)	408 (9.2)	139 (3.2)		445 (6.4)	325 (9.3)	120 (3.4)	
	Yes	291 (3.3)	247 (5.5)	44 (1.0)		241 (3.4)	202 (5.8)	39 (1.1)	
Capsular invasion, n (%)	No	3,900 (44.6)	1,557 (34.9)	2,343 (54.6)	<0.001	3,123 (44.6)	1,217 (34.8)	1,906 (54.5)	<0.001
	Unknown	547 (6.3)	408 (9.2)	139 (3.2)		445 (6.4)	325 (9.3)	120 (3.4)	
	Yes	4,304 (49.2)	2,491 (55.9)	1,813 (42.2)		3,430 (49.0)	1,957 (55.9)	1,473 (42.1)	

PTC, papillary thyroid carcinoma; PTMC, papillary thyroid microcarcinoma; N/n, number; SD, standard deviation.

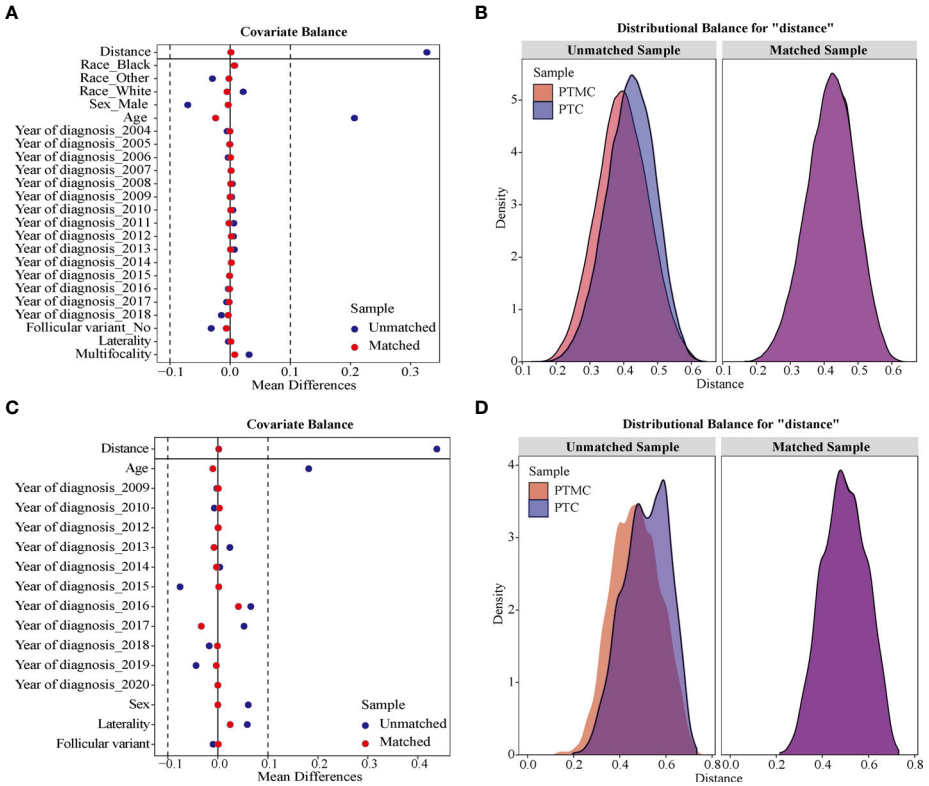

FIGURE 3
The assessment of sample distribution and covariate balance before and after propensity score matching. **(A, B)** For the data from SEER database and **(C, D)** for the data from our institution. **(A, C)** Mean standardized difference analysis showed that all matched covariates were less than 10%, indicating good matching effect. **(B, D)** Kernel density estimation indicated that, compared with the unmatched sample, the matched sample showed almost complete overlap, suggesting better comparability between the two cohorts.

for patients with PTMC (p = 1), and no patients died due to PTMC in both cohorts. Therefore, for patients with PTMC at stage T1N0M0, AS with good medical compliance may be a potentially feasible management strategy. However, for PTC patients, the differences were significant for both OS and CSS (Figures 6A, C).

Discussion

In recent years, with the increasing incidence of THCA but stable mortality (7), overtreatment of PTC has become a major concern. Consequently, an increasing number of studies are exploring the feasibility of AS in PTC treatment. In this study,

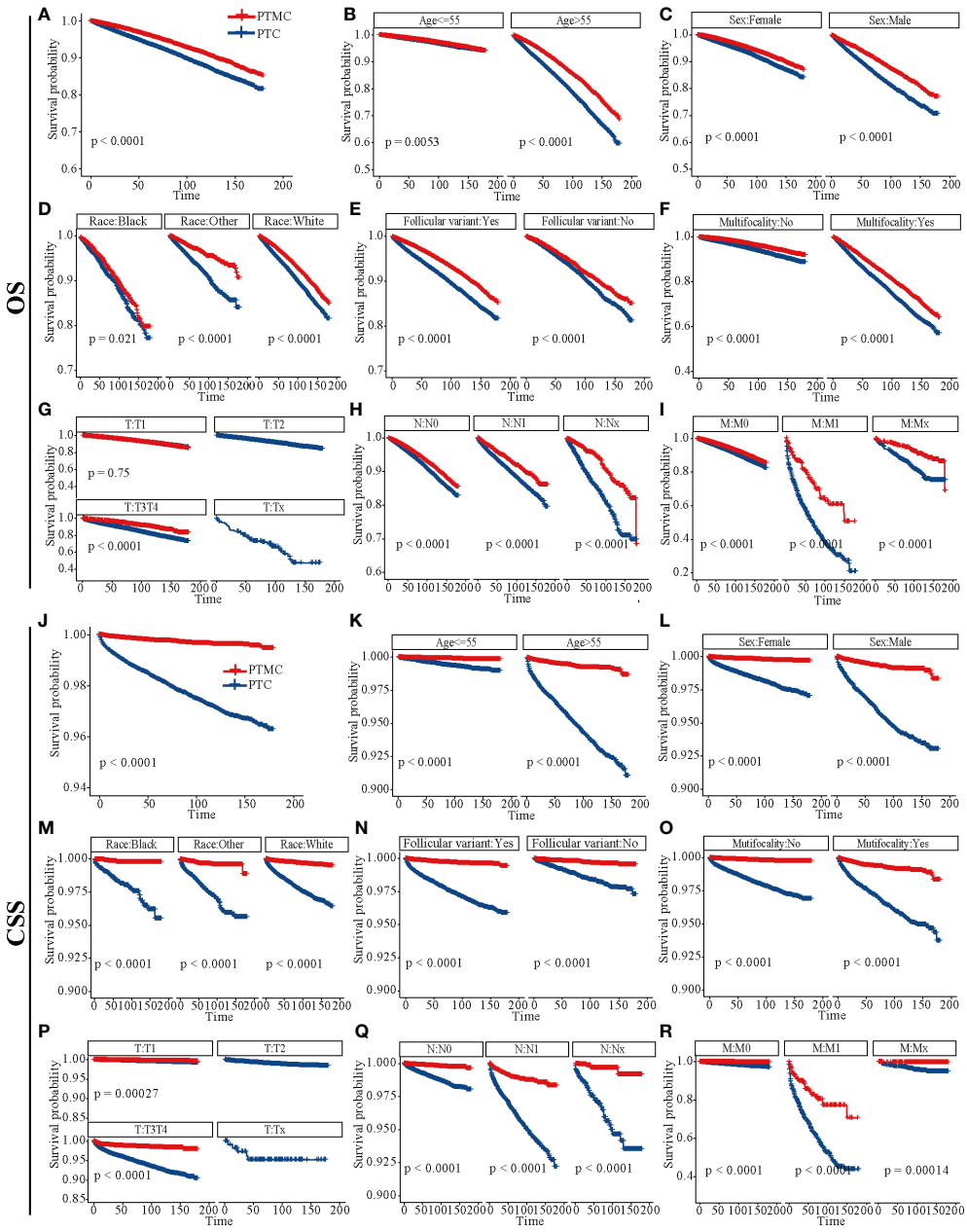

FIGURE 4
Survival analysis of OS and CSS for patients with PTC and PTMC at different stages or with different characteristics. **(A–I)** OS analysis and **(J–R)** CSS analysis. **(A, J)** All factors; **(B, K)** age; **(C, L)** sex; **(D, M)** race; **(E, N)** follicular variant; **(F, O)** multifocality; **(G, P)** T stage; **(H, Q)** N stage; **(I, R)** M stage. OS, overall survival; CSS, cancer-specific survival; PTC, papillary thyroid carcinoma; PTMC, papillary thyroid microcarcinoma.

using PSM, we elucidated clinicopathological differences between PTC and PTMC based on data of 145,951 patients with PTC from the SEER database and validated them with data of 8,751 patients with PTC in our institution. It was concluded that PTMC generally presented higher biological indolence than PTC, which meant a higher OS and CSS rate for patients. In addition, survival analysis suggests no significant difference in CSS between patients with PTMC at stage T1N0M0 with and without surgery (p = 0.36). This meant that surgery could not confer significant survival benefits for these patients, and AS may be a potentially more viable alternative management strategy than surgery. Taken together, the results of this population-based PSM analysis confirm differences in the biological behavior and prognosis of PTC and PTMC

TABLE 3 An overall estimation of prognosis for different types of patients based on survival analysis.

Categories	OS		CSS	
	5-year	10-year	5-year	10-year
PTC	94%	88%	98%	97%
PTMC	96%	91%	>99%	>99%
Patients with PTC with surgery	95%	90%	99%	98%
Patients with PTC without surgery	62%	50%	86%	82%
Patients with PTMC with surgery	97%	92%	>99%	>99%
Patients with PTMC without surgery	76%	67%	98%	98%

PTC, papillary thyroid carcinoma; PTMC, papillary thyroid microcarcinoma; OS, overall survival; CSS, cancer-specific survival.

and provide evidence for AS in patients with PTMC at stage T1N0M0.

Although both PTMC and PTC are considered indolent malignancy (23), they receive uniform immediate surgical treatment with no differences in management strategies. Hence, identifying clinicopathological differences between the two could improve management of PTC. This study suggested that PTMC was diagnosed at an older age and had a lower proportion of follicular

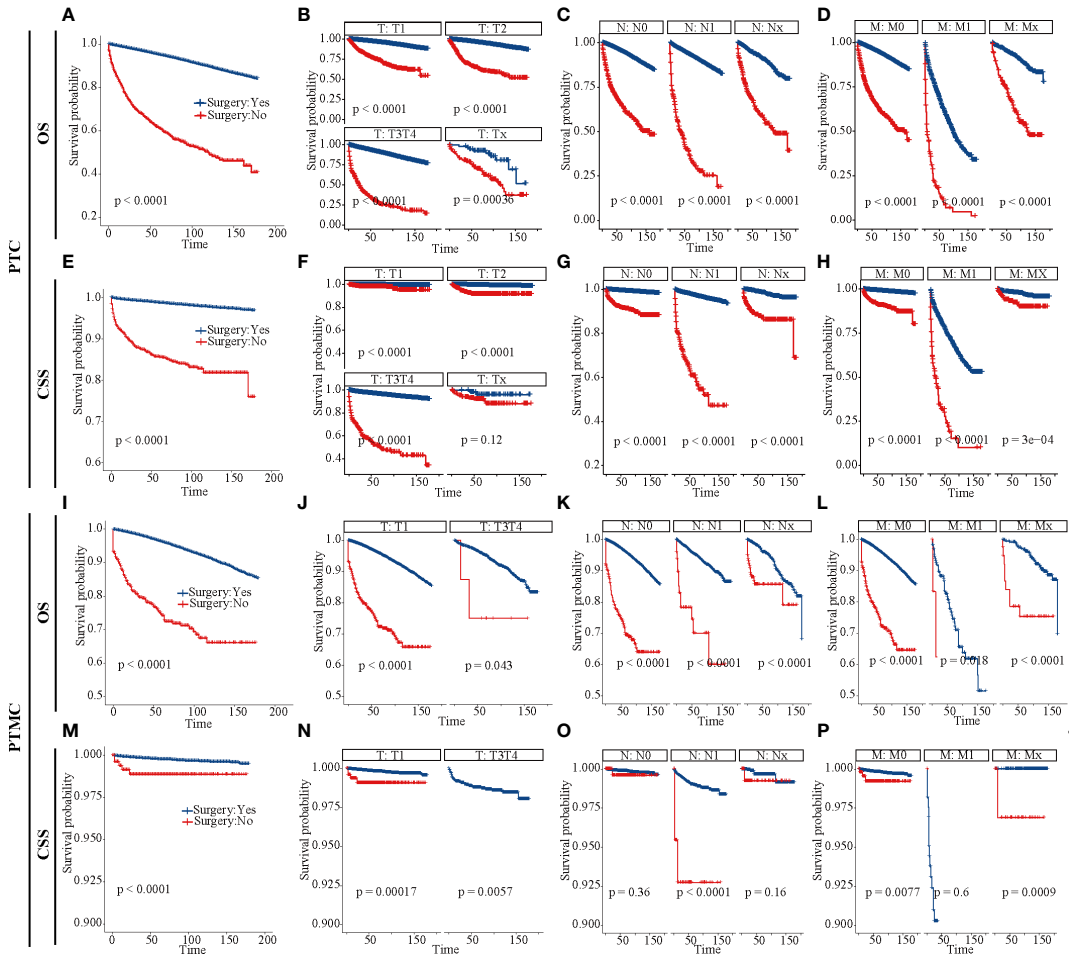

FIGURE 5
Survival analysis of patients with PTC and PTMC with or without surgery at different stages. **(A–D)** OS for patients with PTC; **(E–H)** CSS for patients with PTC; **(I–L)** OS for patients with PTMC; **(M–P)**: CSS for patients with PTMC. **(A, E, I, M)** All factors; **(B, F, J, N)** T stage; **(C, G, K, O)** N stage; **(D, H, L, P)** M stage. OS, overall survival; CSS, cancer-specific survival; PTC, papillary thyroid carcinoma; PTMC, papillary thyroid microcarcinoma.

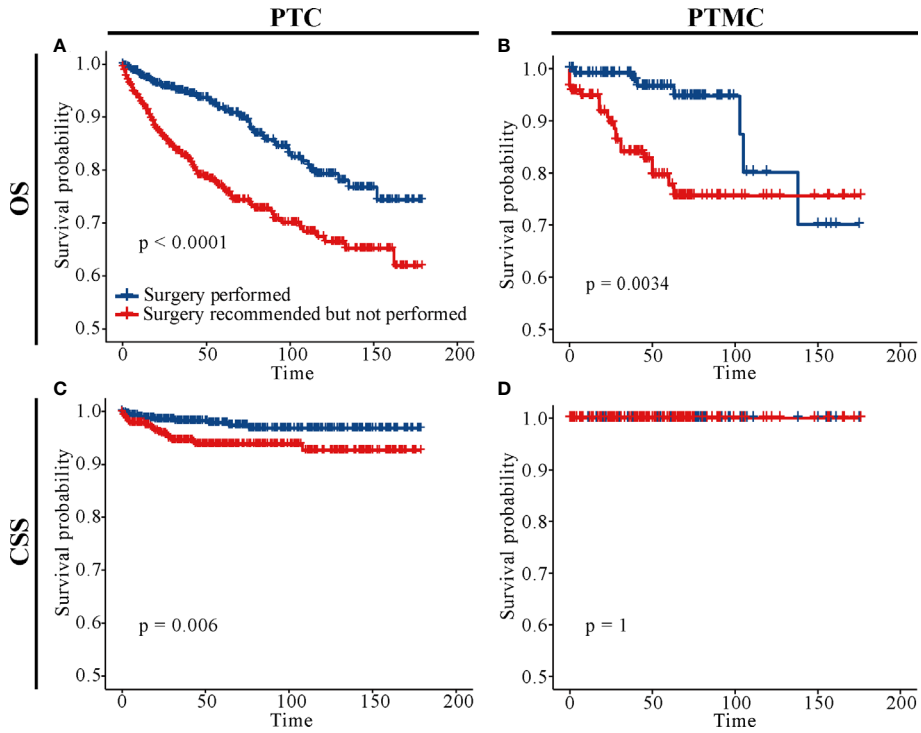

FIGURE 6
Survival analysis of patients with PTC and PTMC who underwent surgery and those who were recommended but did not undergo surgery. **(A)** OS for PTC patients; **(B)** OS for patients with PTMC; **(C)** CSS for PTC patients; **(D)** CSS for patients with PTMC; OS, overall survival; CSS, cancer-specific survival; PTC, papillary thyroid carcinoma; PTMC, papillary thyroid microcarcinoma.

variants, intraglandular dissemination, extraglandular invasion, and capsular invasion than PTC (Tables 1, 2). Previous studies have identified younger age (≤45 years) at diagnosis, extraglandular invasion and capsular invasion as risk factors for PTC recurrence (24) and LN metastases (19, 25, 26). Ito et al. concluded that PTMC may be more progressive in young patients than in older patients (27). In addition, a previous report confirmed that PTC displays a distinct gene expression pattern from PTC (28). Thus, these clinicopathological features may partly elucidate the higher biological indolence of PTMC, OS, and CSS compared with PTC. In addition, as the tumor was at an earlier stage and the risk was lower, patients with PTMC received a lower proportion of radiotherapy, chemotherapy, and total thyroidectomy but a higher proportion of lobectomy and/or isthmectomy than PTC patients. In addition, both data from the SEER database and our institution suggested that PTMC exhibited higher proportion of multifocality compared with PTC, consistent with the high multifocality of PTMC reported in the literature (29). Research suggested that even patients with multiple PTMC were good candidates for AS (30).

Although AS for low-risk PTMC was introduced into the management guidelines of THCA in Japan and the United States in 2010 and 2015, respectively, long-term follow-up data for patients included in AS are still limited. As a result, some clinicians or patients are reluctant to perform it. This study retrospectively analyzed long-term follow-up results of patients with or without surgery, providing an evidence for clinical management of PTC and PTMC. As shown in Figure 5O, CSS was not significant different between patients with PTMC at stage T1N0M0 with and without surgery. This result was consistent with the Consensus Statements from the Japan Association of Endocrine Surgery Task Force on Management for Papillary Thyroid Microcarcinoma (31). As shown in Figure 6D, further survival analysis showed no statistical difference in CSS between patients who underwent surgery and those who were recommended but did not undergo surgery for patients with PTMC ($p = 1$). Further, no patients died of PTMC in both cohorts. Similarly, in a prospective study of 230 patients with asymptomatic PTMC, 90% of PTMC remained stable during the 17-year observation period, and no patient developed distant metastasis or died due to PTMC (32). Moreover, a study of quality of life of patients with low-risk PTMC reported that patients in the immediate surgery group had more complaints and were more anxious and depressed than those in the AS group (33). In a cohort of patients with PTMC observed for more than 50 years, only three patients (0.3%) died of PTMC, compared with 29% of patients dying of other causes (34). Consistently, patients with PTMC at stage T1N0M0 who did not undergo surgery had significantly lower OS than those who underwent it (Figures 5K, 6B). This may be partly due to

excessive psychological stress and poor medical compliance. Therefore, it was necessary to eliminate the psychological burden of patients with PTMC under AS, urge them to carry out standardized AS and maintain good medical compliance, and minimize the effect of comorbidities. Appropriate medical education of the patients may reduce cancer and surveillance-related stress in patients, facilitate patient compliance with AS protocols, and improve follow-up (10). In conclusion, for patients with PTMC at stage T1N0M0, AS may be a potentially feasible management strategy.

AS is defined in literature as the life-long application of meticulous diagnostic modalities to monitor changes in the status of a disease without immediate therapeutic measures until the progression of the disease is evident, through regular testing and assessment of cancer progression (35). It has been successfully applied to the prostate cancer, which is also considered low risk (36). Ito et al. proposed the following strategy of AS for low-risk PTMC: Patients enrolled in AS were required to revisit hospital after 6 months, and if no signs of progression such as enlargement (increase by more than 3mm) or LN metastases were detected, then their next visit was scheduled 1 year later (4). Otherwise AS would be terminated, and immediate surgery would be performed. In addition, if the patient felt overwhelmed with the psychological burden of not undergoing treatment or changed preferences, then he or she should be switched to surgery therapy. By comparison, several suggestions for AS have been proposed in literature (10, 31): (1) accurately identify and exclude aggressive tumors at the beginning and during AS; (2) develop a standardized thyroid ultrasound examination and recording system; (3) provide appropriate education of patients and clinicians to fully understand follow-up protocols; (4) evaluate factors affecting patient compliance with follow-up; and (5) provide necessary psychological support to ensure a good quality of life.

This study has limitations that must be acknowledged. First, as a retrospective study, there were inherent biases and uncontrollable confounding factors. Second, the validation cohort from our center lacked follow-up data to validate prognostic differences concluded by SEER data under different clinicopathological parameters. Finally, the number of patients who were recommended but did not undergo surgery was low, resulting in loss of large amounts of data from the matched cohorts during PSM analysis, which may weaken our conclusions. Therefore, more prospective randomized controlled trials with large samples are warranted to further confirm these findings.

Conclusion

Generally, PTMC showed higher biological indolence than PTC, which meant higher OS and CSS for patients. For patients with PTMC at stage T1N0M0, AS may be a potentially feasible management strategy. However, the maintenance of good medical compliance and the management of psychological burden should be prioritized for the patients included in AS.

Data availability statement

The raw data supporting the conclusions of this article will be made available by the authors, without undue reservation.

Ethics statement

Ethical review and approval was not required for the study on human participants in accordance with the local legislation and institutional requirements. The patients/participants provided their written informed consent to participate in this study.

Author contributions

Conception and design: XQ and TH; administrative support: XQ, LM, and TH; collection and assembly of data: BQ and JZ; data analysis and interpretation: BQ and LH; manuscript writing: BQ; critical revision of the manuscript: SZ; final approval of manuscript: All authors.

Acknowledgments

We acknowledge the efforts of the SEER Program tumor registries in providing high quality open resources for researchers.

Conflict of interest

The authors declare that the research was conducted in the absence of any commercial or financial relationships that could be construed as a potential conflict of interest.

Publisher's note

Supplementary material

The Supplementary Material for this article can be found online at: https://www.frontiersin.org/articles/10.3389/fendo.2022.944758/full#supplementary-material

References

1. Siegel RL, Miller KD, Jemal A. Cancer statistics. (2020) *CA Cancer J Clin* (2020) 70(1):7–30. doi: 10.3322/caac.21590

2. Krajewska J, Kukulska A, Oczko-Wojciechowska M, Kotecka-Blicharz A, Drosik-Rutowicz K, Haras-Gil M, et al. Early diagnosis of low-risk papillary thyroid cancer results rather in overtreatment than a better survival. *Front Endocrinol (Lausanne)* (2020) 11:571421. doi: 10.3389/fendo.2020.571421

3. Hung ML, Wu JX, Li N, Livhits MJ, Yeh MW. Association of radioactive iodine administration after reoperation with outcomes among patients with recurrent or persistent papillary thyroid cancer. *JAMA Surg* (2018) 153(12):1098–104. doi: 10.1001/jamasurg.2018.2659

4. Ito Y, Miyauchi A. Active surveillance as first-line management of papillary microcarcinoma. *Annu Rev Med* (2019) 70(1):369–79. doi: 10.1146/annurev-med-051517-125510

5. Davies L, Morris LG, Haymart M, Chen AY, Goldenberg D, Morris J, et al. American Association of clinical endocrinologists and American college of endocrinology disease state clinical review: The increasing incidence of thyroid cancer. *Endocr Pract* (2015) 21(6):686–96. doi: 10.4158/EP14466.DSCR

6. Davies L, Welch HG. Current thyroid cancer trends in the united states. *JAMA Otolaryngol Head Neck Surg* (2014) 140(4):317–22. doi: 10.1001/jamaoto.2014.1

7. Ahn HS, Kim HJ, Welch HG. Korea's thyroid-cancer "Epidemic"–screening and overdiagnosis. *N Engl J Med* (2014) 371(19):1765–7. doi: 10.1056/NEJMp1409841

8. Sutherland R, Tsang V, Clifton-Bligh RJ, Gild ML. Papillary thyroid microcarcinoma: Is active surveillance always enough? *Clin Endocrinol* (2021) 95 (6):811–7. doi: 10.1111/cen.14529

9. Harach HR, Franssila KO, Wasenius VM. Occult papillary carcinoma of the thyroid. a "Normal" finding in finland. a systematic autopsy study. *Cancer* (1985) 56(3):531–8.

10. Haser GC, Tuttle RM, Su HK, Alon EE, Bergman D, Bernet V, et al. Active surveillance for papillary thyroid microcarcinoma: New challenges and opportunities for the health care system. *Endocr Pract* (2016) 22(5):602–11. doi: 10.4158/EP151065.RA

11. Takami H, Ito Y, Okamoto T, Yoshida A. Therapeutic strategy for differentiated thyroid carcinoma in Japan based on a newly established guideline managed by Japanese society of thyroid surgeons and Japanese association of endocrine surgeons. *World J Surg* (2011) 35(1):111–21. doi: 10.1007/s00268-010-0832-6

12. Haugen BR, Alexander EK, Bible KC, Doherty GM, Mandel SJ, Nikiforov YE, et al. 2015 American Thyroid association management guidelines for adult patients with thyroid nodules and differentiated thyroid cancer: The American thyroid association guidelines task force on thyroid nodules and differentiated thyroid cancer. *Thyroid* (2016) 26(1):1–133. doi: 10.1089/thy.2015.0020

13. Ito Y, Miyauchi A, Kudo T, Oda H, Yamamoto M, Sasai H, et al. Trends in the implementation of active surveillance for low-risk papillary thyroid microcarcinomas at kuma hospital: Gradual increase and heterogeneity in the acceptance of this new management option. *Thyroid* (2018) 28(4):488–95. doi: 10.1089/thy.2017.0448

14. Baek S, Park SH, Won E, Park YR, Kim HJ, et al. Propensity score matching: A conceptual review for radiology researchers. *Korean J Radiol* (2015) 16(2):286–96. doi: 10.3348/kjr.2015.16.2.286

15. Tatonetti NP, Ye PP, Daneshjou R, Altman RB. Data-driven prediction of drug effects and interactions. *Sci Transl Med* (2012) 4(125):125ra31. doi: 10.1126/scitranslmed.3003377

16. Agha R, Abdall-Razak A, Crossley E, Dowlut N, Iosifidis C, Mathew G. STROCSS 2019 guideline: Strengthening the reporting of cohort studies in surgery. *Int J Surg* (2019) 72:156–65. doi: 10.1016/j.ijsu.2019.11.002

17. Austin PC. An introduction to propensity score methods for reducing the effects of confounding in observational studies. *Multivariate Behav Res* (2011) 46 (3):399–424. doi: 10.1080/00273171.2011.568786

18. Zhang Z. Propensity score method: A non-parametric technique to reduce model dependence. *Ann Transl Med* (2017) 5(1):7. doi: 10.21037/atm.2016.08.57

19. Qian B, Guo S, Zhou J, Qu X, Zhang S. Intraglandular dissemination is a risk factor for lymph node metastasis in papillary thyroid carcinoma: A propensity score matching analysis. *Gland Surg* (2021) 10(12):3169–80. doi: 10.21037/gs-21-470

20. Stuart EA. Matching methods for causal inference: A review and a look forward. *Stat Sci* (2010) 25(1):1–21. doi: 10.1214/09-STS313

21. Rubin D. Using propensity scores to help design observational studies: Application to the tobacco litigation. *Health Serv Outcomes Res Method* (2001) 2(3-4):169–88. doi: 10.1023/A:1020363010465

22. Yao XI, Wang X, Speicher PJ, Hwang ES, Cheng P, Harpole DH, et al. Reporting and guidelines in propensity score analysis: A systematic review of cancer and cancer surgical studies. *J Natl Cancer Inst* (2017) 109(8). doi: 10.1093/jnci/djw323

23. Nikiforov YE, Seethala RR, Tallini G, Baloch ZW, Basolo F, Thompson LD, et al. Nomenclature revision for encapsulated follicular variant of papillary thyroid carcinoma: A paradigm shift to reduce overtreatment of indolent tumors. *JAMA Oncol* (2016) 2(8):1023–9. doi: 10.1001/jamaoncol.2016.0386

24. Roti E, degli Uberti EC, Bondanelli M, Braverman LE. Thyroid papillary microcarcinoma: A descriptive and meta-analysis study. *Eur J Endocrinol* (2008) 159(6):659–73. doi: 10.1530/EJE-07-0896

25. Zhang L, Wei WJ, Ji QH, Zhu YX, Wang ZY, Wang Y, et al. Risk factors for neck nodal metastasis in papillary thyroid microcarcinoma: A study of 1066 patients. *J Clin Endocrinol Metab* (2012) 97(4):1250–7. doi: 10.1210/jc.2011-1546

26. Huang H, Xu S, Wang X, Liu S, Liu J. Patient age is significantly related to distant metastasis of papillary thyroid microcarcinoma. *Front Endocrinol* (2021) 12. doi: 10.3389/fendo.2021.748238

27. Ito Y, Miyauchi A, Kihara M, Higashiyama T, Kobayashi K, Miya A. Patient age is significantly related to the progression of papillary microcarcinoma of the thyroid under observation. *Thyroid* (2014) 24(1):27–34. doi: 10.1089/thy.2013.0367

28. Hsu YC, Lee JJ, Chien MN, Chen MJ, Leung CH, Cheng SP. Is papillary thyroid microcarcinoma a biologically different disease? a propensity score-matched analysis. *J Surg Oncol* (2019) 120(6):1023–30. doi: 10.1002/jso.25670

29. So YK, Kim MW, Son YI. Multifocality and bilaterality of papillary thyroid microcarcinoma. *Clin Exp Otorhinol* (2015) 8(2):174–8. doi: 10.3342/ceo.2015.8.2.174

30. Nagaoka R, Ebina A, Toda K, Jikuzono T, Saitou M, Sen M, et al. Multifocality and progression of papillary thyroid microcarcinoma during active surveillance. *World J Surg* (2021) 45(9):2769–76. doi: 10.1007/s00268-021-06185-2

31. Sugitani I, Ito Y, Takeuchi D, Nakayama H, Masaki C, Shindo H, et al. Indications and strategy for active surveillance of adult low-risk papillary thyroid microcarcinoma: Consensus statements from the Japan association of endocrine surgery task force on management for papillary thyroid microcarcinoma. *Thyroid* (2021) 31(2):183–92. doi: 10.1089/thy.2020.0330

32. Sugitani I, Toda K, Yamada K, Yamamoto N, Ikenaga M, Fujimoto Y. Three distinctly different kinds of papillary thyroid microcarcinoma should be recognized: Our treatment strategies and outcomes. *World J Surg* (2010) 34(6):1222–31. doi: 10.1007/s00268-009-0359-x

33. Nakamura T, Miyauchi A, Ito Y, Ito M, Kudo T, Tanaka M, et al. Quality of life in patients with low-risk papillary thyroid microcarcinoma: Active surveillance versus immediate surgery. *Endocr Pract* (2020) 26(12):1451–7. doi: 10.4158/EP-2020-0201

34. Hay ID, Hutchinson ME, Gonzalez-Losada T, McIver B, Reinalda ME, Grant CS, et al. Papillary thyroid microcarcinoma: A study of 900 cases observed in a 60-year period. *Surgery* (2008) 144(6):980–7; discussion 7-8. doi: 10.1016/j.surg.2008.08.035

35. Zhang H, Zheng X, Liu J, Gao M, Qian B. Active surveillance as a management strategy for papillary thyroid microcarcinoma. *Cancer Biol Med* (2020) 17(3):543–54. doi: 10.20892/j.issn.2095-3941.2019.0470

36. Matulewicz RS, Weiner AB, Schaeffer EM. Active surveillance for prostate cancer. *Jama* (2017) 318(21):2152. doi: 10.1001/jama.2017.17222

frontiers | Frontiers in Endocrinology

TYPE Original Research
PUBLISHED 11 August 2022
DOI 10.3389/fendo.2022.960682

OPEN ACCESS

EDITED BY
Jose Federico Carrillo,
National Institute of Cancerology (INCAN), Mexico

REVIEWED BY
Khawla S. Al-Kuraya,
King Faisal Specialist Hospital and Research Centre, Saudi Arabia
Li Zhu,
Shanghai Jiao Tong University, China

*CORRESPONDENCE
Hengqiang Zhao
zhaochewh@whu.edu.cn
Yiping Gong
gongyp@whu.edu.cn

SPECIALTY SECTION
This article was submitted to Thyroid Endocrinology, a section of the journal Frontiers in Endocrinology

RECEIVED 03 June 2022
ACCEPTED 21 July 2022
PUBLISHED 11 August 2022

CITATION
Zhao H and Gong Y (2022) Radioactive iodine in low- to intermediate-risk papillary thyroid cancer. *Front. Endocrinol.* 13:960682. doi: 10.3389/fendo.2022.960682

Radioactive iodine in low- to intermediate-risk papillary thyroid cancer

Hengqiang Zhao* and Yiping Gong*

Department of Breast and Thyroid Surgery, Renmin Hospital of Wuhan University, Wuhan, China

It remains controversial whether papillary thyroid cancer (PTC) patients with low- to intermediate-risk disease should receive radioactive iodine (RAI) after total thyroidectomy (TT). We aim to identify those who might benefit from RAI treatment in PTC patients with cervical nodal metastasis after TT. Patients were divided into TT and TT+RAI groups from the Surveillance, Epidemiology, and End Results (SEER) database (2004–2018). Overall survival (OS) and cancer-specific survival (CSS) were compared, and propensity score matching (PSM) was performed between groups. A total of 15,179 patients were enrolled, including 3,387 (22.3%) who underwent TT and 11,792 (77.7%) who received TT+RAI. The following characteristics were more likely to present in the TT+RAI group: multifocality, capsular extension, T3, N1b, and more metastatic cervical lymph nodes. RAI was associated with better OS in low- to intermediate-risk PTC patients in the multivariate Cox regression model. The subgroup analysis showed that RAI predicted better OS in patients ≥55 years, American Joint Committee on Cancer (AJCC) stage II, and capsular extension with a hazard ratio (HR) (95% CI) of 0.57 (0.45–0.72), 0.57 (0.45–0.72), and 0.68 (0.51–0.91), respectively. However, RAI failed to improve the prognoses of patients with age <55 years, AJCC stage I, PTC ≤1 cm, and capsular invasion. In the PSM cohort with 3,385 paired patients, TT+RAI treatment predicted better OS compared with TT alone. In addition, TT+RAI predicted better OS in patients with metastatic cervical lymph nodes ≥2, multifocality, extracapsular extension, and American Thyroid Association (ATA) intermediate risk. In conclusion, RAI was associated with better OS in low- to intermediate-risk PTC patients with age ≥55 years, multifocality, extrathyroidal extension, and ATA intermediate risk. However, the survival benefit from RAI may be limited in patients with AJCC stage I, PTC ≤1 cm, unifocality, capsular invasion, and ATA low-risk diseases; these patients even showed pathological cervical lymph node metastasis.

KEYWORDS

papillary thyroid carcinoma, total thyroidectomy, radioactive iodine, prognosis, propensity score matching

Introduction

The incidence of papillary thyroid carcinoma (PTC) has increased substantially in recent decades (1). PTC is the most frequent subtype of thyroid cancer, accounting for more than 90% of all thyroid cancers. The standard treatment toward PTC includes thyroid surgery, thyrotropin inhibition, and radioactive iodine (RAI) (2). Thyroidectomy and thyroid hormone therapy are routinely performed on PTC patients. However, the administration of RAI is mainly based on postoperative risk stratification.

RAI is routinely recommended for high-risk PTC patients after total thyroidectomy (TT), while RAI is not recommended for papillary thyroid microcarcinoma (PTMC) patients in the absence of other adverse features according to the American Thyroid Association (ATA) guidelines (3). More specifically, patients with gross extrathyroidal extension and distant metastases were recommended for RAI, while patients with PTMC in the absence of cervical lymph node and distant metastases were not recommended for RAI therapy (3).

However, PTC patients with low to intermediate risk are not routinely recommended for RAI for conflicting observational evidence, and thus more research is needed to uncover the therapeutic efficacy in various subgroups of patients in the ATA low- to intermediate-risk category (3, 4). In the present study, we aimed to investigate the effect of RAI on the prognosis of PTC patients with cervical lymph node metastasis after TT. We collected the data from the largest public database and balanced the variables between groups using propensity score matching (PSM) method. The present study provided new evidence for better treatment of PTC.

Patients and methods

Ethics statement

Patients were obtained from the Surveillance, Epidemiology, and End Results (SEER) database from 2004 to 2018 (SEERStat user name: 21208-Nov2020). The SEER database collected patients with deidentified information; thus, this study was granted exempt status by our institutional review board.

Study population

The SEER*Stat Database named "Incidence-SEER Research Plus Data, 18 Registries, Nov 2020 Sub (2000–2018)" was selected for the following research. The exclusion criteria were as follows: patients with multiple (≥2) primary tumors, age <18 years, non-positive histology, chemotherapy, and distant metastasis. All patients underwent TT and cervical lymph node dissection. Patients with T4 were excluded. In the present study, tumor extrathyroidal extension represents those with minimal extrathyroidal extension including strap muscles and pericapsular soft tissue. Only patients with cervical lymph node metastasis were included, and cervical lymph node metastases were categorized into N1a (central compartment lymph node metastases), N1b (lateral neck lymph node metastases), and N1NOS. Patients with unknown or indefinite information on the included variables such as tumor number, capsular extension, tumor stage, T/N stage, RAI therapy, cause-specific death, lymph node examined, and positive lymph nodes were excluded. Patients with International Classification of Diseases for Oncology (third edition) codes of 8050, 8260, 8340, 8341, 8342, 8343, 8344, and 8350 were enrolled. Tumor stage was based on the American Joint Committee on Cancer (AJCC) eighth edition. Patients were divided into three races: White, Black, and Other (Asian or Pacific Islander and American Indian/Alaska Native).

Statistical analysis

The chi-square test, Mann–Whitney *U* test, and Student's t-test were used to analyze the category variables, data with skewed distribution (age and year of diagnosis), and the number of lymph nodes between groups, respectively. Kaplan–Meier curves of cancer-specific survival (CSS) and overall survival (OS) were analyzed using log-rank test. Risk factors for CSS and OS were estimated by Cox proportional hazards model with hazard ratio (HR) and a 95% confidence interval (CI).

PSM analysis was performed between groups to balance the statistical differences of the clinicopathologic features such as year of diagnosis, multifocality, capsular extension, T/N stage, and positive regional lymph nodes between TT and TT+RAI groups. PSM of 1:1 matching with a caliper of 0.1 was selected using R software (ver. 3.3.3) as we previously described (5). Two-sided $P < 0.05$ was considered statistically significant.

Results

Patient characteristics

The flowchart of the selection process was shown in Figure 1. Finally, a total of 15,179 patients were enrolled, including 3,387 (22.3%) with TT alone and 11,792 (77.7%) receiving additional RAI therapy (Table 1). The following characteristics of patients were more likely to present in the TT+RAI group compared with the TT group: multifocality, extracapsular extension, T3, N1b, more cervical lymph node examined, and more metastatic cervical lymph nodes (Table 1).

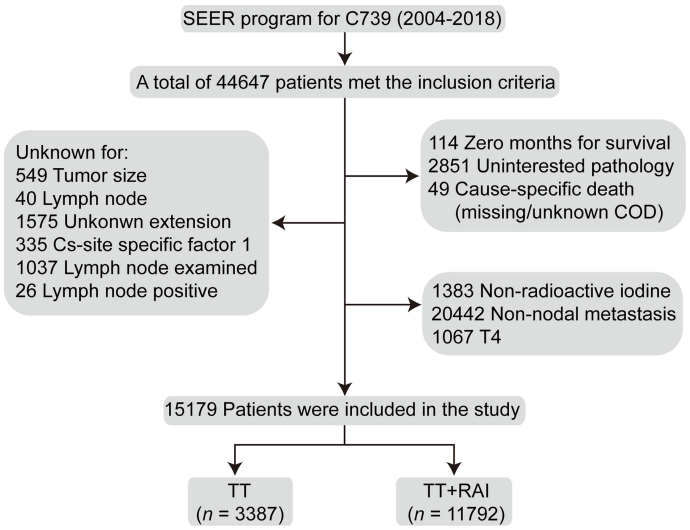

FIGURE 1
Flowchart of the selection process of the patients who underwent TT and additional RAI treatment from the Surveillance, Epidemiology, and End Results database. TT, total thyroidectomy; RAI, radioactive iodine.

Predictors for cancer-specific survival and overall survival of patients with papillary thyroid microcarcinoma

After adjustment for patient age, year of diagnosis, sex, race, capsular extension, multifocality, T/N stage, cervical lymph node examined, and positive cervical lymph nodes in the multivariate Cox regression model, RAI treatment was associated with better OS with an HR (95% CI) of 0.66 (0.54–0.80), while RAI failed to improve CSS with an HR (95% CI) of 0.89 (0.62–1.27) compared with TT treatment alone (Table 2).

Subgroup analysis

The subgroup analyses stratified by the clinicopathologic characteristics were performed to assess the robustness of the results. TT+RAI treatment was associated with better OS in most subgroups (Table 3). However, RAI use was not associated with better OS in patients with age <55 years, black patients, AJCC stage I, PTMC, and capsular invasion with HRs (95% CI) of 0.88 (0.62–1.26), 0.95 (0.30–2.97), 0.88 (0.62–1.26), 0.79 (0.49–1.25), and 0.97 (0.42–2.24), respectively, compared with TT alone. In addition, RAI was not associated with better CSS in the subgroup analyses. We further found that PTMC patients failed to gain better CSS and OS with the addition of RAI treatment. Patients were divided into low-risk and intermediate-risk subgroups according to ATA risk stratification. Compared with TT alone, TT+RAI treatment was associated with better OS in ATA low-risk and intermediate-risk subgroups with HRs (95% CI) of 0.71 (0.51–0.97) and 0.63 (0.49–0.80), respectively (Table 3).

Kaplan–Meier curves before and after propensity score matching

Kaplan–Meier curves showed that RAI therapy was associated with better OS with an HR (95% CI) of 1.52 (1.23–1.88) before PSM (Figure 2A). We further divided patients into N1a and N1b subsets. Similarly, RAI was associated with better OS in patients with N1a with an HR (95% CI) of 1.39 (1.03-1.87) (Figure 2B), and in patients with N1b with an HR (95% CI) of 1.76 (1.23–2.53) (Figure 2C).

To increase the between-group comparability, we performed PSM analysis to balance the clinicopathologic characteristics between TT and TT+RAI groups. The PSM process yielded 3,385 paired patients. After PSM, the differences of baseline characteristics between the two groups were obviously reduced (Supplementary Table S1). After PSM, RAI was associated with better OS with an HR (95% CI) of 1.47 (1.15–1.88) (Figure 3A). Consistently, RAI was associated with better OS in N1a patients with an HR (95% CI) of 1.48 (1.03–2.12) and in N1b patients with an HR (95% CI) of 1.49 (1.01–2.20) (Figures 3B, C).

In the PSM cohort, we further stratified patients into one metastatic lymph node vs. ≥2 metastatic lymph nodes, unifocality vs. multifocality, extracapsular extension vs. intrathyroidal and capsular invasion tumor. There were no significant statistical differences in OS between TT+RAI and TT groups in patients

TABLE 1 Characteristics of the study population (n = 15,179).

Variables	TT (n = 3,387	TT+RAI (n = 11,792)	P-value
Age	41 (32–52)	41 (32–52)	0.426
<55 years	2,698 (79.7)	9,475 (80.4)	0.372
≥55 years	689 (20.3)	2,317 (19.6)	
Year of diagnosis	2011 (2008–2013)	2011 (2008–2013)	0.036
Sex			
Men	924 (27.3)	3,400 (28.8)	0.078
Women	2,463 (72.7)	8,392 (71.2)	
Race			
White	2,832 (83.6)	9,795 (83.1)	0.410
Black	104 (3.1)	334 (2.8)	
Other	451 (13.3)	1,663 (14.1)	
Multifocality			
No	1,541 (45.5)	5,017 (42.5)	0.002
Yes	1,846 (54.5)	6,775 (57.5)	
Capsular extension			
Intrathyroidal tumor	2,161 (63.8)	6,670 (56.6)	<0.001
Capsular invasion	272 (8.0)	905 (7.7)	
Extracapsular extension	954 (28.2)	4,217 (35.8)	
AJCC stage eighth			
I	2,698 (79.7)	9,475 (80.4)	0.372
II	689 (20.3)	2,317 (19.6)	
T stage			
T1	1,589 (46.9)	4,836 (41.0)	<0.001
T2	654 (19.3)	2,187 (18.5)	
T3	1,144 (33.8)	4,769 (40.4)	
N stage			
N1a	2,055 (60.7)	6,821 (57.8)	<0.001
N1b	937 (27.7)	3,886 (33.0)	
N1NOS	395 (11.7)	1,085 (9.2)	
CLN examined	13.5 ± 16.9	14.9 ± 17.9	<0.001
CLN positive	4.7 ± 6.0	5.4 ± 6.2	<0.001
Number of deaths			
CSS	40	126	–
OS	149	345	–

Age and year of diagnosis were expressed as median with interquartile range; other variables were expressed as n (%).
TT, total thyroidectomy; RAI, radioactive iodine; CLN, cervical lymph node; CSS, cancer-specific survival; OS, overall survival.

with one metastatic lymph node, unifocality, and intrathyroidal and capsular invasion tumor (Figures 4A, C, E). Compared with TT +RAI, TT alone was associated with poorer OS in patients with ≥2 metastatic lymph nodes, multifocality, and extracapsular extension with HRs (95% CI) of 1.51 (1.11–2.05), 1.70 (1.22–2.37), and 1.54 (1.06–2.25), respectively (Figures 4B, D, F). We further divided patients into ATA low-risk vs. ATA intermediate-risk subgroups. In the ATA low-risk patients, there was no significant difference in OS between patients with TT and TT+RAI with an HR (95% CI) of 1.43 (0.96–2.13) (Figure 5A). In the ATA intermediate-risk subgroup, TT was associated with poorer OS compared with TT +RAI treatment with an HR (95% CI) of 1.52 (1.11–2.07) (Figure 5B).

Discussion

In this study, we examined the effect of RAI treatment on the prognoses of PTC patients who underwent TT and cervical lymph node dissection. All of the enrolled patients showed cervical lymph node metastasis and were not diseases of T4 and/or distant metastasis. We found that RAI+TT treatment was associated with better OS compared with TT alone before and after PSM in the low- to intermediate-risk PTC patients. The subgroup analyses showed that RAI was associated with better OS in patients with age ≥55 years, AJCC stage II, and extracapsular extension. However, RAI failed to improve prognoses in patients with age <55 years, AJCC stage I, and capsular invasion compared with the TT group. In the PSM cohort, Kaplan–Meier curves showed that RAI treatment was associated with better OS in patients with ≥2 metastatic lymph nodes, multifocality, extracapsular extension, and ATA intermediate risk.

The difficulty in performing RAI is to identify patients who are most likely to benefit from RAI therapy while avoiding unnecessary exposure to ionizing radiation in the majority of low- to intermediate-risk thyroid cancer patients (6). Except for the strong recommendation for RAI treatment in patients with gross tumor extension and distant metastases and non-recommendation for RAI in PTMC patients without risk clinicopathologic features, RAI use remains controversial in most cases (7). Consistent with the ATA recommendation, our study found that PTMC patients did not benefit from RAI administration, while patients with extrathyroidal extension had better OS with the addition of RAI. A previous study showed that differentiated thyroid cancer ≤2 cm without risk factors such as multifocality, extrathyroidal extension, lymph node, and/or distant metastasis may exempt from RAI and receive less extensive surgery (8).

In our study, about 80% of patients were AJCC stage I (eighth edition), and these patients failed to benefit from RAI administration. Of note, these patients were those <55 years for the enrollment of patients with nodal metastasis in our study. On the contrary, patients with older age (≥55 years) benefited from RAI therapy with the improvement of OS, which may reflect the survival benefit from RAI in patients with AJCC stage II. One important finding in our study was that both patients with N1a and N1b benefited from RAI therapy. In clinical practice, the proportion of N1b subtype was about 13.5% in PTC patients (9), and about 50% of PTC patients present with pathological N1a disease (10). Increasing metastatic lymph nodes were associated with compromised survival in PTC patients (11). Therefore, we can expect that a change point of the number of metastatic lymph nodes in the central compartment may exist, and patients

TABLE 2 Multivariate Cox regression analysis for cancer-specific survival and overall survival of PTC patients.

Category	Cancer-specific survival		Overall survival	
	HR (95% CI)	*P*-value	HR (95% CI)	*P*-value
Age	1.11 (1.10–1.12)	<0.001	1.10 (1.09–1.10)	<0.001
Year of diagnosis	0.94 (0.89–0.99)	0.030	0.96 (0.93–0.99)	0.012
Sex				
Men	Ref		Ref	
Women	0.84 (0.61–1.16)	0.286	0.58 (0.48–0.69)	<0.001
Race				
White	Ref		Ref	
Black	2.07 (0.96–4.47)	0.063	1.83 (1.18–2.85)	0.007
Other	0.99 (0.64–1.53)	0.950	0.78 (0.58–1.04)	0.090
Multifocality				
No	Ref		Ref	
Yes	0.78 (0.57–1.06)	0.108	0.97 (0.81–1.16)	0.748
Capsular extension				
Intrathyroidal tumor	Ref		Ref	
Capsular invasion	1.22 (0.62–2.41)	0.566	1.03 (0.71–1.49)	0.870
Extracapsular extension	0.66 (0.38–1.14)	0.132	0.85 (0.57–1.27)	0.431
T stage				
T1	Ref		Ref	
T2	2.60 (1.45–4.65)	0.001	1.05 (0.79–1.39)	0.757
T3	6.25 (3.26–11.97)	<0.001	1.67 (1.12–2.51)	0.013
N stage				
N1a	Ref		Ref	
N1b	1.62 (1.11–2.37)	0.013	1.10 (0.89–1.37)	0.371
N1NOS	1.86 (1.15–3.00)	0.011	1.16 (0.86–1.55)	0.332
RAI				
No	Ref		Ref	
Yes	0.89 (0.62–1.27)	0.524	0.66 (0.54–0.80)	<0.001
CLN examined	1.00 (0.99–1.01)	0.752	1.00 (0.99–1.01)	0.907
CLN positive	1.05 (1.02–1.08)	<0.001	1.04 (1.02–1.06)	<0.001

PTC, papillary thyroid cancer; HR (95% CI), hazard ratio (95% confidence interval); RAI, radioactive iodine; CLN, cervical lymph node.

with more metastatic lymph nodes were more likely to benefit from RAI treatment. In the PSM cohort, the mean and median number of metastatic lymph nodes were 5.2 and 3.0, respectively. We found that PTC patients with ≥2 metastatic lymph nodes can benefit from RAI use, while patients with only one metastatic lymph node failed to benefit from RAI treatment. This should be validated in the following studies. A recent study by Sun et al. (12) found that RAI therapy predicted better OS in both N1a and N1b subtypes in the multivariate Cox regression model, which was consistent with our results. However, they did not examine the robustness of results stratified by N1a and N1b subsets in a PSM cohort (12). Wang et al. (13) found that there was no difference in the 5-year central compartment nodal recurrence-free survival between PTC patients treated with RAI and those without RAI treatment. However, the 104 patients and the median follow-up of 53 months may be limited in the evaluation of the recurrence risk of PTC (13). A recent study showed that the recurrence-free survival curve of the intermediate-risk PTC patients who received postoperative RAI therapy (n = 208) did not differ significantly from that of the patients who did not receive it (n = 141), especially for patients with negative extranodal spread and low number (<5) of metastatic lymph nodes (14). However, they did not focus on OS of PTC patients.

New evidence showed that RAI utilization declined from 61.0% in 2004 to 43.9% in 2016, especially in patients with T1a (tumor ≤1 cm in diameter), N0/X, M0 PTC without extrathyroidal extension (34.8% in 2004 to 9.5% in 2015) in the United States (15). Similarly, a recent study showed that the declining use of RAI represented the most pronounced change in the management of PTCs <4 cm (44%–18% during the period 2006–2018), including PTMC (26%–6% during the period 2007–

TABLE 3 Subgroup analysis for cancer-specific survival and overall survival of TT with RAI vs. TT alone by multivariate Cox regression analysis.

Category	Cancer-specific survival		Overall survival	
	HR (95% CI)	*P*-value	HR (95% CI)	*P*-value
Age				
<55 years	1.37 (0.57–3.29)	0.478	0.88 (0.62–1.26)	0.493
≥55 years	0.72 (0.48–1.07)	0.102	0.57 (0.45–0.72)	<0.001
Sex				
Men	0.78 (0.46–1.32)	0.354	0.60 (0.46–0.79)	<0.001
Women	0.98 (0.60–1.62)	0.946	0.71 (0.54–0.95)	0.018
Race				
White	0.87 (0.58–1.29)	0.481	0.64 (0.52–0.78)	<0.001
Black	0.74 (0.07–7.74)	0.802	0.95 (0.30–2.97)	0.927
Multifocality				
No	0.95 (0.56–1.64)	0.864	0.67 (0.49–0.91)	0.009
Yes	0.85 (0.52–1.38)	0.508	0.65 (0.50–0.84)	0.001
Capsular extension				
Intrathyroidal tumor	0.81 (0.43–1.53)	0.523	0.61 (0.46–0.81)	0.001
Capsular invasion	3.21 (0.37–27.85)	0.290	0.97 (0.42–2.24)	0.949
Extracapsular extension	0.81 (0.51–1.27)	0.353	0.68 (0.51–0.91)	0.009
AJCC stage eighth				
I	1.37 (0.57–3.29)	0.478	0.88 (0.62–1.26)	0.493
II	0.72 (0.48–1.07)	0.102	0.57 (0.45–0.72)	<0.001
T stage				
PTMC	1.44 (0.41–5.10)	0.568	0.79 (0.49–1.25)	0.307
T1	1.07 (0.39–2.92)	0.890	0.71 (0.51–0.99)	0.045
T2	0.89 (0.32–2.48)	0.829	0.53 (0.32–0.88)	0.015
T3	0.82 (0.54-1.25)	0.351	0.67 (0.51–0.88)	0.004
N stage				
N1a	1.47 (0.74–2.93)	0.270	0.72 (0.54–0.95)	0.021
N1b	0.64 (0.39–1.04)	0.072	0.59 (0.43–0.81)	0.001
ATA risk stratification				
ATA low risk	1.83 (0.71–4.78)	0.212	0.71 (0.51–0.97)	0.032
ATA intermediate risk	0.75 (0.51–1.11)	0.148	0.63 (0.49–0.80)	<0.001

HRs were adjusted for age, year of diagnosis, sex, race, multifocality, capsular extension, T/N stage, RAI, and number of metastatic lymph nodes.
RAI, radioactive iodine; TT, total thyroidectomy; PTC, papillary thyroid cancer; HR (95% CI), hazard ratio (95% confidence interval); PTMC, papillary thyroid microcarcinoma; ATA, American Thyroid Association.

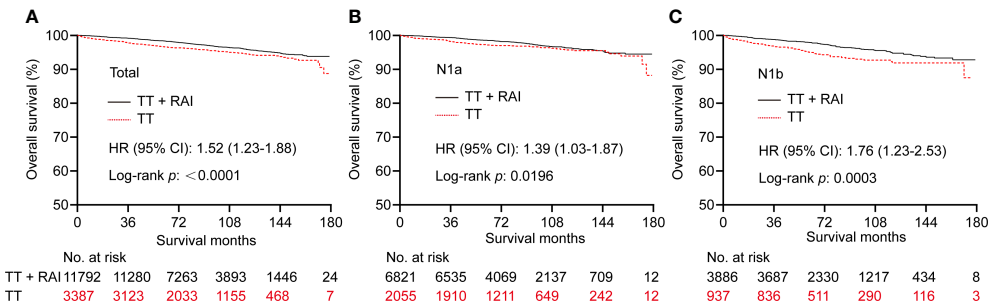

FIGURE 2
Kaplan–Meier curves of OS in PTC patients who underwent TT vs. TT+RAI before PSM in total patients **(A)**, N1a patients **(B)**, and N1b patients **(C)**. OS, overall survival; PTC, papillary thyroid carcinoma; TT, total thyroidectomy; RAI, radioactive iodine; PSM, propensity score matching.

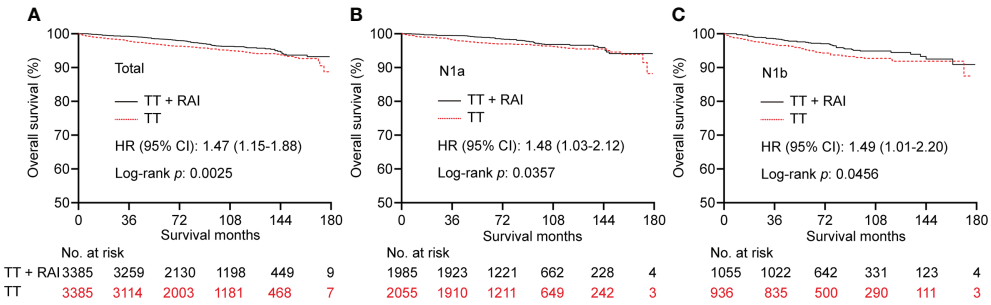

FIGURE 3
Kaplan–Meier curves of OS in PTC patients who underwent TT vs. TT+RAI after PSM in total patients **(A)**, N1a patients **(B)**, and N1b patients **(C)**. OS, overall survival; PTC, papillary thyroid carcinoma; TT, total thyroidectomy; RAI, radioactive iodine; PSM, propensity score matching.

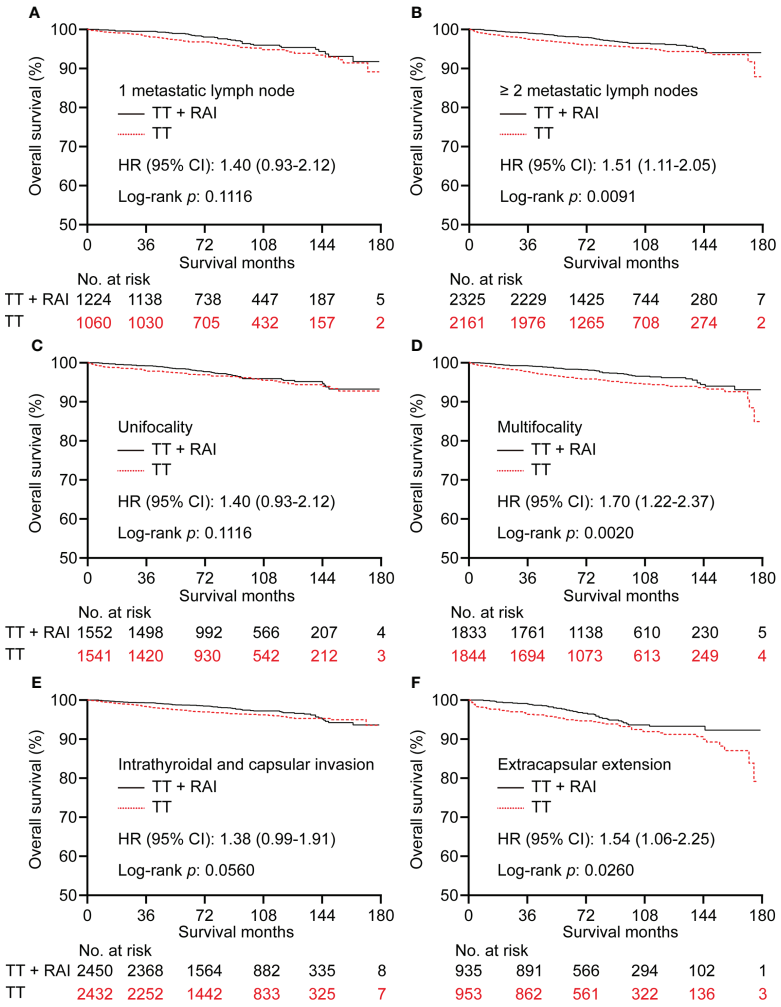

FIGURE 4
Kaplan–Meier curves of OS in PTC patients who underwent TT vs. TT+RAI after PSM stratified by the number of metastatic lymph nodes **(A, B)**, tumor number **(C, D)**, and tumor extension **(E, F)**. OS, overall survival; PTC, papillary thyroid carcinoma; TT, total thyroidectomy; RAI, radioactive iodine; PSM, propensity score matching.

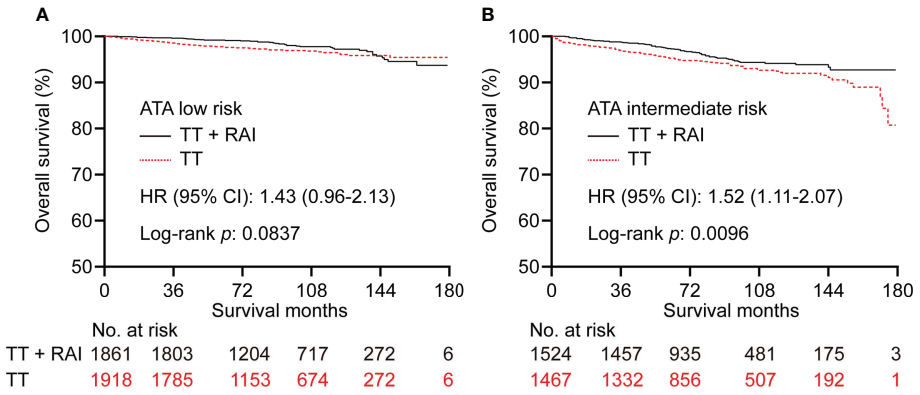

FIGURE 5
Kaplan–Meier curves of OS in PTC patients underwent TT vs. TT+RAI after PSM in low-risk **(A)** and intermediate-risk **(B)** patients stratified by the ATA risk stratification. OS, overall survival; PTC, papillary thyroid carcinoma; TT, total thyroidectomy; RAI, radioactive iodine; PSM, propensity score matching; ATA, American Thyroid Association.

2018). For pediatric patients (<20 years), use of RAI peaked in 2009 (59%), then decreased markedly to 11% (2018) (16). A recent survey showed that more than half of the patients (55.8%) feel that they did not have an RAI choice, while the majority of patients (75.9%) received RAI, suggesting a need for more shared decision-making to reduce overtreatment (17). Nearly 25% of low-risk PTC patients (defined T1 without metastasis) received RAI. Predictors of overtreatment with RAI included age <45 years, age 45–64 years, male sex, Hispanic and Asian race, and extensive lymphadenectomy (18). Efforts to reduce the overuse of RAI in low-risk thyroid cancer should include interventions targeted toward physicians (19). It seems apparent that RAI administration changes with the implementation and dissemination of evidence-based guidelines toward PTC with RAI use, and prudent use of RAI should be considered in low-risk patients (20).

Our study has several advantages compared with previous studies. Firstly, we used the largest database with more pathological variables included such as tumor multifocality, extrathyroidal extension, and metastatic lymph nodes, and variables with unknown information were excluded compared with previous studies with the same topic (12, 21). In addition, we adopted the updated AJCC stage to assess the therapeutic effect of RAI use for the first time. We further validated the limited survival benefit in PTMC patients, which might reduce the potentially unnecessary RAI use in the majority of PTMC patients. We also demonstrated that patients with minimal extrathyroidal extension gained better OS after RAI use. Additionally, we used the PSM analysis to balance the clinicopathologic differences between groups; this procedure improved the comparability and reliability of the results. However, some limitations must be acknowledged. The retrospective design prevented proving causality between RAI use and the better prognosis of PTC patients. However, the population-based nature may reflect the "real-world" management outcomes found outside of the well-controlled trials. In addition, the SEER database cannot evaluate patients' comorbidities and disease recurrence. Additionally, the dosages of RAI were not recorded in the SEER database. We therefore cannot determine the optimal dosages of RAI that will benefit PTC patients most. Last but not least, TT+RAI treatment was not associated with better CSS compared with TT alone in this study. This may be caused by the excellent prognosis of PTC and limited follow-up period. RAI treatment should be narrowed down to only those cases that will truly benefit from RAI treatment. Nowadays, the usual medical practice is to conduct a genetic search for drug therapy and decide whether to treat the patient according to the results of the companion diagnosis. The amount of sodium/iodide symporter (NIS) expression in tumor tissue and the presence or absence of genetic abnormalities that could alter NIS expression should be used as indicators to determine future indications for RAI treatment (22). Apart from postoperative risk assessment, radioactive iodine imaging, preferences of local disease management, assessment of potential side effect, and patients' preferences are additional key elements that must be considered when deciding whether an individual patient could benefit from RAI treatment (23).

In conclusion, this PSM-based study suggested that RAI treatment predicted better OS in low- to intermediate-risk PTC patients, especially in those with advanced diseases like AJCC stage II, age ≥55 years, multifocality, extracapsular extension, and ATA intermediate-risk, while RAI may not bring survival

benefit in patients with age <55 years, AJCC stage I, capsular invasion, PTMC, and ATA low-risk diseases. A large cohort study with a longer follow-up period is warranted to confirm the present findings.

Data availability statement

The original contributions presented in the study are included in the article/Supplementary Material. Further inquiries can be directed to the corresponding authors.

Ethics statement

Ethical review and approval was not required for the study on human participants in accordance with the local legislation and institutional requirements. Written informed consent for participation was not required for this study in accordance with the national legislation and the institutional requirements.

Author contributions

HZ: conception, data acquisition. HZ and YG: data analysis and drafting the article. HZ and YG: revised it critically for important intellectual content. HZ: investigation, project administration, and supervision. Both authors read and approve the final version of the manuscript.

Funding

This study was supported by Open Foundation of Hubei Key Laboratory of Renmin Hospital of Wuhan University (grant number 2021KFY009).

Conflict of interest

The authors declare that the research was conducted in the absence of any commercial or financial relationships that could be construed as a potential conflict of interest.

Publisher's note

Supplementary material

The Supplementary Material for this article can be found online at: https://www.frontiersin.org/articles/10.3389/fendo.2022.960682/full#supplementary-material

References

1. Lim H, Devesa SS, Sosa JA, Check D, Kitahara CM. Trends in thyroid cancer incidence and mortality in the united states, 1974-2013. *JAMA* (2017) 317:1338–48. doi: 10.1001/jama.2017.2719

2. Cabanillas ME, McFadden DG, Durante C. Thyroid cancer. *Lancet* (2016) 388:2783–95. doi: 10.1016/s0140-6736(16)30172-6

3. Haugen BR, Alexander EK, Bible KC, Doherty GM, Mandel SJ, Nikiforov YE, et al. 2015 American Thyroid association management guidelines for adult patients with thyroid nodules and differentiated thyroid cancer: The American thyroid association guidelines task force on thyroid nodules and differentiated thyroid cancer. *Thyroid* (2016) 26:1–133. doi: 10.1089/thy.2015.0020

4. James DL, Ryan EJ, Davey MG, Quinn AJ, Heath DP, Garry SJ, et al. Radioiodine remnant ablation for differentiated thyroid cancer: A systematic review and meta-analysis. *JAMA Otolaryngol Head Neck Surg* (2021) 147:544–52. doi: 10.1001/jamaoto.2021.0288

5. Zhao H. The prognosis of invasive ductal carcinoma, lobular carcinoma and mixed ductal and lobular carcinoma according to molecular subtypes of the breast. *Breast Cancer* (2020) 28:187–95. doi: 10.1007/s12282-020-01146-4

6. Tuttle RM, Sabra MM. Selective use of RAI for ablation and adjuvant therapy after total thyroidectomy for differentiated thyroid cancer: a practical approach to clinical decision making. *Oral Oncol* (2013) 49:676–83. doi: 10.1016/j.oraloncology.2013.03.444

7. Mayson SE, Chan CM, Haugen BR. Tailoring the approach to radioactive iodine treatment in thyroid cancer. *Endocr Relat Cancer* (2021) 28:T125–40. doi: 10.1530/erc-21-0161

8. Momesso DP, Vaisman F, Caminha LS, Pessoa CH, Corbo R, Vaisman M. Surgical approach and radioactive iodine therapy for small well-differentiated thyroid cancer. *J Endocrinol Invest* (2014) 37:57–64. doi: 10.1007/s40618-013-0015-z

9. Zhao H, Huang T, Li H. Risk factors for skip metastasis and lateral lymph node metastasis of papillary thyroid cancer. *Surgery* (2019) 166:55–60. doi: 10.1016/j.surg.2019.01.025

10. Zhao H, Li H, Huang T. High iodine intake and central lymph node metastasis risk of papillary thyroid cancer. *J Trace Elem Med Biol* (2019) 53:16–21. doi: 10.1016/j.jtemb.2019.01.015

11. Adam MA, Pura J, Goffredo P, Dinan MA, Reed SD, Scheri RP, et al. Presence and number of lymph node metastases are associated with compromised survival for patients younger than age 45 years with papillary thyroid cancer. *J Clin Oncol* (2015) 33:2370–5. doi: 10.1200/jco.2014.59.8391

12. Sun Y, Gong J, Guo B, Shang J, Cheng Y, Xu H. Association of adjuvant radioactive iodine therapy with survival in node-positive papillary thyroid cancer. *Oral Oncol* (2018) 87:152–7. doi: 10.1016/j.oraloncology.2018.10.041

13. Wang LY, Palmer FL, Migliacci JC, Nixon IJ, Shaha AR, Shah JP, et al. Role of RAI in the management of incidental N1a disease in papillary thyroid cancer. *Clin Endocrinol (Oxf)* (2016) 84:292–5. doi: 10.1111/cen.12828

14. Han K, Noh HM, Jeong HM, Lim YC. Is postoperative adjuvant radioactive iodine ablation therapy always necessary for intermediate-risk papillary thyroid cancer patients with central neck metastasis? *Ann Surg Oncol* (2021) 28:7533–44. doi: 10.1245/s10434-021-10164-1

15. Jacobs D, Breen CT, Pucar D, Holt EH, Judson BL, Mehra S. Changes in population-level and institutional-level prescribing habits of radioiodine therapy for papillary thyroid cancer. *Thyroid* (2021) 31:272–9. doi: 10.1089/thy.2020.0237

16. Pasqual E, Sosa JA, Chen Y, Schonfeld SJ, Berrington de Gonzalez A, Kitahara CM. Trends in the management of localized papillary thyroid carcinoma in the united states (2000-2018). *Thyroid* (2022) 32:397–410. doi: 10.1089/thy.2021.0557

17. Wallner LP, Reyes-Gastelum D, Hamilton AS, Ward KC, Hawley ST, Haymart MR. Patient-perceived lack of choice in receipt of radioactive iodine for treatment of differentiated thyroid cancer. *J Clin Oncol* (2019) 37:2152–61. doi: 10.1200/JCO.18.02228

18. Moten AS, Zhao H, Willis AI. The overuse of radioactive iodine in low-risk papillary thyroid cancer patients. *Surg Oncol* (2019) 29:184–9. doi: 10.1016/j.suronc.2019.05.011

19. Wallner LP, Banerjee M, Reyes-Gastelum D, Hamilton AS, Ward KC, Lubitz C, et al. Multilevel factors associated with more intensive use of radioactive iodine for low-risk thyroid cancer. *J Clin Endocrinol Metab* (2021) 106:e2402–12. doi: 10.1210/clinem/dgab139

20. Sacks W, Wong RM, Bresee C, Braunstein GD. Use of evidence-based guidelines reduces radioactive iodine treatment in patients with low-risk differentiated thyroid cancer. *Thyroid* (2015) 25:377–85. doi: 10.1089/thy.2014.0298

21. Orosco RK, Hussain T, Noel JE, Chang DC, Dosiou C, Mittra E, et al. Radioactive iodine in differentiated thyroid cancer: a national database perspective. *Endocr Relat Cancer* (2019) 26:795–802. doi: 10.1967/s002449910500

22. Oh JM, Ahn BC. Molecular mechanisms of radioactive iodine refractoriness in differentiated thyroid cancer: Impaired sodium iodide symporter (NIS) expression owing to altered signaling pathway activity and intracellular localization of NIS. *Theranostics* (2021) 11:6251–77. doi: 10.7150/thno.57689

23. Tuttle RM, Ahuja S, Avram AM, Bernet VJ, Bourguet P, Daniels GH, et al. Controversies, consensus, and collaboration in the use of (131)I therapy in differentiated thyroid cancer: A joint statement from the American thyroid association, the European association of nuclear medicine, the society of nuclear medicine and molecular imaging, and the European thyroid association. *Thyroid* (2019) 29:461–70. doi: 10.1089/thy.2018.0597

frontiers | Frontiers in Endocrinology

TYPE Original Research
PUBLISHED 02 September 2022
DOI 10.3389/fendo.2022.948285

OPEN ACCESS

EDITED BY
Erivelto Martinho Volpi,
Centro de referencia no ensino do diagnóstico por imagem (CETRUS), Brazil

REVIEWED BY
Jing Li,
First Affiliated Hospital of China Medical University, China
Jufeng Xia,
The University of Tokyo, Japan
Yukun Li,
Third Hospital of Hebei Medical University, China
Kemal Beksac,
Dr. Abdurrahman Yurtaslan Ankara Oncology Training and Research Hospital, Turkey

*CORRESPONDENCE
Ling-Qing Yuan
allenylq@csu.edu.cn

SPECIALTY SECTION
This article was submitted to Cancer Endocrinology, a section of the journal Frontiers in Endocrinology

RECEIVED 19 May 2022
ACCEPTED 02 August 2022
PUBLISHED 02 September 2022

CITATION
Li C-C, Ullah MHE, Lin X, Shan S-K, Guo B, Zheng M-H, Wang Y, Li F and Yuan L-Q (2022) Identifying key genes of classic papillary thyroid cancer in women aged more than 55 years old using bioinformatics analysis. *Front. Endocrinol.* 13:948285. doi: 10.3389/fendo.2022.948285

Identifying key genes of classic papillary thyroid cancer in women aged more than 55 years old using bioinformatics analysis

Chang-Chun Li[1], Muhammad Hasnain Ehsan Ullah[1], Xiao Lin[2], Su-Kang Shan[1], Bei Guo[1], Ming-Hui Zheng[1], Yi Wang[1], Fuxingzi Li[1] and Ling-Qing Yuan[1]*

[1]National Clinical Research Center for Metabolic Diseases, Department of Metabolism and Endocrinology, The Second Xiangya Hospital, Central South University, Changsha, China, [2]Department of Radiology, The Second Xiangya Hospital, Central South University, Changsha, China

Background: The incidence rate of thyroid carcinoma (THCA) markedly increased in the recent few decades and has been likely over-diagnosed, especially papillary thyroid cancer (PTC) in women. However, the incidence of advanced-stage papillary thyroid cancer is also rising. According to earlier studies, tumors with identical pathology might have different clinical outcomes, which implies some variances in papillary thyroid cancer. Although the mortality of thyroid cancer has remained stable or declined, there is still an important problem in estimating whether it is benign or needs surgery for patients with papillary thyroid cancer.

Methods: After obtaining data from The Cancer Genome Atlas (TCGA) Project-THCA database by R package TCGA bio links, 18 samples (11 at stage IV as high-risk group and 7 at stage I as low-risk group) were obtained using survival package and edgeR to ensure differential expression; ClusterProfiler package was used to carry on gene set enrichment analysis and searched the possible pathways in the Kyoto Encyclopedia of Genes and Genomes (KEGG) database. STRING and Cytoscape were used to construct and modify the protein–protein interaction (PPI) network to get hub genes of differentially expressed genes. Next, the pROC package was used to get the receiver operating characteristic (ROC) curves of hub genes' disease-free survival (DFS). Then, transcription factors (TFs) and miRNAs of key genes were predicted by ENCORI and AnimalTFDB. In the end, TF–target genes–miRNA regulatory network was also constructed by Cytoscape.

Results: Our research obtained the top 9 candidate genes from the whole network (IFNA1, MRC1, LGALS3, LOX, POSTN, TIMP1, CD276, SDC4, and TLR2). According to the ROC results, TIMP1, LOX, CD276, IFNA1, TLR2, and POSTN were considered to play a more critical role in malignant papillary thyroid

cancer or immature cancer of papillary thyroid cancer. Our analysis concludes that TIMP1, LOX, CD276, IFNA1, TLR2, and POSTN are identified as thyroid cancer biomarkers, which lead to the different clinical courses of a woman older than 55 years old with papillary thyroid cancer. Especially CD276, POSTN, and IFNA1 may be considered as new biomarkers associated with the prognosis of thyroid cancer.

Conclusions: TIMP1, LOX, CD276, IFNA1, TLR2, and POSTN have different expressions in PTCs, which lead to the various clinical courses of a woman older than 55 years old with papillary thyroid cancer. Especially CD276, POSTN, and IFNA1 may be considered as new potential biomarkers associated with the prognosis of thyroid cancer. In addition, TF–miRNA–target gene regulatory network may help further reach for PTC.

KEYWORDS

thyroid carcinoma, R package, gene ontology, Kyoto Encyclopedia of Genes and Genomes, protein–protein interaction, biomarkers, prognosis thyroid carcinoma, prognosis

Introduction

The incidence rate of thyroid carcinoma (THCA) markedly increased in the recent few decades (1) and has been likely over-diagnosed because ultrasonography or other modern diagnostic techniques have been widely used to discover previously undetectable thyroid nodules (2). Differentiated thyroid cancer is the most common thyroid cancer, particularly the category of papillary thyroid cancer (PTC) in women diagnosed by methods such as fine-needle aspiration (FNA) after imaging tests. However, the incidence of advanced-stage PTC (large tumors and locally advanced and/or metastatic) rises (3). The fact that tumors with identical pathologies might have distinct clinical outcomes suggests some variances in PTC, according to previous studies (4, 5). Although the mortality of THCA has remained stable or declined, there is still an important problem in estimating if it is benign or needs surgery for patients with PTC.

Controversial issues in thyroid cancer management mainly focus on treatment options for different thyroid cancers (DTCs) (6). Recently, detecting genetic changes in thyroid cancer has been generally stressed and applied as an essential means to guide treatment (7). DNA sequencing technology has been frequently used to detect a different group of diagnoses. Bioinformatics technology has also been employed to identify those different gene expressions (DEGs). The BRAF and RAS family's mutations are usually found in THCA and mitogen-activated protein kinase (MAPK) cellular signaling pathway and PI3K/AKT/mTOR pathway (8, 9). Those findings have greatly improved our understanding of studying THCA with different clinical outcomes.

This research performed many analyses through a wide-ranging bioinformatics study to classify the critical hub gene in thyroid cancer with a poor prognosis. A total of 994 genes upregulated in the high-risk group were obtained from TCGA-THCA data by edgeR (10, 11). Then, GO and KEGG pathway enrichment and the construction of protein–protein interaction (PPI) network and survival analysis were performed in these differentially expressed genes (DEGs) (12–14). Finally, key genes, transcription factors, and miRNA relations that might be important in THCA with poor prognosis were identified.

Methods

Datasets selection and DEGs identification

The Cancer Genome Atlas (TCGA) research network has collected many public clinical and molecular profiling of more than 10,000 tumor patients across 33 different tumor types. We obtained the clinical and transcriptome profiling of THCA from the TCGA-THCA database by TCGA-biolinks packages, which provide several useful functions to search, download, and prepare TCGA samples for data analysis (15), using the following criteria: (A) PTC-classic/usual, (B) female, (C) age ≥55 years old, (D) datasets including stage I and IV samples, and (E) replicated samples value being saved with unique bcr patient barcode. Next, Cox proportional hazards model was performed by survival packages of R for those data, and the result was presented by forest plot packages (16, 17). Furthermore, the edgeR packages were

used to distinguish the DEGs in each sample in R (Version 4.1.2) (10, 11). The standard for DEGs has been considered a false discovery rate of <0.05. The groups' criteria were |log2FC (fold change)| ≥ 1.

GO and KEGG enrichment analyses of DEGs

Gene Ontology (GO) and Kyoto Encyclopedia of Genes and Genomes (KEGG) were performed to reveal the functional enrichment analysis of DEGs. BiomaRt packages that include over 800 different biological datasets spanning were used to convert gene ID from other types (18, 19). ClusterProfiler packages that automate enrichment analysis of gene clusters were used to progress GO enrichment analyses, which include cellular component (CC), biological process (BP), and molecular function (MF), and KEGG pathways analysis (20, 21). Finally, GOplot and ggplot2 packages were used to make figures of those results (22, 23).

PPI network construction

STRING (https://string-db.org/), an online database, was used to establish the protein–protein interaction (PPI) network of the candidate genes, which evaluates the interacting units with protein-coding gene loci (represented by their main, canonical protein isoform) (24), and the minimum required score was set as the medium confidence (0.400). Moreover, Cytoscape (Version 3.9.1) was used to visualize, model, and analyze molecular and genetic interaction networks (25). Next, the analysis network of Cytoscape tool, Molecular Complex Detection (MCODE), was applied to screen modules of the PPI network with a degree cutoff = 2, node score cutoff = 0.2, k-core = 2, and max. depth = 100.

Survival analysis

The receiver operating characteristic (ROC) curve is a commonly used graphical summary to evaluate the predictive value of biomarkers (26). To verify the prognosis results of hub genes, disease-free survival (DFS) data obtained from TCGA and pROC package were used to make the ROC curve figure (27).

TF and miRNA regulatory network construction

After the reference sequence (RefSeq) of the key genes were obtained from National Center for Biotechnology Information (NCBI) RefSeq database (https://www.ncbi.nlm.nih.gov/), transcription factors were predicted by AnimalTFDB (http://bioinfo.life.hust.edu.cn/AnimalTFDB/#!/) and selected by score >20 (28, 29). ENCORI (https://rna.sysu.edu.cn/encori/index.php) was used to predict miRNAs that bind to hub genes and apply standards including CLIP-Data ≥3, pan-cancer ≥1, and miRNA, with the least intersections in three databases selected (30).

Results

Patient characteristics

The clinical characteristics of 359 cases of classic PTC were obtained from the TCGA-THCA project, including days to the last follow-up, days to death, disease-free status, age at diagnosis, TNM classification, and tumor stage. After Cox analysis, age at diagnosis and tumor stage were significant for disease-free status (Figure 1A). Compared to age <55 years, the order indicated a poor prognosis that corresponds with previous research. At the same time, ages between 55 and 65 still have no noticeable difference with age <55 years old, suggesting that there might some of the patients with a preferable prognosis. Consequently, with age more than 55 years, 7 cases of stage I as a low-risk group and 11 cases of stage IV as a high-risk group were finally obtained after filtering the following criteria. The different expressions between the two groups were analyzed by edgeR and shown in the volcano plot (Figure 1B).

Function annotation of DEGs

GO enrichment analysis was completed to explore the biological functions of all DEGs of the upregulated gene obtained after edgeR. The GO term biological process analysis corroborated that the DEGs were enriched in external encapsulating structure organization, extracellular matrix organization, and extracellular structure organization. The GO term cellular component was enriched in the collagen-containing extracellular matrix, cornified envelope, and endoplasmic reticulum lumen. Apart from that, the molecular function classification of GO was enriched in extracellular matrix structural constituent, integrin binding, and cytokine activity (Figure 2).

The enrichment analysis of the KEGG pathway demonstrated that DEGs were correlated with proteoglycans in cancer, PI3K-Akt signaling pathway, and p53 signaling pathway (Figure 3).

Construction of PPI network

The STRING database identified the interaction of these upregulated DEGs. The combined score >0.4

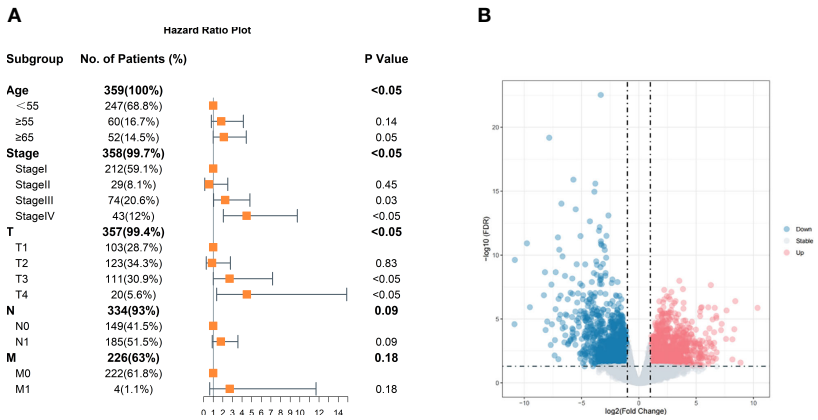

FIGURE 1
Clinical characteristics of classic PTC and volcano plot of DEGs. **(A)** Age, stage, and tumor size are significant. The reference of age is <55 years old. The reference of stage is stage I, and references of TNM are T1, N0, and M0. **(B)** Volcano plot of DEGs. Those blue dots represent downregulation in high-risk group thyroid carcinoma compared with low-risk group samples; red represents upregulation, and gray dots show no significant difference in the two groups.

(medium confidence score) was considered statistically significant. Then, a PPI network was made with Cytoscape. A total of 905 nodes and 4,941 edges were included in that PPI network. Additionally, the modules in the PPI network were analyzed by MCODE, and >8 was set as cutoff criteria with the default parameters (degree cutoff, 2; node score cutoff, 2; K-score, 2; and max depth = 100) (Figure 4). Next, the top 3 genes of every cluster (IFNA1, MRC1, LGALS3, LOX, POSTN, TIMP1, CD276, SDC4, and TLR2) were obtained as hub genes after being ranked by MCODE score.

Survival analysis

pROC packages made the receiver operating characteristic (ROC) curve to explore the patient's prognosis with high-expression hub genes. According to the results of the ROC curve, TIMP1, LOX, CD276, IFNA1, TLR2, and POSTN as key genes are more relevant to THCA (Figure 5). The heatmap of key gene expression in sample patients was made after normalization. Compared to IFNA1, high expressions of other genes are more common in the high-risk group (Figure 6).

FIGURE 2
Gene Ontology analyses of differentially expressed genes. Biological process (BP) was enriched in the external encapsulating structure organization, extracellular matrix organization, and extracellular structure organization. The cellular component (CC) was enriched in the collagen-containing extracellular matrix, cornified envelope, and endoplasmic reticulum lumen. Molecular function (MF) was enriched in extracellular matrix structural constituent, integrin binding, and cytokine activity.

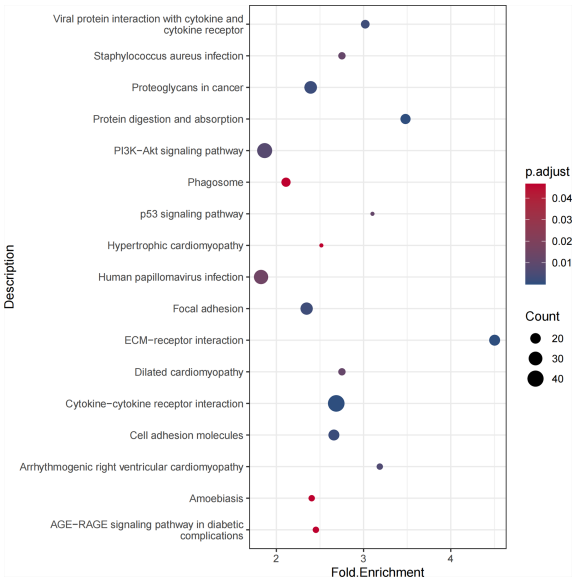

FIGURE 3
KEGG pathways of differentially expressed genes. The KEGG pathway could find proteoglycans in cancer, PI3K-Akt signaling pathway, and p53 signaling pathway related to thyroid carcinoma.

TF and miRNA regulatory network

A total of 47 miRNAs and 44 transcription factors that could be bound to key genes are predicted. TF, miRNA, and target gene relations were revealed in the regulatory network (Figure 7).

Discussion

In recent years, thyroid carcinoma has had a worldwide and dramatic incidence, especially in women. However, thyroid cancer treatment options are limited, and they mostly need to have surgery and supply of thyroxine for the whole of their later life. The high-intensity treatment for most tumor diameters over 1 cm, especially patients with differentiated thyroid cancer or papillary thyroid cancer, has also been controversial after PTC prognosis is more remarkable than that of other tumors. The fact that advanced thyroid cancer is found with the increase in cardinality estimate also promotes more research to distinguish the difference from PTC so that more suitable and precise therapeutics could be suggested to each of the patients.

For the above target, it is critical to know the prognosis of carcinoma, especially for PTC, which has a high risk of incidence and is likely over-diagnosed. Many studies have utilized bioinformatics technology to uncover biomarkers in THCA or PTC. However, the majority of them compared carcinoma and normal samples. According to the 8th American Joint Committee on Cancer (AJCC) and other experts, there may be distinct influencing factors for varying clinical outcomes in patients with PTC who are over 55 years old (31–34). In the current study, based on the hypothesis of difference in PTC, we explore the potential difference between PTC classification in women over 55 years old who have the worst prognosis and those with favorable forecasts based on data from TCGA.

In the present study, 994 upregulated genes were obtained from TCGA-THCA data using the edgeR package. GO was enriched in cell connection and extracellular matrix organization. KEGG pathway enrichment analysis of those DEGs could be linked to thyroid cancer growth and metastasis

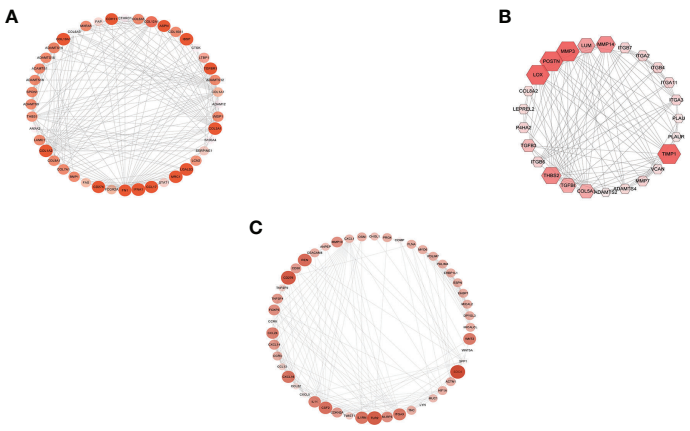

FIGURE 4
MCODE cluster. Cluster calculated by MCODE after protein–protein interaction network constructed, and different sizes and colors represent different MCODE scores. **(A)** Cluster 1 (score, 10.1). **(B)** Cluster 2 (score, 9.8). **(C)** Cluster 3 (score, 8.5).

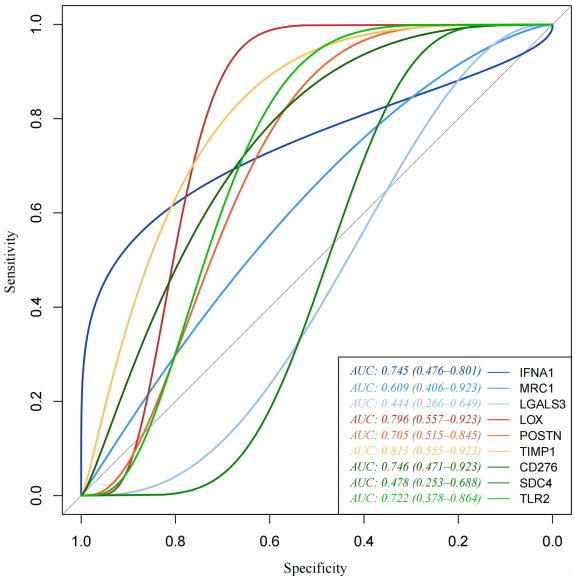

FIGURE 5
Receiver operating characteristic (ROC) curve. Receiver operating characteristic (ROC) curve made by pROC. TIMP1, LOX, CD276, IFNA1, TLR2, and POSTN as key genes are more relevant to THCA.

pathways such as proteoglycans in cancer, PI3K-Akt signaling pathway, and p53 signaling pathway. After using MCODE and Cytoscape network analysis tools of Cytoscape, nine hub genes with greater degrees were finally obtained (IFNA1, MRC1, LGALS3, LOX, POSTN, TIMP1, CD276, SDC4, and TLR2), which were considerably overexpressed in PTC with a poor prognosis compared to those with a better prognosis. In comparison to the survival analysis of nine hub genes, TIMP1, LOX, CD276, IFNA1, TLR2, and POSTN as key genes are more relevant to THCA.

Tissue inhibitor of metalloproteinase 1 (TIMP1) belongs to the TIMP gene family, and its encoded protein can promote cell proliferation. TIMP1 was found to be overexpressed in classic and follicular variants of PTC in different age and gender groups and in the BRAF-MUT group compared to that in BRAF-WT patients in previous research (35, 36). It binds CD63 on the cell surface membrane and activates AKT signaling pathway to make antiapoptotic activity and predict aggressive behaviors (37, 38). Lysyl oxidase (LOX) was found to be overexpressed in aggressive cancers and related to MMPs and TIMPs by regulating SNA12 expression (39). In addition, LOX upregulation is also associated with anaplastic thyroid cancer progression and aggressive tall cell variant of PTC (TC-PTC) compared with the differentiated thyroid cancers [classic PTC (cPTC) and follicular variant of PTC (FV-PTC)] that may respond to BRAF activation (40–42). Toll-like receptor 2 (TLR2) is a member of the Toll-like receptor (TLR) family; it was found to be mediated by Akt phosphorylation by GT1b (trisialoganglioside 1b) and activated PI3K/Akt signaling pathway (43). POSTN-encoded protein binds to integrins to support adhesion, migration of epithelial cells, and participation in cancer stem cell maintenance and metastasis. Previous research once found a wide variability of POSTN expression in a different histological subtype of PTC, and high stromal POSTN expression is associated with aggressive tumor behavior (44). Compared to TIMP1 and LOX, the relation between TLR2 and thyroid carcinoma was unclear, especially in PTC. However, previous research indicated that overexpression of TLR2 was associated with a high risk of colorectal cancer,

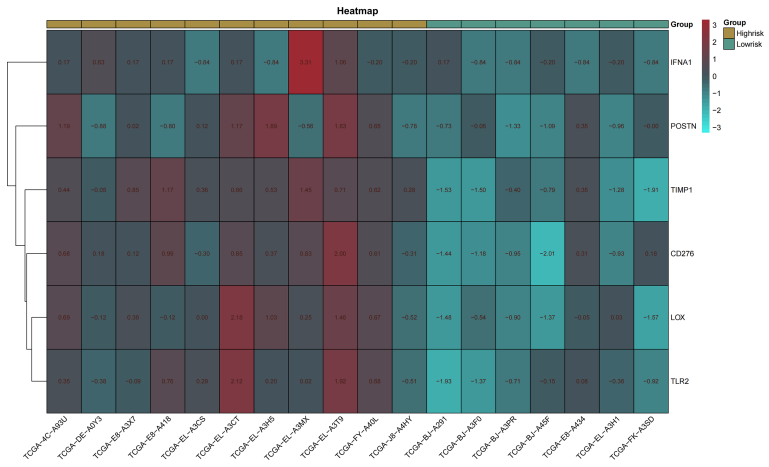

FIGURE 6
Heatmap of key genes. Heatmap made by pheatmap package and normalized by scale function. Different expression of genes in the high- and low-risk groups.

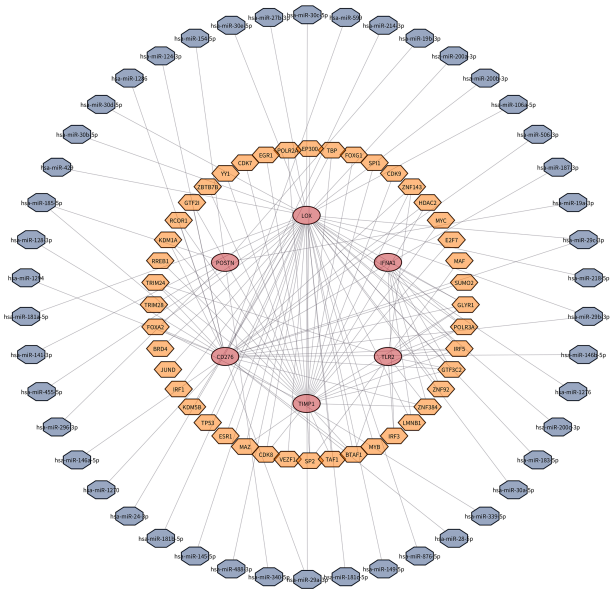

FIGURE 7
TF–miRNA–target gene network. A total of 47 miRNAs and 44 transcription factors that could be bound to key genes are predicted.

cervical cancer, and oral cancer (45–48). CD276, also known as B7-H3, has upregulated expression in many cancer cells and related with tumor cells by pathological angiogenesis (49). CD276 has been found to have an upregulated expression at the protein and mRNA levels in different types of thyroid cancer, and its effect on thyroid carcinoma has also been researched recently. CD276 was overexpressed in advanced thyroid carcinoma such as ATC, which is consistent with our results; its high expression indicates a poor prognosis of different PTCs (50, 51). We found that in the classic PTC, the upregulated CD276 is also related to a poor prognosis. Periostin (POSTN) encoded a secreted extracellular matrix protein and is found to exhibit stromal deposition in invasive portions and cytoplasmic expression of undifferentiated thyroid carcinoma cells (52). Periostin has different expressions in different kinds of PTCs, and upregulated periostin could also be found in PTC compared to non-neoplastic tissues. Upregulation of periostin-introduced invasion and lymph node metastasis may be due to loss of cellular polarity/cohesiveness and epithelial–mesenchymal transition (EMT) (53). This research also was consistent with the above results and found that in classic PTC of female patients aged more than 55 years, POSTN still has a different expression and upregulated POSTN still indicated a poor prognosis. Interferon alpha 1 (IFNA1) could encode a member of the type I interferon, and expression of IFNA1 is associated with HPV-positive head and neck cancers (54). Interferon alpha 1 could be found in normal thyroid cells and differentiated thyroid cancer and also used in some diseases, but long-term interferon (IFN) therapy is frequently associated with side effects on the thyroid gland (55). Although its effect is considered antiproliferative, interferon alpha is also found to influence malignant thyroid cancer by the microenvironment or affect other factors, such as tumor necrosis factor (TNF) or epidermal growth factor (EGF) (56, 57). According to our research, IFNA affects high-risk group PTC with an upregulated expression. More facts about its effect on PTC also need to be explored by further research. Above all, in our results, TIMP1, LOX, and POSTEN had different expressions no matter what type of thyroid cancer and papillary thyroid cancer; even in pure classic PTC, high expression of those genes also predicted a poor prognosis. Although CD276, TLR2, and IFNA1 were not found to have complex functions in thyroid cancer, they all participate in different carcinomas. These results indicate that further study is needed to reveal their roles in thyroid carcinoma.

Data availability statement

The original contributions presented in the study are included in the article/supplementary material. Further inquiries can be directed to the corresponding author.

Author contributions

L-QY designed the analyses. C-CL and MU analyzed the data and wrote the manuscript. XL and S-KS collected the data, YW and FL prepared the figures, and BG and M-HZ revised the

manuscript. All authors contributed to the article and approved the submitted version.

Funding

This work was supported by grants from the National Natural Science Foundation of China (Nos. 82100944, 82100494, 82070910, and 81870623), Natural Science Foundation of Hunan Province (No. 2021JJ40842), and Key R&D Plan Hunan Province (2020SK2078).

Acknowledgments

We want to thank our colleagues in the lab for their assistance.

Conflict of interest

The authors declare that the research was conducted in the absence of any commercial or financial relationships that could be construed as a potential conflict of interest.

Publisher's note

All claims expressed in this article are solely those of the authors and do not necessarily represent those of their affiliated organizations, or those of the publisher, the editors and the reviewers. Any product that may be evaluated in this article, or claim that may be made by its manufacturer, is not guaranteed or endorsed by the publisher.

References

1. Kitahara CM, Sosa JA. The changing incidence of thyroid cancer. *Nat Rev Endocrinol* (2016) 12(11):646–53. doi: 10.1038/nrendo.2016.110

2. Vaccarella S, Lortet-Tieulent J, Colombet M, Davies L, Stiller CA, Schüz J, et al. Global patterns and trends in incidence and mortality of thyroid cancer in children and adolescents: A population-based study. *Lancet Diabetes Endocrinol* (2021) 9(3):144–52. doi: 10.1016/S2213-8587(20)30401-0

3. Sung H, Ferlay J, Siegel RL, Laversanne M, Soerjomataram I, Jemal A, et al. Global cancer statistics 2020: GLOBOCAN estimates of incidence and mortality worldwide for 36 cancers in 185 countries. *CA: A Cancer J Clin* (2021) 71(3):209–49. doi: 10.3322/caac.21660

4. Takano T. Natural history of thyroid cancer. *Endocr J* (2017) 64(3):237–44. doi: 10.1507/endocrj.EJ17-0026

5. Williams D. Thyroid growth and cancer. *Eur Thyroid J* (2015) 4(3):164–73. doi: 10.1159/000437263

6. Tuttle RM. Controversial issues in thyroid cancer management. *J Nucl Med* (2018) 59(8):1187–94. doi: 10.2967/jnumed.117.192559

7. Wang TS, Sosa JA. Thyroid surgery for differentiated thyroid cancer - recent advances and future directions. *Nat Rev Endocrinol* (2018) 14(11):670–83. doi: 10.1038/s41574-018-0080-7

8. Cabanillas ME, McFadden DG, Durante C. Thyroid cancer. *Lancet* (2016) 388(10061):2783–95. doi: 10.1016/S0140-6736(16)30172-6

9. Cohen-Solal KA, Boregowda RK, Lasfar A. RUNX2 and the PI3K/AKT axis reciprocal activation as a driving force for tumor progression. *Mol Cancer* (2015) 14:137. doi: 10.1186/s12943-015-0404-3

10. Robinson MD, McCarthy DJ, Smyth GK. edgeR: a bioconductor package for differential expression analysis of digital gene expression data. *Bioinformatics* (2010) 26(1):139–40. doi: 10.1093/bioinformatics/btp616

11. McCarthy DJ, Chen Y, Smyth GK. Differential expression analysis of multifactor RNA-seq experiments with respect to biological variation. *Nucleic Acids Res* (2012) 40(10):4288–97. doi: 10.1093/nar/gks042

12. Thomas PD. The gene ontology and the meaning of biological function. *Methods Mol Biol* (2017) 1446:15–24. doi: 10.1007/978-1-4939-3743-1_2

13. Xing Z, Chu C, Chen L, Kong X. The use of gene ontology terms and KEGG pathways for analysis and prediction of oncogenes. *Biochim Biophys Acta* (2016) 1860(11 Pt B):2725–34. doi: 10.1016/j.bbagen.2016.01.012

14. Khunlertgit N, Yoon BJ. Incorporating topological information for predicting robust cancer subnetwork markers in human protein-protein interaction network. *BMC Bioinf* (2016) 17(Suppl 13):351. doi: 10.1186/s12859-016-1224-1

15. Colaprico A, Silva TC, Olsen C, Garofano L, Cava C, Garolini D, et al. TCGAbiolinks: an R/Bioconductor package for integrative analysis of TCGA data. *Nucleic Acids Res* (2016) 44(8):e71–e. doi: 10.1093/nar/gkv1507

16. *T T. a package for survival analysis in r* (2022). Available at: https://CRAN.R-project.org/package=survival.

17. Lumley MGAT. *Forestplot: Advanced forest plot using 'Grid' graphics* (2021). Available at: https://CRAN.R-project.org/package=forestplot.

18. Smedley D, Haider S, Durinck S, Pandini L, Provero P, Allen J, et al. The BioMart community portal: An innovative alternative to large, centralized data repositories. *Nucleic Acids Res* (2015) 43(W1):W589–98. doi: 10.1093/nar/gkv350

19. Durinck S, Moreau Y, Kasprzyk A, Davis S, De Moor B, Brazma A, et al. BioMart and bioconductor: A powerful link between biological databases and microarray data analysis. *Bioinformatics* (2005) 21(16):3439–40. doi: 10.1093/bioinformatics/bti525

20. Yu G, Wang LG, Han Y, He QY. clusterProfiler: An r package for comparing biological themes among gene clusters. *OMICS* (2012) 16(5):284–7. doi: 10.1089/omi.2011.0118

21. Wu T, Hu E, Xu S, Chen M, Guo P, Dai Z, et al. clusterProfiler 4.0: A universal enrichment tool for interpreting omics data. *Innovation (N Y)* (2021) 2(3):100141. doi: 10.1016/j.xinn.2021.100141

22. Walter W, Sanchez-Cabo F, Ricote M. GOplot: an r package for visually combining expression data with functional analysis. *Bioinformatics* (2015) 31(17):2912–4. doi: 10.1093/bioinformatics/btv300

23. Wickham H. *ggplot2: Elegant graphics for data analysis*. New York: Springer-Verlag (2016).

24. Szklarczyk D, Morris JH, Cook H, Kuhn M, Wyder S, Simonovic M, et al. The STRING database in 2017: Quality-controlled protein-protein association networks, made broadly accessible. *Nucleic Acids Res* (2017) 45(D1):D362–D8. doi: 10.1093/nar/gkw937

25. Cline MS, Smoot M, Cerami E, Kuchinsky A, Landys N, Workman C, et al. Integration of biological networks and gene expression data using cytoscape. *Nat Protoc* (2007) 2(10):2366–82. doi: 10.1038/nprot.2007.324

26. Michael H, Tian L, Ghebremichael M. The ROC curve for regularly measured longitudinal biomarkers. *Biostatistics* (2019) 20(3):433–51. doi: 10.1093/biostatistics/kxy010

27. Robin X, Turck N, Hainard A, Tiberti N, Lisacek F, Sanchez JC, et al. pROC: an open-source package for r and s+ to analyze and compare ROC curves. *BMC Bioinf* (2011) 12:77. doi: 10.1186/1471-2105-12-77

28. Hu H, Miao YR, Jia LH, Yu QY, Zhang Q, Guo AY. AnimalTFDB 3.0: a comprehensive resource for annotation and prediction of animal transcription factors. *Nucleic Acids Res* (2019) 47(D1):D33–D8. doi: 10.1093/nar/gky822

29. O'Leary NA, Wright MW, Brister JR, Ciufo S, Haddad D, McVeigh R, et al. Reference sequence (RefSeq) database at NCBI: Current status, taxonomic expansion, and functional annotation. *Nucleic Acids Res* (2016) 44(D1):D733–45. doi: 10.1093/nar/gkv1189

30. Li JH, Liu S, Zhou H, Qu LH, Yang JH. starBase v2.0: decoding miRNA-ceRNA, miRNA-ncRNA and protein-RNA interaction networks from large-scale CLIP-seq data. *Nucleic Acids Res* (2014) 42(Database issue):D92–7. doi: 10.1093/nar/gkt1248

31. Uchino S, Ishikawa H, Miyauchi A, Hirokawa M, Noguchi S, Ushiama M, et al. Age- and gender-specific risk of thyroid cancer in patients with familial adenomatous polyposis. *J Clin Endocrinol Metab* (2016) 101(12):4611–7. doi: 10.1210/jc.2016-2043

32. Ito Y, Miyauchi A, Oda H. Low-risk papillary microcarcinoma of the thyroid: A review of active surveillance trials. *Eur J Surg Oncol* (2018) 44(3):307–15. doi: 10.1016/j.ejso.2017.03.004

33. Ito Y, Miyauchi A, Kihara M, Higashiyama T, Kobayashi K, Miya A. Patient age is significantly related to the progression of papillary microcarcinoma of the thyroid under observation. *Thyroid* (2014) 24(1):27–34. doi: 10.1089/thy.2013.0367

34. Kazaure HS, Roman SA, Sosa JA. The impact of age on thyroid cancer staging. *Curr Opin Endocrinol Diabetes Obes* (2018) 25(5):330–4. doi: 10.1097/MED.0000000000000430

35. Smallridge RC, Chindris AM, Asmann YW, Casler JD, Serie DJ, Reddi HV, et al. RNA Sequencing identifies multiple fusion transcripts, differentially expressed genes, and reduced expression of immune function genes in BRAF (V600E) mutant vs BRAF wild-type papillary thyroid carcinoma. *J Clin Endocrinol Metab* (2014) 99 (2):E338–47. doi: 10.1210/jc.2013-2792

36. Jarzab B, Wiench M, Fujarewicz K, Simek K, Jarzab M, Oczko-Wojciechowska M, et al. Gene expression profile of papillary thyroid cancer: Sources of variability and diagnostic implications. *Cancer Res* (2005) 65(4):1587–97. doi: 10.1158/0008-5472.CAN-04-3078

37. Bommarito A, Richiusa P, Carissimi E, Pizzolanti G, Rodolico V, Zito G, et al. BRAFV600E mutation, TIMP-1 upregulation, and NF-kappaB activation: closing the loop on the papillary thyroid cancer trilogy. *Endocr Relat Cancer* (2011) 18(6):669–85. doi: 10.1530/ERC-11-0076

38. Ilie MI, Lassalle S, Long-Mira E, Hofman V, Zangari J, Benaim G, et al. In papillary thyroid carcinoma, TIMP-1 expression correlates with BRAF (V600E) mutation status and together with hypoxia-related proteins predicts aggressive behavior. *Virchows Arch* (2013) 463(3):437–44. doi: 10.1007/s00428-013-1453-x

39. Boufraqech M, Zhang L, Nilubol N, Sadowski SM, Kotian S, Quezado M, et al. Lysyl oxidase (LOX) transcriptionally regulates SNAI2 expression and TIMP4 secretion in human cancers. *Clin Cancer Res* (2016) 22(17):4491–504. doi: 10.1158/1078-0432.CCR-15-2461

40. Boufraqech M, Nilubol N, Zhang L, Gara SK, Sadowski SM, Mehta A, et al. miR30a inhibits LOX expression and anaplastic thyroid cancer progression. *Cancer Res* (2015) 75(2):367–77. doi: 10.1158/0008-5472.CAN-14-2304

41. Jolly LA, Novitskiy S, Owens P, Massoll N, Cheng N, Fang W, et al. Fibroblast-mediated collagen remodeling within the tumor microenvironment facilitates progression of thyroid cancers driven by BrafV600E and pten loss. *Cancer Res* (2016) 76(7):1804–13. doi: 10.1158/0008-5472.CAN-15-2351

42. Hebrant A, Floor S, Saiselet M, Antoniou A, Desbuleux A, Snyers B, et al. miRNA expression in anaplastic thyroid carcinomas. *PLoS One* (2014) 9(8): e103871. doi: 10.1371/journal.pone.0103871

43. Yoo HK, Park H, Hwang HS, Kim HJ, Choi Y-H, Kook KH. Ganglioside GT1b increases hyaluronic acid synthase 2 *via* PI3K activation with TLR2 dependence in orbital fibroblasts from thyroid eye disease patients. *BMB Rep* (2021) 54(2):136–41. doi: 10.5483/BMBRep.2021.54.2.178

44. Giusca SE, Amalinei C, Lozneanu L, Ciobanu Apostol D, Andriescu EC, Scripcariu A, et al. Heterogeneous periostin expression in different histological variants of papillary thyroid carcinoma. *BioMed Res Int* (2017) 2017:8701386. doi: 10.1155/2017/8701386

45. Proenca MA, de Oliveira JG, Cadamuro AC, Succi M, Netinho JG, Goloni-Bertolo EM, et al. TLR2 and TLR4 polymorphisms influence mRNA and protein expression in colorectal cancer. *World J Gastroenterol* (2015) 21(25):7730–41. doi: 10.3748/wjg.v21.i25.7730

46. Zhu L, Yuan H, Jiang T, Wang R, Ma H, Zhang S. Association of TLR2 and TLR4 polymorphisms with risk of cancer: A meta-analysis. *PLoS One* (2013) 8(12): e82858. doi: 10.1371/journal.pone.0082858

47. Yang S, Liu L, Xu D, Li X. The relationship of the TLR9 and TLR2 genetic polymorphisms with cervical cancer risk: A meta-analysis of case-control studies. *Pathol Oncol Res* (2020) 26(1):307–15. doi: 10.1007/s12253-018-0465-x

48. Hussaini HM, Parachuru VPB, Seymour GJ, Rich AM. FoxP3 and TLR2 in co-expression in oral cancer. *Acta Histochem* (2017) 119(7):768. doi: 10.1016/j.acthis.2017.06.006

49. Seaman S, Zhu Z, Saha S, Zhang XM, Yang MY, Hilton MB, et al. Eradication of tumors through simultaneous ablation of CD276/B7-H3-Positive tumor cells and tumor vasculature. *Cancer Cell* (2017) 31(4):501–15.e8. doi: 10.1016/j.ccell.2017.03.005

50. Luo Y, Yang YC, Shen CK, Ma B, Xu WB, Wang QF, et al. Immune checkpoint protein expression defines the prognosis of advanced thyroid carcinoma. *Front Endocrinol (Lausanne)* (2022) 13:859013. doi: 10.3389/fendo.2022.859013

51. Zhao B, Huang Z, Zhu X, Cai H, Huang Y, Zhang X, et al. Clinical significance of the expression of Co-stimulatory molecule B7-H3 in papillary thyroid carcinoma. *Front Cell Dev Biol* (2022) 10:819236. doi: 10.3389/fcell.2022.819236

52. Kusafuka K, Yamashita M, Iwasaki T, Tsuchiya C, Kubota A, Hirata K, et al. Periostin expression and its supposed roles in benign and malignant thyroid nodules: An immunohistochemical study of 105 cases. *Diagn Pathol* (2021) 16 (1):86. doi: 10.1186/s13000-021-01146-8

53. Bai Y, Kakudo K, Nakamura M, Ozaki T, Li Y, Liu Z, et al. Loss of cellular polarity/cohesiveness in the invasive front of papillary thyroid carcinoma and periostin expression. *Cancer Lett* (2009) 281(2):188–95. doi: 10.1016/j.canlet.2009.02.043

54. Zhang J, Chen T, Yang X, Cheng H, Spath SS, Clavijo PE, et al. Attenuated TRAF3 fosters activation of alternative NF-kappaB and reduced expression of antiviral interferon, TP53, and RB to promote HPV-positive head and neck cancers. *Cancer Res* (2018) 78(16):4613–26. doi: 10.1158/0008-5472.CAN-17-0642

55. Selzer E, Wilfing A, Sexl V, Freissmuth M. Effects of type I-interferons on human thyroid epithelial cells derived from normal and tumour tissue. *Naunyn Schmiedebergs Arch Pharmacol* (1994) 350(3):322–8. doi: 10.1007/BF00175039

56. Lahat N, Sheinfeld M, Sobel E, Kinarty A, Kraiem Z. Divergent effects of cytokines on human leukocyte antigen-DR antigen expression of neoplastic and non-neoplastic human thyroid cells. *Cancer* (1992) 69(7):1799–807. doi: 10.1002/1097-0142(19920401)69:7<1799::AID-CNCR2820690723>3.0.CO;2-8

57. Cunha LL, Domingues GAB, Morari EC, Soares FA, Vassallo J, Ward LS. The immune landscape of the microenvironment of thyroid cancer is closely related to differentiation status. *Cancer Cell Int* (2021) 21(1):387. doi: 10.1186/s12935-021-02084-7

frontiers | Frontiers in Endocrinology

TYPE Original Research
PUBLISHED 25 October 2022
DOI 10.3389/fendo.2022.1030143

OPEN ACCESS

EDITED BY
Erivelto Martinho Volpi,
Centro de referencia no ensino do diagnóstico por imagem (CETRUS), Brazil

REVIEWED BY
Edward Grant,
University of Southern California, United States
Fajin Dong,
Jinan University, China

*CORRESPONDENCE
Nianyu Xue
xuenianyu010133@126.com

SPECIALTY SECTION
This article was submitted to Cancer Endocrinology, a section of the journal Frontiers in Endocrinology

RECEIVED 28 August 2022
ACCEPTED 13 October 2022
PUBLISHED 25 October 2022

CITATION
Xue N, Li P, Deng H, Yi J, Xie Y and Zhang S (2022) The spoke wheel color Doppler blood flow signal is a specific sign of papillary thyroid carcinoma. *Front. Endocrinol.* 13:1030143. doi: 10.3389/fendo.2022.1030143

The spoke wheel color Doppler blood flow signal is a specific sign of papillary thyroid carcinoma

Nianyu Xue[1]*, Ping Li[2], Huadong Deng[3], Jing Yi[4], Yu Xie[5] and Shengmin Zhang[1]

[1]Department of Ultrasonography, Ningbo First Hospital, Ningbo, Zhejiang, China, [2]Department of Ultrasonography, Nanjing First Hospital, Jiangsu, China, [3]Department of Ultrasonography, Lishui People's Hospital, Zhejiang, China, [4]Department of Ultrasonography, Renmin Hospital of Wuhan University, Wuhan, Hubei Province, China, [5]Department of Ultrasonography, Meishan People's Hospital, Meishan, China

Background: Papillary thyroid carcinoma (PTC) is the most common type of thyroid cancer. Grayscale ultrasound (US) is the main method used to diagnose benign and malignant thyroid nodules, While color doppler blood flow imaging (CDFI) is not widely recognized when diagnosing thyroid cancer.

Methods: This study used a retrospective analysis. The study included 36 spoked wheel blood flow nodules detected by CDFI in 37,372 patients in five hospitals from January 2020 to June 2021. All thyroid nodules were examined histologically after ultrasound-guided fine needle biopsy or following surgical resection. The value of color doppler in diagnosing papillary thyroid carcinoma was evaluated based on pathological results.

Results: Among 36 thyroid nodules, only 6 were highly suspected of being malignant on grayscale ultrasound (classified as 5, according to ACR TI-RADS). However, these 36 thyroid nodules showed spoke wheel blood flow signal distribution on CDFI. If the spoke wheel blood flow signal is used to diagnose papillary thyroid cancer, then the diagnostic accuracy of this group of papillary thyroid cancers can reach 100%, which is significantly higher than the accuracy of grayscale ultrasound diagnosis, and the difference is statistically significant ($p<0.05$).

Conclusions: The results of this study found that spoke wheel blood flow sign on CDFI can be used to diagnose PTC. PTC with spoke wheel blood flow have benign characteristics on gray-scale ultrasound, which is easy to be misdiagnosed.

KEYWORDS

thyroid neoplasms, ultrasonography, doppler, color, papillary thyroid carcinoma

Introduction

Thyroid nodules are considered to be the most common manifestation of endocrine disease in clinical practice. The incidence of thyroid cancer has rapidly increased throughout the past few decades (1). The increase in the detection of malignant thyroid tumors may be related to the widespread use of high-frequency ultrasound, which is the most preferred diagnostic method for thyroid nodules (2).

Color Doppler blood flow imaging (CDFI) is an imaging technique that exploits the shift in the frequency of US waves when waves are reflected by moving blood (the Doppler effect) (3). In CDFI, the Doppler effect can detect the movement of red blood cells in blood vessels. Therefore, CDFI can provide information on the vascularity of thyroid lesions and is widely used in daily clinical practice to evaluate diffuse thyroid diseases, such as hyperthyroidism. However, CDFI is not valuable in assessing benign and malignant thyroid nodules (4). CDFI information is not considered in the standards of various versions of thyroid classification (including ACR, Korean quark classification, Chinese version classification, etc.) (5–8), which also proves that CDFI is of no value in the differentiating benign and malignant thyroid nodules. Ultrasonographic findings related to malignant tumors included hypoechoicity, solid and irregular edges, taller-than-wide and calcification.

In reviewing cases of misdiagnosed thyroid tumors, the authors found that papillary thyroid carcinomas with spoke wheel blood flow were easily misdiagnosed as benign nodules. To the best of our knowledge, there are no reports in the literature regarding the use of CDFI spoke wheel blood flow distribution to distinguish benign and malignant thyroid nodules. Therefore, we conducted a study that evaluated the value of spoke wheel blood flow distribution in the diagnosis of papillary thyroid carcinoma.

Material and methods

Study population

The study was approved by the ethics committee of our hospital(NO.2022RS042). Individual consent for this retrospective analysis was waived.

From January 2020 to June 2021, among 37,372 thyroid nodules in five hospitals, 38 nodules with spoke wheel blood flow detected by color Doppler ultrasonography were included in the study. The selection criteria were as follows: all patients underwent grayscale ultrasound and color Doppler ultrasound examinations, and pathological results were obtained. Among the 38 patients, 2 patients with thyroid nodules did not obtain pathological results, and the remaining 36 patients (20 males and 16 females, age range, 17–65 years; mean age, 36.5 ± 12.2 years) were included in this study. The patients with thyroid nodules with spoke wheel blood flow were all single. The mean diameter of the thyroid nodules was 2.1 ± 1.1 cm (range, 0.6–4.6 cm). All thyroid nodules were examined histologically after ultrasound-guided fine needle biopsy or following surgical resection.

Ultrasound examinations

All patients in the study underwent grayscale ultrasound and color Doppler ultrasound. When a thyroid nodule was detected, the position, size, echogenicity, composition, margin, shape, echogenic foci and blood flow of the nodule (spoke wheel blood flow distribution and non-spoke wheel blood flow distribution) were recorded. According to the American College of Radiology (ACR) Thyroid Imaging Reporting and Data System (TI-RADS) classification. An ultrasound machine (including Toshiba, GE, Mindray, Philips, Hitachi) with high frequency (7-14 MHz) line array transducers was used in all imaging procedures.

Ultrasound imaging was performed by the same radiologist, who had more than five years of experience in thyroid ultrasound, in each hospital. All images were recorded and transferred to the research staff database. Then, the images were evaluated by two radiologists who had 10 years of experience in thyroid imaging. If there was any disagreement, a third senior radiologist, who had more than 15 years of experience in thyroid ultrasonography, was consulted until a consensus was reached. None of the three radiologists knew the pathological diagnosis of the thyroid nodules.

First, thyroid nodules were diagnosed based on grayscale ultrasound findings, and then thyroid papillary carcinoma was diagnosed based on the color Doppler spoke wheel blood flow distribution. The value of color Doppler in diagnosing papillary thyroid carcinoma was evaluated based on pathological results. Color Doppler spoke wheel blood flow distribution was determined based on the observance of at least three blood vessels in different directions from the center of the nodule to the periphery (Figure 1).

Pathological examination

After the ultrasound examination was completed in all the patients, ultrasound-guided fine-needle aspiration or surgical resection was performed within two weeks to obtain pathological results.

Statistical analysis

The chi-squared test or Fisher's exact test was applied to categorical variables. The statistical analysis was performed, and

histopathology results were considered the diagnostic gold standard. *P values* <0.05 were considered to be statistically significant. Data analysis was performed using the SPSS version 20.0 software package.

Results

A total of 37,372 thyroid nodules were examined, of which 38 with spoke wheel blood flow signals were detected. Two of the patients were refused further examination, thus, no pathological results were obtained. The remaining 36 patients underwent fine-needle aspiration biopsy or surgical resection, and the pathological results confirmed that each patient had papillary carcinoma. Although the incidence of spoke wheel blood flow signals in thyroid nodules is very low (0.1%), it can directly diagnose papillary thyroid carcinoma (specificity as high as 100.0%).

We analyzed and summarized the ultrasound imaging characteristics of these 36 patients with papillary thyroid carcinoma (Table 1). Thirty-six thyroid nodules were identified and no cervical lymph node metastasis was found before ultrasonography. Among the 36 thyroid nodules, only 6 were highly suspected of being malignant on grayscale ultrasound (classified as 5, according to ACR TI-RADS), 15 nodules were identified as indeterminate benign and malignant (classified as 4, according to ACR TI-RADS), and the remaining 15 were determined to be benign (classified as Class 3, according to ACR TI-RADS). However, these 36 thyroid nodules showed spoke wheel blood flow signal distribution on color Doppler blood flow imaging (Figures 2, 3). The spoke wheel blood flow signal was not present in benign thyroid nodules. Therefore, the spoke wheel blood flow signal can be used as a specific ultrasound manifestation of papillary thyroid carcinoma.

If the spoke wheel blood flow signal is used to diagnose patients with papillary thyroid cancer, the diagnostic accuracy of this group of papillary thyroid cancers can reach 100.0%. This was significantly higher than the accuracy of grayscale ultrasound diagnosis (16.7%), and the difference was statistically significant (p<0.05). Regardless of the gray-scale ultrasonic characteristics, as long as the thyroid nodule has a spoke like blood flow, it can be divided into ACR TI-RADS 5.

TABLE 1 Ultrasonic image features of 36 cases of papillary thyroid carcinoma with spoke wheel blood flow.

Characteristics		Number
Gender	Female	16
	Male	20
Age (year)		36.50 ± 12.15
Location	Right lobe	21
	Left lobe	15
Maximum diameter of lesion (cm)		2.05 ± 1.09
Echogenicity	Hypoechoic	13
	Isoechoic	23
Composition	Mixed cystic and solid	3
	Solid or almost completely solid	33
Margin	Smooth	33
	Lobulated or irregular	3
Shape	Taller-than-wide	0
	Wider-than-all	36
Echogenic foci	Punctate echogenic foci	10
	Macrocalcifications	5
	None	21
Color doppler flow imaging	Spoke wheel blood flow	36

Discussion

Papillary thyroid carcinoma (PTC) is the most common type of thyroid cancer (9, 10). Grayscale ultrasound (US) is the main method for diagnosing benign and malignant thyroid nodules. The main ultrasound features that suggest PTC are hypoechoic or very hypoechoic, solid component, lobulated or irregular margins or extra-thyroidal extension, taller-than-wide shape, and calcifications. As greater numbers of the above ultrasound features are observed, the probability of malignancy increases.

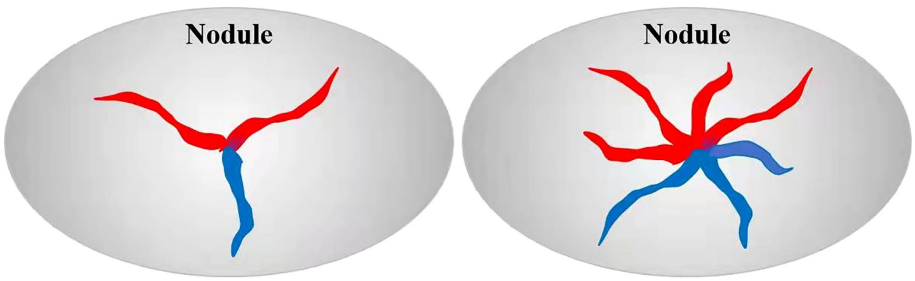

FIGURE 1
Schematic diagram of spoke wheel blood flow. Red: blood flow towards the probe, blue: blood flow away from the probe.

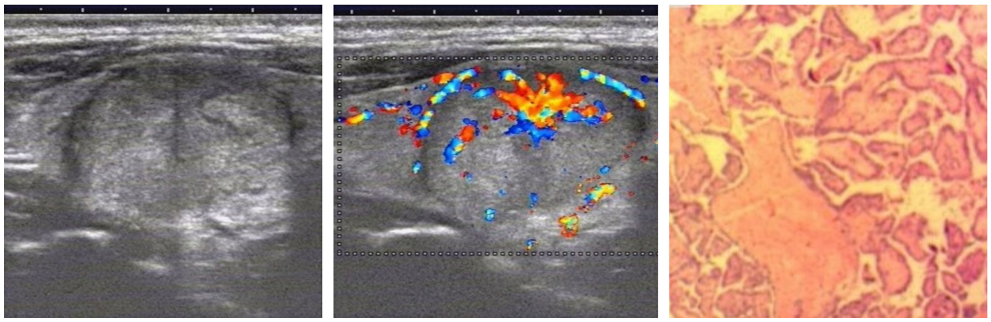

FIGURE 2
Grayscale ultrasonography shows a solid, isoechoic nodule in the right lobe of the thyroid with wider-than-tall and smooth margin and is considered to be a benign nodule on grayscale ultrasonography. Color Doppler ultrasonography showed the distribution of spoke wheel blood flow signals, which was determined to be papillary thyroid carcinoma. Postoperative pathology confirmed papillary thyroid carcinoma.

These ultrasound features are used for risk classification of thyroid imaging reports and data systems. Clearly, color Doppler blood flow imaging is not recognized in various versions of the thyroid risk classification. This suggests that color Doppler blood flow information is not used for the diagnosis of thyroid cancer. Both benign and malignant thyroid nodules can present with or without abundant blood flow.

This study found that the CDFI spoke wheel blood flow signal distribution can be used as a highly specific sign of papillary thyroid carcinoma. Retrospective analysis of the characteristics of this type of papillary thyroid carcinoma was performed. Incidence rates were not significantly different regarding sex and location. Similar to the reported papillary thyroid gland in the literature, the age of onset is approximately 36 years (11–14). The maximum diameter of the mass in this group of patients was approximately 2 cm, which is larger than that reported in the literature on papillary thyroid carcinoma (12–14). This group of papillary carcinomas are speculated to have a rich blood supply and are easier to grow up. However, we did not follow up on its growth rate. The grayscale ultrasound features of this group of PTCs are mainly characterized by nodules that are isoechoic, solid, smooth margin, with a wider than tall, no calcifications and no halo. Except for the solid component, there are few other malignant indicators (hypoechoic or very hypoechoic, solid component, lobulated or irregular margins or extra-thyroidal extension, taller-than-wide shape, and calcifications), so grayscale ultrasound findings can easily suggest that the nodules are benign. In this study, the misdiagnosis rate of gray-scale ultrasound in 36 cases of papillary thyroid carcinoma was significantly higher than that of papillary thyroid carcinoma reported in the literature (15). If the spoke wheel blood flow signal is used to diagnose papillary thyroid cancer, the diagnostic accuracy of this group of papillary thyroid cancers can reach 100%. CDFI can significantly improve the diagnostic accuracy of this type of PTC. The spoke wheel blood flow mainly appears in the larger PTC. PTC papillary

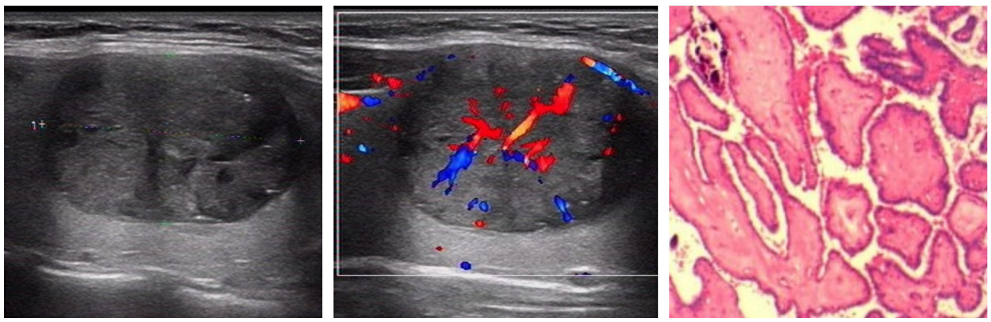

FIGURE 3
Grayscale ultrasonography shows a solid, hypoechoic nodule in the right lobe of the thyroid with wider-than-tall and smooth margin. It was classified as an ACR TI-RADS 4 lesion with moderate suspicion of cancer requiring biopsy. Color Doppler ultrasonography showed the distribution of spoke wheel blood flow signals, which was determined to be papillary thyroid carcinoma. Postoperative pathology confirmed papillary thyroid carcinoma.

structure has fiber vascular axis. Large fiber vessels will branch out. If the branch vessels originate from the center of the mass and the vessels are large enough, they can be detected by CDFI.

This study had several limitations. First, the case samples were limited, and large samples are needed for further research and confirmation. Second, we did not follow up patients for a long time to observe their outcomes. Third, limited by the retrospective study, there is a unified standard for image acquisition of spoke wheel blood flow, which may affect its incidence.

Conclusions

The results of this study found that CDFI can be used to diagnose papillary thyroid cancer that have characteristics of spoke wheel blood flow distribution and using grayscale ultrasound for these cases of PTC often show benign features and is easily misdiagnosed.

Data availability statement

The raw data supporting the conclusions of this article will be made available by the authors, without undue reservation.

Ethics statement

The studies involving human participants were reviewed and approved by Ethics Committee of Ningbo First Hospital. Written informed consent for participation was not required for this study in accordance with the national legislation and the institutional requirements.

Author contributions

SZ and NX designed this study. NX, PL, HD, JY, YX and SZ conducted the study and collected important background data. NX and SZ drafted the manuscript. All authors contributed to the article and approved the submitted version.

Conflict of interest

The authors declare that the research was conducted in the absence of any commercial or financial relationships that could be construed as a potential conflict of interest.

Publisher's note

References

1. Sadrzadeh H, Kline G. Chapter 2. thyroid. In: *Endocrine biomarkers, 1st edition*, vol. 2. The Netherlands: Elsevier (2017). p. 41–93.

2. Haugen BR, Alexander EK, Bible KC, Doherty GM, Mandel SJ, Nikiforov YE, et al. 2015 American Thyroid association management guidelines for adult patients with thyroid nodules and differentiated thyroid cancer: The American thyroid association guidelines task force on thyroid nodules and differentiated thyroid cancer. *Thyroid* (2016) 26:1–133. doi: 10.1089/thy.2015.0020

3. White DN. Johann Christian Doppler And his effect: a brief history. *Ultrasound Med Biol* (1982) 8:583–91. doi: 10.1016/0301-5629(82)90114-4

4. Hong YR, Wu YL, Luo ZY, Wu NB, Liu XM. Impact of nodular size on the predictive values of gray-scale, color-Doppler ultrasound, and sonoelastography for assessment of thyroid nodules. *J Zhejiang Univ Sci B* (2012) 13:707–16. doi: 10.1631/jzus.B1100342

5. Park JY, Lee HJ, Jang HW, Kim HK, Yi JH, Lee W, et al. A proposal for a thyroid imaging reporting and data system for ultrasound features of thyroid carcinoma. *Thyroid* (2009) 19:1257–64. doi: 10.1089/thy.2008.0021

6. Shapira-Zaltsberg G, Miller E, Martinez-Rios C, Bass J, Goldbloom EB, Tank K, et al. Comparison of the diagnostic performance of the 2017 ACR TI-RADS guideline to the kwak guideline in children with thyroid nodules. *Pediatr Radiol* (2019) 49:862–8. doi: 10.1007/s00247-019-04385-6

7. Schott M. *An ultrasonogram reporting system for thyroid nodules stratifying cancer risk for clinical Management.Yearbook of endocrinology*. The Germany: Mosby (2010). pp. 147–9.

8. Grant EG, Tessler FN, Hoang JK, Langer JE, Beland MD, Berland LL, et al. Thyroid ultrasound reporting lexicon: White paper of the ACR thyroid imaging, reporting and data system (TIRADS) committee. *J Am Coll Radiol* (2015) 12:1272–9. doi: 10.1016/j.jacr.2015.07.011

9. Ren J, Liu B, Zhang LL, Li HY, Zhang F, Li S, et al. A taller than-wide shape is a good predictor of papillary thyroid carcinoma in small solid nodules. *J Ultrasound Med* (2015) 34:19–26. doi: 10.7863/ultra.34.1.19

10. Carling T, Udelsman R. Thyroid cancer. *Annu Rev Med* (2014) 65:125–37. doi: 10.1146/annurev-med-061512-105739

11. Huang H, Xu S, Wang X, Liu S, Liu J. Patient age is significantly related to distant metastasis of papillary thyroid microcarcinoma. *Front Endocrinol (Lausanne)* (2021) 12:748238. doi: 10.3389/fendo.2021.748238

12. Liu J, Jia X, Gu Y, Chen X, Guan L, Yan J, et al. Thyroid parenchyma microcalcifications on ultrasound for predicting lymph node metastasis in papillary thyroid carcinoma: A prospective multicenter study in China. *Front Oncol* (2021) 11:609075. doi: 10.3389/fonc.2021.609075

13. Cao YM, Zhang TT, Li BY, Qu N, Zhu YX. Prognostic evaluation model for papillary thyroid cancer: A retrospective study of 660 cases. *Gland Surgb* (2021) 10:2170–9. doi: 10.21037/gs-21-100

14. Li X, Zhang H, Zhou Y, Cheng R. Risk factors for central lymph node metastasis in the cervical region in papillary thyroid carcinoma: a retrospective study. *World J Surg Oncol* (2021) 19:138. doi: 10.1186/s12957-021-02247-w

15. Brito JP, Gionfriddo MR, Al Nofal A, Boehmer KR, Leppin AL, Reading C, et al. The accuracy of thyroid nodule ultrasound to predict thyroid cancer: Systematic review and meta-analysis. *J Clin Endocrinol Metab* (2014) 99:1253–63. doi: 10.1210/jc.2013-2928

frontiers | Frontiers in Endocrinology

TYPE Original Research
PUBLISHED 02 November 2022
DOI 10.3389/fendo.2022.1022438

OPEN ACCESS

EDITED BY
Erivelto Martinho Volpi,
Centro de Referencia no Ensino do Diagnóstico por Imagem (CETRUS), Brazil

REVIEWED BY
Qian Xiaoqin,
Jiangsu University Affiliated People's Hospital, China
Jose Candido Xavier,
Salesian University Center of São Paulo, Brazil

*CORRESPONDENCE
Mingbo Zhang
zhangmingbo@301hospital.com

SPECIALTY SECTION
This article was submitted to Thyroid Endocrinology, a section of the journal Frontiers in Endocrinology

RECEIVED 18 August 2022
ACCEPTED 17 October 2022
PUBLISHED 02 November 2022

CITATION
Wu J, Li Y and Zhang M (2022) Clinical value of FNA puncture feeling in the diagnosis of non-diagnostic and indeterminate thyroid nodules. *Front. Endocrinol.* 13:1022438. doi: 10.3389/fendo.2022.1022438

Clinical value of FNA puncture feeling in the diagnosis of non-diagnostic and indeterminate thyroid nodules

Jintao Wu[1], Yingying Li[2] and Mingbo Zhang[2*]

[1]Department of Ultrasound, Linzi District Maternity and Child Health Care Hospital, Zibo, China, [2]Department of Ultrasound, Chinese PLA General Hospital, Beijing, China

Objective: The aim of this study was to explore the clinical diagnostic value of puncture feeling during fine-needle aspiration (FNA) for non-diagnostic and indeterminate thyroid nodules.

Methods: A retrospective analysis was performed on 176 patients (196 nodules) diagnosed with Bethesda I or III by FNA cytology at the ultrasound department of our hospital between January 2017 and January 2020. Comparisons were made on the differences in puncture feeling (including stiffness and grittiness) between benign and malignant thyroid nodules, and their diagnostic performance was analyzed.

Results: There were significant differences between benign and malignant nodules with respect to the puncture stiffness and puncture grittiness ($P < 0.001$). The presence of a hard stiffness and grittiness demonstrated comparable levels of diagnostic performance for malignant thyroid nodules, with sensitivities, specificities, accuracies, positive predictive values, and negative predicative values of 55.56% and 63.89%, 87.10% and 78.22%, 75.51% and 72.96%, 71.43% and 63.01%, and 77.14% and 78.86%, respectively. The diagnostic performance was most optimal in the presence of at least one puncture feeling (area under the receiver operating characteristic curve: 0.771), exhibiting a sensitivity, specificity, accuracy, positive predictive value, and negative predictive value of 79.17%, 75.00%, 76.53%, 64.77, and 86.11%%, respectively.

Conclusions: Puncture feeling adds clinical value in the diagnosis of thyroid nodules with indeterminate FNA findings.

KEYWORDS

Fine needle aspiration (FNA), thyroid nodules, thyroid cancer, puncture feeling, ultrasound

Introduction

There has been a significantly gradual rise in the incidence of thyroid cancer over the past few years (1). Fine-needle aspiration (FNA) is a cytopathological technique that plays a crucial role in the diagnosis of thyroid cancer (2, 3). The diagnosis through FNA cytology is reliant on the Bethesda System for Reporting Thyroid Cytopathology (4). However, there are ambiguities in its criteria for cytological diagnosis, and 10-15% false negatives has been reported (5, 6). In particular, Bethesda category I and III nodules are non-diagnostic and indeterminate thyroid nodules prone to misdiagnosis, which inevitably cause repeat aspiration or diagnostic operation.

Molecular pathology including gene mutational panel and comprehensive multigene next-generation sequencing panel can be used to diagnosis thyroid cancer (7). However, the cost is expensive and not universally available. Repeat FNA of non-diagnostic and indeterminate thyroid nodules had a positive impact. However, some cases may remain indeterminate even after repeat aspiration of the nodule (8).During the process of FNA, the operator may detect different sensations as the needle enters the nodule (i.e., puncture feeling), such as stiffness, grittiness, etc. The different sensations indicate different internal composition of the nodules, which may contribute to differential diagnosis. Due to the presence of calcifications and psammoma bodies in papillary thyroid carcinomas, the friction may contribute to the sensation of grittiness during the puncture process (9). In addition, most thyroid cancers appear as hard nodules on elastography (10). At present, research on the significance of puncture feeling to the diagnostic performance of thyroid nodule biopsy is relatively scarce, and it remains unclear which types of puncture feeling can better facilitate the diagnosis of thyroid nodules.

In order to further improve diagnostic accuracy on the basis of cytopathological diagnosis and to provide evidence for decision-making by clinicians and interventional sonographers, this study explored the clinical diagnostic value of puncture feeling during FNA biopsy for non-diagnostic and indeterminate nodules and compared the diagnostic performances of different commonly observed puncture feelings.

Materials and methods

Patients

176 patients (196 nodules) diagnosed with Bethesda category I or III nodules by thyroid nodule FNA cytology at the ultrasound department of Qidu Hospital between January 2017 and January 2020 were enrolled in this retrospective study.

The inclusion criteria were as follows (1): patients with well-defined single or multiple thyroid nodules that were suspicious for malignancy and indicated for FNA biopsy; (2) patients who underwent ultrasound-guided FNA at our department; (3) cytopathological findings indicating Bethesda category I or III nodules; (4) patients who underwent repeat aspiration or surgical treatment after FNA. The exclusion criteria: patients with unclear secondary aspiration or postoperative pathological findings.

Instruments and methods

Thyroid examination was performed using the Mindray Resona 7 (Mindray, Shenzhen, Guangdong, China) color Doppler ultrasound system equipped with an L14-5 probe, and the settings were adjusted for thyroid examination (frequency: 5–14 MHz). In accordance with the classification criteria of the American College of Radiology (ACR) Thyroid Imaging, Reporting and Data System (TI-RADS) (2), the thyroid nodules that met the ACR criteria or 2012 Chinese Medical Association Guidelines (11) were recommended for FNA. Prior to the biopsy, informed consent was obtained in writing from the patients and their family members. FNA was performed using 25G × 50 mm biopsy needles (Hakko Co., Ltd., Chikum-Shi, Nagano, Japan).

All FNA procedures were performed by a sonographer with more than 10 years of interventional experience. During the procedure, patients were placed in a supine position, and the puncture site was covered with fenestrated drapes after undergoing disinfection. The sonographer sat at the patient's cranial end. Using the freehand FNA technique, the needle was inserted at the midpoint on the side of the probe. Under ultrasound guidance, the needle tip entered the nodule without negative pressure, and 10–20 needle passes were made in multiple directions. The assistant observed whether bleeding occurred at the end of the needle and prompted the sonographer to stop if bleeding occurred to prevent excessive blood in the biopsy specimen. The puncture feeling was dictated and documented by the operator. Grittiness was defined as a sensation of sandpaper-like friction during the needle insertion, and its presence or absence was recorded. In addition, the stiffness encountered when the needle tip entered the nodule was compared with that entering normal thyroid parenchyma. Nodules with a higher stiffness than normal thyroid parenchyma were defined as hard. Otherwise, they were defined as soft. Once FNA was completed, rapid smear preparation was performed with the cooperation of the assistant, and the specimens were fixed using 95% alcohol for 20 s. The operator then selected 2–3 smears based on visual judgement of the specimen quality for cytopathological examination in the pathology department. The pathological findings were classified according to the Bethesda System for Reporting Thyroid Cytopathology (12). Patients with nodules classified as

category I or category III were recommended for repeat aspiration or surgical treatment, as appropriate.

The medical records of patients with thyroid nodules stored in the ultrasound department were reviewed. Screening was performed using the clinical data and pathological records to select the patients with Bethesda category I or III nodules. The patients' parameters were recorded, which included sex, age, maximum nodule diameter, nodule volume (superior-inferior diameter × left-right diameter × anterior-posterior diameter × 0.52), initial FNA findings and final pathological findings. Comparisons were performed to determine whether the presence/absence of grittiness and nodule puncture texture was associated with the final pathological findings (benign vs. malignant). In addition, we evaluated the clinical value of applying the two types of puncture feelings alone or combined in the diagnosis of thyroid nodules.

Statistical methods

All statistical analyses were performed using SPSS (version 26.0). Measurement data are expressed as the mean ± standard deviation, whereas the count data are expressed as the number of cases and percentage. Comparisons of differences were performed using the chi-squared test or Fisher's exact test. The diagnostic performance of puncture feeling for thyroid nodules was evaluated using its sensitivity, specificity, accuracy, positive predictive value (PPV), negative predictive value (NPV), receiver operating characteristic (ROC) curve and area under the ROC curve (AUROC). $P < 0.05$ was used to indicate statistical significance.

Results

Clinical and pathological data

A total of 176 patients with 196 nodules were enrolled, including 21 males (11.9%) and 155 females (88.1%), and the patients had a mean age of 43.48 ± 11.39 years (20–72 years). The maximum nodule diameter was 2.42 ± 1.59 cm (0.5–6.6 cm), and the nodule volume was 7.78 ± 2.01 (0.065–66.25 cm^3). The initial FNA findings indicated that 115 (58.7%) were Bethesda category III nodules and 81(41.3%) were category I nodules. The final pathological confirmation indicated that 124 were benign nodules, including 61 (49.2%) nodular goiter, 5 (4.0%) subacute thyroiditis, 40 (32.3%) thyroid adenoma and 18 (14.5%) localized Hashimoto's thyroiditis; whereas 72 were malignant nodules, including 70 (97.2%) papillary thyroid carcinoma and 2 (2.8%) follicular thyroid carcinoma. Of all the nodules enrolled in our study, their tumor size, location and ultrasound characteristics were displayed in Table 1.

TABLE 1 Imaging features of the thyroid nodules.

Parameter	Result	Pathology	
		Malignant	Benign
Diameter (cm)		1.49±1.08	2.95±1.59
Location	Left lobe	30 (41.67)	57 (45.97)
	Right lobe	35 (48.61)	58 (46.77)
	Isthmus	7 (9.72)	9 (7.26)
echogenicity	Hypoechogenicity	59 (81.94)	75 (60.48)
	Isoechogenicity	2 (2.78)	4 (3.23)
	Hyperechogenicity	1 (1.39)	2 (1.61)
	Mixed echogenicity	10 (13.89)	43 (34.68)
Composition	Mixed cystic and solid	11 (15.28)	37 (29.84)
	Solid or almost solid	61 (84.72)	87 (70.16)
Shape	Wider-than-tall	40 (55.56)	109 (87.90)
	Taller-than-wide	32 (44.44)	15 (12.10)
Echogenic foci	Microcalcification	14 (19.44)	21 (16.94)
	Macrocalcification	29 (40.28)	23 (18.55)
	Peripheral calcification	19 (26.39)	4 (3.23)
	None	10 (13.89)	76 (61.29)
Vascular pattern	intratumoral	22 (30.56)	79 (63.71)
	Periphtumoral	37 (51.39)	14 (11.29)
	Both	13 (18.06)	31 (25.00)
Total		72	124

Values are presented as number and percentage (parenthesis).

Of all the 72 malignant nodules, 9 of them (12.5%) were presence with psamoma on histology. And tumor variant results showed 2(2.8%) medullary carcinoma, 3(4.2%) follicular papillary carcinoma, 15(20.8%) micro-carcinoma and 52 (72.2%) classical papillary carcinoma. 64(88.9%) received surgery and 8(11.1%) received ultrasound guided thermal ablation. Of the 64 patients who underwent surgery, the results of the T-staging showed 59(92.2%) T1, three (4.7%) T2 and two (3.1%) T4. Their N-staging showed 27(42.2%) N1 and 37(57.8%) N0. Occult cancers were detected in 12(18.8%) cases. The 8 patients who underwent ablation were all confirmed as classical papillary carcinoma by CNB before ablation, and the ablation was successfully completed, with more than 1 year's follow-up. No tumor recurrence and lymph node metastasis were detected in the 8 ablation cases.

Diagnostic performance of puncture feeling in thyroid nodules with indeterminate FNA findings

As shown in Table 2, there were significant differences between benign and malignant nodules with respect to the nodule texture (hard vs. soft) ($P < 0.001$) and presence of grittiness ($P < 0.001$) during the puncture.

As shown in Table 3, the puncture stiffness exhibited a diagnostic sensitivity of 55.56%, specificity of 87.10%, accuracy of 75.51%, PPV of 71.43%, and NPV of 77.14% in the diagnosis of benign and malignant thyroid nodules; while the puncture grittiness exhibited a diagnostic sensitivity of 63.89%, specificity of 78.22%, accuracy of 72.96%, PPV of 63.01%, and NPV of 78.86% in the differential diagnosis of benign and malignant thyroid nodules.

In the differential diagnosis of benign and malignant thyroid nodules with indeterminate FNA findings, the presence of stiffness produced an AUROC of 0.713, while the presence of grittiness produced an AUROC of 0.711. When at least one of the both feelings were present, we can get the highest sensitivity, accuracy, NPC and AUROC of 0.778, 0.811, 0.853 and 0.764; when both hard texture and grittiness were present, the AUROC was 0.653 with the highest specificity of 90.32%. The diagnostic ROC curves are shown in Figure 1.

Due to the inflammatory processes can affect the feeling of stiffness and grittiness, we perform an analysis between the inflammatory lesion and malignant thyroid nodules. The puncture stiffness exhibited a diagnostic sensitivity of 55.56%, specificity of 86.96%, accuracy of 63.16%, PPV of 93.02%, and NPV of 38.46%; while the puncture grittiness exhibited a diagnostic sensitivity of 63.89%, specificity of 78.26%, accuracy of 67.37%, PPV of 90.20%, and NPV of 41.86% in the differential diagnosis of inflammatory and malignant thyroid nodules.

Discussion

FNA is one of the most reliable techniques for the diagnosis of thyroid malignancies and selection of treatment methods and has been recommended by numerous guidelines published in China and abroad (2, 13, 14). However, due to the ambiguities in the FNA findings, nodules with indeterminate pathological reports will often require patients to undergo repeat biopsy. In this study, we demonstrated that puncture feeling had some value in assisting the diagnosis of thyroid nodules with indeterminate pathological findings. Thus, reporting the puncture feeling can provide clinicians with auxiliary diagnostic evidence in cases with indeterminate pathological diagnosis.

Our findings revealed that the sensations of nodule texture perceived during puncture can serve as an auxiliary diagnostic method. Previous studies have demonstrated that malignant tumors exhibited a loss of normal orderly arrangement and an increase in density (15). Furthermore, the presence of proliferative stromal fibrosis in thyroid cancer tissues contributes to tumor hardening. In addition, the presence of calcifications, especially macrocalcifications, in malignant thyroid tumors can also increase their stiffness. Studies using

TABLE 2 Differences in the puncture feeling of thyroid nodules with indeterminate FNA findings.

Parameter	Result	Pathology		χ^2	*P* value
		Malignant	Benign		
Puncture texture	Hard	40	16	40.61	<0.001
	Soft	32	108		
Grittiness	Present	46	27	34.57	<0.001
	Absent	26	97		
Number of puncture feelings	Both	29	12	25.78	<0.001
	Either	28	19	13.88	<0.001
	At least one	57	31	54.02	<0.001
	None	15	93	54.02	<0.001

TABLE 3 Diagnostic performance of puncture feeling for thyroid nodules with indeterminate FNA findings.

Parameter	Sensitivity	Specificity	Accuracy	PPV	NPV	AUROC	95%CI
Stiffness	55.56%	87.10%	75.51%	71.43%	77.14%	0.713±0.040	0.634~0.793
Grittiness	63.89%	78.22%	72.96%	63.01%	78.86%	0.711±0.040	0.633~0.788
Presence of both	40.28%	90.32%	71.94%	70.73%	72.26%	0.653±0.043	0.569~0.737
Presence of either	38.89%	84.68%	67.86%	59.57%	70.47%	0.618±0.043	0.534~0.702
At least one feeling	79.17%	75.00%	76.53%	64.77%	86.11%	0.771±0.036	0.701~0.841
Absence of both	20.83%	25.00%	13.89%	35.23%	23.47%	0.229±0.036	0.159~0.299

PPV, positive predictive value; NPV, negative predictive value; AUROC, area under the receiver operating characteristic curve; CI, confidential interval.

ultrasound elastography have demonstrated that malignant thyroid tumors exhibit a significant higher stiffness than benign tumors (16). However, sonoelastography is more operator-dependent and may be subjected to some interfering factors (17). Moreover, the instrumentation requirements of this technique are not conducive to its widespread promotion in primary care settings. Despite the lack of an objective indicator for evaluating nodule stiffness in this study, the use of puncture feeling to determine the nodule stiffness was more direct. Therefore, this indicator can exclude patients with benign tumors more effectively, which in favor of reducing unnecessary repeat aspirations and diagnostic operation.

Our findings also indicate that puncture grittiness has clinical significance in aiding the diagnosis. The feeling of grittiness encountered during puncture may result from the friction between the nodule calcifications and the needle tip, while nodule microcalcifications are one of the distinct manifestations of malignant thyroid tumors, especially papillary thyroid carcinomas (18). According to histopathological studies, microcalcifications chiefly manifest as psammoma bodies. Psammoma bodies are currently defined as round concentric lamellar calcifications observed in the stroma of papillary carcinomas, and the exact mechanisms underlying their pathogenesis are poorly understood (19). However, they are detected in more than 50% of all papillary thyroid carcinomas (20). Owing to its unique nature, the puncture feeling of grittiness obtained good agreement among experienced operators (8), which also served as a basis for its reliability. In addition, compared with puncture texture, grittiness demonstrated a higher sensitivity, which enabled the more-effective screening of suspicious

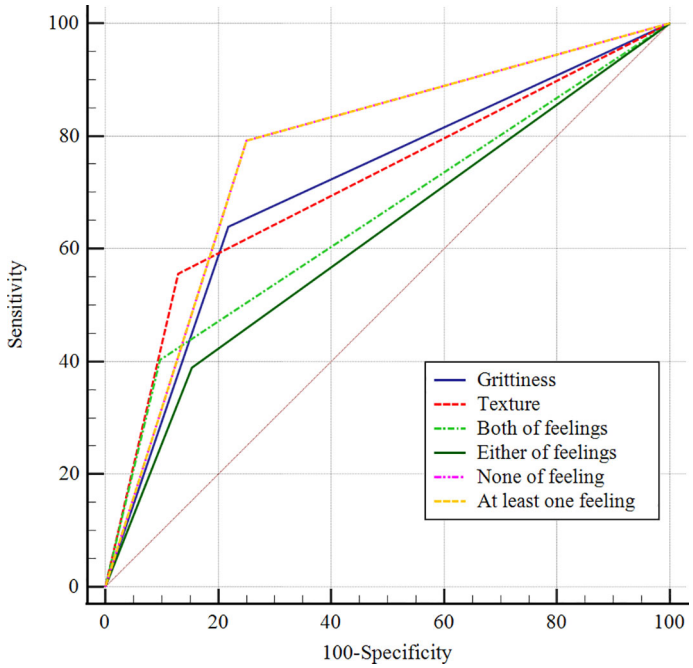

FIGURE 1
ROC curves for puncture feeling in the differential diagnosis of benign and malignant thyroid nodules with indeterminate FNA findings.

patients, thereby reducing a missed diagnosis in cases of an indeterminate pathological diagnosis.

Furthermore, our findings suggest that, for nodules with heterogenous texture, the lesion sites were often located in areas with hard texture and grittiness. Hence, focusing the biopsy to such areas can also improve the accuracy of FNA. In addition, providing timely remarks on the puncture feeling or suspicions in ultrasound diagnosis can also facilitate a targeted cytological diagnosis by pathologists, thereby reducing the risk of misdiagnosis.

The diagnostic performance of combining the two types of puncture feelings was also validated in this study. In the presence of both puncture feelings, the diagnostic specificity was 90.32%, which essentially reduced erroneous diagnosis of thyroid cancer, and reduced the pain and medical expenses caused by repeat aspiration. In the presence of at least one puncture feeling, the sensitivity was 79.17%, which reduced misdiagnosis and can serve as an indication for clinicians to arrange for a repeat aspiration promptly or switch to histological biopsy. Li has reported FNA combined with puncture feeling in the diagnosis of thyroid nodules (21). The result showed that the puncture feeling had a good PPV and NPV, which was similar to our result. However, their study included nodules with all Bethesda categories. 74% of them were classified as category V and VI and only 14% of them were classified as category I and III. In contrast, only non-diagnostic and indeterminate thyroid nodules were included in our study. Therefore, the results of our study are more valuable for the diagnosis of such nodules.

There are several limitations to this study. First, the subjectivity of the evaluation indicator (puncture feeling) may lead to significant disparities among different operators. We did not evaluate the concordance among physicians with different puncture experiences, which can be further explored in subsequent studies. Second, the puncture feeling produced in this study cannot be confirmed using objective indicators at present. Finally, this was a single-center retrospective study with a relatively small sample size, and it also did not include rare malignancies (e.g., undifferentiated carcinoma, metastatic carcinoma, etc.). Thus, the sample size should be further increased and prospective studies should be performed in the future.

In conclusion, puncture feeling during FNA may assist the diagnosis of thyroid nodules with indeterminate cytopathological findings, thereby providing the basis for reducing unnecessary repeat aspirations or preventing missed diagnoses. Hence, it has potential value in clinical application.

Data availability statement

The raw data supporting the conclusions of this article will be made available by the authors, without undue reservation.

Ethics statement

The studies involving human participants were reviewed and approved by Institutional Ethics Committee of the Linzi Maternal and Child Health Care Hospital (Qidu Hospital). The patients/participants provided their written informed consent to participate in this study.

Author contributions

All authors listed have made a substantial, direct, and intellectual contribution to the work and approved it for publication.

Acknowledgments

We are grateful to the patients who participated in this study.

Conflict of interest

The authors declare that the research was conducted in the absence of any commercial or financial relationships that could be construed as a potential conflict of interest.

Publisher's note

References

1. Welch HG, Doherty GM. Saving thyroids - overtreatment of small papillary cancers. *N Engl J Med* (2018) 379:310–2. doi: 10.1056/NEJMp1804426

2. Tessler F, Middleton W, Grant E, Hoang J, Berland L, Teefey S, et al. ACR thyroid imaging, reporting and data system (TI-RADS): White paper of the ACR

TI-RADS committee. *J Am Coll Radiol JACR* (2017) 14:587–95. doi: 10.1016/j.jacr.2017.01.046

3. Tanaka A, Hirokawa M, Suzuki A, Higuchi M, Kanematsu R, Yamao N, et al. Clinical significance and cytological detection of tracheal puncture following thyroid fine-needle aspiration: A retrospective study. *Diagn Cytopathol* (2021) 49:1116–21. doi: 10.1002/dc.24826

4. Cibas ES, Ali SZ. The 2017 Bethesda system for reporting thyroid cytopathology. *Thyroid Off J Am Thyroid Assoc* (2017) 27(11):1341–6. doi: 10.1089/thy.2017.0500

5. Kulstad R. Do all thyroid nodules >4 cm need to be removed? An evaluation of thyroid fine-needle aspiration biopsy in large thyroid nodules *Endocr Pract.* (2016) 22(7):791–8. doi: 10.4158/EP151150

6. Yoon JH, Moon HJ, Kim EK, Kwak JY. Inadequate cytology in thyroid nodules: should we repeat aspiration or follow-up? *Ann Surg Oncol* (2011) 18:1282–9. doi: 10.1245/s10434-011-1605-7

7. Poller DN, Glaysher S. Molecular pathology and thyroid FNA. *CYTOPATHOLOGY* (2017) 28:475–81. doi: 10.1111/cyt.12492

8. Saieg MA, Barbosa B, Nishi J, Ferrari A, Costa F. The impact of repeat FNA in non-diagnostic and indeterminate thyroid nodules: A 5-year single-centre experience. *Cytopathology* (2018) 29(2):196–200. doi: 10.1111/cyt.12508

9. Luo J, Zhang C, Huang F, Chen J, Sun Y, Xu K, et al. Risk of malignancy in thyroid nodules: predictive value of puncture feeling of grittiness in the process of fine-needle aspiration. *Sci Rep* (2017) 7:13109. doi: 10.1038/s41598-017-13391-3

10. Hu L, Liu X, Pei C, Xie L, He N. Assessment of perinodular stiffness in differentiating malignant from benign thyroid nodules. *Endocr Connect* (2021) 10:492–501. doi: 10.1530/EC-21-0034

11. Teng W, Liu Y, Gao M, Huang G, Zhao J, Shan Z, et al. China Anti-cancer associatio head and neck tumor proffessional committee. management guidelines for patients with thyroid nodules and differentiated thyroid cancer. *Chin J Pract Surg* (2011) 31:908–14.

12. Alhashem MH, Alabidi A, Aly MG. The Bethesda system for reporting thyroid cytopathology: A retrospective review of its diagnostic utility at johns Hopkins aramco healthcare, Saudi Arabia. *Am J Otolaryngol* (2021) 42:103088. doi: 10.1016/j.amjoto.2021.103088

13. Haugen B, Alexander E, Bible K, Doherty G, Mandel S, Nikiforov Y, et al. American Thyroid association management guidelines for adult patients with thyroid nodules and differentiated thyroid cancer: The American thyroid association guidelines task force on thyroid nodules and differentiated thyroid cancer. *Thyroid Off J Am Thyroid Assoc* (2015) 2016:26 1–133. doi: 10.1089/thy.2015.0020

14. Zhou J, Yin L, Wei X, Zhang S, Song Y, Luo B, et al. Chinese Guidelines for ultrasound malignancy risk stratification of thyroid nodules: the c-TIRADS. *ENDOCRINE* (2020) 2020:70 256–279. doi: 0.1007/s12020-020-02441-y

15. Mahmud F, Siddique AB, Alam F, Siddique MI. Cytologically indeterminate follicular thyroid nodule on fine needle aspiration cytology is an indication for total thyroidectomy. *Mymensingh Med J* (2019) 28:434–40.

16. Kim H, Kim JA, Son EJ, Youk JH. Quantitative assessment of shear-wave ultrasound elastography in thyroid nodules: diagnostic performance for predicting malignancy. *Eur Radiol* (2013) 23:2532–7. doi: 10.1007/s00330-013-2847-5

17. Adamczewski Z, Stasiak M, Stasiak B, Adamczewska M, Lewiński A. Interobserver agreement and plane-dependent intraobserver variability of shear wave sonoelastography in the differential diagnosis of ectopic thymus tissue. *J Clin Med* (2021) 10(2):214. doi: 10.3390/jcm10020214

18. Brophy C, Stewart J, O'Donovan N, McCarthy J, Murphy M, Sheahan P. Impact of microcalcifications on risk of malignancy in thyroid nodules with indeterminate or benign cytology. *Otolaryngol Head Neck Surg* (2016) 154:46–51. doi: 10.1177/0194599815605326

19. Chernock RD, Lewis JSJr. Classification of psammoma bodies in the revised college of American pathologists thyroid cancer protocol. *Arch Pathol Lab Med* (2015) 139:967. doi: 10.5858/arpa.2014-0483-LE

20. Clement KD, Emslie K, Maniam P, Wilson MSJ. What is the operative cost of managing acute appendicitis in the NHS: The impact of stump technique and perioperative imaging. *World J Surg* (2020) 44:749–54. doi: 10.1007/s00268-019-05306-2

21. Li L, Chen X, Li P, Liu Y, Ma X, Ye YQ. The value of ultrasound-guided fine-needle aspiration cytology combined with puncture feeling in the diagnosis of thyroid nodules. *Acta Cytol.* (2021) 65(5):368–76. doi: 10.1159/000517168

frontiers | Frontiers in Endocrinology

TYPE Original Research
PUBLISHED 09 December 2022
DOI 10.3389/fendo.2022.1038041

OPEN ACCESS

EDITED BY
Erivelto Martinho Volpi,
Centro de referencia no ensino do diagnóstico por imagem (CETRUS), Brazil

REVIEWED BY
Lingyu Bao,
National Institutes of Health (NIH), United States
Lilah Morris-Wiseman,
Johns Hopkins Medicine, United States
Gregorio Scerrino,
University of Palermo, Italy

*CORRESPONDENCE
Kang Chen
cycon_ck@yeah.net
Xuan Wang
endocrine@163.com
Yi Fang
fangyi5zhongxin@163.com

†These authors contributed equally to the work

SPECIALTY SECTION
This article was submitted to Thyroid Endocrinology, a section of the journal Frontiers in Endocrinology

RECEIVED 06 September 2022
ACCEPTED 28 November 2022
PUBLISHED 09 December 2022

CITATION
Zhang T-t, Zeng J, Yang Y, Wang J-j, Kang Y-j, Zhang D-h, Liu X-z, Chen K, Wang X and Fang Y (2022) A visualized dynamic prediction model for survival of patients with geriatric thyroid cancer: A population-based study. *Front. Endocrinol.* 13:1038041. doi: 10.3389/fendo.2022.1038041

A visualized dynamic prediction model for survival of patients with geriatric thyroid cancer: A population-based study

Ting-ting Zhang[1†], Jing Zeng[1†], Yan Yang[1†], Jin-jing Wang[1], Yao-jie Kang[1], Dong-he Zhang[2], Xiao-zhu Liu[3], Kang Chen[4*], Xuan Wang[1*] and Yi Fang[1*]

[1]Department of Endocrinology, The Fifth Medical Center of Chinese PLA General Hospital, Beijing, China, [2]Department of Day Clinic, The Fifth Medical Center of Chinese People's Liberation Army (PLA) General Hospital, Beijing, China, [3]Department of Cardiology, The Second Affiliated Hospital of Chongqing Medical University, Chongqing, China, [4]Department of Endocrinology, The First Medical Center of Chinese People's Liberation Army (PLA) General Hospital, Beijing, China

Objective: Thyroid cancer (TC) is a common malignancy with a poor prognosis with aging. However, no accurate predictive survival model exists for patients with geriatric TC.We aimed to establish prediction models of prognosis in elderly TC.

Methods: We retrospectively reviewed the clinicopathology characteristics of patients with geriatric TC in the Surveillance, Epidemiology, and End Results database (SEER) from 2004 to 2018. The risk predictors used to build the nomograms were derived from the Cox proportional risk regression. These nomograms were used to predict 1-, 3-, and 5-year overall survival and cancer-specific survival in elderly patients with TC. The accuracy and discriminability of the new model were evaluated by the consistency index (C-index) and calibration curve. The clinical applicability value of the model was assessed using the decision curve analysis.

Results: We used the SEER database to include 16475 patients with geriatric TC diagnosed from 2004 to 2018. The patients from 2004 to 2015 were randomly sorted out on a scale of 7:3. They were classified into a training group (n = 8623) and a validation group (n = 3669). Patients with TC diagnosed in 2016–2018 were classified into external validation groups (n = 4183). The overall survival nomogram consisted of 10 variables (age, gender, marital status, histologic type, grade, TNM stage, surgery status, and tumor size). A cancer-specific survival nomogram consisted of eight factors (age, tumor size, grade, histologic type, surgery, and TNM stage). The C-index values for the training, validation, and external validation groups were 0.775 (95% confidence interval [CI] 0.785–0.765), 0.776 (95% CI 0.792–0.760), and 0.895(95% CI 0.873–0.917), respectively. The overall survival was consistent with a nomogram based on the calibration curve. Besides, the decision curve analysis showed excellent clinical application value of the nomogram. Additionally, we found that surgery

could improve the prognosis of patients with geriatric at high-risk (P < 0.001) but not those at low-risk (P = 0.069).

Conclusion: This was the first study to construct predictive survival nomograms for patients with geriatric TC. The well-established nomograms and the actual results could guide follow-up management strategies.

KEYWORDS

thyroid cancer, geriatric patient, nomogram, prediction model, SEER

Introduction

Undoubtedly one of the most common endocrine cancers is thyroid carcinoma (TC) (1). Despite its steady disease-specific mortality (0.5/100,000) (2), the TC incidence rate over the past 20 years has increased by approximately 2.5 times (5.57/100,000-13.98/100,000) (3). By 2030, TC is anticipated to be the fourth most prevalent cancer in the USA (4). However, the South Korean experience indicates that they will need to discourage early thyroid cancer discovery if they wish to stop their own "epidemic".Vital statistics and cancer registry data for South Korea illustrate the effect of thyroid-cancer screening since 1999. Thyroid-cancer incidence increased rapidly after the turn of the century In 2011, the rate of thyroid-cancer diagnoses was 15 times that observed in 1993. This entire increase can be attributed to the detection of papillary thyroid cancer. Furthermore, despite the dramatic increase in incidence, mortality from thyroid cancer remains stable — a combination that is pathognomonic for over diagnosis (5).

With the continuously improved cancer prevention and treatment, the population aged ≥65 years will rise from 15% to 21% by 2030 in USA (6). In 2000, Americans aged ≥80 years represented approximately 3.3% of the population, which is expected to show a 2-fold increase by 2050 (7). Given the advanced age of patients with TC, we must consider the challenges that may arise as a direct result. In the 2015 Korean Central Cancer Registry, thyroid cancer was reported to be the fourth most common cancer in women aged 65 years or older (8).Recent literature shows that particularly poor prognosis is associated with age greater than 60 years (9, 10).Additionally, older individuals typically have more advanced-stage, aggressive, and widespread TC (11). Elderly individuals with TC often have follicular histology, vascular invasion, and extrathyroidal extension (12).In fact, Anaplastic thyroid cancer (ATC) is relatively more common with advanced age (13–16).. In several studies, older patients have had large volume tumor, lymph node metastasis, and distant metastasis at diagnosis and recurrence (17, 18). The survival rate was independently associated with a poorer prognosis starting at 60 years; elderly patients >70 years had the worst prognosis (12)..

TC has a satisfying good prognosis, with an average survival rate of 10 years for 90% of patients (19, 20). The median age of death for patients with TC is 73 years, and >70% of the deaths occur when patients are aged ≥65 years (21). A risk stratification technique that can enhance outcomes is required to predict overall survival (OS) for older patients with TC due to the limits of available treatment choices. Within this context, TNM staging can be used to determine the clinical staging of patients with cancer. However, the TNM classification is still insufficient in covering tumor biology and predicting all TC outcomes and treatment decisions made by elderly patients.

Nomograms have proved superior to the TNM staging system in different cancer studies (22, 23). A nomogram is a simple, user-friendly statistical prediction tool used to predict and quantify individual patient outcomes (24, 25). Population-based statistics show that, nevertheless, no study has created a nomogram of elderly TC persons. With the support of the Surveillance, Epidemiology, and End Results database (SEER) (26), we aimed to construct and verify a web-based survival prediction model for geriatric patients with TC. This model may be useful for individualized therapy, prognostic prediction, and follow-up strategy.

Materials and methods

Patient and screening criteria

The data of geriatric patients with TC were obtained using the SEER∗ Stat software (version 8.3.8). The timeframe for data collection was from 2004 to 2018.

The inclusion criteria were as follows: (1) patients aged ≥65 years; (2) positive histological diagnosis of TC by the 3rd Edition of the International Classification of Diseases for Oncology (ICD-O-3) without an autopsy or death certificate; (3) AJCC stage I–III with a histological grade I–III; (4) a positive follow-up.

The following exclusion criteria were used: (1) patients who had a second primary malignancy, (2) patients who missed follow-ups, and (3) patients who had non-complete clinical data (marital status, cause of death, survival month, tumor size, staging, and follow-up months). Patients were randomly distributed to a training or internal validation group and an external validation group. The study required no local ethical approvals or statements, as all data in the research were selected out of the SEER database.

Variables and outcomes

Based on 14 clinical variables, we examined the age at diagnosis, race (Black, White and other, which including American Indian/Alaska Native and Asian/Pacific Islander), sex (female and male), marital status, years of diagnosis (2004–2009, 2009–2015, and 2016–2018), grade (I–III), histological subtype (papillary, follicular, medullary, or anaplastic), T stage (T1–T4), M stage (M0 or M1), N stage (N0–N1), tumor size, surgery, radiotherapy, and chemotherapy conditions. Patients who were widowed, divorced, separated, or bachelor (with a domestic partner or unmarried) were classified as unmarried. Regarding grading, grade I represented a highly differentiated cancer, grade II represented a moderately differentiated cancer, and grade III represented a poorly differentiated cancer. grade IV represented Undifferentiated cancer. Tumor diameters (0–10, 11–20, 21–40, and >40 mm) were translated into classification variables to test the linear hypothesis. There was no detailed information about radiotherapy regimens and chemotherapy drugs in the SEER database; therefore, these variables could not be further evaluated and controlled in this study. Finally, these TC's variables (radiotherapy and chemotherapy) are used as dichotomous variables. The primary outcomes were OS and cancer-specific survival (CSS).The total survival time from TC diagnosis to TC-related or other causes of death as OS, whereas diagnosis to death or censoring as a result of TC was defined as CSS. For TNM staging, the 6-8th edition of the AJCC clinical staging guidelines was used for the study, which used the data from 2004-2018.

Statistical analysis

The training cohort was used to construct the nomograms and develop the predictive model and risk stratification system. In contrast, the validation cohort was used to test the predictive model and risk stratification system. All eligible cases were randomized into the training and internal validation cohort (split 7:3) from 2004 to 2015. All eligible patients from 2016 to 2018 were used as the external validation group.

Cox Proportional Hazards Regression Models for each putative prognostic variable were used to calculate the associated 95% CIs and hazard ratios (HRs). Multivariate analysis included the relevant factors from a univariate analysis ($P < 0.05$). Besides, the statistical studies contributed to using the program SPSS 24 (SPSS, Chicago, IL). Based on the results of the multivariable analysis, the well-constructed nomogram may provide graphical risk predictions using the RMS and survival packages of R 4.0.2. The nomograms were validated both internally and externally. Nomograms were built as an intuitive scoring plot based on the traditional Cox proportional risk regression model. We combined the predictive power of conventional regression models with user-friendly and easy-to-use performance to construct a nomogram to predict patient survival. The TNM stage system and the net clinical advantages of the prediction model were further evaluated using a decision curve analysis (DCA).

Meanwhile, a risk categorization system was established based on each patient's total nomogram score. The X-Tile program determined the best cut-off value for each patient's total score (Robert L. Camp, Yale University, New Haven, Connecticut, USA). The patients were then divided into two prognostic categories based on the best cut-off value: the low-risk and high-risk groups. The Kaplan–Meier curves and log-rank test were also used to depict and compare the OS and CSS of patients with geriatric in various risk groups.

Results

General clinicopathological features

Between 2004 and 2018, 16475 registered geriatric patients with TC were included from the SEER database according to the eligibility criteria. Figure 1 illustrates the flowchart of the patient selection process. There were no significant differences in demographic information, tumor type, or treatment between the training and validation groups (Table 1), including the training group (n = 8623, diagnosed between 2004 and 2015), and the validation sample comprised 3,669 patients (n = 3669, diagnosed between 2004 and 2015). Table S1 demonstrates the patients (n = 4183, diagnosed between 2016 and 2018) in the external validation group.

In the whole study cohort, the average age was 72.6 (SD: 6.32) years; 8262 (67.2%) patients were female, and 4030 (32.8%) were male. Among all patients, the average age was 72.6 (SD: 6.34) in the training group and 72.6 (SD: 6.27) in the internal validation group. Most tumors (62.8%) were ≥1.0 cm in size. A total of 76.4% of patients received thyroidectomy, and 44.1% of patients received radioactive iodine. Additionally, 53.1% (6,524 out of 12,292), 13.8% (1,695 out of 12,292), 22.3% (2,741 out of 12,292), and 10.8% (1,332 out of 12,292) of patients had T1, T2,

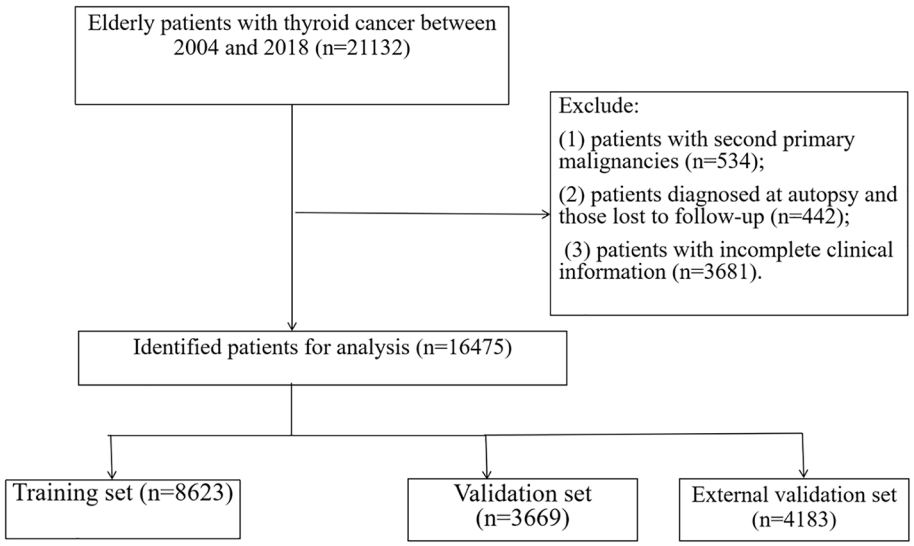

FIGURE 1
The flowchart of including and dividing patients.

TABLE 1 Clinicopathological characteristics of elderly patients with thyroid cancer.

	ALL N = 12292	Training cohort 1 N = 8623	Validation cohort 2 N = 3669	p
Age	72.6 (6.32)	72.6 (6.34)	72.6 (6.27)	0.714
Race				0.986
white	10259 (83.5%)	7195 (83.4%)	3064 (83.5%)	
black	690 (5.61%)	486 (5.64%)	204 (5.56%)	
other	1343 (10.9%)	942 (10.9%)	401 (10.9%)	
Sex				0.322
Male	4030 (32.8%)	2803 (32.5%)	1227 (33.4%)	
Female	8262 (67.2%)	5820 (67.5%)	2442 (66.6%)	
Marital				0.694
No	5127 (41.7%)	3607 (41.8%)	1520 (41.4%)	
Married	7165 (58.3%)	5016 (58.2%)	2149 (58.6%)	
Year of diagnosis				0.418
2004-2009	4799 (39.0%)	3346 (38.8%)	1453 (39.6%)	
2010-2015	7493 (61.0%)	5277 (61.2%)	2216 (60.4%)	
Histologic type				0.753
Papillary	10251 (83.4%)	7211 (83.6%)	3040 (82.9%)	
Follicular	1034 (8.41%)	717 (8.31%)	317 (8.64%)	
Medullary	626 (5.09%)	434 (5.03%)	192 (5.23%)	
Anaplastic	381 (3.10%)	261 (3.03%)	120 (3.27%)	
Grade				0.285
I	1721 (14.0%)	1195 (13.9%)	526 (14.3%)	
II	470 (3.82%)	311 (3.61%)	159 (4.33%)	
III	224 (1.82%)	158 (1.83%)	66 (1.80%)	
IV	479 (3.90%)	330 (3.83%)	149 (4.06%)	
Unknown	9398 (76.5%)	6629 (76.9%)	2769 (75.5%)	

(Continued)

TABLE 1 Continued

	ALL N = 12292	Training cohort 1 N = 8623	Validation cohort 2 N = 3669	p
T				0.197
T1	6524 (53.1%)	4628 (53.7%)	1896 (51.7%)	
T2	1695 (13.8%)	1172 (13.6%)	523 (14.3%)	
T3	2741 (22.3%)	1910 (22.2%)	831 (22.6%)	
T4	1332 (10.8%)	913 (10.6%)	419 (11.4%)	
N				0.142
N0	9684 (78.8%)	6796 (78.8%)	2888 (78.7%)	
N1a	1259 (10.2%)	905 (10.5%)	354 (9.65%)	
N1b	1349 (11.0%)	922 (10.7%)	427 (11.6%)	
M				1.000
M0	11723 (95.4%)	8224 (95.4%)	3499 (95.4%)	
M1	569 (4.63%)	399 (4.63%)	170 (4.63%)	
Tumor.size				0.360
0-10mm	4568 (37.2%)	3232 (37.5%)	1336 (36.4%)	
11-20mm	3114 (25.3%)	2201 (25.5%)	913 (24.9%)	
21-40mm	2828 (23.0%)	1958 (22.7%)	870 (23.7%)	
>40mm	1782 (14.5%)	1232 (14.3%)	550 (15.0%)	
Surgery				0.410
No	701 (5.70%)	474 (5.50%)	227 (6.19%)	
Lobectomy	1777 (14.5%)	1241 (14.4%)	536 (14.6%)	
Subtotal or near total thyroidectomy	428 (3.48%)	307 (3.56%)	121 (3.30%)	
Total thyroidectomy	9386 (76.4%)	6601 (76.6%)	2785 (75.9%)	
Chemotherapy				1.000
No/Unknown	12015 (97.7%)	8429 (97.8%)	3586 (97.7%)	
Yes	277 (2.25%)	194 (2.25%)	83 (2.26%)	
Radiation				0.490
No/Unknown	6871 (55.9%)	4838 (56.1%)	2033 (55.4%)	
Yes	5421 (44.1%)	3785 (43.9%)	1636 (44.6%)	
Survival months	76.5 (42.9)	76.6 (42.9)	76.0 (42.8)	0.474

T3, and T4 tumors, respectively. Furthermore, 78.8% (9,684 of 12,292) of the patients were in the negative N stage, and 21.2% (4,129 of 12,292) were in the positive N stage. The average follow-up duration in the study cohort was 76.5 months (SD: 42.9). Moreover, 85.6% (83.8%–87.4%), 80.6% (79.1%–82.1%), and 78.7% (77.4%–80.1%) represented the 1-, 3-, and 5-year OS rates in the training group, respectively. The 1-, 3-, and 5-year OS rates in the validation group were 87.8% (85.4%–90.2%), 81.5% (79.3%–83.7%), and 78.8% (76.8%–80.8%), respectively.

Univariate and multivariate analyses

In the training group, age, race, sex, marital status, years of diagnosis, histologic type, pathological grade, TNM stage, tumor size, surgery, radiation, and chemotherapy were all determined using the univariate Cox regression analysis with $P < 0.05$. Next, these characteristics were then examined in a multivariate Cox regression model (Table 2), which showed that the clinical features associated with survival included age (HR 1.076, 95% CI 1.07–1.082), sex (HR 0.685, 95% CI 0.63–0.745), marital status (HR 0.779, 95% CI 0.718–0.845), histologic type (papillary as a reference; medullary: HR 1.361, 95% CI 1.167–1.589; anaplastic: HR 1.671, 95% CI 1.243–2.245), tumor grade (grade I as a reference; grade III: HR 1.566, 95% CI 1.234–1.989; grade IV: HR 3.223, 95% CI 2.392–4.344), T stage (T1 as a reference; T4: HR 1.53, 95% CI 1.28–1.83), N stage (N0 as a reference; N1a: HR 1.174, 95% CI 1.032–1.335; N1b: HR 1.469, 95% CI 1.311–1.646), M stage (M0 as a reference; M1: HR 2.848, 95% CI 2.488–3.26), tumor size (0–10 mm as a reference; 21–40 mm: HR 1.481, 95% CI 1.143–1.669; >40 mm: HR1.639, 95% CI 1.369–1.963), and surgery procedure (no surgery as a reference; lobectomy. HR 0.441, 95% CI 0.378–0.516; subtotal or near total thyroidectomy: HR 0.524, 95% CI 0.42–0.653; total thyroidectomy: HR 0.403, 95%

10.3389/fendo.2022.1038041

TABLE 2 Univariate and multivariate analyses of OS in training set.

	Univariate			Multivariate		
	HR	95%CI	P	HR	95%CI	P
Age	1.1	1.09-1.1	<0.001	1.076	1.07-1.082	<0.001
Sex						
Male						
Female	0.67	0.62-0.73	<0.001	0.685	0.63-0.745	<0.001
Race						
white						
black	1.18	1.01-1.37	0.04			
other	0.9	0.79-1.03	0.116			
Year of diagnosis						
2004-2009						
2010-2015	1	0.92-1.09	0.993			
Marital						
No						
Married	0.71	0.66-0.77	<0.001	0.779	0.718-0.845	<0.001
Histologic type						
Papillary						
Follicular	1.28	1.12-1.46	<0.001	0.957	0.83-1.102	0.54
Medullary	1.67	1.44-1.94	<0.001	1.361	1.167-1.589	<0.001
Anaplastic	18.5	16.1-21.26	<0.001	1.671	1.243-2.245	0.001
Grade						
I						
II	1.24	0.98-1.58	0.075	0.98	0.771-1.246	0.869
III	3.85	3.06-4.85	<0.001	1.566	1.234-1.989	<0.001
IV	15.69	13.3-18.51	<0.001	3.223	2.392-4.344	<0.001
Unknown	1.13	0.99-1.28	0.062	0.966	0.851-1.096	0.588
T						
T1						
T2	1.5	1.34-1.69	<0.001	0.914	0.742-1.126	0.397
T3	1.61	1.46-1.78	<0.001	0.961	0.821-1.126	0.622
T4	5.37	4.87-5.93	<0.001	1.53	1.28-1.83	<0.001
N						
N0						
N1a	1.38	1.22-1.56	<0.001	1.174	1.032-1.335	0.015
N1b	2.78	2.52-3.08	<0.001	1.469	1.311-1.646	<0.001
M						
M0						
M1	6.53	5.79-7.36	<0.001	2.848	2.488-3.26	<0.001
Tumor size						
0-10mm						
11-20mm	1.27	1.14-1.42	<0.001	1.107	0.987-1.243	0.083
21-40mm	1.93	1.74-2.14	<0.001	1.381	1.143-1.669	0.001
>40mm	3.77	3.39-4.19	<0.001	1.639	1.369-1.963	<0.001
Surgery						
No						
Lobectomy	0.18	0.16-0.21	<0.001	0.441	0.378-0.516	<0.001
Subtotal or near total thyroidectomy	0.21	0.17-0.26	<0.001	0.524	0.42-0.653	<0.001
Total thyroidectomy	0.17	0.15-0.19	<0.001	0.403	0.354-0.459	<0.001

(Continued)

TABLE 2 Continued

	Univariate			Multivariate		
	HR	95%CI	P	HR	95%CI	P
Radiation						
No/Unknown						
Yes	1	0.92-1.07	0.911			
Chemotherapy						
No/Unknown						
Yes	7.5	6.38-8.81	<0.001			

CI 0.354–0.459). These clinical prognostic variables were included in the constructed OS nomogram for further analysis. We also performed a competitive risk multiple analysis on patients who died from cancer (Table 3).

Nomogram development and validation

This study discovered 10 independent predictive factors based on the multivariate Cox regression results and generated

TABLE 3 Multivariate Cox regression models predict cancer-specific mortality in elderly patients with thyroid cancer.

	CSM		
	HR	95%CI	P
Age	1.038	1.02 - 1.05	<0.001
Sex			
Male			
Female	0.990	0.83 - 1.18	0.91
Race			
white			
black	0.909	0.65 - 1.26	0.57
other	1.135	0.9 - 1.43	0.28
Year of diagnosis			
2004-2009			
2010-2015	0.806	0.68 - 0.96	0.013
Marital			
No			
Married	0.851	0.72 - 1.01	0.066
Histologic type			
Papillary			
Follicular	1.119	0.85 - 1.48	0.4
Medullary	2.320	1.8 - 2.98	<0.001
Anaplastic	1.381	0.94 - 2.03	0.099
Grade			
I			
II	1.347	0.83 - 2.17	0.22
III	2.762	1.87 - 4.07	<0.001
IV	5.185	3.3 - 8.14	<0.001
Unknown	1.068	0.79 - 1.45	0.67
T			
T1			
T2	1.166	0.75 - 1.81	0.5
T3	1.894	1.35 - 2.67	<0.001

(Continued)

10.3389/fendo.2022.1038041

TABLE 3 Continued

	CSM		
	HR	95%CI	P
T4	4.675	3.21 - 6.8	<0.001
N			
N0			
N1a	1.606	1.29 - 2	<0.001
N1b	1.447	1.16 - 1.8	<0.001
M			
M0	3.896	3.1 - 4.89	<0.001
M1			
Tumor size			
0-10mm			
11-20mm	1.392	1.01 - 1.92	0.046
21-40mm	1.910	1.28 - 2.84	<0.001
>40mm	2.461	1.68 - 3.61	<0.001
Surgery			
No			
Lobectomy	0.586	0.42 - 0.81	<0.001
Subtotal or near total thyroidectomy	0.816	0.54 - 1.23	0.33
Total thyroidectomy	0.561	0.43 - 0.74	<0.001
Radiation			
No/Unknown			
Yes	0.978	0.81 - 1.18	0.82
Chemotherapy			
No/Unknown			
Yes	1.210	0.9 - 1.62	0.2

a predictive OS nomogram. Age, sex, marital status, histologic type, tumor grade, T stage, N stage, M stage, tumor size, and operation are all shown in Figure 2A. Each clinical feature was assigned a score. The estimated 1-, 3-, and 5-year OS probabilities were easily calculated by adding the scores for all 10 clinical features and drawing a vertical line between the total score and the survival probability axis. Tumor grade and M stage were found to substantially impact prognosis, followed by surgical type, histologic type, T stage, tumor size, N stage, sex, race, and marital status on the nomogram. The training and validation groups had C-indices of 0.775 (95% CI: 0.785–0.765) and 0.776 (95% CI: 0.792–0.760), respectively.

According to Figure 3, the training group's 1-, 3-, and 5-year areas under the curve (AUCs) were 0.856, 0.806, and 0.787, respectively. On the other hand, the validation group's 1-, 3-, and 5-year AUCs were, respectively, 0.878, 0.815, and 0.787. These findings demonstrated that the model prediction accuracy was high. Calibration curves of the training and validation groups used 1,000 bootstraps, suggesting high agreement between anticipated and actual outcomes (Figure 4). TNM staging was compared with the DCA curve of the training group to assess the clinical viability of the nomogram. According to the results, the nomogram was more vital in predicting 1-, 3-, and 5-year OS in patients with geriatric TC compared to TNM staging (Figure 5).

Additionally, we constructed a competitive risk model to predict patients' CSS (Figure 2B). The 1-, 3-, and 5-year C-indexes of the training group were 93.9, 92.1, and 90.5, respectively. The 1-, 3-, and 5-year C-indexes of the validation group were 95.5, 93.9, and 91.2, respectively. The 1- and 3-year C-indexes of the external validation group were 95.1 and 95.2, respectively. The calibration curve of the competitive risk model also showed that the predicted value is highly consistent with the actual observed value, suggesting that the model has good accuracy (Figures 6A, B). The calibration curve of external validation also showed that the model has good accuracy (Figure 6C).

Risk stratification analysis

Following the optimal cut-off value, patients were divided into two prognostic groups: the low-risk group (total score ≤ 24.9) and the high-risk group (total score > 24.9) (Figures 7A, B).

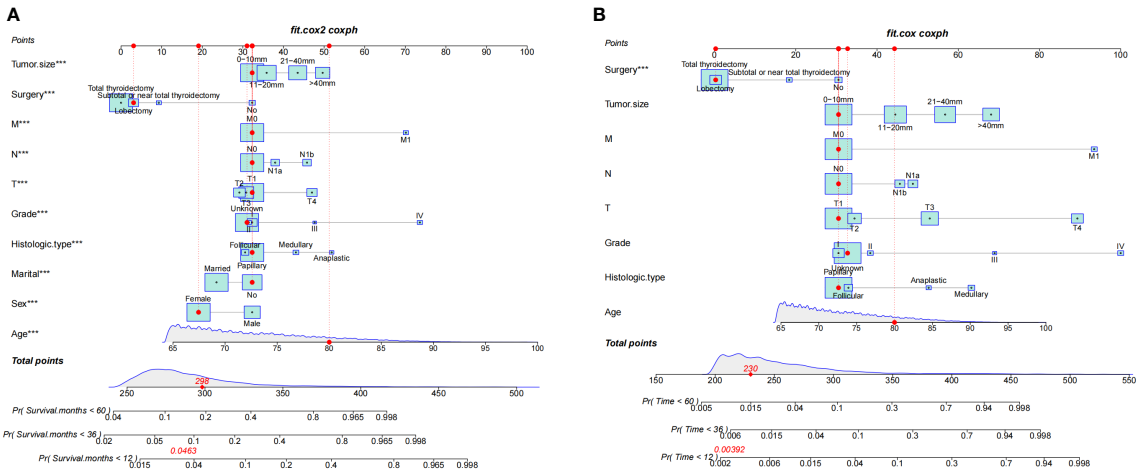

FIGURE 2
Nomograms for 1-, 3-, and 5-year OS **(A)** and CSS **(B)** of patients with TC. ***, a highly significant variable.

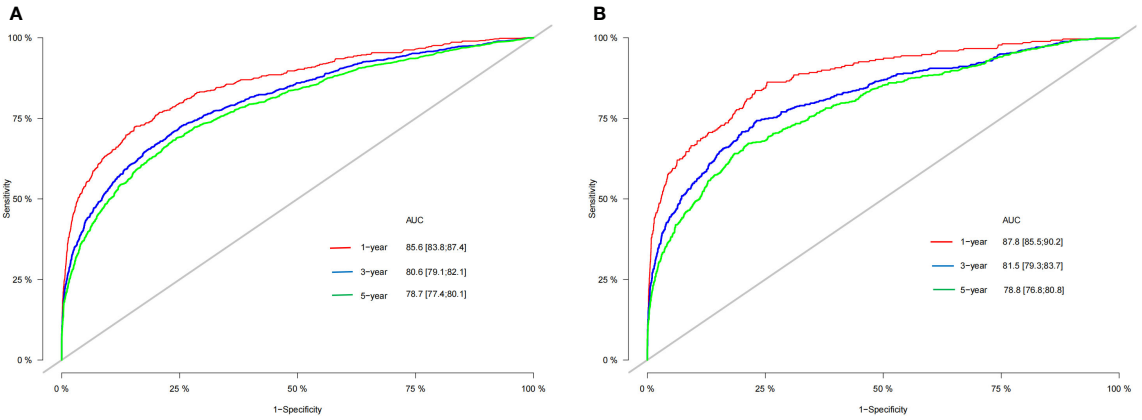

FIGURE 3
The AUC for OS of 1-, 3- and 5-year of training cohort **(A)** and validation cohort **(B)**.

According to the Kaplan–Meier curve, the risk stratification system could accurately recognize the training and validation cohorts from the OS. The high-risk patients had 1-, 3-, and 5-year OS rates of 91.8%, 84.1%, and 76.9%, respectively. On the other hand, the low-risk patients had 1-, 3-, and 5-year OS rates of 99.3%, 97.2%, and 79.50%, respectively.

Effects of surgery on survival in different stratifications

Kaplan–Meier curves were created for the low-risk and high-risk groups to further analyze the benefit of surgery in terms of survival (Figures 8A, B).In addition, the impact of different surgical methods on the survival probability of patients in the low-, and high-risk groups was summarized. In the low-risk group, almost everyone has undergone surgery (Figure 8A). A subset of patients in the high-risk group did not undergo surgery; that group had the lowest survival probability (Figure 8B).

Construction of a web app for easy nomogram access

The online app may be found at https://zhangtingting.shinyapps.io/DynNomapp/ and is designed to help researchers and physicians determine patient survival probabilities.

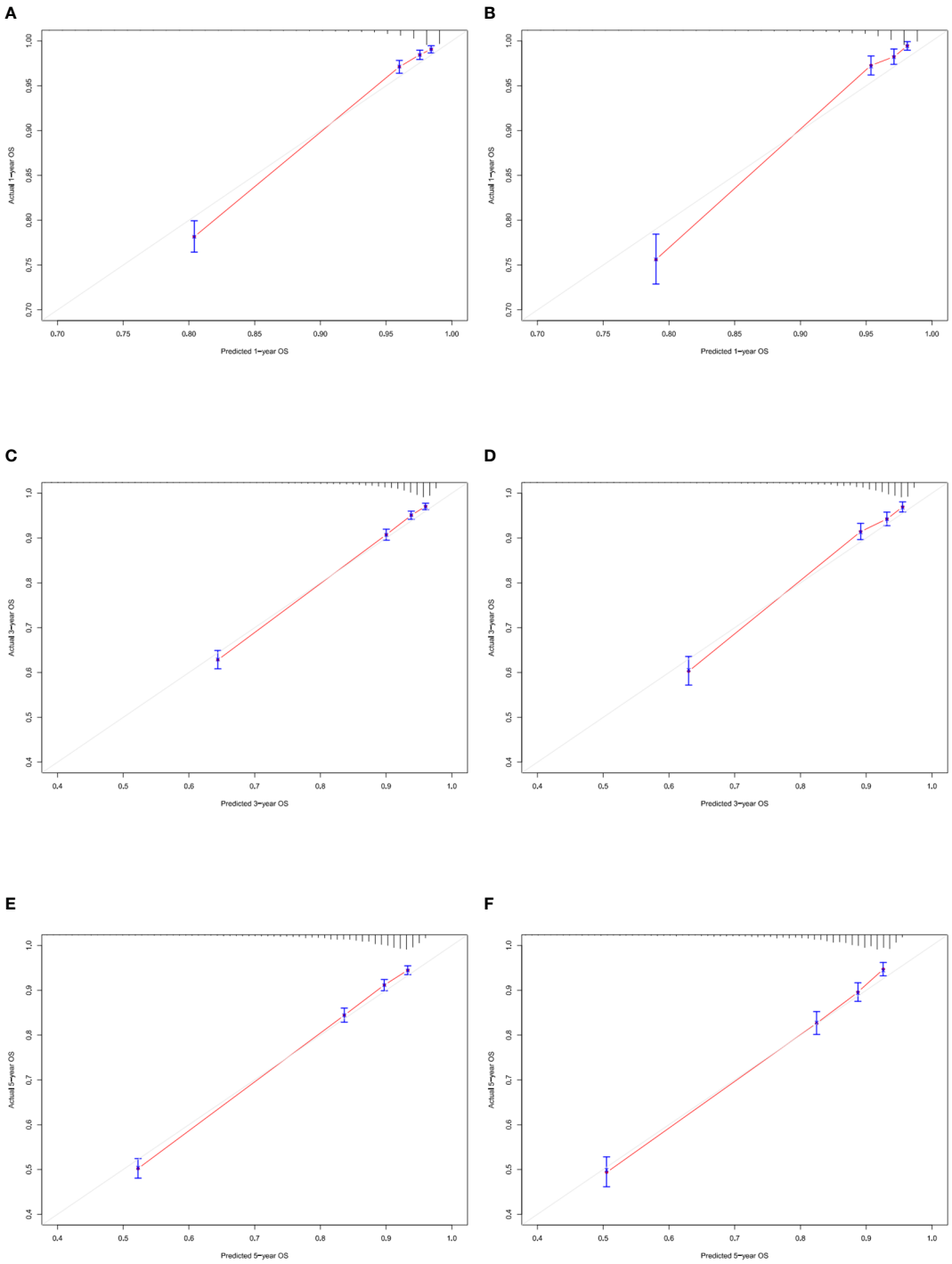

FIGURE 4
Calibration curves of nomogram. **(A–C)** For 1-, 3-, and 5-year OS in training cohort; **(D–F)** For 1-, 3-, and 5-year OS in validation cohort.

Discussion

In this study, 16475 individuals with geriatric TC were included. The histologic type, tumor grade, TNM stage, tumor size, and surgery were determined by the univariate and multivariate Cox analyses. The C-index and calibration charts were used to test the model and revealed good differentiation and calibration. According to DCA, our OS nomogram had a superior clinical net and a more excellent

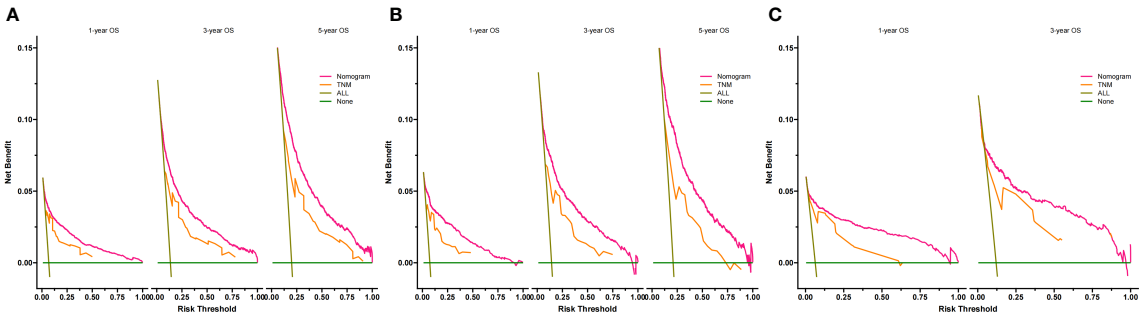

FIGURE 5
Decision curves of the nomogram predicting OS in training cohort **(A)**, validation cohort **(B)** and external validation cohort **(C)**. The y-axis represents the net benefit, and the x-axis represents the threshold probability. When the threshold probability is between 20% and 60%, the net benefit of the model exceeds all deaths or no deaths.

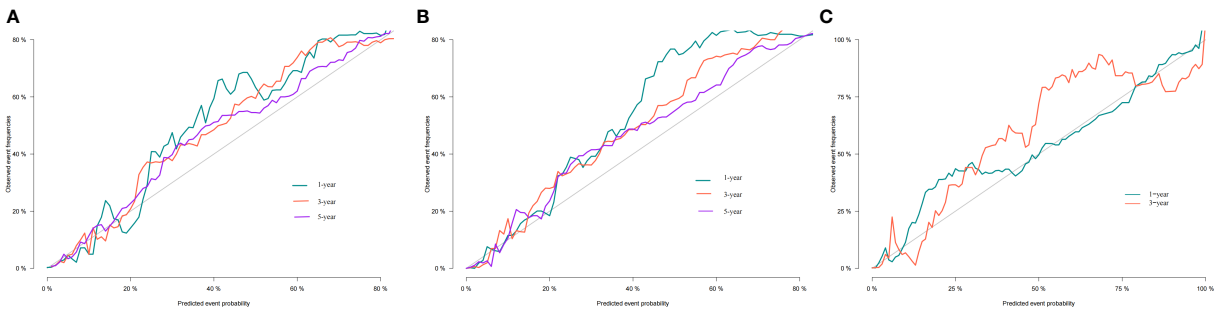

FIGURE 6
Calibration curves of nomogram. **(A)** For 1-, 3-, and 5-year CSS in training cohort; **(B)** For 1-, 3-, and 5-year CSS in validation cohort; **(C)** For 1-, 3-year CSS in external validation cohort.

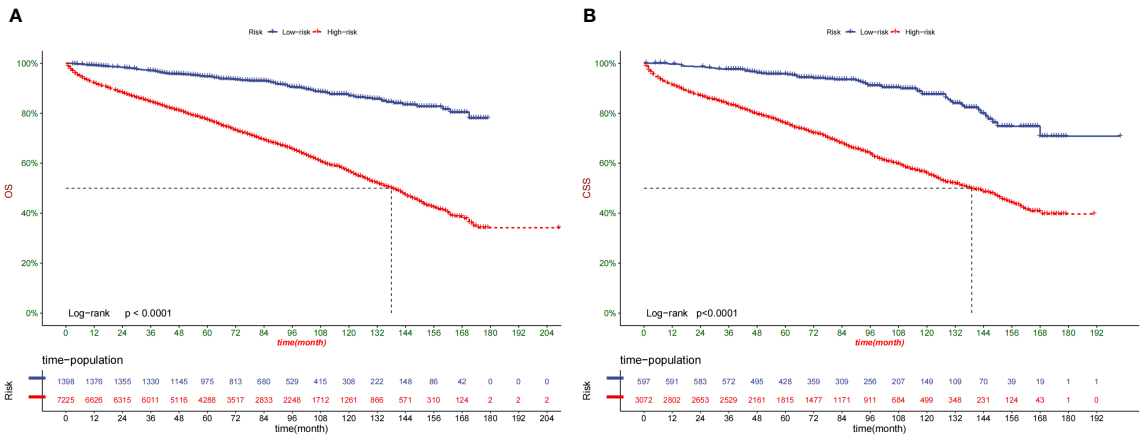

FIGURE 7
Kaplan–Meier curves of OS for patients in the low-, and high-risk groups in the training Cohort **(A)** and validation Cohort **(B)**.

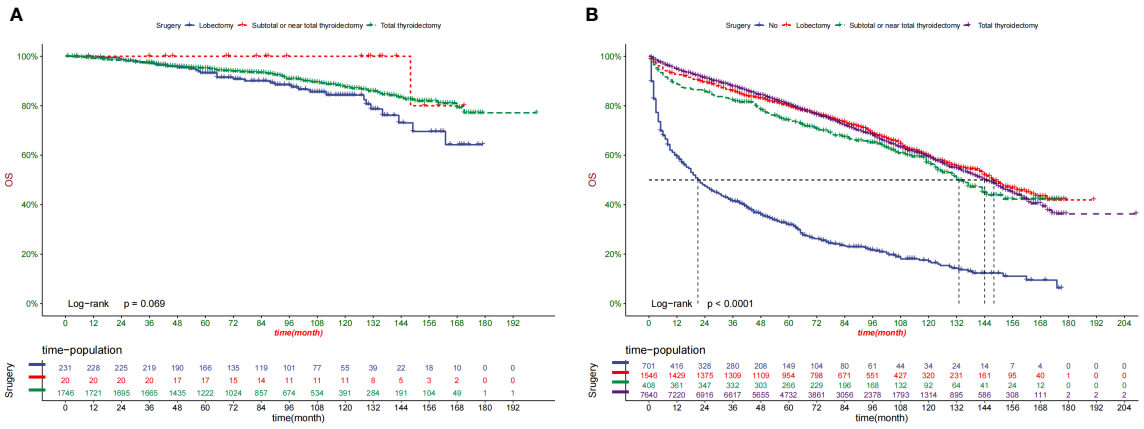

FIGURE 8
OS prediction of patients with different surgery in low- **(A)** and high-risk **(B)** group.

threshold probability range in predicting 1-, 3-, and 5-year OS in the training and validation groups than the usual TNM stage system. Meanwhile, the CSS nomogram was constructed using eight independent parameters: age, tumor size, grade, histologic type, surgery, T stage, N stage, and M stage. Although the prognosis of thyroid cancer varies considerably by histological type, inspired by previous studies (27), we included elderly patients with thyroid cancer of various tissue types and included tissue type as a variable in the regression analysis. Histologic type was included as an important variable in the prediction model's construction with poorer survival for more aggressive histologic subtypes compared to papillary (Table 2, medullary: HR 1.361, 95%CI 1.167–1.589 and anaplastic: HR 1.671, 95% CI 1.243–2.245). In the online APP based on the model construction, clinicians can enter the patient's tissue type. The survival prediction of patients with thyroid cancer including MTC is obtained.

Many scoring systems are used for predictive purposes. Despite a more simplified utilization in the clinic, only a stratified population risk assessment could be conducted for each patient (28). Nomograms are helpful tools for evaluating patient survival outcomes. Statistical modeling and risk quantification are used to handle the difficulty of balancing multiple factors. Their methodical methodology also eliminates the influence of individual physicians' biases or aberrant clinical factors. Nomograms are more accurate than typical stage score methods (29–31). They may also be the most beneficial when the prospective advantages of additional therapy are unknown (32, 33). They are also great for personalized risk assessment and assisting clinicians with clinical care management when there are no definite guidelines.

To the best of our knowledge, this is the first study to describe the development and validation of a nomogram to forecast 5-year OS and CSS in TC-affected elderly individuals. Our nomograms exhibited good calibration and discrimination. The nomograms surpassed the accuracy of the TNM staging mechanism, as seen by the receiver operating characteristic curve. Our nomogram models are straightforward therapeutic aids that can support patient counseling and treatment individualization.

Our nomograms found several independent variables potentially impacting the outcome in elderly patients with TC. First, age is a significant factor for CSS in patients with TC (34). As a separate risk factor, patients with geriatric thyroid cancer have a reduced chance of surviving (35–37). Patients with geriatric TC have unique psychological features compared to younger patients including more comorbidities and shorter life expectancy. Less life expectancy, more comorbidities, and a shorter life expectancy are among these factors. The previous version of the AJCC staging system divided people by 45 years, but the 8th version utilizes 55 years for the same purpose. Age is recognized as a significant prognostic factor independent of the cut-off number.

The gender disparity in TC prevalence has also been thoroughly documented (38). Women are more likely to develop TC than men, although men have worse clinical outcomes (39). The findings of our patients with geriatric were similar to those in prior investigations. In addition to the above-mentioned characteristics, marital status, histologic type, tumor grade, T stage, N stage, M stage, tumor size, and surgery were significant prognostic indicators. However, we discovered that neither gender nor marital status was a risk factor for the 1-, 3-, or 5-year CSS.

The association of marital status and survival was explored in many tumors, including breast cancer, rectal cancer, and non-small cell lung cancer (40–42).We identified that marital status was an independent prognostic factor in the univariate analysis, with married patients having a decreased chance of mortality (43). After adjusting for demographic and clinical characteristics, married patients were shown to have a lower mortality risk than unmarried patients. In a prior study concentrating on differentiated patients with TC, Shi et al. have discovered that single individuals had a higher risk of

tumor death (44). In a study of breast cancer patients aged ≥70 years, marriage has been found to provide higher protection from poorer prognosis (45). According to a study that analyzed more than a million patients diagnosed with various diseases, unmarried individuals have had a greater chance of metastatic cancer and death from cancer (46). Consistent with the findings of the above researches, our results found that marriage was a factor associated with superior survival. There are two possibilities that could explain why married patients live longer than unmarried patients. On the one hand, these married patients were overseen by their spouses for frequent physical checkups before being diagnosed, which helps detect TC early. Meanwhile spouses may also provide more economic support for subsequent treatments. On the other hand, cancer patients are more than four times more likely to suffer from psychological disorders (47). After being diagnosed with cancer, married persons had reduced despair and psychological suffering, which may be attributed to the encouragement and support from their spouses (43, 48).

Our prediction model may be used in clinical practice to estimate patient survival by alerting doctors about the predicted advantages of various therapies. In this study, we found that for elderly patients with TC, almost all patients in the low-risk group undergo thyroidectomy. Regardless of surgical method, patients undergoing surgery have better overall survival. Most high-risk patients did not undergo surgery.

Patients with TC have a variety of risk variables, including age, grade, TNM stage, and tumor size. Elderly patients are more likely to have comorbidities and therefore surgery could reduce the OS rate of patients. However, for the first time, our study found that surgery is advantageous to cancer-specific higher-risk senior individuals with TC ($P < 0.0001$) but not to low-risk groups ($P = 0.069$), providing doctors with suggestions for extending their patients' lives.

This study had some limitations. First, the nomograms were created using historical data. As a result, there was a possibility of selection bias. Second, the SEER does not cover all factors; hence, only 14 variables were included in our analysis. Some critical factors were not included, such as the degree of surgery, radioiodine dose, thyrotropin suppression, etc. Third, as a retrospective cohort research, selection bias might have existed because only patients with comprehensive information on essential characteristics were included. Fourth, the majority of the participants in this study were Americans. As a result, prospective clinical pilot studies are needed to see if the findings can be generalized to different groups.

Conclusion

Based on this study, the first applicable nomograms were created, along with an online application that predicts the personalized long-term OS and CSS of geriatric TC patients. The nomogram performed effectively and had great accuracy and dependability. It is the first nomogram based on a large number of patients with external validation.

Data availability statement

The original contributions presented in the study are included in the article/Supplementary Material. Further inquiries can be directed to the corresponding authors.

Author contributions

T-TZ, YY, and JZ all helped with the idea and design. The data were analyzed by T-TZ, YY, and Y-JK. The manuscript was written by T-TZ. A critical revision of the manuscript was contributed by XW and YF. The final version of the work has been reviewed and approved by all authors.

Funding

This study was supported by The Innovation Fund Youth Cultivation Project (QNPY 2015008).

Acknowledgments

The authors thank the Surveillance, Epidemiology, and End Results program for providing data.

Conflict of interest

The authors declare that the research was conducted in the absence of any commercial or financial relationships that could be construed as a potential conflict of interest.

Publisher's note

Supplementary material

The Supplementary Material for this article can be found online at: https://www.frontiersin.org/articles/10.3389/fendo.2022.1038041/full#supplementary-material

References

1. Siegel RL, Miller KD, Jemal A. Cancer statistics, 2018. *CA Cancer J Clin* (2018) 68(1):7–30. doi: 10.3322/caac.21442

2. Davies L, Welch HG. Increasing incidence of thyroid cancer in the united states, 1973-2002. *JAMA* (2006) 295(18):2164–7. doi: 10.1001/jama.295.18.2164

3. Mao Y, Xing M. Recent incidences and differential trends of thyroid cancer in the USA. *Endocr Relat Cancer*. (2016) 23(4):313–22. doi: 10.1530/ERC-15-0445

4. Deng Y, Li H, Wang M, Li N, Tian T, Wu Y, et al. Global burden of thyroid cancer from 1990 to 2017. *JAMA Netw Open* (2020) 3(6):e208759. doi: 10.1001/jamanetworkopen.2020.8759

5. Ahn HS. And coll: Korea's thyroid-cancer "epidemic"–screening and over diagnosis. *N Engl J Med* (2014) 371(19):1765–7. doi: 10.1056/NEJMp1409841

6. Rahib L, Smith BD, Aizenberg R, Rosenzweig AB, Fleshman JM, Matrisian LM. Projecting cancer incidence and deaths to 2030: the unexpected burden of thyroid, liver, and pancreas cancers in the united states. *Cancer Res* (2014) 74 (11):2913–21. doi: 10.1158/0008-5472.CAN-14-0155

7. Colby SL, Ortman JM. Projections of the size and composition of the US population: 2014 to 2060. In: *Population estimates and projections*. Washington, DC: US Census Bureau (2015). p. 1–13.

8. Sosa JA, Mehta PJ, Wang TS, Boudourakis L, Roman SA. A population-based study of outcomes from thyroidectomy in aging americans: at what cost? *J Am Coll Surg* (2008) 206(6):1097–105. doi: 10.1016/j.jamcollsurg.2007.11.023

9. Jung KW, Won YJ, Oh CM, Kong HJ, Cho H, Lee DH, et al. Prediction of cancer incidence and mortality in Korea, 2015. *Cancer Res Treat* (2015) 47:142–8. doi: 10.4143/crt.2015.066

10. Grogan RH, Kaplan SP, Cao H, Weiss RE, DeGroot LJ, Simon CA, et al. A study of recurrence and death from papillary thyroid cancer with 27 years of median follow-up. *Surgery* (2013) 154:1436–47. doi: 10.1016/j.surg.2013.07.008

11. Durante C, Haddy N, Baudin E, Leboulleux S, Hartl D, Travagli JP, et al. Long-term outcome of 444 patients with distant metastases from papillary and follicular thyroid carcinoma: benefits and limits of radioiodine therapy. *J Clin Endocrinol Metab* (2006) 91:2892–9. doi: 10.1210/jc.2005-2838

12. Park HS, Roman SA, Sosa JA. Treatment patterns of aging americans with differentiated thyroid cancer. *Cancer* (2010) 116(1):20–30. doi: 10.1002/cncr.24717

13. Shi RL, Qu N, Liao T, Wei WJ, Wang YL, Ji QH. The trend of age-group effect on prognosis in differentiated thyroid cancer. *Sci Rep* (2016) 6:27086. doi: 10.1038/srep27086

14. Zivaljevic V, Vlajinac H, Jankovic R, Marinkovic J, Diklic A, Paunovic I. Case-control study of anaplastic thyroid cancer. *Tumori* (2004) 90(1):9–12. doi: 10.1177/030089160409000103

15. Zivaljevic VR, Vlajinac HD, Marinkovic JM, Kalezic NK, Paunovic IR, Diklic AD. Case-control study of anaplastic thyroid cancer: goiter patients as controls. *Eur J Cancer Prev* (2008) 17(2):111–5. doi: 10.1097/CEJ.0b013e3281108036

16. Sorrenti S, Baldini E, Pironi D, Lauro A, D'Orazi V, Tartaglia F, et al. Iodine: Its role in thyroid hormone biosynthesis and beyond. *Nutrients* (2021) 13(12):4469. doi: 10.3390/nu13124469

17. Graceffa G, Salamone G, Contino S, Saputo F, Corigliano A, Melfa G, et al. Risk factors for anaplastic thyroid carcinoma: A case series from a tertiary referral center for thyroid surgery and literature analysis. *Front Oncol* (2022) 12:948033. doi: 10.3389/fonc.2022.948033

18. Amato B, Sivero L, Vigliotti G, Rispoli C, Rocco N, Iannone L, et al. Surgery for cancer in the elderly: state of the art. *Chirurgia* (2013) 26(4):313–5.

19. Vini L, Hyer SL, Marshall J, A'Hern R, Harmer C. Long-term results in elderly patients with differentiated thyroid carcinoma. *Cancer* (2003) 97(11):2736–42. doi: 10.1002/cncr.11410

20. Yang L, Shen W, Sakamoto N. Population-based study evaluating and predicting the probability of death resulting from thyroid cancer and other causes among patients with thyroid cancer. *J Clin Oncol* (2013) 31(4):468–74. doi: 10.1200/JCO.2012.42.4457

21. Liu M, Ruan M, Chen L. Update on the molecular diagnosis and targeted therapy of thyroid cancer. *Med Oncol* (2014) 31(6):973. doi: 10.1007/s12032-014-0973-9

22. NIH National Cancer Institute. *Surveillance, epidemiology, and end results program. cancer stat facts: Thyroid cancer* . Available at: https://seer.cancer.gov/statfacts/html/thyro.html (Accessed October 13, 2020).

23. Balachandran VP, Gonen M, Smith JJ, DeMatteo RP. Nomograms in oncology: more than meets the eye. *Lancet Oncol* (2015) 16:e173–80. doi: 10.1016/S1470-2045(14)71116-7

24. Sternberg CN. Are nomograms better than currently available stage groupings for bladder cancer? *J Clin Oncol* (2006) 24(24):3819–20. doi: 10.1200/JCO.2006.07.1290

25. Karakiewicz PI, Briganti A, Chun FK, Trinh QD, Perrotte P, Ficarra V, et al. Multi-institutional validation of a new renal cancer-specific survival nomogram. *J Clin Oncol* (2007) 25:1316–22. doi: 10.1200/JCO.2006.06.1218

26. Liang W, Zhang L, Jiang G, Wang Q, Liu L, Liu D, et al. Development and validation of a nomogram for predicting survival in patients with resected non-small-cell lung cancer. *J Clin Oncol* (2015) 33(8):861–9. doi: 10.1200/JCO.2014.56.6661

27. Yang T, Hu T, Zhao M, He Q. Nomogram predicts overall survival in patients with stage IV thyroid cancer (TC): A population-based analysis from the SEER database. *Front Oncol* (2022) 12:919740. doi: 10.3389/fonc.2022.919740

28. Yang J, Li Y, Liu Q, Li L, Feng A, Wang T, et al. Brief introduction of medical database and data mining technology in big data era. *J Evid Based Med* (2020) 13 (1):57–69. doi: 10.1111/jebm.12373

29. Amin MB, Greene FL, Edge SB, Compton CC, Gershenwald JE, Brookland RK, et al. The eighth edition AJCC cancer staging manual: Continuing to build a bridge from a population-based to a more "personalized" approach to cancer staging. *CA Cancer J Clin* (2017) 67(2):93–9. doi: 10.3322/caac.21388

30. Roberto M, Botticelli A, Strigari L, Ghidini M, Onesti CE, Ratti M, et al. Prognosis of elderly gastric cancer patients after surgery: a nomogram to predict survival. *Med Oncol* (2018) 35(7):111. doi: 10.1007/s12032-018-1166-8

31. Fang C, Wang W, Feng X, Sun J, Zhang Y, Zeng Y, et al. Nomogram individually predicts the overall survival of patients with gastroenteropancreatic neuroendocrine neoplasms. *Br J Cancer*. (2017) 117(10):1544–50. doi: 10.1038/bjc.2017.315

32. Wan G, Gao F, Chen J, Li Y, Geng M, Sun L, et al. Nomogram prediction of individual prognosis of patients with hepatocellular carcinoma. *BMC Cancer*. (2017) 17(1):91. doi: 10.1186/s12885-017-3062-6

33. Rudloff U, Jacks LM, Goldberg JI, Wynveen CA, Brogi E, Patil S, et al. Nomogram for predicting the risk of local recurrence after breast-conserving surgery for ductal carcinoma in situ. *J Clin Oncol* (2010) 28(23):3762–9. doi: 10.1200/JCO.2009.26.8847

34. Weiser MR, Landmann RG, Kattan MW, Gonen M, Shia J, Chou J, et al. Individualized prediction of colon cancer recurrence using a nomogram. *J Clin Oncol* (2008) 26(3):380–5. doi: 10.1200/JCO.2007.14.1291

35. Shah S, Boucai L. Effect of age on response to therapy and mortality in patients with thyroid cancer at high risk of recurrence. *J Clin Endocrinol Metab* (2018) 103(2):689–97. doi: 10.1210/jc.2017-02255

36. Shen W, Sakamoto N, Yang L. Cancer-specific mortality and competing mortality in patients with head and neck squamous cell carcinoma: a competing risk analysis. *Ann Surg Oncol* (2015) 22(1):264–71. doi: 10.1245/s10434-014-3951-8

37. Skillington SA, Kallogjeri D, Lewis JSJr, Piccirillo JF. Prognostic importance of comorbidity and the association between comorbidity and p16 in oropharyngeal squamous cell carcinoma. *JAMA Otolaryngol Head Neck Surg* (2016) 142(6):568–75. doi: 10.1001/jamaoto.2016.0347

38. Wray CJ, Phatak UR, Robinson EK, Wiatek RL, Rieber AG, Gonzalez A, et al. The effect of age on race-related breast cancer survival disparities. *Ann Surg Oncol* (2013) 20(8):2541–7. doi: 10.1245/s10434-013-2913-x

39. Rahbari R, Zhang L, Kebebew E. Thyroid cancer gender disparity. *Future Oncol* (2010) 6(11):1771–9. doi: 10.2217/fon.10.127

40. Zhang D, Tang J, Kong D, Cui Q, Wang K, Gong Y, et al. Impact of gender and age on the prognosis of differentiated thyroid carcinoma: a retrospective analysis based on SEER. *Horm Cancer.* (2018) 9(5):361–70. doi: 10.1007/s12672-018-0340-y

41. Chen Z, Yin K, Zheng D, Gu J, Luo J, Wang S, et al. Marital status independently predicts non-small cell lung cancer survival: a propensity-adjusted SEER database analysis. *J Cancer Res Clin Oncol* (2020) 146(1):67–74. doi: 10.1007/s00432-019-03084-x

42. Jin JJ, Wang W, Dai FX, Long ZW, Cai H, Liu XW, et al. Marital status and survival in patients with gastric cancer. *Cancer Med* (2016) 5(8):1821–9. doi: 10.1002/cam4.758

43. Wang X, Cao W, Zheng C, Hu W, Liu C. Marital status and survival in patients with rectal cancer: An analysis of the surveillance, epidemiology and end results (SEER) database. *Cancer Epidemiol.* (2018) 54:119–24. doi: 10.1016/j.canep.2018.04.007

44. Shi RL, Qu N, Lu ZW, Liao T, Gao Y, Ji QH. The impact of marital status at diagnosis on cancer survival in patients with differentiated thyroid cancer. *Cancer Med* (2016) 5(8):2145–54. doi: 10.1002/cam4.778

45. Zhai Z, Zhang F, Zheng Y, Zhou L, Tian T, Lin S, et al. Effects of marital status on breast cancer survival by age, race, and hormone receptor status: A population-based study. *Cancer Med* (2019) 8(10):4906–17. doi: 10.1002/cam4.2352

46. Aizer AA, Chen MH, McCarthy EP, Mendu ML, Koo S, Wilhite TJ, et al. Marital status and survival in patients with cancer. *J Clin Oncol* (2013) 31 (31):3869–76. doi: 10.1200/JCO.2013.49.6489

47. Bortolato B, Hyphantis TN, Valpione S, Perini G, Maes M, Morris G, et al. Depression in cancer: The many biobehavioral pathways driving tumor progression. *Cancer Treat Rev* (2017) 52:58–70. doi: 10.1016/j.ctrv.2016.11.004

48. Ai L, Li N, Tan HL, Wei B, Zhao YX, Chen P, et al. Effects of marital status on survival of medullary thyroid cancer stratified by age. *Cancer Med* (2021) 10 (24):8829–37. doi: 10.1002/cam4.4388

frontiers | Frontiers in Endocrinology

TYPE Original Research
PUBLISHED 12 December 2022
DOI 10.3389/fendo.2022.1063998

OPEN ACCESS

EDITED BY
Erivelto Martinho Volpi,
Centro de referencia no ensino do diagnóstico por imagem (CETRUS), Brazil

REVIEWED BY
Andreea Borlea,
UMF Timisoara, Romania
Dana I. Stoian,
Victor Babes University of Medicine and Pharmacy, Romania

*CORRESPONDENCE
Xin-Wu Cui
cuixinwu@live.cn
Ai-jiao Yi
938186822@163.com

†These authors have contributed equally to this work

SPECIALTY SECTION
This article was submitted to Thyroid Endocrinology, a section of the journal Frontiers in Endocrinology

RECEIVED 07 October 2022
ACCEPTED 28 November 2022
PUBLISHED 12 December 2022

CITATION
Wang B, Cao Q, Cui X-W, Dietrich CF and Yi A-j (2022) A model based on clinical data and multi-modal ultrasound for predicting cervical lymph node metastasis in patients with thyroid papillary carcinoma. *Front. Endocrinol.* 13:1063998. doi: 10.3389/fendo.2022.1063998

A model based on clinical data and multi-modal ultrasound for predicting cervical lymph node metastasis in patients with thyroid papillary carcinoma

Bin Wang[1†], Qing Cao[1†], Xin-Wu Cui[2*], Christoph F. Dietrich[3] and Ai-jiao Yi[1*]

[1]Department of Medical Ultrasound, Yueyang Central Hospital, Yueyang, China, [2]Department of Medical Ultrasound, Tongji Hospital, Tongji Medical College, Huazhong University of Science and Technology, Wuhan, China, [3]Department Allgemeine Innere Medizin, Kliniken Hirslanden Beau Site, Salem und Permanence, Bern, Switzerland

Objective: The aim of this study was to explore diagnostic performance based on clinical characteristics, conventional ultrasound, Angio PLUS (AP), shear wave elastography (SWE), and contrast-enhanced ultrasound (CEUS) for the preoperative evaluation of cervical lymph node metastasis (CLNM) in patients with papillary thyroid carcinoma (PTC) and to find a reliable predictive model for evaluating CLNM.

Materials and methods: A total of 206 thyroid nodules in 206 patients were included. AP, SWE, and CEUS were performed for all thyroid nodules. Univariate analysis and multivariate logistic regression analysis were performed to ascertain the independent risk factors. The sensitivity, specificity, and the area under the curve (AUC) of independent risk factors and the diagnostic model were compared.

Results: Sex, age, nodule size, multifocality, contact extent with adjacent thyroid capsule, Emax, and capsule integrity at CEUS were independent risk predictors for CLNM in patients with PTC. A predictive model was established based on the following multivariate logistic regression: Logit (p) = −2.382 + 1.452 × Sex − 1.064 × Age + 1.338 × Size + 1.663 × multifocality + 1.606 × contact extent with adjacent thyroid capsule + 1.717 × Emax + 1.409 × capsule integrity at CEUS. The AUC of the predictive model was 0.887 (95% CI: 0.841–0.933), which was significantly higher than using independent risk predictors alone.

Conclusion: Our study found that male presence, age < 45 years, size ≥ 10 mm, multifocality, contact extent with adjacent thyroid capsule > 25%, Emax ≥ 48.4, and interrupted capsule at CEUS were independent risk predictors for CLNM in

patients with PTC. We developed a diagnostic model for predicting CLNM, which could be a potentially useful and accurate method for clinicians; it might be beneficial to surgical decision-making and patient management and for improving prognosis.

KEYWORDS

contrast-enhanced ultrasound, shear wave elastography, thyroid papillary carcinoma, lymph node metastasis, predictive model

Introduction

Papillary thyroid carcinoma (PTC) is the most common thyroid cancer, with 30%–80% of patients experiencing metastasis to the cervical lymph node (1). Cervical lymph node metastasis (CLNM) can affect surgical options and extent, and it is related to thyroid cancer recurrence and patients' prognosis (2, 3). Therefore, accurate preoperative evaluation of CLNM is extremely important.

Ultrasound is the first-line imaging modality for preoperative CLNM assessment in patients with suspicious malignant nodules (2). Preoperative ultrasound can find suspicious cervical lymphadenopathy in 20%–31% of patients, which might potentially alter the surgical approach (2, 4, 5). However, ultrasound has a low sensitivity in the diagnosis of central lymph node metastasis (10.5%–61%) (6), and metastases are most likely to occur in central lymph nodes. Therefore, it is important to find a method to accurately assess CLNM.

The Angio PLUS microvascular Doppler ultrasound technique (AP) is a novel Doppler technique in the supersonic imaging system. It has been used in other organs such as breast or parathyroid (7, 8) and could detect more low-speed microvessels compared with color Doppler flow imaging. Thus, we expected AP to provide more microvessel information for predicting CLNM.

Shear wave elastography (SWE) can quantitatively assess tissue hardness by obtaining Young's modulus, along with a color-coded elasticity map. Recently, SWE has been widely used in the diagnosis of thyroid nodules, which can be a potential indicator in the diagnosis of thyroid nodules and provide additional information for clinical decision-making (9). However, there were a few studies (6, 10) on the clinical utility of quantitative SWE in predicting CLNM, which found that a high index of thyroid nodules was independently related to CLNM (6), but the optimal cutoff values of Young's modulus were controversial; therefore, it is insufficient to use SWE alone to evaluate CLNM.

Contrast-enhanced ultrasound (CEUS) can present the macro- and micro-vascularization of tumor compared with the surrounding tissues. Recently, CEUS has been widely used in differentiating between benign and malignant thyroid nodules and is a promising noninvasive method in the diagnosis of thyroid nodules (11). Several studies have reported that CEUS is useful for the evaluation of biological behavior and CLNM (12–14), but the enhancement patterns in different studies were inconsistent; thus, it is important to conduct further studies.

CLNM was difficult to evaluate before surgery, especially for central lymph nodes. Clinical characteristics, conventional ultrasound, AP, SWE, and CEUS could provide information for thyroid nodules, which may be useful for the preoperative evaluation of CLNM. To the best of our knowledge, combining the use of clinical characteristics, conventional ultrasound, AP, SWE, and CEUS for the preoperative evaluation of CLNM has rarely been reported. The purpose of this study was to explore the diagnostic performance based on clinical characteristics, conventional ultrasound, AP, SWE, and CEUS for the preoperative evaluation of CLNM and to find a reliable predictive model for CLNM, which would be beneficial to surgical decision-making and for improving patient prognosis.

Materials and methods

This prospective study was approved by the ethics committee of Yueyang Central Hospital, and all patients signed informed consent before CEUS examination and surgery.

Patients

From March 2020 to May 2022, a total of 582 patients with 582 thyroid nodules were evaluated initially. Of these, 206 thyroid nodules in 206 patients were finally enrolled. The inclusion criteria were as follows: (a) the pathology of thyroid nodule in each patient was confirmed as PTC *via* surgery, (b) surgery was conducted within 1 month after SWE and CEUS examination, and (c) age 18 years or older. The exclusion criteria were as follows: (a) had a previous needle biopsy, (b) had previous radiofrequency ablation (RFA), and (c) had a contraindication of CEUS: history of hypersensitivity reactions to sulfur hexafluoride (SonoVue®, Bracco International, Milan, Italy) or to any of the inactive ingredients in SonoVue.

Ultrasound examination

Conventional ultrasound, AP, SWE, and CEUS examinations were conducted using an Aixplorer ultrasound system (Supersonic imaging, France) equipped with an L15-4 linear array transducer for conventional ultrasound or AP and an L10-5 linear array transducer for SWE or CEUS by the same investigator.

Conventional ultrasound examination: The conventional ultrasound was performed with an L15-4 linear array transducer, and the conventional ultrasound images were obtained by scanning the suspicious target thyroid nodules and all regions of cervical lymph nodes, and then the general characteristics were recorded, including location, size, multifocality, composition, echogenicity, shape, margin, echogenic foci (15), and the extent of contact between thyroid nodules and adjacent thyroid capsule (16). All suspicious thyroid nodules were classified as ACR TI-RADS 3 (mildly suspicious), ACR TI-RADS 4 (moderately suspicious), or ACR TI-RADS 5 (highly suspicious) (15), and these nodules were recommended for CEUS and SWE examinations. If there was more than one suspicious thyroid nodule, we chose the highest suspicious thyroid nodule. Multifocality is defined as more than one suspicious thyroid nodule in conventional ultrasound and more than one confirmed malignant nodule by surgical pathology.

AP examination: AP vascularization of nodules was classified into three grades (17): Grade 0, no blood flow in the nodule; Grade I: a few spots of blood flow or one long vessel penetrating into the nodule; Grade II: abundant blood flow with five or more punctate blood flows or two long vessels inside nodules.

SWE examination: After AP examination, the system was changed to SWE mode with an L10-5 linear array transducer. In general, to decrease the effect of artery pulsation on SWE measurement, longitudinal section is usually selected to conduct SWE imaging. Patients should hold their breath for several seconds while the SWE was conducted. The stiffness range of the color map was from blue to red (0–180 kPa). The elasticity characteristics were measured using the quantification box (Q-box), which should contain the whole nodules, excluding the surrounding tissues, and then the system automatically calculated elasticity parameters, including Emin, Emean, and Emax. The median of five measurements was taken.

CEUS examination: After SWE examination, CEUS was performed with the same linear array transducer. The patients should breathe quietly without swallowing, coughing, and talking. To display suspicious target nodules clearly, the double-contrast mode was used. Sulfur hexafluoride was used in this study. A total of 25 mg of sulfur hexafluoride, diluted in 5 ml of 0.9% sodium chloride, was administered to each patient as a 2.4-ml intravenous bolus, followed by a 5-ml saline flush. Then, CEUS imaging was continuously recorded for 90 s in the machine's hard disk.

According to previous studies (14, 18, 19) and our clinical experience, the enhancement patterns of thyroid nodules were evaluated with the following features: peak enhancement intensity (hyper-enhancement, iso-enhancement, or hypo-enhancement); ring enhancement was classified as present or absent; homogeneity of enhancement (homogeneous or heterogeneous); contrast agent arrival time (synchronous with, earlier than, or later than adjacent thyroid tissue); enhancement direction (scattered, centripetal, or centrifugal); enhancement area (equal to, greater than, or less than that on conventional ultrasound); nodule composition at CEUS (nonsolid or solid); enhancement border (the border between the nodule and the surrounding parenchyma at the peak intensity) was classified as well-defined or ill-defined; and capsule integrity at CEUS (the membrane was defined as continuous if the thyroid capsule showed a line-like intact structure) was classified as continuous and interrupted.

Imaging analysis: The same investigator, who had more than 5 years of experience in thyroid conventional ultrasound and 3 years of experience in AP, SWE, and CEUS, carried out all ultrasound examinations. General clinical data, conventional ultrasound, AP, SWE, and CEUS imaging were recorded. According to the pathology after surgery, enrolled patients were divided into the cervical lymph node non-metastasis group and the metastasis group.

Statistical analysis

SPSS 23.0 and MedCalc 19.0 were used for all statistical analysis. A receiver operating characteristic (ROC) curve differentiating the non-metastasis group from the metastasis group was drawn based on Young's modulus for each nodule. The optimal cutoff value and area under the curve (AUC) were calculated. The count data of clinical characteristics, AP, SWE, and the enhancement patterns of CEUS were compared with Kappa analysis or Fisher's exact test. $p < 0.05$ was regarded as the threshold for statistical significance. In order to identify the independent risk factors, variables that show univariate significance for CLNM were added to a multivariate logistic regression analysis. The diagnostic performance of independent risk factors and the diagnostic model was calculated with ROC, and the sensitivity, specificity, and the AUC of independent risk factors and the diagnostic model were compared.

Results

General clinical data and conventional ultrasound features between the non-metastasis group and the metastasis group

We chose the highest suspicious thyroid nodule for patients with more than one suspicious thyroid nodule, which was

confirmed PTC by surgical pathology. Neck dissection was performed in all 206 enrolled patients. In the end, the surgically pathological results showed that 123 nodules were PTC without CLNM and 83 nodules were PTC with CLNM (Figure 1). The rate of CLNM was 40.29% in this study. All the nodules were classified into either the non-metastasis group or the metastasis group. General clinical characteristics and conventional ultrasound features are summarized in Table 1.

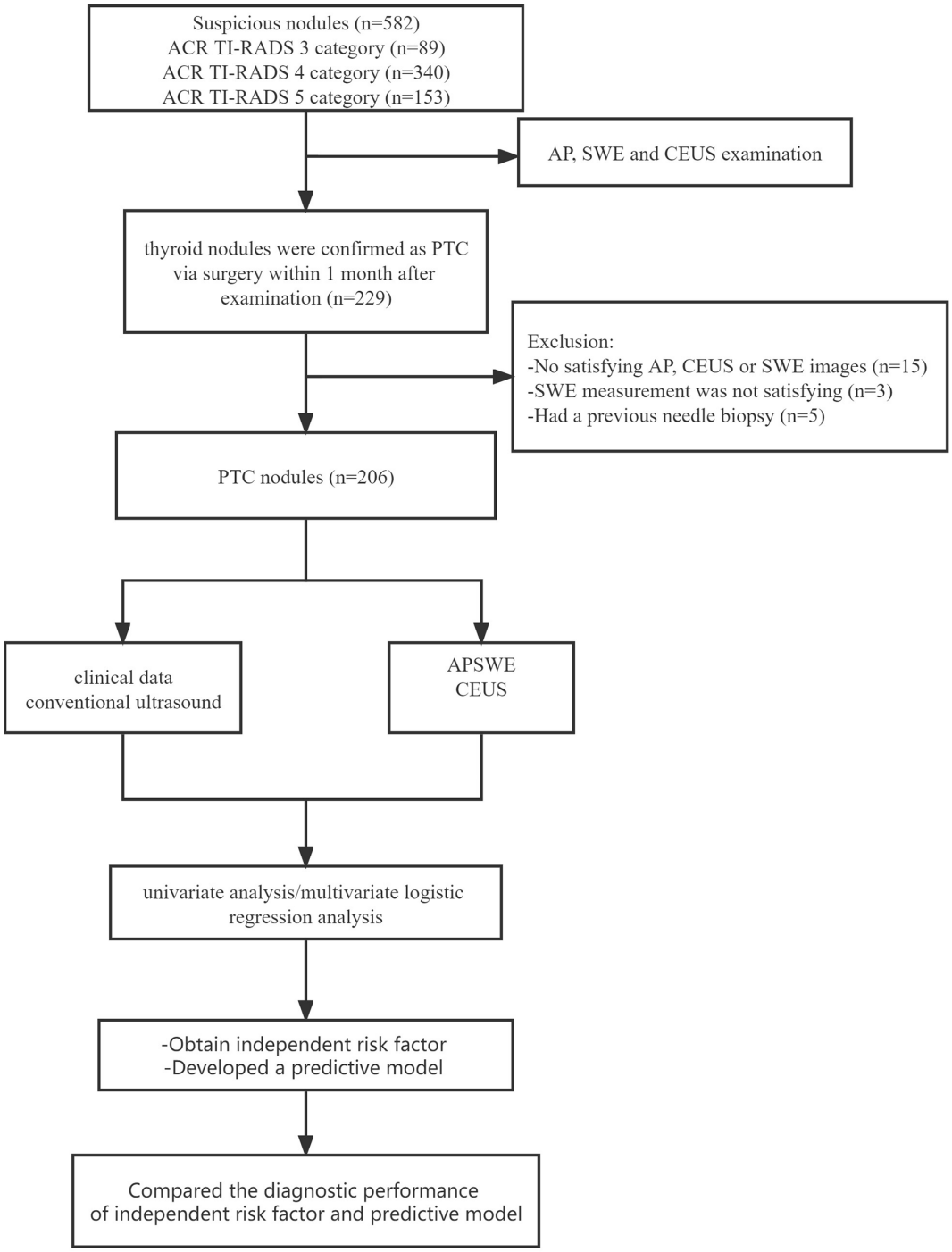

FIGURE 1
The flowchart of selection of thyroid carcinoma patients.

10.3389/fendo.2022.1063998

TABLE 1 Clinical data and conventional ultrasound features between the non-metastasis and metastasis group.

Conventional and clinical features		Non-metastatic group $n = 123$	Metastatic group $n = 83$	χ^2	p-value
Sex	Female	107	59	8.015	0.005
	Male	16	24		
Age	<45	31	36	7.456	0.006
	≥45	92	47		
Location	Upper	21	20	1.549	0.461
	Middle	54	32		
	Lower	43	29		
Multifocality	No	98	47	12.631	0.000
	Yes	25	36		
Composition	Mixed cystic and solid	2	2	0.16	0.689
	Solid or almost completely solid	121	81		
Echogenicity	Isoechoic/hyperechoic	5	4	0.067	0.795
	Hypoechoic/very hypoechoic	118	79		
Shape	Wider than tall	19	21	3.705	0.079
	Taller than wide	104	62		
Margin	Smooth	67	36	5.274	0.022
	Ill-defined/lobulated or irregular	56	57		
Calcification	None or large comet-tail artifacts	53	14	15.527	0.000
	Macrocalcifications or peripheral calcifications or punctate echogenic foci	70	69		
Size	<10 mm	109	35	50.822	0.000
	≥10 mm	14	48		
Contract with the adjacent thyroid capsule	≤25%	86	15	52.763	0.000
	>25%	37	68		
HT	No	77	52	0.000	0.994
	Yes	46	31		

Sex, age, size, multifocality, margin, calcification, and contact extent with adjacent thyroid capsule were statistically different between the non-metastasis group and the metastasis group.

AP, SWE, and CEUS features between the non-metastasis group and the metastasis group

AP, SWE, and CEUS features between the non-metastasis group and the metastasis group are summarized in Table 2. AP vascularization was statistically different between the non-metastasis group and the metastasis group. The CLNM rate of Grade 0–I and Grade II were 34.5% and 52.2%, respectively.

An ROC curve was drawn based on Emin, Emean, and Emax to calculate the optimal cutoff value for discriminating the non-metastasis from the metastasis group. The optimal cutoff value was 26.45 kPa for Emin, 36.05 kPa for Emean, and 48.4 kPa for Emax.

There were significant differences in capsule integrity at CEUS and enhancement border at CEUS between the non-metastasis group and the metastasis group. There were no significant differences in peak enhancement intensity, ring enhancement, homogeneity of enhancement, contrast agent arrival time, enhancement direction, enhancement area, and nodule composition at CEUS.

Univariate and multivariate analysis on the predictors of cervical lymph node metastasis

A summary of the binary logistic regression analysis of clinical data, conventional ultrasound, AP, SWE, and CEUS features is shown in Table 3. Sex, age, nodule size, multifocality, contract extent with adjacent capsule, Emax, and capsule integrity at CEUS were independent risk predictors for CLNM in patients with PTC. A predictive model was established

10.3389/fendo.2022.1063998

TABLE 2 AP, SWE, and CEUS features between the non-metastasis and metastasis group.

		Non-metastatic group $n = 123$	Metastatic group $n = 83$	χ^2	p-value
AP	0	12	9	6.604	0.037
	I	79	39		
	II	32	35		
SWE	Emin <26.45	84	42	6.529	0.011
	Emin ≥26.45	39	41		
	Emean <36.05	80	32	14.014	0.000
	Emean ≥36.05	43	51		
	Emax <48.4	84	26	27.216	0.000
	Emax ≥48.4	39	57		
CEUS					
Ring enhancement	Present	2	3	—	0.394
	Absent	121	80		
Peak intensity	Hyper-enhancement/iso-enhancement	19	9	0.894	0.344
	Hypo-enhancement	104	74		
Homogeneity	Homogeneous	18	5	3.704	0.054
	Heterogeneous	105	78		
Enhancement direction	Scattered	15	11	0.050	0.823
	Centripetal or centrifugal	108	72		
Contrast agent arrival time	Synchronous with normal thyroid tissue	28	19	0.000	0.983
	Earlier or later than normal thyroid tissue	95	64		
Enhancement area	Equal to conventional ultrasound	62	41	0.020	0.887
	Smaller or greater than conventional ultrasound	61	42		
Nodule composition at CEUS	Nonsolid	1	2	—	0.566
	Solid	122	81		
Capsule integrity at CEUS	Continuous	104	27	57.93	0.000
	Interrupted	19	56		
Enhancement border	Clear	48	55	14.71	0.000
	Unclear	75	28		

TABLE 3 Multivariate logistic regression analysis of clinical data, conventional ultrasound, AP, SWE, and CEUS.

Variables	B	p	OR	95% CI for OR	
Sex	1.452	0.010	4.270	1.423	12.817
Age	−1.064	0.023	0.345	0.138	0.866
Size	1.338	0.020	3.811	1.229	11.814
Multifocality	1.663	0.001	5.274	2.014	13.809
Margin	0.715	0.121	2.044	0.827	5.050
Calcification	0.698	0.192	2.009	0.704	5.735
Contact extent	1.606	0.001	4.980	2.009	12.346
AP	−0.797	0.060	0.451	0.196	1.034
Emin	−0.169	0.797	0.845	0.234	3.056
Emean	−1.150	0.184	0.317	0.058	1.730
Emax	1.717	0.021	5.570	1.296	23.942
CEUS border at CEUS	−0.398	0.397	0.672	0.268	1.685
Capsule integrity at CEUS	1.409	0.004	4.092	1.583	10.576
Constant	−2.328	0.002	0.097		

according to the multivariate logistic regression: Logit (p) = −2.382 + 1.452 × Sex − 1.064 × Age + 1.338 × Size + 1.663 × multi-focality + 1.606 × contact extent with adjacent thyroid capsule + 1.717 × Emax + 1.409 × capsule integrity at CEUS.

Comparing the diagnostic performance of independent risk predictors and the predictive model

ROC analysis of the predictive model for evaluating CLNM was performed (Figure 2). The AUC of the predictive model was 0.887 (95% CI: 0.841–0.933), which was significantly higher than using independent risk predictor alone (Table 4). The predictive model also had the best sensitivity and specificity, compared with using independent risk factor alone; the sensitivity and specificity of the predictive model were 69.88% and 93.50%, respectively.

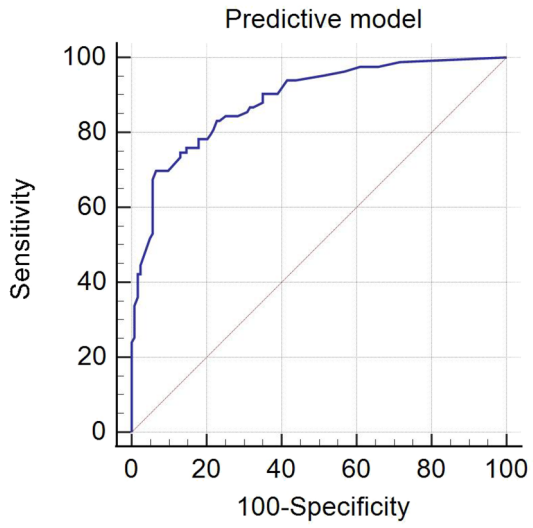

FIGURE 2
The ROC of the predictive model.

Discussion

In this study, we analyzed clinical data, conventional ultrasound feature, AP, SWE, and CEUS enhancement patterns of thyroid nodules in PTC patients to explore their predictive values for CLNM. We found that male presence, age < 45 years, size ≥ 10 mm, multifocality, contact extent with adjacent thyroid capsule > 25%, Emax ≥ 48.4, and interrupted capsule at CEUS were independent risk predictors for CLNM in patients with PTC. A predictive model based on multivariate logistic regression analysis showed better diagnostic performance for CLNM with an AUC of 0.887, compared with using independent risk predictor alone.

Several studies (14, 20) had reported that clinical data of patients including sex or age had predictive values for the aggressiveness of PTC. In this study, we found male and age < 45 years were independent risk factors for predicting CLNM in patients with PTC, which was consistent with previous studies. The CLNM rate of female patients (35.5%) was significantly lower than that of male patients (60.0%) in this study, and the CLNM rate of patients ≥ 45 years (35.5%) was lower than that of patients < 45 years (50%). Thus, one should practice caution in the surgery decision-making regarding and the preoperative evaluation of young male patients.

The size of malignant thyroid nodules ≥10 mm was an independent risk factor for predicting CLNM in patients with PTC, which was consistent with previous studies (21, 22). In general, the characteristics of thyroid nodules might be determined already during the initial formation, and the size of nodules was related to uncontrolled cell division and proliferation. Thus, the larger the PTC nodule was, the faster it grows and the higher the degree of nodule infiltration; hence, it is more prone to CLNM.

Multifocality presents a reported incidence of about 18%–27% in patients with PTC (22), which is related to lymph node

TABLE 4 The AUC of independent risk factors and predictive model.

	Sensitivity	Specificity	AUC	95% Confidence Interval
Sex	28.90%	87.00%	0.580	0.499–0.661
Age	43.40%	74.80%	0.591	0.511–0.671
Size	57.80%	88.60%	0.732	0.658–0.806
Multifocality	43.45%	79.70%	0.615	0.536–0.695
Contact extent with adjacent thyroid capsule	68.70%	54.50%	0.685	0.610–0.760
Emax	68.70%	68.30%	0.685	0.610–0.760
Capsule integrity at CEUS	67.50%	84.60%	0.760	0.690–0.831
Predictive model	69.88%	93.50%	0.887	0.841–0.933

metastasis, recurrence, and prognosis (23). In this study, we defined multifocality as more than one suspicious thyroid nodule in conventional ultrasound and more than one confirmed malignant nodule by surgical pathology. However, microscopic PTC is still difficult to detect prior to surgery. In this study, multifocality was an independent risk factor for predicting CLNM in PTC patients (p = 0.001), which is consistent with a previous study. The OR value of multifocality (OR = 5.274) in this study was significantly higher than previous studies (OR = 1.297–3.235) (14, 18, 24).

The ill-defined, lobulated, or irregular margin of thyroid nodules is generally associated with the irregular growth of the fibrous stroma surrounding the PTC nodules or carcinoma invasion of the surrounding thyroid parenchyma. However, margin was not an independent risk factor for predicting CLNM in patients with PTC in this study, which was consistent with most previous studies (14, 18, 22).

Whether calcification can predict CLNM of PTC is still controversial; some studies (22, 25) reported that micro-calcification could reflect the rapid growth in carcinoma tissues, and ≥5-mm micro-calcifications was an independent risk factor for predicting CLNM in patients with PTC, while several studies (12, 14) did not have the same results. In this study, we found that calcifications were significantly different between the non-metastasis and metastasis group, but it was not an independent risk factor for predicting CLNM according to multivariate logistic regression analysis. Thus, the correlation between calcifications and CLNM in PTC needs to be explored in a multi-center large-sample study in the future.

Previous studies (16) have found that contact extent with adjacent thyroid capsule >25% was the most accurate predictive feature for extra-thyroidal extension in this study, and we found that contact extent with adjacent thyroid capsule >25% was an important independent factor for CLNM. It may be because extra-thyroidal extension breaks the thyroid capsule, and the thyroid gland has a rich lymphatic network, which could easily cause CLNM.

HT is a common autoimmune thyroid disease, and the correlation between HT and PTC has been widely debated and remains controversial (26). Moreover, the enlarged lymph node in the central region caused by thyroiditis is always easily confused with lymph node metastasis. Li (10) found that HT has no significant difference for predicting CLNM in patients with PTC, which is consistent with our study.

A previous study reported that the characteristics of superb microvascular imaging (SMI) in PTC nodules (Grade II) were independent risk predictors for CLNM in patients with PTC, suggesting that the degree of rich and disorderly blood flow in PTC nodules might be helpful to predict CLNM (22). In this study, we found that AP vascularization in PTC nodules was significantly different between the non-metastasis and metastasis group, which was consistent with a previous study (22); the CLNM rate of Grade 0–I and Grade II was 34.5% and 52.2%, respectively. However, we did not obtain the same result by multivariate logistic regression analysis, and the p-value (0.06) was slightly higher than 0.05, which could be affected by the sample size.

SWE has been widely used to quantitatively assess the thyroid nodules. Few studies (6, 10, 27) have explored the values of SWE for predicting CLNM in patients with PTC. Park et al. (6) found that higher elasticity values of PTC were related to CLNM. Another study (27) found that the elasticity characteristics of PTC nodules did not have a significant difference between the non-metastasis and metastasis group. Li et al. (10) reported that Emax was an independent risk factor for CLNM, and the best cutoff value of Emax was >59.0 kPa. Similarly, Emax was an independent risk factor for predicting CLNM based on multivariate logistic regression analysis in this study, which was consistent with a previous study; using Emax > 48.4 kPa, our OR (OR = 5.57) was significantly higher than the OR of previous studies (OR = 1.005–4.934) (6, 10). Thus, the higher the Emax was, the more careful we should be in clinical work.

Several studies have reported that the enhancement patterns of CEUS were useful for predicting CLNM. Zhan et al. (12) found that peak enhancement intensity and homogeneity were significant features in predicting CLNM in PTC patients. Hong et al. (28) reported that hyper-enhancement or iso-enhancement could be an independent risk factor for predicting CLNM in PTC patients. Xue et al. (14) found that hyper-enhancement was not an independent predictor for predicting CLNM. In this study, we found that there was no statistical difference on peak enhancement intensity, ring enhancement, homogeneity of enhancement, contrast agent arrival time, enhancement direction, enhancement area, and nodule composition at CEUS between the non-metastasis and metastasis group, which was different with the previous studies; it may be because the qualitative enhancement patterns of CEUS could be controversial in different observers and ultrasound systems. The interrupted capsule at CEUS was an independent risk factor for predicting CLNM in patients with PTC, which is related to extra-thyroidal extension. Thus, the rate could be higher due to the rich lymphatic network in the gland network. When using the interrupted capsule at CEUS alone for predicting CLNM, the specificity was 84.60%, which showed that the rate of CLNM was low with the continuous capsule at CEUS.

Based on the multivariate logistic regression analysis of clinical characteristics, conventional ultrasound, AP, SWE, and CEUS, we developed a predictive model for predicting CLNM in PTC patients (Figures 3, 4); the model had the best AUC (0.887, 95% CI: 0.841–0.933) compared with using the independent factor alone. Moreover, this predictive model in this study was simple, convenient, and accurate, which could be widely used in clinical work.

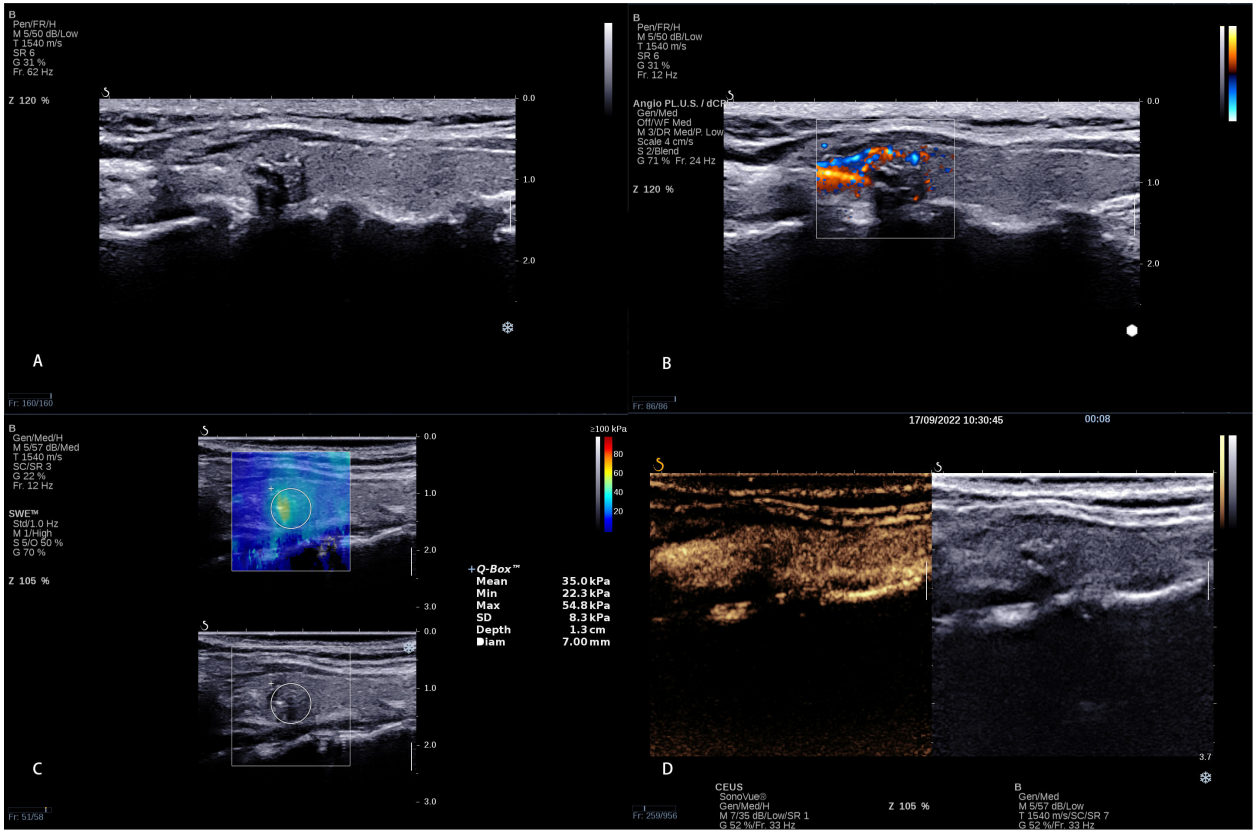

FIGURE 3
A 8 × 6 mm thyroid nodule in the left lobe of a 38-year-old woman. **(A)** Conventional ultrasound showed a solid hypo-echoic, irregular nodule with calcifications; the shape was wider than taller and the contact extent with adjacent thyroid capsule >25%. **(B)** AP shows that the vascularization of nodule could be classified as Grade I **(C)** SWE measurement shows that Emin, Emean, and Emax were 22.3 kPa, 35.0 kPa, and 54.8 kPa, respectively. **(D)** CEUS shows interrupted capsule at CEUS. The calculated predictive value with the logistic regression formula was 2.35 (>2.0805), which was regarded as presence of CLNM.

10.3389/fendo.2022.1063998

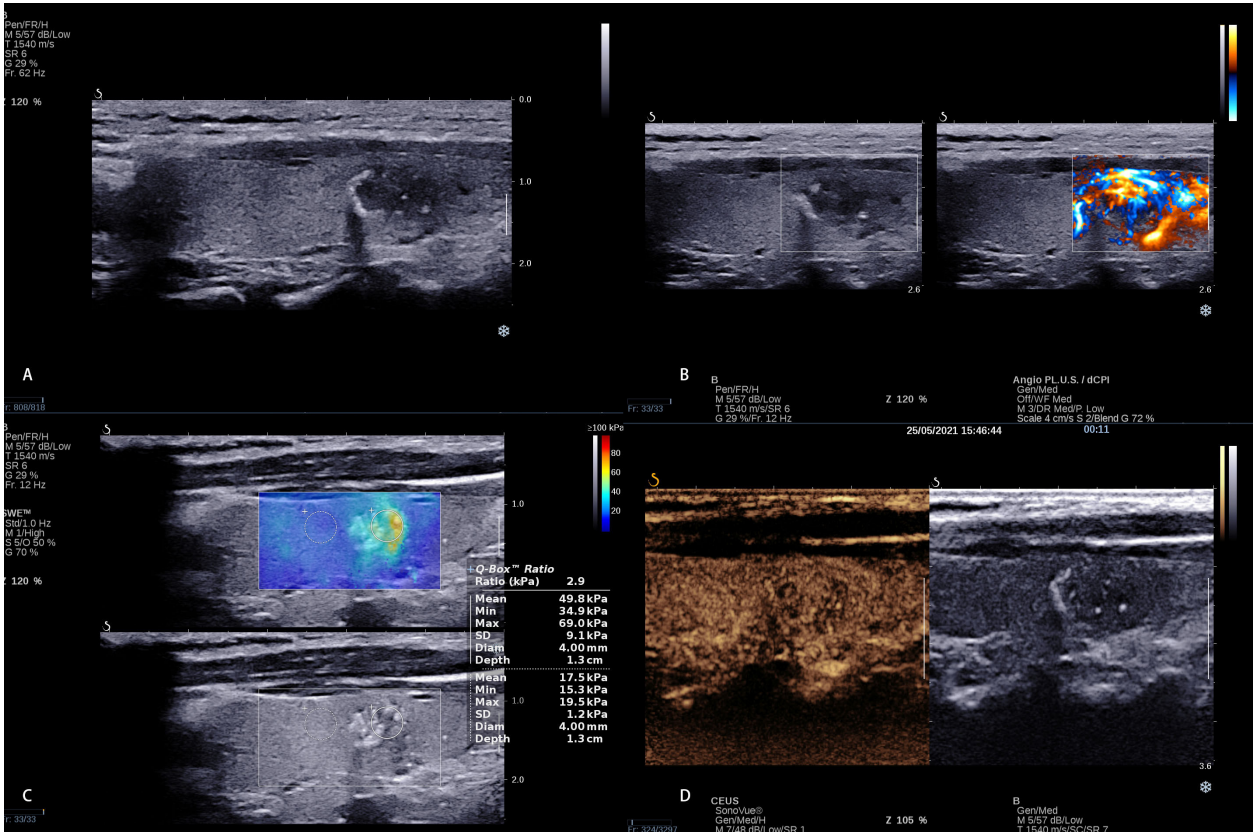

FIGURE 4
A 13 × 7 mm thyroid nodule in the right lobe of a 31-year-old woman. **(A)** Conventional ultrasound showed a solid hypo-echoic, ill-defined nodule with calcifications; the shape was wider than taller and the contact extent with adjacent thyroid capsule <25%. **(B)** AP shows that the vascularization of nodule could be classified as Grade II. **(C)** SWE measurement shows that Emin, Emean, and Emax were 34.9 kPa, 49.8 kPa, and 69.0 kPa, respectively. **(D)** CEUS shows continuous capsule at CEUS. The calculated predictive value with the logistic regression formula was 0.673 (<2.0805), which predicted no CLNM.

10.3389/fendo.2022.1063998

There are several limitations in this study. First, it was a single-center study with a small sample. Second, quantitative CEUS features were not included in this study. Third, we did not compare inter-observer and intra-observer variation.

Conclusion

Based on the multivariate logistic regression analysis of clinical characteristics, conventional ultrasound, SWE, and CEUS, we found that male presence, age < 45 years, size ≥ 10 mm, multifocality, contact extent with adjacent thyroid capsule > 25%, Emax ≥ 48.4, and interrupted capsule at CEUS were independent risk predictors for CLNM in patients with PTC. We developed a diagnostic model for predicting CLNM, which could be a potentially useful and accurate method for clinicians; it would be beneficial to surgical decision-making and patient management and for improving prognosis.

Data availability statement

The raw data supporting the conclusions of this article will be made available by the authors, without undue reservation.

Ethics statement

The studies involving human participants were reviewed and approved by the ethics committee of Yueyang Central Hospital. The patients/participants provided their written informed consent to participate in this study.

Author contributions

Conception and design: BW, A-jY, X-WC, and CD. Drafting of the article: BW, QC, and A-jY. Critical revision of the article for important intellectual content: BW, QC, and X-WC. All authors contributed to the article and approved the submitted version.

Funding

This work was supported by the National Natural Science Foundation of China (Nos. 82071953 and 21878237), the Science and Technology Department of Hunan Province (No. 2020SK52705), and the General Funding Project of Hunan Provincial Health Commission (No. B202309029532).

Conflict of interest

The authors declare that the research was conducted in the absence of any commercial or financial relationships that could be construed as a potential conflict of interest.

Publisher's note

All claims expressed in this article are solely those of the authors and do not necessarily represent those of their affiliated organizations, or those of the publisher, the editors and the reviewers. Any product that may be evaluated in this article, or claim that may be made by its manufacturer, is not guaranteed or endorsed by the publisher.

References

1. Sherman SI. Thyroid carcinoma. *Lancet* (2003) 361(9356):501–11. doi: 10.1016/s0140-6736(03)12488-9

2. Haugen BR, Alexander EK, Bible KC, Doherty GM, Mandel SJ, Nikiforov YE, et al. 2015 American Thyroid association management guidelines for adult patients with thyroid nodules and differentiated thyroid cancer: The American thyroid association guidelines task force on thyroid nodules and differentiated thyroid cancer. *Thyroid* (2016) 26(1):1–133. doi: 10.1089/thy.2015.0020

3. Lundgren CI, Hall P, Dickman PW, Zedenius J. Clinically significant prognostic factors for differentiated thyroid carcinoma: A population-based, nested case-control study. *Cancer* (2006) 106(3):524–31. doi: 10.1002/cncr.21653

4. Kouvaraki MA, Shapiro SE, Fornage BD, Edeiken-Monro BS, Sherman SI, Vassilopoulou-Sellin R, et al. Role of preoperative ultrasonography in the surgical management of patients with thyroid cancer. *Surgery* (2003) 134(6):946–54; discussion 954-5. doi: 10.1016/s0039-6060(03)00424-0

5. Stulak JM, Grant CS, Farley DR, Thompson GB, van Heerden JA, Hay ID, et al. Value of preoperative ultrasonography in the surgical management of initial and reoperative papillary thyroid cancer. *Arch Surg* (2006) 141(5):489–94; discussion 494-6. doi: 10.1001/archsurg.141.5.489

6. Park AY, Kim JA, Son EJ, Youk JH. Shear-wave elastography for papillary thyroid carcinoma can improve prediction of cervical lymph node metastasis. *Ann Surg Oncol* (2016) 23(Suppl 5):722–9. doi: 10.1245/s10434-016-5572-x

7. Liu H, Liao Q, Wang Y, Hu Y, Zhu Q, Wang L, et al. A new tool for diagnosing parathyroid lesions: Angio plus ultrasound imaging. *J Thorac Dis* (2019) 11(11):4829–34. doi: 10.21037/jtd.2019.11.29

8. Wang B, Chen YY, Yang S, Chen ZW, Luo J, Cui XW, et al. Combined use of shear wave elastography, microvascular Doppler ultrasound technique, and BI-RADS for the differentiation of benign and malignant breast masses. *Front Oncol* (2022) 12:906501. doi: 10.3389/fonc.2022.906501

9. Bamber J, Cosgrove D, Dietrich CF, Fromageau J, Bojunga J, Calliada F, et al. EFSUMB guidelines and recommendations on the clinical use of ultrasound elastography. part 1: Basic principles and technology. *Ultraschall Med* (2013) 34 (2):169–84. doi: 10.1055/s-0033-1335205

10. Li T, Li H, Xue J, Miao J, Kang C. Shear wave elastography combined with gray-scale ultrasound for predicting central lymph node metastasis of papillary thyroid carcinoma. *Surg Oncol* (2021) 36:1–6. doi: 10.1016/j.suronc.2020.11.004

11. Sidhu PS, Cantisani V, Dietrich CF, Gilja OH, Saftoiu A, Bartels E, et al. The EFSUMB guidelines and recommendations for the clinical practice of contrast-enhanced ultrasound (CEUS) in non-hepatic applications: Update 2017 (Long version). *Ultraschall Med* (2018) 39(2):e2–e44. doi: 10.1055/a-0586-1107

12. Zhan J, Zhang LH, Yu Q, Li CL, Chen Y, Wang WP, et al. Prediction of cervical lymph node metastasis with contrast-enhanced ultrasound and association between presence of BRAFV600E and extrathyroidal extension in papillary thyroid

carcinoma. *Ther Adv Med Oncol* (2020) 12:1758835920942367. doi: 10.1177/1758835920942367

13. Zhan J, Diao X, Chen Y, Wang W, Ding H. Predicting cervical lymph node metastasis in patients with papillary thyroid cancer (PTC) - why contrast-enhanced ultrasound (CEUS) was performed before thyroidectomy. *Clin Hemorheol Microcirc* (2019) 72(1):61–73. doi: 10.3233/CH-180454

14. Xue T, Liu C, Liu JJ, Hao YH, Shi YP, Zhang XX, et al. Analysis of the relevance of the ultrasonographic features of papillary thyroid carcinoma and cervical lymph node metastasis on conventional and contrast-enhanced ultrasonography. *Front Oncol* (2021) 11:794399. doi: 10.3389/fonc.2021.794399

15. Tessler FN, Middleton WD, Grant EG, Hoang JK, Berland LL, Teefey SA, et al. ACR thyroid imaging, reporting and data system (TI-RADS): White paper of the ACR TI-RADS committee. *J Am Coll Radiol* (2017) 14(5):587–95. doi: 10.1016/j.jacr.2017.01.046

16. Kwak JY, Kim EK, Youk JH, Kim MJ, Son EJ, Choi SH, et al. Extrathyroid extension of well-differentiated papillary thyroid microcarcinoma on US. *Thyroid* (2008) 18(6):609–14. doi: 10.1089/thy.2007.0345

17. Adler DD, Carson PL, Rubin JM, Quinn-Reid D. Doppler Ultrasound color flow imaging in the study of breast cancer: Preliminary findings. *Ultrasound Med Biol* (1990) 16(6):553–9. doi: 10.1016/0301-5629(90)90020-D

18. Wang Y, Nie F, Wang G, Liu T, Dong T, Sun Y. Value of combining clinical factors, conventional ultrasound, and contrast-enhanced ultrasound features in preoperative prediction of central lymph node metastases of different sized papillary thyroid carcinomas. *Cancer Manag Res* (2021) 13:3403–15. doi: 10.2147/CMAR.S299157

19. Ruan J, Xu X, Cai Y, Zeng H, Luo M, Zhang W, et al. A practical CEUS thyroid reporting system for thyroid nodules. *Radiol* (2022) 305(1):149–59. doi: 10.1148/radiol.212319

20. Han DY, Sohn YM, Seo M, Yun SJ, Park WS, Jeon SH, et al. Shear-wave elastography in thyroid ultrasound: Can be a predictor of extrathyroidal extension and cervical lymph node metastasis in papillary thyroid carcinoma? *Med (Baltimore)* (2020) 99(52):e23654. doi: 10.1097/MD.0000000000023654

21. Jin WX, Ye DR, Sun YH, Zhou XF, Wang OC, Zhang XH, et al. Prediction of central lymph node metastasis in papillary thyroid microcarcinoma according to clinicopathologic factors and thyroid nodule sonographic features: A case-control study. *Cancer Manag Res* (2018) 10:3237–43. doi: 10.2147/CMAR.S169741

22. Guang Y, He W, Zhang W, Zhang H, Zhang Y, Wan F. Clinical study of ultrasonographic risk factors for central lymph node metastasis of papillary thyroid carcinoma. *Front Endocrinol (Lausanne)* (2021) 12:791970. doi: 10.3389/fendo.2021.791970

23. Pacini F, Schlumberger M, Dralle H, Elisei R, Smit JW, Wiersinga W. European Consensus for the management of patients with differentiated thyroid carcinoma of the follicular epithelium. *Eur J Endocrinol* (2006) 154(6):787–803. doi: 10.1530/eje.1.02158

24. Liu W, Cheng R, Ma Y, Wang D, Su Y, Diao C, et al. Establishment andvalidation of the scoring system for preoperative prediction of central lymph node metastasis in papillary thyroid carcinoma. *Sci Rep* (2018) 8(1):6962. doi: 10.1038/s41598-018-24668-6

25. Iannuccilli JD, Cronan JJ, Monchik JM. Risk for malignancy of thyroid nodules as assessed by sonographic criteria: The need for biopsy. *J Ultrasound Med* (2004) 23(11):1455–64. doi: 10.7863/jum.2004.23.11.1455

26. Noureldine SI, Tufano RP. Association of hashimoto's thyroiditis and thyroid cancer. *Curr Opin Oncol* (2015) 27(1):21–5. doi: 10.1097/CCO.0000000000000150

27. Park YJ, Kim JA, Son EJ, Youk JH, Park CS. Quantitative shear wave elastography as a prognostic implication of papillary thyroid carcinoma (PTC): elasticity index can predict extrathyroidal extension (ETE). *Ann Surg Oncol* (2013) 20(8):2765–71. doi: 10.1245/s10434-013-2927-4

28. Hong YR, Yan CX, Mo GQ, Luo ZY, Zhang Y, Wang Y, et al. Conventional US, elastography, and contrast enhanced US features of papillary thyroid microcarcinoma predict central compartment lymph node metastases. *Sci Rep* (2015) 5:7748. doi: 10.1038/srep07748

frontiers | Frontiers in Endocrinology

TYPE Original Research
PUBLISHED 20 December 2022
DOI 10.3389/fendo.2022.1062571

OPEN ACCESS

EDITED BY
Jose Federico Carrillo,
National Institute of Cancerology (INCAN), Mexico

REVIEWED BY
Jianing Zhu,
Zhejiang University, China
Xiaozhu Liu,
Second Affiliated Hospital of Chongqing Medical University, China

*CORRESPONDENCE
Xiubo Lu
doctorluxiubo@126.com
Meng Jia
dr_jiameng@163.com

SPECIALTY SECTION
This article was submitted to Thyroid Endocrinology, a section of the journal Frontiers in Endocrinology

RECEIVED 06 October 2022
ACCEPTED 12 December 2022
PUBLISHED 20 December 2022

CITATION
Yu J, Zhang Y, Zheng J, Jia M and Lu X (2022) Ultrasound images-based deep learning radiomics nomogram for preoperative prediction of *RET* rearrangement in papillary thyroid carcinoma.
Front. Endocrinol. 13:1062571.
doi: 10.3389/fendo.2022.1062571

Ultrasound images-based deep learning radiomics nomogram for preoperative prediction of *RET* rearrangement in papillary thyroid carcinoma

Jialong Yu[1], Yihan Zhang[2], Jian Zheng[1], Meng Jia[1]* and Xiubo Lu[1]*

[1]Department of Thyroid Surgery, The First Affiliated Hospital of Zhengzhou University, Henan, China, [2]Department of Ophthalmology, The First Affiliated Hospital of Zhengzhou University, Henan, China

Purpose: To create an ultrasound -based deep learning radiomics nomogram (DLRN) for preoperatively predicting the presence of *RET* rearrangement among patients with papillary thyroid carcinoma (PTC).

Methods: We retrospectively enrolled 650 patients with PTC. Patients were divided into the *RET*/PTC rearrangement group (n = 103) and the non-*RET*/PTC rearrangement group (n = 547). Radiomics features were extracted based on hand-crafted features from the ultrasound images, and deep learning networks were used to extract deep transfer learning features. The least absolute shrinkage and selection operator regression was applied to select the features of nonzero coefficients from radiomics and deep transfer learning features; then, we established the deep learning radiomics signature. DLRN was constructed using a logistic regression algorithm by combining clinical and deep learning radiomics signatures. The prediction performance was evaluated using the receiver operating characteristic curve, calibration curve, and decision curve analysis.

Results: Comparing the effectiveness of the models by linking the area under the receiver operating characteristic curve of each model, we found that the area under the curve of DLRN could reach 0.9545 (95% confidence interval: 0.9133–0.9558) in the test cohort and 0.9396 (95% confidence interval: 0.9185–0.9607) in the training cohort, indicating that the model has an excellent performance in predicting *RET* rearrangement in PTC. The decision curve analysis demonstrated that the combined model was clinically useful.

10.3389/fendo.2022.1062571

Conclusion: The novel ultrasonic-based DLRN has an important clinical value for predicting *RET* rearrangement in PTC. It can provide physicians with a preoperative non-invasive primary screening method for *RET* rearrangement diagnosis, thus facilitating targeted patients with purposeful molecular sequencing to avoid unnecessary medical investment and improve treatment outcomes.

KEYWORDS

papillary thyroid carcinoma, radiomics, deep learning, nomogram, *RET* rearrangement, prediction

1 Introduction

Thyroid cancer is the most common endocrine tumor; papillary thyroid carcinoma (PTC) is the most common type of pathological cancer, accounting for approximately 80%–90% of all thyroid cancers (1). Yasuhiro et al. studied 5897 patients with PTC and reported that PTC is inert cancer with a low mortality rate and >90% overall survival rate (2). However, some histological subtypes of PTC show aggressive behavior, have a high recurrence and distant metastasis, or lead to death (3, 4). Therefore, early discrimination against these PTCs that require aggressive medical intervention is important.

Several genetic alterations have been used as a tool for diagnosing diseases and predicting prognosis owing to the advancement in molecular genetics (5, 6). On a molecular basis, some genetic alterations are closely associated with the clinicopathological features of PTC. Fusco et al. first reported the *RET* chromosomal rearrangement was in PTC. *RET* is a proto-oncogene that encodes a plasma membrane-bound *RET* tyrosine kinase receptor for ligands of the glial-derived neurotrophic factor family (7). Chromosomal rearrangements cause *RET*/PTC-related carcinogenesis (8).

Thus far, at least 13 different forms of *RET*/PTC rearrangements have been found; these rearrangements are almost exclusively found in PTC (9). Among all rearrangement forms, *RET*/PTC3 and *RET*/PTC1 are the most common, accounting for >90% of all rearrangements. The prognostic role of *RET* rearrangements has been confirmed in other studies as the presence of *RET*/PTC3 rearrangements and both large tumors size and advanced tumor stage at the time of diagnosis are positively associated; these studies highlight that *RET*/PTC3 has a significant role in metastatic spread (10–13). However, *RET*/PTC1 rearrangement is more prevalent than *RET*/PTC3 in less aggressive classical variants (14, 15).

Ultrasound is the primary imaging technique for the evaluation of thyroid nodules. Predicting molecular alterations in PTC by analyzing conventional ultrasound features is controversial, mainly due to the limitation of conventional ultrasound images and high interobserver variability (16). Radiomics can automatically extract innumerable high-dimensional features from images; however, these features cannot be assessed visually. Radiomics has recently shown clinical importance in the thyroid (17). Radiomics based on ultrasound images has been used to predict molecular properties in thyroid cancer (18–20).

Machine learning is the scientific technique that emphasizes how computers learn from data. It can be found at the intersection of statistics and computer science (21). Deep transfer learning (DTL) is a new type of machine learning method developed *via* the advancement of artificial neural networks. DTL depends on a network of computational units that gradually extract higher-lever features from the input data (22). DTL is widely used in medicine, including in the field of the thyroid (23, 24).

To our knowledge, there are no published studies aimed at identifying the presence of *RET* rearrangement in PTC using ultrasound radiomics combined with DTL. Therefore, we evaluated the association between *RET* rearrangement and ultrasound radiomics DTL and established a deep learning radiomics nomogram (DLRN) to predict *RET* rearrangement in PTC.

2 Materials and methods

2.1 Ethics statement

This study was approved by the Ethics Committee of the First Affiliated Hospital of Zhengzhou University (Number: 2022-KY-1002-002).

2.2 Clinical data

Between June 2020 and June 2022, we enrolled consecutive patients from the Department of Thyroid Surgery of the First Affiliated Hospital of Zhengzhou University; informed consent from patients was exempted. The inclusion criteria were as

follows: (1) patients who were treated for the first time; (2) patients who preoperatively underwent ultrasound examination within 2 weeks; (3) patients who had pathologically confirmed PTC; and (4) patients with well-preserved clinical data, imaging data, and pathological specimens. The exclusion criteria were as follows: (1) patients who underwent preoperative radiotherapy, chemotherapy, or radiofrequency ablation; (2) patients who presented with other head and neck tumor diseases; (3) patients with multifocal or bilateral PTC; and (4) patients with poor quality ultrasound images. Figure 1 shows the patient recruitment pathway. The patients were divided into training and test cohorts using a 5-fold cross-validation method.

2.3 Ultrasound examination and image acquisition

All enrolled patients underwent a preoperative neck ultrasound examination. The ultrasound machines included HITACHI HI VISION Ascendus (Japan), TOSHIBA aplio500 (Japan), SAMSUNG LA3-16A (Korea), and PHILIPS RPIQ5 (Netherlands). The ultrasound examinations were performed with a 5–12 MHz transducer by radiologists with 5–10 years of experience in thyroid ultrasound evaluation. After placing the patients in the supine position, longitudinal and transverse continuous scanning were performed to obtain longitudinal and transverse images of the thyroid nodules. All selected thyroid nodules were evaluated for the following ultrasound feature composition (mixed cystic and solid, cystic, or solid), echogenicity (hypoechoic, isoechoic, or hyperechoic), tumor margin (irregular, ill-defined, or smooth), vertical and horizontal diameter ratio (<1 or ≥1), shape (irregular, ill-defined, or regular), and calcification (macrocalcification, microcalcification, non-calcification, or cluster calcification); the American College of Radiology Thyroid Imaging Reporting and Data System (ACR-TI-RADS) score of each nodule was calculated by the same radiologists. Supplement Tables 1, 2 show the detailed process of calculating the ACR-TI-RADS score and category.

2.4 Region of interest segmentation

Two radiologists with >3 years of experience who were blinded to the pathological results reviewed the ultrasound images of the enrolled patients using Picture Archiving and Communication Systems, selected appropriate images, stored the selected images in BMP format, and then converted them to NII format. The open-source software 3D Slicer (version 4.1.13.0, available at https://www.slicer.org/) was used for texture analysis. The region of interest of the target nodule was manually segmented using a 3D Slicer. The interobserver

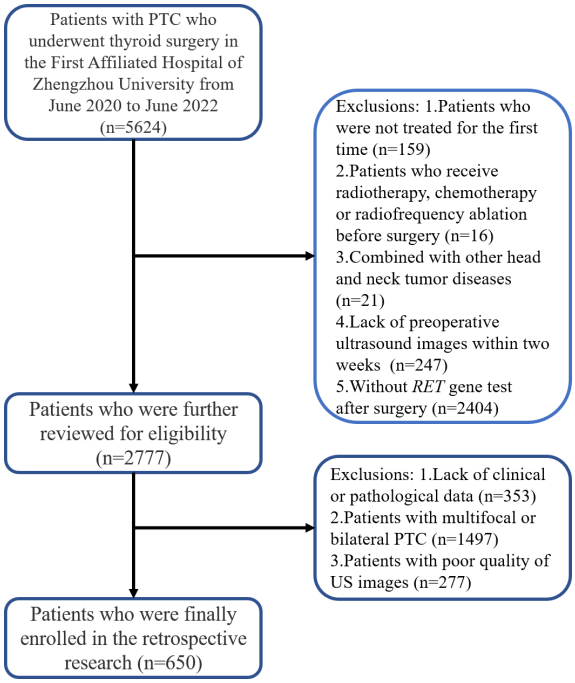

FIGURE 1
The patient recruitment pathway.

and intraobserver agreements were measured using random 130 nodules delineated by a radiologist twice within 2 weeks. The interclass correlation coefficient was used to evaluate the interobserver and intraobserver agreement of the feature extraction. An interclass correlation coefficient larger than 0.75 was considered a satisfactory agreement.

2.5 Features extraction and signature building

All handcrafted features were extracted using an in-house feature analysis program implemented in Pyradiomics (http://pyradiomics.readthedocs.io); 1477 handcrafted features were extracted from each ultrasound image. After the least absolute shrinkage and selection operator (LASSO) feature screening, we input the final features into the machine learning models such as LR, SVM, random forest, XGBoost, and so on for prediction model construction.

Deep learning features were extracted from pre-trained convolutional neural networks *via* transfer learning. In this study, resnet50 was chosen as the pre-trained convolutional neural network model18. The resnet50 model was trained on the ILSVRC-2012 dataset. The image that had the largest tumor area was selected to represent each patient; the gray values were normalized to the range [−1, 1] using min-max transformation. Then, each cropped subregion image was resized to 224 × 224 with the nearest interpolation. The obtained images were used as the model input. Since the dimension of deep migration features was 2048, we used the principal component analysis to reduce the dimension of deep migration features and ensure the balance between features. We reduced the dimension of deep learning to 128 dimensions for improving the generalization ability of the model and reducing the risk of overfitting. After compressing the deep learning feature by principal component analysis, all compressed features were standardized using the Z-score method, and the mean and variance (standard deviation) of each column of features were calculated. Each column of features was subtracted from the mean, divided by variance, and transformed into a standard normal distribution. We used the least absolute shrinkage and selection operator (LASSO) to filter out features whose coefficients were not 0, selected and reduced the dimension of fusion features, and obtained the optimal subset of fusion features.

Based on the selected radiomics features and 128 compressed DTL features, we aimed to create a deep learning radiomics (DLR) signature. We followed the same path as the radiomics signature or DTL signature. After LASSO feature screening, we input the final features into the machine learning models for predictive model construction to obtain the final DLR signature.

2.6 Construction of DLRN and predictive performance

We referred to clinical data with the conventional ultrasound features commonly referred to as clinical features. First, the features used for building clinical signatures were selected by baseline statistics with a p-value of <0.05. We also used the same machine learning model in the radiomics signature-building process.

DLRN was prepared in combination with clinical and DLR signatures. The diagnostic efficacy of the nomogram was tested in the test cohort; the receiver operating characteristic curves were drawn to assess the diagnostic efficacy of the nomogram. The calibration efficiency of the nomogram was estimated by drawing calibration curves; the Hosmer–Lemeshow analytical fit was used to evaluate the calibration ability of the nomogram. Decision curve analysis (DCA) was mapped to evaluate the clinical utility of predictive models. Figure 2 shows the whole process of model building.

2.7 Detection of *RET*/PTC rearrangements

Genomic DNA was extracted from postoperative specimens using AmoyDX provided by Amoy Diagnostics Co., Ltd. (Xiamen, China). *RET* rearrangements were analyzed using the next-generation sequencing method. Amplification and analysis were conducted on an ABI 7500 Real-Time PCR System (Applied Biosystem, CA, USA). Next, we performed a real-time fluorescence amplification refractory mutation system-polymerase chain reaction. Each rearrangement was further confirmed by direct Sanger sequencing; the results of *RET* rearrangement to be tested were finally read.

2.8 Statistical analysis

Descriptive statistics of continuous variables were expressed as mean ± standard deviation; categorical variables were presented as median (interquartile range) and frequency (%). The independent sample t-test was used for continuous factors with normal distribution; the Mann–Whitney U test was used for continuous factors without normal distribution. The categorical variables were compared using the χ^2 test or Fisher exact test. The Delong's test was used to compare the area under the curve (AUC). The Hosmer–Lemeshow test was used to assess whether the expected and actual probabilities were calculated with the prediction model. $P < 0.05$ was considered statistically significant.

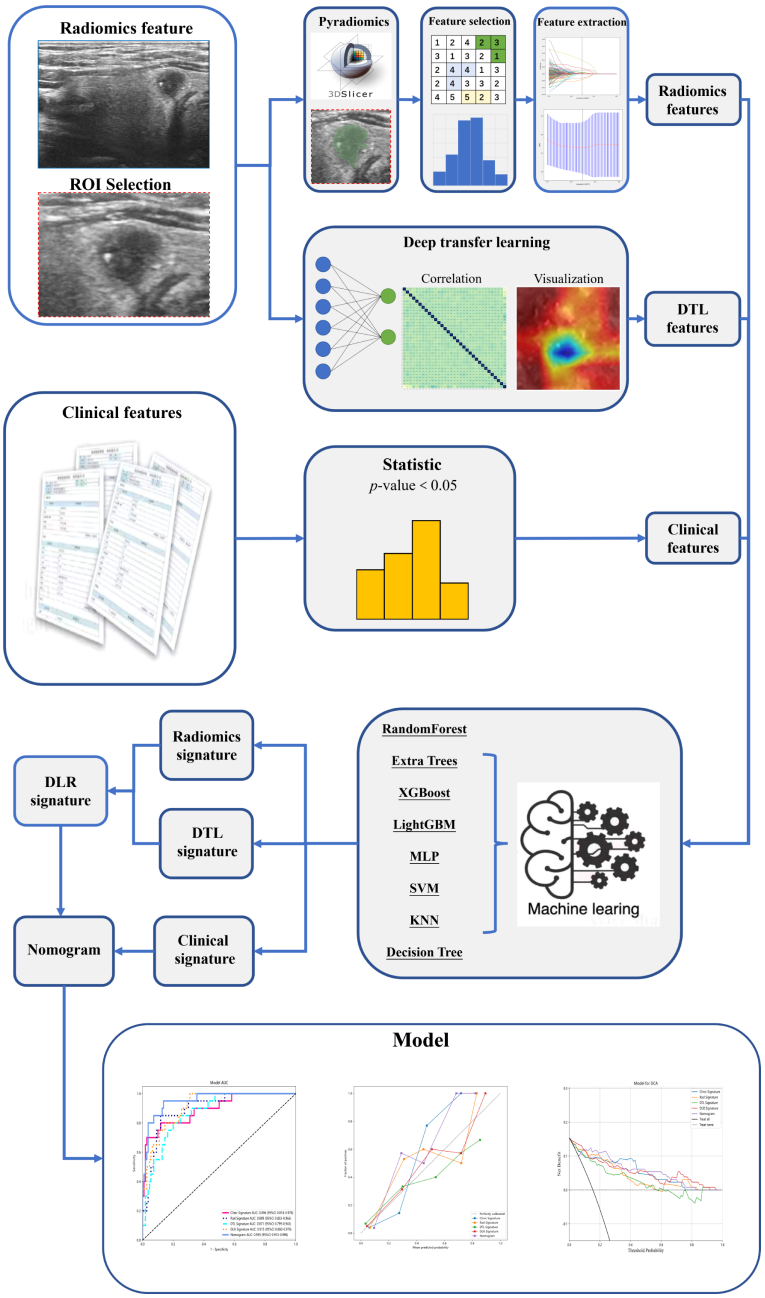

FIGURE 2
The process of model building.

3 Results

3.1 Features statistics

We enrolled 650 patients with PTC: 103 patients had *RET*/PTC rearrangement and 547 had non-*RET*/PTC rearrangement. Table 1 shows the clinical features of all patients. Significant differences were noted in the clinical characteristics between the two cohorts, including age, tumor size, sex, TPOAb, TGAb, echogenicity, vertical and horizontal diameter ratio, calcification, and ACR-TI-RADS score.

In radiomics, 1477 handcrafted features were extracted, including 306 first-order features, 14 shape features, and the last texture features. In DTL, we compared and visualized the

10.3389/fendo.2022.1062571

TABLE 1 The clinical features of all enrolled patients.

Feature name	All	*RET*/PTC rearrangement		p-value
		No	Yes	
Age, mean ± SD (years)	42.8 ± 11.2	43.7 ± 11.0	37.9 ± 11.2	<0.001
Tumor size, mean ± SD (mm)	9.3 ± 6.9	8.5 ± 6.4	13.6 ± 7.9	<0.001
Sex				
Female	505 (77.7)	417 (76.2)	88 (85.4)	0.0396
Male	145 (22.3)	130 (23.8)	15 (14.6)	
TPOAb				
Normal	520 (80.0)	472 (86.3)	48 (46.6)	<0.001
Abnormal	130 (20.0)	75 (13.7)	55 (53.4)	
TGAb				
Normal	513 (78.9)	459 (83.9)	54 (52.4)	<0.001
Abnormal	137 (21.1)	88 (16.1)	49 (47.6)	
Primary site				
Right lobe	334 (51.4)	290 (53.0)	44 (42.7)	0.1446
Isthmus	22 (3.4)	14 (2.6)	8 (7.8)	
Left lobe	294 (45.2)	243 (44.4)	51 (49.5)	
Tumor location				
Upper pole	162 (24.9)	140 (25.6)	22 (21.4)	0.2072
Lower pole	221 (34.0)	188 (34.4)	33 (32.0)	
Middle	267 (41.1)	219 (40.0)	48 (46.6)	
Composition				
Mixed cystic and solid	23 (3.5)	19 (3.5)	4 (3.9)	0.8384
Cystic	1 (0.2)	1 (0.2)	0 (0)	
Solid	626 (96.3)	527 (96.3)	99 (96.1)	
Echogenicity				
Hypoechoic	610 (93.9)	526 (96.2)	84 (81.6)	<0.001
Isoechoic	30 (4.6)	20 (3.7)	10 (9.7)	
Hyperechoic	10 (1.5)	1 (0.1)	9 (8.7)	
Tumor margin				
Irregular	319 (49.1)	278 (50.8)	41 (39.8)	0.4145
Ill-defined	269 (41.4)	215 (39.3)	54 (52.4)	
Smooth	62 (9.5)	54 (9.9)	8 (7.8)	
The vertical and horizontal diameter ratio				
<1	300 (46.2)	219 (40.0)	81 (78.6)	<0.001
≥1	350 (53.8)	328 (60.0)	22 (21.4)	
Shape				
Irregular	220 (33.9)	173 (31.6)	47 (45.6)	0.2833

(Continued)

TABLE 1 Continued

Feature name	All	*RET*/PTC rearrangement		p-value
		No	Yes	
Ill-defined	283 (43.5)	255 (46.6)	28 (27.2)	
Regular	147 (22.6)	119 (21.8)	28 (27.2)	
Calcification				
Macrocalcification	62 (9.5)	54 (9.9)	8 (7.8)	<0.001
Microcalcification	209 (32.2)	170 (31.1)	39 (37.9)	
Non-calcification	235 (36.2)	227 (41.5)	8 (7.7)	
Cluster calcification	144 (22.1)	96 (17.5)	48 (46.6)	
ACR-TI-RADS category				
3 (Mildly suspicious)	18 (2.8)	13 (2.4)	5 (4.9)	<0.001
4 (Moderately suspicious)	367 (56.4)	330 (60.3)	37 (35.9)	
5 (Highly suspicious)	265 (40.8)	204 (37.3)	61 (59.2)	

PTC, papillary thyroid carcinoma; TGAb, thyroglobulin antibody; TPOAb, thyroid peroxidase antibody; ACR-TI-RADS, American College of Radiology Thyroid Imaging Reporting and Data System.

correlation coefficients of the deep learning features. We established that the collinearity between the features was weak, indicating that deep learning still further captured the differences.

For investigating the interpretability of the DLR, we visualized the network by applying the gradient-weighted class activation mapping, which could provide a rough localization map highlighting the import regions for the classification target. The last convolutional layer of the last res-block was made transparent (Figure 3).

Next, 19 features of nonzero coefficients were selected from radiomics features and deep learning features to obtain the DLR-score with a LASSO logistic regression model in the training cohort. Coefficients, mean standard error of 10 folds validation, and the value of the coefficients in the final selected none zero features are shown in Figure 4. The DLR score is shown below:

DLR_score = 0.15893069804681456−− 0.000667 × exponential_gldm_SmallDependenceLowGrayLevelEmphasis + 0.010403 × gradient_firstorder_Range + 0.005532 × lbp_3D_m2_glszm_GrayLevelNonUniformity − 0.039521 × original_shape_Elongation + 0.002556 × square_gldm_GrayLevelNonUniformity + 0.005940 × squareroot_firstorder_90Percentile + 0.003671 × wavelet_HHH_firstorder_Mean − 0.013805 × wavelet_HHH_glszm_ZonePercentage − 0.032163 × wavelet_HLL_firstorder_Mean + 0.016144 × wavelet_HLL_glcm_JointAverage + 0.005555 × wavelet_LLH_firstorder_RobustMeanAbsoluteDeviation + 0.007702 × wavelet_LLL_glcm_DifferenceVariance + 0.019646 × wavelet_LLL_glszm_GrayLevelVariance − 0.053602 × DL-0 − 0.050075 × DL-1 − 0.057482 × DL-2 − 0.030163 × DL-4 + 0.025809 × DL-9 − 0.008247 × DL-16

3.2 Signature efficiency comparison

A 5-fold cross-validation method was used; we divided all patients into the training and test cohorts, and the test cohort was to be fixed for a fair comparison. To compare the efficiency of each signature, we further selected the best model from each signature-building process.

The optimal model was obtained using radiomics features compared with an LR, SVM, KNN, Decision Tree, Random Forest, Extra Trees, XGBoost, and LightGBM classifier. The features of other categories were similarly related and modeled. LR performs almost the best performance in each model of the *RET*/PTC rearrangement respectively. Figure 5 shows the receiver operating characteristic analysis of different models on the test cohort.

3.3 Establishment and validation of the Nomogram

In the training cohort, with both clinical signature AUC = 0.8442 [95% confidence interval (CI): 0.8009–0.8874] and radiomics signature AUC = 0.8638 (95% CI: 0.8262–0.9014), DLR is combined radiomics and DTL features achieved AUC = 0.9335 (95% CI: 0.9119–0.9551). In the test cohort, with both clinical signature AUC = 0.8959 (95% CI: 0.8141–0.9777) and radiomics signature AUC = 0.8991 (95% CI: 0.8325–0.9656), DLR was also the best model between radiomics signature and DLR signature [(DLR: 0.9150) vs. (Rad: 0.8991, DTL: 0.8709)]. DLRN using the logistic regression algorithm was performed to combine the clinical signature and DLR signature, which shows

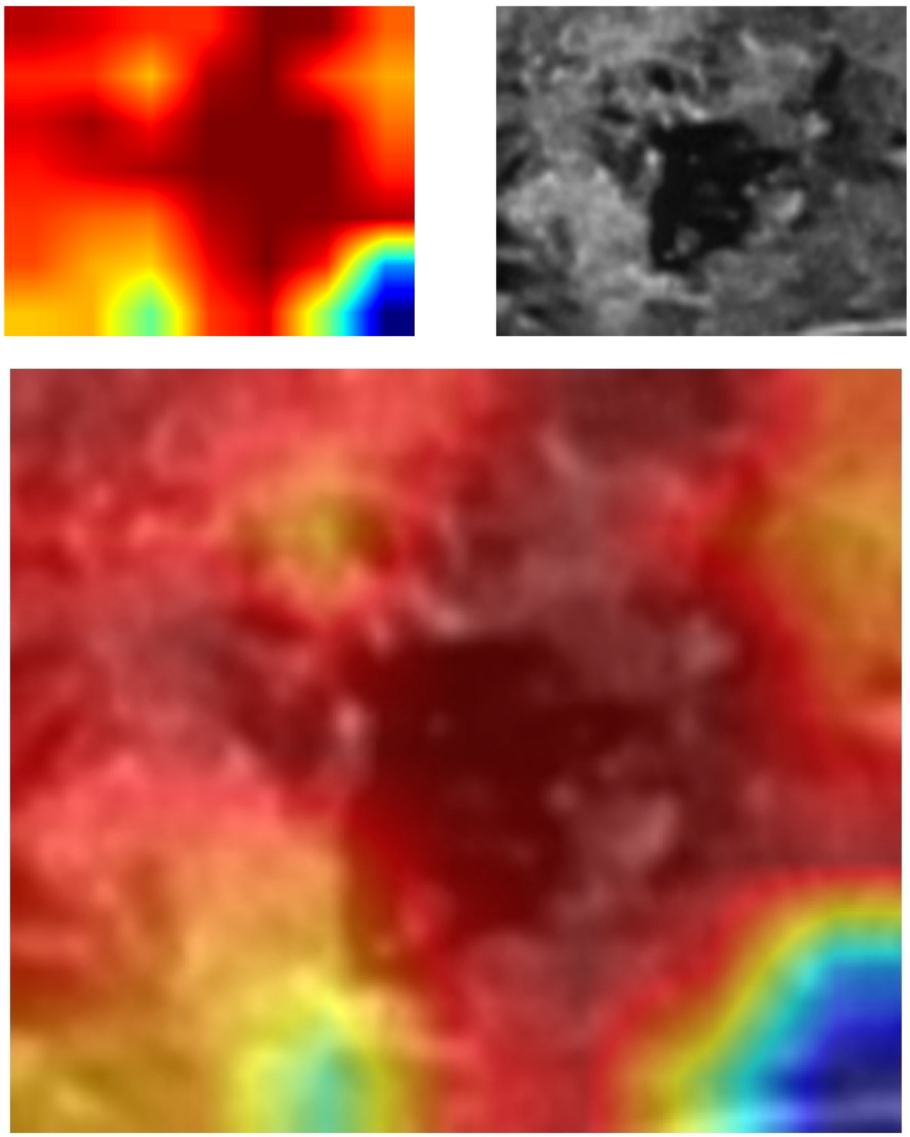

FIGURE 3
Grad-CAM visualization. Grad-CAM, gradient-weighted class activation mapping.

that the best performance AUC was 0.9545 (95% CI 0.9133–0.9958). Table 2 shows all models that we used to predict the *RET*/PTC rearrangement. Figure 6 shows the AUC in both the training and test cohorts. To compare the clinical signature, DTL signature, DLR signature, radiomics signature, and Nomogram, the Delong test was used (Table 3).

The Nomogram calibration curves showed good agreement between the predicted and observed *RET*/PTC rearrangement in the training and test cohorts. The *p*-values of the Hosmer–Lemeshow test were 0.5655, 0.4756, 0.3451, 0.9988, and 0.2142 inspections of clinical signature, radiomics signature, DTL signature, DLR signature, and Nomogram (Table 4). This shows that Nomogram perfectly fits in both the training and test cohorts. Figure 7 shows the calibration curves in the training and test cohorts.

We also evaluated each model through DCA. DCA for the clinical signature, radiomics signature, DTL signature, DLR signature, and Nomogram is presented in Figure 8. The preoperative prediction of *RET*/PTC rearrangement using a radiomics nomogram has been shown to have better clinical benefits.

Based on the clinical signature and DLR signature, we established the nomogram to predict the *RET*/PTC rearrangement (Figure 9).

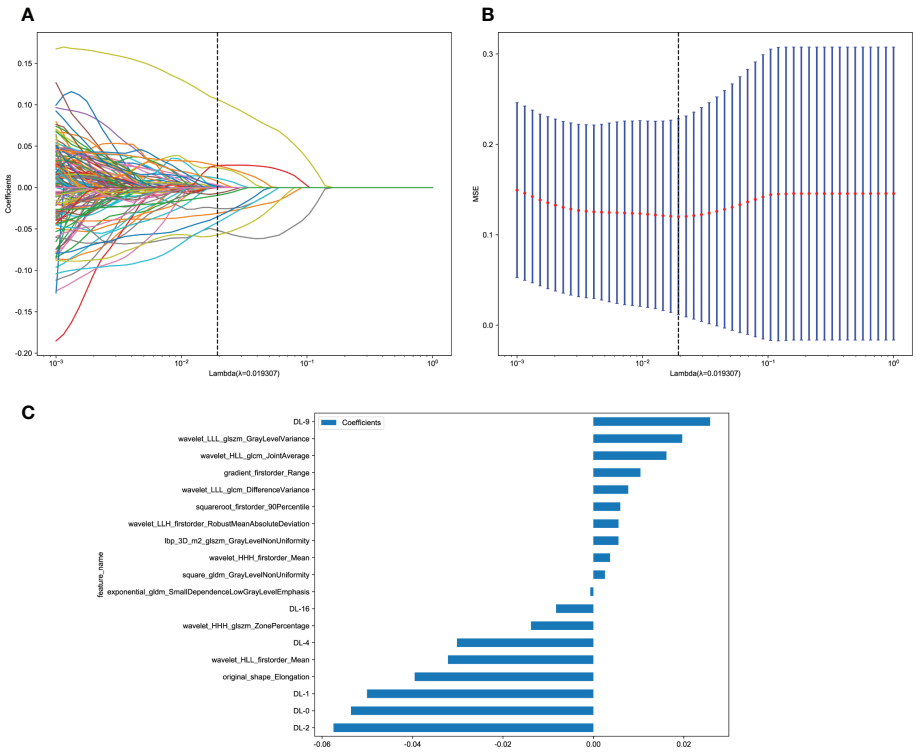

FIGURE 4
Deep learning radiomics (DLR) feature selection using the least absolute shrinkage and selection operator (LASSO) logistic regression model in the training cohort and the histogram of the DLR-score based on the selected features. **(A)** Coefficients of 10-fold cross-validation. **(B)** Mean square error of 10-fold validation. **(C)** The histogram of the DLR-score based on the selected features. Depending on the regulation weight λ, LASSO shrinks all regression coefficients towards zero and sets the coefficients of many irrelevant features exactly to zero. To find an optimal λ, 10-fold cross-validation with minimum criteria was employed, where the final value of λ yielded minimum cross-validation error. The retained features with nonzero coefficients were used for regression model fitting and combined into a DLR signature. Subsequently, we obtained a DLR score for each patient by a linear combination of retained features weighed by their model coefficients.

4 Discussion

Most patients with PTC have an excellent prognosis for long-term survival; however, some subtypes of PTC have an aggressive tumor process wherein *RET* rearrangements are positively associated with high-risk pathological factors for PTC, such as early occurrence, large tumor, rapid growth, and high metastatic capacity (12). *RET* rearrangements play an important role in the occurrence and development of PTC and can be used as a significant indicator for the diagnosis of PTC. The *RET*/PTC3 rearrangement is more aggressive than the *RET*/PTC1 rearrangement, among the most common subtypes of *RET* rearrangements (14). Therefore, preoperative determination of *RET* rearrangement will successfully assist in making more aggressive treatment strategies for patients with high-risk PTC. However, due to the low incidence of *RET* rearrangement in sporadic PTC (approximately 20%), as a routine preoperative examination, the *RET* gene test is not of good clinical utility.

In this study, we created a novel model built by ultrasound radiomics combined with DTL for the preoperative prediction of *RET* rearrangement in patients with PTC. We developed and validated five models, the clinical, radiomics, DTL, DLR, and DLRN signatures, for the prediction of the presence of *RET*/PTC rearrangement by quantitative analysis of thyroid ultrasound images. In both training and test cohorts, DLRN demonstrated the best-predicted performance compared with the other models. The AUC of DLRN in the test cohort could reach 0.9545 (95% CI: 0.9133–0.9558) in the test cohort and 0.9396 (95% CI: 0.9185–0.9607) in the training cohort. DCA showed that DLRN can improve preoperative *RET* rearrangement prediction. Thus, our results are valuable and can be distinguished from previous studies as the first attempt at combining DLR based on ultrasound images and the clinically rare *RET*/PTC rearrangement; we also demonstrated the clinical feasibility of DLRN. Furthermore, our study provides a preoperative method to non-invasively assess *RET* information and assist in design-making when clinicians are faced with

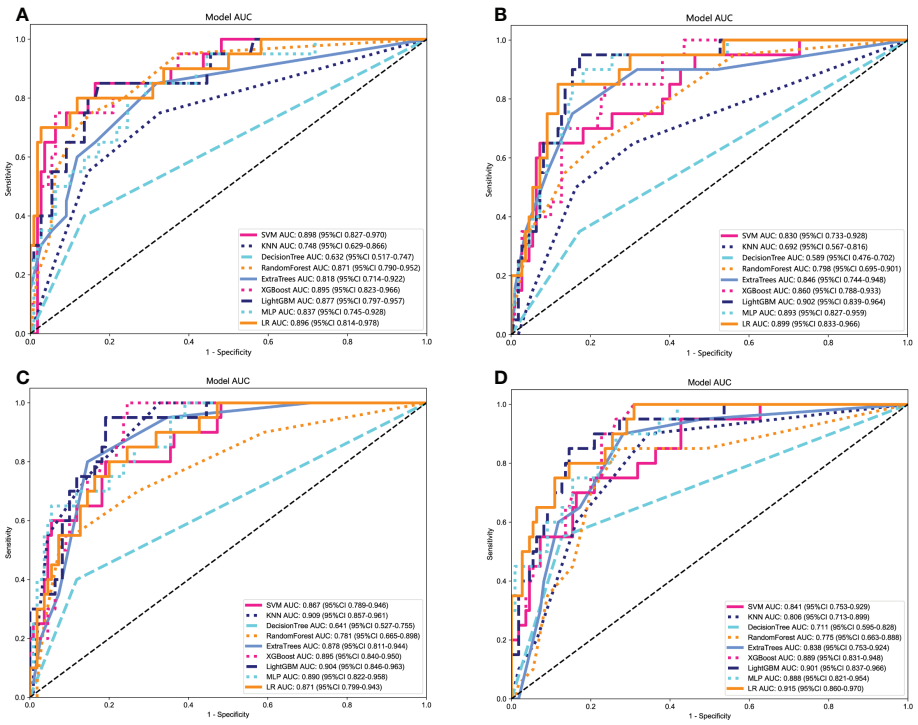

FIGURE 5
Receiver operating characteristic (ROC) curves of different models in the test cohort. **(A)** ROC curves of different models on Clinical signature. **(B)** ROC curves of different models on Rad signature. **(C)** ROC curves of different models on DTL signature. **(D)** ROC curves of different models on DLR signature.

ultrasound images that are difficult to determine with the naked eye.

Radiomics uses high-throughput automated extraction algorithms to evaluate the geometry, texture, and echo intensity of nodules; it also shifts from the traditional use of images for visual interpretation to their conversion to quantitative features (25, 26). Radiomics has been used to predict the molecular characteristics of various tumors (27). Concerning thyroid, radiomics has been proposed based on ultrasound images to predict the *BRAF* mutation (19, 20, 28); however, the models showed limited ability. Moreover, the *BRAF* mutation is the most representative mutation in PTC and has low specificity among all molecular features. Meanwhile, the significance of traditional ultrasound features for prediction is neglected. Although conventional ultrasound examinations rely only on the radiologist's visual description of the nodal features and cannot dig deeper into the information and the interpretation of ultrasound images is operator-dependent, there is interobserver variability. By designing the DLR model using ultrasound images and clinical factors, we simultaneously incorporated the DLR and traditional ultrasound features. In this study, four traditional ultrasound features, such as hypoechoic, vertical and horizontal diameter ratio of <1, cluster calcification, and ACR-TI-RADS 5 (highly suspicious), were associated with *RET*/PTC rearrangement. However, data on the association between *RET* rearrangement and traditional ultrasound features of PTC are very scarce and frequently inconsistent (16). Previous studies have pointed out that the *BRAF* mutation of PTC is associated with ultrasound features, such as hypoechoic, microcalcification, and irregular margins (29). Therefore, the traditional ultrasound features with *RET*/PTC rearrangement in our study were not very representative; however, our results can be used as a reference for further study of *RET*/PTC rearrangement in ultrasound radiomics. Compared with the DLR signature based on only containing DLR features, incorporating traditional ultrasound features of the nomogram showed a better predictive performance. The ultrasound features are supposed to be included in the analysis along with radiomics parameters for enhancing the diagnostic ability of gene mutation.

Deep learning has shown remarkable progress in medical image analysis, advancing the field forward at a quick pace. DLR has more advantages than hand-crafted and radiomics features. For example, deep learning can extract multilevel features from original images *via* a hierarchical neural network and automatically identify tumor boundaries. In this study, 19

TABLE 2 Predictive efficacy of all models in training cohort and test cohort.

	Training Cohort					Test Cohort				
Signature	Clinic Signature	Rad Signature	DTL Signature	DLR Signature	Nomogram	Clinic Signature	Rad Signature	DTL Signature	DLR Signature	Nomogram
Accuracy	0.8096	0.7615	0.8192	0.8154	0.8538	0.8692	0.8769	0.7692	0.7385	0.8769
AUC	0.8442	0.8638	0.9283	0.9335	0.9396	0.8959	0.8991	0.8709	0.9150	0.9545
95%CI	0.8009 - 0.8874	0.8262 - 0.9014	0.9035 - 0.9531	0.9119 - 0.9551	0.9185 - 0.9607	0.8141 - 0.9777	0.8325 - 0.9656	0.7986 - 0.9432	0.8601 - 0.9699	0.9133 - 0.9958
Sensitivity	0.6988	0.8313	0.9398	0.9639	0.9157	0.8000	0.8500	0.8500	1.0000	0.9500
Specificity	0.8307	0.7483	0.7963	0.7872	0.8421	0.8818	0.8818	0.7545	0.6909	0.8636
PPV	0.4394	0.3855	0.4671	0.4624	0.5241	0.5517	0.5667	0.3864	0.3704	0.5588
NPV	0.9356	0.9589	0.9858	0.9914	0.9813	0.9604	0.9700	0.9651	1.0000	0.9896
Precision	0.4394	0.3855	0.4671	0.4624	0.5241	0.5517	0.5667	0.3864	0.3704	0.5588
Recall	0.6988	0.8313	0.9398	0.9639	0.9157	0.8000	0.8500	0.8500	1.0000	0.9500
F1	0.5395	0.5267	0.6240	0.6250	0.6667	0.6531	0.6800	0.5313	0.5405	0.7037
Threshold	0.2115	0.1400	0.1255	0.1103	0.1123	0.2194	0.1974	0.0798	0.0876	0.1463

AUC, area under curve; CI, confidence interval; PPV, positive predictive value; NPV, negative predictive value.

10.3389/fendo.2022.1062571

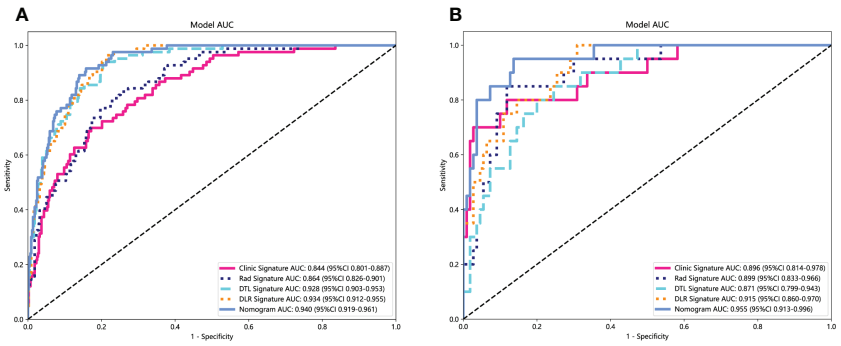

FIGURE 6
Receiver operating characteristic (ROC) curves of clinic signature, Rad signature, DTL signature, DLR signature and Nomogram. **(A)** in training cohort; **(B)** in test cohort.

TABLE 3 Delong test for each model.

Cohort	Nomogram Vs Clinical	Nomogram Vs Rad	Nomogram Vs DTL	Nomogram Vs DLR
Train	<0.0001	<0.0001	0.2898	0.2027
Test	0.1020	0.0771	0.0176	0.0626

TABLE 4 Hosmer–Lemeshow test.

Cohort	Clinic Signature	Rad Signature	DTL Signature	DLR Signature	Nomogram
Train	0.8457	0.7195	0.9141	0.5513	0.0787
Test	0.5655	0.4756	0.3451	0.9988	0.2142

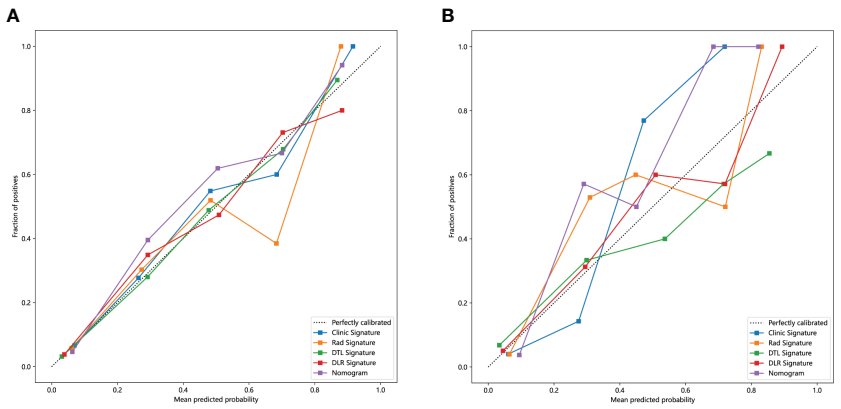

FIGURE 7
The calibration curves clinic signature, Rad signature, DTL signature, DLR signature and Nomogram. **(A)** in the training cohort; **(B)** in the test cohort.

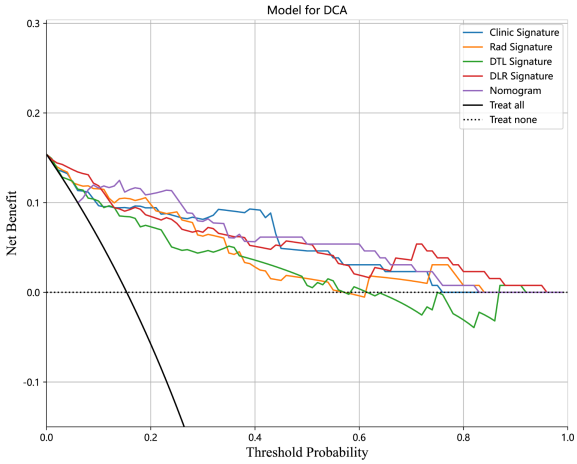

FIGURE 8
Decision curve analysis (DCA) for the Clinical signature, Rad signature, DTL signature, DLR signature, and Nomogram in the test cohort.

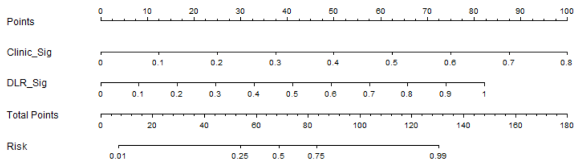

FIGURE 9
The nomogram to predict *RET*/PTC rearrangement.

features with nonzero coefficients were filtered from radiomics and DTL features to create the DLR signature. Among the selected DTL features, there were four most significant and robust features associated with *RET* rearrangement. For the selected radiomics features, most reflected the image texture and voxel intensity. The human visual system cannot recognize these features; however, these DLR features can serve as an auxiliary tool for the prediction of *RET* rearrangement in PTC.

There are certain limitations to our study: (1) First, the samples of *RET* rearrangement were not compared by different subtypes, such as *RET*/PTC1 and *RET*/PTC3, due to the insufficient sample size, concluding that this study could only perform primary screening of patients with *RET* rearrangement in PTC and not predict the specific subtypes. (2) Second, as this was a retrospective study, a selection bias may exist. Therefore, we aim to conduct a prospective study in the future to control for confounding variables. (3) Lastly, there was a lack of external validation as it was a single-center, small-sample study; therefore, this model needs to be further validated in a multi-center, larger sample size survey.

Data availability statement

The raw data supporting the conclusions of this article will be made available by the authors, without undue reservation.

Ethics statement

The studies involving human participants were reviewed and approved by The Ethics Committee of the First Affiliated Hospital of Zhengzhou University. Written informed consent from the participants' legal guardian/next of kin was not required to participate in this study in accordance with the national legislation and the institutional requirements.

Author contributions

JY: collected the all data from our hospital, statistical analysis, and drafting of the manuscript. YZ: contributed to

analysis and manuscript preparation. JZ and MJ: the accuracy of the data and proof reader. XL: supervision and proof reader. All authors contributed to the article and approved the submitted version.

Funding

This work was supported by the National Nature Science Foundation of China Youth Science Fund Project (No.81902881); Academic Leader of Young and Middle-aged Health in Henan Province (No.NSWJW-2020004) and Leading talents Plan in Henan Province (No.ZYYCYU202012116).

Acknowledgments

The authors appreciate assistance with the access of data from Information Management Center of the First Affiliated Hospital of Zhengzhou University.

Conflict of interest

The authors declare that the research was conducted in the absence of any commercial or financial relationships that could be construed as a potential conflict of interest.

Publisher's note

Supplementary material

The Supplementary Material for this article can be found online at: https://www.frontiersin.org/articles/10.3389/fendo.2022.1062571/full#supplementary-material

References

1. Siegel RL, Miller KD, Fuchs HE, Jemal A. Cancer statistics, 2021. *CA Cancer J Clin* (2021) 71(1):7–33. doi: 10.3322/caac.21654

2. Ito Y, Miyauchi A, Kihara M, Fukushima M, Higashiyama T, Miya A. Overall survival of papillary thyroid carcinoma patients: A single-institution long-term follow-up of 5897 patients. *World J Surg* (2018) 42(3):615–22. doi: 10.1007/s00268-018-4479-z

3. Grogan RH, Kaplan SP, Cao H, Weiss RE, Degroot LJ, Simon CA, et al. A study of recurrence and death from papillary thyroid cancer with 27 years of median follow-up. *Surgery* (2013) 154(6):1436–46;discussion 46-7. doi: 10.1016/j.surg.2013.07.008

4. Gan T, Huang B, Chen Q, Sinner HF, Lee CY, Sloan DA, et al. Risk of recurrence in differentiated thyroid cancer: A population-based comparison of the 7th and 8th editions of the American joint committee on cancer staging systems. *Ann Surg Oncol* (2019) 26(9):2703–10. doi: 10.1245/s10434-019-07275-1

5. Xing M. Molecular pathogenesis and mechanisms of thyroid cancer. *Nat Rev Cancer* (2013) 13(3):184–99. doi: 10.1038/nrc3431

6. Chu YH, Wirth LJ, Farahani AA, Nose V, Faquin WC, Dias-Santagata D, et al. Clinicopathologic features of kinase fusion-related thyroid carcinomas: An integrative analysis with molecular characterization. *Mod Pathol* (2020) 33 (12):2458–72. doi: 10.1038/s41379-020-0638-5

7. Li AY, McCusker MG, Russo A, Scilla KA, Gittens A, Arensmeyer K, et al. Ret fusions in solid tumors. *Cancer Treat Rev* (2019) 81:101911. doi: 10.1016/j.ctrv.2019.101911

8. Fagin JA, Mitsiades N. Molecular pathology of thyroid cancer: Diagnostic and clinical implications. *Best Pract Res Clin Endocrinol Metab* (2008) 22(6):955–69. doi: 10.1016/j.beem.2008.09.017

9. Romei C, Elisei R. Ret/Ptc translocations and clinico-pathological features in human papillary thyroid carcinoma. *Front Endocrinol (Lausanne)* (2012) 3:54. doi: 10.3389/fendo.2012.00054

10. Zafon C, Obiols G, Castellví J, Tallada N, Baena JA, Simó R, et al. Clinical significance of Ret/Ptc and P53 protein expression in sporadic papillary thyroid carcinoma. *Histopathology* (2007) 50(2):225–31. doi: 10.1111/j.1365-2559.2006.02555.x

11. Fisher SB, Cote GJ, Bui-Griffith JH, Lu W, Tang X, Hai T, et al. Genetic characterization of medullary thyroid cancer in childhood survivors of the Chernobyl accident. *Surgery* (2019) 165(1):58–63. doi: 10.1016/j.surg.2018.08.029

12. Adeniran AJ, Zhu Z, Gandhi M, Steward DL, Fidler JP, Giordano TJ, et al. Correlation between genetic alterations and microscopic features, clinical manifestations, and prognostic characteristics of thyroid papillary carcinomas. *Am J Surg Pathol* (2006) 30(2):216–22. doi: 10.1097/01.pas.0000176432.73455.1b

13. Ullmann TM, Thiesmeyer JW, Lee YJ, Beg S, Mosquera JM, Elemento O, et al. Ret fusion-positive papillary thyroid cancers are associated with a more aggressive phenotype. *Ann Surg Oncol* (2022) 29(7):4266–73. doi: 10.1245/s10434-022-11418-2

14. Cancer Genome Atlas Research N. Integrated genomic characterization of papillary thyroid carcinoma. *Cell* (2014) 159(3):676–90. doi: 10.1016/j.cell.2014.09.050

15. Di Cristofaro J, Vasko V, Savchenko V, Cherenko S, Larin A, Ringel MD, et al. Ret/Ptc1 and Ret/Ptc3 in thyroid tumors from Chernobyl liquidators: Comparison with sporadic tumors from Ukrainian and French patients. *Endocr Relat Cancer* (2005) 12(1):173–83. doi: 10.1677/erc.1.00884

16. Lewinski A, Adamczewski Z, Zygmunt A, Markuszewski L, Karbownik-Lewinska M, Stasiak M. Correlations between molecular landscape and sonographic image of different variants of papillary thyroid carcinoma. *J Clin Med* (2019) 8(11):1916. doi: 10.3390/jcm8111916

17. Park VY, Lee E, Lee HS, Kim HJ, Yoon J, Son J, et al. Combining radiomics with ultrasound-based risk stratification systems for thyroid nodules: An approach for improving performance. *Eur Radiol* (2021) 31(4):2405–13. doi: 10.1007/s00330-020-07365-9

18. Yoon JH, Han K, Lee E, Lee J, Kim EK, Moon HJ, et al. Radiomics in predicting mutation status for thyroid cancer: A preliminary study using radiomics features for predicting Brafv600e mutations in papillary thyroid carcinoma. *PloS One* (2020) 15(2):e0228968. doi: 10.1371/journal.pone.0228968

19. Kwon MR, Shin JH, Park H, Cho H, Hahn SY, Park KW. Radiomics study of thyroid ultrasound for predicting braf mutation in papillary thyroid carcinoma: Preliminary results. *AJNR Am J Neuroradiol* (2020) 41(4):700–5. doi: 10.3174/ajnr.A6505

20. Wang YG, Xu FJ, Agyekum EA, Xiang H, Wang YD, Zhang J, et al. Radiomic model for determining the value of elasticity and grayscale ultrasound diagnoses for predicting Braf(V600e) mutations in papillary thyroid carcinoma. *Front Endocrinol (Lausanne)* (2022) 13:872153. doi: 10.3389/fendo.2022.872153

21. Handelman GS, Kok HK, Chandra RV, Razavi AH, Lee MJ, Asadi H. Edoctor: Machine learning and the future of medicine. *J Internal Med* (2018) 284 (6):603–19. doi: 10.1111/joim.12822

22. Hosny A, Parmar C, Quackenbush J, Schwartz LH, Aerts H. Artificial intelligence in radiology. *Nat Rev Cancer* (2018) 18(8):500–10. doi: 10.1038/s41568-018-0016-5

23. Jiang Y, Yang M, Wang S, Li X, Sun Y. Emerging role of deep learning-based artificial intelligence in tumor pathology. *Cancer Commun (Lond)* (2020) 40 (4):154–66. doi: 10.1002/cac2.12012

24. Bini F, Pica A, Azzimonti L, Giusti A, Ruinelli L, Marinozzi F, et al. Artificial intelligence in thyroid field-a comprehensive review. *Cancers (Basel)* (2021) 13 (19):4740. doi: 10.3390/cancers13194740

25. Sorrenti S, Dolcetti V, Radzina M, Bellini MI, Frezza F, Munir K, et al. Artificial intelligence for thyroid nodule characterization: Where are we standing? *Cancers (Basel)* (2022) 14(14):3357. doi: 10.3390/cancers14143357

26. Mayerhoefer ME, Materka A, Langs G, Haggstrom I, Szczypinski P, Gibbs P, et al. Introduction to radiomics. *J Nucl Med* (2020) 61(4):488–95. doi: 10.2967/jnumed.118.222893

27. Qi Y, Zhao T, Han M. The application of radiomics in predicting gene mutations in cancer. *Eur Radiol* (2022) 32(6):4014–24. doi: 10.1007/s00330-021-08520-6

28. Tang J, Jiang S, Ma J, Xi X, Li H, Wang L, et al. Nomogram based on radiomics analysis of ultrasound images can improve preoperative braf mutation diagnosis for papillary thyroid microcarcinoma. *Front Endocrinol (Lausanne)* (2022) 13:915135. doi: 10.3389/fendo.2022.915135

29. Shangguan R, Hu YP, Huang J, Yang SJ, Ye L, Lin RX, et al. Association between Braf(V600e) mutation and the American college of radiology thyroid imaging, reporting and data system in solitary papillary thyroid carcinoma. *Acad Radiol* (2019) 26(2):154–60. doi: 10.1016/j.acra.2018.05.010

frontiers | Frontiers in Endocrinology

TYPE Original Research
PUBLISHED 04 January 2023
DOI 10.3389/fendo.2022.1039494

OPEN ACCESS

EDITED BY
Jose Federico Carrillo,
National Institute of Cancerology (INCAN), Mexico

REVIEWED BY
Mudiana Muhamad,
MARA University of Technology, Malaysia
Weibo Xu,
Fudan University, China

*CORRESPONDENCE
Sarni Mat Junit
sarni@um.edu.my

SPECIALTY SECTION
This article was submitted to Thyroid Endocrinology, a section of the journal Frontiers in Endocrinology

RECEIVED 08 September 2022
ACCEPTED 07 December 2022
PUBLISHED 04 January 2023

CITATION
Eng ZH, Abdullah MI, Ng KL, Abdul Aziz A, Arba'ie NH, Mat Rashid N and Mat Junit S (2023) Whole-exome sequencing and bioinformatic analyses revealed differences in gene mutation profiles in papillary thyroid cancer patients with and without benign thyroid goitre background. *Front. Endocrinol.* 13:1039494. doi: 10.3389/fendo.2022.1039494

Whole-exome sequencing and bioinformatic analyses revealed differences in gene mutation profiles in papillary thyroid cancer patients with and without benign thyroid goitre background

Zing Hong Eng[1], Mardiaty Iryani Abdullah[1,2], Khoon Leong Ng[3], Azlina Abdul Aziz[1], Nurul Hannis Arba'ie[3], Nurullainy Mat Rashid[1] and Sarni Mat Junit[1]*

[1]Department of Molecular Medicine, Faculty of Medicine, Universiti Malaya, Kuala Lumpur, Malaysia, [2]Department of Biomedical Science, Kulliyyah of Allied Health Sciences, International Islamic University Malaysia, Kuantan, Pahang, Malaysia, [3]Department of Surgery, Faculty of Medicine, Universiti Malaya, Kuala Lumpur, Malaysia

Background: Papillary thyroid cancer (PTC) is the most common thyroid malignancy. Concurrent presence of cytomorphological benign thyroid goitre (BTG) and PTC lesion is often detected. Aberrant protein profiles were previously reported in patients with and without BTG cytomorphological background. This study aimed to evaluate gene mutation profiles to further understand the molecular mechanism underlying BTG, PTC without BTG background and PTC with BTG background.

Methods: Patients were grouped according to the histopathological examination results: (i) BTG patients (n = 9), (ii) PTC patients without BTG background (PTCa, n = 8), and (iii) PTC patients with BTG background (PTCb, n = 5). Whole-exome sequencing (WES) was performed on genomic DNA extracted from thyroid tissue specimens. Nonsynonymous and splice-site variants with MAF of ≤ 1% in the 1000 Genomes Project were subjected to principal component analysis (PCA). PTC-specific SNVs were filtered against OncoKB and COSMIC while novel SNVs were screened through dbSNP and COSMIC databases. Functional impacts of the SNVs were predicted using PolyPhen-2 and SIFT. Protein-protein interaction (PPI) enrichment of the tumour-related genes was analysed using Metascape and MCODE algorithm.

Results: PCA plots showed distinctive SNV profiles among the three groups. OncoKB and COSMIC database screening identified 36 tumour-related genes including *BRCA2* and *FANCD2* in all groups. *BRAF* and 19 additional genes were found only in PTCa and PTCb. "Pathways in cancer", "DNA repair" and "Fanconi anaemia pathway" were among the top networks shared by all groups.

10.3389/fendo.2022.1039494

However, signalling pathways related to tyrosine kinases were the most significantly enriched in PTCa while "Jak-STAT signalling pathway" and "Notch signalling pathway" were the only significantly enriched in PTCb. Ten SNVs were PTC-specific of which two were novel; *DCTN1* c.2786C>G (p.Ala929Gly) and *TRRAP* c.8735G>C (p.Ser2912Thr). Four out of the ten SNVs were unique to PTCa.

Conclusion: Distinctive gene mutation patterns detected in this study corroborated the previous protein profile findings. We hypothesised that the PTCa and PTCb subtypes differed in the underlying molecular mechanisms involving tyrosine kinase, Jak-STAT and Notch signalling pathways. The potential applications of the SNVs in differentiating the benign from the PTC subtypes requires further validation in a larger sample size.

KEYWORDS

benign thyroid goitre, whole-exome sequencing, thyroid tumourigenesis, single nucleotide variants, papillary thyroid cancer

1 Introduction

Abnormal focal growth of thyroid cells resulting in thyroid nodules are very common in the general population. Although the majority of them are diagnosed as benign thyroid goitre (BTG), malignancies occur in 5% to 10% of nodules (1). Thyroid cancer, the most prevalent endocrine malignancy (2), is in the top ten of the most common cancer types in the world's female population, including Malaysia (3). Papillary thyroid cancer (PTC) is thyroid follicular cell-derived, constituting approximately 80% of all thyroid cancer cases (4). Mutations that trigger oncogenic activation of mitogen-activated protein kinase (MAPK) signalling pathway such as the $BRAF^{V600E}$ mutation are frequently linked to many malignancies including melanoma, colorectal cancer, and PTC (5).

Fine-needle aspiration cytology (FNAC) is a standard pre-operative, minimally invasive procedure to determine thyroid nodule malignancy status. However, up to one-fourth of the cases usually falls into the indeterminate Bethesda categories III and IV (6). Malignancy status is usually confirmed by histopathological examination (HPE) of thyroid tissue samples following partial or total thyroidectomy. HPE is the gold standard for thyroid nodule diagnosis, and yet only 40% of the indeterminate nodules were confirmed to be malignant after HPE (6, 7). Particularly, some of the confirmed PTC through HPE biopsies were found to have a BTG cytomorphological structure. Whether these PTCs are unique PTC subtypes, or the intermediate state of BTG transformation to PTC, remains unknown. Differences in tissue and serum protein profiles were reported in PTC patients with and without BTG background (8) indicative of differences in the underlying mechanisms between the two PTC subtypes and/or differences in their disease progression. This study aimed to evaluate gene mutation profiles to further understand the molecular mechanism underlying BTG, PTC without BTG background and PTC with BTG background. The presence of distinct tumour-related genetic profiles may be able to differentiate the two PTC subtypes in this cohort of patients.

2 Materials and methods

2.1 Subjects

This study was approved by the University of Malaya Medical Centre (UMMC)'s Medical Research Ethics Committee (MREC ID NO: 2019619-7540) in accordance with the ICH GCP guidelines and the Declaration of Helsinki. Written informed consent was obtained from all patients before the study was carried out.

The malignancy status of the patients was assessed through FNA cytology (FNAC) and was further confirmed by histopathological examination (HPE) of tissue specimens following partial or total thyroidectomy. All thyroid tissue specimens were placed in Allprotect tissue reagent (Qiagen, Hilden, Germany) at the time of retrieval and then stored at –80°C until further analysis. The patients were categorised into three groups based on the HPE reports: i) BTG (n = 9), ii) PTC without a BTG cytomorphological background (PTCa) (n = 8) and iii) PTC with a background of BTG (PTCb) (n = 5).

2.2 Genomic DNA extraction from thyroid tissue

Freshly excised thyroid tissue sample from each individual in the respective groups was submerged overnight in Allprotect tissue reagent (Qiagen, Hilden, Germany) at 4°C before storage at –80°C. Genomic DNA (gDNA) was extracted from the tissue samples using Qiagen AllPrep DNA/RNA/Protein Mini Kit (Qiagen, Hilden, Germany) according to the manufacturer's protocol. The concentration and purity of the extracted gDNA were determined by Invitrogen Qubit dsDNA BR Assay kit (Thermo Fisher Scientific, Massachusetts, USA) on Qubit 2.0 Fluorometer, and by Thermo Scientific NanoDrop™ 2000c Spectrophotometer (Thermo Fisher Scientific, Massachusetts, USA), respectively. The gDNA integrity test was then performed using 1% agarose gel electrophoresis.

2.3 Whole-exome sequencing analysis

Genomic DNA (gDNA) samples of the patients; BTG (n = 9), PTCa (n = 8), and PTCb (n = 5) were sent to BGI Biotechnology Company (Shenzhen, China) for whole-exome sequencing (WES) analysis. The qualified gDNA was randomly fragmented into fragments with a range of 150-200 bp using the Adaptive Focused Acoustics® (AFA®) technology of Covaris Ltd. The adapter-ligated templates were purified using the AgencourtAMPure Solid Phase Reversible Immobilisation (SPRI) beads and fragments with an insert size of about 200 bp were excised. Extracted adapter-ligated templates were then amplified by ligation-mediated polymerase chain reaction (LM-PCR), purified, and hybridised to the SureSelect Biotinylated RNA baits for enrichment and measured using the Agilent 2100 Bioanalyzer. The captured products were then circularised before rolling circle amplification (RCA) was used to produce DNA Nanoballs (DNBs). The captured libraries were then sequenced using the BGISEQ-500 sequencing platform and processed by BGISEQ base-calling Software with default parameters. The filtered WES data in FASTQ format were aligned to Reference Genome of human genome built 37 (http://hgdownload.cse.ucsc.edu/goldenPath/hg19/bigZips/) using Burrows-Wheeler Aligner (BWA) software. Genomic variations were detected by HaplotypeCaller of Genome Analysis Toolkit (GATK) (v3.6). The hard-filtering method was applied to obtain high confident variant calls. All the SNVs were then annotated using the SnpEff program (http://snpeff.sourceforge.net/). The WES results were validated by $BRAF^{V600E}$ mutation screening using PCR-direct DNA sequencing (9). Primers targeting the *BRAF* mutation were designed using Primer3 (https://primer3.ut.ee/). The primer sequence is as follows; Forward: 5'-CTCTTCATAATGCTTGCTCTGATAG-3'; Reverse: 5'-CCTCAATTCTTACCATCCAC-3'.

2.4 Variant filtering and principal component analysis

The variants with the following criteria were retained for further analyses: (i) minor allele frequency (MAF) ≤ 0.01 in the 1000 Genomes Project control database; and (ii) nonsynonymous and splice-site variants. Principal component analysis (PCA) was carried out on the retained SNVs using Python 3.6 software from a single computer workstation equipped with 3.1 GHz Dual-Core Intel Core i5 and 8 GB RAM. All the software and Python libraries used in the study work were from open sources. The following four variables of categorical data were used to represent an SNV molecular component chosen for the PCA: sample ID (e.g. patients 1, 2 etc), mutant genes (e.g. *AATF*), specific mutation (e.g. NM_012138:c.G872A:p.G291D) and genotype status (heterozygous/homozygous) as well as three classes of the disease type (BTG, PTCa and PTCb). One hot encoding was then run to convert the categorical variables into the numerical interpretation. A new dimension data of 22,427 rows and 22,850 columns were produced. All data were standardised in such a manner that it has mean as 0 and standard deviation as 1. During model training, the PCA algorithm was carried out to reduce high dimensional data into a minimum number of dimensions with 90% of the retained variance.

2.5 Database search of single nucleotide variants in tumour-related genes

The variants were filtered against two cancer-related gene panels from Oncology Knowledge Base (OncoKB) and Catalogue Of Somatic Mutation In Cancer (COSMIC) Cancer Gene Census databases (10, 11). The filtered variants were then screened through the Single Nucleotide Polymorphisms Database (dbSNP, http://www.ncbi.nlm.nih.gov/snp) and COSMIC database for identification of those that were novel. To determine PTC-specific SNVs, those that were identified in more than one PTC patients were further subjected to the Allele Frequency Aggregator (ALFA) project and the genome Aggregation Database (gnomAD) through Ensembl database (https://asia.ensembl.org/index.html) of which SNVs with MAF < 0.01 were retained. The PTC-specific SNVs were then analysed for their potential functional impact using Polymorphism Phenotype 2 (PolyPhen-2, http://genetics.bwh.harvard.edu/pph2/) and Sorting Intolerant from Tolerant (SIFT, https://sift.bii.a-star.edu.sg/). The variants predicted to be deleterious were further validated using Sanger sequencing method.

2.6 Protein-protein interaction network enrichment analysis

PPI enrichment analysis was carried out through Metascape tool (http://metascape.org) with the following databases: STRING, BioGrid, OmniPath, InWeb_IM9 using default parameters. Tumour-related genes that were found to be mutated in each disease group were used as the input gene sets. STRING (physical score > 0.132) and BioGrid were used to identify the protein-protein physical interactions. The Molecular Complex Detection (MCODE) algorithm was then applied to identify densely connected network components in the PPI analysis results. Pathway and process enrichment analyses were then carried out on the MCODE modules based on the GO Biological Processes and KEGG Pathway biological pathway databases.

3 Results

3.1 Nonsynonymous and splice-site variants identification and PCA analysis

A total of 15703 nonsynonymous and splice-site variants were identified in the three cohorts of patients (Figure 1A). PTCa patients had the highest average variant count (≈ 1156) followed by PTCb (≈ 1029) and BTG (893) patients. Missense mutation was found to be the most common type of variant type among all subjects. PCA plots of the filtered WES data for the three groups are shown in Figure 1B. In general, distinctive patterns of the four variables were observed for the BTG (Figure 1B(i)), PTCa (Figure 1B(ii)) and PTCb (Figure 1B(iii)) when the data were analysed separately. A similar distinctive pattern was observed when the datasets from the three disease groups were co-analysed. The variable profiles for PTCa showed a higher degree of dispersal compared to PTCb in relation to BTG. In addition, BTG, PTCa and PTCb showed some extent of similarities in their patterns represented by the shared area at the centre of the PCA plot [Figure 1B(iv)].

3.2 Analysis of mutated tumour-related genes in BTG, PTCa and PTCb

The 15703 nonsynonymous and splice-site variants were found in a total of 7875 genes in the three groups of patients. When the 7875 genes were filtered against OncoKB and COSMIC cancer gene census databases, a total of 259 tumour-related genes were identified (Figure 2A). OncoKB was able to identify more tumour-related genes in our cohort of patients (410 genes) compared to the COSMIC database (318 genes). Among the 259 mutated tumour-related genes, 149 were found in the BTG group, followed by 144 and 111 in the PTCa and PTCb groups, respectively (Figure 2B). Thirty-six tumour-related genes including *ALK*, *AR*, *BRCA2*, *FANCD2* and *CBL* were found to be mutated in all the three disease groups. An

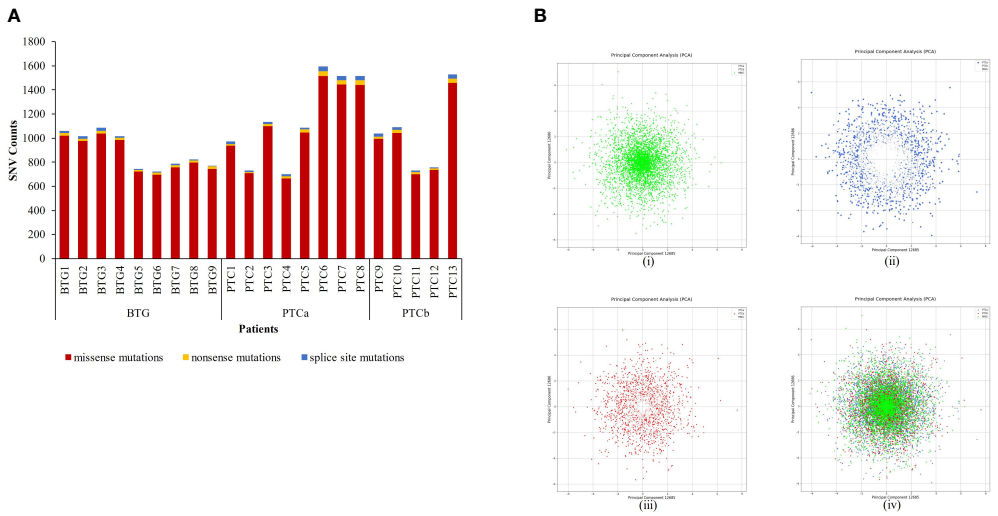

FIGURE 1
Analysis of nonsynonymous and splice-site single nucleotide variants (SNVs) identified through whole exome sequencing in patients with benign thyroid goitre (BTG), papillary thyroid cancer without BTG background (PTCa) and with BTG background (PTCb). **(A)** Nonsynonymous SNVs identified in each patient were filtered against 1000 Genome Projects (MAF ≤ 0.01). **(B)** Principal Component Analysis (PCA) of SNV profiles (gene, mutation, and genotype status) of the filtered nonsynonymous SNVs in (i) BTG, (ii) PTCa in relation to BTG, (iii) PTCb in relation to BTG and (iv) all disease groups.

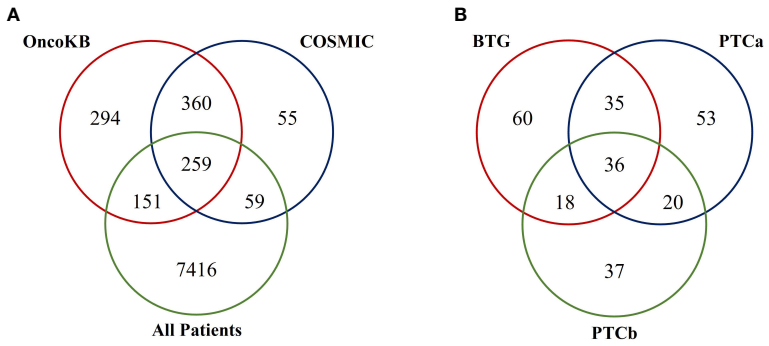

FIGURE 2
Venn diagrams illustrating findings from the database search of mutated tumour-related genes in this cohort of patients. **(A)** A total of 259 mutated tumour-related genes were listed in both the OncoKB and COSMIC databases. **(B)** Among the 259 mutated tumour-related genes, there were 36 genes found to be mutated in all three disease groups.

additional 35 genes including *ATR* and *IRS4* were found only in the BTG and PTCa. Another 18 tumour-related genes such as *NCOR2* and *PALB2* were found to be mutated in BTG and PTCb only. In addition, genes including *BRAF*, *DCTN1* and *RAD51B* were among the 20 tumour-related genes that were found to be mutated only in the PTCa and PTCb patients. The list of mutated tumour-related genes in each disease group is presented in Supplementary Table 1. A representative of the Sanger sequencing result of the $BRAF^{V600E}$ is shown in Supplementary Figure 1.

3.3 Protein-protein interaction network enrichment analysis of the mutated tumour-related genes found in BTG, PTCa and PTCb

The top enriched KEGG ontology terms in the PPI networks of the three groups are shown in Figure 3A. "Pathways in cancer" (hsa05200), "Fanconi anaemia pathway" (hsa03460) and "Homologous recombination" (hsa03440) were significantly enriched in the three groups with "Pathways in cancer" and "Fanconi anaemia pathway" were the most enriched in PTCa while "Homologous recombination" was the most enriched in PTCb. "EGFR tyrosine kinase inhibitor resistance" (hsa01521) was exclusively enriched in PTCa while "Jak-STAT signalling pathway" (hsa04630), "Notch signalling pathway" (hsa04330) and "Endocrine resistance" (hsa01522) were only enriched in PTCb.

"DNA repair" (GO:0006281), "cellular response to DNA damage stimulus" (GO:0006974) and "double-strand break repair" (GO:0006302) were the enriched Gene Ontology (GO) terms shared among the three groups with the highest significance observed in PTCb followed by PTCa and BTG (Figure 3B). Three GO networks were only significantly enriched in the malignant groups namely "peptidyl-tyrosine phosphorylation" (GO:0018108), "peptidyl-tyrosine modification" (GO:0018212) and "regulation of kinase activity" (GO:0043549), with higher significance shown in PTCa compared to PTCb. "Mismatch repair" (GO:0006298),

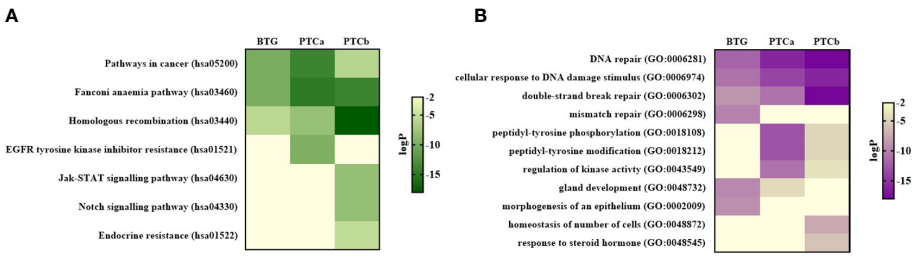

FIGURE 3
Protein-protein interaction (PPI) network analysis showing the top enriched pathways for the three disease groups based on the **(A)** KEGG database and **(B)** GO ontology database. Pathways with p-value < 0.01 (LogP < −2) was considered as significant. BTG, Benign thyroid goitre; PTCa, Papillary thyroid cancer without BTG background; PTCb, Papillary thyroid cancer with BTG background.

"gland development" (GO:0048732) and "morphogenesis of an epithelium" (GO:0002009) were highly enriched in the BTG group while "homeostasis of number of cells" (GO:0048872) and "response to steroid hormone" (GO:0048545) were only enriched in PTCb.

The enriched terms were categorised into three main modules: (a) Cancer-related pathways, (b) DNA damage and repair-related pathways, and (c) Signalling Pathways and the tumour-related genes that were involved in each module are shown in Figure 4. Although there was no shared gene among the three groups in the Cancer-related pathways, three genes were shared between the two malignant groups namely *AR*, *HSP90AB1* and *GNAS* (Figure 4A). *NOTCH2* was the only gene shared between BTG and PTCb. In the DNA damage and repair-related pathways, *BRCA2 (FANCD1)* and *FANCD2* were the only two genes shared by the three groups (Figure 4B). In addition to the two genes, *ERCC4, NBN, FANCA*, *FANCE* and *FANCG* were shared between BTG and PTCa; *WRN*, *POLD1* and *PALB2* were shared between BTG and PTCb groups while *BRIP1* and *RAD51B* were identified in PTCa and PTCb only. As shown in Figure 4C, none of the genes in the Signalling pathways were shared between the two malignant groups. BTG had none of the enriched term for this module.

3.4 Identification of potential molecular markers for PTC

A total of 108 SNVs were identified in more than one subjects. The complete list of the SNVs is presented in Supplementary Table 2. Comparative analysis against the ALFA project and gnomAD dataset through Ensembl database (https://asia.ensembl.org/index.html) identified 10 PTC-specific SNVs (Table 1). Four of the SNVs, *ATR* c.7817G>A (p.Arg2606Gln), *IRS4* c.605A>G (p.Lys202Arg), *PCM1* c.3520A>G (p.Thr1174Ala) and *TRRAP* c.8735G>C (p.Ser2912Thr) were only detected in PTCa. Two SNVs, *DCTN1* c.2786C>G (p.Ala929Gly) and *TRRAP* c.8735G>C (p.Ser2912Thr) were presumed novel as they could not be found in the dbSNP and COSMIC databases. *In silico* functional analysis through Polyphen2 predicted that the two novel mutations were "possibly damaging" while SIFT predicted that *DCTN1* c.2786C>G (p.Ala929Gly) and *TRRAP* c.8735G>C (p.Ser2912Thr) was "tolerated" and "deleterious" respectively. Another six previously reported SNVs namely *ARID1B* c.1181C>G (p.Ala394Gly), *BRAF* c.1799T>A (p.Val600Glu), *PDE4DIP* c.4073T>C (p.Ile1358Thr), *ATR* c.7817G>A (p.Arg2606Gln), *IRS4* c.605A>G (p.Lys202Arg), and *PCM1* c.3520A>G (p.Thr1174Ala) were also predicted to be deleterious. Although predicted to be of benign variants, *TET2* c.2440C>T (p.Arg814Cys) and *USP6* c.287G>T (p.Arg96Leu) showed PTC-specificity.

Allelic frequency comparison of six SNPs: *BRAF* c.1799T>A (p.Val600Glu), *TET2* c.2440C>T (p.Arg814Cys), *USP6* c.287G>T (p.Arg96Leu), *ATR* c.7817G>A (p.Arg2606Gln), *IRS4* c.605A>G (p.Lys202Arg) and *PCM1* c.3520A>G (p.Thr1174Ala) with various normal populations is presented in Figure 5. The minor allele for the six PTC-specific SNVs were either totally absent (*BRAF* c.1799T>A (p.Val600Glu) and *IRS4* c.605A>G (p.Lys202Arg) or present in less than 1% in the world (ALL), African (AFR), American (AMR), East Asian (EAS), European (EUR) and South Asian (SAS) populations. Population genetic data for the other four SNVs; *ARID1B*

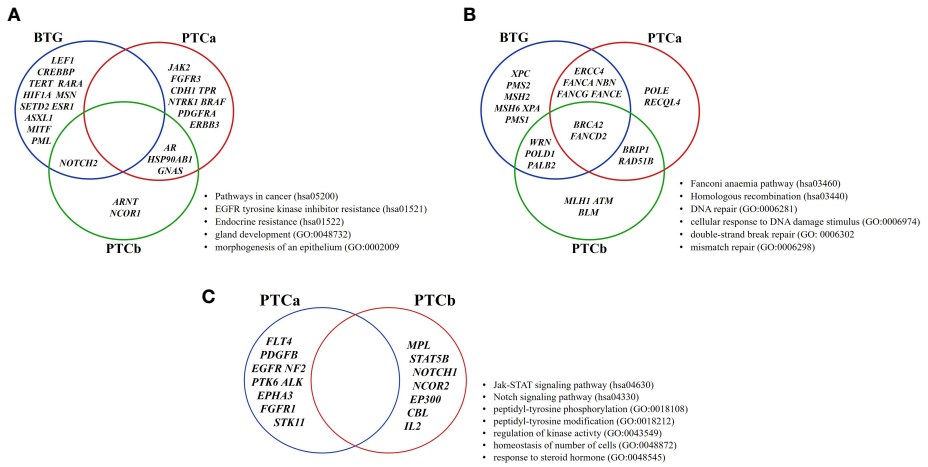

FIGURE 4
Distribution of genes of the enriched pathways in BTG, PTCa and PTCb. The enriched ontology terms are categorised according to the MCODE algorithm modules: **(A)** Cancer-related pathways and **(B)** DNA damage and repair-related pathways and **(C)** Signalling pathways. BTG, Benign thyroid goitre; PTCa, Papillary thyroid cancer without BTG background; PTCb, Papillary thyroid cancer with BTG background.

TABLE 1 Ten PTC-specific SNVs and their *in silico* functional impact predictions.

Gene	dbSNP	Transcript	Codon Change	Amino acid Change	SNV counts		PolyPhen2		SIFT	
					BTG	PTC	Score	Prediction	Score	Prediction
ARID1B	rs1778971493	NM_020732	c.1181C>G	p.Ala394Gly	0	3	0.766	Possibly Damaging	Not scored	
DCTN1	Novel	NM_004082	c.2786C>G	p.Ala929Gly	0	3	0.849	Possibly Damaging	0.370	Tolerated
BRAF	rs113488022	NM_004333	c.1799T>A	p.Val600Glu	0	3	0.923	Possibly Damaging	0.010	Deleterious
TET2	rs192553789	NM_001127208	c.2440C>T	p.Arg814Cys	0	2	0.034	Benign	0.120	Tolerated
USP6	rs113754955	NM_001304284	c.287G>T	p.Arg96Leu	0	2	0.069	Benign	0.193	Tolerated
PDE4DIP	rs2066638374	NM_001198834	c.4073T>C	p.Ile1358Thr	0	2	0.993	Probably Damaging	0.010	Deleterious
ATR	rs199948706	NM_001184	c.7817G>A	p.Arg2606Gln	0	2	0.935	Possibly Damaging	0.210	Tolerated
IRS4	rs753584516	NM_003604	c.605A>G	p.Lys202Arg	0	2	0.890	Possibly Damaging	0.280	Tolerated
PCM1	rs143680240	NM_006197	c.3520A>G	p.Thr1174Ala	0	2	0.005	Benign	0.018	Deleterious
TRRAP	Novel	NM_001244580	c.8735G>C	p.Ser2912Thr	0	2	0.976	Probably Damaging	0.020	Deleterious

BTG, Benign thyroid goitre; PTC, Papillary thyroid cancer. SNVs with PolyPhen2 score ranged from 0.15 to 1.0 are predicted to be possibly damaging, those with score > 0.85 are more confidently predicted to be damaging. SNVs with SIFT score < 0.05 are considered deleterious.

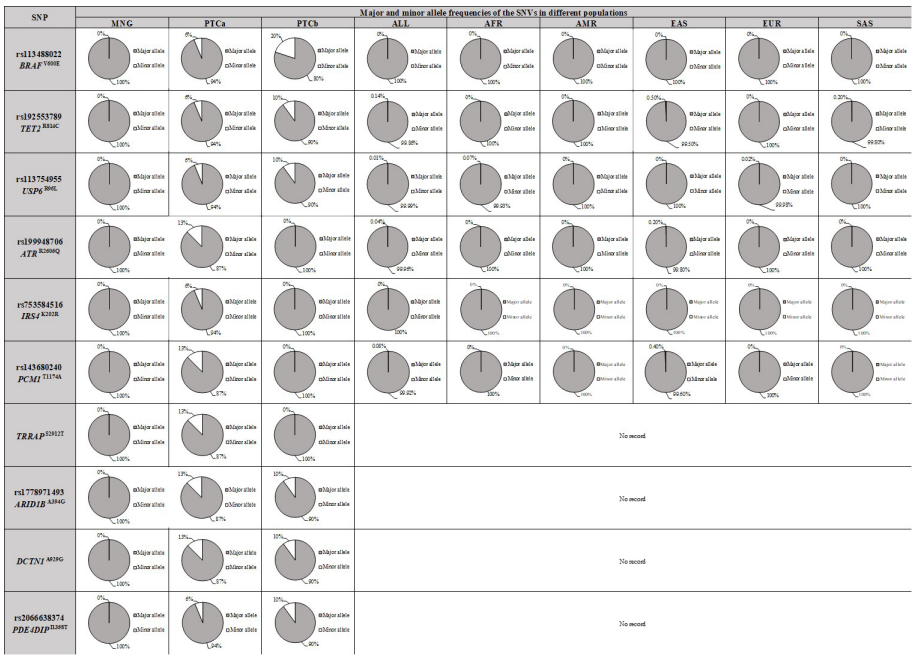

FIGURE 5
Comparison of allelic frequencies of ten PTC-specific SNPs in BTG, PTCa, PTCb and various populations. The data of different populations were obtained from Ensembl population genetic database (https://asia.ensembl.org/index.html). ALL, all populations; AFR, African; AMR, American; EAS, East Asian; EUR, European; SAS, South Asian. Major allele refers to the wildtype allele; minor allele refers to the mutant allele. BTG, Benign thyroid goitre; PTCa, Papillary thyroid cancer without BTG background; PTCb, Papillary thyroid cancer with BTG background.

c.1181C>G (p.Ala394Gly), *DCTN1* c.2786C>G (p.Ala929Gly), *PDE4DIP* c.4073T>C (p.Ile1358Thr) and *TRRAP* c.8735G>C (p.Ser2912Thr) were not available in the database for allelic frequency comparison to be made.

4 Discussion

To understand the underlying genetic alterations in PTCa and PTCb, WES data of the two groups were compared to those in BTG. WES is one of the NGS platforms that can detect variations in the protein-coding area of genes (exons), which account for approximately 3.09% of the whole genome (12). Its function and application to detect disease-causing mutations have been previously demonstrated in papillary thyroid cancer cases (13–16) and other clinical studies (17, 18).

In this study, nonsynonymous variants with MAF ≤ 1% were prioritised due to their direct impact on the functionality and the available tools to interrogate their pathogenic effects (19, 20). The three groups showed similarities in the type of variants of which missense variants being the most common, followed by splice-site and nonsense variants. However, among the three groups, PTCa had the highest total number of variants, followed by PTCb and BTG. DNA damage is common, and it is usually repaired by various DNA repair machineries. The equilibrium between the occurrence of DNA damage and repair, if skewed, leads to DNA damage accumulation, and might start the cancer onset (21). DNA damage accumulation might have contributed towards the higher number of variants in both the malignant PTCa and PTCb groups as compared to the BTG. The different average number of variants between PTCa and PTCb may indicate differences in the underlying disease progression mechanisms or differences in the phases/states during the transformation from the benign to malignant condition. Since the transformed WES data had superhigh dimensions, PCA was done to reduce the dimensionality to find distinct patterns within the data without losing its original information. Ninety percent of variance were set during the model training to get the best visualisation of the distinct patterns while retaining as much information in the datasets as possible (22). The 10% loss in information is to be expected during the dimensional reduction and other factors including duplication, less informative or the complex nature of the information (23). Distinctive profiles were also observed when the filtered WES data for PTCa and PTCb in relation to BTG, were further visualised through PCA plots. This may also point to differences in the underlying molecular mechanisms. Despite the distinctive profiles, some extent of similar patterns in PCA plots were also observed among the BTG, PTCa and PTCb. The pattern similarities could be interpreted that both PTCa and PTCb originate from BTG or PTCb could be an intermediate state in the BTG to PTCa transformation.

To further understand the similarities and differences in the underlying molecular mechanisms behind PTCa and PTCb in relation to BTG, the gene variants identified in all patients were subjected to comparative analyses against OncoKB and COSMIC cancer gene census databases followed by PPI pathway enrichment analyses. MCODE algorithm was applied to identify the densely connected network components in the PPI analysis. The three groups shared significant enrichment of the Cancer-related pathways and DNA damage repair-related pathways. Although no specific tumour-related gene was shared among the three groups, *NOTCH2* was shared between BTG and PTCb while *AR*, *HSP90AB1* and *GNAS* were shared between BTG and PTCa suggesting their possible roles in the BTG-to-PTCb and BTG-to-PTCa transformation, respectively. These observations also suggest that the mechanism of transformation from BTG to PTCa differs from that of BTG to PTCb. In general, the DNA damage and repair-related pathways were more significantly enriched in both PTCa and PTCb compared to BTG. "Fanconi anaemia pathway" was most enriched in PTCa while "Homologous recombination" and "mismatch repair" were most enriched in PTCb and BTG respectively. Notably, *BRCA2* and *FANCD2* were shared by three groups indicating that the two genes possibly playing key roles in triggering the transformation of BTG to both PTCa and PTCb. DNA lesions can be caused by either endogenous or exogenous agents, such as reactive oxygen species (ROS) produced during cell metabolism or ionising radiation (13). As such, cells are equipped with different DNA repair systems, including base excision repair (BER), nucleotide excision repair (NER), mismatch repair (MMR), homologous recombination (HR) and non-homologous end-joining (NHEJ) against different types of DNA damages and active throughout different cell cycle stages, maintaining our genome stability. Aberrant DNA repair might drive accumulation of the DNA damages, followed by cancer onset. DNA damage in thyroid disorders is common, due to the reliance on ROS in thyroid hormone biosynthesis (14, 15).

Fanconi anaemia (FA) pathway has been found to be important in DNA repair mechanisms (24, 25), although none of our patients had haematologic disorders. Based on the literatures, upon recognition and binding of FA core complex that comprises seven complementary groups (A, B, C, E, F, L and M) to the DNA lesions, the ubiquitination activated FANCD2-I will then localise to the damaged DNA loci. The FA pathway then regulates the subsequent repair processes including DNA replication, cell-cycle arrest, and DNA damage repair. BRCA2 is a recombination mediator that co-localises with ubiquitinated FANCD2 and facilitates the formation of Rad51 nucleofilaments, linking the FA pathways to homologous recombination (26). *BRCA2* mutation has been linked to many cancer types, including breast cancer, ovarian cancer, pancreatic cancer and glioblastoma (27–30). Generally, cancer patients with the *BRCA2* mutations were reported to have a more aggressive phenotype compared to those with *FANCD2* mutation (24). In this study, in addition to *BRCA2* and *FANCD2*, another three genes in the FA pathways, *FANCA*, *FANCE* and *FANCG*, were exclusively shared

between BTG and PTCa indicating their importance in the transformation of BTG to PTCa with an aggressive phenotype.

In addition to *BRCA2* and *FANCD2, PALB2* is another gene node which was found in both BTG and PTCb. PALB2 has been reported to be indispensable to BRCA1 and BRCA2 in DNA repair mechanisms (31, 32). In contrast to FANCD2 monoubiquitination which has a mild impact on HR, BRCA2 activity is essential for DNA double-strand break (DSB) repair (24). *PALB2* and *BRCA*s genes have been well-reported due to their high prevalence in breast cancer where patients with *PALB2* gene mutation were found to have shorter survival years (33–35). It was also reported that approximately 49.1% of thyroid cancer patients were found to have breast tumours (36). *PALB2* codes for a protein that serves as a bridge protein between BRCA1 and BRCA2 proteins to form a complex that initiates HR of the DSB (37, 38). Mutations in PALB2 might lead to its BRCAs binding function loss, which leads to the impaired HR pathway, and the accumulation of DNA DSB lesions. The *ATM* gene found in PTCb's PPI network further strengthens our speculation. *ATM* gene codes for the checkpoint kinase ataxia telangiectasia mutated, which activates the intra-S checkpoint in response to DSBs to arrest DNA replication, the possible loss of this kinase function might lead to further DNA lesions accumulation in the PTCb group. Further assessment on DSBs in PTCb with concomitant presence of breast cancer is thus warranted.

While there were degrees of similarities and differences in DNA damage repair-related pathways gene enrichment, in PTCa and PTCb, the "Signalling pathways" enriched network were distinctive in the two groups. Genomic instability has been suggested to be an early event in cancer development, where the consecutive genetic alterations that affect the normal cell cycle machinery might promote progression from a relatively benign proliferative cells lump to malignant tumour (39–41). Oncogenic mutations that lead to abnormal synthesis of receptors or ligands involved in signalling pathways, such as growth factor receptor tyrosine kinases (RTKs) and serine/threonine kinase, can cause hyperactive oncogenic signalling pathways and dysregulate cell cycle machinery (40). Signalling pathways related to tyrosine kinases were the most significantly enriched in PTCa while "Jak-STAT signalling pathway" and "Notch signalling pathway" were the only significantly enriched in PTCb. BTG was found to have none of the enriched term for this module. Oncogenic activation of the MAPK signalling cascade was found to be indispensable to the PTC development (31). The oncogenic activation of MAPK cascade upregulates the expression of the receptor tyrosine kinase and its binding to the ligands, such as growth factors, might lead to the oncogenic cell proliferation. However, the absence of this MCODE network in the PTCb group further revealed the different underlying mechanisms in the PTCa and PTCb disease progression. Jak-STAT and Notch signalling pathways were shown to be affected in the PTCb group. Jak-STAT signalling pathway has been reported to have tumour effects in PTC development (42). An additional study had also reported the potential role of affected STAT3 pathway and MAPK signalling cascade due to prolonged H_2O_2 insult in the thyroid gland and leading to the PTC progression (43, 44). The role of Notch signalling in cancer progression remains controversial, as it was found to be oncogenic and tumour suppressive in different studies. Increased Notch1 and Notch2 expression in PTC cases were found to be associated with more aggressive phenotypes (45). The upregulated Notch1 signalling pathway was linked to metastasis, increased tumour size, and led to a poor prognosis in PTC patients (45, 46). The affected Notch signalling pathway in the PTCb patients in the present study might result in the poor prognosis of PTCb where their presence of BTG cytomorphological structure is in the background. However, discordant findings were also reported (47, 48).

Taken together, findings from the *in-silico* PPI network enrichment analysis suggest that erroneous DNA repair mechanism might be the primary cause of thyroid tumour development of BTG. Further oncogenic mutations that affect the signalling pathways then drive the transformation of PTCa and PTCb from BTG. The transformation of BTG to PTCa follows a different mechanism which involves a more aggressive tyrosine kinase-related pathways while the transformation of BTG to PTCb is linked to presumably a less aggressive JAK-STAT/Notch signalling pathways. Further confirmation on this is required. The difference in the signalling pathways will allow a more personalised therapeutic target for PTCa and PTCb. The proposed mechanism of transformation from BTG to PTCa and PTCb is summarised in Figure 6.

Through the WES sequencing analysis, there were ten SNVs showing PTC-specific characteristic where also predicted to be functionally deleterious in *in-silico* functional analysis *BRAF* c.1799T>A (p.Val600Glu) is one of ten SNVs that were found to be PTC-specific. $BRAF^{V600E}$ mutation, which was detected in approximately 60% of PTC cases, is associated with disease aggressiveness, recurrence and increased mortality (17, 18, 49–52). Its high prevalence in PTC patients has led to the suggestion of its potential use as a diagnostic and prognostic genetic biomarker (53–55). In the current study, $BRAF^{V600E}$ was confirmed to be PTC-specific. Its relatively low occurrence of 23.1% suggests that $BRAF^{V600E}$ is not a common underlying mutation in our cohort of patients. The prevalence of $BRAF^{V600E}$ mutation in PTC patients in Malaysia and in the rest of the Southeast Asia region remains largely unknown (56). While this mutation had been reported to be associated with intra-axial brain tumour patients in Malaysia (57), our study is the first to report the presence of this mutation in PTC patients in Malaysia. Further screening of the $BRAF^{V600E}$ mutation in a larger sample size will better reflect its prevalence in the Malaysian PTC population. While $BRAF^{V600E}$ was able to differentiate the BTG from the malignant PTC cases, it was unable to differentiate between PTCa and PTCb in this study.

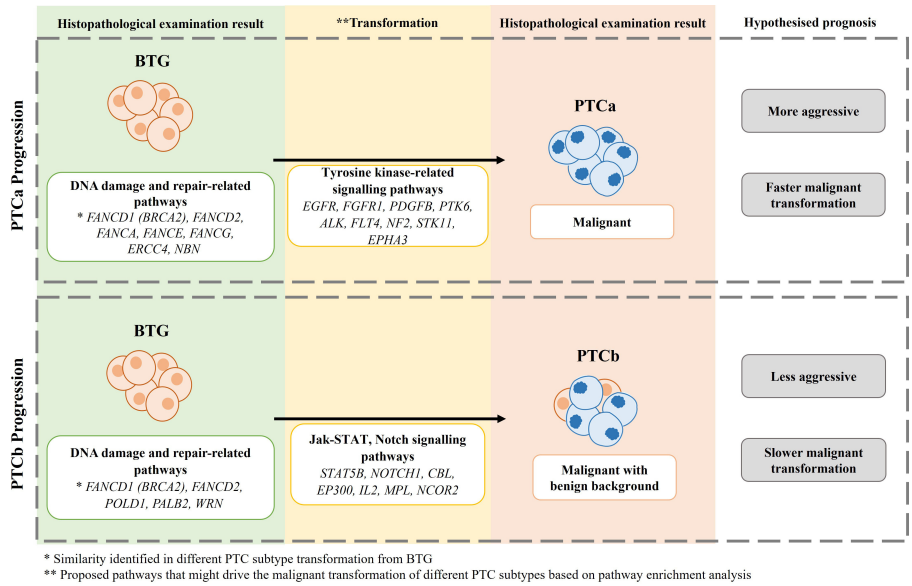

FIGURE 6
The proposed mechanism of BTG transformation to PTCa and PTCb in this cohort of patients.

Six SNPs, *BRAF* c.1799T>A (p.Val600Glu), *TET2* c.2440C>T (p.Arg814Cys), *USP6* c.287G>T (p.Arg96Leu), *ATR* c.7817G>A (p.Arg2606Gln), *IRS4* c.605A>G (p.Lys202Arg) and *PCM1* c.3520A>G (p.Thr1174Ala) were present in less than 1% of the world population as the African (AFR), American (AMR), East Asian (EAS), European (EUR) and South Asian (SAS) populations further suggesting that these were pathological instead of neutral mutations. The allelic frequency of another four SNVs {*ARID1B* c.1181C>G (p.Ala394Gly), *DCTN1* c.2786C>G (p.Ala929Gly), *PDE4DIP* c.4073T>C (p.Ile1358Thr) and *TRRAP* c.8735G>C (p.Ser2912Thr)} in the various populations were unknown due to data unavailability. While the ten SNVs were PTC-specific, four of the mutations; *ATR*, *IRS4*, *PCM1* and *TRRAP* were present only in PTCa. *ATR* encodes for serine/threonine-protein kinase ATR, is important for DNA damage sensors, activating DNA damage checkpoint against replication stress. The potential loss of function of ATR due to rs199948706 (p.Arg2606Gln) was suggested to increase the DNA damage, initiating the PTCa progression from BTG. Insulin receptor substrate 4 (IRS4) can induce hyperactivation of PI3K/AKT pathway and promote tumourigenesis, in the absence of insulin or other growth factors (56). *IRS4* mRNA is expressed in various human tissues including pituitary, thyroid, ovary, prostate, fibroblasts, however, with a low expression level (58). Upregulated *IRS4* was detected in various cancer cell lines, and high phosphatidylinositol triphosphate level was also identified (59, 60). *PCM1* codes for pericentriolar material 1, chromosomal aberrations of this gene have been linked to various malignancies. RET/PCM1 translocation had been identified in PTC patient, however its role in tumourigenesis is not fully elucidated. *TRRAP* mutation which was identified in *BRAF* wildtype PTC patients (61), plays an important role in the recruitment of histone acetyltransferase (HAT) complexes to the chromatin, regulating transcription and DNA repair. Its FATC domain can bind to Myc, regulating Myc oncogenic activities (62, 63). In this present study, the *TRRAP* p.S2912T mutation is located within the FAT domain, where the function and protein-protein interaction of this domain remains largely unknown. The ten SNVs may be useful as a diagnostic tool to determine malignancy status of thyroid nodules to complement the existing diagnostic methods pending further validation in a clinical setting and in a larger sample size.

In conclusion, distinctive gene mutation patterns were detected in BTG, PTCa and PTCb which corroborated the previous findings on protein profiles in similar cohort of patients. Based on the current study, it is hypothesised that *FANCD1* (*BRCA2*) and *FANCD2* along with other genes that encode for various components of the DNA damage and repair-related pathways, play a key role in the progression of BTG to PTC. Gene mutation patterns did not indicate that PTCb is the intermediate state of transformation of BTG to PTCa. Instead, PTCa and PTCb are subtypes that differ in the underlying molecular mechanisms involving tyrosine kinase-related signalling for the former and Jak-STAT and Notch signalling pathways for the latter. However, *in vitro* functional analysis would need to be carried out to further validate our speculations. The potential applications of the SNVs, especially the ten PTC-

specific, in differentiating the benign from the PTC subtypes requires further validation in a larger sample size.

Data availability statement

The data presented in the study are deposited in the Figshare repository, doi: 10.6084/m9.figshare.21714812.

Ethics statement

The studies involving human participants were reviewed and approved by The University of Malaya Medical Centre (UMMC)'s Medical Research Ethics Committee (MREC ID NO: 2019619-7540) in accordance with the ICH GCP guidelines and the Declaration of Helsinki. The patients/participants provided their written informed consent to participate in this study.

Author contributions

ZE participated in the study design, performed a major part of the experiments, analysed and interpreted the data, drafted the manuscript, prepared figures, and tables. MA performed part of the experiments, and reviewed manuscript drafts. KN performed surgeries, involved in specimen collection process, and contributed the clinical data of the patients and reviewed manuscript drafts. AA analysed the data, and reviewed manuscript drafts. NA collected samples, analysed the data, and reviewed drafts of the paper. NR analysed the data, and reviewed drafts of the paper. SJ conceived and designed the experiments, analysed, and interpreted the data, reviewed drafts, and critically revised the final manuscript. All authors contributed to the article and approved the submitted version.

Funding

This work was supported by the FRGS/1/2018/SKK08/UM/02/16 grant from the Ministry of Higher Education Malaysia, and the funder had no role in the study design, data collection and analysis, decision to publish, or manuscript preparation.

Conflict of interest

The authors declare that the research was conducted in the absence of any commercial or financial relationships that could be construed as a potential conflict of interest.

Publisher's note

Supplementary material

The Supplementary Material for this article can be found online at: https://www.frontiersin.org/articles/10.3389/fendo.2022.1039494/full#supplementary-material

References

1. Patel KN, Yip ÃYL, Lubitz CC, Grubbs EG, Miller BS, Shen W, et al. The American association of endocrine surgeons guidelines for the definitive surgical management of thyroid disease in adults. *Ann Surg* (2020) 271(3):e21–93. doi: 10.1097/SLA.0000000000003580

2. Jin M, Li Z, Sun Y, Zhang M, Chen X, Zhao H, et al. Association analysis between the interaction of RAS family genes mutations and papillary thyroid carcinoma in the han Chinese population. *Int J Med Sci* (2021) 18(2):441–7. doi: 10.7150/ijms.50026

3. Manan AA, Basri H, Kaur N, Rahman SZA, Amir PN, Ali N, et al. *Malaysia National cancer registry report (MNCRR) 2012-2016*. Malaysia: National Cancer Registry (2019) p. 1–116. Available at: https://www.moh.gov.my/moh/resources/Penerbitan/Laporan/Umum/2012-2016%20(MNCRR)/MNCR_2012-2016_FINAL_(PUBLISHED_2019).pdf.

4. Kim J-K, Seong CY, Bae IE, Yi JW, Yu HW, Kim S-J, et al. Comparison of immunohistochemistry and direct sequencing methods for identification of the BRAF(V600E) mutation in papillary thyroid carcinoma. *Ann Surg Oncol* (2018) 25(6):1775–81. doi: 10.1245/s10434-018-6460-3

5. Cohn AL, Day B-M, Abhyankar S, McKenna E, Riehl T, Puzanov I. BRAF (V600) mutations in solid tumors, other than metastatic melanoma and papillary thyroid cancer, or multiple myeloma: A screening study. *Onco Targets Ther* (2017) 10:965–71. doi: 10.2147/OTT.S120440

6. Wang H, Mehrad M, Ely KA, Liang J, Solórzano CC, Neblett WWIII, et al. Incidence and malignancy rates of indeterminate pediatric thyroid nodules. *Cancer Cytopathol* (2019) 127(4):231–9. doi: 10.1002/cncy.22104

7. Paulson VA, Rudzinski ER, Hawkins DS. Thyroid cancer in the pediatric population. *Genes (Basel)* (2019) 10(9):723. doi: 10.3390/genes10090723

8. Abdullah MI, Lee CC, Junit SM, Ng KL, Hashim OH. Tissue and serum samples of patients with papillary thyroid cancer with and without benign background demonstrate different altered expression of proteins. *PeerJ* (2016) 4:e2450. doi: 10.7717/peerj.2450

9. Lee CC, Harun F, Jalaludin MY, Heh CH, Othman R, Novel MJSA. Homozygous c.1502T>G (p.Val501Gly) mutation in the thyroid peroxidase gene in Malaysian sisters with congenital hypothyroidism and multinodular goiter. *Int J Endocrinol* (2013) 2013:987186. doi: 10.1155/2013/987186

10. Chakravarty D, Gao J, Phillips S, Kundra R, Zhang H, Wang J, et al. OncoKB: A precision oncology knowledge base. *JCO Precis Oncol* (2017) 1:PO.17.00011. doi: 10.1200/PO.17.00011

11. Tate JG, Bamford S, Jubb HC, Sondka Z, Beare DM, Bindal N, et al. COSMIC: The catalogue of somatic mutations in cancer. *Nucleic Acids Res* (2019) 47(D1):D941–7. doi: 10.1093/nar/gky1015

12. Suwinski P, Ong C, Ling MHT, Poh YM, Khan AM, Ong HS. Advancing personalized medicine through the application of whole exome sequencing and big data analytics. *Front Genet* (2019) 10:49. doi: 10.3389/fgene.2019.00049

13. Chakarov S, Petkova R, Russev GC, Zhelev N. DNA Damage and mutation. types of DNA damage. *Biodiscovery* (2014) 11(1):e8957. doi: 10.7750/BioDiscovery.2014.11.1

14. Ameziane El Hassani R, Buffet C, Leboulleux S, Dupuy C. Oxidative stress in thyroid carcinomas: Biological and clinical significance. *Endocr Relat Cancer* (2019) 26(3):R131–43. doi: 10.1530/ERC-18-0476

15. Donmez-Altuntas H, Bayram F, Bitgen N, Ata S, Hamurcu Z, Baskol G. Increased chromosomal and oxidative DNA damage in patients with multinodular goiter and their association with cancer. *Int J Endocrinol* (2017) 2017:2907281. doi: 10.1155/2017/2907281

16. Fang Y, Ma X, Zeng J, Jin Y, Hu Y, Wang J, et al. The profile of genetic mutations in papillary thyroid cancer detected by whole exome sequencing. *Cell Physiol Biochem* (2018) 50(1):169–78. doi: 10.1159/000493966

17. Chong JX, Buckingham KJ, Jhangiani SN, Boehm C, Sobreira N, Smith JD, et al. The genetic basis of mendelian phenotypes: Discoveries, challenges, and opportunities. *Am J Hum Genet* (2015) 97(2):199–215. doi: 10.1016/j.ajhg.2015.06.009

18. Jeste SS, Geschwind DH. Disentangling the heterogeneity of autism spectrum disorder through genetic findings. *Nat Rev Neurol* (2014) 10(2):74–81. doi: 10.1038/nrneurol.2013.278

19. Cooper GM, Shendure J. Needles in stacks of needles: Finding disease-causal variants in a wealth of genomic data. *Nat Rev Genet* (2011) 12(9):628–40. doi: 10.1038/nrg3046

20. Gelfman S, Wang Q, McSweeney KM, Ren Z, La Carpia F, Halvorsen M, et al. Annotating pathogenic non-coding variants in genic regions. *Nat Commun* (2017) 8(1):236. doi: 10.1038/s41467-017-00141-2

21. Loeb KR, Loeb LA. Significance of multiple mutations in cancer. *Carcinogenesis* (2000) 21(3):379–85. doi: 10.1093/carcin/21.3.379

22. Cangelosi R, Goriely A. Component retention in principal component analysis with application to cDNA microarray data. *Biol Direct* (2007) 2(1):2. doi: 10.1186/1745-6150-2-2

23. Björklund M. Be careful with your principal components. *Evol (N Y).* (2019) 73(10):2151–8. doi: 10.1111/evo.13835

24. Moldovan G-L, D'Andrea AD. How the fanconi anemia pathway guards the genome. *Annu Rev Genet* (2009) 43:223–49. doi: 10.1146/annurev-genet-102108-134222

25. Walden H, Deans AJ. The fanconi anemia DNA repair pathway: structural and functional insights into a complex disorder. *Annu Rev Biophys* (2014) 43:257–78. doi: 10.1146/annurev-biophys-051013-022737

26. Nakanishi K, Yang Y-G, Pierce AJ, Taniguchi T, Digweed M, D'Andrea AD, et al. Human fanconi anemia monoubiquitination pathway promotes homologous DNA repair. *Proc Natl Acad Sci USA* (2005) 102(4):1110–5. doi: 10.1073/pnas.0407796102

27. Ramus SJ, Harrington PA, Pye C, DiCioccio RA, Cox MJ, Garlinghouse-Jones K, et al. Contribution of BRCA1 and BRCA2 mutations to inherited ovarian cancer. *Hum Mutat* (2007) 28(12):1207–15. doi: 10.1002/humu.20599

28. Tai YC, Domchek S, Parmigiani G, Chen S. Breast cancer risk among male BRCA1 and BRCA2 mutation carriers. *J Natl Cancer Inst* (2007) 99(23):1811–4. doi: 10.1093/jnci/djm203

29. Pilarski R. The role of BRCA testing in hereditary pancreatic and prostate cancer families. *Am Soc Clin Oncol Educ B* (2019) 39):79–86. doi: 10.1200/EDBK_238977

30. Raufi A, Alsharedi M, Khelfa Y, Tirona M. Bilateral triple-negative invasive breast cancer with a BRCA2 mutation, and glioblastoma: A case report and literature review. *J Breast cancer* (2017) 20:108–11. doi: 10.4048/jbc.2017.20.1.108

31. Zaballos MA, Santisteban P. Key signaling pathways in thyroid cancer. *J Endocrinol* (2017) 235(2):R43–61. doi: 10.1530/JOE-17-0266

32. Wu S, Zhou J, Zhang K, Chen H, Luo M, Lu Y, et al. Molecular mechanisms of PALB2 function and its role in breast cancer management. *Front Oncol* (2020) 10:301. doi: 10.3389/fonc.2020.00301

33. Cybulski C, Kluźniak W, Huzarski T, Wokołorczyk D, Kashyap A, Jakubowska A, et al. Clinical outcomes in women with breast cancer and a PALB2 mutation: A prospective cohort analysis. *Lancet Oncol* (2015) 16(6):638–44. doi: 10.1016/S1470-2045(15)70142-7

34. Li A, Geyer FC, Blecua P, Lee JY, Selenica P, Brown DN, et al. Homologous recombination DNA repair defects in PALB2-associated breast cancers. *NPJ Breast Cancer* (2019) 5(1):23. doi: 10.1038/s41523-019-0115-9

35. Szczerba E, Kamińska K, Mierzwa T, Misiek M, Kowalewski J, Lewandowska MA. BRCA1/2 mutation detection in the tumor tissue from selected polish patients with breast cancer using next generation sequencing. *Genes (Basel)* (2021) 12(4):519. doi: 10.3390/genes12040519

36. Kamihara J, LaDuca H, Dalton E, Speare V, Garber JE, Black MH. Germline mutations in cancer predisposition genes among patients with thyroid cancer. *J Clin Oncol* (2017) 35(15_suppl):1581. doi: 10.1200/JCO.2017.35.15_suppl.1581

37. Zhang F, Ma J, Wu J, Ye L, Cai H, Xia B, et al. PALB2 links BRCA1 and BRCA2 in the DNA-damage response. *Curr Biol* (2009) 19(6):524–9. doi: 10.1016/j.cub.2009.02.018

38. Xia B, Sheng Q, Nakanishi K, Ohashi A, Wu J, Christ N, et al. Control of BRCA2 cellular and clinical functions by a nuclear partner, PALB2. *Mol Cell* (2006) 22(6):719–29. doi: 10.1016/j.molcel.2006.05.022

39. Sever R, Brugge JS. Signal transduction in cancer. *Cold Spring Harb Perspect Med* (2015) 5(4):a006098. doi: 10.1101/cshperspect.a006098

40. Yip HYK, Papa A. Signaling pathways in cancer: Therapeutic targets, combinatorial treatments, and new developments. *Cells* (2021) 10(3):659. doi: 10.3390/cells10030659

41. Campbell PJ, Getz G, Korbel JO, Stuart JM, Jennings JL, Stein LD, et al. Pan-cancer analysis of whole genomes. *Nature* (2020) 578(7793):82–93. doi: 10.1038/s41586-020-1969-6

42. Couto JP, Daly L, Almeida A, Knauf JA, Fagin JA, Sobrinho-Simões M, et al. STAT3 negatively regulates thyroid tumorigenesis. *Proc Natl Acad Sci USA* (2012) 109(35):E2361–70. doi: 10.1073/pnas.1201232109

43. Kim WW, Ha TK, Bae SK. Clinical implications of the BRAF mutation in papillary thyroid carcinoma and chronic lymphocytic thyroiditis. *J Otolaryngol - Head Neck Surg* (2018) 47(1):1–6. doi: 10.1186/s40463-017-0247-6

44. Lee CC, Abdullah MI, Junit SM, Ng KL, Wong SY, Fatimah Ramli NS, et al. Malignant transformation of benign thyroid nodule is caused by prolonged H2O2 insult that interfered with the STAT3 pathway? *Int J Clin Exp Med* (2016) 9(9):18601–17.

45. Gallo C, Fragliasso V, Donati B, Torricelli F, Tameni A, Piana S, et al. The bHLH transcription factor DEC1 promotes thyroid cancer aggressiveness by the interplay with NOTCH1. *Cell Death Dis* (2018) 9(9):871. doi: 10.1038/s41419-018-0933-y

46. Piana S, Zanetti E, Bisagni A, Ciarrocchi A, Giordano D, Torricelli F, et al. Expression of NOTCH1 in thyroid cancer is mostly restricted to papillary carcinoma. *Endocr Connect* (2019) 8(8):1089–96. doi: 10.1530/EC-19-0303

47. Xiao X, Ning L, Chen H. Notch1 mediates growth suppression of papillary and follicular thyroid cancer cells by histone deacetylase inhibitors. *Mol Cancer Ther* (2009) 8(2):350–6. doi: 10.1158/1535-7163.MCT-08-0585

48. Yu X-M, Jaskula-Sztul R, Georgen MR, Aburjania Z, Somnay YR, Leverson G, et al. Notch1 signaling regulates the aggressiveness of differentiated thyroid cancer and inhibits SERPINE1 expression. *Clin Cancer Res* (2016) 22(14):3582–92. doi: 10.1158/1078-0432.CCR-15-1749

49. Chang C, Chang Y, Huang H, Yeh K, Liu T, Chang J. Determination of the mutational landscape in Taiwanese patients with papillary thyroid cancer by whole-exome sequencing. *Hum Pathol* (2018) 78:151–8. doi: 10.1016/j.humpath.2018.04.023

50. Lee WK, Lee SG, Yim SH, Kim D, Kim H, Jeong S, et al. Whole exome sequencing identifies a novel hedgehog-interacting protein G516R mutation in locally advanced papillary thyroid cancer. *Int J Mol Sci* (2018) 91(10):2867. doi: 10.3390/ijms19102867

51. Xing M. BRAF V600E mutation and papillary thyroid cancer. *JAMA* (2013) 310(5):535. doi: 10.1001/jama.2013.8592

52. Xing M, Liu R, Liu X, Murugan AK, Zhu G, Zeiger MA, et al. BRAF V600E and TERT promoter mutations cooperatively identify the most aggressive papillary thyroid cancer with highest recurrence. *J Clin Oncol* (2014) 32(25):2718–26. doi: 10.1200/JCO.2014.55.5094

53. Nam JK, Jung CK, Song BJ, Lim DJ, Chae BJ, Lee NS, et al. Is the BRAF (V600E) mutation useful as a predictor of preoperative risk in papillary thyroid cancer? *Am J Surg* (2012) 203(4):436–41. doi: 10.1016/j.amjsurg.2011.02.013

54. Xing M, Clark D, Guan H, Ji M, Dackiw A, Carson KA, et al. BRAF mutation testing of thyroid fine-needle aspiration biopsy specimens for preoperative risk stratification in papillary thyroid cancer. *J Clin Oncol* (2009) 27(18):2977–82. doi: 10.1200/JCO.2008.20.1426

55. Trimboli P, Treglia G, Condorelli E, Romanelli F, Crescenzi A, Bongiovanni M, et al. BRAF-mutated carcinomas among thyroid nodules with prior indeterminate FNA report: A systematic review and meta-analysis. *Clin Endocrinol (Oxf)* (2016) 84(3):315–20. doi: 10.1111/cen.12806

56. Rashid FA, Munkhdelger J, Fukuoka J, Bychkov A. Prevalence of BRAF(V600E) mutation in Asian series of papillary thyroid carcinoma-a contemporary systematic review. *Gland Surg* (2020) 9(5):1878–900. doi: 10.21037/gs-20-430

57. Mohamed Yusoff AA, Abd Radzak SM, Mohd Khair SZN, Abdullah JM. Significance of BRAF(V600E) mutation in intra-axial brain tumor in Malaysian patients: Case series and literature review. *Exp Oncol* (2021) 43(2):159–67. doi: 10.32471/exp-oncology.2312-8852.vol-43-no-2.16076

58. Sesti G, Federici M, Hribal ML, Lauro D, Sbraccia P, Lauro R. Defects of the insulin receptor substrate (IRS) system in human metabolic disorders. *FASEB J* (2001) 15(12):2099–111. doi: 10.1096/fj.01-0009rev

59. Hoxhaj G, Dissanayake K, MacKintosh C. Effect of IRS4 levels on PI 3-kinase signalling. *PloS One* (2013) 8(9):e73327. doi: 10.1371/journal.pone.0073327

60. Li X, Zhong L, Wang Z, Chen H, Liao D, Zhang R, et al. Phosphorylation of IRS4 by CK1γ2 promotes its degradation by CHIP through the ubiquitin/lysosome pathway. *Theranostics* (2018) 8(13):3643–53. doi: 10.7150/thno.26021

61. Demeure MJ, Aziz M, Rosenberg R, Gurley SD, Bussey KJ, Carpten JD. Whole-genome sequencing of an aggressive BRAF wild-type papillary thyroid cancer identified EML4-ALK translocation as a therapeutic target. *World J Surg* (2014) 38(6):1296–305. doi: 10.1007/s00268-014-2485-3

62. Park J, Kunjibettu S, McMahon SB, Cole MD. The ATM-related domain of TRRAP is required for histone acetyltransferase recruitment and myc-dependent oncogenesis. *Genes Dev* (2001) 15(13):1619–24. doi: 10.1101/gad.900101

63. Liu X, Tesfai J, Evrard YA, Dent SYR, Martinez E. C-myc transformation domain recruits the human STAGA complex and requires TRRAP and GCN5 acetylase activity for transcription activation. *J Biol Chem* (2003) 278(22):20405–12. doi: 10.1074/jbc.M211795200

frontiers | Frontiers in Endocrinology

TYPE Original Research
PUBLISHED 30 January 2023
DOI 10.3389/fendo.2023.1101705

OPEN ACCESS

EDITED BY
Erivelto Martinho Volpi,
Centro de referencia no ensino do diagnóstico por imagem (CETRUS), Brazil

REVIEWED BY
Serena Ippolito,
ASL Napoli 1 centro, Italy
Sana Ghaznavi,
University of Calgary, Canada
Anupam Kotwal,
University of Nebraska Medical Center, United States

*CORRESPONDENCE
Lisa A. Orloff
lorloff@stanford.edu

SPECIALTY SECTION
This article was submitted to Thyroid Endocrinology, a section of the journal Frontiers in Endocrinology

RECEIVED 18 November 2022
ACCEPTED 04 January 2023
PUBLISHED 30 January 2023

CITATION
Cohen SM, Noel JE, Baroody M and Orloff LA (2023) Prognostication of papillary thyroid microcarcinoma based on preoperative ultrasound. *Front. Endocrinol.* 14:1101705. doi: 10.3389/fendo.2023.1101705

Prognostication of papillary thyroid microcarcinoma based on preoperative ultrasound

Samuel M. Cohen, Julia E. Noel, Michael Baroody and Lisa A. Orloff*

Department of Otolaryngology-Head and Neck Surgery, Stanford University School of Medicine, Stanford, CA, United States

Background: Diagnosis of papillary thyroid microcarcinoma, defined as papillary thyroid carcinoma measuring 1cm or less in greatest diameter, has increased with improvements in ultrasound technology and widespread familiarity and utilization. Given the indolent course of papillary thyroid carcinoma, active surveillance is considered an acceptable alternative to surgical resection for select patients. Candidacy for active surveillance is determined by a number of patient and tumor characteristics. Specifically, the location of the tumor within the thyroid gland plays one of the key roles in decision making. Here we evaluate characteristics of the primary tumor and distance to the thyroid capsule in association with locoregional metastases to help guide risk assessment.

Methods: Retrospective chart review of all thyroid surgeries performed by two surgeons at one medical center from 2014-2021 to evaluate characteristics of papillary thyroid microcarcinoma on preoperative ultrasound that are associated with locoregional metastatic disease.

Results: Our data show a sensitivity of 65% and specificity of 95% for identifying regional metastases in papillary thyroid microcarcinoma using preoperative ultrasound. We found no correlation between regional metastasis and size of tumor, distance to thyroid capsule or trachea, tumor contour, or presence of autoimmune thyroiditis. Nodules in the superior or midpole were associated with central or lateral neck metastases, whereas nodules in the isthmus or inferior pole were only associated with central neck metastases.

Conclusions: Active surveillance may be a reasonable option for even those papillary thyroid microcarcinomas adjacent to the thyroid capsule.

KEYWORDS

papillary thyroid microcarcinoma, active surveillance, ultrasound, papillary throid carcinoma, thyroid nodular disease

Introduction

Papillary thyroid microcarcinoma (PTMC) is defined by the World Health Organization as papillary thyroid carcinoma (PTC) with a maximum diameter of 1 cm or less. The prevalence of PTMC has dramatically increased in the past fifty years largely with the evolution of ultrasound technology and ultrasound-guided FNA (1). While rates of PTMC have risen throughout the world, rates of mortality from thyroid cancer have remained stable, raising concern for overtreatment (2–4).

Accordingly, the traditional treatment modality of surgical resection for PTMC has been reconsidered. Prospective clinical trials from Japan demonstrate that active surveillance (AS) is a safe option for management of low-risk (T1aN0M0) PTMC (5, 6). Professional organizations in Japan and the United States adopted active surveillance as an alternative management strategy in 2010 and 2015, respectively (7, 8).

In 2016, Brito et al. published a clinical framework for risk stratification when considering AS for PTMC (9). This approach considers tumor/neck ultrasound characteristics, patient demographic characteristics, and treatment characteristics, including availability of a multidisciplinary team. To date, several features have been identified that may increase the risk of nodal metastases and impact candidacy for AS, including age <45, male sex, tumor size >5mm, multifocal disease, and extrathyroidal extension (10–13). Location of the primary tumor must also be considered, particularly if growth may affect critical structures or increase surgical risk. Prior study has suggested AS may be appropriate for tumors <7mm or even low-risk PTMCs < 7mm abutting the trachea with an acute angle between the tumor and the tracheal surface, or near the anticipated location of the recurrent laryngeal nerve but with a normal rim of thyroid in the direction of the nerve (14). However, data and validation guiding clinical practice based on preoperative assessment remains limited.

Specifically, in this study we analyze preoperative ultrasound images to identify ultrasound characteristics of PTMC nodules associated with increased risk of regional metastases. Several ultrasound characteristics were identified that may help determine appropriate candidacy for AS.

Materials and methods

Study design and patients

This study was approved by the Stanford Institutional Review Board.

A retrospective chart review of all thyroid cancer surgeries performed by two surgeons (J.E.N. and L.A.O.) between 1/1/2014 and 3/1/2021 was performed. All operative and pathology reports were reviewed, and cases were included if a total thyroidectomy or thyroid lobectomy was performed with final pathology indicating PTC equal to or less than 1.0 cm in greatest diameter. Patients were excluded if they had a concurrent PTC >1cm or were undergoing surgery for recurrent disease. Patients with multifocal PTMC were not excluded. In total, 185 PTMC nodules from 158 individuals were identified.

Demographic features (age, gender, race/ethnicity) were collected from the medical record (Table 1) and clinical features (indication for surgery, laterality of disease, size of nodule by surgical pathology, presence of adverse features on pathology [extrathyroidal extension, angioinvasion, lymphatic invasion, positive margins], presence of regional metastases, concurrent autoimmune thyroiditis) were collected from preoperative notes, operative reports, laboratory values, and pathology reports. Presence of suspicious lymphadenopathy was collected from preoperative ultrasound reports. To simplify our analysis and optimize statistical power, we combined N1a and N1b into one group. 65 out of 185 PTMC nodules were identified incidentally (resection of PTMC was not the indication for surgery).

TABLE 1 Demographic information for data included in our overall analysis (left column) and in our ultrasound analysis (right column).

	Total (%)	Ultrasound Analysis (%)
Individuals	158	84
Nodules	185	88
Age: mean (range)	50.4 (16-88)	49.0 (23-88)
Sex		
Female	117 (74%)	63 (75%)
Male	41 (26%)	21 (25%)
Race		
Asian	42 (27%)	31 (37%)
Hispanic	17 (11%)	7 (8.3%)
White	83 (53%)	40 (48%)
Black	1 (0.63%)	0 (0%)
Other	15 (10%)	6 (7.1%)
Autoimmune Thyroiditis	61 (39%)	34 (40%)

When available, preoperative ultrasound images were reviewed. Nodules were included in ultrasound analysis if they could be confidently identified on the preoperative ultrasound in one of two scenarios: 1) preoperative FNA confirming PTC, or 2) clearly visible nodule on ultrasound that correlated in size and location with PTMC on surgical pathology without heterogeneous thyroid background or other confounding nodules. 8 out of the 88 nodules used in our ultrasound analysis were identified incidentally. For those nodules included, the following ultrasound features were collected: size, smoothness or lobulation of contour, position within thyroid gland, relationship to trachea, distance to anterior thyroid capsule, distance to posterior thyroid capsule (Figure 1). The distance to the anterior and posterior thyroid capsule was independently measured by two of the authors in a blinded fashion (S.M.C. and J.E.N.) and the mean of each of these values was used for analysis.

Statistical analysis

All statistical analysis was performed using Prism (Graphpad Software, San Diego, CA). Significance tests were two-sided and a p-value <0.05 was considered significant. Analysis of Variance (ANOVA) and t-tests were used to determine if differences between the means of the parameters measured were statistically significant.

Results

185 PTMC nodules were identified from 158 individuals. 102 nodules (55%) were associated with N0 disease and 46 nodules (25%) were associated with pathologic N1 disease. 37 nodules were associated with Nx disease (no pathological data from lymph nodes available) and were excluded from subsequent analysis. The primary analyses in our study were repeated by combining N0 and Nx data, and no significant differences were found compared to when Nx was excluded (data not shown). For 88 of the original 185 nodules, the PTMC nodule could be confidently identified on preoperative ultrasound images; many nodules were discovered only retrospectively on pathology and we were unable to identify them on preoperative ultrasound due to multinodular disease or small size. 41 of these 88 nodules were associated with N0 disease and 33 nodules were associated with N1 disease. 14 nodules were associated with Nx disease and were excluded from ultrasound analysis.

Appropriate management of thyroid disease requires accurate assessment of nodule size. In our data set, nodules ranged in size from 0.2cm to 2.7cm on preoperative ultrasound and from 0.15cm to 1.0cm on pathology (Figure 2A). As PTMC is defined by surgical pathologic size, our dataset contains nodules with ultrasound dimensions greater than 1cm that still ultimately classify as PTMC. 57 nodules (65%) were 1cm or less on preoperative ultrasound and 31 nodules (35%) were >1cm. When ultrasound and pathology values for each nodule (Figure 2A) or metastatic lymph node (Figure 2B) were compared, most values fell above a line with a slope of 1 passing through (0,0). Ultrasound measurements *in vivo* tended to exceed the size of disease compared with *ex vivo* histopathology. We next analyzed the distance between nodules and the thyroid capsule. There was a poor correlation between distance measured on ultrasound and pathologic margins (Figure 2C, R squared = 0.17). There was no significant difference in distance to thyroid capsule (measured on ultrasound) between thyroid nodules with a pathologic margin of <5mm or >5mm (p>0.05). Pathologic margin size was not reported when it exceeded 5mm, limiting sample size for analysis of this characteristic.

Preoperative ultrasound is a valuable tool to assess for regional metastasis. We analyzed the success rate of ultrasound in accurately capturing nodal disease, compared to final pathology (Figure 3A). Among patients with N1 disease, the preoperative ultrasound accurately predicted suspicious lymph nodes in 30 out of 46 of PTMC nodules; we report a sensitivity of 65% for preoperative ultrasound to rule out regional metastasis in PTMC. Among patients with N0 disease, preoperative ultrasound was free of visible lymphadenopathy in the central neck in 97 out of 102 cases, corresponding to a specificity of 95% for confirming regional metastasis.

Understanding which factors may predispose to regional metastasis is an area of significant clinical interest. On examination of pathology reports, PTMC nodules associated with N1 disease were larger than those associated with N0 disease (Figure 3B, mean: N0 [0.51cm], N1 [0.63cm], p<0.05). In contrast to histopathological data, however, preoperative ultrasound did not capture any difference in size of nodules associated with N0 vs N1 disease (Figure 3C, mean: N0 [1.03cm], N1 [0.92cm], p>0.05). There was also no difference in rate of metastatic disease amongst PTMC nodules measuring ≤5mm vs

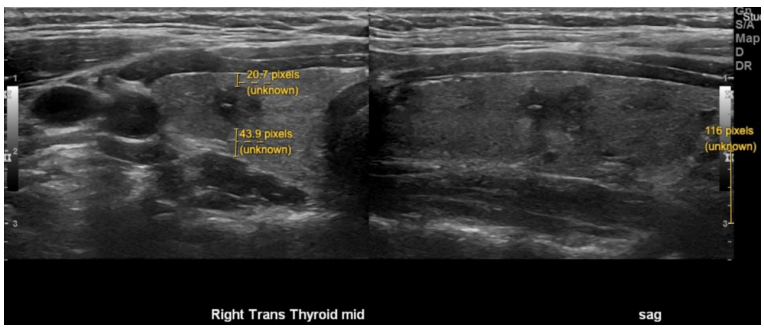

FIGURE 1
Representative image demonstrating preoperative ultrasound measurements of thyroid nodules. Size of nodule (white). Distance to anterior and posterior capsule (yellow). The pixel size was calibrated for each image using the scale provided by the ultrasound software (bottom right of image).

10.3389/fendo.2023.1101705

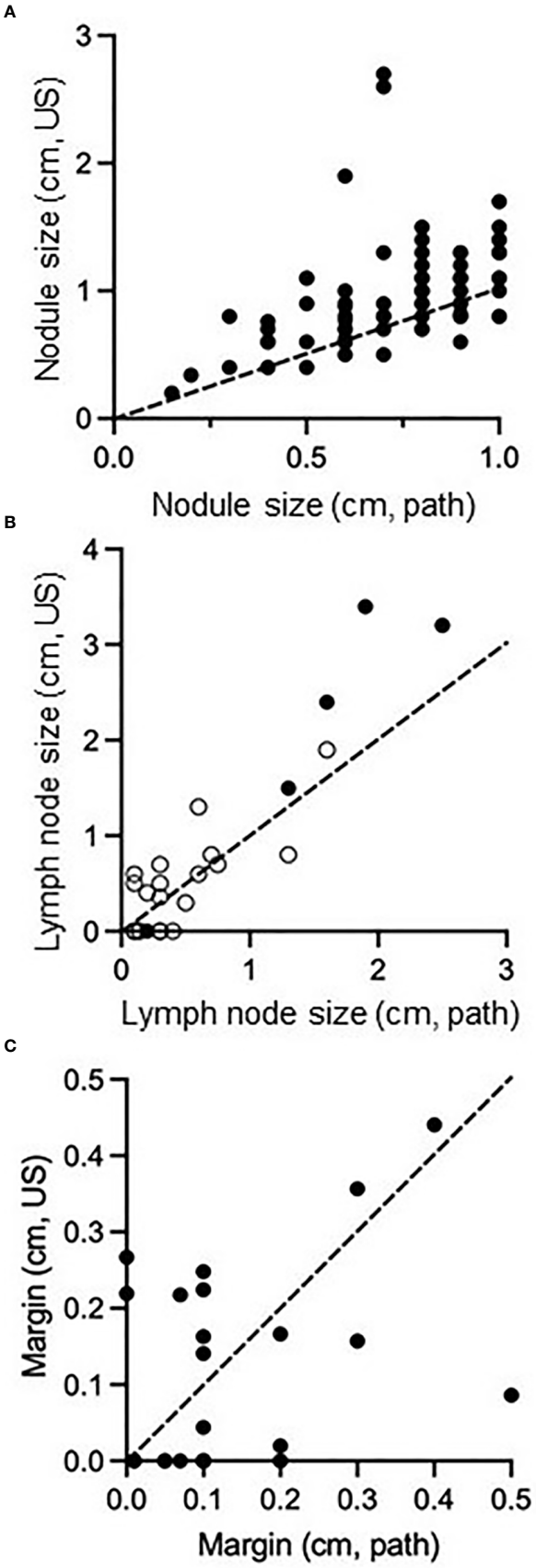

FIGURE 2
Comparison of size of PTMC nodules **(A)**, size of regional metastatic disease **(B)**, and distance of tumor margin from thyroid capsule/surgical resection boundary **(C)** as measured on preoperative ultrasound compared to surgical pathology. Dashed line passes through (0,0) and (1,1), representing equivalent size on both measurements. In **(B)**, open circles represent central neck nodes and closed circles represent lateral neck nodes.

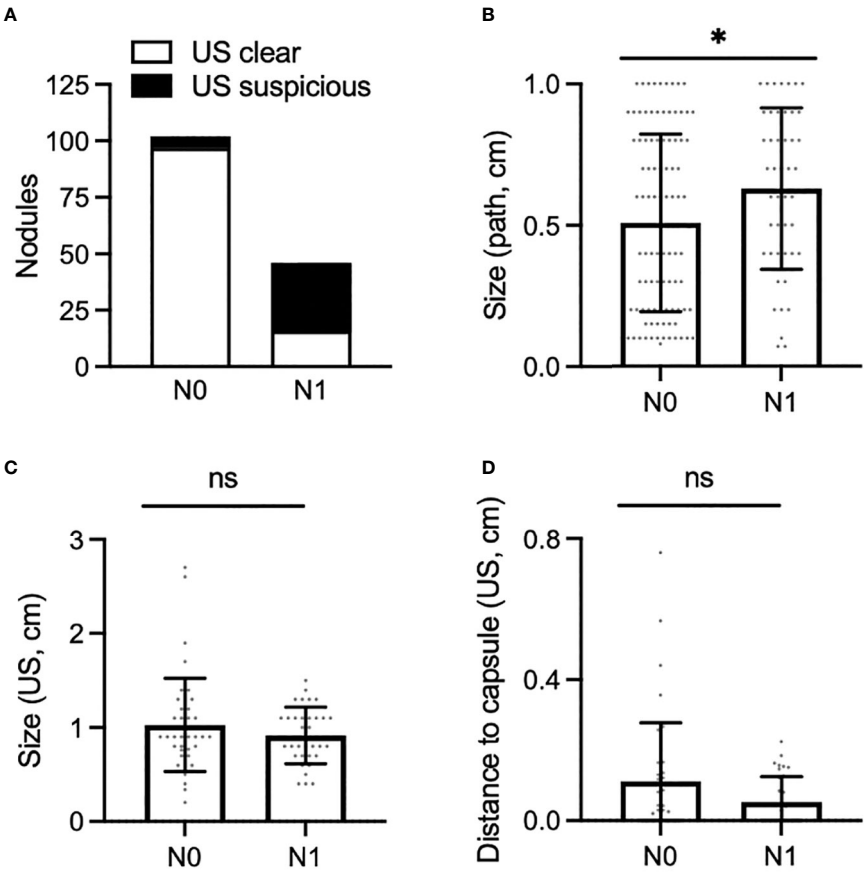

FIGURE 3
(A) Proportion of PTMC nodules associated with N0 neck (left) and N1 neck (right), for which the preoperative ultrasound was clear of disease (white bar) or was suspicious for pathologic nodes (black bar). **(B,C)** Size of PTMC nodules associated with N0 or N1 disease as measured on surgical pathology **(B)** and preoperative ultrasound **(C)**. **(D)**, Shortest distance to the anterior or posterior thyroid capsule as measured on preoperative ultrasound in PTMC nodules associated with N0 or N1 disease. *, $p < 0.05$. ns, not stastistically significant.

>5mm. This result was consistent when size was measured on ultrasound ($p > 0.05$) or on final pathology ($p > 0.05$).

We next determined whether distance of a nodule to the thyroid capsule may increase the likelihood of metastasis. Distance of each nodule to the anterior and posterior thyroid capsule was measured, and the smaller of these two measurements was used for analysis; no difference was seen between nodules associated with N0 or N1 disease (Figures 1 and 3D, mean: N0 [0.11cm], N1 [0.0.5cm], $p > 0.05$). Of note, 34 of 88 of nodules (39%) were adjacent to either the anterior or posterior thyroid capsule, measured as a minimum distance to the capsule of 0cm. Extrathyroidal extension was identified on pathology for 2 of 88 PTMC nodules (2%), one of which abutted the posterior thyroid capsule. Positive margins were identified on pathology for 2 of 88 PTMC nodules (2%), but were distinct from the 2 nodules with extrathyroidal extension.

Previous data suggest that observation is safe for certain PTMCs abutting the trachea (14).

In our data set, of 13 PTMC nodules abutting the trachea, only 1 was associated with positive margins on pathology and none with extrathyroidal extension. There was no difference between the rate of positive margin (Figure 4A) or the rate of metastatic disease (Figure 4B) between those nodules abutting the trachea and those not abutting the trachea, although analysis was limited by small sample size. Ito and colleagues have described certain "high risk" characteristics of PTMC nodules abutting the trachea, including an obtuse angle with relation to the trachea and a size larger than 7mm (14). Consistent with those data, our single nodule with positive margins had an obtuse angle and was larger than 7mm. Of the remaining 12 nodules, 10 had acute angles, 1 had an obtuse angle, and 1 had a 90 degree angle with regard to the trachea. 6 of these nodules were 7mm or larger and 6 nodules were smaller than 7mm.

Finally, we analyzed several additional factors which have been suggested to be associated with risk of metastases from PTMC. Presence or absence of autoimmune thyroiditis was not associated with a difference in rates of metastatic disease amongst patients with PTMC (Figure 4C). Furthermore, there was no difference in rates of metastatic disease associated with PTMC nodules with irregular as opposed to smooth contours (Figure 4D). The location of PTMC nodules within the thyroid, however, did show differing results. While nodules found in the superior or mid thyroid pole were significantly associated with both central and lateral neck metastases, those in the isthmus and inferior pole were associated only with central metastases (Figure 5).

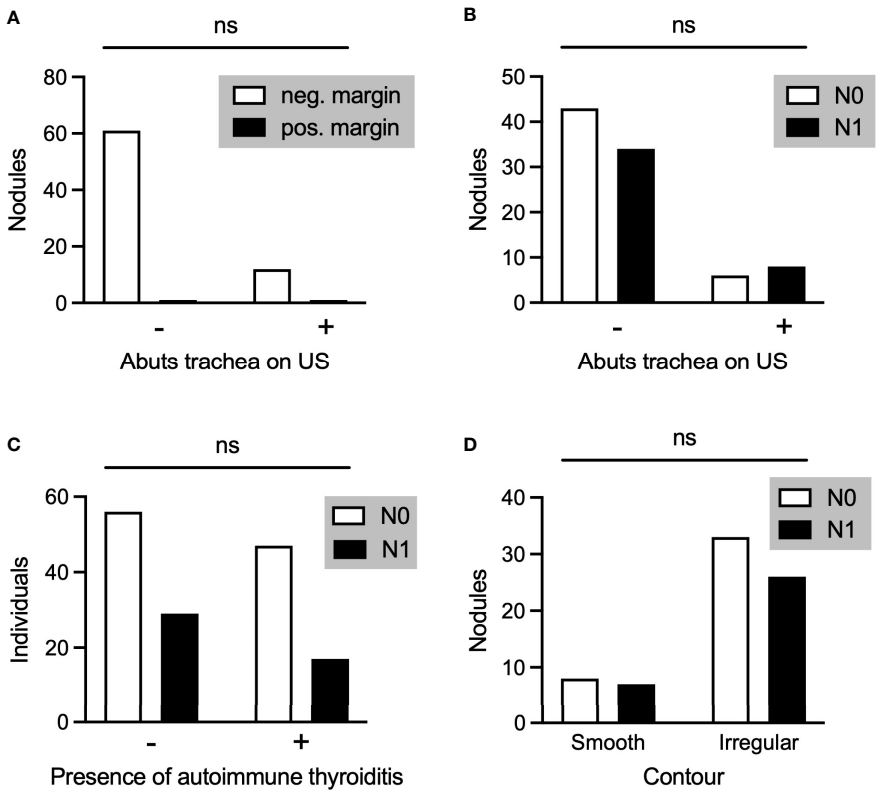

FIGURE 4
(A) PTMC nodules associated with negative or positive pathological margins in those nodules that did (+) or did not **(-)** abut the trachea on preoperative ultrasound. **(B-D)** Comparison of PTMC nodules associated with N0 or N1 disease with regard to whether the nodule abutted the trachea **(B)**, the individual had autoimmune thyroiditis **(C)**, and the contour of the nodule **(D)**. ns, not stastistically significant.

Discussion

The question of which PTMCs are candidates for observation is increasingly pressing as acceptance of active surveillance has become mainstream. Our data demonstrate that ultrasound measurements overestimate nodule size compared to final pathology, which is the metric by which PTMC is defined. As one third of PTMC nodules in our data set measured greater than 1cm on preoperative ultrasound, an ultrasound size cutoff of 1.5cm or 2cm rather than a pathology size cutoff of 1cm may be more clinically relevant for future studies. Nonetheless, our study provides informative data to help guide the decision-making process in determining surveillance candidacy.

We found a sensitivity of 65% and specificity of 95% for identifying PTMC regional metastases, consistent with prior data. Two recent meta-analyses reported ultrasound sensitivity for identifying central and lateral neck metastases of 28-33% and 70-73%, respectively, with a specificity of 93-95% and 84-89%, respectively (15, 16). The discrepancy in sensitivity between our study and prior data likely relate to our combining central and lateral neck metastasis.

Considering the relatively poor sensitivity to rule out regional, especially central, metastases, identification of ultrasound characteristics of high risk PTMC nodules is paramount. Our data suggest that proximity to or contact with the thyroid capsule alone should not necessarily discourage a physician from offering active surveillance (Figure 3D). This finding is consistent with one retrospective study of 1,622 patients (12); however, a meta-analysis of 43,750 patients found that >25% PTMC contact with the thyroid capsule was significantly associated with lateral neck metastases (13). Within our dataset, nodule contour was classified as smooth or irregular based on ultrasound, but there was no association between PTMC contour and regional metastases. Previous meta-analysis found that PTMC contour and also shape (taller than wide) conveyed no increased risk of lateral neck metastases (13). Together, these data suggest that PTMC nodules regardless of contour may be safely observed. This analysis also suggests that some PTMC nodules abutting the trachea may be safely observed, as described in Ito et al. (14) This prospective study of 1143 patients with PTMC concluded that nodules with an obtuse angle to the trachea should undergo surgical resection. However, many nodules may be observed, including those <7mm even if abutting trachea, those ≥ 7 mm with an acute angle to the trachea, and those with a normal rim of thyroid tissue separating the nodule from the course of the recurrent laryngeal nerve (14).

Prior data suggest that PTMC >5mm are higher risk for regional lymph node metastases than those ≤5mm (11, 12). We caution against relying on size of PTMC as measured on ultrasound. While there may be differences in pathological size, such slight variations in size may not be reliably captured on clinic ultrasound. Our cohort contained few nodules ≤5mm, which is not surprising considering the difficulty of accurately assessing and performing biopsy on such small nodules, and the discouragement of intervening on such small lesions. Furthermore, we found no relationship between mean size on ultrasound and regional metastasis. Thus, none of our results refute

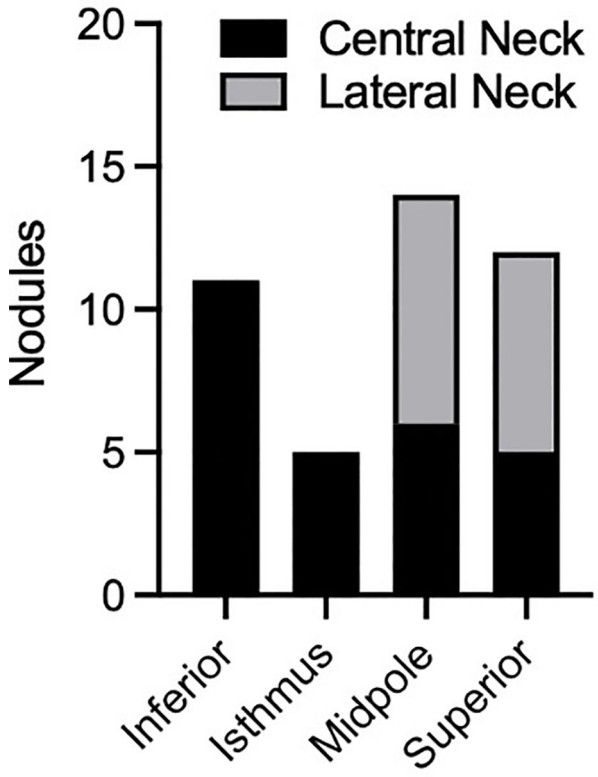

FIGURE 5
Analysis of PTMC nodules with regional metastasis. Plot displays location of nodules within the thyroid and location of notal metastasis (central or lateral neck). In TNM staging, central and lateral neck metastases are referred to as N1a and N1b disease, respectively.

prior data or recommendations that nodules ≤5mm in size may safely be observed. One caveat is the assumption that such nodules, even if malignant, are PTMC. It is important to remember that medullary thyroid carcinoma is in the differential diagnosis and has overlapping sonographic features with PTC. While rare, medullary carcinoma should be considered during the history-taking, physical examination, and possible laboratory testing of patients with thyroid nodules.

Our data did demonstrate the tendency of superior pole nodules to metastasize to the lateral neck, and inferior thyroid nodules to metastasize to the central neck. This finding is consistent with a prior meta-analysis (13) and with the anatomy of the lymphovascular drainage pathway of the thyroid gland. Considering that N1b disease has a higher mortality than N1a for patients over 55 yo, surgery may be considered more strongly for superior/midpole PTMCs in this age group, compared to isthmus or inferior pole nodules. Regardless, ultrasonography of the entire neck, including bilateral central and lateral compartments, is warranted during the ultrasound evaluation and surveillance of PTMC.

There was no correlation between the presence of autoimmune thyroiditis and identification of metastatic disease. In general, data on the relationship between autoimmune thyroid disease and the extent of disease is variable. For example, a meta-analysis of over 15,000 patients reported that, although the presence of thyroiditis increased the risk of harboring PTC, it protected against lateral neck metastasis (17), whereas another large meta-analysis of 43,750 patients found no association with metastatic disease (13). Given the conflicting data, the presence of thyroiditis is not an independent factor in determining candidacy for active surveillance.

Limitations

This study was limited by a small sample size; we designed the study primarily to include preoperative ultrasound analysis of nodules as this was lacking in the literature. We chose to exclude Nx disease to increase clarity of results, but by doing so our sample size was further decreased. Other limitations are the retrospective nature of the study, the lack of preoperative cytologic confirmation of 65/185 PTMC nodules included in our study, and the lack of follow-up data for recurrence or survival.

Conclusions

For patients with PTMC, the sensitivity of preoperative ultrasound to rule out regional metastasis in PTMC, albeit potentially micro metastasis, is mediocre. Surgery is recommended when ultrasound identifies frank extrathyroidal extension or lymph node metastases, or when adverse clinical features are present such as vocal fold paralysis or active increase in nodule size on interval exam. Younger age (less than 45 years) is also associated with long-term disease progression and favors intervention (10). Many other tumor and demographic factors, however, have less clear implications on candidacy for surveillance, and there remains insufficient data for strong recommendations. The data presented here suggest that active surveillance may be a reasonable option for even those papillary thyroid microcarcinomas adjacent to the thyroid capsule, certain nodules abutting the trachea, and those with irregular margins, regardless of autoimmune disease status, in the absence of the risk factors noted above. Nevertheless, and as previously reported, candidates for observation should be managed by an experienced multidisciplinary team with the capability of high-quality ultrasonography and a mechanism to ensure proper follow up.

Data availability statement

The raw data supporting the conclusions of this article will be made available by the authors, without undue reservation.

Ethics statement

The studies involving human participants were reviewed and approved by Stanford Institutional Review Board. Written informed consent for participation was not required for this study in accordance with the national legislation and the institutional requirements.

Author contributions

SC: Devised study outline, collected patient data, analyzed data, wrote manuscript. JN: Devised study outline, collected patient data, analyzed data, wrote manuscript. MB: Wrote manuscript. LO: Devised

study outline, collected patient data, wrote manuscript. All authors contributed to the article and approved the submitted version.

Conflict of interest

The authors declare that the research was conducted in the absence of any commercial or financial relationships that could be construed as a potential conflict of interest.

Publisher's note

References

1. Vaccarella S, Dal Maso L, Laversanne M, Bray F, Plummer M, Franceschi S. The impact of diagnostic changes on the rise in thyroid cancer incidence: A population-based study in selected high-resource countries. *Thyroid Oct* (2015) 25(10):1127–36. doi: 10.1089/thy.2015.0116

2. Davies L, Welch HG. Increasing incidence of thyroid cancer in the united states, 1973-2002. *JAMA* (2006) 295(18):2164–7. doi: 10.1001/jama.295.18.2164

3. Lim H, Devesa SS, Sosa JA, Check D, Kitahara CM. Trends in thyroid cancer incidence and mortality in the united states, 1974-2013. *JAMA* (2017) 317(13):1338–48. doi: 10.1001/jama.2017.2719

4. Ahn HS, Kim HJ, Welch HG. Korea's thyroid-cancer "epidemic"–screening and overdiagnosis. *N Engl J Med* (2014) 371(19):1765–7. doi: 10.1056/NEJMp1409841

5. Ito Y, Uruno T, Nakano K, Takamura Y, Miya A, Kobayashi Kaoru, et al. An observation trial without surgical treatment in patients with papillary microcarcinoma of the thyroid. *Thyroid* (2003) 13(4):381–7. doi: 10.1089/105072503321669875

6. Ito Y, Miyauchi A, Inoue H, Fukushima M, Kihara M, Higashiyama T, et al. An observational trial for papillary thyroid microcarcinoma in Japanese patients. *World J Surg* (2010) 34(1):28–35. doi: 10.1007/s00268-009-0303-0

7. Takami H, Ito Y, Noguchi H, Yoshida A, Okamoto T. *Treatment of thyroid tumor: Japanese clinical guidelines*. Hyogo, Japan: Japan Association of Endocrine Surgeons Japanese Society of Thyroid Surgery (2010).

8. Haugen BR, Alexander EK, Bible KC, Doherty GM, Mandel SJ, Nikiforov YE, et al. 2015 American Thyroid association management guidelines for adult patients with thyroid nodules and differentiated thyroid cancer: The American thyroid association guidelines task force on thyroid nodules and differentiated thyroid cancer. *Thyroid Jan* (2016) 26(1):1–133. doi: 10.1089/thy.2015.0020

9. Brito JP, Ito Y, Miyauchi A, Tuttle RM. A clinical framework to facilitate risk stratification when considering an active surveillance alternative to immediate biopsy and surgery in papillary microcarcinoma. *Thyroid Jan* (2016) 26(1):144–9. doi: 10.1089/thy.2015.0178

10. Ito Y, Miyauchi A, Kihara M, Higashiyama T, Kobayashi K, Miya A. Patient age is significantly related to the progression of papillary microcarcinoma of the thyroid under observation. *Thyroid* (2014) 24(1):27–34. doi: 10.1089/thy.2013.0367

11. Qu N, Zhang L, Ji QH, Chen J-Y, Zhu Y-X, Cao Y-M, et al. Risk factors for central compartment lymph node metastasis in papillary thyroid microcarcinoma: A meta-analysis. *World J Surg* (2015) 39(10):2459–70. doi: 10.1007/s00268-015-3108-3

12. Zhu M, Zheng W, Xiang Y, Gu J, Wang K, Shang J. The relationship between central lymph node metastasis and the distance from tumor to thyroid capsule in papillary thyroid microcarcinoma without capsule invasion. *Gland Surg* (2020) 9(3):727–36. doi: 10.21037/gs-20-478

13. Xue S, Han Z, Lu Q, Wang P, Chen G. Clinical and ultrasonic risk factors for lateral lymph node metastasis in papillary thyroid microcarcinoma: A systematic review and meta-analysis. *Front Oncol* (2020) 10:436. doi: 10.3389/fonc.2020.00436

14. Ito Y, Miyauchi A, Oda H, Kobayashi K, Kihara M, Miya A. Revisiting low-risk thyroid papillary microcarcinomas resected without observation: Was immediate surgery necessary? *World J Surg* (2016) 40(3):523–8. doi: 10.1007/s00268-015-3184-4

15. Alabousi M, Alabousi A, Adham S, Pozdnyakov A, Ramadan S, Chaudhari H, et al. Diagnostic test accuracy of ultrasonography vs computed tomography for papillary thyroid cancer cervical lymph node metastasis: A systematic review and meta-analysis. *JAMA Otolaryngol Head Neck Surg* (2022) 148(2):107–18. doi: 10.1001/jamaot<o.2021.3387

16. Zhao H, Li H. Meta-analysis of ultrasound for cervical lymph nodes in papillary thyroid cancer: Diagnosis of central and lateral compartment nodal metastases. *Eur J Radiol* (2019) 112:14–21. doi: 10.1016/j.ejrad.2019.01.006

17. Xu J, Ding K, Mu L, Huang J, Ye F, Peng Y, et al. Hashimoto's thyroiditis: A "Double-edged sword" in thyroid carcinoma. *Front Endocrinol (Lausanne)* (2022) 13:801925. doi: 10.3389/fendo.2022.801925

frontiers | Frontiers in Endocrinology

TYPE Original Research
PUBLISHED 02 February 2023
DOI 10.3389/fendo.2023.1075598

OPEN ACCESS

EDITED BY
Erivelto Martinho Volpi,
Centro de referencia no ensino do diagnóstico por imagem (CETRUS), Brazil

REVIEWED BY
Andrii Dinets,
Taras Shevchenko National University of Kyiv, Ukraine
Gloria Angélica González Villaseñor,
Instituto Mexicano del Seguro Social, Mexico

*CORRESPONDENCE
Yafei Shi
jysyf@mail.jnmc.edu.cn

SPECIALTY SECTION
This article was submitted to Thyroid Endocrinology, a section of the journal Frontiers in Endocrinology

RECEIVED 20 October 2022
ACCEPTED 23 January 2023
PUBLISHED 02 February 2023

CITATION
Ma T, Wang L, Zhang X and Shi Y (2023) A clinical and molecular pathology prediction model for central lymph node metastasis in cN0 papillary thyroid microcarcinoma. *Front. Endocrinol.* 14:1075598. doi: 10.3389/fendo.2023.1075598

A clinical and molecular pathology prediction model for central lymph node metastasis in cN0 papillary thyroid microcarcinoma

Teng Ma[1,2], Lulu Wang[3], Xueyan Zhang[2] and Yafei Shi[1]*

[1]Department of Thyroid Surgery, Affiliated Hospital of Jining Medical University, Jining, Shandong, China, [2]Qingdao Medical College, Qingdao University, Qingdao, Shandong, China, [3]Department of Cardiovascular Surgery, Affiliated Hospital of Qingdao University, Qingdao, Shandong, China

Background: The frequency of thyroid cancer has rapidly increased in recent years globally. Thus, more papillary thyroid microcarcinoma (PTMC) patients are being diagnosed, including clinical lymph node-negative (cN0) patients. Our study attempted to develop a prediction model for assessing the probability of central lymph node metastasis (CLNM) in cN0 PTMC patients.

Methods: A total of 595 patients from the Affiliated Hospital of Qingdao University (training cohort: 456 patients) and the Affiliated Hospital of Jining Medical University (verification cohort: 139 patients) who underwent thyroid surgery between January 2020 and May 2022 were enrolled in this study. Their clinical and molecular pathology data were analyzed with multivariate logistic regression to identify independent factors, and then we established a prediction model to assess the risk of CLNM in cN0 PTMC patients.

Results: Multivariate logistic regression analysis revealed that sex, Hashimoto's thyroiditis (HT), tumor size, extrathyroidal extension, TERT promoter mutations and NRAS mutation were independent factors of CLNM. The prediction model demonstrated good discrimination ability (C-index: 0.757 and 0.753 in the derivation and validation cohorts, respectively). The calibration curve of the model was near the optimum diagonal line, and decision curve analysis (DCA) showed a noticeably better benefit.

Conclusion: CLNM in cN0 PTMC patients is associated with male sex, tumor size, extrathyroidal extension, HT, TERT promoter mutations and NRAS mutation. The prediction model exhibits good discrimination, calibration and clinical usefulness. This model will help to assess CLNM risk and make clinical decisions in cN0 PTMC patients.

KEYWORDS

papillary thyroid microcarcinoma, central lymph node metastasis, molecular pathology markers, nomogram, prediction model

Introduction

The most prevalent endocrine malignancy is thyroid carcinoma, and papillary thyroid carcinoma (PTC) accounts for nearly 90%, including probably 50% microcarcinoma (PTMC) (1, 2). PTC with a maximal diameter of less than 1 cm is referred to PTMC. In the past, most PTMCs were diagnosed after the excision of benign thyroid tumors, but now with the popularity of health checkups and widespread use of ultrasound-guided fine needle aspiration biopsy (US-FNAB), the diagnosis rate of PTMC is on the rise (3).

Papillary thyroid carcinoma itself has relatively indolent biological characteristics and superadd the small tumor burden; PTMC patients usually have a good prognosis after treatment (4). The 2022 National Comprehensive Cancer Network (NCCN) advises against utilizing prophylactic CLND to treat T1 and T2 cN0 PTC (5). Nevertheless, the sensitivity of preoperative detection, such as ultrasound, is low for assessing the central lymph node (CLN) state (6); thus, the high probability of occult CLNM cannot be ignored even in cN0 PTMCs (7).

Numerous studies have analyzed the risk factors for CLNM in cN0 PTMC. Our study aimed to create a validated predictive model including preoperatively determinable clinical data and molecular markers, hoping to provide valuable information for clinicians about facilitating the individualized prediction of CLNM in cN0 PTMC patients and guide precise treatment.

Materials and methods

Study design and population

Our study enrolled 2 independent sets of patients from 2 independent medical centers. A total of 456 patients diagnosed with cN0 PTMC in the Thyroid Surgery Department of the Affiliated Hospital of Qingdao University from January 2020 to May 2022 were included as the training cohort. A total of 139 patients were diagnosed with cN0 PTMC in the Thyroid Surgery Department of the Affiliated Hospital of Jining Medical University at the same time as the validation cohort. All operations were performed by surgeons who completed more than 400 surgeries per year. This study was approved by the Affiliated Hospital of Jining Medical University ethics committee (2022C103). Consent has been obtained from each patient or subject after a full explanation of the purpose and nature of all procedures used.

The inclusion criteria were as follows: (1) patients were diagnosed with cN0 PTMC through preoperative ultrasonography (US), computed tomography (CT) and US-FNAB; (2) patients underwent total thyroidectomy with CLND, unilateral thyroid lobectomy and isthmectomy with CLND; and (3) patients underwent BRAF V600E, TERT, RET, HRAS, KRAS, and NRAS genetic testing.

The exclusion criteria were as follows: (1) patients diagnosed with recurrent thyroid tumors (only primary thyroid carcinoma patients were included); (2) patients who had previously undergone neck radiation therapy or other types of surgery; and (3) patients with incomplete medical records.

Data collection

Data collected included sex, age, surgical method, thyroid peroxidase antibody (TPOAb), thyroglobulin antibody (TGAb), thyroid hormone receptor antibody (TRAb), microcalcification foci, positive lymph node number, BRAF gene mutation(V600E), TERT promoter mutation(C228, C250), RET/PTC chromosomal rearrangement(RET/PTC1, RET/PTC3), HRAS gene mutation(Q61), KRAS gene mutation(G12, G13), and NRAS gene mutation(Q61). All data from preoperative examinations and postoperative pathological reports, such as cervical ultrasonic and CT, laboratory examination, and gene test results, were evaluated.

All preoperative examinations were confirmed by a radiologist and chief surgeon, who confirmed the number, size, and calcification of carcinoma and evaluated the lymph node state. Metastatic lymph nodes were suspected when lymph nodes showed increased size (>0.5 cm), demarcation of the cortex and medulla was unclear or the structure of the medulla disappeared, gravel-like calcification or cystic degeneration, rounded bulging shape, and abnormal blood flow or vascularity. Hashimoto's thyroiditis (HT) was diagnosed when the thyroid gland was diffusely enlarged with hypoechogenicity, and the gland parenchyma was inhomogeneous with grid-like or compartment-like changes or appeared abnormal TPOAb, TGAb, TRAb results (8, 9). A gene mutation detection kit (Shanghai Anjia Biological Technology Co., Ltd.) was used to detect BRAF, TERT, HRAS, KRAS, NRAS mutations and RET/PTC rearrangements according to the manufacturer's instructions. The scope of CLND was superior to the hyoid bone, lateral to the carotid sheath, inferior to the sternum notch or the innominate artery, medial to the trachea and dorsal to the prevertebral fascia.

Statistical analysis

The t test (normally distributed data) and Mann–Whitney test (nonnormally distributed data) were used to compare continuous data, and the χ^2 test was used to compare categorical data. Multivariate analysis was carried out with logistic regression; therefore, independent predictors were used to construct a predictive model to evaluate the CLNM risk of cN0 PTMC.

Then, we developed a nomogram as a pictorial representation of the model. The nomogram featured a scoring range at the top from 0 to 100 for each factor variable. Predictor factors are shown below, and bars scaled their effects, displaying the importance of each factor clearly and enabling the awarding of points for each significant clinical feature. Each predictor point's overall value and the corresponding probability of CLNM can be read from the bottom 2 rows.

The predicted accuracy and conformity of the model were assessed using the calibration curve and receiver operating characteristic (ROC) curve. The goodness of fit of the model was evaluated using the Hosmer –Lemeshow test. The net benefit for patients was shown by decision curve analysis (DCA), and 1000 bootstrap repetitions were performed in both discrimination and calibration. In the statistical analyses, $P<0.05$ was considered significant. Statistical analyses were performed using SPSS (version 22.0) and R (version 3.4.1).

Results

Baseline characteristics

Clinical information from a total of 531 patients was acquired from the Affiliated Hospital of Qingdao University for the training cohort, and 75 met the exclusion criteria due to the absence of medical records and recurrent thyroid tumors (Figure 1). Therefore, 456 patients were enrolled in this cohort (97 males, 359 females; mean age 43.04 ± 13.68 years). Among them, 184 patients (40.35%) had CLNM. Clinical information from a total of 139 patients was acquired from the Affiliated Hospital of Jining Medical University for the validation cohort (21 males, 118 females; mean age 44.47 ± 11.54 years). Among them, 48 patients (34.53%) had CLNM. Finally, 595 patients were included in this study. The patients' clinical, pathology and molecular characteristics are listed in Table 1.

Univariate and multivariate analysis

Within the training cohort, univariable analysis demonstrated that sex, HT, tumor size, tumor number, extrathyroidal extension, BRAF mutation, TERT promoter mutations and NRAS mutations were relative influencing factors of CLNM ($P<0.05$). These factors were included in multivariate logistic regression analysis. As shown in Table 2, the results revealed six independent factors, of which male sex, increased tumor size, extraglandular infiltration, TERT promoter mutations and NRAS mutation increased the risk of CLNM, while HT was a protective factor ($P<0.05$). Accordingly, a prediction model was built.

The nomogram for predicting PTC recurrence

To visualize the model, we plotted a nomogram based on six independent factors (sex, HT, tumor size, extrathyroidal extension, TERT promoter mutations and NRAS mutation) in the training cohort. For each risk factor, an ascending line was drawn in the nomogram to obtain a point value in Line 1. The risk possibility of CLNM in cN0 PTMC patients might be estimated by plotting the total of all six points on the final risk axis (Line 8), as shown in Figure 2.

Subsequently we drew the ROC curve to assess the discriminating ability of the model. The area under the ROC was 0.757 (95% CI, 0.711-0.802) and 0.753 (95% CI, 0.682-0.851) in the training cohort and validation cohort, respectively. The model demonstrated a strong capacity to discriminate CLNM in cN0 PTMC (this result is shown in Figure 3).

The calibration curve illustrated the model's potent capacity to calibrate (Figure 4). In both the training cohort and the validation group, the model's predicted values and the observed variables showed good agreement. According to the Hosmer–Lemeshow test, the model's goodness of fit was 0.243.

To determine the net benefit of the nomogram, we built a decision curve analysis (DCA) (Figure 5). The curve demonstrated that the nomogram could be useful when the threshold probability of the patients was between 0.15 and 0.70. In the prediction model, the DCA's net benefit was noticeably higher.

Discussion

The most frequent pathological type of thyroid carcinoma is PTC (10), which is characterized by high differentiation and low malignancy. Most patients have a good prognosis, especially PTMC patients, whose cancer-related mortality rate is merely 0.34% after treatment (11, 12). Whereas PTMC patients have a high CLNM rate, studies have pointed out that 28% of PTMC patients are diagnosed with CLNM (13, 14). Thyroid cancer diagnosis and treatment guidelines (2022) published by the National Health Commission of the People's Republic of China recommended prophylactic CLND should be performed for PTC patients as long as

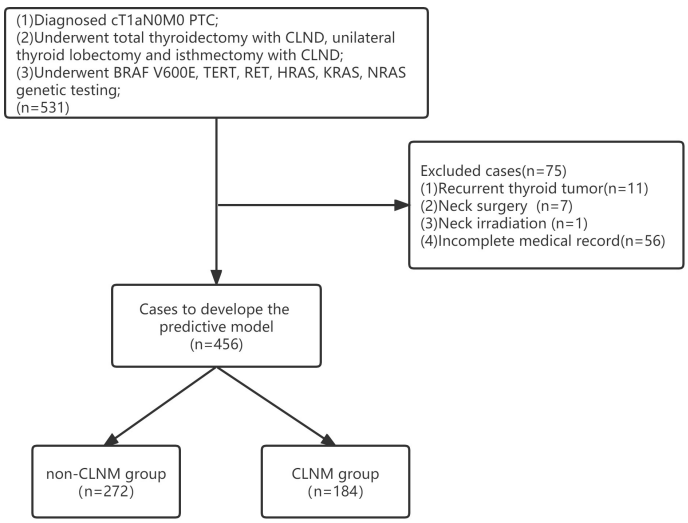

FIGURE 1
Flow chart for patient selection.

10.3389/fendo.2023.1075598

TABLE 1 Baseline characteristics of all patients.

	Training cohort (n=456)			Validation cohort (n=139)		
	Non-CLNM group (n=272)	CLNM group (n=184)	P	Non-CLNM group (n=91)	CLNM group (n=48)	P
Age(Mean ± SD)(y)	42.39 ± 13.79	44.01 ± 13.50	0.216	46.40 ± 11.60	40.81 ± 10.58	0.008
Sexuality			0.006			0.176
Male	226	133		80	38	
Female	46	51		11	10	
Surgery Method			0.669			0.176
Unilateral	187	123		60	37	
Bilateral	85	61		31	11	
HT			0.006			0.054
Absence	177	142		51	26	
Presence	95	42		40	22	
Calcification foci			0.167			0.930
Absence	167	101		50	26	
Presence	105	83		41	22	
Tumor size (Mean ± SD) (mm)	5.66 ± 2.13	6.27 ± 2.36	0.004	6.98 ± 2.20	5.26 ± 2.52	0.000
Tumor number (Mean ± SD)	1.07 ± 0.29	1.07 ± 0.35	0.119	1.17 ± 0.48	1.10 ± 0.30	0.311
Extrathyroidal infiltration			0.001			0.002
Absence	224	126		82	33	
Presence	48	58		9	15	
BRAF V600E mutation			0.044			0.004
Negative	137	75		52	15	
Positive	135	109		39	33	
TERT promoter mutation			0.001			0.009
Negative	262	161		86	38	
Positive	10	23		5	10	
RET mutation			0.396			0.765
Negative	258	171		82	44	
Positive	14	13		9	4	
HRAS mutation			0.202			0.243
Negative	266	176		89	45	
Positive	6	8		2	3	
KRAS mutation			0.504			0.545
Negative	265	181		89	48	
Positive	7	3		2	0	
NRAS mutation			0.009			0.114
Negative	266	170		89	44	
Positive	6	14		2	4	

10.3389/fendo.2023.1075598

TABLE 2 Univariate and multivariate analysis of CLNM in the training cohort.

	Univariate Logistic Regression		Multivariate Logistic Regression	
	OR (95% CI)	P Value	OR (95% CI)	P Value
Age	1.009(0.995-1.023)	0.216	NA	NA
Sexuality	1.884(1.198-2.962)	0.006	4.360(2.446-7.769)	<0.001
Surgery method	1.091(0.731-1.628)	0.669	NA	NA
Calcification foci	1.307(0.894-1.910)	0.167	NA	NA
HT	0.551(0.360-0.843)	0.006	0.090(0.046-0.179)	<0.001
Tumor size	1.130(1.039-1.229)	0.004	1.208(1.093-1.334)	<0.001
Tumor number	1.597(0.887-2.877)	0.119	NA	NA
Extrathyroidal infiltration	2.148(1.383-3.337)	0.001	4.754(2.665-8.480)	<0.001
BRAF	1.475(1.011-2.153)	0.044	1.390(0.898-2.151)	0.140
TERT	3.743(1.737-8.067)	0.001	7.291(3.067-17.333)	<0.001
RET	1.401(0.643-3.054)	0.396	NA	NA
HRAS	2.015(0.687-5.907)	0.202	NA	NA
KRAS	0.627(0.160-2.459)	0.504	NA	NA
NRAS	3.651(1.376-9.685)	0.009	7.956(2.516-25.161)	<0.001

NA, Not Available.

the parathyroid gland and recurrent laryngeal nerve can be protected (15). Moreover, the 2021 Chinese Society of Clinical Oncology (CSCO) Guidelines of Differentiated Thyroid Cancer recommended that PTMC patients with metastatic lymph nodes should undergo CLND (16). However, some studies still show that preventive dissection does not improve patient survival (17), and patients cannot benefit from it; conversely, it will increase the risk of nerve injury and hypoparathyroidism (18). How can metastasis be discriminated? Currently, the most common preoperative diagnostic method is ultrasound, the sensitivity of which for CLNM diagnosis is only 10.9%-38% (19). No practical way was found to raise the CLNM detection rate before surgery, which means that a large number of cN0 PTMC patients actually belong to pN1. Accordingly, identifying the risk factors for CLNM and evaluating the preoperative lymph node state accurately are of major clinical importance in cN0 PTMC patients, and some unnecessary prophylactic CLND can be avoided.

We conducted a large retrospective study including 595 patients from 2 independent medical centers and established a prediction model to assess the risk of CLNM in cN0 PTMC. The results showed that sex, HT, tumor size, extrathyroidal extension, TERT promoter mutations and NRAS mutation were independent factors.

Previous studies have shown that the incidence of PTC in males is lower than that in females, but the incidence of CLNM is higher (20). This is consistent with our findings that males showed a significant trend of CLNM ($P < 0.001$).

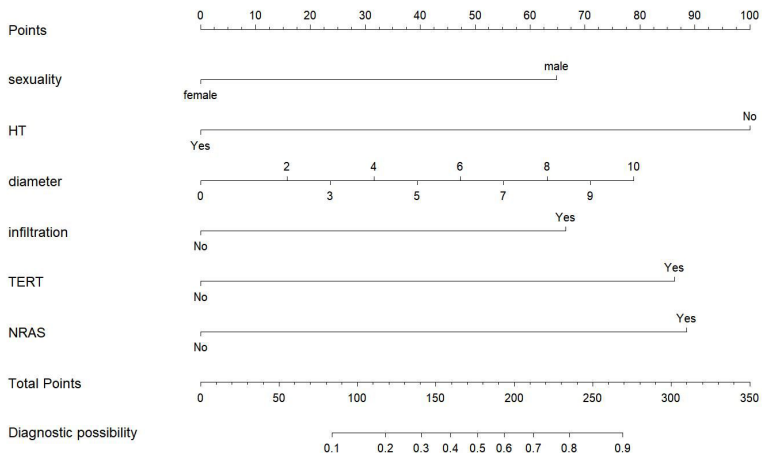

FIGURE 2
Nomogram for prediction model.

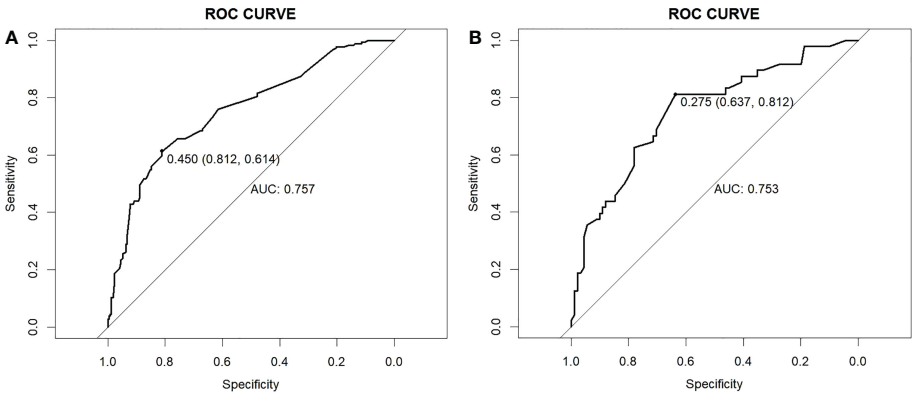

FIGURE 3
ROC curves. **(A)** Training cohort. **(B)** Validation cohort. ROC, receiver operating characteristic; AUC, area under the ROC curve.

Tumor size reflects the stage and prognosis, such as lymph node status (5). In our study, the risk of CLNM in PTC increased with the enlargement of tumor size ($P < 0.001$), similar to other studies.

Extraglandular infiltration refers to the thyroid capsule being invaded by the tumor, and the tumor is more prone to infect lymph nodes through the thyroid capsule's surface lymphatic channels after it has been breached (21). This result is consistent with our findings ($P < 0.001$).

HT is characterized by enrichment of inflammatory factors, also known as autoimmune thyroiditis. It produces a significant amount of lymphocytes and macrophages, both of which naturally possess antitumor activity, and the autoimmune antibodies released by HT-related lymphocytes can also destroy the follicles, contributing to their shrinkage and fibrosis (22, 23). Therefore, PTC tissues with HT usually exhibit a microscopic fibrous cell layer wrapping around the primary lesion, indicating that the combination of HL has a limiting effect on the progression of the primary lesion, which can significantly impede the spread and infiltration of tumor cells (24), reduce the invasiveness of the primary lesion (25), and decrease CLNM chance (26). Kim's studies have shown that PTC patients with HT have lower clinical stage, lower incidence of vascular invasion, lower incidence of CLNM and better prognosis (27). Jara found that the incidence of CLNM in PTC patients with HT was 39% lower than that of PTC alone (28). Zhu analyzed 763 PTMC patients and showed that the presence of HT reduced the lymph node metastasis rate in PTMC patients (29). These results coincide with our study ($P < 0.001$). It is worth mentioning that the effect of HT may vary depending on the criteria used to define HT, Konturek found that the CLNM rate was four times higher in PTC patients coexisting with HT than non-HT patients (30).

The rapid development of fine-needle aspiration techniques makes preoperative genetic testing possible. Thus, surgeons can obtain preoperative genetic test results, such as BRAF gene mutation, TERT gene mutation, HRAS gene mutation, KRAS gene mutation, NRAS gene mutation and RET/PTC rearrangement.

BRAF, one of the three serine-threonine kinase RAF genes (the others being ARAF and CRAF), is crucial to the mitogen-activated protein kinase (MAPK) pathway (31). BRAF V600E is reported to be the most common mutation in PTC, with a probability of 29-69% (32). Although some studies revealed that BRAF genetic testing was valuable in PTC diagnosis (33), its utility in PTC prognosis remains controversial (34). According to several researchers, BRAF mutation is related to aggressiveness, such as lymph node metastases (35). In our study, the mutation incidence in the CLNM group (59.24%) was higher than that in the non-CLNM group (49.63%), but BRAF V600E mutation was not a relative influencing factor in CLNM (P=0.140). Probably because some BRAF V600E mutation testing was conducted preoperatively when patients could not be definitively diagnosed with

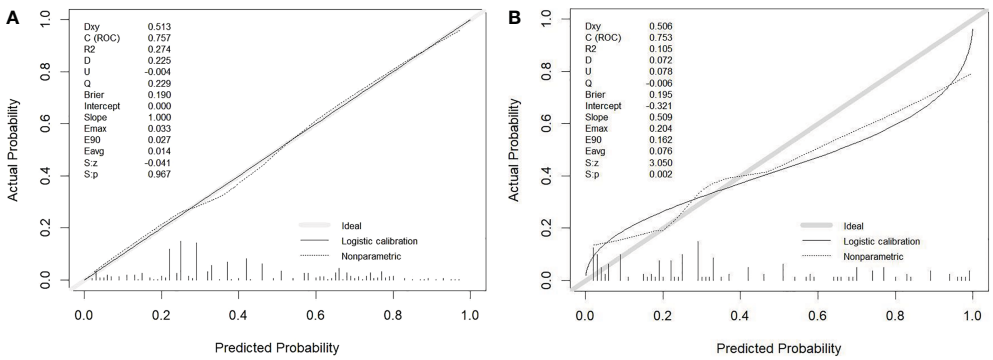

FIGURE 4
Calibration curve for prediction model. **(A)** Training cohort. **(B)** Validation cohort.

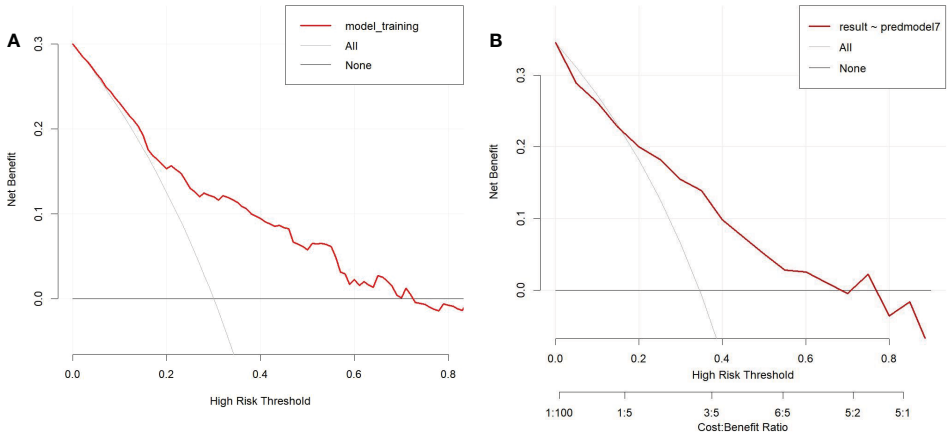

FIGURE 5
Decision curve analysis in prediction model **(A)** Training cohort. **(B)** Validation cohort.

PTC by US-FNAB pathology testing, which perhaps increased the proportion of BRAF V600E mutations patients inadvertently and affected its efficacy in CLNM diagnosis.

TERT promoter mutation has been deeply studied in various cancers, such as nervous system tumors, hepatocellular carcinoma, and bladder cancer (36). Recently, research on thyroid carcinoma has increased. Some articles have reported that the incidence of TERT promoter mutations is approximately 7.5-27% in PTC (37), and the mutation is correlated with particularly aggressive clinicopathological parameters, such as extrathyroidal extension, larger tumor size, and lymph node metastases (38–40). A meta-analysis study including 173 TERT promoter mutant and 1587 TERT promoter wild-type thyroid carcinoma patients showed that the LNM probability ratios were 53.18% and 37.30%, respectively, and a significant association existed between TERT promoter mutation and LNM (41). In Yang's study, the TERT promoter mutation rate was 10.6% (1027/9653), which was significantly associated with PTC LNM (42). And Liu demonstrated that TERT promoter mutations occurred frequently in follicular derived PTC and associated with aggressive disease and poor outcome (43). These studies suggest that TERT promoter mutations can promote lymph node metastasis, which is consistent with our results. Nevertheless, most of the studies focus on advanced thyroid carcinoma (44), and studies on PTMC, especially CLNM, have rarely been conducted. In our study, TERT promoter mutation played an important role in diagnostic value and was an independent predictor of CLNM ($p<0.001$).

The second most frequent mutation is a RAS mutation in preoperative thyroid FNA. RAS mutations include 3 subtypes: HRAS, KRAS, and NRAS, the most common of which is NRAS (45). RAS mutations promote invasion mainly in follicular tumors, relate to local lymph node metastasis and distant metastasis (46). However, the encapsulated follicular type of papillary carcinoma, which is typically indolent and has a good prognosis, also frequently exhibits RAS mutations (47, 48). RAS mutations may only be present in thyroid carcinomas that are well-differentiated and prone to dedifferentiation and metastasis, but it is unlikely that this point mutation will serve as a general prognostic indicator for all varieties of thyroid carcinoma (49). In our study, NRAS was an independent factor for cN0 CLNM ($p<0.001$), perhaps just because of a specific subset, such as follicular papillary carcinoma.

There were many predictive models for assessing CLNM possibility in cN0 PTMC, but their models only incorporated clinical baseline data such as tumor characteristics, ultrasound and CT examination features or just included BRAF mutation result (50–52). Our study built the first predictive model that incorporates such molecular markers and included a large sample size. Finally, we identified 6 independent factors from preoperatively determinable clinical data and molecular markers and then built a predictive model to quantify the likelihood of CLNM in cN0 PTMC patients. The model exhibits good discrimination, calibration and clinical usefulness.

Nevertheless, it also had several limitations. First, our data were all obtained in one province, selection bias is inevitable, and the distribution of pathological subtypes and clinical features may differ in other regions. Second, the molecular pathology markers that were included in this study were limited, and important markers such as PTEN mutation, TRK rearrangement, and PAX8/PPARγ rearrangement were not involved. Third, our study requires further validation in prospective studies, and we are proceeding with a larger-scale, multicenter study in follow-up research. We hope our predictive model can provide valuable information for clinicians about facilitating the individualized prediction of CLNM in cN0 PTMC and guiding precise treatment.

Data availability statement

The original contributions presented in the study are included in the article/supplementary material. Further inquiries can be directed to the corresponding author.

Author contributions

TM designed the study, analyzed the data, and commented on the manuscript at all stages. LW and XZ collected the data. YS provided the research direction. All authors contributed to the article and approved the submitted version.

Funding

Our research was funded by Academician He Lin Research Foundation of Affiliated Hospital of Jining Medical University (JYHL2022FMS10).

Conflict of interest

The authors declare that the research was conducted in the absence of any commercial or financial relationships that could be construed as a potential conflict of interest.

Publisher's note

References

1. Siegel RL, Miller KD, Fuchs HE, Jemal A. Cancer statistics, 2022. *CA Cancer J Clin* (2022) 72(1):7–33. doi: 10.3322/caac.21708

2. Davies L, Welch HG. Increasing incidence of thyroid cancer in the united states, 1973-2002. *JAMA* (2006) 295(18):2164–7. doi: 10.1001/jama.295.18.2164

3. Slijepcevic N, Zivaljevic V, Diklic A, Jovanovic M, Oluic B, Paunovic I. Risk factors associated with intrathyroid extension of thyroid microcarcinomas. *Langenbecks Arch Surg* (2018) 403(5):615–22. doi: 10.1007/s00423-018-1680-3

4. Tagliabue M, Giugliano G, Mariani MC, Rubino M, Grosso E, Chu F, et al. Prevalence of central compartment lymph node metastases in papillary thyroid microcarcinoma: A retrospective evaluation of predictive preoperative features. *Cancers* (2021) 13(23):6028. doi: 10.3390/cancers13236028

5. Haddad RI, Bischoff L, Ball D, Bernet V, Blomain E, Busaidy NL, et al. Thyroid carcinoma, version 2.2022, NCCN clinical practice guidelines in oncology. *J Natl Compr Canc Netw* (2022) 20(8):925–51. doi: 10.6004/jnccn.2022.0040

6. Liu Z, Wang R, Zhou J, Zheng Y, Dong Y, Luo T, et al. Ultrasound lymphatic imaging for the diagnosis of metastatic central lymph nodes in papillary thyroid cancer. *Eur Radiol* (2021) 31(11):8458–67. doi: 10.1007/s00330-021-07958-y

7. Shu X, Tang L, Hu D, Wang Y, Yu P, Yang Z, et al. Prediction model of pathologic central lymph node negativity in cN0 papillary thyroid carcinoma. *Front Oncol* (2021) 11:727984. doi: 10.3389/fonc.2021.727984

8. Anderson L, Middleton WD, Teefey SA, Reading CC, Langer JE, Desser T, et al. Hashimoto thyroiditis: Part 1, sonographic analysis of the nodular form of hashimoto thyroiditis. *AJR Am J Roentgenol* (2010) 195(1):208–15. doi: 10.2214/AJR.09.2459

9. Anderson L, Middleton WD, Teefey SA, Reading CC, Langer JE, Desser T, et al. Hashimoto thyroiditis: Part 2, sonographic analysis of benign and malignant nodules in patients with diffuse hashimoto thyroiditis. *AJR Am J Roentgenol* (2010) 195(1):216–22. doi: 10.2214/AJR.09.3680

10. Shirley LA, Jones NB, Phay JE. The role of central neck lymph node dissection in the management of papillary thyroid cancer. *Front Oncol* (2017) 7:122. doi: 10.3389/fonc.2017.00122

11. Huang Y, Yin Y, Zhou W. Risk factors for central and lateral lymph node metastases in patients with papillary thyroid micro-carcinoma: Retrospective analysis on 484 cases. *Front Endocrinol* (2021) 12:640565. doi: 10.3389/fendo.2021.640565

12. Aliyev E, Ladra-González MJ, Sánchez-Ares M, Abdulkader-Nallib I, Piso-Neira M, Rodríguez-Carnero G, et al. Thyroid papillary microtumor. *Am J Surg Pathol* (2020) 44(9):1161–72. doi: 10.1097/PAS.0000000000001522

13. Gao R, Jia X, Liang Y, Fan K, Wang X, Wang Y, et al. Papillary thyroid micro carcinoma: The incidence of high-risk features and its prognostic implications. *Front Endocrinol* (2019) 10:74. doi: 10.3389/fendo.2019.00074

14. Fu GM, Wang ZH, Chen YB, Li CH, Zhang YJ, Li XJ, et al. Analysis of risk factors for lymph node metastases in elderly patients with papillary thyroid micro-carcinoma. *Cancer Manag Res* (2020) 12:7143–9. doi: 10.2147/CMAR.S248374

15. Health Commission Of The People's Republic Of China National. National guidelines for diagnosis and treatment of thyroid cancer 2022 in China (English version). *Chin J Cancer Res* (2022) 34(3). doi: 10.21147/j.issn.1000-9604.2022.03.01

16. Guidelines of Chinese Society of Clinical Oncology (CSCO). Differentiated thyroid Cancer(2021). *J Cancer Control And Treat* (2021) 34(12):1164–201. doi: 10.3969/j.issn.1674-0904.2021.12.013

17. De Napoli L, Matrone A, Favilla K, Piaggi P, Galleri D, Ambrosini CE, et al. Role of prophylactic central compartment lymph node dissection on the outcome of patients with papillary thyroid carcinoma and synchronous ipsilateral cervical lymph node metastases. *Endocrine Pract* (2020) 26(8):807–17. doi: 10.4158/EP-2019-0532

18. Mulla M, Schulte K. Central cervical lymph node metastases in papillary thyroid cancer: a systematic review of imaging-guided and prophylactic removal of the central compartment. *Clin Endocrinol* (2012) 76(1):131–6. doi: 10.1111/j.1365-2265.2011.04162.x

19. Xue T, Liu C, Liu JJ, Hao YH, Shi YP, Zhang XX, et al. Analysis of the relevance of the ultrasonographic features of papillary thyroid carcinoma and cervical lymph node metastasis on conventional and contrast-enhanced ultrasonography. *Front Oncol* (2021) 11:794399. doi: 10.3389/fonc.2021.794399

20. Oh HS, Park S, Kim M, Kwon H, Song E, Sung TY, et al. Young age and Male sex are predictors of Large-volume central neck lymph node metastasis in clinical N0 papillary thyroid microcarcinomas. *Thyroid* (2017) 27(10):1285–90. doi: 10.1089/thy.2017.0250

21. Seifert R, Schäfers M, Heitplatz B, Kerschke L, Riemann B, Noto B. Minimal extrathyroidal extension in papillary thyroid microcarcinoma is an independent risk factor for relapse through lymph node and distant metastases. *J Nucl Med* (2021) 62 (12):1702–9. doi: 10.2967/jnumed.121.261898

22. Zhang QY, Ye XP, Zhou Z, Zhu CF, Li R, Fang Y, et al. Lymphocyte infiltration and thyrocyte destruction are driven by stromal and immune cell components in hashimoto's thyroiditis. *Nat Commun* (2022) 13(1):775. doi: 10.1038/s41467-022-28120-2

23. Ajjan RA, Weetman AP. The pathogenesis of hashimoto's thyroiditis: Further developments in our understanding. *Horm Metab Res* (2015) 47(10):702–10. doi: 10.1055/s-0035-1548832

24. Donangelo I, Walts AE, Bresee C, Braunstein GD. Lymphocytic thyroiditis is associated with increased number of benign cervical nodes and fewer central neck compartment metastatic lymph nodes in patients with differentiated thyroid cancer. *Endocrine Pract* (2016) 22(10):1192–8. doi: 10.4158/E151078.OR

25. Wen X, Wang B, Jin Q, Zhang W, Qiu M. Thyroid antibody status is associated with central lymph node metastases in papillary thyroid carcinoma patients with hashimoto's thyroiditis. *Ann Surg Oncol* (2019) 26(6):1751–8. doi: 10.1245/s10434-019-07256-4

26. Song E, Jeon MJ, Park S, Kim M, Oh HS, Song DE, et al. Influence of coexistent hashimoto's thyroiditis on the extent of cervical lymph node dissection and prognosis in papillary thyroid carcinoma. *Clin Endocrinol* (2018) 88(1):123–8. doi: 10.1111/cen.13475

27. Kim SJ, Lee SE, Kim YI, Nam-Goong IS, Jung HW, Kim ES. Papillary thyroid cancer with hashimoto's thyroiditis attenuates the tumour aggressiveness through the up-regulation of e-cadherin and TGF-beta expression. *Clin Exp Med* (2022). doi: 10.1007/s10238-022-00857-6

28. Jara SM, Carson KA, Pai SI, Agrawal N, Richmon JD, Prescott JD, et al. The relationship between chronic lymphocytic thyroiditis and central neck lymph node metastasis in north American patients with papillary thyroid carcinoma. *Surgery* (2013) 154(6):1272–1280, 1280-1282. doi: 10.1016/j.surg.2013.07.021

29. Zhu F, Shen YB, Li FQ, Fang Y, Hu L, Wu YJ. The effects of hashimoto thyroiditis on lymph node metastases in unifocal and multifocal papillary thyroid carcinoma: A retrospective Chinese cohort study. *Med (Baltimore)* (2016) 95(6):e2674. doi: 10.1097/MD.0000000000002674

30. Konturek A, Barczynski M, Wierzchowski W, Stopa M, Nowak W. Coexistence of papillary thyroid cancer with hashimoto thyroiditis. *Langenbecks Arch Surg* (2013) 398 (3):389–94. doi: 10.1007/s00423-012-1021-x

31. Chu Y, Wirth LJ, Farahani AA, Nosé V, Faquin WC, Dias-Santagata D, et al. Clinicopathologic features of kinase fusion-related thyroid carcinomas: An integrative analysis with molecular characterization. *Modern Pathol* (2020) 33(12):2458–72. doi: 10.1038/s41379-020-0638-5

32. Melo M, Gaspar DRA, Batista R, Vinagre J, Martins MJ, Costa G, et al. TERT, BRAF, and NRAS in primary thyroid cancer and metastatic disease. *J Clin Endocrinol Metab* (2017) 102(6):1898–907. doi: 10.1210/jc.2016-2785

33. Choi JE, Bae JS, Lim DJ, Jung SL, Jung CK. Atypical histiocytoid cells and multinucleated giant cells in fine-needle aspiration cytology of the thyroid predict lymph node metastasis of papillary thyroid carcinoma. *Cancers* (2019) 11(6):816. doi: 10.3390/cancers11060816

34. Zhan J, Zhang L, Yu Q, Li CL, Chen Y, Wang WP, et al. Prediction of cervical lymph node metastasis with contrast-enhanced ultrasound and association between presence of BRAFV600E and extrathyroidal extension in papillary thyroid carcinoma. *Ther Adv Med Oncol* (2020) 12:386355740. doi: 10.1177/1758835920942367

35. Liu S, Liu C, Zhao L, Wang K, Li S, Tian Y, et al. A prediction model incorporating the BRAFV600E protein status for determining the risk of cervical lateral lymph node metastasis in papillary thyroid cancer patients with central lymph node metastasis. *Eur J Surg Oncol* (2021) 47(11):2774–80. doi: 10.1016/j.ejso.2021.08.033

36. Vinagre J, Almeida A, Populo H, Batista R, Lyra J, Pinto V, et al. Frequency of TERT promoter mutations in human cancers. *Nat Commun* (2013) 4:2185. doi: 10.1038/ncomms3185

37. Panebianco F, Nikitski AV, Nikiforova MN, Nikiforov YE. Spectrum of TERT promoter mutations and mechanisms of activation in thyroid cancer. *Cancer Med* (2019) 8(13):5831–9. doi: 10.1002/cam4.2467

38. Landa I, Pozdeyev N, Korch C, Marlow LA, Smallridge RC, Copland JA, et al. Comprehensive genetic characterization of human thyroid cancer cell lines: A validated panel for preclinical studies. *Clin Cancer Res* (2019) 25(10):3141–51. doi: 10.1158/1078-0432.CCR-18-2953

39. Yang T, Huang L, Chen C, Luo H, Jiang Y. Comparison between clinicopathological characteristics, BRAF V600E and TERT promoter mutation of familial non-medullary thyroid carcinomas, and sporadic case. *Front Oncol* (2021) 11:616974. doi: 10.3389/fonc.2021.616974

40. Geng J, Liu Y, Guo Y, Wang H, Tai J, Jin Y, et al. Correlation between TERT C228T and clinic-pathological features in pediatric papillary thyroid carcinoma. *Sci China Life Sci* (2019) 62(12):1563–71. doi: 10.1007/s11427-018-9546-5

41. Yin DT, Yu K, Lu RQ, Li X, Xu J, Lei M, et al. Clinicopathological significance of TERT promoter mutation in papillary thyroid carcinomas: A systematic review and meta-analysis. *Clin Endocrinol (Oxf)* (2016) 85(2):299–305. doi: 10.1111/cen.13017

42. Yang J, Gong Y, Yan S, Chen H, Qin S, Gong R. Association between TERT promoter mutations and clinical behaviors in differentiated thyroid carcinoma: a systematic review and meta-analysis. *Endocrine* (2020) 67(1):44–57. doi: 10.1007/s12020-019-02117-2

43. Liu T, Wang N, Cao J, Sofiadis A, Dinets A, Zedenius J, et al. The age- and shorter telomere-dependent TERT promoter mutation in follicular thyroid cell-derived carcinomas. *Oncogene* (2014) 33(42):4978–84. doi: 10.1038/onc.2013.446

44. Yoo SK, Song YS, Lee EK, Hwang J, Kim HH, Jung G, et al. Integrative analysis of genomic and transcriptomic characteristics associated with progression of aggressive thyroid cancer. *Nat Commun* (2019) 10(1):2764. doi: 10.1038/s41467-019-10680-5

45. Carneiro T, Bim LV, Buzatto VC, Galdeno V, Asprino PF, Lee EA, et al. Evidence of cooperation between hippo pathway and RAS mutation in thyroid carcinomas. *Cancers (Basel)* (2021) 13(10). doi: 10.3390/cancers13102306

46. Landa I, Ibrahimpasic T, Boucai L, Sinha R, Knauf JA, Shah RH, et al. Genomic and transcriptomic hallmarks of poorly differentiated and anaplastic thyroid cancers. *J Clin Invest* (2016) 126(3):1052–66. doi: 10.1172/JCI85271

47. Hernandez-Prera JC, Valderrabano P, Creed JH, de la Iglesia JV, Slebos RJC, Centeno BA, et al. Molecular determinants of thyroid nodules with indeterminate cytology and RAS mutations. *Thyroid* (2021) 31(1):36–49. doi: 10.1089/thy.2019.0650

48. Angell TE. RAS-positive thyroid nodules. *Curr Opin Endocrinol Diabetes Obes* (2017) 24(5):372–6. doi: 10.1097/MED.0000000000000354

49. Marotta V, Bifulco M, Vitale M. Significance of RAS mutations in thyroid benign nodules and non-medullary thyroid cancer. *Cancers (Basel)* (2021) 13(15). doi: 10.3390/cancers13153785

50. Wang Y, Guan Q, Xiang J. Nomogram for predicting central lymph node metastasis in papillary thyroid microcarcinoma: A retrospective cohort study of 8668 patients. *Int J Surg* (2018) 55:98–102. doi: 10.1016/j.ijsu.2018.05.023

51. Luo QW, Gao S, Lv X, Li SJ, Wang BF, Han QQ, et al. A novel tool for predicting the risk of central lymph node metastasis in patients with papillary thyroid microcarcinoma: a retrospective cohort study. *BMC Cancer* (2022) 22(1):606. doi: 10.1186/s12885-022-09655-5

52. Siddiqui S, White MG, Antic T, Grogan RH, Angelos P, Kaplan EL, et al. Clinical and pathologic predictors of lymph node metastasis and recurrence in papillary thyroid microcarcinoma. *Thyroid* (2016) 26(6):807–15. doi: 10.1089/thy.2015.0429

frontiers | Frontiers in Endocrinology

TYPE Original Research
PUBLISHED 10 February 2023
DOI 10.3389/fendo.2023.1076640

OPEN ACCESS

EDITED BY
Jose Federico Carrillo,
National Institute of Cancerology (INCAN), Mexico

REVIEWED BY
Xiaopei Shen,
Fujian Medical University, China
Minghua Ge,
Zhejiang Provincial People's Hospital, China

*CORRESPONDENCE
Haipeng Xiao
xiaohp@mail.sysu.edu.cn
Shubin Hong
hongshb3@mail.sysu.edu.cn

SPECIALTY SECTION
This article was submitted to Thyroid Endocrinology, a section of the journal Frontiers in Endocrinology

RECEIVED 21 October 2022
ACCEPTED 31 January 2023
PUBLISHED 10 February 2023

CITATION
He W, Sun Y, Ge J, Wang X, Lin B, Yu S, Li Y, Hong S and Xiao H (2023) STRA6 regulates tumor immune microenvironment and is a prognostic marker in BRAF-mutant papillary thyroid carcinoma.
Front. Endocrinol. 14:1076640.
doi: 10.3389/fendo.2023.1076640

STRA6 regulates tumor immune microenvironment and is a prognostic marker in BRAF-mutant papillary thyroid carcinoma

Weiman He[1], Yijia Sun[1], Jiawei Ge[1], Xuejie Wang[1], Bo Lin[2], Shuang Yu[1], Yanbing Li[1], Shubin Hong[1*] and Haipeng Xiao[1*]

[1]Department of Endocrinology, The First Affiliated Hospital of Sun Yat-sen University, Guangzhou, China, [2]Department of Thyroid Surgery, The First Affiliated Hospital of Sun Yat-sen University, Guangzhou, China

Background: BRAF mutation is one of the most common genetic alterations contributing to the initiation and progression of papillary thyroid carcinoma (PTC). However, the prognostic value of BRAF mutation for PTC is limited. Novel markers are needed to identify BRAF-mutant patients with poor prognosis.

Methods: Transcriptional expression data were downloaded from the Cancer Genome Atlas (TCGA) and Gene Expression Omnibus (GEO) datasets. Pathway enrichment was performed by Kyoto Encyclopedia of Genes and Genomes (KEGG) analysis and gene set enrichment analysis (GSEA). Protein-protein interaction networks were predicted by the GeneMANIA. The correlation between STRA6 expression and immune infiltration was analyzed by tumor immune estimation resource (TIMER) and tumor-immune system interaction database (TISIDB). Immunohistochemistry was used to detect the STRA6 protein expression level of PTC. Infiltration of regulatory T cells (Tregs) and CD8+ T cells in tumor samples were analyzed by fluorescent multiplex immunohistochemistry.

Results: In BRAF-mutant PTC, STRA6 was extremely upregulated and predicted unfavorable survival, which was an independent risk factor for increased mortality risk. Bioinformatic analyses indicated that STRA6 might activate the MAPK pathway synergistically with $BRAF^{V600E}$. The expression of STRA6 was associated with immune infiltrates and T cell exhaustion. Fluorescent multiplex immunohistochemistry showed that STRA6 increased Tregs abundance and decreased CD8+ T cells infiltration in PTC. Moreover, STRA6 promoted epithelial-mesenchymal transition *via* increased cancer-associated fibroblasts infiltration.

Conclusions: Our study demonstrates STRA6 may serve as a prognostic marker for BRAF-mutated PTC, which may drive thyroid carcinogenesis *via* activation of oncogenic pathway and regulation of tumor immunosuppressive microenvironment.

KEYWORDS

papillary thyroid carcinoma (PTC), BRAF mutation, STRA6, prognosis, tumor immune microenvironment

Introduction

Thyroid carcinoma (TC) is the most common endocrine malignancy with an increasing incidence worldwide (1). Most of TCs arise from thyroid follicular epithelial cells, among which 80% are papillary thyroid carcinoma (PTC) (2). Initiation and progression of TC involve multiple genetic alterations, of which the most common oncogenic mutation is $BRAF^{V600E}$ (3, 4). Although $BRAF^{V600E}$ mutation is associated with poorer recurrence-free probability (5), it was suggested that not all of the PTCs with $BRAF^{V600E}$ mutation belonged to high-risk recurrence in American Thyroid Association Management Guidelines (6) or even were associated with aggressive clinicopathological outcomes (7, 8). Thus, novel markers are needed to identify BRAF-mutant PTC patients with poor prognosis.

STRA6, functions as a Vitamin A transporter and cytokine receptor (9), has been reported in multiple cancers. STRA6 activated the Wnt/β-catenin signaling in gastric cancer and served as a prognostic biomarker (10, 11). Upregulation of STRA6 in colon cancer was correlated with poor oncologic prognosis and transduced JAK2-STAT signaling, which contributes to colon tumorigenesis (12, 13). Moreover, STRA6 polymorphisms were correlated with clinical characteristics and might be potential markers in locally-advanced and metastatic non-small cell lung cancer (14). However, the prognostic value of STRA6 in PTC remains unknown.

Tumor microenvironment, composed of tumor cells, immune cells, cytokines, etc., plays an essential role in cancer metastasis, progression and recurrence. The escape of tumor cells often occurs in an immunosuppressive microenvironment (15). It was reported that regulatory T cells (Tregs) were enriched in primary thyroid tumors (16) and had higher infiltration in lymph node metastases (17). Besides, the density of tumor-associated macrophages was increased in advanced thyroid cancer, which correlated with decreased survival rate of patients (18). Recent study revealed that STRA6 was associated with infiltration of antigen-presenting cells in stomach adenocarcinoma, which could serve as a potential mRNA vaccine candidate (19). Nevertheless, the engagement of STRA6 in tumor immune microenvironment of TC remains elusive.

In this study, we demonstrate STRA6 is upregulated in BRAF-mutant PTC. High STRA6 expression is associated with unfavorable prognosis for individuals with $BRAF^{V600E}$. Immune infiltration and pathway enrichment were investigated in samples with high STRA6 expression. STRA6 may contribute to the progression of BRAF-mutant PTC *via* regulation of immunosuppressive tumor microenvironment and activation of oncogenic pathway.

Materials and methods

Transcriptional data

Transcriptional expression data and clinicopathological information of the Cancer Genome Atlas (TCGA) cohort were downloaded from UCSC Xena (https://xena.ucsc.edu/). GSE199023 was downloaded from Gene Expression Omnibus (GEO) datasets (https://www.ncbi.nlm.nih.gov/). The RNA sequencing data of the FAH-SYSU cohort was obtained from our previous study (20).

Tumor immune estimation

Tumor immune estimation resource (TIMER) 2.0 (http://timer.cistrome.org/) is a web server for comprehensive analysis of immune infiltrates with diverse algorithms. It was applied to analyze STRA6 expression level in pan-cancer based on the TCGA dataset. The correlation of STRA6 expression between BRAF mutation status was further explored by Timer 2.0. It was also used to analyze the correlation of immune infiltrates with STRA6 expression and BRAF mutation status. The relation between immunomodulators and STRA6 expression was evaluated *via* tumor-immune system interaction database (TISIDB) (http://cis.hku.hk/TISIDB/index.php).

Differential expression analysis and functional annotations

NetworkAnalyst (https://www.networkanalyst.ca/) is a platform for comprehensive gene expression profiling analysis. We divided the BRAF-mutant PTC from the TCGA cohort into two groups according to STRA6 expression. After uploading a gene expression table, differently expressed genes (DEGs) were analyzed by the platform and followed with Kyoto Encyclopedia of Genes and Genomes (KEGG) analysis. Additionally, principal component analysis (PCA) between two groups was performed on Clustvis website (https://biit.cs.ut.ee/clustvis/). Protein-protein interaction (PPI) was predicted by GeneMANIA (http://genemania.org/).

Gene set enrichment analysis

GSEA software was downloaded from the website (http://www.gsea-msigdb.org/gsea/index.jsp). We performed analysis in 50 patients with high STRA6 expression and 50 patients with low STRA6 expression of the TCGA cohort. Hallmark gene sets were used to explore the mechanism of STRA6 in thyroid carcinoma progression.

Immunohistochemistry

The study was approved by the Institutional Research Ethics Committee of The First Affiliated Hospital of Sun Yat-sen University (no. [2021] 109). 30 pairs of PTC tissues were collected from the First Affiliated Hospital of Sun Yat-sen University with informed consent from patients. Paraffin embedded tissues were deparaffinized with xylene for two times and dehydrated with a series of ethanol. Antigen retrieval was performed by boiling the slides in EDTA buffer (C1034, Solarbio). After cooling, the slides were blocked with 20% goat serum at room temperature for 30 min and incubated with STRA6 primary antibody (diluted 1:200, H00064220-D01P, Novus) at 4°C overnight. Followed by rinse with PBS for 3 times, the slices were incubated with secondary antibody at room temperature for 30 min. Detection of protein expression was performed with a 3,3'-diaminobenzidine (DAB) peroxidase substrate kit (K5007; Dako) under a microscope. Subsequently, the slides were counterstained with Harris hematoxylin, followed by dehydration in graded alcohol and incubation in xylene. The immunohistochemistry (IHC) staining score was calculated with the following formula: IHC score = extent score × intensity score. The staining extent was scored as 0 (1%–4% positive cells), 1(5%–25% positive cells), 2 (26%–50% positive cells), 3 (51%–75% positive cells), 4 (≥75% positive cells). The staining intensity was scored as 0-3, corresponding to no staining, weak staining, intermediate staining and strong staining, respectively.

Fluorescent multiplex immunohistochemistry

Fluorescent multiplex immunohistochemistry (mIHC) was applied to characterize immune infiltration in PTC. After incubation with primary antibody, the slides were incubated with an HRP-conjugated secondary antibody and fluorophore-conjugated Tyramide Signal Amplification reagent (Cat. 10003100100, Panovue). Multiplex panel design was as follows: FoxP3 (diluted 1:100, ab215206, abcam), Opal 570 TSA (diluted 1:200); CD8 (diluted 1:100, 70306S, CST), Opal 690 TSA (diluted 1:200). Finally, the slides were stained with DAPI (4', 6-diamidino-2-phenylindole) and mounted with anti-fated reagent.

Statistical analysis

Experimental data was analyzed with GraphPad Prism 8.0 and presented as mean ± standard deviation (SD). Comparison between two groups was analyzed with Mann-Whitney U test or Student's t test. The correlation between STRA6 expression and clinicopathological features in the TCGA cohort was analyzed with a chi-squared test. Kaplan–Meier analysis with a log-rank test was used to evaluate the prognostic value of STRA6 in BRAF-mutant PTC. Univariate Cox regression analysis was performed to investigate the correlation between variables and survival. After multivariate adjustment for age, gender, tumor size, multifocality, extrathyroidal extension and lymph node metastasis, multivariate Cox regression analysis further accessed whether high STRA6 expression was an independent risk factor for recurrence and mortality. A P value of <0.05 was considered statistically significant.

Results

STRA6 is upregulated in BRAF-mutated PTC.

To unveil the expression pattern of STRA6 across different cancers, we analyzed the mRNA expression level of STRA6 in the TCGA cohort. STRA6 was upregulated in most cancers including thyroid carcinoma (Figure 1A). Notably, the expression of STRA6 was positively correlated with BRAF mutation in TC and melanoma (Figure S1A). Compared with BRAF wild-type (WT) PTC, STRA6 was significantly upregulated in BRAF-mutated samples (Figure 1B). Based on a public dataset GSE199023, zebrafish thyroid tumors transfected with $BRAF^{V600E}$ oncogenes showed higher expression of STRA6 as compared to those transfected with CCDC6-RET fusion (Figure 1C). We further analyzed the mRNA expression in our cohort based on distinct molecular subtypes. STRA6 was remarkably upregulated in BRAF subtype compared with other PTC subtypes and benign nodules (Figure 1D). Overexpression of STRA6 protein level in $BRAF^{V600E}$ PTC was also confirmed by IHC (Figure 1E). Taken together, STRA6 is upregulated in thyroid cancer and exhibits extremely higher expression in BRAF-mutant PTC.

Upregulation of STRA6 predicts aggressive outcomes and unfavorable prognosis for BRAF-mutant PTC

We investigated the relationship between STRA6 expression and clinicopathological features in the TCGA cohort. High STRA6 expression was associated with BRAF mutation (P = 0.001) and distant metastasis (P = 0.019) (Table 1). Then we divided PTC patients into two groups according to the genotype of BRAF. Intriguingly, high STRA6 expression was significantly associated with aggressive clinicopathological outcomes in BRAF-mutant PTC, but not in BRAF WT groups. For individuals with BRAF mutation, rates of distant metastasis were 2/130 (1.5%) vs. 3/26 (11.5%) (P = 0.033) in low-STRA6 group vs. high-STRA6 group, respectively. The recurrence rates were significantly higher in high-STRA6 PTC than low-STRA6 PTC [11/40 (27.5%) vs. 20/212 (9.4%), P = 0.003]. As for mortality, it was robustly higher in PTC with high STRA6 expression than those with low STRA6 expression [5/40 (12.5%) vs. 4/212 (1.9%), P = 0.004] (Table 2). Kaplan-Meier analysis showed higher STRA6 expression significantly predicted poorer recurrence free survival

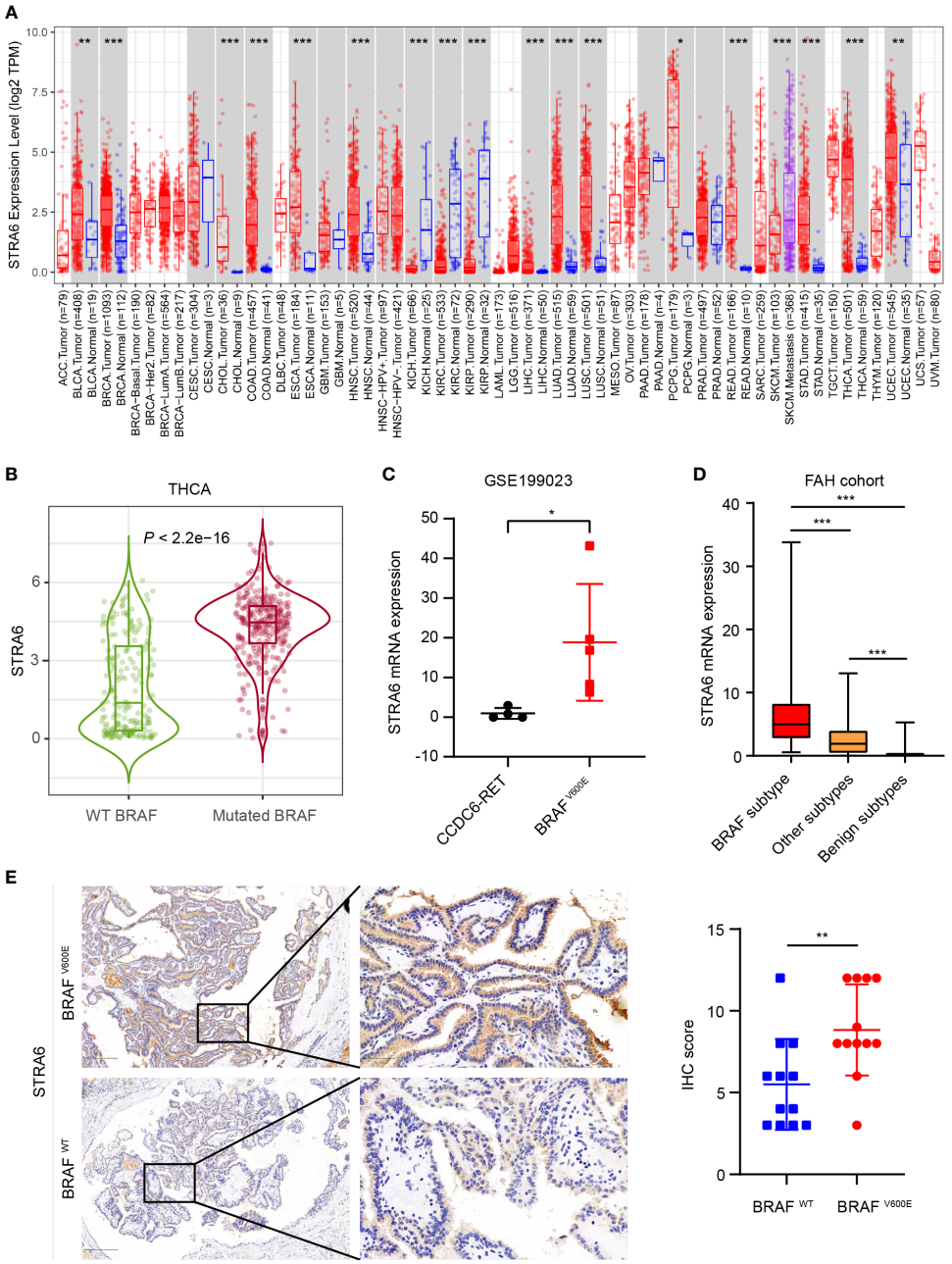

FIGURE 1
STRA6 is upregulated in BRAF-mutated PTC. **(A)** mRNA expression of STRA6 in various cancers according to the TCGA cohort. **(B)** STRA6 mRNA expression based on BRAF genotype in THCA cohort. **(C)** STRA6 mRNA expression of zebrafish thyroid tumors with oncogenic transfection gene in GSE199023. **(D)** mRNA abundance in FAH cohort with respect to different molecular subtypes. **(E)** Immunohistochemistry (IHC) staining of STRA6 protein level based on the BRAF mutation status in PTC samples. (*p < 0.05, **p < 0.01, ***p < 0.001. The data are shown as the mean ± SD).

(RFS) (P = 0.0007) and overall survival (OS) (P = 0.0006) (Figures 2A, B).

High STRA6 expression is an independent risk factor for mortality in BRAF-mutated PTC

Furthermore, we explored the hazard ratios (HRs) of STRA6-related risk (Table 3). In the entire TCGA cohort, univariate Cox regression analysis showed that upregulation of STRA6 was an independent risk factor for recurrence and mortality, with HRs being 2.98 (1.62-5.48) (P < 0.001) and 4.67 (1.69-12.87) (P = 0.003), respectively. After multivariate adjustment for age, gender, tumor size, multifocality, extrathyroidal extension and lymph node metastasis, HRs of recurrence and mortality remained significantly (P = 0.013 and P = 0.017). Then we divided patients into two groups according to BRAF mutation status. In BRAF wild-type patients, neither recurrence rates nor mortality rates was associated with STRA6 expression. In BRAF-mutant patients, STRA6-related recurrence risk was 3.32 (1.59-6.96) (P =0.001) and became 1.97 (0.81-4.81) (P = 0.135) after multivariate adjustment (Figure 2C).

10.3389/fendo.2023.1076640

TABLE 1 The association between STRA6 expression and clinicopathologic characteristics in the TCGA cohort.

	Total	Low-STRA6	High-STRA6	*P* value
	n (%)	n (%)	n (%)	
Age ≥55 years	167/504 (33.1%)	142/447 (31.8%)	25/57 (43.9%)	0.068
Sex (female)	368/504 (73.0%)	330/447 (73.8%)	38/57 (66.7%)	0.251
Multifocality	227/494 (46.0%)	202/438 (46.1%)	25/56 (44.6%)	0.835
Tumor size (≥2.0 cm)	151/406 (37.2%)	130/356 (36.5%)	21/50 (42.0%)	0.453
Extrathyroidal extension	153/486 (31.5%)	131/430 (30.5%)	22/56 (39.3%)	0.181
BRAF mutation	252/495 (50.9%)	212/439 (48.3%)	40/56 (71.4%)	0.001
Lymph node metastasis	224/454 (49.3%)	195/402 (48.5%)	29/52 (55.8%)	0.324
Distant metastasis	9/291 (3.1%)	5/253 (2.0%)	4/38 (10.5%)	0.019[a]
Stage (III/IV)	166/502 (33.1%)	141/445 (31.7%)	25/57 (43.9%)	0.066

[a]Continuity Correction.

STRA6 overexpression was a risk factor for mortality with an HR being 7.12 (1.91-26.56) (P = 0.003), which became more significant with an HR being 19.02 (3.48-103.94) (P = 0.001) after multivariate adjustment (Figure 2D). Therefore, individuals with high STRA6 expression show increased mortality risk in BRAF-mutated PTC.

STRA6 plays oncogenic and immunoregulatory roles in BRAF-mutated PTC progression

To explore the mechanism of STRA6 contributing to the poor prognosis in BRAF-mutant PTC, we divided patients into two groups according to STRA6 expression. Principal component analysis (PCA) showed separation between high-STRA6 PTC and low-STRA6 PTC (Figure 3A). Differential expression genes (DEGs) between two groups were shown in Figure 3B. Of which, most genes were involved in malignant tumor progression, such as OBP2B, TNNT1, KLK6, KRT17 etc. Moreover, chemokine signaling pathway and cytokine-cytokine receptor interaction were enriched with the upregulated genes in high-STRA6 groups, indicating STRA6 may engage in the regulation of the immune interaction (Figure 3C). We also found that STRA6 expression was associated with immunomodulators in the TCGA cohort (Figures S1B, C), which indicated that STRA6 may function as an immunoregulator in TC progression. Additionally, the MAPK signaling pathway, which has emerged as one of the frequently activated pathways in thyroid tumorigenesis, was also remarkably enriched with the upregulated genes in high-STRA6 PTC. Downregulation of genes enriched in thyroid hormone synthesis further suggested the oncogenic role of STRA6 in TC progression (Figure 3C). PPI networks of STRA6 were constructed by GeneMANIA. It was predicted that 20 proteins were binding to STRA6. Of note, STRA6 interacted with several proteins modulated by the MAPK signaling pathway, including DIO3, BMP4 and DUSP6 (Figure 3D). Therefore, our results demonstrate that STRA6 may contribute to BRAF-mutated PTC progression by regulating oncogenic pathways and immune microenvironment.

TABLE 2 Correlation between STRA6 expression and clinicopathological characteristics of PTC in the TCGA cohort based on the BRAF genotypes.

	Wild-type BRAF			BRAF V600E mutation		
	Low-STRA6	High-STRA6	*P* value	Low-STRA6	High-STRA6	*P* value
Age ≥55 years	76/227 (33.5%)	6/16 (37.5%)	0.742	63/212 (29.7%)	18/40 (45.0%)	0.058
Sex (female)	168/227 (74.0%)	10/16 (62.5%)	0.476[a]	157/212 (74.1%)	27/40 (67.5%)	0.392
Multifocality	103/220 (46.8%)	5/16 (31.3%)	0.227	94/210 (44.8%)	20/39 (51.3%)	0.453
Tumor size (≥2.0 cm)	67/177 (37.9%)	7/13 (53.8%)	0.254	60/171 (35.1%)	13/36 (36.1%)	0.907
Extrathyroidal extension	48/216 (22.2%)	7/16 (43.8%)	0.099[a]	81/207 (39.1%)	14/39 (35.9%)	0.704
Lymph node metastasis	90/202 (44.6%)	9/16 (56.3%)	0.366	105/195 (53.8%)	19/35 (54.3%)	0.962
Distant metastasis	3/118 (2.5%)	1/11 (9.1%)	0.303[b]	2/130 (1.5%)	3/26 (11.5%)	0.033[b]
Stage (III/IV)	65/226 (28.8%)	4/16 (25.0%)	0.972[a]	72/211 (34.1%)	20/40 (50.0%)	0.056
Recurrence	18/227 (7.9%)	3/16 (18.8%)	0.304[a]	20/212 (9.4%)	11/40 (27.5%)	0.003[a]
Mortality	6/227 (2.6%)	1/16 (6.3%)	0.383[b]	4/212 (1.9%)	5/40 (12.5%)	0.004[a]

[a]Continuity Correction.
[b]Fisher's Exact Test.

10.3389/fendo.2023.1076640

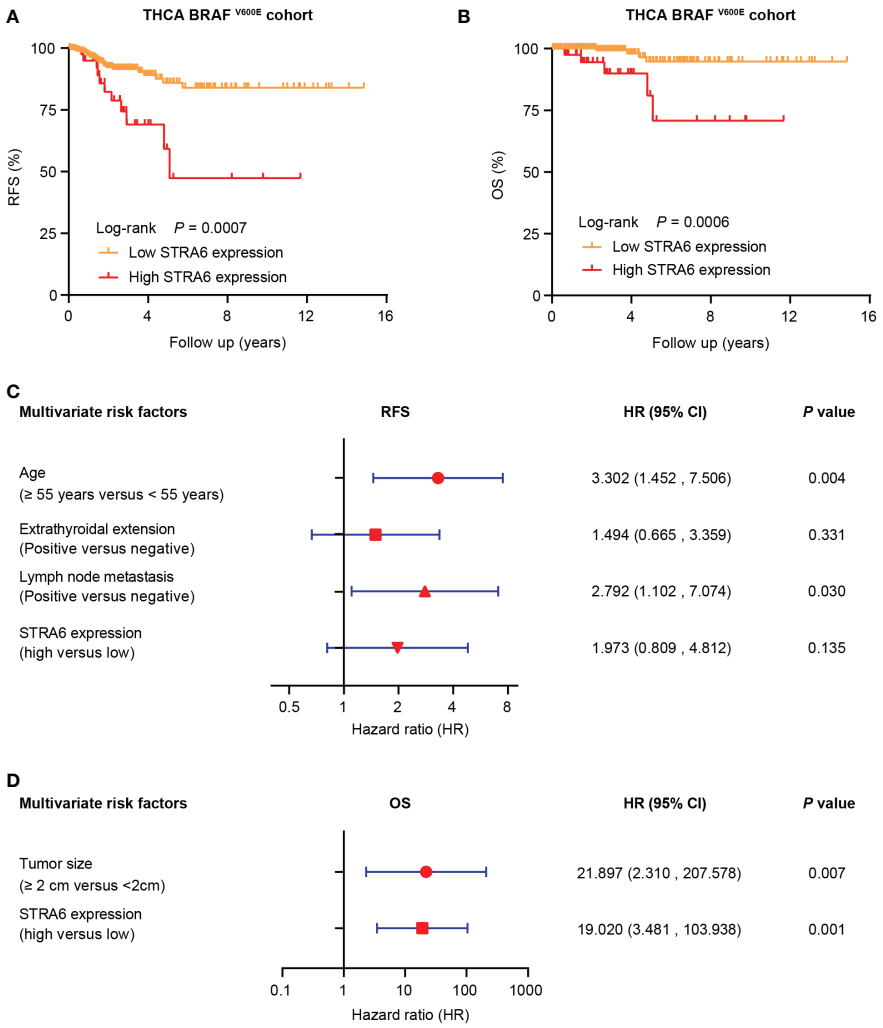

FIGURE 2
STRA6 predicts poor prognosis for BRAF-mutant PTC. **(A)** Kaplan–Meier survival curves of recurrence-fee survival (RFS) according to STRA6 expression in BRAF-mutant PTC. Prognostic cutoff value was identified as 10.3 using X-Tile. **(B)** Kaplan-Meier analysis of overall survival (OS) based on STRA6 expression in PTC patients with BRAF mutation. **(C)** Multivariate Cox regression analysis of the risk factors for recurrence in BRAF-mutant PTC. All bars represented 95% confidence intervals (95% CI). **(D)** Multivariate Cox regression analysis of the risk factors for mortality in BRAF-mutant PTC. All bars corresponded to 95% CI.

STRA6 is correlated with immune infiltration in thyroid carcinoma

Given immune infiltration takes part in tumor progression, we performed Gene Set Enrichment Analysis (GSEA) with transcriptome data from the TCGA cohort. The results showed that samples with high STRA6 expression enriched in the IL2-STAT5 signaling pathway (Figure 4A). STRA6 expression was positively correlated with the mRNA level of IL2, STAT5a and STAT5b (Figure 4B). IL2 is a critical immunomodulatory cytokine, which increases Tregs and induces CD8+ T cell exhaustion *via* activation of STAT5. Thus, we evaluated the association between STRA6 expression and immune cell infiltration in PTC samples. After purity adjustment, upregulation of STRA6 was correlated with abundance of Tregs. However, STRA6 expression was negatively correlated with the infiltration of CD8+ T cells (Figure 4C). We also assessed the expression of exhausted T cells markers, including LAG3, PDCD1G2, CTLA4, HAVCR2, PRDM1 and GZMB in the TCGA cohort. STRA6 was positively correlated with most T cell exhaustion markers (Figure 4D). Pan-caner analysis also revealed the role of STRA6 in inducing T cell exhaustion (Figure 4E). Tregs were significantly abundant in high-STRA6 PTC, while CD8+ T cells had a lower infiltration level (Figure 4F). The infiltration of other immune cells was also correlated with STRA6 expression, including NK cells, neutrophils, MDSCs, macrophages, myeloid dendritic cells, monocytes and B cells (Figure S2A).

To confirm the role of STRA6 in Tregs and CD8+ T cells infiltration, we performed fluorescent multiplex immunohistochemistry (mIHC) in PTC with different STRA6 expression. Samples with high STRA6 expression were mainly infiltrated with FoxP3+ Tregs while CD8+ T cells were mainly observed in samples with low STRA6 expression (Figures 5A, B). Adjacent thyroid tissues were less infiltrated with immune cells (Figure 5C). Upregulation of STRA6 was associated with lower CD8 + cells and higher Tregs infiltrates (Figure 5D), which was consistent with the infiltration level of immune cells in PTC with BRAF mutation (Figures S3A, B). Therefore, STRA6 may limit antitumor immunity and induce immunosuppressive tumor microenvironment in TC.

10.3389/fendo.2023.1076640

TABLE 3 Hazard ratios of high STRA6 expression vs low STRA6 expression in risk of recurrence and mortality in the THCA cohort with respect to BRAF status.

	HR (95%CI)	*P* value	Adjusted HR (95% CI)	*P* value
Entire TCGA cohort				
Recurrence	2.98 (1.62, 5.48)	<0.001	2.39 (1.20, 4.76)	0.013
Mortality	4.67 (1.69, 12.87)	0.003	4.29 (1.30, 14.16)	0.017
Wild-type BRAF subtype				
Recurrence	2.55 (0.75, 8.69)	0.136	–	–
Mortality	2.53 (0.30, 21.37)	0.395	–	–
BRAF V600E subtype				
Recurrence	3.32 (1.59, 6.96)	0.001	1.97 (0.81, 4.81)	0.135
Mortality	7.12 (1.91, 26.56)	0.003	19.02 (3.48, 103.94)	0.001

"-" means not applicable.

STRA6 promotes epithelial-mesenchymal transition *via* increased cancer-associated fibroblasts infiltration in thyroid carcinoma

(CAF) Cancer-associated fibroblast is one of the important components in tumor microenvironment. CAFs infiltration was positively associated with the expression of STRA6 (Figure 6A). We also analyzed the expression level of CAFs markers in PTC. COLA1, COLA2 and COL3A1 were all upregulated in high-STRA6 samples (Figure 6B). Compared with low-STRA6 group, CAFs were abundant in high-STRA6 group (Figure 6C). Higher infiltration level of CAFs was also observed in BRAF-mutant PTC (Figure S3C). CAFs play important roles in cancer development *via* regulation of metastasis. The results of GSEA showed that the TNFα/NF-κB signaling pathway and Epithelial-Mesenchymal Transition (EMT) hallmark gene set was significantly enriched in high-STRA6 PTC (Figures 6D, E). Consistently, the mRNA expression of STRA6 was positively correlated with the expression of EMT markers, including Vimentin (r = 0.1446), MMP7 (r = 0.5345), MMP9 (r = 0.3594), MMP14 (r = 0.4984) (Figure 6F). Taken together, STRA6 may promote TC metastasis *via* CAF-mediated EMT process.

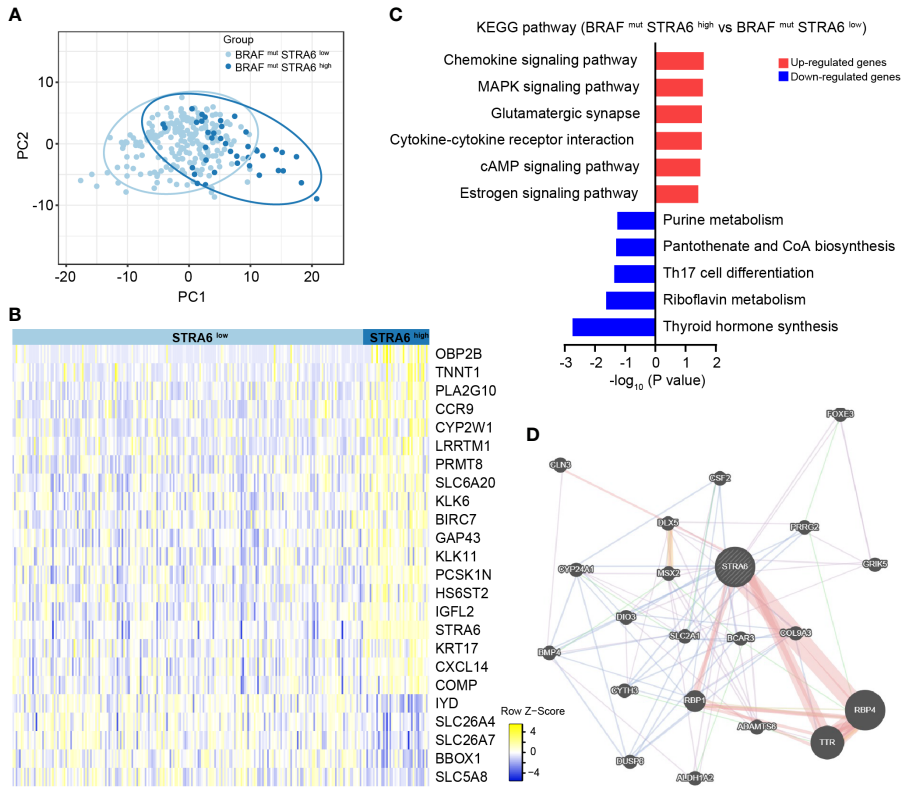

FIGURE 3
STRA6 plays immunoregulatory and oncogenic roles in BRAF-mutated PTC. **(A)** Principal component analysis (PCA) plot of BRAF-mutated samples based on STRA6 expression. **(B)** Differently expressed genes (DEGs) between high-STRA6 group and low-STRA6 group. **(C)** Kyoto Encyclopedia of Genes and Genomes (KEGG) pathway enrichment analysis based on upregulated genes and downregulated genes. **(D)** Proteins interacted with STRA6 were predicted by GeneMANIA.

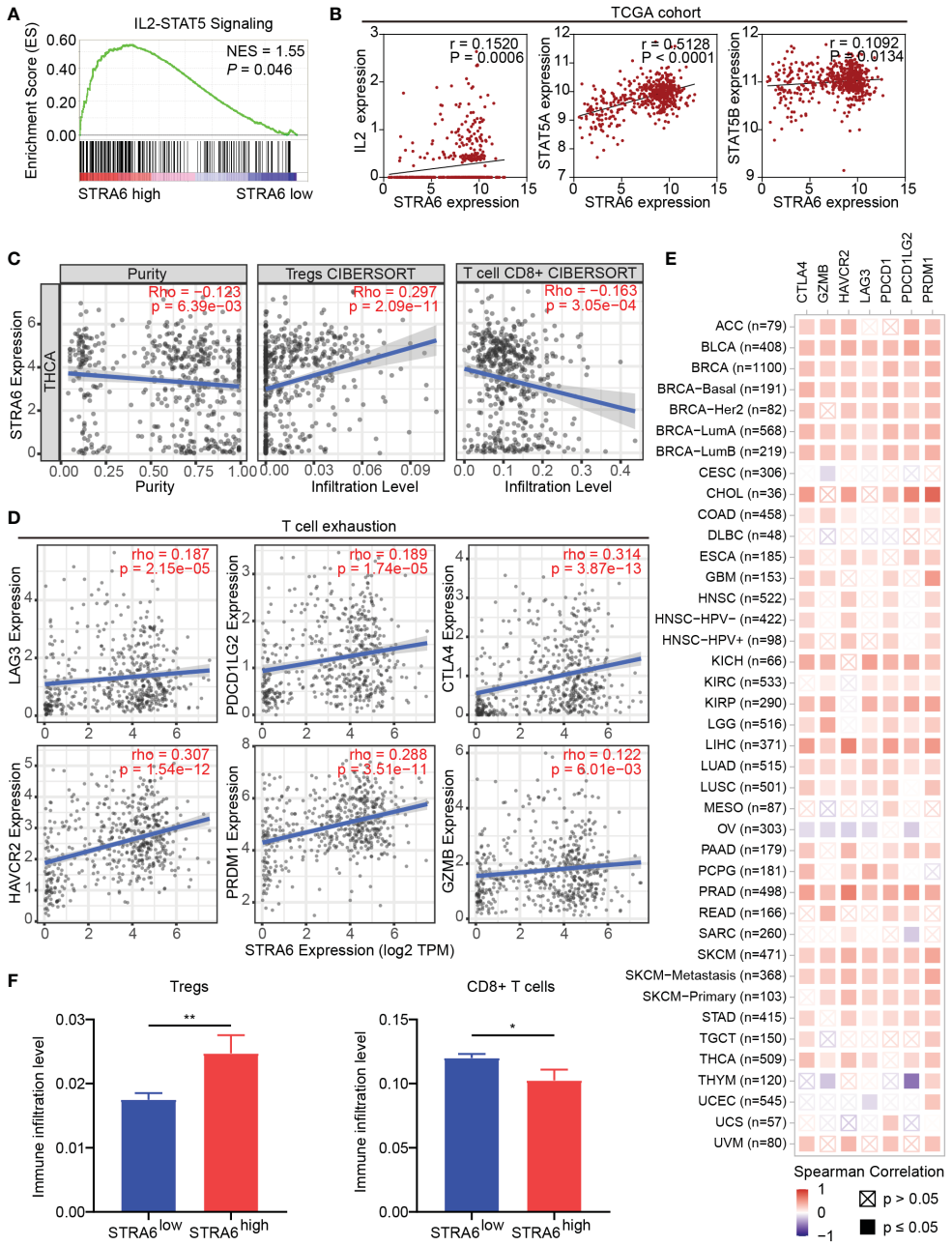

FIGURE 4
STRA6 regulates immunosuppressive microenvironment *via* the IL2-STAT5 signaling pathway. **(A)** Gene set enrichment analysis (GSEA) of the IL2-STAT5 signaling pathway enriched in samples with high-STRA6 expression. **(B)** Correlation of the expression of STRA6 and key molecules in the IL2-STAT5 pathway. **(C)** The correlation of STRA6 expression with infiltration of Tregs and CD8+ T cells according to the TCGA datasets. **(D)** Scatterplots of correlations between STRA6 expression and T cell exhaustion markers in the TCGA cohort. **(E)** Spearman correlations between STRA6 expression and T cell exhaustion markers in pan-cancer. **(F)** Immune infiltration level of Tregs and CD8+ T cells in PTC based on STRA6 expression. (*p < 0.05, **p < 0.01. The data are shown as the mean ± SEM).

Discussion

As the most common genetic alteration in PTC, the prevalence of BRAF mutation differs in races. Compared with western populations (3), the incidence of BRAF mutation was much higher in Chinese population (4, 21), which was detected in about 75% PTC patients. However, BRAF mutation may not be a single and independent prognostic marker for PTC. Studies revealed that BRAF mutation may not totally associate with clinicopathological characteristics or survival (22, 23). In our study, we found STRA6 is associated with BRAF genotype. Upregulation of STRA6 predicts poor RFS and OS in BRAF-mutant PTC, which is an independent risk factor for mortality. Previous study showed that $BRAF^{V600E}$ mutation was significantly correlated with PTC-related mortality in an unadjusted analysis and the association was no longer significant after adjusting for multiple clinical factors (24). Thus, our study indicated that STRA6 may act as a prognostic marker, which may provide

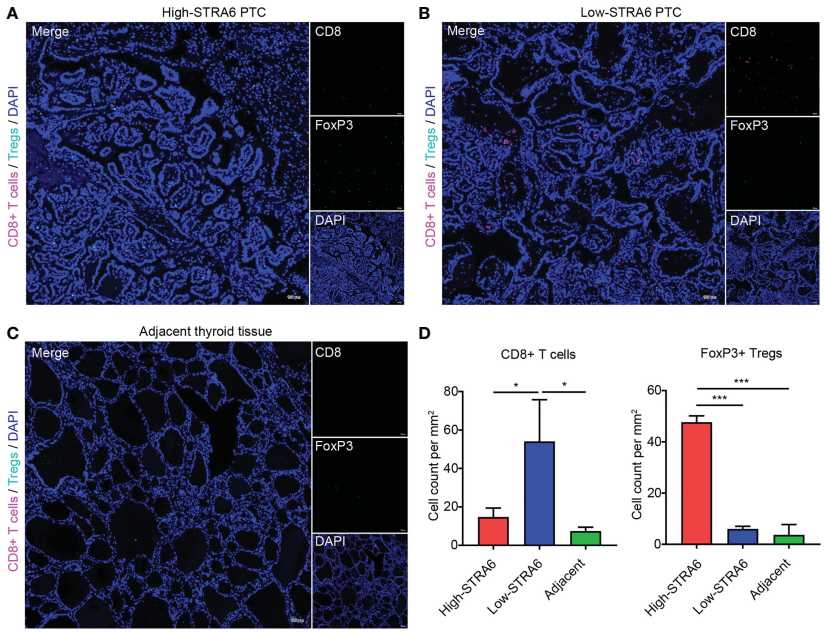

FIGURE 5
STRA6 increases Tregs abundance and inhibits CD8+ T cells infiltration in PTC. **(A–C)** Representative images of fluorescent multiplex immunohistochemistry (mIHC) in high-STRA6 PTC, low-STRA6 PTC and adjacent thyroid tissue. CD8+ T cells were stained with CD8α and Tregs were stained with FoxP3. Nuclei were stained with DAPI. **(D)** Positive Tregs and CD8+ T cells were counted in each group. (*p < 0.05, ***p < 0.001. The data are shown as the mean ± SD).

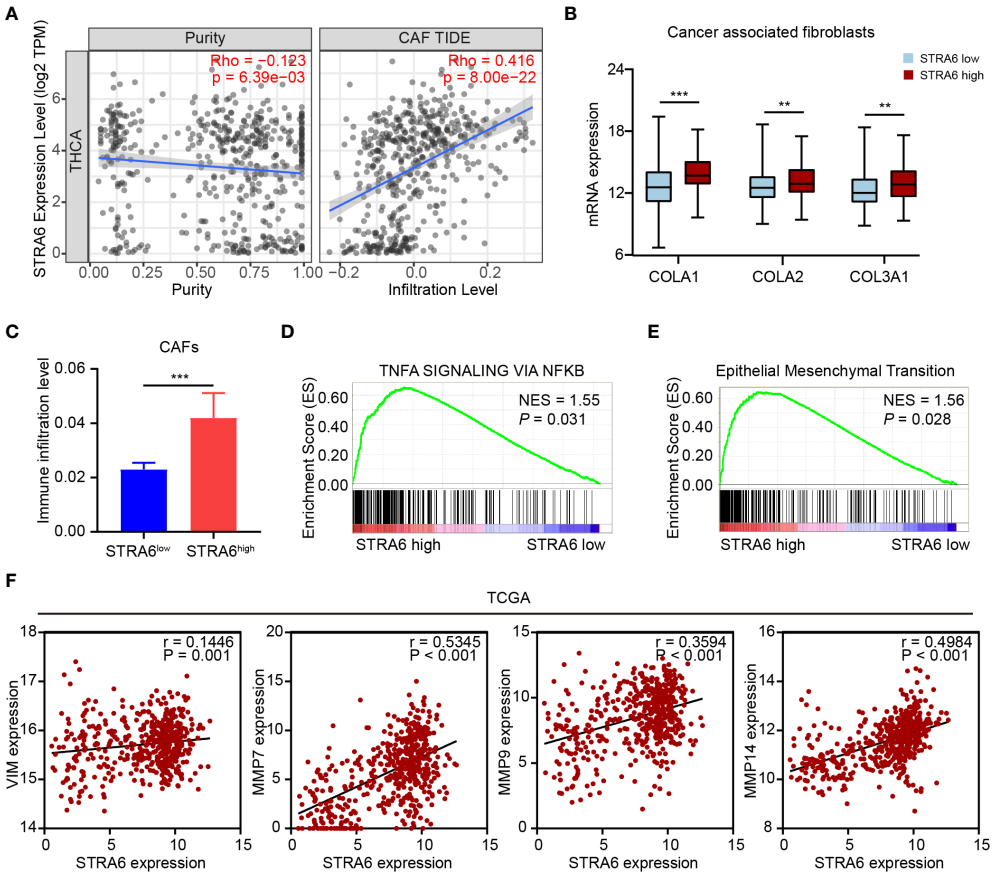

FIGURE 6
STRA6 promotes EMT process *via* increased CAFs infiltration. **(A)** The correlation of STRA6 expression with CAFs infiltration after purity adjustment. **(B)** mRNA expression of CAFs markers in PTC based on STRA6 expression. **(C)** Infiltration level of CAFs in low-STRA6 PTC and high-STRA6 PTC. **(D, E)** GSEA results of TNFα/NF-κB signaling pathway and epithelial mesenchymal transition enrichment according to the TCGA database. **(F)** Scatter plot analysis of correlation between STRA6 mRNA expression and EMT markers. (**p < 0.01, ***p < 0.001. The data are shown as the mean ± SEM).

individualized diagnosis and therapeutic strategy for BRAF-mutant PTC.

We further explored the mechanism of STRA6 in BRAF-mutant PTC progression. Interestingly, when we divided BRAF-mutant PTC into two groups according to STRA6 expression, the MAPK signaling pathway is significantly enriched with the upregulated genes. STRA6 also interacts with several proteins regulated by the MAPK pathway, including BMP4, DIO3, and DUSP6. It was reported that BMP4 can inhibit heat-induced apoptosis by enhancing the activation of ERK (25). DIO3 is increased in PTC through activation of the MAPK pathway (26, 27). DUSP6 is a member of the MAPK phosphatase family and plays pro-tumorigenic role in TC (28, 29). Moreover, BRAF mutation drives aberrant activation of the MAPK pathway (30) and promotes TC tumorigenesis. Dual activation of the MAPK pathway by STRA6 and BRAF mutation, may contribute to the poor survival of BRAF-mutant PTC with high STRA6 expression.

Pathway analyses showed that STRA6 involves in the regulation of the immune interaction and activation of the IL2-STAT5 pathway. Our study also revealed that STRA6 expression is correlated with the infiltration of multiple immune cells. Notably, upregulation of STRA6 results in higher Tregs abundance and lower CD8+ T cells infiltration. Additionally, STRA6 is correlated with T cell exhaustion. In support of our results, IL-2 is mainly produced by activated CD4+ T cells and induces the expansion of Tregs (31). Persistent activation of the IL2-STAT5 pathway triggers CD8+ T cells into exhausted status (32). Decreased infiltration of CD8+ T cells and a low CD8/regulatory T cell ratio in tumors are critical for unfavorable prognosis of cancers (33, 34). Our results also showed that high STRA6 expression is associated with increased CAFs and promotes EMT process, which further explains the worse prognosis in BRAF-mutant PTC. CAFs are one of the most abundant stromal components in the tumor microenvironment. By secreting TGF-β, CCL2, CCL5, IL-6 etc., CAFs recruit immunosuppressive cells into the tumor stroma, which contributes to cancer metastasis and progression (35). The secretion of various cytokines promotes aggressive phenotypes in tumor cells *via* the activation of EMT process (36). We also confirmed $BRAF^{V600E}$ mutation was associated with suppressive immune cell infiltration (37). In hence, immune suppression mediated by STRA6 and BRAF contributes to PTC progression synergistically.

Taken together, STRA6 is overexpressed in TC and associated with BRAF mutation. Upregulation of STRA6 predicts unfavorable prognosis for BRAF-mutant PTC. High STRA6 expression is correlated with decreased CD8+ T cells as well as abundant Tregs and CAFs, which induces immunosuppressive microenvironment in TC. Moreover, STRA6 may play an oncogenic role *via* the MAPK pathway and EMT process. In conclusion, STRA6 might be a prognostic marker for BRAF-mutant PTC and individualized therapeutic strategies for the patients are needed.

Data availability statement

The original contributions presented in the study are included in the article/Supplementary Material. Further inquiries can be directed to the corresponding authors.

Ethics statement

The studies involving human participants were reviewed and approved by the Institutional Research Ethics Committee of The First Affiliated Hospital of Sun Yat-sen University. The patients/participants provided their written informed consent to participate in this study.

Author contributions

HX, SH and WH conceived and designed the study. WH, JG, and XW performed the bioinformatic analysis. WH and YS performed immunohistochemistry and fluorescent multiplex immunohistochemistry. WH analyzed the data and wrote the manuscript with the approval of all other authors. BL collected tissue samples. SY and YL gave critical comments. HX and SH supervised the study. All authors contributed to the article and approved the submitted version.

Funding

This work was supported by the General Program of the National Natural Science Foundation of China (No. 82072956) and the Youth Program of the National Natural Science Foundation of China (No. 81802677).

Conflict of interest

The authors declare that the research was conducted in the absence of any commercial or financial relationships that could be construed as a potential conflict of interest.

Publisher's note

Supplementary material

The Supplementary Material for this article can be found online at: https://www.frontiersin.org/articles/10.3389/fendo.2023.1076640/full#supplementary-material

References

1. Bray F, Ferlay J, Soerjomataram I, Siegel RL, Torre LA, Jemal A. Global cancer statistics 2018: GLOBOCAN estimates of incidence and mortality worldwide for 36 cancers in 185 countries. *CA Cancer J Clin* (2018) 68(6):394–424. doi: 10.3322/caac.21492

2. Zaballos MA, Santisteban P. Key signaling pathways in thyroid cancer. *J Endocrinol* (2017) 235(2):R43–61. doi: 10.1530/JOE-17-0266

3. Cancer Genome Atlas Research N. Integrated genomic characterization of papillary thyroid carcinoma. *Cell* (2014) 159(3):676–90. doi: 10.1016/j.cell.2014.09.050

4. Wang Z, Tang P, Hua S, Gao J, Zhang B, Wan H, et al. Genetic and clinicopathologic characteristics of papillary thyroid carcinoma in the Chinese population: High BRAF mutation allele frequency, multiple driver gene mutations, and RET fusion may indicate more advanced TN stage. *Onco Targets Ther* (2022) 15:147–57. doi: 10.2147/OTT.S339114

5. Xing M, Alzahrani AS, Carson KA, Shong YK, Kim TY, Viola D, et al. Association between BRAF V600E mutation and recurrence of papillary thyroid cancer. *J Clin Oncol* (2015) 33(1):42–50. doi: 10.1200/JCO.2014.56.8253

6. Haugen BR, Alexander EK, Bible KC, Doherty GM, Mandel SJ, Nikiforov YE, et al. 2015 American Thyroid association management guidelines for adult patients with thyroid nodules and differentiated thyroid cancer: The American thyroid association guidelines task force on thyroid nodules and differentiated thyroid cancer. *Thyroid* (2016) 26(1):1–133. doi: 10.1089/thy.2015.0020

7. Li X, Kwon H. The impact of BRAF mutation on the recurrence of papillary thyroid carcinoma: A meta-analysis. *Cancers (Basel)* (2020) 12(8):2056. doi: 10.3390/cancers12082056

8. Niederer-Wust SM, Jochum W, Forbs D, Brandle M, Bilz S, Clerici T, et al. Impact of clinical risk scores and BRAF V600E mutation status on outcome in papillary thyroid cancer. *Surgery* (2015) 157(1):119–25. doi: 10.1016/j.surg.2014.07.015

9. Zhong M, Kawaguchi R, Costabile B, Tang Y, Hu J, Cheng G, et al. Regulatory mechanism for the transmembrane receptor that mediates bidirectional vitamin a transport. *Proc Natl Acad Sci U S A.* (2020) 117(18):9857–64. doi: 10.1073/pnas.1918540117

10. Lin L, Xiao J, Shi L, Chen W, Ge Y, Jiang M, et al. STRA6 exerts oncogenic role in gastric tumorigenesis by acting as a crucial target of miR-873. *J Exp Clin Cancer Res* (2019) 38(1):452. doi: 10.1186/s13046-019-1450-2

11. Nakamura S, Kanda M, Shimizu D, Sawaki K, Tanaka C, Hattori N, et al. STRA6 expression serves as a prognostic biomarker of gastric cancer. *Cancer Genomics Proteomics* (2020) 17(5):509–16. doi: 10.21873/cgp.20207

12. Berry DC, Levi L, Noy N. Holo-retinol-binding protein and its receptor STRA6 drive oncogenic transformation. *Cancer Res* (2014) 74(21):6341–51. doi: 10.1158/0008-5472.CAN-14-1052

13. Karunanithi S, Levi L, DeVecchio J, Karagkounis G, Reizes O, Lathia JD, et al. RBP4-STRA6 pathway drives cancer stem cell maintenance and mediates high-fat diet-induced colon carcinogenesis. *Stem Cell Rep* (2017) 9(2):438–50. doi: 10.1016/j.stemcr.2017.06.002

14. Muniz-Hernandez S, Velazquez-Fernandez JB, Diaz-Chavez J, Mondragon-Fonseca O, Mayen-Lobo Y, Ortega A, et al. STRA6 polymorphisms are associated with EGFR mutations in locally-advanced and metastatic non-small cell lung cancer patients. *Front Oncol* (2020) 10:579561. doi: 10.3389/fonc.2020.579561

15. Schreiber RD, Old LJ, Smyth MJ. Cancer immunoediting: integrating immunity's roles in cancer suppression and promotion. *Science* (2011) 331(6024):1565–70. doi: 10.1126/science.1203486

16. French JD, Weber ZJ, Fretwell DL, Said S, Klopper JP, Haugen BR. Tumor-associated lymphocytes and increased FoxP3+ regulatory T cell frequency correlate with more aggressive papillary thyroid cancer. *J Clin Endocrinol Metab* (2010) 95(5):2325–33. doi: 10.1210/jc.2009-2564

17. French JD, Kotnis GR, Said S, Raeburn CD, McIntyre RCJr., Klopper JP, et al. Programmed death-1+ T cells and regulatory T cells are enriched in tumor-involved lymph nodes and associated with aggressive features in papillary thyroid cancer. *J Clin Endocrinol Metab* (2012) 97(6):E934–43. doi: 10.1210/jc.2011-3428

18. Ryder M, Ghossein RA, Ricarte-Filho JC, Knauf JA, Fagin JA. Increased density of tumor-associated macrophages is associated with decreased survival in advanced thyroid cancer. *Endocr Relat Cancer* (2008) 15(4):1069–74. doi: 10.1677/ERC-08-0036

19. You W, Ouyang J, Cai Z, Chen Y, Wu X. Comprehensive analyses of immune subtypes of stomach adenocarcinoma for mRNA vaccination. *Front Immunol* (2022) 13:827506. doi: 10.3389/fimmu.2022.827506

20. Hong S, Xie Y, Cheng Z, Li J, He W, Guo Z, et al. Distinct molecular subtypes of papillary thyroid carcinoma and gene signature with diagnostic capability. *Oncogene* (2022) 41(47):5121-5132. doi: 10.1038/s41388-022-02499-0

21. Liang J, Cai W, Feng D, Teng H, Mao F, Jiang Y, et al. Genetic landscape of papillary thyroid carcinoma in the Chinese population. *J Pathol* (2018) 244(2):215–26. doi: 10.1002/path.5005

22. Al-Masri M, Al-Shobaki T, Al-Najjar H, Iskanderian R, Younis E, Abdallah N, et al. BRAF V600E mutation in papillary thyroid carcinoma: it's relation to clinical features and oncologic outcomes in a single cancer centre experience. *Endocr Connect* (2021) 10(12):1531–7. doi: 10.1530/EC-21-0410

23. Ito Y, Yoshida H, Maruo R, Morita S, Takano T, Hirokawa M, et al. BRAF mutation in papillary thyroid carcinoma in a Japanese population: its lack of correlation with high-risk clinicopathological features and disease-free survival of patients. *Endocr J* (2009) 56(1):89–97. doi: 10.1507/endocrj.K08E-208

24. Xing M, Alzahrani AS, Carson KA, Viola D, Elisei R, Bendlova B, et al. Association between BRAF V600E mutation and mortality in patients with papillary thyroid cancer. *JAMA* (2013) 309(14):1493–501. doi: 10.1001/jama.2013.3190

25. Deng H, Ravikumar TS, Yang WL. Bone morphogenetic protein-4 inhibits heat-induced apoptosis by modulating MAPK pathways in human colon cancer HCT116 cells. *Cancer Lett* (2007) 256(2):207–17. doi: 10.1016/j.canlet.2007.06.008

26. Romitti M, Wajner SM, Ceolin L, Ferreira CV, Ribeiro RV, Rohenkohl HC, et al. MAPK and SHH pathways modulate type 3 deiodinase expression in papillary thyroid carcinoma. *Endocr Relat Cancer* (2016) 23(3):135–46. doi: 10.1530/ERC-15-0162

27. Romitti M, Wajner SM, Zennig N, Goemann IM, Bueno AL, Meyer EL, et al. Increased type 3 deiodinase expression in papillary thyroid carcinoma. *Thyroid* (2012) 22(9):897–904. doi: 10.1089/thy.2012.0031

28. Degl'Innocenti D, Romeo P, Tarantino E, Sensi M, Cassinelli G, Catalano V, et al. DUSP6/MKP3 is overexpressed in papillary and poorly differentiated thyroid carcinoma and contributes to neoplastic properties of thyroid cancer cells. *Endocr Relat Cancer* (2013) 20(1):23–37. doi: 10.1530/ERC-12-0078

29. Lee JU, Huang S, Lee MH, Lee SE, Ryu MJ, Kim SJ, et al. Dual specificity phosphatase 6 as a predictor of invasiveness in papillary thyroid cancer. *Eur J Endocrinol* (2012) 167(1):93–101. doi: 10.1530/EJE-12-0010

30. Xing M. Molecular pathogenesis and mechanisms of thyroid cancer. *Nat Rev Cancer* (2013) 13(3):184–99. doi: 10.1038/nrc3431

31. Boyman O, Sprent J. The role of interleukin-2 during homeostasis and activation of the immune system. *Nat Rev Immunol* (2012) 12(3):180–90. doi: 10.1038/nri3156

32. Liu Y, Zhou N, Zhou L, Wang J, Zhou Y, Zhang T, et al. IL-2 regulates tumor-reactive CD8(+) T cell exhaustion by activating the aryl hydrocarbon receptor. *Nat Immunol* (2021) 22(3):358–69. doi: 10.1038/s41590-020-00850-9

33. Piersma SJ, Jordanova ES, van Poelgeest MI, Kwappenberg KM, van der Hulst JM, Drijfhout JW, et al. High number of intraepithelial CD8+ tumor-infiltrating lymphocytes is associated with the absence of lymph node metastases in patients with large early-stage cervical cancer. *Cancer Res* (2007) 67(1):354–61. doi: 10.1158/0008-5472.CAN-06-3388

34. Sato E, Olson SH, Ahn J, Bundy B, Nishikawa H, Qian F, et al. Intraepithelial CD8+ tumor-infiltrating lymphocytes and a high CD8+/regulatory T cell ratio are associated with favorable prognosis in ovarian cancer. *Proc Natl Acad Sci U S A.* (2005) 102(51):18538–43. doi: 10.1073/pnas.0509182102

35. Chen X, Song E. Turning foes to friends: targeting cancer-associated fibroblasts. *Nat Rev Drug Discovery* (2019) 18(2):99–115. doi: 10.1038/s41573-018-0004-1

36. Fiori ME, Di Franco S, Villanova L, Bianca P, Stassi G, De Maria R. Cancer-associated fibroblasts as abettors of tumor progression at the crossroads of EMT and therapy resistance. *Mol Cancer* (2019) 18(1):70. doi: 10.1186/s12943-019-0994-2

37. Angell TE, Lechner MG, Jang JK, Correa AJ, LoPresti JS, Epstein AL. BRAF V600E in papillary thyroid carcinoma is associated with increased programmed death ligand 1 expression and suppressive immune cell infiltration. *Thyroid* (2014) 24(9):1385–93. doi: 10.1089/thy.2014.0134

frontiers | Frontiers in Endocrinology

TYPE Original Research
PUBLISHED 10 February 2023
DOI 10.3389/fendo.2023.1109439

OPEN ACCESS

EDITED BY
Jose Federico Carrillo,
National Institute of Cancerology (INCAN), Mexico

REVIEWED BY
Renfei Wang,
Shanghai Jiao Tong University Affiliated Sixth People's Hospital, China
Chentian Shen,
Shanghai Sixth People's Hospital, China

*CORRESPONDENCE
Jun Liang
liangjun1959@aliyun.com
Yansong Lin
linys@pumch.cn

†These authors have contributed equally to this work and share first authorship

SPECIALTY SECTION
This article was submitted to Thyroid Endocrinology, a section of the journal Frontiers in Endocrinology

RECEIVED 27 November 2022
ACCEPTED 27 January 2023
PUBLISHED 10 February 2023

CITATION
Meng C, Song J, Long W, Mu Z, Sun Y, Liang J and Lin Y (2023) A user-friendly nomogram for predicting radioiodine refractory differentiated thyroid cancer. *Front. Endocrinol.* 14:1109439. doi: 10.3389/fendo.2023.1109439

A user-friendly nomogram for predicting radioiodine refractory differentiated thyroid cancer

Chao Meng[1,2,3,4†], Juanjuan Song[5†], Wen Long[6], Zhuanzhuan Mu[2,3], Yuqing Sun[2,3], Jun Liang[1,4*] and Yansong Lin[2,3*]

[1]Department of Oncology, Key Laboratory of Carcinogenesis and Translational Research (Ministry of Education/Beijing), Peking University Cancer Hospital & Institute, Beijing, China, [2]Department of Nuclear Medicine, State Key Laboratory of Complex Severe and Rare Diseases, Peking Union Medical College (PUMC) Hospital, Chinese Academy of Medical Sciences & PUMC, Beijing, China, [3]Beijing Key Laboratory of Molecular Targeted Diagnosis and Therapy in Nuclear Medicine, Beijing, China, [4]Department of Oncology, Peking University International Hospital, Beijing, China, [5]Department of Nuclear Medicine, Peking University International Hospital, Beijing, China, [6]Department of Nuclear Medicine, State Key Laboratory of Oncology in South China, Sun Yat-sen University Cancer Center, Guangzhou, China

Background: The diagnosis of radioiodine refractory differentiated thyroid cancer (RAIR-DTC) is primarily based on clinical evolution and iodine uptake over the lesions, which is still time-consuming, thus urging a predictive model for timely RAIR-DTC informing. The aim of this study was to develop a nomogram model for RAIR prediction among DTC patients with distant metastases (DM).

Methods: Data were extracted from the treatment and follow-up databases of Peking Union Medical College Hospital between 2010 and 2021. A total of 124 patients were included and divided into RAIR (n=71) and non-RAIR (n=53) according to 2015 ATA guidelines. All patients underwent total thyroidectomy followed by at least two courses of RAI treatment. Serological markers and various clinical, pathological, genetic status, and imaging factors were integrated into this study. The pre-treatment stimulated Tg and pre- and post-treatment suppressed Tg at the first and second course RAI treatment were defined as s-Tg1, s-Tg2, sup-Tg1, and sup-Tg2, respectively. Δs-Tg denoted s-Tg1/s-Tg2, and Δs-TSH denoted s-TSH1/s-TSH2. Multivariate logistic regression and correlation analysis were utilized to determine the independent predictors of RAIR. The performance of the nomogram was assessed by internal validation and receiver operating characteristic (ROC) curve, and benefit in clinical decision-making was assessed using decision curve.

Results: In univariate logistic regression, nine possible risk factors were related to RAIR. Correlation analysis showed four of the above factors associated with RAIR. Through multivariate logistic regression, Δs-Tg/Δs-TSH<1.50 and age upon diagnosis were obtained to develop a convenient nomogram model for predicting RAIR. The model was internally validated and had good predictive efficacy with an AUC of 0.830, specificity of 0.830, and sensitivity of 0.755. The decision curve also showed that if the model is used for clinical decision-making when the probability threshold is between 0.23 and 0.97, the net benefit of patients is markedly higher than that of the TreatAll and TreatNone control groups. By using

1.50 as a cut-off ofΔs-Tg/Δs-TSH, differing biochemical progression among the generally so-called RAIR can be further stratified as meaningfully rapidly or slowly progressive patients (P=0.012).

Conclusions: A convenient user-friendly nomogram model was developed with good predictive efficacy for RAIR. The progression of RAIR can be further stratified as rapidly or slowly progressive by using 1.50 as a cut-off value of Δs-Tg/Δs-TSH.

KEYWORDS

neoplasm metastasis, thyroid cancer, thyroglobulin, radioiodine refractory, nomogram

Introduction

The incidence of thyroid cancer has kept rising globally (1). Differentiated thyroid cancer (DTC)accounts for more than 90% of thyroid cancers and consists mainly of papillary thyroid cancer (PTC) and follicular thyroid cancer (FTC) (2, 3). Most DTCs carry a favorable prognosis after thyroidectomy, selective radioactive iodine (RAI) treatment, and thyroid stimulating hormone (TSH) -suppressive treatment. However, roughly 7-23% of DTC patients develop distant metastases (DM) (4–6). Among these patients, two-thirds become radioiodine refractory DTC (RAIR-DTC) and have a much lower 10-year survival rate than those RAI responsive patients (10 vs. 56%), which is the most common cause of cancer-related deaths, and pose a great challenge in the management of DTC (7–9). Given the lack of benefit of repeated RAI treatment to these patients and the increasing risk of side effects, timely identifying the RAIR-DTC is imperative for such patients to avoid unnecessary RAI treatment and gain more time for the effective treatment regimen like Multi-Kinase Inhibitors (MKIs).

The definition of RAIR has been outlined in the 2015 ATA guidelines (10), which are mainly based on imaging manifestation characterized by the loss of radioiodine uptake and increasing level of the tumor marker thyroglobulin (Tg). Of note, the diagnosis of RAIR-DTC is primarily based on clinical evolution and iodine uptake characteristics rather than pathological characteristics. While controversies existed particularly in terms of the predictive value of ^{131}I whole body scan (^{131}I-WBS) imaging and imaging heterogeneity among multiple metastases (11). Thus the ultimate identification still requires long-term follow-up after RAI treatment, which is time-consuming and often induces a delayed judgment that deprives access to timely and effective therapeutic approaches.

Over recent years, clinicopathological characteristics, as well as molecular features, have been recognized as meaningful indicators that could be utilized for RAIR prediction. And factors like older age, larger primary tumor size, extrathyroidal extension (ETE), BRAF^{V600E} mutation, TERT promoter mutation, and high-risk histological subtypes were reported to be correlated with RAIR-DTC respectively, according to different retrospective studies, with an unfavorable median overall survival (OS) (12–14). While factors identified in each study alone still showed poor performance in predicting individual risk of RAIR, thus a predictive model is needed to integrate multiple factors as a whole. The nomogram is an effective model that takes the weights of relevant factors into consideration and integrates the independent factors for predicting the risk probability of a special clinical event, which is valuable for clinical decision-making and risk stratification (15, 16). Only two studies have reported the nomogram model to predict RAIR-DTC so far to our knowledge, which mainly took static clinicopathologic and costly ^{18}F-FDG PET/CT molecular imaging features into account, while both of which lacked dynamic assessment and were not universally available due to economic burden (17, 18). While Tg as the most critical real-time tumor marker was ignored, which has an irreplaceable role in the follow-up and management of thyroid cancer after surgery to predict recurrence and metastasis and assess long-term survival (19–22).

This study aims to develop a prediction nomogram model of RAIR by integrating serological markers such as Tg, various clinical, pathological, genetic status, and imaging factors for predicting RAIR among patients with DM-DTC.

Patients and methods

The study protocol was approved by the ethical board of the Chinese Academy of Medical Sciences and Peking Union Medical College Hospital (PUMCH).

Patients

In this retrospective study, we extracted data for all DM-DTC patients (n=369) from 2205 thyroid cancer patients treated with total or near-total thyroidectomy followed by RAI treatment between 2010 and 2021, with follow-up through November 1, 2021. Patients with DM-DTC were defined with any of the following: ① metastatic lesions confirmed by pathology, ② focal or diffuse uptake in metastatic lesions on ^{131}I-WBS after excluding the contamination and physiological RAI uptake, with or without positive findings on other complementary imaging modalities (chest CT, x-rays, MRI, bone scintigraphy or ^{18}F-FDG PET/CT) or elevated Tg levels, ③ positive findings on ^{18}F-FDG PET/CT after excluding other malignancies and benign diseases, with a rising Tg level, despite of the negative ^{131}I-WBS results, ④ negative findings on functional imaging, but structural lesions suggested by other imaging instruments with a rising Tg level after excluding other malignancies and benign diseases. Patients' exclusion criteria with either of the following: ① no distant metastatic lesions identified on

imaging, ② absence of serial serological data, ③ absence of information on the first two rounds of RAI treatment, ④ absence of follow-up information.

RAIR definition was based on the 2015 ATA guidelines: (i) the malignant/metastatic tissue does not ever concentrate RAI (no uptake outside the thyroid bed at the first therapeutic WBS), (ii) the tumor tissue loses the ability to concentrate RAI after previous evidence of RAI-avid disease (in the absence of stable iodine contamination), (iii) RAI is concentrated in some lesions but not in others; and (iv) metastatic disease progresses despite significant concentration of RAI (10). A total of 124 DM-DTC patients were finally enrolled (Figure 1). The overall median follow-up was 51.5 months (interquartile range:32.75,70.00 months). Patients were further divided into non-RAIR and RAIR.

Postoperative RAI treatment

A serum thyroid stimulating hormone (TSH) level higher than 30mU/L was achieved by thyroid hormone withdrawal (THW) before RAI treatment. All patients were instructed with a low iodine diet from the beginning of THW to 3 weeks after RAI treatment. Patients were administrated with a range of 3.7–7.4GBq (100-200mCi) RAI treatment dose. Repeated RAI treatment was usually performed 6 to 12 months after the previous treatment.

Stimulated or suppressed Tg (s-Tg or sup-Tg), TSH, and thyroglobulin antibody (TgAb) were usually tested 1 day before and 2–3 months after RAI treatment. S-Tg was defined as Tg measured after THW with a TSH level>30 mU/L. The s-Tg and TSH on the day of the first (s-Tg1, s-TSH1) and second (s-Tg2, s-TSH2) course of RAI

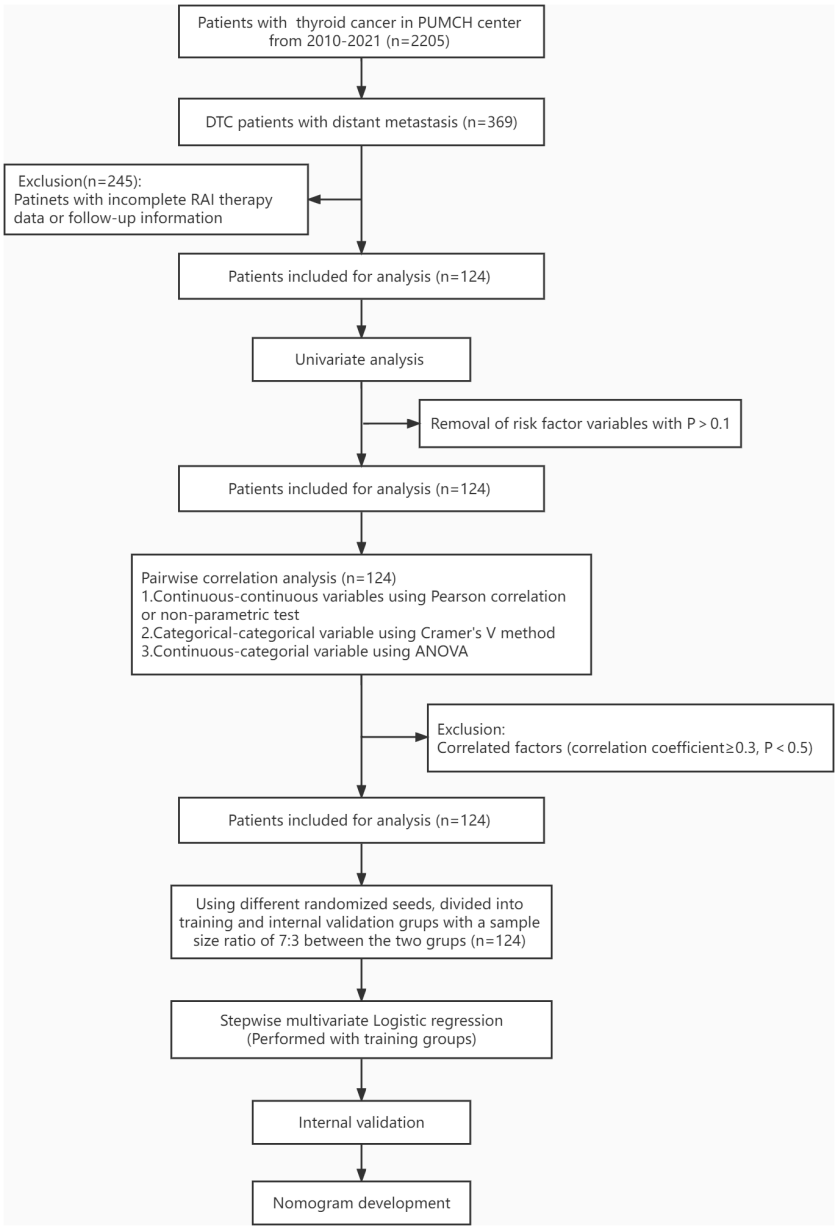

FIGURE 1
Workflow for patient selection and development of the nomogram model to predict RAIR among DM-DTC patients. PUMCH, Peking Union Medical College Hospital; RAIR, radioiodine refractory; DM, distant metastases; DTC, differentiated thyroid cancer.

treatment and the suppressed Tg at 1 to 3 months before (sup-Tg1) and 3 months after (sup-Tg2) the second RAI treatment were further analyzed to detect the prediction value. Post-therapeutic whole-body scan (Rx-WBS) was performed 5–7 days after RAI treatment. CT without contrast was carried out as needed. All patients were under TSH suppressive treatment using sodium levothyroxine to achieve a TSH level<0.1μIU/mL during courses of RAI treatment and subsequent follow-up.

Measurement of Tg, TgAb and TSH

Tg and TgAb levels were determined by electrochemiluminescence immunoassay (Roche Diagnostics GmbH, Mannheim, Germany) with a functional sensitivity of 0.100 ng/mL and 10 IU/mL, respectively. TSH was determined by chemiluminescence immunoassay (Siemens Healthcare Diagnostics Inc, New York, New York, USA), with a measuring range from 0.004 to 150μIU/mL. TgAb values>115 IU/mL were considered positive. Rx-WBS was obtained in the anterior and posterior projections using dual-head gamma cameras (Infinia Hawkeye; GE, Fairfield, Connecticut, USA) equipped with high-energy parallel-hole collimators, and a 20% energy window was centered at 364 keV, at a table speed of 20 cm/min for a total time of 15 min (256×1024 matrix).

Biochemical progression

The sup-Tg level in all samples with TSH level<0.1μIU/mL and TgAb negativity (≤115IU/mL) was examined. Biochemical progression was defined as>20% increase in sup-Tg level at follow-up compared with that after thyroid remnant ablation (23).

Gene analysis

Genomic DNA was extracted from either primary or lymph-node metastatic DTC tumors, which were sliced into 5μm-thick sections, fixed with formalin and embedded in paraffin. BRAF and TERT mutations were analyzed by real-time fluorescent quantitative polymerase chain reaction (PCR). Exon 15 of the BRAF gene containing the site for the T1799A (V600E) mutation was amplified using primers 5'- TGCTTGCTCTGA TAGGAAAA TG-3'(sense) and 5'-AGCCTCAA TTCTTACCA TCCA-3'(antisense). The TERT promoter includes two mutation hotspots: C228T and C250T. A 193-bp fragment of the TERT promoter was amplified by PCR using approximately 100 ng of genomic DNA and primers 5'-CACCCGTCCTGCCCCTTCACCTT-3'(sense) and 5'-GGCTTCCCACGTGCGCAGCAGGA-3'(antisense). The real-time fluorescent quantitative PCR protocol comprised an initial denaturation for 5 min at 95°C, 15 cycles of template enrichment (denaturation for 25 s at 95°C, annealing for 20 s at 64°C, and extension for 20 s at 72°C), and 31 amplification cycles (denaturation for 25 s at 93°C, annealing for 35 s at 60°C, and amplification cycles (denaturation for 25 s at 93°C, annealing for 35 s at 60°C, and DNA Analyzer.

Data processing and statistical analysis

All factors included in the analysis were divided into categorical and continuous variables, with no special processing for the former. Continuous variable were handled as follows: ① remove outliers: Data less than the 1st quartile minus1.5 times the quartile difference were replaced with the 5% quantile and data greater than the 3rd quartile plus 1.5 times the quartile difference were replaced with the 95% quantile; ② remove the Tg for TgAb>115 IU/ml; ③ ROC curves were plotted for each continuous variable against the RAIR status, and variables with AUC value>0.7 were then transformed to corresponding categorical variables. A dataset was then derived after removing highly subjective variables such as TSH levels, cumulative dose, and cumulative number of RAI treatment. Very incomplete variables were removed to get the final dataset. Univariate and multivariate logistic regression was then applied to this dataset. Figure 1 shows the workflow chart for patient selection and model construction.

Statistical analysis was performed using the R software (version 4.1.2). The packages in R that were used in this study are reported in the Data Supplementary. The reported statistical significance levels between groups were all two-sided, with statistical significance set at 0.05.

The Kaplan-Meier and log-rank analyses were used to assess Tg progression-free survival (Tg-PFS).

Results

Clinicopathologic characteristics of patients

Of 124 patients included in the analysis, 118 (95.2%) had PTC, 5 (4.0%) had FTC and 1 (0.8%) had PTC combined with FTC. The baseline clinicopathologic characteristics of 124 DM-DTC patients, including 42 men and 82 women, with a male/female ratio of 1:1.95, are summarized in Table 1. With the criteria for judgment, 71 patients were identified as RAIR, 53 as non-RAIR, and one RAIR case fulfilled criteria ii and iii. Patients with RAIR were more likely to be older upon diagnosis and with more advanced T staging (P=0.021 and 0.015, respectively). RAIR tended to have higher capsular invasion rate and larger tumor size (P=0.059 and 0.147, respectively). There were no statistical differences in terms of gender, tumor lesion, multifocality, and N staging.

Serological characteristics in RAIR and non-RAR patients

Serological follow-up was performed on 124 patients with DM-DTC before and after the first and second RAI treatment (Table 1). TSH, Tg and TgAb results did not differ between the two groups before and after the first RAI treatment. Both s-Tg2 and sup-Tg2 were significantly higher in RAIR group (P=0.02, and 0.027, respectively). Additionally, Δs-Tg (s-Tg1/s-Tg2) was remarkably lower in RAIR than the in non-RAIR group (P<0.001). To minimize the influence of TSH, Δs-Tg/Δs-TSH (s-TSH1/s-TSH2) was also calculated in the analyses. Δs-Tg/Δs-TSH in RAIR was significantly lower compared to non-RAIR (P<0.001) and was also more evident than that of Δs-Tg. A cut-off value of Δs-Tg/Δs-TSH at 1.50 was obtained with a sensitivity of 0.831, specificity of 0.792, and AUC of 0.818, respectively (Figure 2).

10.3389/fendo.2023.1109439

TABLE 1 Clinicopathologic Characteristics of 124 Patients with DM-DTC.

Characteristics	Total (N=124)	Non-RAIR (N=53)	RAIR (N=71)	*P*
Age upon diagnosis (year) [mean (SD)]	35.10 (15.60)	31.38 (12.59)	37.89 (17.08)	0.021
Gender [n (%)]				0.578
Mela	42 (33.90)	16 (30.20)	26 (36.6)	
Female	82 (66.10)	37 (69.80)	45 (63.40)	
Tumor largest dimension (cm) [mean (SD)]	2.58 (1.72)	2.31 (1.59)	2.80 (1.80)	0.147
Cervical lymph node dissection [n (%)]				0.418
Yes	117 (94.40)	52 (98.10)	65 (91.50)	
No	7 (5.60)	1 (1.90)	6 (8.50)	
Pathological subtype [n (%)]				0.098
Classic PTC	29 (23.40)	15 (28.30)	14 (19.70)	
Follicular-variant PTC	36 (29.00)	19 (35.80)	17 (23.90)	
Other subtypes	21 (16.90)	6 (11.30)	15 (21.10)	
Unavailable	38 (30.60)	13 (24.50)	25 (35.20)	
Tumor lesion [n (%)]				0.441
Unilateral	59 (47.60)	28 (52.80)	31 (43.70)	
Bilateral	64 (51.60)	25 (47.20)	39 (54.90)	
Unavailable	1 (0.80)	0 (0.00)	1 (1.40)	
Multifocality [n (%)]				0.351
One lesion	36 (29.00)	19 (35.80)	17 (23.90)	
More than one lesion	80 (64.50)	31 (58.50)	49 (69.00)	
Unavailable	8 (6.50)	3 (5.70)	5 (7.00)	
Capsular invasion [n (%)]				0.059
Yes	102 (82.30)	40 (75.50)	62 (87.30)	
No	12 (9.70)	9 (17.00)	3 (4.20)	
Unavailable	10 (8.10)	4 (7.50)	6 (8.50)	
$BRAF^{V600E}$ mutation [n (%)]				0.085
Yes	44 (35.50)	14 (26.40)	30 (42.30)	
No	63 (50.80)	33 (62.30)	30 (42.30)	
Unavailable	17 (13.70)	6 (11.30)	11 (15.50)	
TERT mutation [n (%)]				0.04
Yes	12 (9.70)	1 (1.90)	11 (15.50)	
No	46 (37.10)	21 (39.60)	25 (35.20)	
Unavailable	66 (53.20)	31 (58.50)	35 (49.30)	
AJCC-T Stage [n (%)]				0.015
T1	31 (25.0)	21 (39.6)	10 (14.10)	
T2	12 (9.7)	4 (7.5)	8 (11.30)	
T3	17 (13.7)	4 (7.5)	13 (18.30)	
T4	55 (44.4)	21 (39.6)	34 (47.90)	
Unavailable	9 (7.3)	3 (5.7)	6 (8.50)	

(Continued)

TABLE 1 Continued

Characteristics	Total (N=124)	Non-RAIR (N=53)	RAIR (N=71)	*P*
AJCC-N Stage [n (%)]				0.235
N0	3 (2.40)	1 (1.90)	2 (2.80)	
N1a	12 (9.70)	6 (11.30)	6 (8.50)	
N1b	100 (80.60)	45 (84.90)	55 (77.50)	
Unavailable	9 (7.30)	1 (1.90)	8 (11.30)	
Serological characteristics (ng/mL) [median (IQR)]				
s-Tg1	344.10 (62.74,500.0)	361.40 (93.14,500.0)	342.20 (60.34-500.0)	0.636
sup-Tg1	14.31 (4.75,77.51)	12.73 (2.76-69.0)	16.30 (5.03-80.04)	0.573
s-Tg2	189.96 (57.23, 500.6)	119.8 (38.44, 466)	250.2 (78.89, 603.6)	0.02
sup-Tg2	11.10 (3.15, 70.44)	7.73 (2.0, 42.37)	16.94 (6.2, 87.49)	0.027
Δs-Tg [median (IQR)]	1.06 (0.92, 1.71)	1.69 (1.00,3.7)	1.00 (0.75,1.27)	<0.001
Δs-Tg/Δs-TSH [median (IQR)]	1.37 (0.95, 2.68)	2.42 (1.58-4.11)	1.05 (0.79-1.4)	<0.001
Δs-Tg/Δs-TSH<1.50 [n (%)]				<0.001
Yes	69 (55.6)	11 (20.8)	58 (81.7)	
No	55 (44.4)	42 (79.2)	13 (18.3)	
Cumulative RAI dose (mCi) [median (IQR)]	340 (300, 450)	450.00 (300, 540)	300.00 (300, 450)	0.05
Number of RAI treatment [n (%)]				0.263
2	63 (50.8)	22 (41.5)	41 (57.7)	
3	35 (28.2)	16 (30.2)	19 (26.8)	
4	12 (9.7)	9 (17.0)	3 (4.2)	
>4	14 (11.3)	6 (11.3)	8 (11.3)	
RAIR according to 2015 ATA guidelines [n (%)]				
i			36 (50.7)	
ii			5 (7.04)	
iii			15 (21.13)	
iv			16 (22.54)	

DM, distant metastases; DTC, differentiated thyroid cancer; RAI, radioactive iodine; Δs-Tg, s-Tg1/s-Tg2; Δs-TSH, s-TSH1/ s-TSH2.

Results of univariate logistic regression and correlation analysis

Univariate logistic regression demonstrated that sup-TgAb1, s-Tg2, sup-Tg2, Δs-Tg, Δs-Tg/Δs-TSH, Δs-Tg/Δs-TSH<1.50, age upon diagnosis, $BRAF^{V600E}$ mutation, and AJCC-T stage were opted risk factors for RAIR (*P*<0.1, Table 2), among which sup-TgAb1, sup-Tg2, $BRAF^{V600E}$ mutation, and AJCC-T stage were removed from dataset due to data incompleteness. The remaining possible risk factors were included into the correlation analysis. Risk factors with a correlation coefficient greater than 0.3 were considered to be correlated factors. In correlation analysis, Δs-Tg was removed because of correlation with both s-Tg2 (correlation factor=-0.323) and Δs-Tg/Δs-TSH(correlation factor=0.743), leaving the following four factors to be opt-independent risk factors: s-Tg2, Δs-Tg/Δs-TSH, Δs-Tg/Δs-TSH<1.50, and age upon diagnosis.

Multivariate analysis, internal validation, and logistic model construction

Totally, 70% of cases were randomly selected as the training set, and then stepwise multivariate logistic regression was performed using the MASS package (7.3-54) of R. The left 30% of cases were selected as the validation set. Two independent risk factors, Δs-Tg/Δs-TSH<1.50 and age upon diagnosis, were eventually screened for predicting RAIR. The above procedure was performed five times with different randomization seeds, and the results were reliable (Figure 3, Table 3). We then used the two factors (Δs-Tg/Δs-TSH<1.50 and age upon diagnosis) as independent risk factors to generate a linear Logistic regression model to predict RAIR. Based on the two independent factors obtained in stepwise multiple Logistic regression analysis, a nomogram characterized by scale line and score weight reflected to RAIR-DTC prediction was established in

10.3389/fendo.2023.1109439

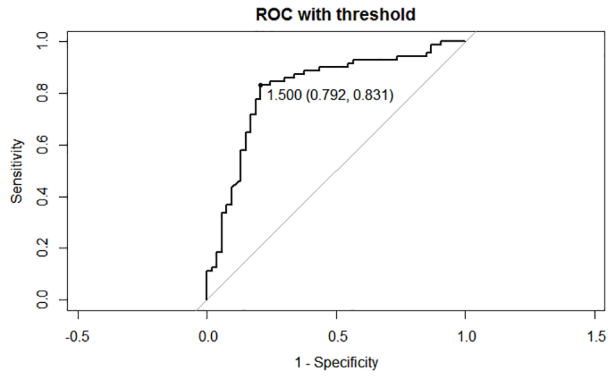

FIGURE 2
Receiver operating characteristic (ROC) curves of the cut-off of Δs-Tg/Δs-TSH. AUC: 0.818, cutoff value:1.50, sensitivity:0.831, specificity: 0.792. Δs-Tg: s-Tg1/ s-Tg2, Δs-TSH: s-TSH1/ s-TSH2, AUC: Area Under Curve.

Figures 4A, B; the AUC of the model is 0.830, with a specificity of 0.830 and sensitivity of 0.755. The calibration and decision curves for our final model are also shown in Figures 4C, D, with the p-value for the Hosmer-Lemeshow test for the former being greater than 0.05, indicating our model's probability of predicting RAIR is not significantly different from the actual RAIR situation. The latter shows that our model outperforms the two control groups of TreatAll and TreatNone in terms of the net benefit to patients' clinical decision-making over a relatively significant threshold probability range of 0.24-0.97.

Impact of Δs-Tg/Δs-TSH cut-off value of 1.50 on Tg-PFS in RAIR patients

The results of the Kaplan-Meier and log-rank analyses of Tg-PFS in patients with RAIR are provided below. The median Tg-PFS (mTg-PFS) in 124 patients was 37 months (95% CI: 37.83-48.82 months). The mTg-PFS was 24.4 months (95% CI: 25.93-38.23 months) and 56 months (95% CI:49.91-66.88months) for RAIR and non-RAIR patients, respectively. An obviously shorter Tg-PFS was observed in RAIR than in non-RAIR ($\chi2$ = 43.345, *P*=0.000) (Figure 5A).

In the RAIR group, the mTg-PFS was 20.49 months (95% CI: 21.89-33.71 months) for 58 patients with Δs-Tg/Δs-TSH<1.50 and 43.00 months (95% CI:31.58-70.76 months) for 13 patients with Δs-Tg/Δs-TSH≥1.50. The log-rank test showed a significantly shorter Tg-PFS in the former patients compared to the latter ($\chi2$ = 6.316, P =0.012) (Figure 5B).

Discussion

In the present study, we retrospectively developed and validated a nomogram model for predicting RAIR in patients with DM-DTC by integrating serological markers and various clinical, pathological, genetic status, and imaging factors. Based on univariate logistic regression, nine possible risk factors were significantly related to RAIR. And correlation analysis showed that four of the above factors displayed associations with RAIR. Two independent predictors of RAIR were finally confirmed in multivariate logistic regression analysis: Δs-Tg/Δs-TSH and age upon diagnosis, with the former parameter derived from Tg, which would be a dichotomous variable reflecting the dynamic s-Tg changing rate with the cut-off of 1.50. Internal validation was used to determine that the model had good predictive power to predict RAIR. The decision curve with net benefits was further used to assess the model's better clinical predictive value.

Tg has been reported to be a specific biomarker produced by thyroid tissue and DTC lesions, which is well acknowledged as convenient, reproducible, and sensitive to be monitored, particularly after remnant thyroid ablation (10). It plays an essential role in the surveillance of thyroid cancer after surgery to reveal recurrence, metastasis and assess long-term survival (24). Previous researches from our team have shown that qualitative assessment of the Tg levels can help to grade the risk of recurrence and predict metastasis and RAIR in DTC patients with pulmonary metastases (20, 25). The change of Tg during TSH stimulation, such as ΔTg/ΔTSH, can be used as a specific early biochemical marker for DM-DTC (22). Wang C et al. further analyzed the percentage change of Tg before and after RAI treatment, namely ΔTg, during the first two courses in DM-DTC patients receiving multiple RAIs and showed that it was informative for RAIR (25). Based upon the above findings, Δs-Tg/

TABLE 2 Results of univariate logistic regression.

Characteristics	*P*	Characteristics	*P*
Age upon diagnosis	0.023*	s-Tg1	0.13
Gender	0.127	sup-Tg1	0.287
Tumor largest dimension	0.153	sup-TgAb1	0.092*
Cervical lymph node dissection	0.111	s-Tg2	0.050*
Tumor lesion	0.288	sup-Tg2	0.039*
Multifocality	0.16	Δs-Tg	0.020*
$BRAF^{V600E}$ mutation	0.037*	Δs-Tg/Δs-TSH	0.001*
AJCC-T Stage	0.083*	Δs-Tg/Δs-TSH<1.5	<0.01*
AJCC-N Stage	0.392		

*P<0.05, Δs-Tg: s-Tg1/s-Tg2, Δs-TSH: s-TSH1/ s-TSH2.

10.3389/fendo.2023.1109439

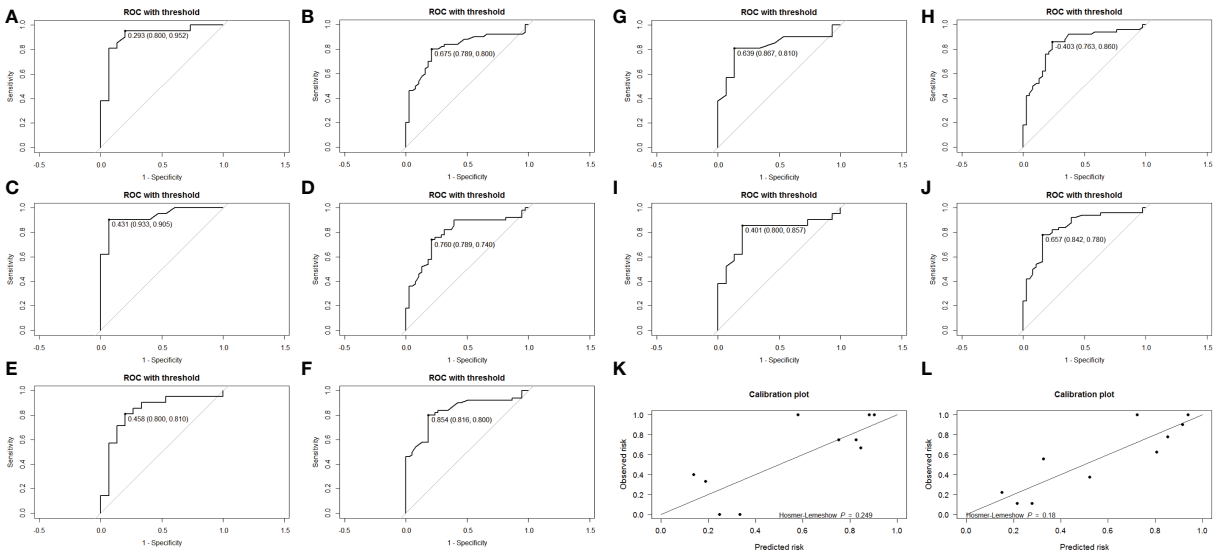

FIGURE 3
Receiver operating characteristic (ROC) curves for the internal validation set **(A, C, E, G, I)** and the training set **(B, D, F, H, J)**. Calibration plots for the last internal validation of the model, training set **(L)**, and validation set **(K)**.

TABLE 3 Results of stepwise multivariate logistic regression on five random samples.

Independent risk factors	training set AUC	Internal validation set		
		AUC	Sensitivity	Specificity
Δs-Tg/Δs-TSH<1.50, Age upon diagnosis	0.810	0.913	0.952	0.800
	0.788	0.933	0.905	0.933
	0.834	0.832	0.810	0.800
	0.837	0.825	0.810	0.867
	0.842	0.805	0.857	0.800

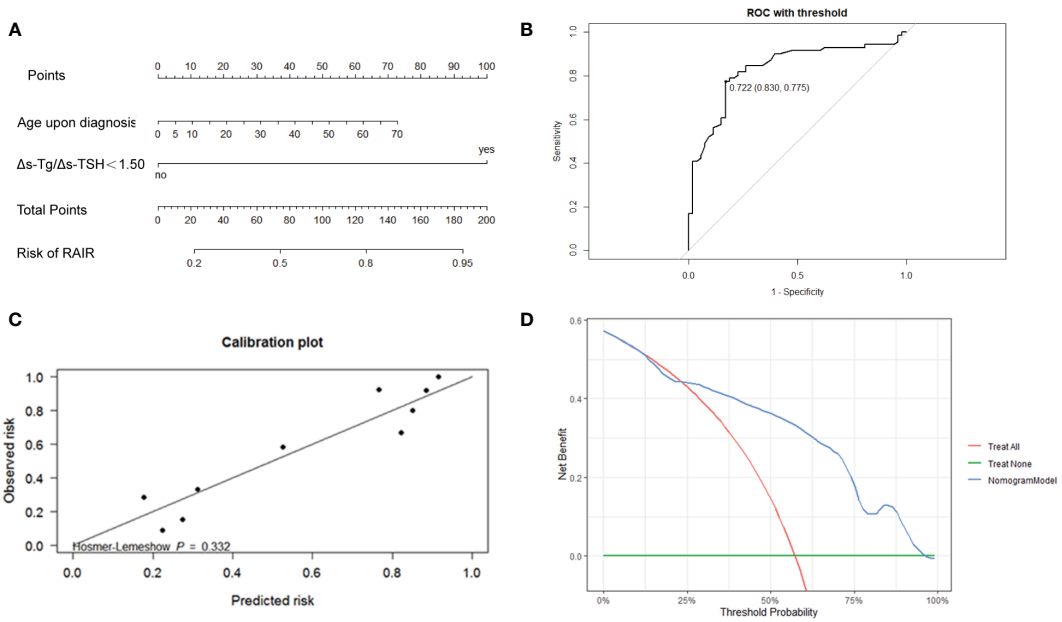

FIGURE 4
(A) Nomogram to develop the risk of RAIR-DTC in DTC patients with distant metastasis. **(B)** ROC curves of the nomogram model for predicting RAIR. AUC:0.830, sensitivity:0.775, specificity: 0.830. The cut-off value of risk of RAIR is 0.722. **(C)** Calibration curve. **(D)** Decision curve.

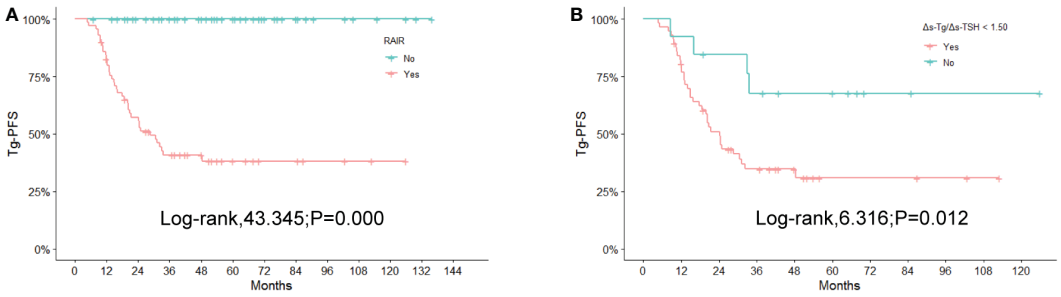

FIGURE 5
Kaplan-Meier curves for Tg-PFS **(A)** between non-RAIR and RAIR patients, **(B)** between RAIR patients with 1.50 of Δs-Tg/Δs-TSH as the cutoff value. RAIR, radioiodine refractory; Tg-PFS, thyroglobulin progression-free survival.

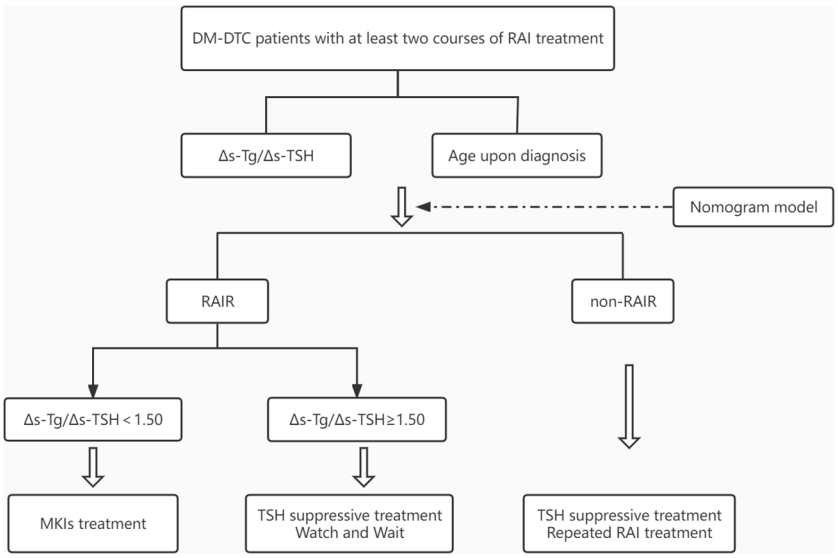

FIGURE 6
Flowchart for predicting RAIR and active surveillance of patients with DM-DTC. DM, distant metastases; DTC, differentiated thyroid cancer; TSH, thyroid stimulating hormone; MKIs, multi-kinase inhibitors.

Δs-TSH was applied for the first time in this study to predict RAIR. Different from the previous Tg-relevant indicators, such a parameter not only associates Tg with TSH to make it standardized and comparable but also reflects the biochemical efficacy from RAI treatment longitudinally.

Age upon diagnosis was another important independent factor manifested in this study. Age has been associated with thyroid cancer staging, RAIR prediction, and risk of death. Age above 45 and over 55 years old were significant stratification factors in the TNM staging of thyroid cancer to differentiate the risk of death, in its 7th, and 8th editions, respectively (26, 27). Other researchers have reported a significant inverse correlation between RAI avidity and different age cut-offs, such as >45, ≥46, or >55-years-old (13, 25, 28). A predictive value for OS of RAIR can be observed by using 45- and 75-years-old as cut-off, respectively (29). In a nomogram model to predict RAIR developed recently, an age cut-off of 48-years-old has also been integrated as an independent factor (18). Our finding revealed that age was also proved to be a significant predictor for RAIR as a continuous rather than a dichotomous variable in previous studies, which presumably related to the wide range of age in the entire population in our research. Thus, it allows a specific personalized nomogram scoring in patients with different ages upon diagnosis.

Thus, unlike other scoring systems in identifying RAIR with either complex or high-cost index such as ^{18}F-FDG-PET (18), we developed this nomogram model with promising predictive RAIR efficacy using two readily accessible factors described above. We believe it might be a user-friendly tool in routine clinical practice, particularly in China where recombinant human TSH (rhTSH) remains unavailable currently and thyroid hormone withdrawal is the only modality for TSH stimulation, which makes rhTSH aided-diagnostic RAI whole-body scan (DxWBS) for RAIR identification impossible. And due to its economic feasibility and practicability, our nomogram model might be an alternative for some other developing countries, where rhTSH cannot be affordable for most of the patients.

Interestingly, when we further evaluated the biochemical progression using a 20% change of Tg among all the generally so-called RAIR patients defined by ATA criteria, differing biochemical progression can be identified as rapidly or slowly progressive patients

with 1.50 as the Δs-Tg/Δs-TSH cut-off value. Patients with Δs-Tg/Δs-TSH <1.5 were apparently more progressive with a worse prognosis than those ≥1.50. The biochemical response of Tg has been reported to reflect the general tumor burden and progression, and is associated with structural response or relapse assessed by RECIST criteria (23, 30–32). The classification of RAIR has long been argued with controversy, as the four or five clinical scenarios may have different underlying genetic backgrounds and clinical progressions but were dealt with solid arbitrary management (33, 34). With the index derived from our study, different clinical progression might be further identified, which may shed light on the personalized management in RAIR patients, and even be helpful to optimize the currently watchful waiting strategy, and to tailor the timing of initiating systemic therapy such as MKIs from a clinical perspective. A workable flowchart was also suggested in this study to guide the active surveillance among RAIR patients (Figure 6).

Although $BRAF^{V600E}$ mutation has been shown to be associated with RAIR (12, 35, 36), it was not manifested in the present study. We suppose the local genetic features reflected by the primary or regional tumor sites, or the heterogeneity between which might not thoroughly reflect the whole-body tumor genetic background, particularly the inaccessibility of distant metastasis due to ethic concern, while Tg, as a circulating marker, could comprehensively represent the overall biochemical tumor burden.

Our study is inevitably limited by its retrospective and single-center nature. Studies with larger sample sizes as well as multi-centers validation will be conducted subsequently.

In conclusion, we developed a convenient nomogram model integrating with Tg and age, which showed good predictive power for RAIR. By utilizing 1.50 as the cut-off value for Δs-Tg/Δs-TSH, the progression of RAIR may be further classified as a rapidly or slowly progressing group.

Data availability statement

The raw data supporting the conclusions of this article will be made available by the authors, without undue reservation.

Author contributions

JL and YL conceived and designed the study. CM and JS were the major contributors in performing the analysis, writing the manuscript, and preparing the figures and tables with support of WL. CM, JS, ZM, and YS collected samples and clinical parameters. JL and YL participated in the study design and edited the manuscript. All authors contributed to the article and approved the submitted version.

Funding

This work was supported by the Project on National High Level Hospital Clinical Research Funding (No. 2022-PUMCH-B-072) and CAMS Innovation Fund for Medical Sciences (CIFMS) (No. 2020-I2M-2-003).

Conflict of interest

The authors declare that the research was conducted in the absence of any commercial or financial relationships that could be construed as a potential conflict of interest.

Publisher's note

Supplementary material

The Supplementary Material for this article can be found online at: https://www.frontiersin.org/articles/10.3389/fendo.2023.1109439/full#supplementary-material

References

1. Sung H, Ferlay J, Siegel RL, Laversanne M, Soerjomataram I, Jemal A, et al. Global cancer statistics 2020: GLOBOCAN estimates of incidence and mortality worldwide for 36 cancers in 185 countries. *CA: Cancer J Clin* (2021) 71(3):209–49. doi: 10.3322/caac.21660

2. Lim H, Devesa SS, Sosa JA, Check D, Kitahara CM. Trends in thyroid cancer incidence and mortality in the united states, 1974-2013. *Jama* (2017) 317(13):1338–48. doi: 10.1001/jama.2017.2719

3. Sherman SI. Thyroid carcinoma. *Lancet (London England)* (2003) 361(9356):501–11. doi: 10.1016/s0140-6736(03)12488-9

4. Wang LY, Palmer FL, Nixon IJ, Thomas D, Patel SG, Shaha AR, et al. Multi-organ distant metastases confer worse disease-specific survival in differentiated thyroid cancer. *Thyroid* (2014) 24(11):1594–9. doi: 10.1089/thy.2014.0173

5. Mazzaferri EL, Kloos RT. Clinical review 128: Current approaches to primary therapy for papillary and follicular thyroid cancer. *J Clin Endocrinol Metab* (2001) 86(4):1447–63. doi: 10.1210/jcem.86.4.7407

6. Nixon IJ, Whitcher MM, Palmer FL, Tuttle RM, Shaha AR, Shah JP, et al. The impact of distant metastases at presentation on prognosis in patients with differentiated carcinoma of the thyroid gland. *Thyroid* (2012) 22(9):884–9. doi: 10.1089/thy.2011.0535

7. Berdelou A, Lamartina L, Klain M, Leboulleux S, Schlumberger M. Treatment of refractory thyroid cancer. *Endocrine-related Cancer* (2018) 25(4):R209–23. doi: 10.1530/erc-17-0542

8. Durante C, Haddy N, Baudin E, Leboulleux S, Hartl D, Travagli JP, et al. Long-term outcome of 444 patients with distant metastases from papillary and follicular thyroid carcinoma: benefits and limits of radioiodine therapy. *J Clin Endocrinol Metab* (2006) 91(8):2892–9. doi: 10.1210/jc.2005-2838

9. Antonelli A, Ferri C, Ferrari SM, Sebastiani M, Colaci M, Ruffilli I, et al. New targeted molecular therapies for dedifferentiated thyroid cancer. *J Oncol* (2010) 2010:921682. doi: 10.1155/2010/921682

10. Haugen BR, Alexander EK, Bible KC, Doherty GM, Mandel SJ, Nikiforov YE, et al. American Thyroid association management guidelines for adult patients with thyroid nodules and differentiated thyroid cancer: The American thyroid association guidelines task force on thyroid nodules and differentiated thyroid cancer. *Thyroid* (2015) 26(1):1–133. doi: 10.1089/thy.2015.0020

11. Mu ZZ, Zhang X, Lin YS. Identification of radioactive iodine refractory differentiated thyroid cancer. *Chonnam Med J* (2019) 55(3):127–35. doi: 10.4068/cmj.2019.55.3.127

12. Luo Y, Jiang H, Xu W, Wang X, Ma B, Liao T, et al. Clinical, pathological, and molecular characteristics correlating to the occurrence of radioiodine refractory differentiated thyroid carcinoma: A systematic review and meta-analysis. *Front Oncol* (2020) 10:549882. doi: 10.3389/fonc.2020.549882

13. Kersting D, Seifert R, Kessler L, Herrmann K, Theurer S, Brandenburg T, et al. Predictive factors for RAI-refractory disease and short overall survival in PDTC. *Cancers* (2021) 13(7):1728. doi: 10.3390/cancers13071728

14. Liu J, Liu R, Shen X, Zhu G, Li B, Xing M. The genetic duet of BRAF V600E and TERT promoter mutations robustly predicts loss of radioiodine avidity in recurrent papillary thyroid cancer. *J Nucl Med* (2020) 61(2):177–82. doi: 10.2967/jnumed.119.227652

15. Mao Q, Xia W, Dong G, Chen S, Wang A, Jin G, et al. A nomogram to predict the survival of stage IIIA-N2 non-small cell lung cancer after surgery. *J Thorac Cardiovasc Surg* (2018) 155(4):1784–92.e1783. doi: 10.1016/j.jtcvs.2017.11.098

16. Lv J, Liu YY, Jia YT, He JL, Dai GY, Guo P, et al. A nomogram model for predicting prognosis of obstructive colorectal cancer. *World J Surg Oncol* (2021) 19(1):337. doi: 10.1186/s12957-021-02445-6

17. Li G, Lei J, Song L, Jiang K, Wei T, Li Z, et al. Radioiodine refractoriness score: A multivariable prediction model for postoperative radioiodine-refractory differentiated thyroid carcinomas. *Cancer Med* (2018) 7(11):5448–56. doi: 10.1002/cam4.1794

18. Liu Y, Wang Y, Zhang W. Scoring system and a simple nomogram for predicting radioiodine refractory differentiated thyroid cancer: a retrospective study. *EJNMMI Res* (2022) 12(1):45. doi: 10.1186/s13550-022-00917-8

19. Yang X, Liang J, Li T, Zhao T, Lin Y. Preablative stimulated thyroglobulin correlates to new therapy response system in differentiated thyroid cancer. *J Clin Endocrinol Metab* (2016) 101(3):1307–13. doi: 10.1210/jc.2015-4016

20. Yang X, Liang J, Li TJ, Yang K, Liang DQ, Yu Z, et al. Postoperative stimulated thyroglobulin level and recurrence risk stratification in differentiated thyroid cancer. *Chin Med J* (2015) 128(8):1058–64. doi: 10.4103/0366-6999.155086

21. Tian T, Xu Y, Zhang X, Liu B. Prognostic implications of preablation stimulated tg: A retrospective analysis of 2500 thyroid cancer patients. *J Clin Endocrinol Metab* (2021) 106(11):e4688-97. doi: 10.1210/clinem/dgab445

22. Zhao T, Liang J, Li T, Guo Z, Vinjamuri S, Lin Y. Value of serial preablative thyroglobulin measurements: can we address the impact of thyroid remnants? *Nucl Med Commun* (2016) 37(6):632–9. doi: 10.1097/mnm.0000000000000485

23. Mu ZZ, Zhang YQ, Sun D, Lu T, Lin YS. Effect of BRAF(V600E) and TERT promoter mutations on thyroglobulin response in patients with distant-metastatic differentiated thyroid cancer. *Endocrine Pract* (2022) 28(3):265–70. doi: 10.1016/j.eprac.2021.12.005

24. Matthews TJ, Chua E, Gargya A, Clark J, Gao K, Elliott M. Elevated serum thyroglobulin levels at the time of ablative radioactive iodine therapy indicate a worse prognosis in thyroid cancer: an Australian retrospective cohort study. *J Laryngol Otol* (2016) 130(Suppl 4):S50–3. doi: 10.1017/s0022215116008331

25. Wang C, Zhang X, Li H, Li X, Lin Y. Quantitative thyroglobulin response to radioactive iodine treatment in predicting radioactive iodine-refractory thyroid cancer with pulmonary metastasis. *PloS One* (2017) 12(7):e0179664. doi: 10.1371/journal.pone.0179664

26. Onitilo AA, Engel JM, Lundgren CI, Hall P, Thalib L, Doi SA. Simplifying the TNM system for clinical use in differentiated thyroid cancer. *J Clin Oncol* (2009) 27 (11):1872–8. doi: 10.1200/jco.2008.20.2382

27. Kim M, Kim YN, Kim WG, Park S, Kwon H, Jeon MJ, et al. Optimal cut-off age in the TNM staging system of differentiated thyroid cancer: is 55 years better than 45 years? *Clin Endocrinol* (2017) 86(3):438–43. doi: 10.1111/cen.13254

28. Shobab L, Gomes-Lima C, Zeymo A, Feldman R, Jonklaas J, Wartofsky L, et al. Clinical, pathological, and molecular profiling of radioactive iodine refractory differentiated thyroid cancer. *Thyroid* (2019) 29(9):1262–8. doi: 10.1089/thy.2019.0075

29. Saïe C, Wassermann J, Mathy E, Chereau N, Leenhardt L, Tezenas du Montcel S, et al. Impact of age on survival in radioiodine refractory differentiated thyroid cancer patients. *Eur J Endocrinol* (2021) 184(5):667–76. doi: 10.1530/eje-20-1073

30. Bachelot A, Cailleux AF, Klain M, Baudin E, Ricard M, Bellon N, et al. Relationship between tumor burden and serum thyroglobulin level in patients with papillary and follicular thyroid carcinoma. *Thyroid* (2002) 12(8):707–11. doi: 10.1089/105072502760258686

31. Ciappuccini R, Hardouin J, Heutte N, Vaur D, Quak E, Rame JP, et al. Stimulated thyroglobulin level at ablation in differentiated thyroid cancer: the impact of treatment preparation modalities and tumor burden. *Eur J Endocrinol* (2014) 171(2):247–52. doi: 10.1530/eje-14-0192

32. Spaas M, Decallonne B, Laenen A, Billen J, Nuyts S. Prognostic value of stimulated thyroglobulin levels at the time of radioiodine administration in differentiated thyroid cancer. *Eur Thyroid J* (2018) 7(4):211–7. doi: 10.1159/000489849

33. Tuttle RM, Ahuja S, Avram AM, Bernet VJ, Bourguet P, Daniels GH, et al. Controversies, consensus, and collaboration in the use of (131)I therapy in differentiated thyroid cancer: A joint statement from the American thyroid association, the European association of nuclear medicine, the society of nuclear medicine and molecular imaging, and the European thyroid association. *Thyroid* (2019) 29(4):461–70. doi: 10.1089/thy.2018.0597

34. Van Nostrand D. Radioiodine refractory differentiated thyroid cancer: Time to update the classifications. *Thyroid* (2018) 28(9):1083–93. doi: 10.1089/thy.2018.0048

35. Yang K, Wang H, Liang Z, Liang J, Li F, Lin Y. BRAFV600E mutation associated with non-radioiodine-avid status in distant metastatic papillary thyroid carcinoma. *Clin Nucl Med* (2014) 39(8):675–9. doi: 10.1097/rlu.0000000000000498

36. Tchekmedyian V, Dunn L, Sherman E, Baxi SS, Grewal RK, Larson SM, et al. Enhancing radioiodine incorporation in BRAF-mutant, radioiodine-refractory thyroid cancers with vemurafenib and the anti-ErbB3 monoclonal antibody CDX-3379: Results of a pilot clinical trial. *Thyroid* (2022) 32(3):273–82. doi: 10.1089/thy.2021.0

frontiers | Frontiers in Endocrinology

TYPE Original Research
PUBLISHED 17 February 2023
DOI 10.3389/fendo.2023.1122517

OPEN ACCESS

EDITED BY
Erivelto Martinho Volpi,
Centro de Referência no Ensino do Diagnóstico por Imagem (CETRUS), Brazil

REVIEWED BY
Mehmet Haciyanli,
Izmir Katip Celebi University, Türkiye
Guobing Yin,
Second Affiliated Hospital of Chongqing Medical University, China

*CORRESPONDENCE
Liang Shi
liangshi@njmu.edu.cn
Feng Wang
fengwangcn@hotmail.com

†These authors have contributed equally to this work and share first authorship

SPECIALTY SECTION
This article was submitted to Thyroid Endocrinology, a section of the journal Frontiers in Endocrinology

RECEIVED 13 December 2022
ACCEPTED 07 February 2023
PUBLISHED 17 February 2023

CITATION
Yu F, Wu W, Zhang L, Li S, Yao X, Wang J, Ni Y, Meng Q, Yang R, Wang F and Shi L (2023) Cervical lymph node metastasis prediction of postoperative papillary thyroid carcinoma before ^{131}I therapy based on clinical and ultrasound characteristics. *Front. Endocrinol.* 14:1122517. doi: 10.3389/fendo.2023.1122517

Cervical lymph node metastasis prediction of postoperative papillary thyroid carcinoma before ^{131}I therapy based on clinical and ultrasound characteristics

Fei Yu[1†], Wenyu Wu[1†], Liuting Zhang[2†], Shaohua Li[1], Xiaochen Yao[1], Jun Wang[1], Yudan Ni[1], Qingle Meng[1], Rui Yang[1], Feng Wang[1*] and Liang Shi[1*]

[1]Department of Nuclear Medicine, Nanjing First Hospital, Nanjing Medical University, Nanjing, China, [2]Department of Functional Examination, Nanjing First Hospital, Nanjing Medical University, Nanjing, China

Background: The status of lymph nodes is crucial to determine the dose of radioiodine-131(^{131}I) for postoperative papillary thyroid carcinoma (PTC). We aimed to develop a nomogram for predicting residual and recurrent cervical lymph node metastasis (CLNM) in postoperative PTC before ^{131}I therapy.

Method: Data from 612 postoperative PTC patients who underwent ^{131}I therapy from May 2019 to December 2020 were retrospectively analyzed. Clinical and ultrasound features were collected. Univariate and multivariate logistic regression analyses were performed to determine the risk factors of CLNM. Receiver operating characteristic (ROC) analysis was used to weigh the discrimination of prediction models. To generate nomograms, models with high area under the curves (AUC) were selected. Bootstrap internal validation, calibration curves and decision curves were used to assess the prediction model's discrimination, calibration, and clinical usefulness.

Results: A total of 18.79% (115/612) of postoperative PTC patients had CLNM. Univariate logistic regression analysis found serum thyroglobulin (Tg), serum thyroglobulin antibodies (TgAb), overall ultrasound diagnosis and seven ultrasound features (aspect transverse ratio, cystic change, microcalcification, mass hyperecho, echogenicity, lymphatic hilum structure and vascularity) were significantly associated with CLNM. Multivariate analysis revealed higher Tg, higher TgAb, positive overall ultrasound and ultrasound features such as aspect transverse ratio ≥ 2, microcalcification, heterogeneous echogenicity, absence of lymphatic hilum structure and abundant vascularity were independent risk factors for CLNM. ROC analysis showed the use of Tg and TgAb combined with ultrasound (AUC = 0.903 for "Tg+TgAb+Overall ultrasound" model, AUC = 0.921 for "Tg+TgAb+Seven ultrasound features" model) was superior to any single variant. Nomograms constructed for the above two models were validated

internally and the C-index were 0.899 and 0.914, respectively. Calibration curves showed satisfied discrimination and calibration of the two nomograms. DCA also proved that the two nomograms were clinically useful.

Conclusion: Through the two accurate and easy-to-use nomograms, the possibility of CLNM can be objectively quantified before ^{131}I therapy. Clinicians can use the nomograms to evaluate the status of lymph nodes in postoperative PTC patients and consider a higher dose of ^{131}I for those with high scores.

KEYWORDS

papillary thyroid carcinoma, lymph node metastasis, nomogram, ^{131}I, Tg, TgAb, ultrasound

Introduction

The incidence of thyroid cancer has a rapid increase worldwide, and differentiated thyroid cancer (DTC) accounts for more than 90% of thyroid cancer cases (1–3). Papillary thyroid carcinoma (PTC) is the most common type of DTC and cervical lymph node metastasis (CLNM) frequently occurs in PTC (4, 5). Previous researches identified the rate of CLNM reaches approximately 20-30% DTC after systemic treatment (4, 6). CLNM can be classified as central and lateral lymph node metastasis. CLNM was an important risk factor for recurrence in PTC (7, 8). We admit that, although with controversy, lateral lymph node metastasis but not central lymph node metastasis affected the recurrence-free survival as some recent studies reported (9–11).

Ultrasonography has been widely applied to detect CLNM in PTC but displays a relatively low sensitivity (12, 13). Precisely identifying CLNM plays a vital role in the determination of whether central lymph node dissection and/or lateral lymph node dissection should be performed during surgery. To date, some prediction models have been established for preoperative prediction of CLNM in PTC patients. It was discovered that clinical characteristics including age, gender, tumor size, extrathyroidal invasion, multifocality, serum thyroglobulin (Tg), serum thyroglobulin antibodies (TgAb), radiomic and ultrasound characteristics might predict CLNM in PTC (12, 14–17).

Prophylactic central lymph node dissection is frequently performed in PTC patients with moderate and high-risk, while prophylactic lateral lymph node dissection is not generally recommended as a standard treatment (18). In practice, a significant number of lateral lymph node metastasis can remain after surgery and present as recurrence (19). Residual CLNM after initial surgery are mainly due to overlook of lymph node involvement before surgery or during thyroidectomy, or incomplete removal of involved lymph nodes in surgery (20). Radioiodine-131 (^{131}I) therapy that can successfully ablate thyroid cancer cells in both primary and metastatic lesions has been accepted as conventional management for treating moderate and high-risk DTC after operation (18, 21). Radioactive Iodine Ablation reduces the risk of recurrence or death from thyroid cancer patients. The recommended dose for patients receiving it as remnant ablative therapy was 100 mCi. Nonetheless, the ^{131}I dose generally needs to be increased to 100-150 mCi and 150-200 mCi when treating patients with CLNM and/or extra-thyroid extension and distant metastasis, respectively (22). Nevertheless, few models were constructed for predicting residual and recurrent CLNM in postoperative PTC patients before ^{131}I therapy. Effective prediction of the residual and recurrent CLNM status may provide a reference for nuclear medicine doctors to give appropriate and sufficient ^{131}I doses that have enough tumoricidal effects but without increased risk of adverse effects.

Therefore, we aimed to filter out important predictors from medical information and to develop a brief and reliable prediction model (nomogram) for accurate residual and recurrent CLNM in postoperative PTC patients before ^{131}I therapy.

Materials and methods

Patients

The study was approved by the Ethics Committee of Nanjing First Hospital. Consecutive moderate and high-risk PTC patients who underwent ^{131}I therapy from May 2019 to December 2020 at the Department of Nuclear Medicine of Nanjing First Hospital were enrolled. The records of patients were retrospectively reviewed and the exclusion criteria were as follows (1): non-PTCs or other subtypes than classic PTC (such as mixed PTC and so on) (2); age younger than 18 years old (3); patients who underwent non-curable surgery (4); patients with another malignancy (5); patients with distant metastasis (6); history of ^{131}I therapy (7); history of neck radiation (8); incomplete clinical data or missing follow-up. According to the above criteria, 612 patients with PTC were enrolled in this study. All patients underwent total/near-total thyroidectomy and central lymph node dissection with/without lateral lymph node dissection. The flow chart of the selection process was shown in Figure 1.

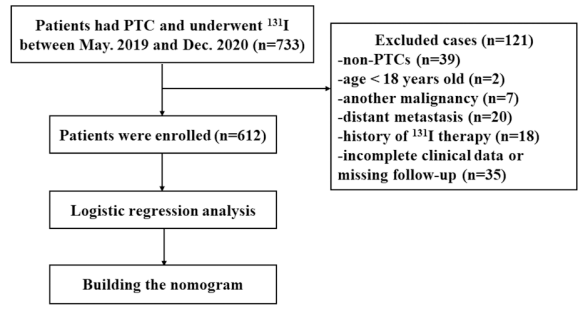

FIGURE 1
Flow chart of the study selection.

Data collection

Clinicopathological factors included age, gender, histological type, stage, tumor size, multifocal or not, serum Tg level, serum TgAb level, results of cervical ultrasound exams, history of ^{131}I therapy and neck radiation were extracted from electronic medical records in our hospital. Multifocality was defined as two or more tumors in the thyroid. The time interval for the first ^{131}I therapy was 3 to 6 months after surgery. Serum Tg level, serum TgAb level and results of ultrasound were measured within one week before ^{131}I therapy in our hospital. Metastasis status of lymph node evaluated by ultrasound was recorded as yes or no. According to overall ultrasound results, one suspicious (when overall ultrasound reported suspicious metastasis) or one normal lymph node (when overall ultrasound reported negative metastasis) was selected to collect ultrasound features including aspect transverse ratio (≥ 2/< 2), cystic change (yes/no), microcalcification (yes/no), mass hyperecho (yes/no), echogenicity (heterogeneous *vs.* homogeneous), lymphatic hilum structure (presence *vs.* absence) and vascularity (abundant *vs.* non-abundant). The ultrasound features were read and recorded by two experienced ultrasound doctors. The golden standard of metastasis status of cervical lymph nodes before ^{131}I was based on cervical SPECT/CT imaging after ^{131}I treatment and follow-up (follow-up time was 12 months). In this study, any residual activity noted on ^{131}I SPECT/CT scan, pathology-proved CLNM during follow-up and imaging revealed suspicious lymph nodes with continuous abnormal Tg during follow-up were defined as CLNM.

Statistical analyses

All statistical analyses were performed using R software version 4.2.1. Continuous variables with normal distribution were expressed as the means ± standard deviations (SD), continuous variables with abnormal distribution were expressed as the median (interquartile range), and categorical variables were reported as numbers and percentages.

A t-test, log-rank test, Pearson's chi-square test or Fisher's exact test was used to compare the baseline characteristics of different groups. Univariate and multivariate backward stepwise logistic regression analyses were used to assess risk factors for CLNM in postoperative PTC patients. Receiver operating characteristic (ROC) curves were used to test the discrimination of our established prediction models and area under the curves (AUC) were compared by Delong test. For models with high AUC values, nomograms were developed to calculate the probability of CLNM. The performance of the nomogram was further evaluated by the calibration chart, which plotted the predicted probability of the nomogram against the observed probability. Bootstrap method (1,000-times) was used for internal validation of the model. A decision curve analysis was also performed to test the clinical usefulness of the nomogram. All tests are two-sided tests and statistical significance level was established at $P < 0.05$.

Results

Patients and clinical characteristics

Baseline characteristics of patients are summarized in Table 1. Among the 612 postoperative PTC patients, including 225 men and 387 women, the average age was 42.44 ± 12.23 years old (ranging from 18 to 79 years old). CLNM was found in 115(18.79%) patients. There were no significant differences in terms of patient age, gender, stage, tumor size and multifocality in the postoperative PTC patients with and without CLNM. The positive rate of ultrasound diagnosis was significantly higher in patients with CLNM (73.91%) than those without CLNM (2.01%). Patients with CLNM had a median Tg level of 8.98 ug/l (interquartile range: 0.89-39.60), while patients without CLNM had a median Tg level of 3.00 ug/l (interquartile range: 0.48-10.23) ($P < 0.001$). Additionally, we found a marginally significant ($P = 0.081$) difference of TgAb (IU/ml) between the two groups (with CLNM: median 2.02, interquartile range 1.02-24.20; without CLNM: median 1.71, interquartile range 0.98-7.15).

Univariate and multivariate predictors for CLNM

The present study identified the potential risk factors for CLNM using univariate and multivariate logistic regression analysis. As shown in Table 2, The univariate analysis identified that levels of Tg ($P < 0.001$), levels of TgAb ($P = 0.009$), overall ultrasound ($P < 0.001$) and seven ultrasound features (all $P < 0.001$) were statistically significant associated with CLNM. CLNM was not significantly related to age, gender, stage, tumor size and multifocal ($P > 0.05$). In the multivariate backward stepwise analysis, Tg ($P = 2.290\times10^{-3}$), TgAb ($P = 6.910\times10^{-3}$) and overall ultrasound ($P < 0.001$) were significantly associated with CLNM. When considering seven ultrasound features, Tg, TgAb and all seven ultrasound features were finally retained in the multivariate model. However, TgAb, cystic change, and mass hyperecho didn't reach statistical significance (P =0.147, 0.060 and 0.091, respectively). These results revealed that levels of Tg, levels of TgAb, and ultrasound may be independent risk factors associated with CLNM in PTC patients before ^{131}I therapy.

10.3389/fendo.2023.1122517

TABLE 1 Demographics and clinical characteristics of patients.

Variables	PTC with CLNM (n=115)	PTC without CLNM (n=497)	*P*
Age (years)			
Mean ± SD	42.55 ± 11.98	42.42 ± 12.29	0.918
Gender [n (%)]			
male	40 (34.78)	185 (37.22)	
female	75 (65.21)	312 (62.78)	0.703
Stage [n (%)]			
I	106 (92.17)	437 (87.93)	
II	9 (7.82)	45 (9.05)	
III	0 (0)	10 (2.01)	
IV	0 (0)	5 (1.01)	0.395
Tumor size (cm)			
median (interquartile range)	1.30 (0.90-2.00)	1.40 (1.00-2.00)	0.704
Multifocality [n (%)]			
No	64 (55.65)	277 (55.73)	
Yes	61 (44.34)	220 (44.27)	1.000
Ultrasound [n (%)]			
negative	30 (26.09)	487 (97.99)	
positive	85 (73.91)	10 (2.01)	< 0.001
Tg (ug/l)			
median (interquartile range)	8.98 (0.89-39.60)	3.00 (0.48-10.23)	< 0.001
TgAb (IU/ml)			
median (interquartile range)	2.02 (1.02-24.20)	1.71 (0.98-7.15)	0.081

CLNM, cervical lymph node metastasis; SD, Standard deviation; Tg, Thyroglobulin; TgAb, thyroglobulin antibodies.

ROC analysis of different models

Figure 2 illustrates the ROC curves of the CLNM prediction results of the thirteen models. According to the results, the AUCs of the models achieved 0.608 (Tg), 0.552 (TgAb), 0.860 (overall ultrasound), 0.756 (aspect transverse ratio), 0.556 (cystic change), 0.708 (microcalcification), 0.559 (mass hyperecho), 0.834 (echogenicity), 0.612 (lymphatic hilum structure), 0.620 (vascularity), 0.892 (seven ultrasound features), 0.903 (Tg+TgAb+Overall ultrasound), and 0.921 (Tg+TgAb+seven ultrasound features), respectively. The corresponding quantitative indexes of all the above models were summarized in Table 3. Based on Delong test, seven ultrasounds aspects combined model performed better than the overall ultrasound model (P = 0.0321), "Tg+TgAb+Overall ultrasound" model performed better than Tg, TgAb, and Overall ultrasound models (all P < 0.01), "Tg+TgAb+Seven ultrasound features" model performed better than Tg, TgAb, each ultrasound feature and seven ultrasound features combined models (all P < 0.01). Nevertheless, we didn't observe a better performance of "Tg+TgAb +Seven ultrasound features" model than "Tg+TgAb+Overall ultrasound" model (P = 0.248).

Construct a nomogram for predicting risk of CLNM

We chose two models which showed good discrimination (AUC exceeding 0.9) to construct nomograms. As shown in Figure 3A, the nomogram was constructed and incorporated variables including Tg, TgAb, and overall ultrasound. Nomogram in Figure 4A contained Tg, TgAb, and seven ultrasound features. For individualized prediction, draw an upward vertical line from the patient's characteristics to calculate total points. Then, the risk of CLNM in each patient can be determined based on the total points. The two nomograms were cross-validated internally by the 1000 repetitions of bootstrap samples and the C-index were 0.899 and 0.914, respectively. Figures 3B, 4B showed the calibration curves of "Tg+TgAb+Overall ultrasound" model and "Tg+TgAb+Seven ultrasound features" model. The unreliability test yielded a P value of 0.966 and 0.927, respectively, indicating a good concordance between the predicted and actual outcomes. Ultimately, we used decision analysis curves to estimate the clinical utility of our nomograms, and results showed that the two nomograms had satisfactory net benefits among most of the threshold probabilities (Figures 3C, 4C).

10.3389/fendo.2023.1122517

TABLE 2 Univariate and multivariate stepwise logistic regression analysis of risk factors for CLNM in postoperative PTC before ^{131}I therapy.

Variables	Univariate analysis		Multivariate analysis [a]		Multivariate analysis [b]	
	OR (95% CI)	*P*	OR (95% CI)	*P*	OR (95% CI)	*P*
Age (>40 *vs.* ≤40 years) *	1.08 (0.72-1.62)	0.707	NA		NA	
Gender (female *vs.* male)	1.11 (0.73-1.71)	0.625	NA		NA	
Stage (II-IV *vs.* I)	0.62 (0.28-1.23)	0.198	NA		NA	
Tumor size (>1.4 cm *vs.* ≤1.4 cm) *	0.92 (0.61-1.38)	0.689	NA		NA	
Multifocality (yes *vs.* no)	1.00 (0.67-1.51)	0.987	NA		NA	
Tg (>12.58 *vs.* ≤12.58 ug/l) #	3.16 (2.06-4.86)	<0.001	3.23 (1.52-6.94)	2.290×10^{-3}	3.13 (1.53-6.45)	1.797×10^{-3}
TgAb (>13.20 *vs.* ≤13.20 IU/ml) #	1.83 (1.16-2.86)	8.580×10^{-3}	2.96 (1.34-6.54)	6.910×10^{-3}	1.75 (0.81-3.70)	0.147
Overall ultrasound (positive *vs.* negative)	137.98 (67.90-308.87)	<0.001	125.31 (60.49-286.61)	<0.001	NA	
Ultrasound features:			NA			
Aspect transverse ratio (≥2 *vs.* <2)	10.34 (6.60-16.49)	<0.001			3.69 (1.96-6.92)	<0.001
Cystic change (yes *vs.* no)	63.22 (12.39-1154.83)	<0.001			8.54 (1.28-172.28)	0.060
Microcalcification (yes *vs.* no)	27.49 (14.78-54.25)	<0.001			3.99 (1.52-11.11)	6.217×10^{-3}
Mass hyperecho (yes *vs.* no)	34.31 (9.40-220.66)	<0.001			4.55 (0.92-35.17)	0.091
Echogenicity (heterogeneous *vs.* homogeneous)	37.40 (22.11-65.20)	<0.001			6.46 (2.69-15.24)	<0.001
Lymphatic hilum structure (absence *vs.* presence)	11.63 (6.01-23.54)	<0.001			5.64 (2.16-14.98)	<0.001
Vascularity (abundant *vs.* non-abundant)	27.59 (11.88-75.42)	<0.001			4.00 (1.28-14.08)	0.022

* Patients were grouped by median of the variable from all patients, # Patients were grouped by cut-off value of receiver operating characteristic curve analysis, [a] Multivariate stepwise logistic regression analysis of overall ultrasound and other variables, [b] Multivariate stepwise logistic regression analysis of ultrasound features and other variables.
CLNM, cervical lymph node metastasis; PTC, papillary thyroid carcinoma; Tg, Thyroglobulin; TgAb, thyroglobulin antibodies; OR, Odd ratio; CI, Confidence intervals; NA, Unavailable.

Discussion

Due to unrecognized occult lymph nodes preoperatively or incomplete removal of metastatic lymph nodes during surgery, residual CLNM after initial surgical treatment for PTC is common (20). Radioactive iodine ablation is highly effective for treating CLNM in postoperative PTC patients (23). As thyroid cancer cells can't uptake the radioactive iodine as easily as normal thyroid cells, higher administered activities (up to 150 mCi) are generally recommended for PTC patients with remnant CLNM to achieve a good therapeutic effect (18). Therefore, accurate identification of CLNM can help provide personalized ^{131}I doses and then improve the prognosis of PTC patients. In the current study, 115 (18.79%) PTC patients presented residual and recurrent CLNM before taking ^{131}I. We identified independent risk factors associated with CLNM as follow: higher Tg, higher TgAb, positive overall ultrasound and ultrasound features such as aspect transverse ratio ≥ 2, microcalcification, heterogeneous echogenicity, absence of lymphatic hilum structure and abundant vascularity.

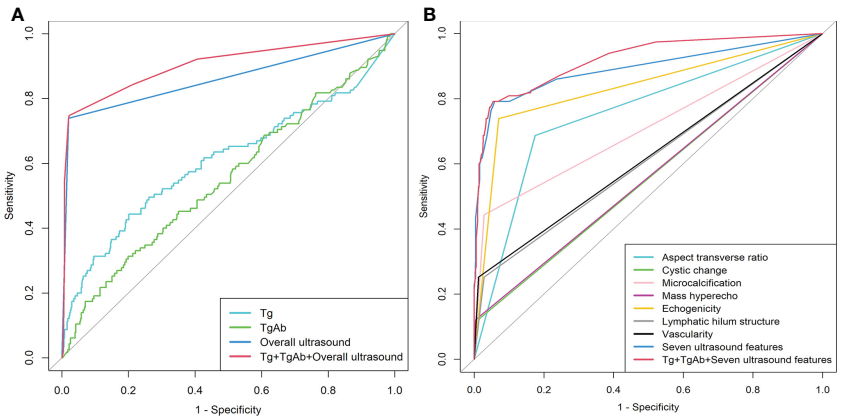

FIGURE 2
Receiver operating characteristic curve analysis of different prediction models for predicting CLNM in postoperative PTC before ^{131}I therapy. **(A)** ROC curves for Tg, TgAb, overall ultrasound and combined models. **(B)** ROC curves for seven ultrasound features and combined models.

TABLE 3 Quantitative indexes of different models.

Models	AUC	Cut-off	Sensitivity	Specificity
Tg	0.608 (0.543-0.674)	12.58	0.443	0.799
TgAb	0.552 (0.491-0.614)	13.20	0.313	0.801
Overall ultrasound	0.860 (0.819-0.900)	/	0.739	0.980
Aspect transverse ratio	0.756 (0.710-0.802)	/	0.687	0.825
Cystic change	0.556 (0.526-0.585)	/	0.113	0.998
Microcalcification	0.708 (0.662-0.754)	/	0.443	0.972
Mass hyperecho	0.559 (0.529-0.589)	/	0.122	0.996
Echogenicity	0.834 (0.793-0.876)	/	0.739	0.93
Lymphatic hilum structure	0.612 (0.572-0.653)	/	0.252	0.972
Vascularity	0.620 (0.580-0.660)	/	0.252	0.988
Seven ultrasound features	0.892 (0.853-0.932)	/	0.791	0.942
Tg+TgAb+Overall ultrasound	0.903 (0.866-0.940)	/	0.748	0.978
Tg+TgAb+Seven ultrasound features	0.921 (0.890-0.951)	/	0.791	0.946

AUC, area under curve; Tg, Thyroglobulin; TgAb, thyroglobulin antibodies.

Our study found serum Tg levels higher than 12.58 ug/l and TgAb higher than 13.20 IU/ml were related to higher CLNM risk in postoperative PTC patients. Serum Tg and TgAb are two important biomarkers that serial measurements of them are beneficial to the postoperative management of DTC patients (24, 25). Previous researches also proved the role of Tg and TgAb in predicting CLNM in DTC patients before and after surgery. Zou et al. found that ipsilateral lateral CLNM was more likely to occur before surgery when Tg > 100.01 ug/l or TgAb > 89.43 IU/ml (26). Tg and TgAb detection from fine-needle aspiration of cervical lymph node can determine metastasis with a cut-off value of 227.1 ug/l and 10.85 IU/ml, respectively (27). On the other hand, Zhang et al. identified serum Tg but not TgAb can detect recurrence and metastasis of DTC after surgery and ^{131}I treatment with an accuracy of 77.5% (28). In DTC patients complicated by Hashimoto thyroiditis after surgery and ^{131}I treatment, Chai et al. revealed the optimal cut-off value associated with metastasis in serum Tg and TgAb was 1.48 μg/L (AUC = 0.907) and 45 IU/ml (AUC = 0.650), respectively (29). Recent studies have demonstrated that PTC might lead to an autoimmune thyroid inflammation characterized by TgAb and anti-thyroperoxidase (TPOAb) (30, 31). In theory, production of TgAb can also be triggered by the presence of Tg (32). Elevated serum TgAb indicated that the tumor is active (33) and our study suggested that TgAb can be an independent predictor for residual and recurrent CLNM in PTC patients. Positive TgAb can interfere with Tg measurement and reduce the reliability of Tg level (34). The inclusion of both Tg and TgAb in our model reduced the risk of underestimating CLNM due to measurement interference to some extent.

In the present study, it was also discovered that general ultrasound and specific ultrasound characteristics, including aspect transverse ratio, microcalcification, echogenicity, lymphatic

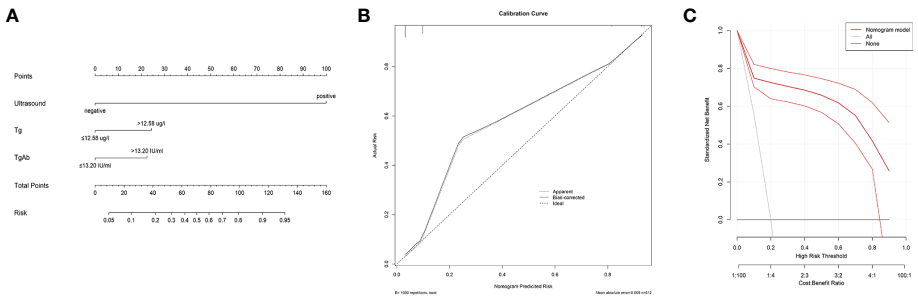

FIGURE 3
The nomogram, calibration curve and decision analysis curve of "Tg+TgAb+Overall ultrasound" model for predicting CLNM in postoperative PTC before ^{131}I therapy. **(A)** A nomogram incorporating serum Tg, serum TgAb and overall ultrasound was constructed. **(B)**The calibration curve of the nomogram model. The x-axis showed the predictive risk by nomogram, and the y-axis represented the actual CLNM risk. The ideal and bias-corrected risk were presented with the dotted black and solid black lines, respectively. **(C)** Decision curve analysis of the model. The x-axis showed threshold probability and the y-axis represented net benefit. The solid red line displayed the benefit and 95% confidence interval of the developed nomogram.

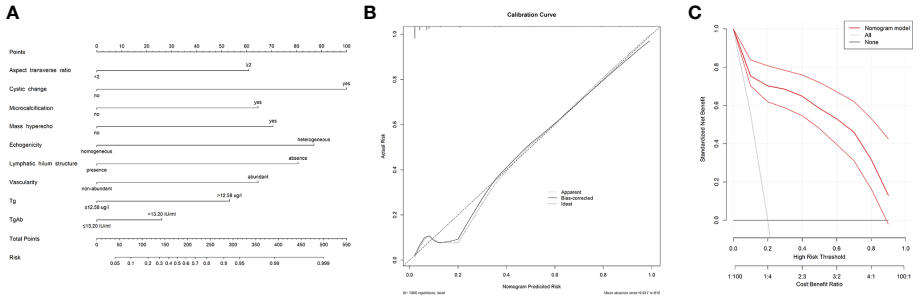

FIGURE 4
The nomogram, calibration curve and decision analysis curve of "Tg+TgAb+ Seven ultrasound features" model for predicting CLNM in postoperative PTC before ^{131}I therapy. **(A)** A nomogram incorporating serum Tg, serum TgAb and seven ultrasound features was constructed. **(B)** The calibration curve of the nomogram model. The x-axis showed the predictive risk by nomogram, and the y-axis represented the actual CLNM risk. The ideal and bias-corrected risk were presented with the dotted black and solid black lines, respectively. **(C)** Decision curve analysis of the model. The x-axis showed threshold probability and the y-axis represented net benefit. The solid red line displayed the benefit and 95% confidence interval of the developed nomogram.

hilum structure, and vascularity, are independent risk factors for CLNM in postoperative PTC patients. Past research works demonstrated that the sensitivity, specificity and accuracy of ultrasonic diagnosis of CLNM after treatment of DTC were 78.5%, 60.0%, and 75.0%, respectively (28). Our study showed a comparable sensitivity (0.739) and a higher specificity (0.980) in overall ultrasound. Former researchers focused on ultrasound characteristics of thyroid nodules related to CLNM preoperatively and found microcalcifications, abundant blood flow, and an irregular shape were significant risk factors (12, 14, 35, 36). Ultrasound parameters including cystic change and mass hyperecho slightly missed the margin of significance and showed poor discrimination values of AUC (<0.6) in this investigation. Our results indicated that ultrasound doctors should pay more attention to aspect transverse ratio, microcalcification, echogenicity, lymphatic hilum structure, and vascularity when judging CLNM.

The nomogram, a simple and useful tool, was widely used for predicting individual probabilities of clinical events (37, 38). Recently, effective nomograms have been constructed to indicate the risk of lymph node metastasis in different types of cancers (39–42). Similar work has been done before to establish a nomogram for preoperatively predicting central lymph node metastasis in PTC patients (15, 43, 44). Nevertheless, they focused on preoperative prediction of CLNM and ignored the importance of predicting residual and recurrent CLNM risk before ^{131}I therapy. Moreover, some studies established the nomogram depends on clinical factors (15, 44) and the accuracy of the model is not high enough (C-index slightly above 0.7). Min et al. collected comprehensive variables like clinical factors, thyroid function tests, and ultrasound features and consequently established a novel nomogram with a favorable C-index of 0.815 (43). To fill the gap that there is no established nomogram for predicting postoperatively residual and recurrent CLNM risk before ^{131}I therapy, we collected multiple variates containing clinical, ultrasonic, and hematological data and incorporated risk factors into two easy-to-use nomograms: one based on overall ultrasound and another based on ultrasound features. The two combined models (C-index 0.903 for "Tg+TgAb +Overall ultrasound" model, C-index 0.921 for "Tg+TgAb+seven ultrasound features" model) both showed better diagnostic performance than any single method in differentiating postoperative PTC patients with metastatic and non-metastatic lymph nodes. Internal validation also showed favorable discrimination and calibration. DCA proved that utilizing the two nomograms to predict CLNM before ^{131}I therapy would be beneficial at almost any threshold probability. We recommended prior usage of "Tg+TgAb+seven ultrasound features" model to calculate CLNM probability. When ultrasound features cannot be obtained, "Tg+TgAb+overall ultrasound" model is alternative and more convenient to use.

There are some limitations in our research that cannot be ignored. First, this was a retrospective study, which could inevitably cause some selection bias, information bias or confounding bias. Second, several specific data could not be obtained from the medical records, or were missing, including extrathyroidal extension and BRAF mutation status. Third, central lymph node metastasis (N1a) and lateral lymph node metastasis (N1b) showed different prognosis and they will show higher clinical value if we divided CLNM into N1a and N1b. However, the small sample size in N1a prevented us from the stratified analysis. Fourth, this study was conducted in a single institutional center with a limited sample size. In the future, external validation with more cases from multiple centers is needed.

Conclusion

Based on the clinical information including serum Tg, serum TgAb and ultrasound of postoperative PTC patients, we plotted two nomograms with high accuracy and reliability that could predict residual and recurrent CLNM in PTC patients before ^{131}I. We believe that our nomograms can assist clinicians to determine personalized ^{131}I dose for PTC patients.

Data availability statement

The raw data supporting the conclusions of this article will be made available by the authors, without undue reservation.

Ethics statement

The studies involving human participants were reviewed and approved by the Ethics Committee and Institutional Review Board of Nanjing First Hospital. The patients/participants provided their written informed consent to participate in this study.

Author contributions

LS and FW contributed to the design of the study. The first draft of the manuscript was written by FY, WW, and LZ. LS contributed to the manuscript review and editing. WW and LZ collect the data. FY performed the data analysis. All authors contributed to the article and approved the submitted version.

Funding

This work was supported by National Natural Science Foundation of China (No. 82001865, 82003532), Natural Science Foundation of Jiangsu Province (BK20200145), Nanjing Health Science and Technology Development Project (YKK22114).

Acknowledgments

We thank all the patients for their invaluable participation and the staff of Nanjing First Hospital for their contribution to the study. We also thank the help of Nasir Ahmad Haidari for modifying the language.

Conflict of interest

The authors declare that the research was conducted in the absence of any commercial or financial relationships that could be construed as a potential conflict of interest.

Publisher's note

References

1. Pizzato M, Li M, Vignat J, Laversanne M, Singh D, La Vecchia C, et al. The epidemiological landscape of thyroid cancer worldwide: GLOBOCAN estimates for incidence and mortality rates in 2020. *Lancet Diabetes Endocrinol* (2022) 10(4):264–72. doi: 10.1016/S2213-8587(22)00035-3

2. Miranda-Filho A, Lortet-Tieulent J, Bray F, Cao B, Franceschi S, Vaccarella S, et al. Thyroid cancer incidence trends by histology in 25 countries: A population-based study. *Lancet Diabetes Endocrinol* (2021) 9(4):225–34. doi: 10.1016/S2213-8587(21)00027-9

3. Glikson E, Alon E, Bedrin L, Talmi YP. Prognostic factors in differentiated thyroid cancer revisited. *Israel Med Assoc J IMAJ* (2017) 19(2):114–8.

4. Spanu A, Nuvoli S, Marongiu A, Gelo I, Mele L, Piras B, et al. Neck lymph node metastasis detection in patients with differentiated thyroid carcinoma (DTC) in long-term follow-up: a (131)I-SPECT/CT study. *BMC Cancer* (2020) 20(1):239. doi: 10.1186/s12885-020-06744-1

5. Choi YJ, Yun JS, Kook SH, Jung EC, Park YL. Clinical and imaging assessment of cervical lymph node metastasis in papillary thyroid carcinomas. *World J Surg* (2010) 34(7):1494–9. doi: 10.1007/s00268-010-0541-1

6. Pastorcic Grgic M, Stubljar B, Perse P, Zekan Vucetic M, Sitic S. Total thyroidectomy with central node dissection is a valuable option in papillary thyroid cancer treatment. *Acta clinica Croatica* (2020) 59(Suppl 1):102–7. doi: 10.20471/acc.2020.59.s1.13

7. Tufano RP, Clayman G, Heller KS, Inabnet WB, Kebebew E, Shaha A, et al. Management of recurrent/persistent nodal disease in patients with differentiated thyroid cancer: a critical review of the risks and benefits of surgical intervention versus active surveillance. *Thyroid Off J Am Thyroid Assoc* (2015) 25(1):15–27. doi: 10.1089/thy.2014.0098

8. Yeh MW, Bauer AJ, Bernet VA, Ferris RL, Loevner LA, Mandel SJ, et al. American Thyroid association statement on preoperative imaging for thyroid cancer surgery. *Thyroid Off J Am Thyroid Assoc* (2015) 25(1):3–14. doi: 10.1089/thy.2014.0096

9. Feng JW, Qin AC, Ye J, Pan H, Jiang Y, Qu Z. Predictive factors for lateral lymph node metastasis and skip metastasis in papillary thyroid carcinoma. *Endocrine Pathol* (2020) 31(1):67–76. doi: 10.1007/s12022-019-09599-w

10. Yao X, Meng Y, Guo R, Lu G, Jin L, Wang Y, et al. Value of ultrasound combined with immunohistochemistry evaluation of central lymph node metastasis for the prognosis of papillary thyroid carcinoma. *Cancer Manage Res* (2020) 12:8787–99. doi: 10.2147/CMAR.S265756

11. Maksimovic S, Jakovljevic B, Gojkovic Z. Lymph node metastases papillary thyroid carcinoma and their importance in recurrence of disease. *Med Arch* (2018) 72(2):108–11. doi: 10.5455/medarh.2018.72.108-111

12. Li F, Pan D, He Y, Wu Y, Peng J, Li J, et al. Using ultrasound features and radiomics analysis to predict lymph node metastasis in patients with thyroid cancer. *BMC Surg* (2020) 20(1):315. doi: 10.1186/s12893-020-00974-7

13. Zhao H, Li H. Meta-analysis of ultrasound for cervical lymph nodes in papillary thyroid cancer: Diagnosis of central and lateral compartment nodal metastases. *Eur J Radiol* (2019) 112:14–21. doi: 10.1016/j.ejrad.2019.01.006

14. Liu C, Xiao C, Chen J, Li X, Feng Z, Gao Q, et al. Risk factor analysis for predicting cervical lymph node metastasis in papillary thyroid carcinoma: a study of 966 patients. *BMC Cancer* (2019) 19(1):622. doi: 10.1186/s12885-019-5835-6

15. Feng Y, Min Y, Chen H, Xiang K, Wang X, Yin G. Construction and validation of a nomogram for predicting cervical lymph node metastasis in classic papillary thyroid carcinoma. *J endocrinological Invest* (2021) 44(10):2203–11. doi: 10.1007/s40618-021-01524-5

16. Tong Y, Li J, Huang Y, Zhou J, Liu T, Guo Y, et al. Ultrasound-based radiomic nomogram for predicting lateral cervical lymph node metastasis in papillary thyroid carcinoma. *Acad Radiol* (2021) 28(12):1675–84. doi: 10.1016/j.acra.2020.07.017

17. Chang Q, Zhang J, Wang Y, Li H, Du X, Zuo D, et al. Nomogram model based on preoperative serum thyroglobulin and clinical characteristics of papillary thyroid carcinoma to predict cervical lymph node metastasis. *Front Endocrinol* (2022) 13:937049. doi: 10.3389/fendo.2022.937049

18. Haugen BR, Alexander EK, Bible KC, Doherty GM, Mandel SJ, Nikiforov YE, et al. 2015 American Thyroid association management guidelines for adult patients with thyroid nodules and differentiated thyroid cancer: The American thyroid association guidelines task force on thyroid nodules and differentiated thyroid cancer. *Thyroid Off J Am Thyroid Assoc* (2016) 26(1):1–133. doi: 10.1089/thy.2015.0020

19. So YK, Kim MJ, Kim S, Son YI. Lateral lymph node metastasis in papillary thyroid carcinoma: A systematic review and meta-analysis for prevalence, risk factors, and location. *Int J Surg* (2018) 50:94–103. doi: 10.1016/j.ijsu.2017.12.029

20. Miller JE, Al-Attar NC, Brown OH, Shaughness GG, Rosculet NP, Avram AM, et al. Location and causation of residual lymph node metastasis after surgical treatment of regionally advanced differentiated thyroid cancer. *Thyroid Off J Am Thyroid Assoc* (2018) 28(5):593–600. doi: 10.1089/thy.2017.0434

21. Hundahl SA, Cady B, Cunningham MP, Mazzaferri E, McKee RF, Rosai J, et al. Initial results from a prospective cohort study of 5583 cases of thyroid carcinoma treated in the united states during 1996. U.S. and German thyroid cancer study group. an American college of surgeons commission on cancer patient care evaluation study. *Cancer* (2000) 89(1):202–17. doi: 10.1002/1097-0142(20000701)89:1<202::aid-cncr27>3.0.co;2-a

22. Rui Z, Wu R, Zheng W, Wang X, Meng Z, Tan J. Effect of (1)(3)(1)I therapy on complete blood count in patients with differentiated thyroid cancer. *Med Sci monitor Int Med J Exp Clin Res* (2021) 27:e929590. doi: 10.12659/MSM.929590

23. Wu X, Gu H, Gao Y, Li B, Fan R. Clinical outcomes and prognostic factors of radioiodine ablation therapy for lymph node metastases from papillary thyroid carcinoma. *Nucl Med Commun* (2018) 39(1):22–7. doi: 10.1097/MNM.0000000000000777

24. Algeciras-Schimnich A. Thyroglobulin measurement in the management of patients with differentiated thyroid cancer. *Crit Rev Clin Lab Sci* (2018) 55(3):205–18. doi: 10.1080/10408363.2018.1450830

25. Rosario PW, Cortes MCS, Franco Mourao G. Follow-up of patients with thyroid cancer and antithyroglobulin antibodies: A review for clinicians. *Endocrine-related Cancer* (2021) 28(4):R111–9. doi: 10.1530/ERC-21-0012

26. Zou Y, Zhang H, Li W, Guo Y, Sun F, Shi Y, et al. Prediction of ipsilateral lateral cervical lymph node metastasis in papillary thyroid carcinoma: A combined dual-energy CT and thyroid function indicators study. *BMC Cancer* (2021) 21(1):221. doi: 10.1186/s12885-021-07951-0

27. Wu X, Liu Y, Li K, Yang Y, Lai P, Li J, et al. Predictive value of FNA-tg and TgAb in cervical lymph node metastasis of papillary thyroid carcinoma. *Technol Cancer Res Treat* (2022) 21:15330338221127605. doi: 10.1177/15330338221127605

28. Zhang L, Zou G. Role of thyroid ultrasound combined with thyroglobulin in the diagnosis of postoperative recurrence of thyroid cancer. *Minerva endocrinologica* (2019) 44(2):192–8. doi: 10.23736/S0391-1977.18.02740-2

29. Chai H, Zhu ZJ, Chen ZQ, Yu YL. Diagnostic value of tg and TgAb for metastasis following ablation in patients with differentiated thyroid carcinoma coexistent with hashimoto thyroiditis. *Endocrine Res* (2016) 41(3):218–22. doi: 10.3109/07435800.2015.1010210

30. Boi F, Pani F, Mariotti S. Thyroid autoimmunity and thyroid cancer: Review focused on cytological studies. *Eur Thyroid J* (2017) 6(4):178–86. doi: 10.1159/000468928

31. Vasileiadis I, Boutzios G, Charitoudis G, Koukoulioti E, Karatzas T. Thyroglobulin antibodies could be a potential predictive marker for papillary thyroid carcinoma. *Ann Surg Oncol* (2014) 21(8):2725–32. doi: 10.1245/s10434-014-3593-x

32. Morbelli S, Ferrarazzo G, Pomposelli E, Pupo F, Pesce G, Calamia I, et al. Relationship between circulating anti-thyroglobulin antibodies (TgAb) and tumor metabolism in patients with differentiated thyroid cancer (DTC): prognostic implications. *J endocrinological Invest* (2017) 40(4):417–24. doi: 10.1007/s40618-016-0578-6

33. Wen X, Wang B, Jin Q, Zhang W, Qiu M. Thyroid antibody status is associated with central lymph node metastases in papillary thyroid carcinoma patients with hashimoto's thyroiditis. *Ann Surg Oncol* (2019) 26(6):1751–8. doi: 10.1245/s10434-019-07256-4

34. Jo K, Lim DJ. Clinical implications of anti-thyroglobulin antibody measurement before surgery in thyroid cancer. *Korean J Internal Med* (2018) 33(6):1050–7. doi: 10.3904/kjim.2018.289

35. Guang Y, He W, Zhang W, Zhang H, Zhang Y, Wan F. Clinical study of ultrasonographic risk factors for central lymph node metastasis of papillary thyroid carcinoma. *Front Endocrinol* (2021) 12:791970. doi: 10.3389/fendo.2021.791970

36. Liu W, Wang S, Xia X. Risk factor analysis for central lymph node metastasis in papillary thyroid microcarcinoma. *Int J Gen Med* (2021) 14:9923–9. doi: 10.2147/IJGM.S346143

37. Gao SJ, Jin L, Meadows HW, Shafman TD, Gross CP, Yu JB, et al. Prediction of distant metastases after stereotactic body radiation therapy for early stage NSCLC: Development and external validation of a multi-institutional model. *J Thorac Oncol Off Publ Int Assoc Study Lung Cancer* (2022) S1556-0864(22):01909-8. doi: 10.1016/j.jtho.2022.11.007

38. Chen D, Fu M, Chi L, Lin L, Cheng J, Xue W, et al. Prognostic and predictive value of a pathomics signature in gastric cancer. *Nat Commun* (2022) 13(1):6903. doi: 10.1038/s41467-022-34703-w

39. Huang YQ, Liang CH, He L, Tian J, Liang CS, Chen X, et al. Development and validation of a radiomics nomogram for preoperative prediction of lymph node metastasis in colorectal cancer. *J Clin Oncol Off J Am Soc Clin Oncol* (2016) 34(18):2157–64. doi: 10.1200/JCO.2015.65.9128

40. Wang Y, Liu W, Yu Y, Liu JJ, Xue HD, Qi YF, et al. CT radiomics nomogram for the preoperative prediction of lymph node metastasis in gastric cancer. *Eur Radiol* (2020) 30(2):976–86. doi: 10.1007/s00330-019-06398-z

41. Wang Z, Zhang S, Ma Y, Li W, Tian J, Liu T. A nomogram prediction model for lymph node metastasis in endometrial cancer patients. *BMC Cancer* (2021) 21(1):748. doi: 10.1186/s12885-021-08466-4

42. Lai SW, Fan YL, Zhu YH, Zhang F, Guo Z, Wang B, et al. Machine learning-based dynamic prediction of lateral lymph node metastasis in patients with papillary thyroid cancer. *Front Endocrinol* (2022) 13:1019037. doi: 10.3389/fendo.2022.1019037

43. Min Y, Huang Y, Wei M, Wei X, Chen H, Wang X, et al. Preoperatively predicting the central lymph node metastasis for papillary thyroid cancer patients with hashimoto's thyroiditis. *Front Endocrinol* (2021) 12:713475. doi: 10.3389/fendo.2021.713475

44. Wei X, Min Y, Feng Y, He D, Zeng X, Huang Y, et al. Development and validation of an individualized nomogram for predicting the high-volume (> 5) central lymph node metastasis in papillary thyroid microcarcinoma. *J endocrinological Invest* (2022) 45(3):507–15. doi: 10.1007/s40618-021-01675-5

frontiers | Frontiers in Endocrinology

TYPE Original Research
PUBLISHED 27 February 2023
DOI 10.3389/fendo.2023.1110987

OPEN ACCESS

EDITED BY
Erivelto Martinho Volpi,
Centro de Referência no Ensino do Diagnóstico por Imagem (CETRUS), Brazil

REVIEWED BY
Malgorzata Trofimiuk-Muldner,
Jagiellonian University Medical College, Poland
Mehmet Haciyanli,
Izmir Katip Celebi University, Türkiye

*CORRESPONDENCE
Hong Qiao
qiaohong@hrbmu.edu.cn

SPECIALTY SECTION
This article was submitted to Thyroid Endocrinology, a section of the journal Frontiers in Endocrinology

RECEIVED 29 November 2022
ACCEPTED 14 February 2023
PUBLISHED 27 February 2023

CITATION
Li S, Ran M-Y and Qiao H (2023) A cell cycle–related lncRNA signature predicts the progression-free interval in papillary thyroid carcinoma.
Front. Endocrinol. 14:1110987.
doi: 10.3389/fendo.2023.1110987

A cell cycle–related lncRNA signature predicts the progression-free interval in papillary thyroid carcinoma

Shuang Li[1], Ming-Yu Ran[2] and Hong Qiao[1]*

[1]Department of Endocrinology, The Second Affiliated Hospital of Harbin Medical University, Harbin, China, [2]College of Bioinformatics Science and Technology, Harbin Medical University, Harbin, China

The cell cycle plays a vital role in tumorigenesis and progression. Long non-coding RNAs (lncRNAs) are key regulators of cell cycle processes. Therefore, understanding cell cycle–related lncRNAs (CCR-lncRNAs) is crucial for determining the prognosis of papillary thyroid carcinoma (PTC). RNA-seq and clinical data of PTC were acquired from The Cancer Genome Atlas, and CCR-lncRNAs were selected based on Pearson's correlation coefficients. According to univariate Cox regression, least absolute shrinkage and selection operator (LASSO), and multivariate Cox regression analyses, a five-CCR-lncRNA signature (*FOXD2-AS1*, *LOC100507156*, *BSG-AS1*, *EGOT*, and *TMEM105*) was established to predict the progression-free interval (PFI) in PTC. Kaplan–Meier survival, time-dependent receiver operating characteristic curve, and multivariate Cox regression analyses proved that the signature had a reliable prognostic capability. A nomogram consisting of the risk signature and clinical characteristics was constructed that effectively predicted the PFI in PTC. Functional enrichment analyses indicted that the signature was involved in cell cycle– and immune-related pathways. Furthermore, we also analyzed the correlation between the signature and immune cell infiltration. Finally, we verified the differential expression of CCR-lncRNAs *in vitro* using quantitative real-time polymerase chain reaction. Overall, the newly developed prognostic risk signature based on five CCR-lncRNAs may become a marker for predicting the PFI in PTC.

KEYWORDS

papillary thyroid carcinoma, cell cycle, long non-coding RNA, progression-free interval, prognostic signature

1 Introduction

Thyroid cancer (TC) is the most common endocrine system malignancy and accounts for 3.4% of all cancers diagnosed globally each year (1), of which approximately 85% of TC cases are papillary thyroid carcinoma (PTC) (2). Although PTC has a good outcome, with a five-year survival rate of more than 97% (3), approximately 30% of patients exhibit

recurrence and metastasis after conventional treatment (4) and have a poor prognosis. Satisfactory tools for accurately assessing prognosis are still lacking. Therefore, it is essential to develop a new reliable biomarker to accurately determine the prognosis of PTC patients.

Cell cycle dysregulation and genetic alterations in cell cycle–related regulatory proteins lead to the limitless proliferation and growth of tumor cells (5), and research has shown that various genes affect tumor cell progression by regulating the cell cycle. For instance, *PTBP3* promotes the proliferation of lung squamous cell carcinoma cells by *CDC25A*-mediated cell cycle progression (6), and *ZNF703* knockdown inhibits triple-negative breast cancer cell progression by inducing G1-phase arrest (7). Hence, targeting cell cycle control is a promising therapeutic strategy (8). In addition, the prognostic value of cell cycle–related genes (CCRGs) has been reported in certain tumors (9–11).

Long non-coding RNAs (lncRNAs) are defined as RNAs that are longer than 200 nucleotides and do not encode proteins (12). They primarily participate in epigenetic regulation, including chromatin modifications, splicing, and transcriptional and post-transcriptional regulation (13). In addition, lncRNAs are engaged in various cellular processes, including autophagy, differentiation, cell cycle regulation, proliferation, apoptosis, and mesenchymal stem cell differentiation (14). Many lncRNAs that are closely involved in the occurrence and progression of PTC have been reported, including lncRNA *H19* (15), *lnc-MPEG1-1* (16), and lncRNA *MIAT* (17). Furthermore, lncRNA signatures have been developed to determine prognosis in PTC (18–20). However, prognostic signatures based on cell cycle–related lncRNAs (CCR-lncRNAs) for PTC have not been developed.

In this study, we developed a cell cycle–related lncRNA signature (CCRLSig) for the prediction of the progression-free interval (PFI) in PTC using data from The Cancer Genome Atlas (TCGA). We validated the prognostic value of this CCRLSig and established a nomogram. Moreover, functional enrichment analysis and an analysis of immune cell infiltration were performed to explore the mechanism by which the signature contributes to prognosis. Finally, we used quantitative real-time polymerase chain reaction (qRT–PCR) to detect the differential expression of CCR-lncRNAs in PTC. Our results provide the first demonstration that a CCRLSig can effectively determine the prognosis of PTC and provide new perspectives for the development of therapeutic strategies.

2 Materials and methods

2.1 Data collection

HTseq-FPKM and HTseq-count data of TC samples were obtained from TCGA (https://cancergenome.nih.gov/, accessed January 24, 2022). After removing TC samples of other pathological types, a total of 502 PTC samples and 58 adjacent normal samples as well as the corresponding clinical information were obtained from TCGA.

2.2 Identification of CCR-lncRNAs

The CCRG sets were extracted from MsigDB (http://www.gsea-msigdb.org/gsea/index.jsp, accessed January 24, 2022). Differentially expressed genes (DEGs) between PTC and normal tissues were screened using DEseq2 (|log Fold Change (FC)| > 1, p.adjust< 0.05). Next, 266 differentially expressed CCRGs were identified from the intersection of CCRGs and DEGs. CCR-lncRNAs were acquired by Pearson correlation coefficient analysis between the 266 CCRGs and differentially expressed lncRNAs (DElncRNAs) in the PTC samples, and the Benjamini–Hochberg (BH) method was used for p-value correction ($|R|$> 0.4, BH< 0.05).

2.3 Construction and validation of a CCR-lncRNA prognostic signature

Post-operative recurrence and metastasis are the main factors leading to the poor prognosis of PTC; accordingly, the PFI was chosen as the endpoint of this study, instead of overall survival. A total of 498 PTC samples with complete PFI information were included after removing samples with incomplete clinical information and prognosis less than 30 days. The samples were categorized into training (249) and test (249) cohorts at a 1:1 ratio by the "caret" package. Univariate Cox regression analyses were primarily used to screen CCR-lncRNAs that were associated with PFI in the training cohort (p< 0.05). To reduce noise caused by gene interactions and co-expression patterns, we applied LASSO-Cox regression to filter lncRNAs; the formula is as follows:

$$\min_{\beta} \sum_{i=1}^{n}(y_i - \sum_{j=1}^{q}\beta_j x_{ij})^2, \ subject \ to \ \sum_{j=1}^{q}|\beta_j| \leq \pi$$

where the β is the regression coefficient, x is the gene expression level, and π is an adjusted parameter decided by 10-fold cross validation. Parameter optimization was repeated 1000 times for all lncRNAs. These lncRNAs were utilized to construct a Cox proportional hazards model. The Akaike information criterion was adopted to select the appropriate model. The risk score for each patient (P_{RS}) was calculated with the following formula:

P_{RS} = [0.84919 ∗ normalized expression value of FOXD2-AS1] - [3.86735∗ normalized expression value of LOC100507156] + [0.67474∗ normalized expression value of BSG-AS1]+[0.76288∗ normalized expression value of EGOT]+ [0.46501∗ normalized expression value of TMEM105]

Thereafter, the cut-off value for the risk score was determined using the "survminer" package and patients were separated into high- and low-risk groups. The optimal cut-off values for the training, test and entire cohort were 2.026, 1.998 and 2.038, respectively. Kaplan–Meier (K–M) survival curves was plotted using the "survival" package. Time-dependent receiver operating characteristic (ROC) curves was generated using the "timeROC"

package to assess the predictive accuracy of the model. In addition, clinicopathological differences between the high- and low-risk groups were analyzed using the Wilcoxon rank sum test.

2.4 Independent prognostic value determination and nomogram construction

To validate the CCRLSig as an independent prognostic indicator for PFI in PTC, the signature risk score and clinical parameters (age, gender, tumor size, T stage, N stage, AJCC stage, multifocality, aggressiveness, anatomic site of the tumor, and BRAFV600E mutation status) were subjected to univariate and multivariate Cox regression analyses.

A nomogram incorporating clinical and pathological factors and the risk score was established using the "survival" and "rms" R packages to predict 1-, 3- and 5-year PFI in the entire cohort. The calibration curves and ROC curves were used to estimate the predictive accuracy of the nomogram.

2.5 Functional enrichment analysis

DEGs between the high- and low-risk groups based on the CCRLSig were identified using DEseq2 with a |log FC| > 0.5 and p.adjust< 0.05 as thresholds, after which Gene Ontology (GO), Kyoto Encyclopedia of Genes and Genomes (KEGG) pathway, and gene set enrichment analysis (GSEA) of these DEGs were conducted using the R "clusterProfiler" package.

2.6 Tumor mutation burden (TMB) and immune cell infiltration

The somatic mutation data of PTC patients were acquired from TCGA. The TMB was compared between the high- and low-risk groups using the "maftools" package. The TMB was measured as follows: (total mutations/total covered bases) × 10^6 for each patient with PTC.

To further explore if the risk signature was associated with immune cell infiltration in PTC, immunity-associated data were extracted from xCell (http://xCell.ucsf.edu/) and parameters were compared between the high- and low-risk groups by the Wilcoxon rank sum test. In addition, correlations between the CCR-lncRNAs and immune cell fractions were evaluated.

2.7 Cell culture

The human normal thyroid cell line (Nthy-ori3–1) was provided by Professor Hongmei Shen (Center for Endemic Disease Control, Chinese Center for Disease Control and Prevention, Harbin Medical University, Harbin, China). The human PTC cell line (TPC-1) was obtained from the School of Public Health, Shandong First Medical University & Shandong Academy of Medical Sciences. The cell lines were certified by short tandem repeat (STR) validation. TPC-1 and Nthy-ori3–1 cells were cultured in RPMI 1640 supplemented with 10% fetal bovine serum (Moregate, Bulimba, Australia) and 1% penicillin/streptomycin solution (Beyotime Biotechnology, Shanghai, China) at 37°C and 5% CO_2 conditions.

2.8 Quantitative real-time PCR validation

Total RNA was extracted from the cell lines using TRIzol reagent (Thermo Fisher Scientific, Waltham, MA, USA), and reverse transcribed into cDNA using the Roche Reverse Transcription Kit (Roche, Basel, Switzerland). QRT-PCR was performed using a real-time PCR instrument (Q5). Glyceraldehyde 3-phosphate dehydrogenase (*GAPDH*) served as a control. The primers for lncRNAs were provided by Sangon Biotech (Shanghai, China) and are listed in Table S1. The relative expression level of each lncRNA was calculated by the $2^{-\triangle\triangle CT}$ method.

2.9 Statistical analysis

The R statistical environment (V4.1.2) and GraphPad Prism 8.0 were used for statistical analyses. Analysis of variance, Wilcoxon rank sum test, and Student's t-tests were applied to evaluate differences between groups. The K–M analysis and log-rank test were adopted for comparing PFIs between groups. Values of $p< 0.05$ were considered statistically significant difference for all analyses.

3 Results

3.1 Identification of CCR-lncRNAs

We identified 655 DElncRNAs and 266 CCRGs in a comparison between 502 PTC and 58 adjacent normal samples (|log FC| > 1, p.adjust< 0.05). Based on Pearson correlation coefficients between the CCRGs and lncRNAs (|R| > 0.4, p< 0.05), we obtained 446 CCR-lncRNAs.

3.2 Construction of a CCRLSig predicting PFI in PTC

The 498 PTC samples with complete clinical information were divided into training and test cohorts at a ratio of 1:1. In the training cohort, 31 CCR-lncRNAs associated with PFI were selected by univariate Cox analyses. Subsequently, we applied LASSO-Cox regression analysis and established a prognostic signature consisting of five CCR-lncRNAs (*FOXD2-AS1*, *LOC100507156*, *BSG-AS1*, *EGOT*, and *TMEM105*; Figures 1A, B). The K–M survival curves for the five CCR-lncRNAs relating to the PFI are shown in Supplementary Figures S1A–E. Next, the risk score for each patient in the training cohort was calculated using the

10.3389/fendo.2023.1110987

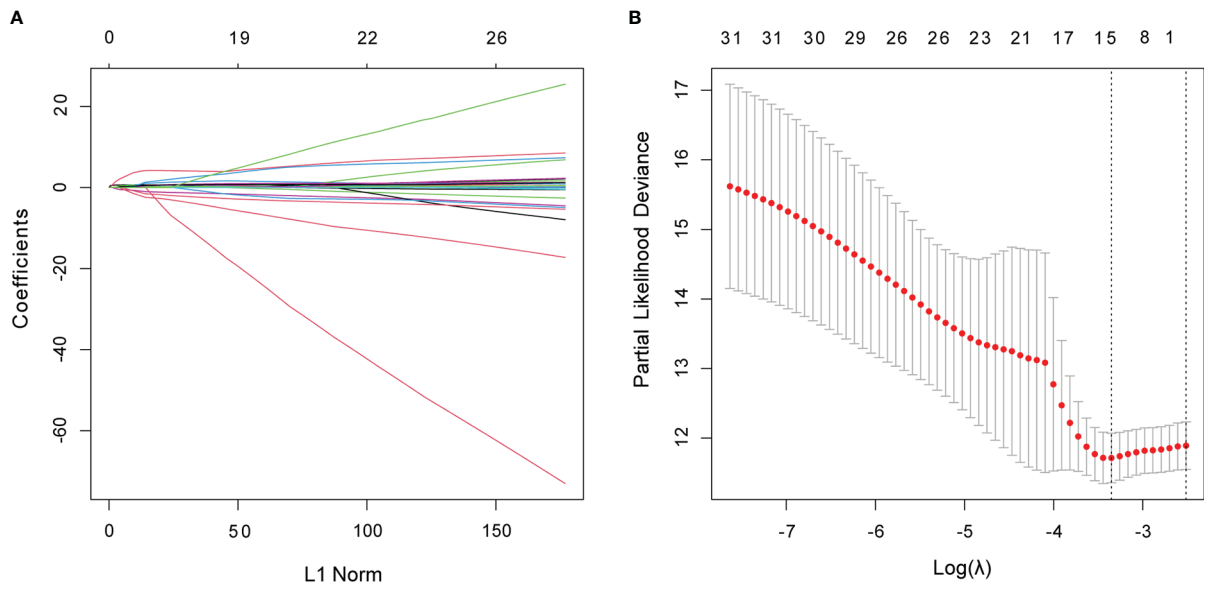

FIGURE 1
Identification of CCR-lncRNAs associated with PFI of PTC. **(A, B)** LASSO coefficient profiles of the PFI-associated CCR-lncRNAs. CCR-lncRNAs, cell cycle–related long non-coding RNAs; PFI, progression-free interval; PTC, papillary thyroid carcinoma; LASSO, least absolute shrinkage and selection operator.

following formula: risk score = [(0.84919) × normalized expression value of *FOXD2-AS1*] – [(3.86735) × normalized expression value of *LOC100507156*] – [(0.67474) × normalized expression value of *BSG-AS1*] – [(0.76288) × normalized expression value of *EGOT*] – [(0.46501) × normalized expression value of *TMEM105*]. Next, according to the optimal cut-off value of the risk score, patients were grouped into high- and low-risk groups. As the risk score increased, patients' prognosis worsened (Figures 2A, B). The expression levels of *TMEM105*, *EGOT*, *FOXD2-AS1*, and *BSG-AS1* in the CCRLSig increased and the expression level of *LOC100507156* decreased as the risk score increased (Figure 2C). K–M analysis showed that PTC patients in the high-risk group had a shorter PFI than that of patients in the low-risk group (Figure 2D). The area under the ROC curve (AUC) values for the risk score for 1-, 3-, and 5-year PFI were 0.784, 0.722, and 0.681, respectively (Figure 2E).

3.3 Validation of the CCRLSig

To validate the accuracy of the signature, patients in the test cohort and the entire cohort were separated into high- and low-risk groups according to the optimal cut-off value for each dataset. The risk curves, PFI status, and heatmaps of risk lncRNA expression profiles in the test cohort and entire cohort were consistent with those of the training cohort (Figures 2F–H, K–M). Similarly, a K–M curve analysis of the test cohort and entire cohort indicated that the high-risk groups had a shorter PFI than the low-risk groups (Figures 2I, N). In the test cohort, the AUC values for the risk score for 1-, 3-, and 5-year PFI were 0.723, 0.677, and 0.668, separately (Figure 2J). In the entire cohort, the AUC values for the risk score for 1-, 3-, and 5-year PFI were 0.757, 0.693, and 0.673, separately (Figure 2O). These results suggest that the five-CCR-lncRNA risk signature has good predictive performance for PFI in PTC.

3.4 Independent prognostic value of the CCRLSig

Univariate and multivariate Cox regression analyses were employed to explore whether the risk score based on the CCRLSig predicts PFI in PTC. Univariate Cox analyses showed that the risk score was notably correlated to the PFI in the training, test, and entire cohorts (Figures 3A–C). A multivariate Cox analysis proved that the risk score was an independent predictor for the PFI of PTC in the training, test, and entire cohorts (Figures 3D–F).

3.5 Correlations between the CCRLSig and clinicopathological characteristics

In correlation analyses, the risk scores based on the CCRLSig were higher for patients older than 55 years than for patients younger than 55 years (Figure 4B). The risk scores of tumor size >2 cm were higher than those for tumor size ≤ 2 (Figure 4C). The risk scores for N1 were higher than those for N0 (Figure 4D). We also found that the risk score tended to increase with T stage and AJCC stage (Figures 4E, F), implying the critical role of the signature in the progression of PTC. Additionally, the risk score was significantly higher in patients with the *BRAFV600E* mutation than in those without the mutation (Figure 4H). Nevertheless, there were no significant correlations between the risk score and gender or M stage ($p > 0.05$, Figures 4A, G).

10.3389/fendo.2023.1110987

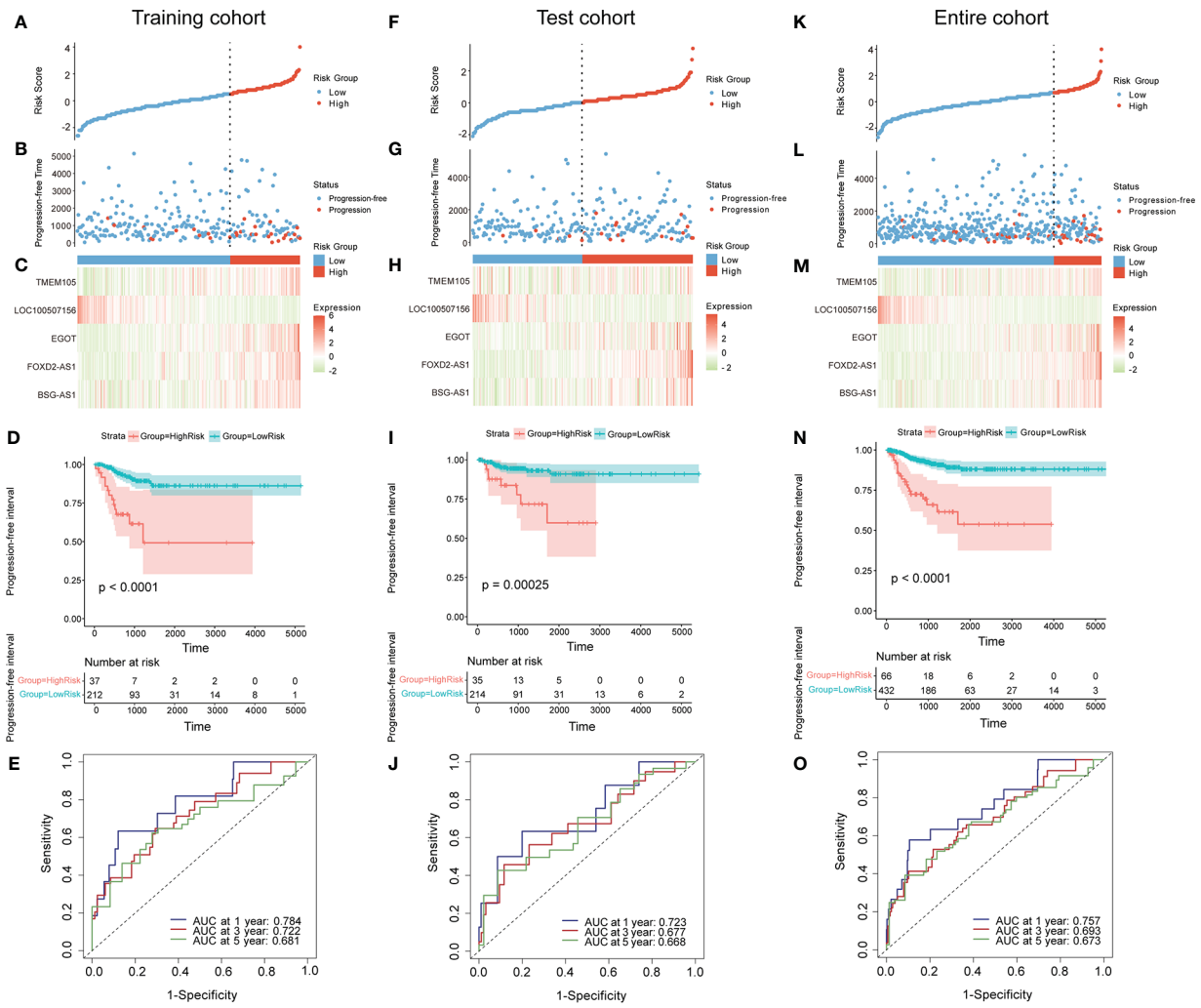

FIGURE 2
Construction and validation of a CCR-lncRNA-based prognostic signature. **(A, F, K)** PTC patients were sorted by risk score in the training, test, and entire cohort **(B, G, L)** PFI status of PTC patients in the training, test, and entire cohort. **(C, H, M)** Heatmap of the expression of five CCR-lncRNAs in the training, test, and entire cohort. **(D, I, N)** Kaplan–Meier curve analysis of the high- and low-risk groups in the training, test, and entire cohort. **(E, J, O)** Time-dependent ROC curves for 1-, 3-, and 5-year PFI predictions for the signature in the training, test, and entire cohort. CCR-lncRNAs, cell cycle–related long non-coding RNAs; PTC, papillary thyroid carcinoma; PFI, progression-free interval.

3.6 Construction and assessment of a nomogram

In the entire cohort, we built a nomogram for the prediction of the 1-, 3-, and 5-year PFI of PTC based on the signature's risk score and significant clinicopathological features (P< 0.05) identified in univariate Cox regression analyses, including the pathological T stage, N stage, AJCC stage, tumor size, age, and aggressiveness (Figure 5A). The calibration curve indicated that the nomogram-predicted PFI at one, three, and five years was highly consistent with the practically observed PFI (Figures 5B–D). Furthermore, the AUCs of the nomogram for evaluation of 1-, 3-, and 5-year PFI were 0.796, 0.711, and 0.681, respectively, and the predictive performances were superior to those of other clinical characteristics (age and N stage; Figures 5E–G). These results suggest that the nomogram reliably predicts the 1-, 3-, and 5-year PFI in PTC.

3.7 Functional enrichment analysis

To investigate the molecular mechanisms and pathways by which the signature is related to the risk of PTC progression, we carried out GO and KEGG enrichment analyses and GSEA of DEGs between the two risk groups. The GO enrichment analysis demonstrated that the DEGs were enriched in multiple biological processes and molecular functions, including cellular calcium ion homeostasis, positive regulation

10.3389/fendo.2023.1110987

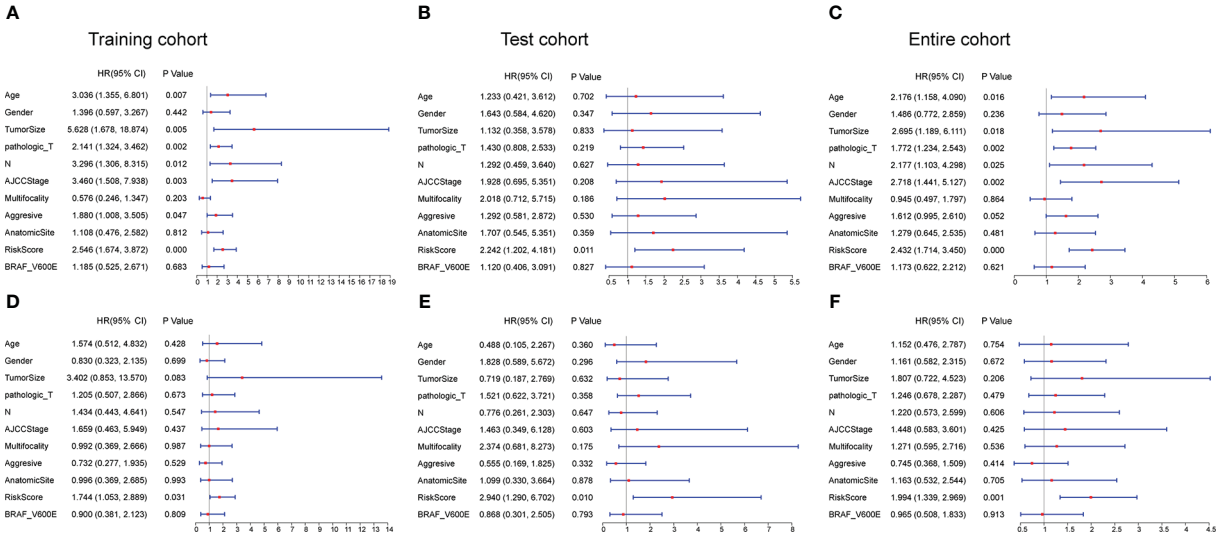

FIGURE 3
Univariate and multivariate Cox regression analyses of the signature and clinical characteristics. **(A–C)** Univariate Cox regression analysis of the signature risk score and clinical characteristics in the training, test, and entire cohort. **(D–F)** Multivariate Cox regression analysis of the signature risk score and clinical characteristics in the training, test, and entire cohort.

of MAPK cascade, cell-substrate adhesion, positive regulation of cell-cell adhesion, humoral immune response, T cell mediated immunity, and chemokine activity (Figure 6A). The KEGG analysis showed that the DEGs were involved in the PI3K-Akt, MAPK signaling pathway, cytokine-cytokine receptor interaction, cell adhesion molecules, antigen processing and presentation, and IL-17 signaling pathway (Figure 6B). The GSEA revealed that the DEGs were enriched in the cell cycle pathway and several immune-related biological processes (Figure 6C), including the cell cycle, P53 signaling pathway, cell cycle checkpoints, innate immune system, antigen response, and MHC class II antigen presentation.

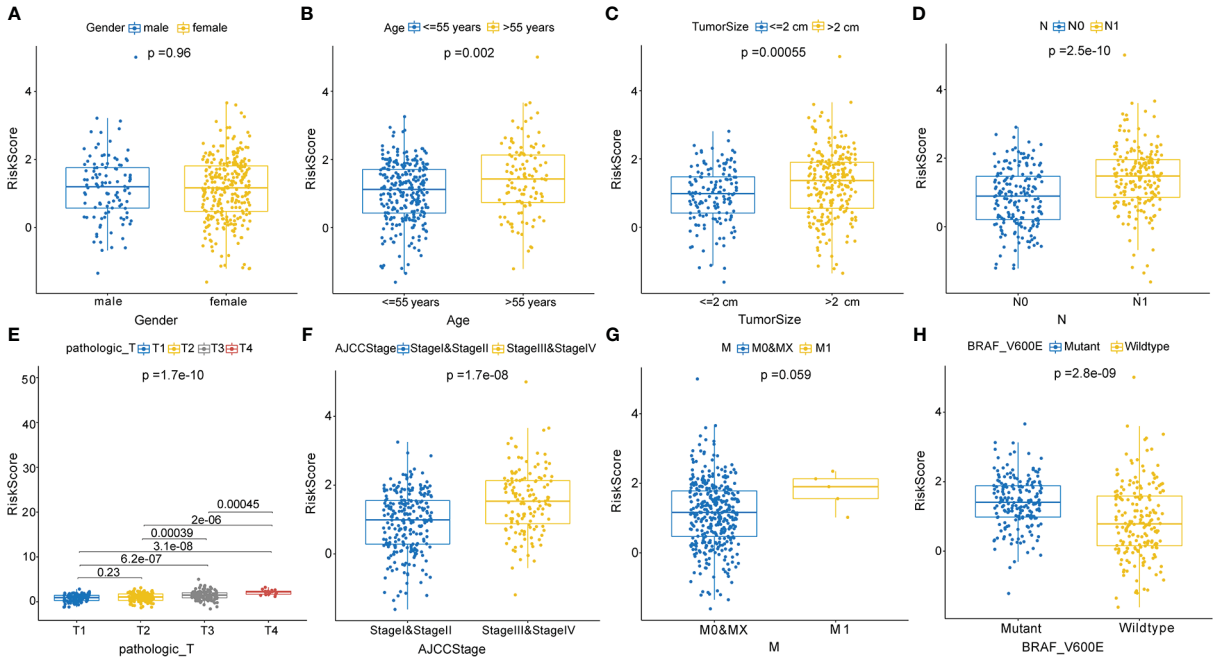

FIGURE 4
Correlations between the risk score based on the signature and clinical characteristics. **(A)** Male and female. **(B)** Age ≤ 55 years and > 55 years. **(C)** Tumor size ≤2 cm and > 2 cm. **(D)** N0 and N1 stage. **(E)** T1, T2, T3, and T4 stage. **(F)** AJCC stages I and II and stages III and V. **(G)** M0, MX, and M1stage. **(H)** Mutant and wild-type BRAFV600E.

10.3389/fendo.2023.1110987

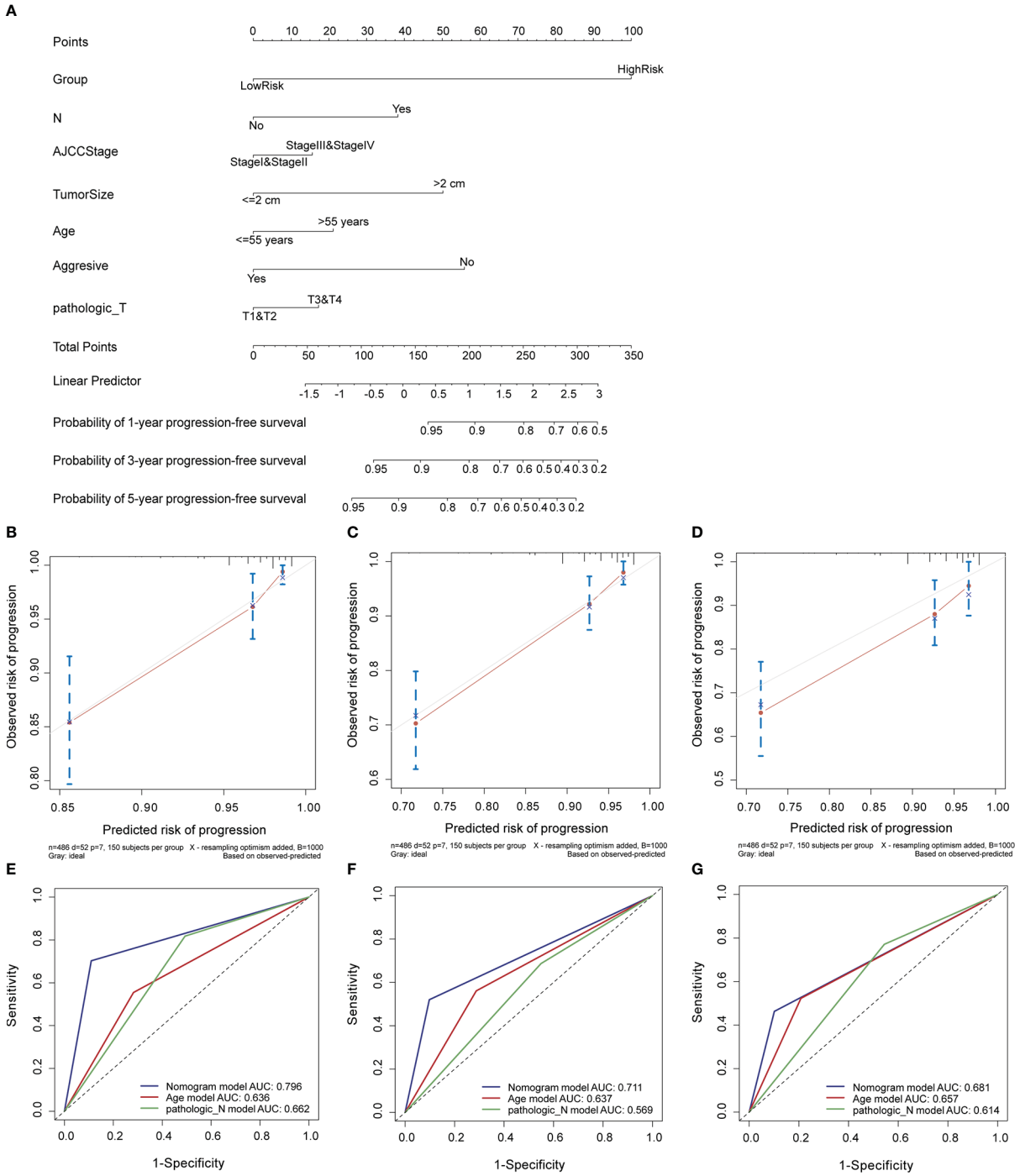

FIGURE 5
Construction and evaluation of a nomogram in the entire cohort. **(A)** Nomogram established to predict 1-, 3-, and 5-year PFI of PTC. **(B–D)** Calibration curves assessed the concordance between predicted and observed 1-, 3-, and 5-year PFI. **(E–G)** The ROC curves of the nomogram and other clinical characteristics at 1-, 3-, and 5-year time points. PFI, progression-free interval.

3.8 Analysis of TMB

To reveal genetic variation in risk score subtypes, we compared the TMB between the high- and low-risk groups. Compared with the low-risk group, the high-risk group had a markedly higher TMB ($p < 0.01$, Supplementary Figure S2A). The top 20 mutated genes in two risk group are shown in Supplementary Figures S2B, C. We observed that the mutation rate of *BRAF* was markedly higher in the high-risk group (84%) than in the low-risk group (56%). Supplementary Figures S2D, E show a complete view of the somatic mutations in the high- and low-risk groups.

10.3389/fendo.2023.1110987

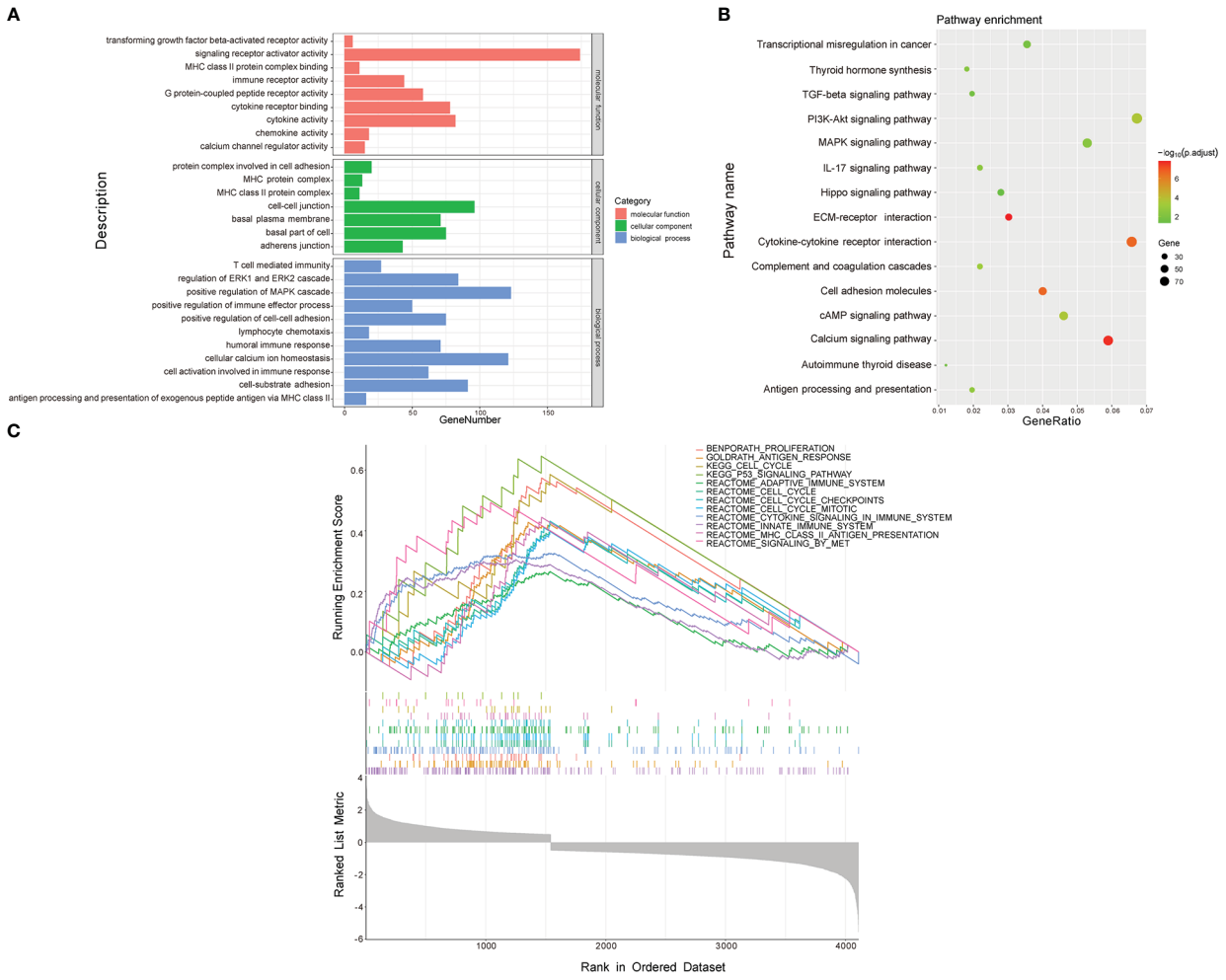

FIGURE 6
Functional enrichment analysis of DEGs between low- and high-risk groups. **(A)** GO analysis. **(B)** KEGG pathway analysis. **(C)** GSEA.

3.9 Relationship between the signature and immune cell infiltration

The functional enrichment analysis displayed that the CCRLSig may be associated with immunity. Hence, we further analyzed the relationships between the signature and immune cell infiltration. The relative frequencies of infiltrating immune cells in all PTC patients are shown in Figure 7A. The high-risk group exhibited higher immune scores than the low-risk group (Figure 7B). The fractions of B-cells, CD4+ memory T cells, class-switched memory B-cells, DC, macrophages, NKT, Th2 cells, and Tregs in the high-risk group were markedly higher than those in the low-risk group ($p< 0.05$). In contrast, the fractions of CD4+ Tcm, CD8+ T cells, and CD8 + Tcm cells in the high-risk group were lower than those in the low-risk group (Figure 7C). Additionally, we explored correlations between the expression levels of the five lncRNAs in the signature and the infiltration of multiple immune cells in PTC (Figure 7D). These results implied that the signature is linked to immune cell infiltration and may regulate immune processes in PTC.

3.10 Validation of the expression levels of five CCR-lncRNAs in cell lines

We analyzed the differential expression of the five lncRNAs between normal and PTC tissues in TCGA data, as illustrated in Figure 8A, and thereafter verified the results in cell lines. The expression levels of *FOXD2-AS1*, *LOC100507156*, *BSG-AS1*, *EGOT*, and *TMEM105* were notably higher in TPC-1 cells than in Nthy-ori3–1 cells (Figures 8B–F), which was in line with the results of the bioinformatics analysis, thereby supporting the accuracy of our analysis.

4 Discussion

The cell cycle is closely related to the growth and proliferation of cancer cells (21), and numerous lncRNAs related to the progression of cancers *via* cell cycle regulation have been identified (22). Understanding the expression levels of these lncRNAs and their combined regulatory patterns is crucial for determining patient outcomes and prognosis. Therefore, we constructed a cell cycle–

10.3389/fendo.2023.1110987

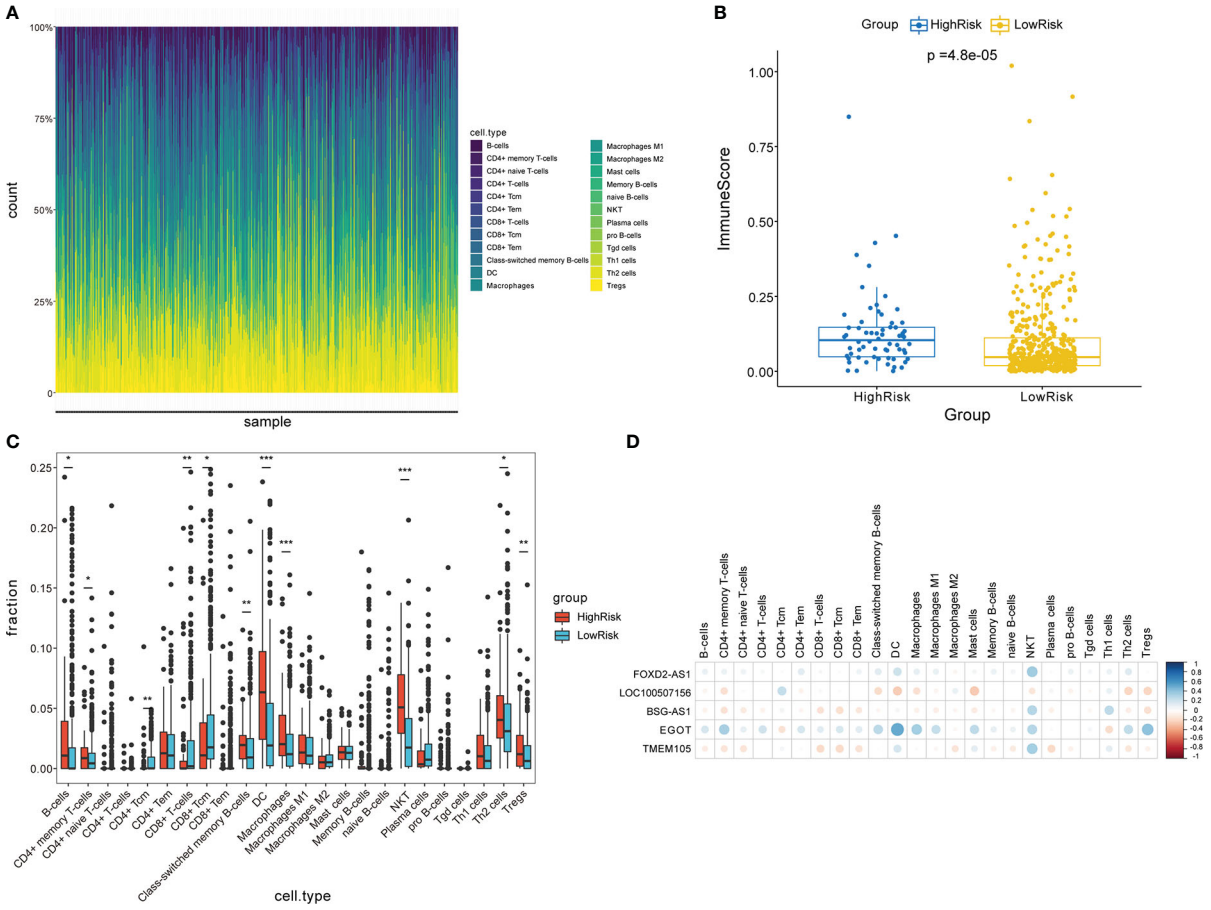

FIGURE 7
Analysis of immune cell infiltration in two risk groups stratified by the signature. **(A)** Overview of immune cell infiltration in each patient with PTC in the entire cohort. **(B)** Comparison of immune scores between two risk groups. **(C)** Analysis of immune cell infiltration in two risk groups. **(D)** Correlation analyses between five CCR-lncRNAs and immune cell infiltration. PTC, papillary thyroid carcinoma; CCR-lncRNAs, cell cycle–related long non-coding RNAs. (*P< 0.05, **P< 0.01, ***P< 0.001).

related lncRNA signature and explored its prognostic capability in PTC patients.

We screened out CCR-lncRNAs and divided PTC samples into training and test cohorts to establish and validate a prognostic signature. Univariate Cox and LASSO-Cox regression analyses were employed to construct a CCRLSig for predicting the PFI of PTC in the training cohort. The prognostic value of the CCRLSig was supported by K–M curve analysis, ROC curve analyses, and multivariate Cox analysis. Furthermore, a nomogram illustrated that the signature has excellent predictive power. To further understand the clinical application of the CCRLSig, we investigated its association with clinicopathological characteristics and observed that a high risk score was positively correlated with age, tumor size, BRAFV600E mutation, AJCC stage, N stage, and T stage. These results indicated that the CCRLSig effectively predicts outcome and can better guide risk stratification for PTC management.

To better understand the underlying mechanisms by which this CCRLSig affects the prognosis of PTC, we performed a functional enrichment analysis of DEGs between the two risk groups. GO and KEGG analyses indicated that these DEGs were enriched in the following terms and pathways: cell-substrate adhesion, cell adhesion molecules, PI3K-Akt signaling pathway, MAPK signaling pathway, humoral immune response, T cell mediated immunity, and the IL-17 signaling pathway, all of which are associated with tumor proliferation, migration and immunity. GSEA also demonstrated that these DEGs were primarily engaged in cell cycle– and immune-related signaling pathways. These results imply that CCR-lncRNAs can affect the progression of PTC by regulating cell cycle– and immune-related signaling pathways, providing new directions for the treatment of PTC.

Recent studies had indicated the key roles of lncRNAs in the regulation of cancer immunity, including lncRNAs involved in immune cell differentiation, proliferation, trafficking, and infiltration (23). For example, the lncRNA *HOXA-AS2* promotes Treg proliferation and immune tolerance in glioma (24), and *LINC00887* promotes clear cell renal cell carcinoma progression by inhibiting the infiltration of CD8+ T cells (25). CCRG signatures are potential indicators of immune cell infiltration, immune evasion, and immune responses (26–28). Our previous functional enrichment analysis has shown that the CCRLSig was involved in immune processes. Thus, we further analyzed immune cell

10.3389/fendo.2023.1110987

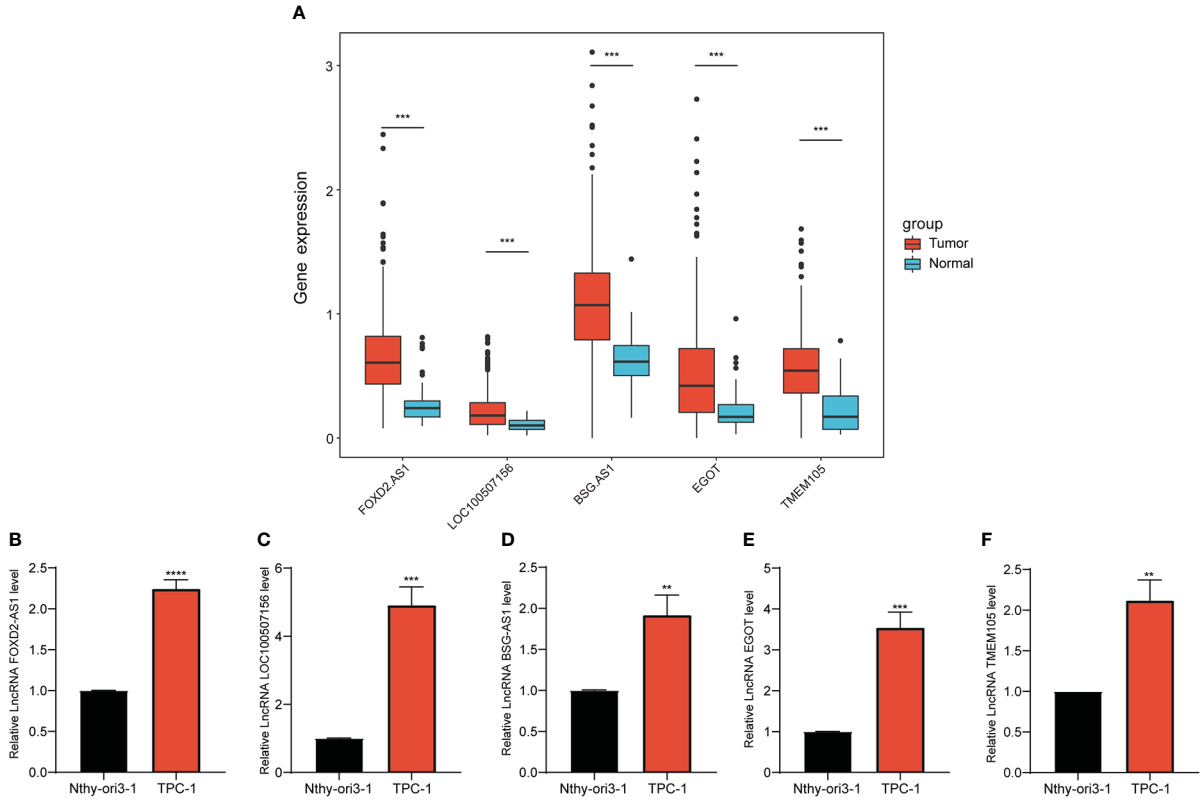

FIGURE 8
Expression of selected CCR-lncRNAs in cell lines. **(A)** Differential expression of five CCR-lncRNAs between normal tissues and tumor tissues of PTC of TCGA. **(B–F)** Relative expression of five CCR-lncRNAs in a PTC cell line and normal human thyroid cell line. CCR-lncRNAs, cell cycle–related long non-coding RNAs; PTC, papillary thyroid carcinoma (*P< 0.05, **P< 0.01, ***P< 0.001).

infiltration in the two risk groups. The high-risk group had infiltrates with higher proportions of B-cells, CD4+ memory T cell, DC, macrophages, NKT, Th2, and Tregs than the low-risk group, and the low-risk group primarily showed the infiltration of CD8+T cells, CD4+ Tcm, and CD8+Tcm cells. Studies have shown that Tregs and DCs play crucial roles in tumor immune escape (29–31) and promote tumor progression. However, CD8+ T cells exert an antitumor effect in PTC (32). Our results demonstrated that low-risk patients had a lower risk of immune evasion and may be more responsive to immunotherapy. Additionally, in PTC, DCs are significantly related to tumor T stage (T3/T4) and lymph node metastasis (33). Tregs show elevated infiltration in the thyroid tissue of PTC patients and were positively correlated with an advanced disease stage (34). CD8+ T cell infiltration is correlated with a lower incidence of lymph node metastasis and favorable prognosis in TC (35, 36). These findings further suggest that the low-risk group has a better prognosis. In summary, our findings suggested that the CCRLSig is associated with tumor immunity and can predict the immune landscape in PTC patients. In addition, these CCR-lncRNAs may be targets for immunotherapy.

Most of the lncRNAs in our signature have been previously reported to be implicated in cancers. For example, lncRNA *FOXD2-AS1* has been discovered to be upregulated in PTC and correlated with a poor prognosis (37), consistent with our results. In addition, lncRNA *FOXD2-AS1* promotes the progression of multiple cancers by participating in several biological processes, such as chemoresistance, proliferation, migration and invasion (38–40). The lncRNA *EGOT* may play different roles in different types of cancers. It promotes the progression of hepatocellular carcinoma (41), colon cancer (42), and gastric cancer (43). However, another study has shown that the lncRNA *EGOT* inhibits the progression of breast carcinoma (44) and renal cell carcinoma (45). The lncRNA *TMEM105*, a ferroptosis and immune-related lncRNA, serves as prognostic and diagnostic biomarker for patients with breast-infiltrating duct and lobular carcinoma (46). The lncRNA *BSG-AS1* contributes to the proliferation and metastasis of hepatocellular carcinoma *via* maintaining *BSG* mRNA stability (47). However, *LOC100507156* has not yet been reported in cancer and requires further investigations. These previous findings indicate that CCR-lncRNAs participate in the progression of multiple types of tumors, further indicating that it is reasonable to develop a risk signature based on CCR-lncRNAs to determine prognosis in PTC. In addition, the expression differences of the five CCR-lncRNAs were verified at the cellular level.

Although the newly constructed CCRLSig may be applied to predict the outcome of PTC, our study had some deficiencies. First, the dataset used to construct and validate the prognostic signature based on CCR-lncRNAs was obtained only from TCGA. Additional external data from other public databases are needed to evaluate the reliability of the signature. Second, we conducted a preliminary

expression study of five CCR-lncRNAs in the signature at the cellular level. However, further functional analyses and mechanistic studies are needed. We will conduct more in-depth studies to verify the performance of our CCRLSig.

In summary, we developed a new CCRLSig that can reliably predict the PFI of PTC, providing a new direction for the prognostic management and treatment of PTC.

Data availability statement

The datasets presented in this study can be found in online repositories. The names of the repository/repositories and accession number(s) can be found in the article/Supplementary Material.

Author contributions

SL and HQ conceived and designed the study, SL wrote the manuscript, SL and MR collected the data and performed bioinformatics analysis. All authors contributed to the article and approved the submitted version

Funding

The present study was supported by the National Natural Science Foundation of China (Nos:82073491 and 81872560).

Acknowledgments

We acknowledge TCGA database and everyone who contributed to this article. And we would like to thank Editage (www.editage.cn) for English language editing.

Conflict of interest

The authors declare that the research was conducted in the absence of any commercial or financial relationships that could be construed as a potential conflict of interest.

Publisher's note

Supplementary material

The Supplementary Material for this article can be found online at: https://www.frontiersin.org/articles/10.3389/fendo.2023.1110987/full#supplementary-material

References

1. Chmielik E, Rusinek D, Oczko-Wojciechowska M, Jarzab M, Krajewska J, Czarniecka A, et al. Heterogeneity of thyroid cancer. *Pathobiology* (2018) 85(1-2):117–29. doi: 10.1159/000486422

2. Fagin JA, Wells SAJr. Biologic and clinical perspectives on thyroid cancer. *N Engl J Med* (2016) 375(11):1054–67. doi: 10.1056/NEJMra1501993

3. Schneider DF, Chen H. New developments in the diagnosis and treatment of thyroid cancer. *CA Cancer J Clin* (2013) 63(6):374–94. doi: 10.3322/caac.21195

4. Zhang HM, Li ZY, Dai ZT, Wang J, Li LW, Zong QB, et al. Interaction of Mrpl9 and ggct promotes cell proliferation and migration by activating the Mapk/Erk pathway in papillary thyroid cancer. *Int J Mol Sci* (2022) 23(19):11989. doi: 10.3390/ijms231911989

5. Ding L, Cao J, Lin W, Chen H, Xiong X, Ao H, et al. The roles of cyclin-dependent kinases in cell-cycle progression and therapeutic strategies in human breast cancer. *Int J Mol Sci* (2020) 21(6):1960. doi: 10.3390/ijms21061960

6. Chen Y, Ji Y, Liu S, Liu Y, Feng W, Jin L. Ptbp3 regulates proliferation of lung squamous cell carcinoma cells *Via* Cdc25a-mediated cell cycle progression. *Cancer Cell Int* (2022) 22(1):19. doi: 10.1186/s12935-022-02448-7

7. Zhang X, Mu X, Huang O, Wang Z, Chen J, Chen D, et al. Znf703 promotes triple-negative breast cancer cells through cell-cycle signaling and associated with poor prognosis. *BMC Cancer* (2022) 22(1):226. doi: 10.1186/s12885-022-09286-w

8. Suski JM, Braun M, Strmiska V, Sicinski P. Targeting cell-cycle machinery in cancer. *Cancer Cell* (2021) 39(6):759–78. doi: 10.1016/j.ccell.2021.03.010

9. Jiang W, Xu J, Liao Z, Li G, Zhang C, Feng Y. Prognostic signature for lung adenocarcinoma patients based on cell-Cycle-Related genes. *Front Cell Dev Biol* (2021) 9:655950. doi: 10.3389/fcell.2021.655950

10. Zhang LQ, Zhou SL, Li JK, Chen PN, Zhao XK, Wang LD, et al. Identification of a seven-cell cycle signature predicting overall survival for gastric cancer. *Aging (Albany NY)* (2022) 14(9):3989–99. doi: 10.18632/aging.204060

11. Zhou Y, Lei D, Hu G, Luo F. A cell cycle-related 13-mrna signature to predict prognosis in hepatocellular carcinoma. *Front Oncol* (2022) 12:760190. doi: 10.3389/fonc.2022.760190

12. Gao N, Li Y, Li J, Gao Z, Yang Z, Li Y, et al. Long non-coding rnas: The regulatory mechanisms, research strategies, and future directions in cancers. *Front Oncol* (2020) 10:598817. doi: 10.3389/fonc.2020.598817

13. Statello L, Guo CJ, Chen LL, Huarte M. Gene regulation by long non-coding rnas and its biological functions. *Nat Rev Mol Cell Biol* (2021) 22(2):96–118. doi: 10.1038/s41580-020-00315-9

14. Murugan AK, Munirajan AK, Alzahrani AS. Long noncoding rnas: Emerging players in thyroid cancer pathogenesis. *Endocr Relat Cancer* (2018) 25(2):R59–82. doi: 10.1530/ERC-17-0188

15. Rolla M, Jawiarczyk-PrzybyLowska A, KolaCkov K, Bolanowski M. H19 in endocrine system tumours. *Anticancer Res* (2021) 41(2):557–65. doi: 10.21873/anticanres.14808

16. Huang C, Su X, Zhou DL, Xu BH, Liu Q, Zhang X, et al. A diagnostic and predictive lncrna lnc-Mpeg1-1 promotes the proliferation and metastasis of papillary thyroid cancer cells by occupying mir-766-5p. *Mol Ther Nucleic Acids* (2022) 28:408–22. doi: 10.1016/j.omtn.2022.03.023

17. Guo K, Qian K, Shi Y, Sun T, Wang Z. Lncrna-miat promotes thyroid cancer progression and function as cerna to target Ezh2 by sponging mir-150-5p. *Cell Death Dis* (2021) 12(12):1097. doi: 10.1038/s41419-021-04386-0

18. Dong X, Jin C, Chen D, Chen Y, Ye ZQ, Zhang X, et al. Genomic instability-related lncrna signature predicts the prognosis and highlights Linc01614 is a tumor microenvironment-related oncogenic lncrna of papillary thyroid carcinoma. *Front Oncol* (2021) 11:737867. doi: 10.3389/fonc.2021.737867

19. Wang K, Xu J, Zhao L, Liu S, Liu C, Zhang L. Prognostic lncrna, mirna, and mrna signatures in papillary thyroid carcinoma. *Front Genet* (2020) 11:805. doi: 10.3389/fgene.2020.00805

20. Wang W, Bai N, Li X. Comprehensive analysis of the prognosis and drug sensitivity of differentiation-related lncrnas in papillary thyroid cancer. *Cancers (Basel)* (2022) 14(5):1353. doi: 10.3390/cancers14051353

21. Liu J, Mei J, Li S, Wu Z, Zhang Y. Establishment of a novel cell cycle-related prognostic signature predicting prognosis in patients with endometrial cancer. *Cancer Cell Int* (2020) 20:329. doi: 10.1186/s12935-020-01428-z

22. Ghafouri-Fard S, Shoorei H, Anamag FT, Taheri M. The role of non-coding rnas in controlling cell cycle related proteins in cancer cells. *Front Oncol* (2020) 10:608975. doi: 10.3389/fonc.2020.608975

23. Wu M, Fu P, Qu L, Liu J, Lin A. Long noncoding rnas, new critical regulators in cancer immunity. *Front Oncol* (2020) 10:550987. doi: 10.3389/fonc.2020.550987

24. Zhong C, Tao B, Li X, Xiang W, Peng L, Peng T, et al. Hoxa-As2 contributes to regulatory T cell proliferation and immune tolerance in glioma through the mir-302a/Kdm2a/Jag1 axis. *Cell Death Dis* (2022) 13(2):160. doi: 10.1038/s41419-021-04471-4

25. Wu J, Lin R, Zhang L, Wei Y, Zhang R, Cai W, et al. Linc00887 fosters development of clear cell renal cell carcinoma *Via* inhibiting Cd8+ T cell immune infiltration. *Comput Math Methods Med* (2022) 2022:2582474. doi: 10.1155/2022/2582474

26. Chen F, Song J, Ye Z, Xu B, Cheng H, Zhang S, et al. Integrated analysis of cell cycle-related and immunity-related biomarker signatures to improve the prognosis prediction of lung adenocarcinoma. *Front Oncol* (2021) 11:666826. doi: 10.3389/fonc.2021.666826

27. Jiang D, Li Y, Cao J, Sheng L, Zhu X, Xu M. Cell division cycle-associated genes are potential immune regulators in nasopharyngeal carcinoma. *Front Oncol* (2022) 12:779175. doi: 10.3389/fonc.2022.779175

28. Liu Z, Pan R, Li W, Li Y. Comprehensive analysis of cell cycle-related genes in patients with prostate cancer. *Front Oncol* (2021) 11:796795. doi: 10.3389/fonc.2021.796795

29. Li C, Jiang P, Wei S, Xu X, Wang J. Regulatory T cells in tumor microenvironment: New mechanisms, potential therapeutic strategies and future prospects. *Mol Cancer* (2020) 19(1):116. doi: 10.1186/s12943-020-01234-1

30. Ling Z, Shao L, Liu X, Cheng Y, Yan C, Mei Y, et al. Regulatory T cells and plasmacytoid dendritic cells within the tumor microenvironment in gastric cancer are correlated with gastric microbiota dysbiosis: A preliminary study. *Front Immunol* (2019) 10:533. doi: 10.3389/fimmu.2019.00533

31. Yu H, Huang X, Liu X, Jin H, Zhang G, Zhang Q, et al. Regulatory T cells and plasmacytoid dendritic cells contribute to the immune escape of papillary thyroid cancer coexisting with multinodular non-toxic goiter. *Endocrine* (2013) 44(1):172–81. doi: 10.1007/s12020-012-9853-2

32. Xie Z, Li X, He Y, Wu S, Wang S, Sun J, et al. Immune cell confrontation in the papillary thyroid carcinoma microenvironment. *Front Endocrinol (Lausanne)* (2020) 11:570604. doi: 10.3389/fendo.2020.570604

33. Bergdorf K, Ferguson DC, Mehrad M, Ely K, Stricker T, Weiss VL. Papillary thyroid carcinoma behavior: Clues in the tumor microenvironment. *Endocr Relat Cancer* (2019) 26(6):601–14. doi: 10.1530/ERC-19-0074

34. Gogali F, Paterakis G, Rassidakis GZ, Kaltsas G, Liakou CI, Gousis P, et al. Phenotypical analysis of lymphocytes with suppressive and regulatory properties (Tregs) and nk cells in the papillary carcinoma of thyroid. *J Clin Endocrinol Metab* (2012) 97(5):1474–82. doi: 10.1210/jc.2011-1838

35. Aghajani MJ, Yang T, McCafferty CE, Graham S, Wu X, Niles N. Predictive relevance of programmed cell death protein 1 and tumor-infiltrating lymphocyte expression in papillary thyroid cancer. *Surgery* (2018) 163(1):130–6. doi: 10.1016/j.surg.2017.04.033

36. Cunha LL, Morari EC, Guihen AC, Razolli D, Gerhard R, Nonogaki S, et al. Infiltration of a mixture of immune cells may be related to good prognosis in patients with differentiated thyroid carcinoma. *Clin Endocrinol (Oxf)* (2012) 77(6):918–25. doi: 10.1111/j.1365-2265.2012.04482.x

37. Li H, Han Q, Chen Y, Chen X, Ma R, Chang Q, et al. Upregulation of the long non-coding rna Foxd2-As1 is correlated with tumor progression and metastasis in papillary thyroid cancer. *Am J Transl Res* (2019) 11(9):5457–71.

38. Li R, Chen S, Zhan J, Li X, Liu W, Sheng X, et al. Long noncoding rna Foxd2-As1 enhances chemotherapeutic resistance of laryngeal squamous cell carcinoma *Via* Stat3 activation. *Cell Death Dis* (2020) 11(1):41. doi: 10.1038/s41419-020-2232-7

39. Liu H, Zhang J, Luo X, Zeng M, Xu L, Zhang Q, et al. Overexpression of the long noncoding rna Foxd2-As1 promotes cisplatin resistance in esophageal squamous cell carcinoma through the mir-195/Akt/Mtor axis. *Oncol Res* (2020) 28(1):65–73. doi: 10.3727/096504019X15656904013079

40. Nong Q, Yu S, Hu H, Hu X. Knockdown of lncrna Foxd2-As1 inhibits proliferation, migration, and drug resistance of breast cancer cells. *Comput Math Methods Med* (2021) 2021:9674761. doi: 10.1155/2021/9674761

41. Zhang Y, Chen D, Yang M, Qian X, Long C, Zheng Z. Comprehensive analysis of competing endogenous rna network focusing on long noncoding rna involved in cirrhotic hepatocellular carcinoma. *Anal Cell Pathol (Amst)* (2021) 2021:5510111. doi: 10.1155/2021/5510111

42. Liu Y, Zhang B, Cao WB, Wang HY, Niu L, Zhang GZ. Study on clinical significance of lncrna egot expression in colon cancer and its effect on autophagy of colon cancer cells. *Cancer Manag Res* (2020) 12:13501–12. doi: 10.2147/CMAR.S285254

43. Peng W, Wu J, Fan H, Lu J, Feng J. Lncrna egot promotes tumorigenesis *Via* hedgehog pathway in gastric cancer. *Pathol Oncol Res* (2019) 25(3):883–7. doi: 10.1007/s12253-017-0367-3

44. Qiu S, Chen G, Peng J, Liu J, Chen J, Wang J, et al. Lncrna egot decreases breast cancer cell viability and migration *Via* inactivation of the hedgehog pathway. *FEBS Open Bio* (2020) 10(5):817–26. doi: 10.1002/2211-5463.12833

45. Jin L, Quan J, Pan X, He T, Hu J, Li Y, et al. Identification of lncrna egot as a tumor suppressor in renal cell carcinoma. *Mol Med Rep* (2017) 16(5):7072–9. doi: 10.3892/mmr.2017.7470

46. Wei T, Zhu N, Jiang W, Xing XL. Development and validation of ferroptosis- and immune-related lncrnas signatures for breast infiltrating duct and lobular carcinoma. *Front Oncol* (2022) 12:844642. doi: 10.3389/fonc.2022.844642

47. Ma Y, Sun W, Zhang Q, Gao B, Cai W, Liu Q, et al. Lncrna bsg-As1 is hypoxia-responsive and promotes hepatocellular carcinoma by enhancing bsg mrna stability. *Biochem Biophys Res Commun* (2021) 566:101–7. doi: 10.1016/j.bbrc.2021.06.002

frontiers | Frontiers in Endocrinology

TYPE Original Research
PUBLISHED 22 March 2023
DOI 10.3389/fendo.2023.1103434

OPEN ACCESS

EDITED BY
Erivelto Martinho Volpi,
Centro de Referencia no Ensino do Diagnóstico por Imagem (CETRUS), Brazil

REVIEWED BY
Adnan Işgör,
Memorial Sisli Hospital, Türkiye
Adnan Muhammad,
Hayatabad Medical Complex (HMC), Pakistan

*CORRESPONDENCE
Zhijiang Han
hzj1022@zju.edu.cn
Peiying Wei
dahai1658@126.com

†These authors have contributed equally to this work and share first authorship

SPECIALTY SECTION
This article was submitted to Thyroid Endocrinology, a section of the journal Frontiers in Endocrinology

RECEIVED 20 November 2022
ACCEPTED 10 March 2023
PUBLISHED 22 March 2023

CITATION
Zhu J, Tian M, Zhang T, Zhu H, Wei P and Han Z (2023) Diagnostic value of CT enhancement degree in lymph node metastasis of papillary thyroid cancer: A comparison of enhancement, ratio, and difference.
Front. Endocrinol. 14:1103434.
doi: 10.3389/fendo.2023.1103434

Diagnostic value of CT enhancement degree in lymph node metastasis of papillary thyroid cancer: A comparison of enhancement, ratio, and difference

Jiying Zhu[1†], Min Tian[1†], Tong Zhang[1], Hanlin Zhu[2], Peiying Wei[1*] and Zhijiang Han[1*]

[1]Department of Radiology, Affiliated Hangzhou First People's Hospital, Zhejiang University School of Medicine, Hangzhou, China, [2]Department of Radiology, Hangzhou Ninth People's Hospital, Hangzhou, China

Objectives: To evaluate the value of computed tomography (CT) enhancement degree in diagnosing lymph node (LN) metastasis in papillary thyroid carcinoma (PTC) by determining the ratio and difference between the Hounsfield units (HU) of CT enhancement and plain scan of the LNs, as well as between the HU of CT-enhanced LNs and the sternocleidomastoid muscle.

Methods: The plain and enhanced CT findings of 114 metastasis-positive LNs in 89 cases and 143 metastasis-negative LNs in 114 cases of PTC were analyzed retrospectively. Plain HU of LNs (PN_{HU}), enhanced HU of LNs (EN_{HU}), and enhanced HU of the sternocleidomastoid muscle (EM_{HU}) were measured. The EN_{HU}, difference between EN_{HU} and PN_{HU} ($EN\text{-}PN_{HU}$), ratio of EN_{HU} to PN_{HU} (EN/PN_{HU}), difference between EN_{HU} and EM_{HU} ($EN\text{-}EM_{HU}$), and ratio of EN_{HU} to EM_{HU} (EN/EM_{HU}) in metastasis-positive and metastasis-negative LN groups were calculated, the corresponding diagnostic efficacy for differentiating metastasis-positive from metastasis-negative LNs in PTC were sought using the receiver-operating curve. The interobserver agreement between readers was assessed using the interobserver correlation coefficient (ICC).

Results: The EN_{HU} of 114 metastasis-positive LNs and 143 metastasis-negative LNs was 113.39 ± 24.13 and 77.65 ± 15.93, $EN\text{-}PN_{HU}$ was 65.84 ± 21.72 HU and 34.07 ± 13.63 HU, EN/PN_{HU} was 2.36 (1.98, 2.75) and 1.76 (1.54, 2.02), $EN\text{-}EM_{HU}$ was 49.42 ± 24.59 HU and 13.27 ± 15.41 HU, and EN/EM_{HU} was 1.79 ± 0.40 and 1.21 ± 0.24, respectively (all $P < 0.001$). The area under the curve, cutoff value, sensitivity, specificity, and accuracy of EN_{HU} for identifying metastasis-positive and metastasis-negative LNs were 0.895, 97.3 HU, 0.746, 0.895, and 0.829, $EN\text{-}PN_{HU}$ was 0.894, 47.8 HU, 0.807, 0.874, and 0.844, EN/PN_{HU} was 0.831, 1.9, 0.877, 0.650, and 0.751, $EN\text{-}EM_{HU}$ was 0.890, 26.4 HU, 0.807, 0.839, and 0.825, and EN/EM_{HU} was 0.888, 1.5, 0.728, 0.902, and 0.825, respectively. The readers had an excellent interobserver agreement on these five parameters (ICC = 0.874–0.994).

10.3389/fendo.2023.1103434

Conclusion: In the preoperative evaluation of LN metastasis in PTC, EN_{HU}, EN-PN_{HU}, EN-EM_{HU}, and EN/EM_{HU} had similarly high diagnostic efficacy, with EN_{HU}, EN-PN_{HU}, and EN/EM_{HU} having higher specificity and EN-PN_{HU} and EN-EM_{HU} having higher sensitivity.

KEYWORDS

lymph node metastasis, thyroid nodule, thyroid tumor, tomography, x-ray computer

1 Introduction

Papillary thyroid carcinoma (PTC) is the most common malignant tumor of the thyroid, accounting for 83.6%–88% of cases (1, 2). Although the 5-year and 10-year survival rates of low-risk PTC are nearly 100% (3, 4), 20%–90% of patients with PTC have cervical lymph node (LN) metastasis at the time of diagnosis (5), especially central LN metastasis. Metastatic LNs can invade the peripheral blood vessels, trachea, and esophagus, causing the stenosis of the corresponding lumen, and invade the recurrent laryngeal nerve, causing hoarseness. Prophylactic LN dissection can reduce the residual metastatic LNs, but it is bound to increase the risk of the parathyroid gland and recurrent laryngeal nerve injury (6). Therefore, accurately identifying and prophylactically removing the central metastasis-positive LN or high-risk groups at risk of LN metastasis while removing the primary tumor of PTC is important.

Ultrasonography is the most commonly used imaging modality during the preoperative evaluation and monitoring of cervical LN metastasis in PTC. Typical ultrasound (US) images of LN metastasis often show signs such as LNs with transverse/long diameter > 0.5, blurred corticomedullary demarcation, disappearance of medullary structures, microcalcifications, and cystic changes (7, 8). While assessing LN metastasis in the lateral cervical levels, the sensitivity and accuracy of ultrasonography diagnosis ranged 64%–74.3% and 70.0%–89.2%, respectively (9–13). However, in the assessment of LNs in the central levels, ultrasonography was often interfered with by gases in the trachea and esophagus, as well as occlusion of the sternum and clavicle; also, the efficacy of its assessment was not satisfactory, with the sensitivity and accuracy of 17.3%–38% and 58.5%–71%, respectively (9, 11–13). Compared with ultrasonography, computed tomography (CT) examination is not limited by gas and bone and can better show the central level LNs. However, micrometastases in the cervical LNs of PTC are more common, and most of these LNs do not have typical CT metastasis signs such as short diameter >1 cm, central necrosis or cystic degeneration, and microcalcifications. Besides, no accurate quantitative value is available for judging LN metastasis based on the criterion of "the degree of enhancement is higher than that of muscle as a suspicious LN." Therefore, the sensitivity and accuracy of the CT examination are not superior to those of US, with 23.5%–50% and 55.7%–75%, respectively (11–13).

In the present study, we propose for the first time a comparative study of the LNs in one cervical level confirmed to be all metastasis-positive or all metastasis-negative, and the metastasis-positive LNs determined by fine-needle aspiration cytology (FNAC) under US-CT fusion navigation. The plain Hounsfield unit of LNs (PN_{HU}), enhanced Hounsfield unit of lymph nodes (EN_{HU}), enhanced Hounsfield unit of the sternocleidomastoid muscle (EM_{HU}), difference between EN_{HU} and PN_{HU} (EN – PN_{HU}), ratio of EN_{HU} to PN_{HU} (EN/PN_{HU}), difference between EN_{HU} and EM_{HU} (EN – EM_{HU}),and ratio of EN_{HU} to EM_{HU} (EN/EM_{HU}) were measured, aiming to find the optimal threshold for differentiating the metastatic LNs and provide an important basis for clinicians to individualize treatment options.

2 Materials and methods

2.1 Participants

The study was performed following the ethical guidelines of the Helsinki Declaration. The ethics committee of Affiliated Hangzhou First People's Hospital (IRB-2020-154) approved the study. Written informed consent for participation was waived due to the retrospective nature of the study and the use of anonymized patient data. We retrospectively analyzed 4621 cases of papillary carcinoma confirmed by surgery and pathology in Affiliated Hangzhou First People's Hospital from January 2015 to January 2022. The inclusion criteria were as follows (should have (1) and (2), or (1) and(3)): (1) patients with PTC confirmed by surgery and pathology; (2) pathology after LN dissection confirmed that the LNs in one cervical level were all metastasis-positive or all metastasis-negative; and (3) the FNAC under US-CT fusion navigation confirmed the LN was metastasis-positive. The exclusion criteria were as follows (having one of them requiring exclusion): (1) LN dissection or the FNAC under US-CT fusion navigation was not performed, or the latter confirmed the LNs were metastasis-negative; (2) pathology after LN dissection confirmed that no LN metastasis was detected; (3) pathology after LN dissection confirmed that partial LNs were metastasis-positive; (4) the largest LN diameter < 3 mm; (5) observation of LN affected by artifacts of clavicle or intravenous contrast agent sclerosis; (6) the image could not be observed due to other technical factors; and (7)

patients with cervical lymphoma or tuberculosis. Finally, 114 metastasis-positive LNs in 89 cases (28 LNs in 22 cases confirmed by the FNAC under US-CT fusion navigation and 86 LNs in 67 cases confirmed by surgery and pathology) and 143 negative LNs in 114 cases (all confirmed by surgery and pathology) met the inclusion criteria of this study. Figure 1 shows the characteristics of the study participants in a flow chart.

2.2 CT examination

The LNs were scanned with Lightspeed 16 (GE Company, Milwaukee, WI, USA) using the following scanning parameters: 120kV, 250 mA, collimation 0.625 mm × 8, pitch 0.875, and frame rotation time 0.5 s. Patients were positioned supine with scans ranging from the oropharynx to the supraclavicular margin with a slice thickness of 3.75 mm and a slice spacing of 3.75 mm. The contrast agent was iopromide (Bayer Company, Germany) or ioverol (Jiangsu Hengrui Pharmaceuticals Co., Ltd.), with an iodine concentration of 300–350 mgI/mL. The iodine concentration was 300–350 mgI/mL, the injection dose was 60–80 mL, the injection rate was 3–3.5 mL/s, and the patients were scanned 50 s after injection. The average interval between CT examination and surgery was 8 (0–15) days.

2.3 Image analysis

Two head and neck doctors, Han (21 years of work experience) and Zhu (17 years of work experience), separately analyzed the CT data of the picture achieving and communication system (PACS) including the selection of LNs and the measurement of PN_{HU}, EN_{HU}, and EM_{HU}. When selecting LNs, the LN with the largest short diameter was selected. If ≥ 2 LNs had the same short diameter, the LN with the highest enhancement degree was selected to avoid measuring multiple fused or ill-defined LNs. When measuring the Hounsfield units (HU) of LNs, the largest slice of LNs after enhancement was first selected, and the HU of the most obvious enhanced area was measured and recorded. Then, the region of interest (ROI) measurement area of LNs on the plain CT scan was determined according to the three-dimensional positioning technology (Figures 2–4), avoiding calcification, cystic degeneration, and vascular structures during measurement. The ROIs of LNs were all measured by 3 × 3 pixels. When measuring the CT HU of the sternocleidomastoid muscle, the level of the lower border of the ipsilateral cricoid cartilage was preferred, followed by the level of the glottis, and the thickest region of the muscle was measured using a circular ROI as large as possible. All the parameters were calculated as follows: $EN\text{-}PN_{HU} = EN_{HU} - PN_{HU}$, $EN/PN_{HU} = EN_{HU}/PN_{HU}$, $EN\text{-}EM_{HU} = EN_{HU} - EM_{HU}$, and $EN/EM_{HU} = EN_{HU}/EM_{HU}$. Finally, the data from Han were used for statistical analysis.

2.4 Statistical analysis

Statistical analyses were performed using R software (version 4.1.0, https://www.r-project.org/) and SPSS software (version 25, IBM Corporation, NY, USA). Continuous data with normal distribution were represented by means and standard deviations. Continuous data with non-normal distribution were represented by medians and quartiles. Classification variables were expressed as a constituent ratio (percentage). The *t* test was used for continuous variables with normal distribution, the Wilcoxon test was used for continuous variables with non-normal distribution, and the χ^2 test was used for classification variables. The interobserver correlation coefficient (ICC) was used to evaluate the repeatability of the quantitative indicators measured

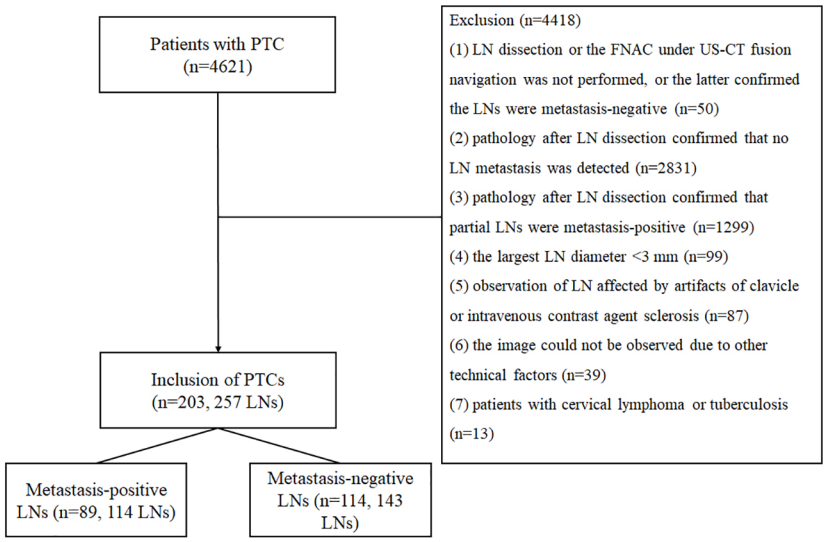

FIGURE 1
Flow chart of the study participants.

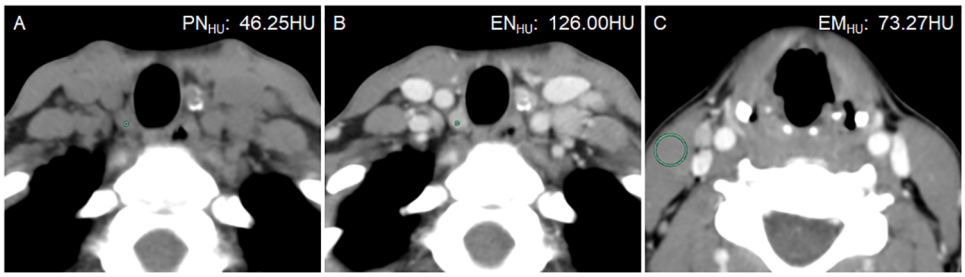

FIGURE 2
A 21-year-old woman with bilateral PTC. Postoperative pathology confirmed that all lymph nodes in the right level VI were metastasis-positive (5/5). **(A)** PN_{HU} was 46.25 HU. **(B)** EN_{HU} was 126 HU. **(C)** EM_{HU} was 73.27 HU. EN-PN_{HU}, EN/PN_{HU}, EN-EM_{HU}, and EN/EM_{HU} were 79.75 HU, 2.72, 52.73 HU, and 1.72, respectively.

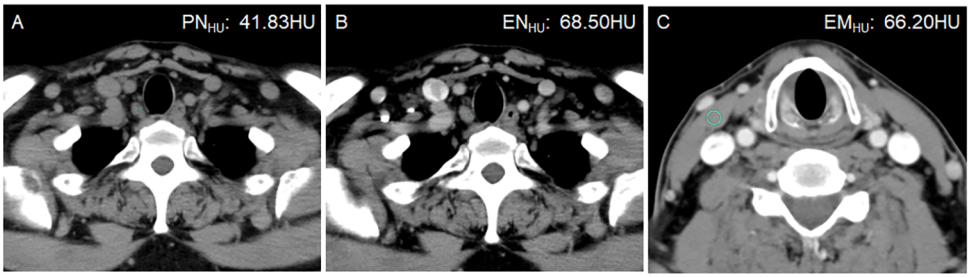

FIGURE 3
A 50-year-old man with bilateral PTC. Postoperative pathology confirmed that all lymph nodes in the right level VI were metastasis-negative (0/5). **(A)** PN_{HU} was 41.83 HU. **(B)** EN_{HU} was 68.50 HU. **(C)** EM_{HU} was 66.20 HU. EN-PN_{HU}, EN/PN_{HU}, EN-EM_{HU}, and EN/EM_{HU} were 26.67 HU, 1.64, 2.3 HU, and 1.02, respectively.

by two doctors, and ICC > 0.75 was considered to indicate the reproducibility of quantitative indicators. The receiver-operating characteristic (ROC) curve of participants was drawn to evaluate the diagnostic performance of quantitative indicators. The evaluation indicators included area under the ROC curve (AUC), sensitivity, specificity, and accuracy. A P value < 0.05 indicated a statistically significant difference.

3 Results

3.1 Distribution of sex, age, Hashimoto thyroiditis, antithyroid peroxidase antibody, and antithyroglobulin antibody levels

The distribution of sex, age, Hashimoto's thyroiditis, TPO-Ab, and TG-Ab levels in metastasis-positive and metastasis-negative LN groups of PTC is shown in Table 1. Age was not statistically different between the two groups (P = 0.116). Male patients were more common in the metastasis-positive LN group than female patients (P = 0.033). Hashimoto's thyroiditis was more common in the metastasis-negative LN group (P < 0.001). The TPO-Ab (P = 0.046) and TG-Ab levels (P < 0.001) in the metastasis-negative LN group were higher than in the LN metastasis-positive group.

3.2 Distribution of LN size, LN division, PN_{HU}, EN_{HU}, and EM_{HU}

The ICC was 0.874–0.994, in which EN_{HU} had the largest CT value, PN_{HU} had the smallest CT value, and EM_{HU} was intermediate (0.951). The distribution of LN size, LN division, PN_{HU}, EN_{HU}, and EM_{HU} is shown in Table 2. No difference in LN size (P = 0.975) and EM_{HU} (P = 0.561) was found between metastasis-positive and metastasis-negative groups. The incidence of LN metastasis was higher in level VI than in other levels in the metastasis-positive group (P < 0.001). PN_{HU}, EN_{HU}, EN-PN_{HU}, EN/PN_{HU}, EN-EM_{HU}, and EN/EM_{HU} in LN metastasis-positive group were higher than those in the LN metastasis-negative group (P < 0.001) (Figures 2–4). The PN_{HU} of the cases complicated with Hashimoto 's thyroiditis (Figure 4) and non-complicated with Hashimoto' s thyroiditis (Figure 3) was 44.38 (40.02, 48.00) and 44.00 (39.00, 48.00) (Z = 0.371, P = 0.711), and EN_{HU} was 76.38 (69.62, 89.86) and 77.50 (64.00, 87.00) (Z = 0.999, P = 0.322), respectively, in the metastasis-negative group.

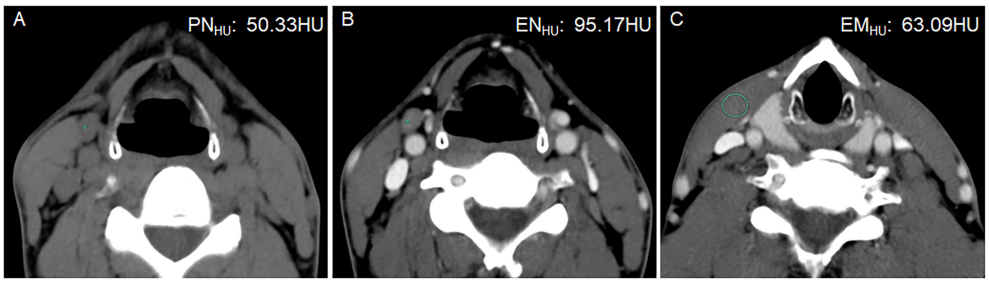

FIGURE 4
A 42-year-old man with PTC complicated with Hashimoto's thyroiditis in the left lobe of the thyroid gland. Postoperative pathology confirmed that all lymph nodes in the right level III were metastasis negative. **(A)** PN_{HU} was 50.33 HU. **(B)** EN_{HU} was 95.17 HU. **(C)** EM_{HU} was 63.09 HU. EN-PN_{HU}, EN/PN_{HU}, EN-EM_{HU}, and EN/EM_{HU} were 44.84 HU, 1.89, 32.08 HU, and 1.51, respectively.

TABLE 1 Distribution of sex, age, Hashimoto thyroiditis, TPO-Ab, and TG-Ab levels.

	Pathology or cytology		χ^2/Z	*P*
	Metastasis-positive LNs (*n* = 89)	Metastasis-negative LNs (*n* = 114)		
Sex (%)			4.550[a]	0.033
Male	36 (40.4%)	30 (26.3%)		
Female	53 (59.6%)	84 (73.7%)		
Age	39.00 (31.00, 55.00)	45.00 (37.25, 53.00)	1.571[b]	0.116
Hashimoto 's thyroiditis (%)			19.447[a]	<0.001
Yes	11 (12.4%)	46 (40.4%)		
No	78 (87.6%)	68 (59.6%)		
TPO-Ab	33.65 (28.00, 47.70)	39.70 (28.00, 727.00)	1.998[b]	0.046
TG-Ab	23.15 (15.00, 32.00)	39.90 (19.80, 144.70)	3.877[b]	<0.001

[a]χ^2 test; [b]Wilcoxon test.

3.3 Diagnostic efficacy of EN_{HU}, EN-PN_{HU}, EN/PN_{HU}, EN-EM_{HU}, and EN/EM_{HU} for LN metastasis in PTC

The ROC curves of EN_{HU}, EN-PN_{HU}, EN/PN_{HU}, EN-EM_{HU}, and EN/EM_{HU} for differentiating metastasis-positive nodes from metastasis-positive nodes in PTC are shown in Figure 5. The AUC and accuracy of EN_{HU}, EN/EM_{HU}, EN-PN_{HU}, and EN-EM_{HU} were highly consistent. EN_{HU} and EN/EM_{HU} had higher specificity, whereas EN-PN_{HU} and EN-EM_{HU} had higher sensitivity. However, EN/PN_{HU} had the highest sensitivity; its AUC, specificity, and accuracy were significantly lower than those of the other four parameters (Table 3).

3.4 Cytological examination guided by US-CT fusion navigation

In this study, 103 LNs in 73 cases were examined by FNAC with the guidance of US-CT fusion navigation. Finally, 28 LNs in 22 cases were confirmed as metastasis positive. Figure 6 shows the application of US-CT fusion imaging.

4 Discussion

The diagnostic value of CT signs, such as necrosis, cystic degeneration, microcalcification, and significant enhancement in PTC LN metastasis, has been widely recognized (2, 10, 11). Among these signs, cystic degeneration has the highest specificity (96.3%–99.7%) in the judgment of LN metastasis in PTC but the lowest sensitivity (15.1%–24.3%); it was common in patients with extensive LN metastasis (10, 14). The specificity of microcalcification in judging PTC LN metastasis was second only to cystic degeneration, being about 78.5%–96.2%; its sensitivity was equal to or slightly higher than that of cystic degeneration, being about 21.5%–30.0% (10, 14). Significant enhancement refers to a higher degree of LN enhancement than the adjacent sternocleidomastoid muscle (10, 12, 15). Although this standard is simple to use and easy to remember, extensive overlap exists between metastasis-positive and metastasis-negative LNs. In

10.3389/fendo.2023.1103434

TABLE 2 Distribution of LN size, division, and HU.

	Pathology or cytology		χ^2/t/Z	P
	Metastasis-positive LNs (*n* = 114)	Metastasis-negative LNs (*n* = 143)		
LN division (%)			29.814[a]	<0.001
Level VI	67 (58.8%)	36 (25.2%)		
Level non-VI	47 (41.2%)	107 (74.8%)		
LN size	5.20 (4.30, 7.00)	5.20 (4.45, 6.60)	0.031[c]	0.975
PN_{HU}	48.12 (41.00, 53.94)	44.00 (39.35, 48.00)	3.530[c]	<0.001
EN_{HU}	113.39 ± 24.13	77.65 ± 15.93	13.624[b]	<0.001
EM_{HU}	63.97 ± 6.14	64.37 ± 4.81	0.582[b]	0.561
EN-PN_{HU}	65.84 ± 21.72	34.07 ± 13.63	13.625[b]	<0.001
EN/PN_{HU}	2.36 (1.98, 2.75)	1.76 (1.54, 2.02)	9.133[c]	<0.001
EN-EM_{HU}	49.42 ± 24.59	13.27 ± 15.41	8.826[b]	<0.001
EN/EM_{HU}	1.79 ± 0.40	1.21 ± 0.24	12.160[b]	<0.001

[a]χ^2 test. [b]t test, and [c]Wilcoxon test.

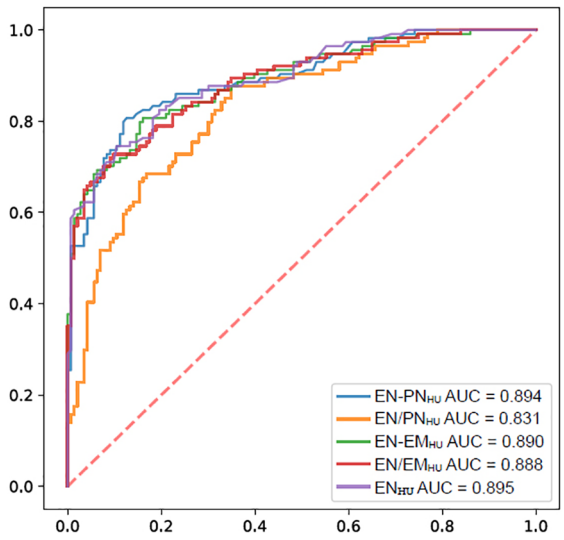

FIGURE 5
ROC of the EN_{HU}, EN-PN_{HU}, EN/PN_{HU}, EN-EM_{HU}, and EN/EM_{HU} for the diagnostic efficacy of LNs metastasis in PTC.

our study, 99.1% (113/114) and 78.3% (112/143) of metastasis-positive and metastasis-negative LNs showed significant enhancement, respectively, which was far from meeting the need for clinical diagnosis. Therefore, quantifying the degree of LN enhancement is important for improving the efficacy of the preoperative diagnosis of LNs.

At present, large differences exist in the delayed CT scanning time of cervical LN metastasis in PTC, such as 25 s, 35 s, 40 s, 45, 50 s, 60 s, 70 s, and 80 s (10–12, 15–18), using one or two phases. It is not difficult to understand that the conclusions drawn may differ using different scanning times; even if the scanning parameters are the same, the results may differ due to individual differences. For example, different conclusions have been drawn by the following scholars with the same delayed 25 s scanning after enhancement. Park et al. (16) analyzed 102 LNs in 42 patients, and the sensitivity and specificity were, respectively, 83%–87% and 93.7%–97.9%, at a cutoff value of EN_{HU} 99 HU. Gürsoy et al. (17) studied 272 LNs in 43 patients, and the results showed that the sensitivity and specificity were, respectively, 93.4% and 99.3%, with the cutoff value of EN_{HU} 109 HU. Su et al. (18) studied 59 LNs in 34

TABLE 3 Diagnostic efficacy of EN_{HU}, $EN\text{-}PN_{HU}$, EN/PN_{HU}, $EN\text{-}EM_{HU}$, and EN/EM_{HU} for LN metastasis in PTC.

	AUC	Cutoff value	Sensitivity	Specificity	Accuracy
EN_{HU}	0.895	97.3 HU	0.746	0.895	0.829
$EN\text{-}PN_{HU}$	0.894	47.8 HU	0.807	0.874	0.844
EN/PN_{HU}	0.831	1.9	0.877	0.650	0.751
$EN\text{-}EM_{HU}$	0.890	26.4 HU	0.807	0.839	0.825
EN/EM_{HU}	0.888	1.5	0.728	0.902	0.825

PN_{HU}, plain Hounsfield units of LNs; EN_{HU}, enhanced Hounsfield units of LNs; EM_{HU}, enhanced Hounsfield units of the sternocleidomastoid muscle; $EN\text{-}PN_{HU}$, difference between EN_{HU} and PN_{HU}; EN/PN_{HU}, ratio of EN_{HU} to PN_{HU}; $EN\text{-}EM_{HU}$, difference between EN_{HU} and EM_{HU}; EN/EM_{HU}, ratio of EN_{HU} to EM_{HU}; AUC, area under the curve.

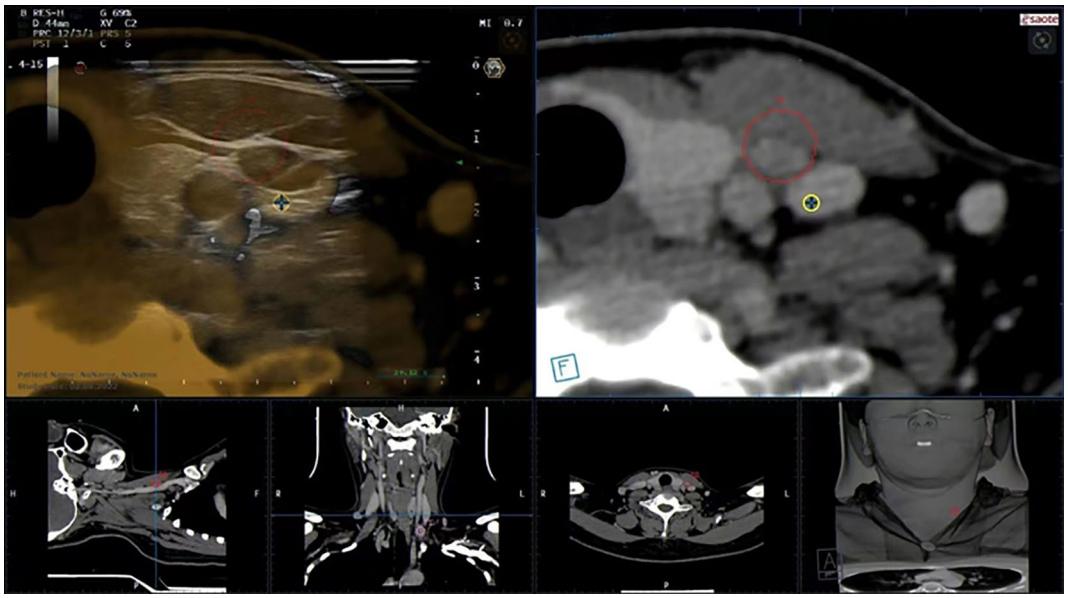

FIGURE 6
US-CT fusion imaging shows that the LN marked after image fusion was in the red circle, and LN metastasis in PTC was confirmed by FNAC.

patients and showed that the sensitivity and specificity were 90.62% and 77.78%, respectively, at a cutoff value of EN_{HU} 81.377 HU. The shortcomings of the studies by Park et al. (16) and Gürsoy et al. (17) included the possible deviation of sample representativeness (too many LNs were selected in one patient) and the fact that the LNs did not reach or completely reach the level of comparison between pathology and imaging. The small sample size was the limitation of the study by Su et al. (18). Yoon et al. (10) compared the enhancement degree of lateral cervical LNs and sternocleidomastoid muscle, and the results showed that the diagnostic efficiency was the highest when the difference between them was 35.7 HU, and the sensitivity, specificity, and accuracy were 0.686, 0.788, and 0.730, respectively. However, the limitation of their study was that the LNs did not reach the level of node-to-node contrast between imaging and pathology.

Our medical center adopted a single-phase delayed scan for 50 s to minimize the patient's radiation exposure, which was similar to the venous scan time used by Yoon et al. (10) and Kim et al. (11), and consistent with that used by Su et al. (18). The following three modifications were made in this study based on the findings of Park et al. (16), Gürsoy et al. (17), Su et al. (18), and Yoon et al. (10), including: (1) the LNs in one cervical level confirmed to be all metastasis-positive or all metastasis-negative, as well as the metastasis-positive LNs confirmed by FNAC under US-CT fusion navigation, were adopted, to ensure that each LN was definitely metastatic or nonmetastatic. Meanwhile, only one LN in the all metastasis-positive or all metastasis-negative level was selected as the study subject so that the sample was more representative (257 LNs were derived from 204 cases); (2) the measurement area of the sternocleidomastoid muscle (the level of the lower edge of the ipsilateral cricoid cartilage) was defined, mainly due to the thicker muscle in this area and uniform density, which were not easily affected by muscle atrophy and partial volume effect; also, the difference between different observers was small (ICC = 0.951); (3) PTC LN metastases were rich in blood supply and showed significant enhancement on CT enhanced images. This study used a

small ROI (3 × 3 pixels) was used to measure the most significantly enhanced area. The results reflected the CT HU of LN metastasis to a greater extent, and the difference between different observers was smaller (ICC = 0.994). Our results showed that EN_{HU}, EN/EM_{HU}, $EN\text{-}PN_{HU}$, and EN/PN_{HU} had similar diagnostic efficacy and were significantly higher than those reported by Yoon et al. (10), in which EN_{HU} and EN/EM_{HU} had higher specificity. In contrast, $EN\text{-}PN_{HU}$ and $EN\text{-}EM_{HU}$ had higher sensitivity. Although the sensitivity of EN/PN_{HU} was higher, the specificityand accuracy were lower and should not be used alone for the judgment of LN metastasis in PTC.

Hashimoto thyroiditis is an autoimmune disease. Positive TPO-Ab was found in 90%–95% of patients and positive TG-Ab was observed in 60%–80% of patients (19–21). In this study, the number of patients in the metastasis-negative group with Hashimoto's thyroiditis was higher than that in the metastasis-positive group, which might well explain why TPO-Ab and TG-Ab in the metastasis-negative group were higher than those in the metastasis-positive group. Hashimoto's thyroiditis is often accompanied by cervical LN enlargement, especially in the central group. No reliable report is available on whether Hashimoto's thyroiditis alters the degree of enhancement of the metastasis-positive or metastasis-negative LNs in PTC. The data of LN metastasis-negative PTC cases were analyzed. The results showed that the plain HU and enhanced HU of LNs in the group with Hashimoto's thyroiditis were not different from those in the group without Hashimoto's thyroiditis. Unfortunately, cases of Hashimoto's thyroiditis were few in the PTC LN metastasis-positive group (only 11 cases). Hence, it was impossible to explore whether Hashimoto's thyroiditis would change the degree of enhancement of metastasis-positive LNs in PTC.

US-CT fusion navigation is the registration and fusion of US and CT images, which integrates the advantages of high resolution and high detection rate of CT and real-time guidance of US. It has been widely used in the interventional therapy of abdominal organs such as the liver, prostate, and kidney (22), and reported in cervical LN metastasis only by Na et al. (12).

The present study had several limitations. First, most patients with negative LN metastasis had no LNs or small LNs, or enlarged LNs with Hashimoto's thyroiditis in level VI. Therefore, in this study, the metastasis-negative LNs mostly came from levels non-VI (74.8%). Second, the measured data were obtained from two senior head and neck radiologists. Although the radiologists demonstrated excellent interobserver agreement on PN_{HU}, EN_{HU}, and EM_{HU}, the interobserver agreement between junior radiologists still needed further confirmation through controlled studies. Finally, our study was a single-center retrospective analysis, thus having some selection bias. Further, prospective multicenter studies should be conducted to validate the findings.

In conclusion, EN_{HU}, $EN\text{-}PN_{HU}$, EN/EM_{HU}, and $EN\text{-}EM_{HU}$ had similarly high diagnostic efficacy in the preoperative evaluation of LN metastasis in PTC, with EN_{HU}, $EN\text{-}PN_{HU}$, and EN/EM_{HU} having higher specificity and $EN\text{-}PN_{HU}$ and $EN\text{-}EM_{HU}$ having higher sensitivity. Also, they were highly repeatable among different operators and hence worth popularizing and applying.

Data availability statement

The raw data supporting the conclusions of this article will be made available by the authors, without undue reservation.

Ethics statement

The studies involving human participants were reviewed and approved by The ethics committee of Affiliated Hangzhou First People's Hospital. Written informed consent for participation was not required for this study in accordance with the national legislation and the institutional requirements. Written informed consent was not obtained from the individual(s) for the publication of any potentially identifiable images or data included in this article.

Author contributions

All authors contributed to the study conception and design. Material preparation, data collection were performed by MT and TZ, and statistical analysis by HZ and PW. The first draft of the manuscript was written by JZ and all authors commented on previous versions of the manuscript. The final review and revision was by ZH. All authors read and approved the final manuscript. All authors contributed to the article and approved the submitted version.

Funding

This work was funded by the Medical Science Research Program of Zhejiang Province (2020RC091, 2021RC024).

Conflict of interest

The authors declare that the research was conducted in the absence of any commercial or financial relationships that could be construed as a potential conflict of interest.

Publisher's note

References

1. Lim H, Devesa SS, Sosa JA, Check D, Kitahara CM. Trends in thyroid cancer incidence and mortality in the United States, 1974-2013. *JAMA* (2017) 317(13):1338–48. doi: 10.1001/jama.2017.2719

2. Hoang JK, Branstetter BF4, Gafton AR, Lee WK, Glastonbury CM. Imaging of thyroid carcinoma with CT and MRI: approaches to common scenarios. *Cancer Imaging* (2013) 13(1):128–39. doi: 10.1102/1470-7330.2013.0013

3. McLeod DS, Sawka AM, Cooper DS. Controversies in primary treatment of low-risk papillary thyroid cancer. *Lancet* (2013) 381(9871):1046–57. doi: 10.1016/S0140-6736(12)62205-3

4. Londero SC, Krogdahl A, Bastholt L, Overgaard J, Trolle W, Pedersen HB, et al. Papillary thyroid carcinoma in Denmark, 1996-2008: Outcome and evaluation of established prognostic scoring systems in a prospective national cohort. *Thyroid* (2015) 25(1):78–84. doi: 10.1089/thy.2014.0294

5. Yang J, Zhang F, Qiao Y. Diagnostic accuracy of ultrasound, CT and their combination in detecting cervical lymph node metastasis in patients with papillary thyroid cancer: a systematic review and meta-analysis. *BMJ Open* (2022) 12(7):e051568. doi: 10.1136/bmjopen-2021-051568

6. Dolidze DD, Shabunin AV, Mumladze RB, Vardanyan AV, Covantsev SD, Shulutko AM, et al. A narrative review of preventive central lymph node dissection in patients with papillary thyroid cancer - a necessity or an excess. *Front Oncol* (2022) 12:906695. doi: 10.3389/fonc.2022.906695

7. Huang JH, Song MY, Shi HY, Huang ZY, Wang SJ, Yin Y, et al. Predictive factor of Large-volume central lymph node metastasis in clinical N0 papillary thyroid carcinoma patients underwent total thyroidectomy. *Front Oncol* (2021) 11:574774. doi: 10.3389/fonc.2021.574774

8. Liu CH, Liu YW, Lei Zhang L, Dong YW, Hu SB, Xia Y, et al. Risk factors for high-volume lymph node metastases in cN0 papillary thyroid microcarcinoma. *Gland Surg* (2019) 8(5):550–6. doi: 10.21037/gs.2019.10.04

9. Zhao H, Li H. Meta-analysis of ultrasound for cervical lymph nodes in papillary thyroid cancer: Diagnosis of central and lateral compartment nodal metastases. *Eur J Radiol* (2019) 112:14–21. doi: 10.1016/j.ejrad.2019.01.006

10. Yoon JH, Kim JY, Moon HJ, Youk JH, Son EJ, Kim EK, et al. Contribution of computed tomography to ultrasound in predicting lateral lymph node metastasis in patients with papillary thyroid carcinoma. *Ann Surg Oncol* (2011) 18(6):1734–41. doi: 10.1245/s10434-010-1527-9

11. Kim E, Park JS, Son KR, Kim JH, Jeon SJ, Na DG. Preoperative diagnosis of cervical metastatic lymph nodes in papillary thyroid carcinoma: comparison of ultrasound, computed tomography, and combined ultrasound with computed tomography. *Thyroid* (2008) 18(4):411–8. doi: 10.1089/thy.2007.0269

12. Na DK, Choi YJ, Choi SH, Kook SH, Park HJ. Evaluation of cervical lymph node metastasis in thyroid cancer patients using real-time CT-navigated ultrasonography: Preliminary study. *Ultrasonography* (2015) 34(1):39–44. doi: 10.14366/usg.14030

13. Alabousi M, Alabousi A, Adham S, Pozdnyakov A, Ramadan S, Chaudhari H, et al. Diagnostic test accuracy of ultrasonography vs computed tomography for papillary thyroid cancer cervical lymph node metastasis: A systematic review and meta-analysis. *JAMA Otolaryngol Head Neck Surg* (2022) 148(2):107–18. doi: 10.1001/jamaoto.2021.3387

14. Ni X, Xu S, Zhan W, Zhou W. A risk stratification model for metastatic lymph nodes of papillary thyroid cancer: A retrospective study based on sonographic features. *Front Endocrinol (Lausanne)* (2022) 13:942569. doi: 10.3389/fendo.2022.942569

15. Ahn JE, Lee JH, Yi JS, Shong YK, Hong SJ, Lee DH, et al. Diagnostic accuracy of CT and ultrasonography for evaluating metastatic cervical lymph nodes in patients with thyroid cancer. *World J Surg* (2008) 32(7):1552–8. doi: 10.1007/s00268-008-9588-7

16. Park JE, Lee JH, Ryu KH, Park HS, Chung MS, Kim HW, et al. Improved diagnostic accuracy using arterial phase CT for lateral cervical lymph node metastasis from papillary thyroid cancer. *AJNR Am J Neuroradiol* (2017) 38(4):782–8. doi: 10.3174/ajnr.A5054

17. Gürsoy Çoruh A, Uzun Ç, Kul M, Akkaya Z, Halil Elhan A, Gökcan K. The impact of arterial phase on the detection of cervical lymph node metastasis from papillary thyroid carcinoma: A quantitative evaluation on multiphasic computed tomography. *J Comput Assist Tomogr* (2020) 44(2):262–8. doi: 10.1097/RCT.0000000000001005

18. Su GY, Xu XQ, Zhou Y, Zhang H, Si Y, Shen MP, et al. Texture analysis of dual-phase contrast-enhanced CT in the diagnosis of cervical lymph node metastasis in patients with papillary thyroid cancer. *Acta Radiol* (2021) 62(7):890–6. doi: 10.1177/0284185120946711

19. Guan H, de Morais NS, Stuart J, Ahmadi S, Marqusee E, Kim MI, et al. Discordance of serological and sonographic markers for hashimoto's thyroiditis with gold standard histopathology. *Eur J Endocrinol* (2019) 181(5):539–44. doi: 10.1530/EJE-19-0424

20. Ragusa F, Fallahi P, Elia G, Gonnella D, Paparo SR, Giusti C, et al. Hashimotos' thyroiditis: Epidemiology, pathogenesis, clinic and therapy. *Best Pract Res Clin Endocrinol Metab* (2019) 33(6):101367. doi: 10.1016/j.beem.2019.101367

21. Durfee SM, Benson CB, Arthaud DM, Alexander EK, Frates MC. Sonographic appearance of thyroid cancer in patients with hashimoto thyroiditis. *J Ultrasound Med* (2015) 34(4):697–704. doi: 10.7863/ultra.34.4.697

22. Ahn SJ, Lee JM, Lee DH, Lee SM, Yoon JH, Kim YJ, et al. Real-time US-CT/MR fusion imaging for percutaneous radiofrequency ablation of hepatocellular carcinoma. *J Hepatol* (2017) 66(2):347–54. doi: 10.1016/j.jhep.2016.09.003

frontiers | Frontiers in Endocrinology

TYPE Original Research
PUBLISHED 06 July 2023
DOI 10.3389/fendo.2023.1108125

OPEN ACCESS

EDITED BY
Jose Federico Carrillo,
National Institute of Cancerology (INCAN), Mexico

REVIEWED BY
Claudio Casella,
University of Brescia, Italy
Giacomo Gaverini,
ASST Spedali Civili di Brescia, Italy

*CORRESPONDENCE
Xinliang Su
201604@hospital.cqmu.edu.cn

†These authors have contributed equally to this work

RECEIVED 25 November 2022
ACCEPTED 19 June 2023
PUBLISHED 06 July 2023

CITATION
Wang D, Hu J, Deng C, Yang Z, Zhu J and Su X (2023) Predictive nomogram for central lymph node metastasis in papillary thyroid microcarcinoma based on pathological and ultrasound features. *Front. Endocrinol.* 14:1108125. doi: 10.3389/fendo.2023.1108125

Predictive nomogram for central lymph node metastasis in papillary thyroid microcarcinoma based on pathological and ultrasound features

Denghui Wang[1†], Ji Hu[2†], Chang Deng[3], Zhixin Yang[4], Jiang Zhu[5] and Xinliang Su[1*]

[1]Department of Endocrine and Breast Surgery, The First Affiliated Hospital of Chongqing Medical University, Chongqing, China, [2]Department of General Surgery, The First People's Hospital of Chongqing Liang Jiang New Area, Chongqing, China, [3]Department of Endocrine and Breast Surgery, The Central Hospital Affiliated Chongqing University of Technology, Chongqing, China, [4]Department of Breast and Thyroid, Guiyang City Maternal and Child Health Care & Guiyang City Children's Hospital, Guiyang, China, [5]Department of Hepatobiliary Surgery, West China Hospital of Sichuan University, Chengdu, China

Background: Central lymph node metastases (CLNM) in papillary thyroid microcarcinoma (PTMC) are common, but management through prophylactic central lymph node dissection (pCLND) remains controversial. In this study, the independent predictors of CLNM in PTMC were retrospectively studied based on ultrasound and pathological data, and we aim to establish the prediction model to predict CLNM in PTMC.

Methods: This study included a total of 1,506 patients who underwent thyroid surgery for PTMC at the First Affiliated Hospital of Chongqing Medical University from 2015 to 2018. Ultrasound and clinicopathological features were summarized and analyzed. Univariate and multivariate analyses were performed to determine the risk factors associated with CLNM. The prediction model is established and verified according to the multivariate analysis results. The Kaplan–Meier curve was used to evaluate the effect of CLNM on survival.

Results: The CLNM rate was 44.5% (670/1,506). Multivariate analysis showed that men, younger age, smaller diameter, ETE, microcalcification, without Hashimoto's thyroiditis, and multifocal were independent risk predictors of CLNM. Nomogram has a good discriminative ability (C-index: 0.755 in the validation group), and the calibration effect is good. In the DCA curve, the CLNM prediction model performed better net benefit given any high-risk thresholds. The median follow-up time was 30 months (12–59 months), 116 cases were lost, and the follow-up rate was 92.8% (1,506/1,622). Of the 1,506 patients included, 12 (0.8%) experienced recurrence.

Conclusion: The likelihood of CLNM can be objectively quantified before surgery by using this reliable and accurate nomogram that combines preoperative ultrasound with clinicopathological features. Clinicians can use this nomogram to assess central lymph node status in patients with PTMC and consider prophylactic CND in patients with high scores.

KEYWORDS

nomogram, PTMC, CLNM, pathological, ultrasound

Introduction

Presently, thyroid carcinoma incidence happens more frequently, making it the most ordinary malignant neoplasm of the endocrine mechanism all around the world. Specifically, papillary thyroid microcarcinoma (PTMC) is defined as a subtype of papillary thyroid carcinoma (PTC) with a maximal size of less than 1 cm, accounting for 30% of PTC cases (1, 2). The reasons for the increased incidence were always controversial, whereas it might be the extensive utilization of high-sensitivity diagnostic tools like ultrasonography that allows the detection concerning smaller nodules. This was despite the fact that PTMC was an indolent tumor with a 10-year disease-free survival rate of >91% and a 15-year disease-free survival rate of >87%. However, the presence of lymph node metastasis (LNM) was always associated with an unfavorable oncological outcome (3–5), with a 0.4% fatality rate (6). Many studies reported the highest risk of central compartment LNM (CLNM), between 18% and 80% (7, 8). CLNM was considered one risk factor for distant metastasis (9), with the potential for recurrence and concomitantly reduced survival rate (4, 9). There were, nevertheless, questions about the implementation of prophylactic central lymph node dissection (pCLND) for PTMC. It was suggested that pCLND might benefit patients with PTMC by reducing local recurrence and enhancing the disease-free survival rate (10–12). Others hold the opposing view that it did not improve survival but rather increased the risk of nerve injury and hypoparathyroidism (13–15). Although the American Thyroid Association (ATA) guidelines (version 2015) stated that thyroidectomy without pCLND was indicated for the noninvasive treatment of marginal (T1 or T2), cN0 PTC (16), the Expert Consensus on the Diagnosis and Treatment of Papillary Thyroid Microcarcinoma (version 2016) edited by Chinese academics, recommended the promotion of pCLND for PTMC in the context of this technical support (17). The rate of preoperative detection of CLNM was relatively low due to limitations in imaging technology and operators. For instance, the diagnostic sensitivity of CLNM in the USA was only 51%–58.3%, with a false-passive rate of 44.6% (18). An appropriate, noninvasive tool to quantify the risk of CLNM in this setting may be helpful in the management of patients with PTMC.

It is important to balance the harms and benefits of pCLND in patients with PTMC for individualized and precise treatment. It is reasonable not to perform pCLND in low-risk PTMC patients. This was because it would reduce the extent of the procedure and the associated perplexities, particularly with regard to the protection of peripheral nerves, and facilitate the patient's postoperative recovery. In high-risk PTMC patients, the implementation of pCLND can achieve effective radical treatment of the tumor. Therefore, this paper not only identified risk factors for CLNM through intraoperative and preoperative findings but also established a predictive model for CLNM in patients with PTMC. This accurate and intuitive nomogram offered the possibility to objectively quantify CLNM preoperatively. At the same time, it achieved good utility and convenience in developing individualized treatment plans for patients.

Materials and methods

Patient information

The local institutional ethics committee backed up this retrospective research. Informed consent was waived after careful review by the ethics committee as there was no patient interest or privacy involved. The records of patients with PTMC who underwent surgery from January 2015 to December 2018 at the Department of Endocrinology and Breast of The First Affiliated Hospital of Chongqing Medical University were retrospectively reviewed. The total number of patients went through not less than a physical check, cervical ultrasound checking, and fine needle aspiration (FNA) before receiving surgery. Patients were the most vulnerable.

Patients were excluded from this research on the condition that they owned any of the elements below:

1. Non-PTMCs or mixed-type PTMC (14)
2. Reoperation or other head and neck surgery history (55)
3. Distant metastasis at diagnosis (7)
4. The radiation exposure during childhood or family PTMC history (3)
5. Incomplete clinicopathological data (144)
6. Those not to be follow-up after receiving surgery (116)
7. Adolescent (9)

In total, 350 patients were excluded; additionally, 1,506 eligible patients were ultimately included in this research (Figure 1).

Surgical procedures

After the patient finds a nodule of the thyroid through imaging inspection or palpation for the first time, we first perform the patient's thyroid function test and the neck ultrasonography for diagnosis. Second, for nodules with suspected malignancy, the fine-needle aspiration (FNA) would be implemented. After all inspections are completed, we will communicate with the patient and their family members about the surgical method and surgical risks. The lobectomy plus ipsilateral central lymph node dissection (CLND) was the foundational therapy in a surgical manner. The total thyroidectomy plus bilateral multifocal CLND was deeply implemented for the cases suffering from bilateral multifocal tumors, tumors located in the thyroid isthmus with extrathyroidal extension (ETE), suspicious metastatic lymph nodes by preoperative examination or intraoperative frozen section biopsy showing CLNM. Lobectomy was stated as the removal of the implicated lobe, including the pyramidal lobe and the isthmus. Total thyroidectomy (TT) was stated as the removal of the two lobes: the pyramidal lobe and the isthmus lobe. Central lymph node dissection (CND) encompassed the removal of the pretracheal, prelaryngeal, and both the left and right paratracheal nodal basins (19). We routinely conducted a CLN intraoperative frozen section biopsy to further determine the degree of the lymph node analysis and the demand for total thyroid resection. Three pathologists independently and blindly diagnosed all resected lymph node and thyroid specimens, and a frozen section biopsy revealed CLNM.

Clinicopathological and ultrasonographic data

We included the relevant data from ultrasonography and clinicopathological characteristics in the analysis. Data gathered included tumor size, age, multifocality, sex, ETE, preoperative cancer-related suspicion, central LN status, along with US features including shape, margin, location, echogenicity, length/width rate > 1, microcalcification emergence, the status of blood flow, and discontinuity of the capsule. Age has been dichotomized in view of the present stage criteria at 55 years. The biggest size of the neoplasm has been stated. The multifocalities have been characterized as > 1 overall neoplasm focus (either in the identical lobe or in the disparate lobes). In one single lobe, two or more PTMC foci were unilateral multifocality, whereas two or more PTMC foci in one lobe plus isthmus or both lobes were bilateral multifocality. Diagnosis of Hashimoto's thyroiditis (HT) was made on the basis of the pathological data. ETE was based on pathological data and stated as the primary neoplasm spreading through the thyroid capsule to the perithyroidal soft tissue, including involving strap muscles or perithyroidal fat, or spreading to circumambient structures including trachea, larynx, recurrent laryngeal nerve, esophagus, skin, subcutaneous soft tissue, internal jugular vein, or carotid artery (20). The two radiologists, each of whom has over 15 years of expertise, implemented the overall preoperative US exams. Hypoechoicity, a length/width rate of less than one, fuzzy edges, hypervascularity, irregular forms, and the emergence of microcalcifications were the hallmarks of the malignant nodules. Pathologic lymph nodes (diffuse or focal, round form, cystic changes, internal calcification, and chaotic or peripheral vascularities on Doppler US) were stated as those with or without not less than one suspected US-type (focal or diffusion-like hyperechogenicity) (21). Ultrasound features of every nodule were encompassed as below: classification of the margin as to whether clear or irregular shape; whether the nodule was simply hypoechogenicity (inferior to the cervical band muscle); length/width ratio >1; of microcalcifications with a threshold value of 1

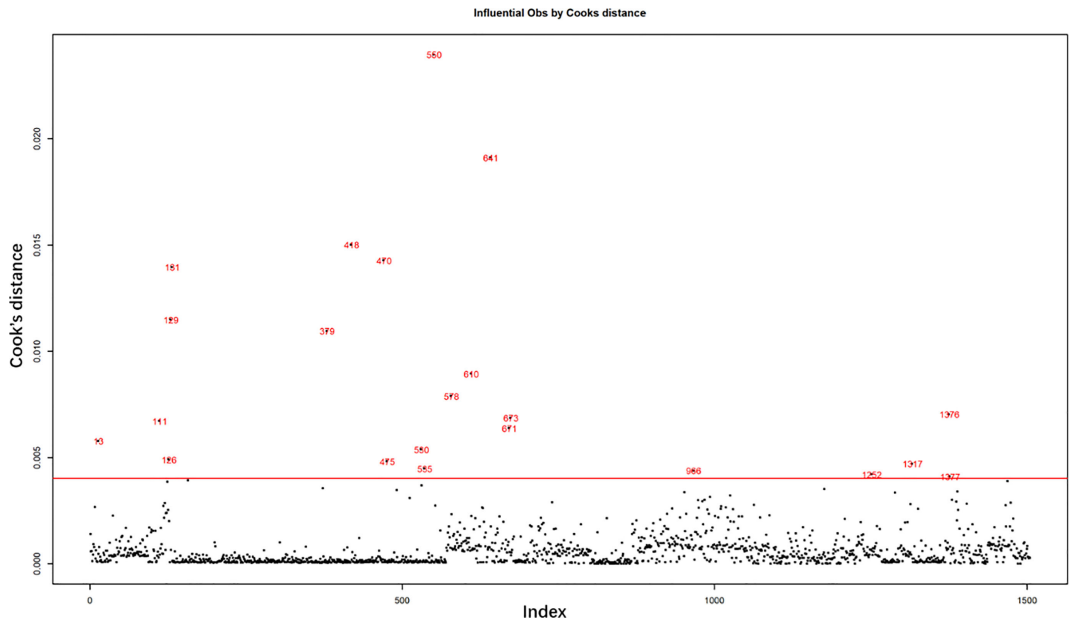

FIGURE 1
Excluded abnormal influential observations by Cook's distance.

mm; discontinuity of the capsule defined as contact of the thyroid mass by means of the thyroid capsule, that is, >25% contacting with the neighbor capsule, is the best indicator for predicting the extrathyroidal spread (22); and rich and not rich blood flow status.

Follow-up

For the total number of sick people, the initial follow-up was set at 1 month postoperatively; moreover, evaluation consisted of palpation and measurement of the levels of serum TSH. Serum thyroglobulin (Tg), along with Tg antibody levels, is merely for the patients who have undergone the overall thyroidectomy. Ultrasonography was performed 6 months after surgery. After that, the patient was re-examined every 6–12 months. On condition that the unstimulated Tg levels ≥ 2 ng/ml and stimulated Tg levels ≥ 20 ng/ml or serially elevated serum Tg (Tg-negative antibodies) are found, or if tumor recurrence is suspected on imaging studies (23), we will perform FNA in these patients, and if tumor recurrence is determined, the overall condition of the patient will be re-evaluated to decide on surgery method or other treatments.

Statistical analysis

Categorical variables were summarized as numbers (percentage), and continuous variables were summarized as means (± standard deviation). One-way ANOVA test was conducted to test the correlation relationship of each variable with CLNM, and the *p*-value was displayed in the univariate analysis. A significance level of 0.05 was considered statistically significant for all statistical analyses. Prior to multivariate analysis, abnormal influential observations were examined using Cook's distance, and the abnormal line was set as greater than six times the mean of Cook's distance. Observations beyond the abnormal line were excluded from the multivariate analysis. The logistic regression model was built for the prediction of CLNM with all candidate factors as an entry in the independent variables, and then the variables were selected stepwise. The estimated coefficient of each selected variable and its corresponding 95% confidence interval were calculated, along with the *p*-value of each estimated coefficient. The model's prediction discrimination was evaluated by C-index and ROC curve. AUC was exhibited with the ROC curve. The model's calibration ability was evaluated by a calibration plot. The Kaplan–Meier curve was plotted for the overall survival grouped by CLNM, and the log-rank test was conducted accordingly. At last, decision curve analysis (DCA) was carried out to evaluate the net benefit of the prediction model with different risk thresholds used. In addition, the clinical impact curve was plotted along with the DCA curve to evaluate the discrepancy between the number of predicted positive and true-positive observations with different risk thresholds used.

Result

Baseline clinical and US characteristics of patients with 1,506 PTMC

The median follow-up time is 29 months. The baseline characteristics of risk factors for CLNM are shown in Table 1. Factors that exhibited significant association with CLNM *via* one-way ANOVA test were sex, length, invasion, preoperative clinical suspicion of CLNM, Hashimoto's thyroiditis, laterality, focal infection, ETE, age, and diameter. Women accounted for 83.3% in the no-CLNM group and 65.2% in the CLNM group. Patients without preoperative clinical suspicion of CLNM accounted for 99.2% in the no-CLNM group and 83.7% in the CLNM group. Unilateral accounted for 93.9% in the no-CLNM group and 82.7% in the CLNM group. Unifocal accounted for 86.7% of the no-CLNM group and 61.2% of the CLNM group. Patients without ETE accounted for 97.6% of the no-CLNM group and 89.0% of the CLNM group. The average age in the no-CLNM group is 45.02 (SD = 12.3), and in the CLNM group, it is 41.46 (SD = 10.68). The average diameter in the no-CLNM group is 6.64 (SD = 2.07), and it is 7.03 (SD = 2.08) in the CLNM group. Apart from these factors, the rest of the factors do not show a strong discrepancy in terms of the distribution between the no-CLNM and CLNM groups.

Result of Cook's distance

The influential observations were examined by Cook's distance, as shown in Figure 1. The horizontal red line is the abnormal line set for excluding abnormal influential observations beyond the line. It was set at six times the mean of Cook's distance. A total of 22 abnormally influential observations were excluded, leaving 1,484 observations for the multivariate analysis.

Comparison of clinical and US factors with CLNM in the training group

A multivariate analysis of the risk factors for CLNM was carried out using a logistic regression model. Data were randomly split by a ratio of 3:2 as training dataset and a validation dataset, respectively. All candidate variables were included at the beginning of the model selection and were selected stepwise. The selected variables are shown in Table 2, along with their odds ratio (OR), corresponding 95% CI, and *p*-value. Among the selected variables, the significant variables were sex, ETE, Hashimoto's thyroiditis, focal infection, age, and diameter. Compared to men, women are less likely to experience CLNM, and their OR is 0.32 (95% CI: 0.22–0.45). Patients with ETE are much more likely to experience CLNM (OR = 10.72; 95% CI: 4.08–28.12). Patients with Hashimoto's thyroiditis are less likely to experience CLNM (OR = 0.53; 95% CI: 0.36–0.80). Compared to unifocal infection, the odds of

10.3389/fendo.2023.1108125

TABLE 1 Univariate analysis of risk factors for central lymph node metastasis.

	n (%) or mean (SD)		*p*-value
	CLNM = No	CLNM = Yes	
Sex			
Male	140 (16.7%)	233 (34.8%)	<0.0001
Female	696 (83.3%)	437 (65.2%)	
Age	45.02 (12.3)	41.46 (10.68)	<0.0001
Diameter	6.64 (2.07)	7.03 (2.07)	0.0003
Tumor location			
Upper	175 (20.9%)	132 (19.7%)	0.144
Middle	396 (47.4%)	310 (46.3%)	
Lower	233 (27.9%)	188 (28.1%)	
Isthmus	32 (3.8%)	39 (5.8%)	
Margin			
Clear	228 (27.3%)	172 (25.7%)	0.395
Near-clear	330 (39.5%)	263 (39.3%)	
Unclear	278 (33.3%)	235 (35.1%)	
Shape			
Regular	193 (23.1%)	140 (20.9%)	0.23
Near-regular	359 (42.9%)	286 (42.7%)	
Irregular or lobulated	284 (34.0%)	244 (36.4%)	
Echogenicity			
Hypoechogenicity	773 (92.5%)	614 (91.6%)	0.614
Isoechoic	61 (7.3%)	55 (8.2%)	
Hyperechoic	2 (0.2%)	1 (0.1%)	
Length			
Width ratio ≤1	572 (68.4%)	490 (73.1%)	0.0462
Width ratio >1	264 (31.6%)	180 (26.9%)	
Calcification			
No	347 (41.5%)	251 (37.5%)	0.663
Microcalcification	424 (50.7%)	385 (57.5%)	
Coarse calcification	65 (7.8%)	34 (5.1%)	
Blood signal			
No blood flow signals	419 (50.1%)	323 48.2%)	0.925
Enriched blood flow signal	68 (8.1%)	77 (11.5%)	
Punctate flow signal	349 (41.7%)	270 (40.3%)	
Invasion			
Continuity of the capsule	783 (93.7%)	609 (90.9%)	0.0439
Discontinuity of the capsule	53 (6.3%)	61 (9.1%)	

(Continued)

TABLE 1 Continued

	n (%) or mean (SD)		*p*-value
	CLNM = No	CLNM = Yes	
Preoperative clinical suspicion of CLNM			
No	829 (99.2%)	560 (83.7%)	<0.0001
Yes	7 (0.8%)	109 (16.3%)	
Hashimoto's thyroiditis			
No	663 (79.3%)	570 (85.1%)	0.0039
Yes	173 (20.7%)	100 (14.9%)	
Laterality			
Unilateral	785 (93.9%)	554 (82.7%)	<0.0001
Bilateral	51 (6.1%)	116 (17.3%)	
Focal infection			
Unifocal	725 (86.7%)	410 (61.2%)	<0.0001
Multifocal	111 (13.3%)	260 (38.8%)	
ETE			
No	816 (97.6%)	596 (89.0%)	<0.0001
Yes	20 (2.4%)	74 (11.0%)	
Recurrence			
No	831 (99.4%)	663 (99.0%)	0.333
Yes	5 (0.6%)	7 (1.0%)	
Month	30.74 (13.63)	30.11 (13.53)	0.372

The frequency of each category across CLNM is calculated for categorical variables along with its percentage; the mean and standard deviation are calculated for continuous variables; the ANOVA test of each variable versus CLNM is conducted to test their associations; and the p-value of the ANOVA test is recorded in the table.

experiencing CLNM is 4.33 (95% CI: 3.04–6.17) times higher for multifocal infection. The age increases by 1 year, and the odds of CLNM would decrease by 0.03 (OR = 0.97; 95% CI: 0.96–0.98). If the diameter increases by 1 mm, the odds of CLNM would increase by 0.08 (OR = 1.08; 95% CI: 1.00–1.16). Patients with microcalcification are more likely to have CLNM (OR = 1.24; 95% CI: 0.91, 1.68), and coarse calcification is a protective factor for the occurrence of CLNM (OR = 0.73; 95% CI: 0.38-1.38).

Validation of the prediction nomogram

The final model achieved a C-index of 0.755 on the validation dataset. ROC curves for the training and validation sets are shown in Figure 2. The AUC on the training and validation sets was all 0.755, which indicates that the model can achieve good accuracy of prediction in both the training and validation sets. In addition, the calibration plots for training and validation are shown in Figure 3, and both calibrated lines are very close to the diagonal line, which indicates that the model was well calibrated. The predicted effect of each variable was visualized in the nomogram (Figure 4). The ETE has the most effective potential to explain the risk points in this study, followed by age, focal infection, sex, and diameter. Hashimoto's thyroiditis and microcalcification had a modest contribution to the risk of CLNM. Finally, the model was further analyzed using DCA. The DCA curve and clinical impact curve were plotted (Figure 5). In the DCA curve (Figure 5A), the CLNM prediction model performed better in terms of net benefit given any high-risk thresholds. In the clinical impact curve (Figure 5B), the discrepancy of the number of CLNM between predicted positives and true positives converged drastically around 0.4. In order to have a better net benefit and a small discrepancy between the number of predicted positives and true positives, 0.4 would be an appropriate cutoff value for the prediction model in this study.

Follow-up status

As last, the survival analysis of CLNM was conducted using the Kaplan–Meier curve. We followed up 1,506 patients (follow-up rate: 92.98%) after the initial surgery until December 2019. The interesting event is a recurrence of the PTMC. The *p*-value for the log-rank test is 0.3, which means that there is no significant difference between CLNM and no-CLNM group in terms of the recurrence rate. Both groups had a very low recurrence rate (Figure 6).

TABLE 2 Multivariate analysis of risk factors for central lymph node metastasis using logistic regression.

	Odds ratio	95% CI	*p*-value
Sex			
Male	Reference		<0.0001
Female	0.32	(0.22, 0.45)	
Age	0.97	(0.96, 0.98)	<0.0001
Diameter	1.08	(1.00, 1.16)	0.0135
ETE			
No	Reference		<0.0001
Yes	10.72	(4.08, 28.12)	
Calcification			
No	Reference		
Microcalcification	1.24	(0.91, 1.68)	0.0178
Coarse calcification	0.73	(0.38, 1.38)	0.0331
Hashimoto's thyroiditis			
No	Reference		0.0026
Yes	0.53	(0.36, 0.80)	
Focal infection			
Unifocal	Reference		<0.0001
Multifocal	4.33	(3.04, 6.17)	

The C-index of the logistic regression model is 0.755.

Discussion

PTMC is a subtype of PTC that is less than 10 mm in diameter. In recent years, its incidence has gradually increased due to advances in ultrasonography and the importance individuals place on physical examination (24, 25). Despite the good prognosis of PTMC, a small number of patients developed local recurrence or distant metastases. Central LNM was only one of the essential factors contributing to their occurrence (26). Ultrasonography was not sensitive to detect metastatic central cervical lymph nodes prior to surgery. This was because they were usually marginal, confused by the overlying thyroid, or had atypical ultrasound features. However, many PTMC patients who were clinically lymph node-negative (cN0) were found to have CLNM metastases during surgery. CLNM (found only on pathological examination) was reported in 49.2%–64.1% of patients with cN0 PTMC (27, 28). In low-risk patients with papillary thyroid cancer, pCLND remained in doubt. Some studies advocated regular CLND during primary thyroidectomy in patients with PTMC. This was because it could benefit mPTC patients by reducing local recurrence and improving disease-specific survival rates (29, 30). It was also opposed because it did not improve survival but rather exacerbated the risk of neurological damage and hypoparathyroidism (14). Even in the research by

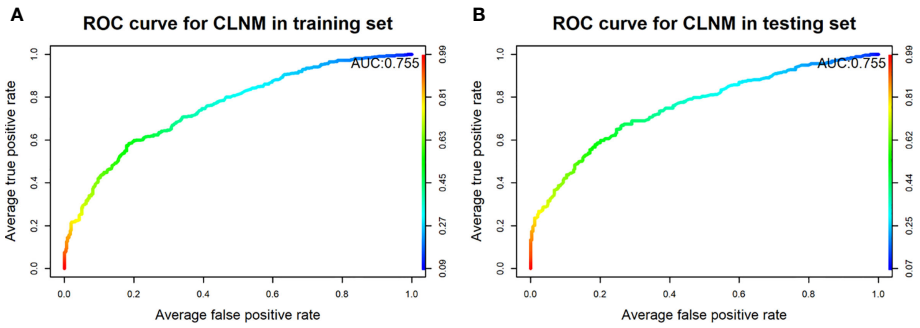

FIGURE 2
Receiver operating characteristic curves of the model for predicting CLNM in the training set **(A)** and testing set **(B)**.

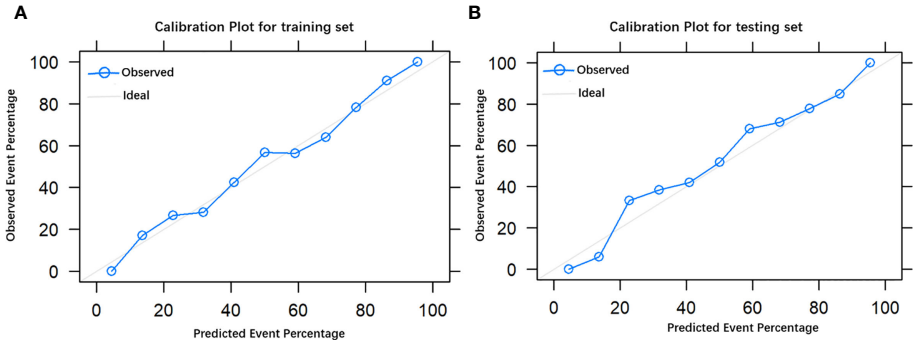

FIGURE 3
The calibration plot of the model in the training group **(A)** and testing group **(B)**.

Sugitani et al. and Ito et al., they found a lower incidence of tumor growth and new LNM in patients with low-risk (T1aN0M0) PTMC through prospective clinical studies. In patients who underwent surgery for tumor growth or new LNM, there were no life-threatening recurrences or deaths from thyroid cancer. There were also no distant metastasis or deaths from thyroid cancer in the active surveillance (AS) (31, 32). Therefore, accurate prediction of CLNM in PTMC is important for individualized treatment.

In this research, the incidence of CLNM was 44.5%, which was in line with the results of earlier studies (7, 8). As one of the important tools for the preoperative assessment of PTMC, ultrasound examination has been used as a routine for PTMC in China. However, the sensitivity and specificity of using ultrasound techniques to assess CLNM were 12.5% and 95.2%, respectively (33), due to a high dependence on the experience of the sonographer and interobserver variability (34). Therefore, the goal of this study was to develop a nomogram that could be used as an emerging strategy to personalize and quantify the likelihood of CLNM in patients with PTMC. The current research indicated that age, gender, tumor dimension, microcalcification, HT, focal infection, and ETE were independent predictors of CLNM. Tumor location, echogenicity, length/width ratio >1, blood signal, capsule invasion, and laterality were not predictive.

For a long time, age was for a clinically important prognostic factor in PTMC. Research by Ito found that younger age was only an independent indicator of PTMC progression (included: (1) increase in volume; (2) new manifestations of LNM; (3) clinical disease progression with an increase in tumor volume of 12 mm or greater; and new manifestations of LNM). In other studies, age had the same effect on PTMC (35, 36), that is, the lowest PTMC promotion rate in older patients and the highest in younger patients (3). In the present study, high age was a separate protective factor for CLNM. In addition, low age had the highest corresponding rank in the nomogram. In clinical practice, a more thorough preoperative assessment of the CLNM status of younger patients is necessary. Moreover, treatment may be different for younger patients than for older patients. Older patients with PTMC are the best candidates for observation, whereas younger patients may require active intervention.

Numerous studies showed that the incidence of PTMC was higher in women than in men, while the incidence of CLNM was low (37, 38). In this research, the ratio of men to women suffering from CLNM was approximately 1:2, and women were an independent protective factor for CLNM in patients with PTMC (OR = 0.32; $p < 0.0001$). It was traditionally assumed that the larger diameter of the tumor, the more aggressive it would be. ATA

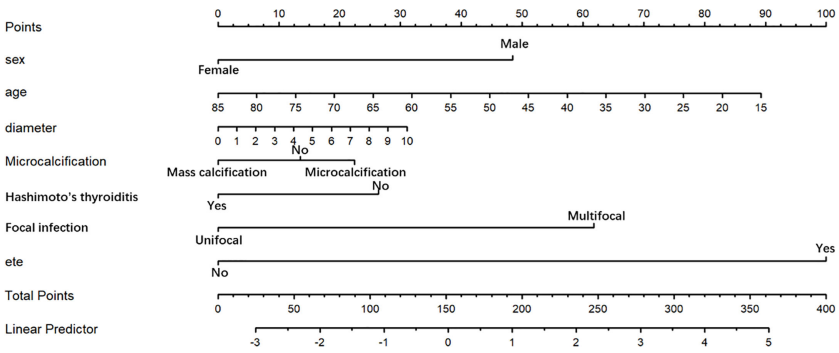

FIGURE 4
Nomogram for prediction of CLNM. A line is drawn straight up to the point axis that corresponds with each patient variable to obtain the points. The sum of these points is located on the total score point axis. A line is drawn downward to the risk axis to determine the possibility of CLNM.

10.3389/fendo.2023.1108125

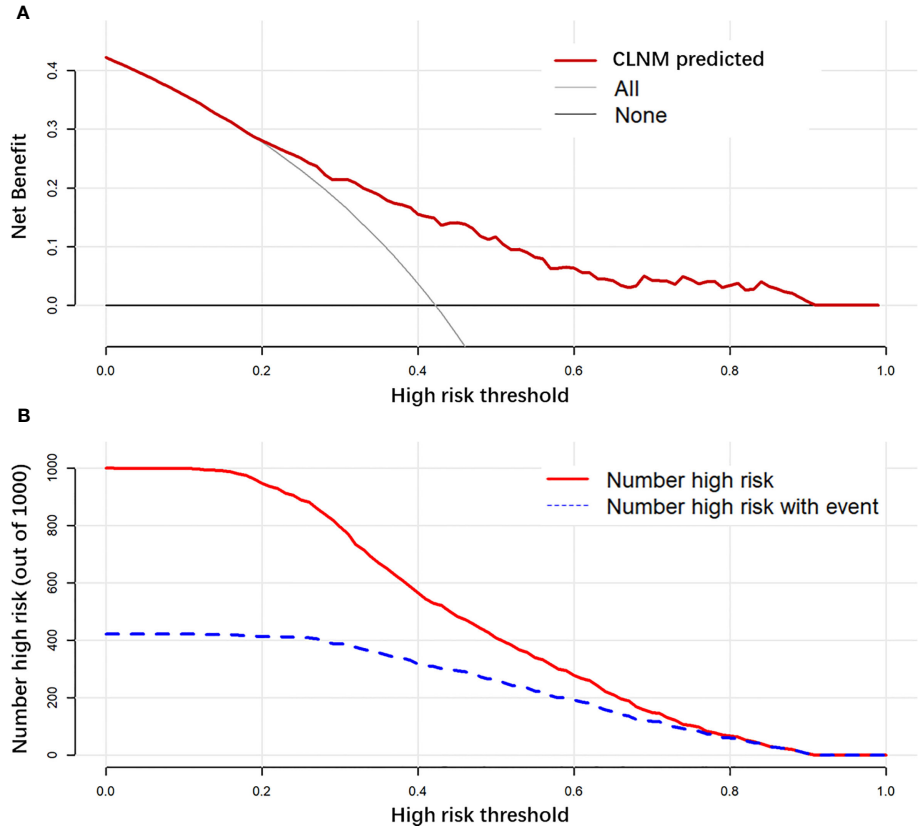

FIGURE 5
Decision curve analysis (DCA) is used to evaluate the net benefit of a prediction model with different risk thresholds used **(A)**. Clinical impact curve to evaluate the discrepancy between the number of predicted-positive and true-positive observations with different risk thresholds used **(B)**.

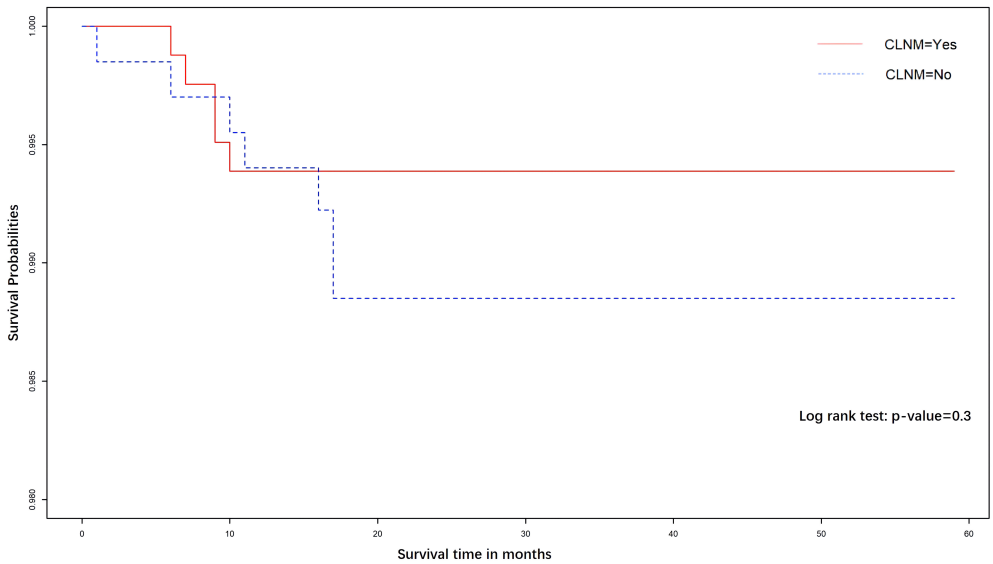

FIGURE 6
The Kaplan–Meier curves for the PTMC patients. There was no significant difference in the DFS rate between the CLNM(+) and CLNM(–) cohorts.

guidelines indicated that pCLND might be considered for patients with advanced primary neoplasms and clinically involved lateral cervical lymph nodes (cN1b). In contrast, in patients with marginal (T1 or T2), clinically negative PTC, and noninvasive patients (16), thyroidectomy may be appropriate instead of PCL. However, the incidence of CLNM in PTMC was usually about 50%, and there might be residual metastatic lymph nodes if pCLND was not performed, leading to resurgery and the risk of serious postoperative complications. For PTMC, some studies suggested that the risk of CLNM metastasis was higher if the diameter was larger (33, 38), and the same conclusion was reached in this study.

HT was the most common autoimmune thyroid disease, with an incidence rate of about 3.5 to five cases per 1,000 people per year (39, 40). The relationship between HT with PTMC has been controversial since it was first described by Dailey et al. in 1955 (41). A few scholars believed that HT was a protective factor for CLNM in PTMC (42, 43), while other studies showed no significant protective effect of HT on CLNM (44). In this study, HT was found to reduce the incidence of CLNM in PTMC. This might bring about fibrosis and atrophy of the thyroid due to HT-induced inflammation. This process involved an associated injury to the adjacent lymphatic vessels, disrupting PTC lymphatic diffusion, and eventually creating problems in reducing the likelihood of CLNM (45).

Bilateral or multifocal tumors might be caused by a single primary tumor spreading through the gland or by multiple concurrent primary tumors (46). It occurred in about 20%–40% of patients with PTMC (47). Although multifocal PTMCS were probably only synchronous tumors and not metastases from the largest primary neoplasm, they were associated with an increased risk of LNM, persistent local disease, distant metastasis, and local recurrence. In this study, it was analyzed in a single-bilateral lesion group and a single-multiple lesion group. The results found that multiple lesions were an independent risk factor for the development of CLNM in patients with PTMC (OR = 3.95; $p < 0.0001$) and the second significant variable in the nomogram.

Ultrasound was a convenient and quick way to evaluate PTMC. It might contain low central lymph nodes (grade VI) due to the presence of the thyroid or some anatomical areas (such as deep bony or air-filled structures and in the retropharyngeal region and mediastinum) that were not clearly visible on ultrasound (48). Retrospective research reported that the sensitivity of high-resolution ultrasound in predicting central LNM in PTC was only 38%. Seven characteristic variables of ultrasound were included in the analysis of this study. Microcalcification was one of the highly specific signs in ATA 2015 (16) and an essential ultrasound finding for suspected malignant nodes. It presented as punctate hyperechoic and was not easily missed. Nodules with microcalcification might be more likely to have cervical LNM. However, as hyperechoic indicated calcification, the ultrasound showed oxalates and concentrated colloids, which made it more difficult for junior doctors to identify microcalcifications. The ultrasound examinations enrolled in this study were performed by experienced sonographers, which marginally improved the diagnostic accuracy of microcalcifications. In this study, microcalcifications had an OR of 1.24 and were an independent risk factor for the occurrence of CLNM, which was consistent with other studies (32, 49). Microcalcifications reflected the rapid proliferation of cancer cells and the deposition of calcium salts due to the enlargement of blood vessels and fibers. As a result, if microcalcifications were found in the nodules, the status of LNs in the intermediate regions would need to be inspected more closely. Meanwhile, coarse calcification was found to be a protective factor for CLNM. This was probably because it was formed by necrosis within the tumor, indicating weak tumor growth activity.

ETE was a tumor that breached the thyroid capsule. After the thyroid capsule ruptured, the tumor was more likely to invade lymph nodes through the lymphatic vessels on the capsule surface. It involved the pharynx, strap muscles (thyroid gland of the sternum, thyrohyoid or mastoid), thyroid-bonding, larynx, prevertebral fascia, esophagus, mediastine, and even carotid artery, along with the PTMC artery. Various studies linked ETE to the invasiveness of PTMC. PTMC occurred when extrathyroidal structures were attacked and was shown to be a risk factor for CLNM (50, 51). According to the 2015 ATA criteria (16), ETE was only one indicator of a poor prognosis. In multivariate analysis, ETE was an independent risk factor for CLNM (OR = 10.72). In addition, ETE has the most effective potential to explain the risk points in the nomogram. This might be due to the fact that once the tumor cells breached the thyroid capsule, they metastasized to the CLNs through the surrounding abundant lymphoid tissue.

The results of the follow-up indicated that few patients suffered from central lymph node recurrence, which confirmed the reliability of examining the pathological status of the central lymph nodes. From the survival analysis, it was concluded that there was no significant difference in recurrence between patients with and without CLNM. However, some subclinical central lymph node metastases may lead to recurrence and distant metastasis. In addition, there is still controversy over whether PTMC patients need to undergo pCLND under domestic and foreign guidelines. Therefore, in order to achieve more accurate and individualized treatment, the model of this study was established to guide clinicians in selecting central lymph node dissection according to the scores, which were calculated based on disease status, so as to avoid unnecessary CLND and reduce postoperative complications. Moreover, in order to avoid recurrence, technical difficulties, hypoparathyroidism, and other complications caused by reoperation, CLND is still recommended when CLNM is found before or during surgery.

This research still had some shortcomings: (1) It was only a single-center retrospective research. Additionally, selection bias was inevitable. (2) Deficiencies in external validation. Relevant prospective multicenter clinical research should be implemented in the coming years to assess the validity of the proposed model. (3) The relatively short follow-up period in this study did not allow for the analysis of potential confounding factors for future metastasis. Therefore, more data and longer follow-ups are needed in the

subsequent work. On the other hand, improving existing proven models, such as by including new variables that have been shown to work (such as BRAF-V600E), can improve the accuracy of the "old" nomogram. In summary, a quantitative CLNM prediction model for PTMC was formulated in this paper. Physicians can use the nomogram in this model to assess patients with PTMC in clinical practice based on clinicopathological features. For PTMC with a high possibility of CLNM, unnecessary pCLND may be avoided.

Above all, our study found that CLNM was independently associated with sex, age, diameter, ETE, calcification in ultrasound, Hashimoto's thyroiditis, and focal infection. Using the above variables, we construct a nomogram. Clinicians can use the nomogram to assess central lymph node status in patients with PTMC. For patients with high scores, pCLND and meticulous postoperative evaluation can be considered.

Data availability statement

The original contributions presented in the study are included in the article/Supplementary Material. Further inquiries can be directed to the corresponding author.

Ethics statement

The studies involving human participants were reviewed and approved by Ethics Committee of the First Affiliated Hospital of Chongqing Medical University. Written informed consent to participate was waivered by the ethics committee.

Author contributions

DW and JH: designed this study, analyzed the data, and wrote this paper. DW, JZ, CD, and ZY: data collection. XS: designed this study, conducted the examination, and modified the manuscript. All authors contributed to the article and approved the submitted version.

Acknowledgments

The authors appreciate all of the staff involved in the preparation of the study.

Conflict of interest

The authors declare that the research was conducted in the absence of any commercial or financial relationships that could be construed as a potential conflict of interest.

Publisher's note

References

1. Usluogullari CA, Onal ED, Ozdemir E, Ucler R, Kiyak G, Ersoy PE, et al. A retrospective analysis of prognostic factors predictive of lymph-node metastasis and recurrence in thyroid papillary microcarcinoma. *Minerva Endocrinol* (2015) 40:15–22. doi: 10.1002/ejic.200400863

2. Krajewska J, Kukulska A, Oczko-Wojciechowska M, Kotecka-Blicharz A, Drosik-Rutowicz K, Haras-Gil M, et al. Early diagnosis of low-risk papillary thyroid cancer results rather in overtreatment than a better survival. *Front Endocrinol (Lausanne)* (2020) 11:571421. doi: 10.3389/fendo.2020.571421

3. Ito Y, Miyauchi A, Kihara M, Higashiyama T, Kobayashi K, Miya A. Patient age is significantly related to the progression of papillary microcarcinoma of the thyroid under observation. *Thyroid* (2014) 24:27–34. doi: 10.1089/thy.2013.0367

4. Gorostis S, Raguin T, Schneegans O, Takeda C, Debry C, Dupret-Bories A. Incidental thyroid papillary microcarcinoma: survival and follow-up. *Laryngoscope* (2019) 129:1722–6. doi: 10.1002/lary.27664

5. Lee YK, Hong N, Park SH, Shin DY, Lee CR, Kang SW, et al. The relationship of comorbidities to mortality and cause of death in patients with differentiated thyroid carcinoma. *Sci Rep* (2019) 9:11435. doi: 10.1038/s41598-019-47898-8

6. Hay ID, Grant CS, van Heerden JA, Goellner JR, Ebersold JR, Bergstralh EJ. Papillary thyroid microcarcinoma: a study of 535 cases observed in a 50-year period. *Surgery* (1992) 112:1139–46. doi: 10.1016/j.surg.2008.08.035

7. Mehanna H, Al-Maqbili T, Carter B, Martin E, Campain N, Watkinson J, et al. Differences in the recurrence and mortality outcomes rates of incidental and nonincidental papillary thyroid microcarcinoma: a systematic review and meta-analysis of 21 329 person-years of follow-up. *J Clin Endocrinol Metab* (2014) 99:2834–43. doi: 10.1210/jc.2013-2118

8. Kouvaraki MA, Shapiro SE, Fornage BD, Edeiken-Monro BS, Sherman SI, Vassilopoulou-Sellin R, et al. Role of preoperative ultrasonography in the surgical management of patients with thyroid cancer. *Surgery* (2003) 134:946–54. doi: 10.1016/s0039-6060(03)00424-0

9. Roti E, degli Uberti EC, Bondanelli M, Braverman LE. Thyroid papillary microcarcinoma: a descriptive and meta-analysis study. *Eur J Endocrinol* (2008) 159:659–73. doi: 10.1530/eje-07-0896

10. Hyun SM, Song HY, Kim SY, Nam SY, Roh JL, Han MW, et al. Impact of combined prophylactic unilateral central neck dissection and hemithyroidectomy in patients with papillary thyroid microcarcinoma. *Ann Surg Oncol* (2012) 19:591–6. doi: 10.1245/s10434-011-1995-6

11. Hughes DT, White ML, Miller BS, Gauger PG, Burney RE, Doherty GM. Influence of prophylactic central lymph node dissection on postoperative thyroglobulin levels and radioiodine treatment in papillary thyroid cancer. *Surgery* (2010) 148:1100–6. doi: 10.1016/j.surg.2010.09.019

12. Su H, Li Y. Prophylactic central neck dissection and local recurrence in papillary thyroid microcarcinoma: a meta-analysis. *Braz J Otorhinolaryngol* (2019) 85:237–43. doi: 10.1016/j.bjorl.2018.05.004

13. Akın Ş, Yazgan Aksoy D, Akın S, Kılıç M, Yetişir F, Bayraktar M. Prediction of central lymph node metastasis in patientswith thyroid papillary microcarcinoma. *Turk J Med Sci* (2017) 47:1723–7. doi: 10.3906/sag-1702-99

14. Ywata de Carvalho A, Chulam TC, Kowalski LP. Long-term results of observation vs prophylactic selective level VI neck dissection for papillary thyroid carcinoma at a cancer center. *JAMA Otolaryngol Head Neck Surg* (2015) 141:599–606. doi: 10.1001/jamaoto.2015.0786

15. Zhao W, You L, Hou X, Chen S, Ren X, Chen G, et al. The effect of prophylactic central neck dissection on locoregional recurrence in papillary thyroid cancer after total thyroidectomy: a systematic review and meta-analysis : pCND for the locoregional recurrence of papillary thyroid cancer. *Ann Surg Oncol* (2017) 24:2189–98. doi: 10.1245/s10434-016-5691-4

16. Haugen BR, Alexander EK, Bible KC, Doherty GM, Mandel SJ, Nikiforov YE, et al. 2015 American Thyroid association management guidelines for adult patients with thyroid nodules and differentiated thyroid cancer: the American thyroid

association guidelines task force on thyroid nodules and differentiated thyroid cancer. *Thyroid* (2016) 26:1–133. doi: 10.1089/thy.2015.0020

17. Gao M, Ge M, Ji Q, Xu Z, Lu H, Cheng R, et al. Chinese Expert consensus on the diagnosis and treatment of thyroid micropapillary carcinoma (version 2016). *Chin J Clin Oncol* (2016) 43:526–. doi: CNKI:SUN:ZGZL.0.2016-10-001

18. Guidoccio F, Grosso M, Orsini F, Boni G, Mariani G, Volterrani D. Thyroid ultrasound and other imaging procedures in the pediatric age. *Curr Pediatr Rev* (2016) 12:253–64. doi: 10.2174/1573396312666161031162436

19. Stack BCJr., Ferris RL, Goldenberg D, Haymart M, Shaha A, Sheth S, et al. American Thyroid association consensus review and statement regarding the anatomy, terminology, and rationale for lateral neck dissection in differentiated thyroid cancer. *Thyroid* (2012) 22:501–8. doi: 10.1089/thy.2011.0312

20. Tuttle RM, Haugen B, Perrier ND. Updated American joint committee on Cancer/Tumor-Node-Metastasis staging system for differentiated and anaplastic thyroid cancer (Eighth edition): what changed and why? *Thyroid* (2017) 27:751–6. doi: 10.1089/thy.2017.0102

21. Du L, Wang Y, Sun X, Li H, Geng X, Ge M, et al. Thyroid cancer: trends in incidence, mortality and clinical-pathological patterns in zhejiang province, southeast China. *BMC Cancer* (2018) 18:291. doi: 10.1186/s12885-018-4081-7

22. Kwak JY, Kim EK, Youk JH, Kim MJ, Son EJ, Choi SH, et al. Extrathyroid extension of well-differentiated papillary thyroid microcarcinoma on US. *Thyroid* (2008) 18:609–14. doi: 10.1089/thy.2007.0345

23. Nascimento C, Borget I, Troalen F, Al Ghuzlan A, Deandreis D, Hartl D, et al. Ultrasensitive serum thyroglobulin measurement is useful for the follow-up of patients treated with total thyroidectomy without radioactive iodine ablation. *Eur J Endocrinol* (2013) 169:689–93. doi: 10.1530/eje-13-0386

24. Morris LG, Sikora AG, Tosteson TD, Davies L. The increasing incidence of thyroid cancer: the influence of access to care. *Thyroid* (2013) 23:885–91. doi: 10.1089/thy.2013.0045

25. Lim H, Devesa SS, Sosa JA, Check D, Kitahara CM. Trends in thyroid cancer incidence and mortality in the united states, 1974-2013. *Jama* (2017) 317:1338–48. doi: 10.1001/jama.2017.2719

26. Lee J, Song Y, Soh EY. Central lymph node metastasis is an important prognostic factor in patients with papillary thyroid microcarcinoma. *J Korean Med Sci* (2014) 29:48–52. doi: 10.3346/jkms.2014.29.1.48

27. Liu LS, Liang J, Li JH, Liu X, Jiang L, Long JX, et al. The incidence and risk factors for central lymph node metastasis in cN0 papillary thyroid microcarcinoma: a meta-analysis. *Eur Arch Otorhinolaryngol* (2017) 274:1327–38. doi: 10.1007/s00405-016-4302-0

28. Wada N, Duh QY, Sugino K, Iwasaki H, Kameyama K, Mimura T, et al. Lymph node metastasis from 259 papillary thyroid microcarcinomas: frequency, pattern of occurrence and recurrence, and optimal strategy for neck dissection. *Ann Surg* (2003) 237:399–407. doi: 10.1097/01.Sla.0000055273.58908.19

29. Kim E, Park JS, Son KR, Kim JH, Jeon SJ, Na DG. Preoperative diagnosis of cervical metastatic lymph nodes in papillary thyroid carcinoma: comparison of ultrasound, computed tomography, and combined ultrasound with computed tomography. *Thyroid* (2008) 18:411–8. doi: 10.1089/thy.2007.0269

30. Ito Y, Tomoda C, Uruno T, Takamura Y, Miya A, Kobayashi K, et al. Clinical significance of metastasis to the central compartment from papillary microcarcinoma of the thyroid. *World J Surg* (2006) 30:91–9. doi: 10.1007/s00268-005-0113-y

31. Ito Y, Uruno T, Nakano K, Takamura Y, Miya A, Kobayashi K, et al. An observation trial without surgical treatment in patients with papillary microcarcinoma of the thyroid. *Thyroid* (2003) 13:381–7. doi: 10.1089/105072503321669875

32. Sugitani I, Fujimoto Y. Symptomatic versus asymptomatic papillary thyroid microcarcinoma: a retrospective analysis of surgical outcome and prognostic factors. *Endocr J* (1999) 46:209–16. doi: 10.1507/endocrj.46.209

33. Huang XP, Ye TT, Zhang L, Liu RF, Lai XJ, Wang L, et al. Sonographic features of papillary thyroid microcarcinoma predicting high-volume central neck lymph node metastasis. *Surg Oncol* (2018) 27:172–6. doi: 10.1016/j.suronc.2018.03.004

34. Chen L, Chen L, Liu J, Nong L, Zhang H. The association among quantitative contrast-enhanced ultrasonography features, thyroid imaging reporting and data system and BRAF V600E mutation status in patients with papillary thyroid microcarcinoma. *Ultrasound Q* (2019) 35:228–32. doi: 10.1097/ruq.0000000000000406

35. Cho JK, Kim JY, Jeong CY, Jung EJ, Park ST, Jeong SH, et al. Clinical features and prognostic factors in papillary thyroid microcarcinoma depends on age. *J Korean Surg Soc* (2012) 82:281–7. doi: 10.4174/jkss.2012.82.5.281

36. Xu Y, Xu L, Wang J. Clinical predictors of lymph node metastasis and survival rate in papillary thyroid microcarcinoma: analysis of 3607 patients at a single institution. *J Surg Res* (2018) 221:128–34. doi: 10.1016/j.jss.2017.08.007

37. Zheng X, Peng C, Gao M, Zhi J, Hou X, Zhao J, et al. Risk factors for cervical lymph node metastasis in papillary thyroid microcarcinoma: a study of 1,587 patients. *Cancer Biol Med* (2019) 16:121–30. doi: 10.20892/j.issn.2095-3941.2018.0125

38. Yu X, Song X, Sun W, Zhao S, Zhao J, Wang Y-G. Independent risk factors predicting central lymph node metastasis in papillary thyroid microcarcinoma. *Horm Metab Res* (2017) 49:201–7. doi: 10.1055/s-0043-101917

39. McLeod DS, Cooper DS. The incidence and prevalence of thyroid autoimmunity. *Endocrine* (2012) 42:252–65. doi: 10.1007/s12020-012-9703-2

40. Vanderpump MP, Tunbridge WM, French JM, Appleton D, Bates D, Clark F, et al. The incidence of thyroid disorders in the community: a twenty-year follow-up of the whickham survey. *Clin Endocrinol (Oxf)* (1995) 43:55–68. doi: 10.1111/j.1365-2265.1995.tb01894.x

41. Dailey ME, Lindsay S, Skahen R. Relation of thyroid neoplasms to hashimoto disease of the thyroid gland. *AMA Arch Surg* (1955) 70:291–7. doi: 10.1001/archsurg.1955.01270080137023

42. Lee JH, Kim Y, Choi JW, Kim YS. The association between papillary thyroid carcinoma and histologically proven hashimoto's thyroiditis: a meta-analysis. *Eur J Endocrinol* (2013) 168:343–9. doi: 10.1530/eje-12-0903

43. Jara SM, Carson KA, Pai SI, Agrawal N, Richmon JD, Prescott JD, et al. The relationship between chronic lymphocytic thyroiditis and central neck lymph node metastasis in north American patients with papillary thyroid carcinoma. *Surgery* (2013) 154:1272–80. doi: 10.1016/j.surg.2013.07.021

44. Zhang Q, Wang Z, Meng X, Duh QY, Chen G. Predictors for central lymph node metastases in CN0 papillary thyroid microcarcinoma (mPTC): a retrospective analysis of 1304 cases. *Asian J Surg* (2019) 42:571–6. doi: 10.1016/j.asjsur.2018.08.013

45. Dayan CM, Daniels GH. Chronic autoimmune thyroiditis. *N Engl J Med* (1996) 335:99–107. doi: 10.1056/nejm199607113350206

46. Bansal M, Gandhi M, Ferris RL, Nikiforova MN, Yip L, Carty SE, et al. Molecular and histopathologic characteristics of multifocal papillary thyroid carcinoma. *Am J Surg Pathol* (2013) 37:1586–91. doi: 10.1097/PAS.0b013e318292b780

47. Koo BS, Lim HS, Lim YC, Yoon YH, Kim YM, Park YH, et al. Occult contralateral carcinoma in patients with unilateral papillary thyroid microcarcinoma. *Ann Surg Oncol* (2010) 17:1101–5. doi: 10.1245/s10434-009-0906-6

48. Khokhar MT, Day KM, Sangal RB, Ahmedli NN, Pisharodi LR, Beland MD, et al. Preoperative high-resolution ultrasound for the assessment of malignant central compartment lymph nodes in papillary thyroid cancer. *Thyroid* (2015) 25:1351–4. doi: 10.1089/thy.2015.0176

49. Guang Y, He W, Zhang W, Zhang H, Zhang Y, Wan F. Clinical study of ultrasonographic risk factors for central lymph node metastasis of papillary thyroid carcinoma. *Front Endocrinol (Lausanne)* (2021) 12:791970. doi: 10.3389/fendo.2021.791970

50. Kim SK, Park I, Woo J-W, Lee JH, Choe J-H, Kim J-H, et al. Predictive factors for lymph node metastasis in papillary thyroid microcarcinoma. *Ann Surg Oncol* (2016) 23:2866–73. doi: 10.1245/s10434-016-5225-0

51. Li C, Guan H, He Q, Zhao Y, Liang N, Zhang J, et al. The relationship between lipotoxicity and risk of extrathyroidal extension in papillary thyroid microcarcinoma. *Endocrine* (2021) 74:646–57. doi: 10.1007/s12020-021-02809-8

Frontiers in Endocrinology

Explores the endocrine system to find new therapies for key health issues

The second most-cited endocrinology and metabolism journal, which advances our understanding of the endocrine system. It uncovers new therapies for prevalent health issues such as obesity, diabetes, reproduction, and aging.

Discover the latest Research Topics

See more →

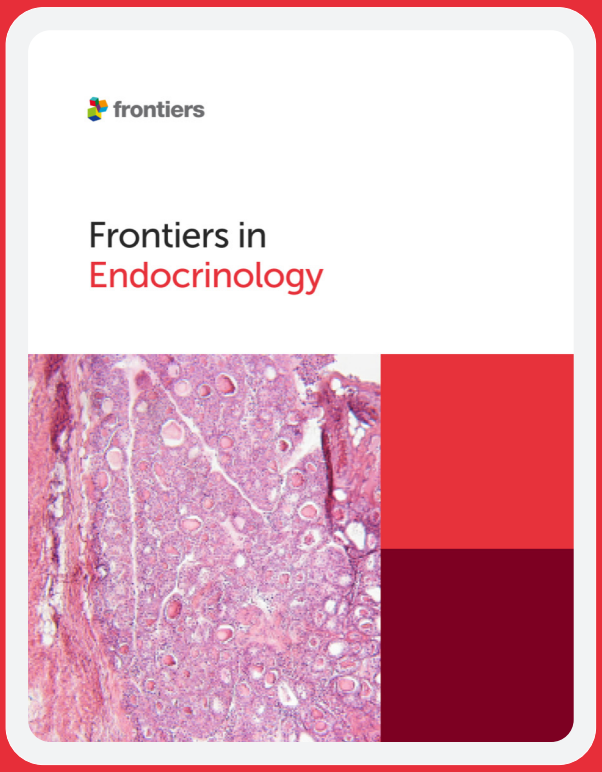

Frontiers

Avenue du Tribunal-Fédéral 34
1005 Lausanne, Switzerland
frontiersin.org

Contact us

+41 (0)21 510 17 00
frontiersin.org/about/contact